The Calcium-Looping process for advancing in the development of both CO_2 capture and thermochemical energy storage systems

Author

Carlos Ortiz Domínguez

Supervisors

Prof. Ricardo Chacartegui Ramírez

Prof. José Manuel Valverde Millán

A Thesis submitted to the
Universidad de Sevilla
for the degree of
DOCTOR OF PHILOSOPHY

Programa de Doctorado de Ingeniería Energética, Química y Ambiental
Escuela Técnica Superior de Ingeniería
Universidad de Sevilla

July 2018

Abstract

The Calcium-Looping process is based on the multicycle calcination-carbonation of calcium carbonate, which is one of the most abundant materials in the Earth. The process shows promising results facing to solve two of the main challenges within the future energy scenario: CO_2 capture from fossil fuel combustion processes and energy storage in renewable-based plants. This thesis is focused in the assessment of the Calcium-Looping allowing a better understanding of the process integration for both applications.

Post-combustion CO_2 capture based on Calcium-Looping process consist of reacting the CO_2 present in the flue gas exiting the fuel power plant with CaO particles according the carbonation reaction, which produces solid $CaCO_3$ as product. CO_2 capture efficiencies over 90% have been proved at MW_{th} pilot-scale. After carbonation, solids are sent to a separated reactor where CaO is regenerated according the endothermic calcination reaction. The heat to carry out the reaction is provided by fuel oxy-fuel combustion to ensure an almost pure CO_2 stream exiting the reactor, which after a purification process is ready to be stored or used in another process. The regenerated CaO is sent again to the carbonator reactor for a new CO_2 capture cycle.

On the other hand, by integrating the Calcium-Looping as thermochemical energy storage system in solar thermal power plants, the process starts performing the calcination reaction from concentrated solar power. CO_2 and CaO streams produced are stored separately for later use. When energy is demanded, both components are brought together to the carbonator where the stored energy is released by the carbonation reaction. The carbonation is highly exothermic and therefore a proper integration of the heat released (i.e. for power production) is fundamental for the process efficiency.

In spite that both applications are based on the same process, the specific operation conditions required leads to a different behaviour which suggest that the process must be analysed in detail according to each application. This thesis is focused on the development of models and process integration schemes based on lab-scale results under specific conditions selected from the analysis of the potential industrial scale implementation. It involves a multidisciplinary approach combining chemical reactions and process engineering to advance in the response of the challenges posed.

This document is structured as follow: the first section introduces the reader to the Calcium-Looping applications, stressing the research opportunities that have motivated the present thesis. This leads to the formulation of the objectives of the work, which are addressed in the presentation and the discussion of the main results of the work. After the conclusions, new research lines to be faced in the near future are summarized.

Acknowledgements

There are many people to whom I would like to thank their collaboration in this thesis. First of all, to my supervisors, Prof. Ricardo Chacartegui and Prof. Jose Manuel Valverde, for giving me opportunity to develop my PhD and for their invaluable support during these three intense years. Also thank Dr. Jose Antonio Becerra for his help in this period.

I am fully grateful to Dr. Matteo Romano for giving me the opportunity of spending a fruitful research stay at the Politecnico di Milano. Thanks to Dr. Marco Binotti for his assistance. I gratefully acknowledge Prof. Luis Pérez-Maqueda and his team, Antonio, Pedro, Mónica and Beatriz, for their collaboration within this edifying work environment.

I would like to thank especially my colleagues Jesús, Pilar, Elisa, Fran, Reyes, Irene and Nabil for making going to work every day so fun. Thanks to Victor, Alessandro, Davide and Giuseppe for the fruitful collaboration.

Thank the department of Electronic and Electromagnetism for hosting me during these years. Thanks to Mª Jesús and Silvia for their help with administrative tasks.

On a more personal note, I would like to thank my parents for their support and confidence. Thanks to my brothers.

Special thanks to Belen, for her unconditional love. I apologize for all the hours that I have not dedicated to you during the realization of this work. Thanks to Guille, our precious baby.

List of publications

This thesis is presented as a compendium of publications according to Article 9 of the regulations governing the regime doctoral thesis (Agreement 9.1/CG 12/04/19) within the framework regulated by the RD 1393/2007. The thesis is supported by several original publications developed by the author and his co-authors during the thesis period. The author has explicit authorization by all his co-authors to use their content as part of this thesis. A complete copy of the publications is presented in Annex 1-10. Moreover, as part of the work carried out in this thesis, several contributions have been made to national and international congresses as well as the application for two patents.

Papers in indexed journals

ANNEX 1

Ortiz C, Chacartegui R, Valverde J, Becerra J, Perez-Maqueda L. ***A new model of the carbonator reactor in the calcium looping technology for post-combustion CO_2 capture****. FUEL 2015;160:328–38. doi:10.1016/j.fuel.2015.07.095.*

ANNEX 2

Ortiz C, Chacartegui R, Valverde JM, Becerra JA. ***A new integration model of the calcium looping technology into coal fired power plants for CO_2 capture.*** *Appl Energy 2016;169:408–20. doi:10.1016/j.apenergy.2016.02.050.*

ANNEX 3

Chacartegui R, Alovisio A, Ortiz C, Valverde JM, Verda V, Becerra JA. ***Thermochemical energy storage of concentrated solar power by integration of the calcium looping process and a CO_2 power cycle.*** *Appl Energy 2016;173:589–605. doi:10.1016/j.apenergy.2016.04.053.*

ANNEX 4

Ortiz C, Valverde JM, Chacartegui R. ***Energy Consumption for CO_2 Capture by means of the Calcium Looping Process: A Comparative Analysis using Limestone, Dolomite, and Steel Slag.*** *Energy Technol 2016:1–12. doi:10.1002/ente.201600390.*

ANNEX 5

Alovisio A, Chacartegui R, Ortiz C, Valverde JM, Verda V. ***Optimizing the CSP-Calcium Looping integration for Thermochemical Energy Storage.*** *Energy Convers Manag 2017;136:85–98. doi:10.1016/j.enconman.2016.12.093.*

ANNEX 6

Ortiz C, Chacartegui R, Valverde JM, Alovisio A, Becerra JA. ***Power cycles integration in concentrated solar power plants with energy storage based on calcium looping****. Energy Convers Manag 2017;149:815–29. doi:10.1016/j.enconman.2017.03.029.*

ANNEX 7

Ortiz C, Valverde JM, Chacartegui R, Benítez-Guerrero M, Perejón A, Romeo LM. ***The Oxy-CaL process: A novel CO_2 capture system by integrating partial oxy-combustion with the Calcium-Looping process****. Appl Energy 2017;196:1–17. doi:10.1016/j.apenergy.2017.03.120.*

ANNEX 8

Bonaventura, D., Chacartegui, R., Valverde, J.M., Becerra, J.A., Ortiz, C., Lizana, J., 2018. ***Dry carbonate process for CO_2 capture and storage: Integration with solar thermal power****. Renew. Sustain. Energy Rev. 82, 1796–1812. https://doi.org/10.1016/j.rser.2017.06.061*

ANNEX 9

Ortiz C, Valverde JM, Chacartegui R, Perez-Maqueda LA. ***Carbonation of Limestone Derived CaO for Thermochemical Energy Storage: From Kinetics to Process Integration in Concentrating Solar Plants.*** *ACS Sustain Chem Eng 2018;6:6404–17. doi:10.1021/acssuschemeng.8b00199.*

ANNEX 10

Ortiz C, Romano MC, Valverde JM, Binotti M, Chacartegui R. ***Process integration of Calcium-Looping thermochemical energy storage system in concentrating solar power plants****. Energy 2018;155:535–51. doi:10.1016/j.energy.2018.04.180.*

In addition, the author has collaborated in other papers not directly related to the subject of the thesis but developed within the research group framework. For this reason, these publications are not included in the annexes:

- *Soltero VM, Chacartegui R, Ortiz C, Velázquez R.* ***Evaluation of the potential of natural gas district heating cogeneration in Spain as a tool for decarbonisation of the economy****. Energy 2016:1–20. doi:10.1016/j.energy.2016.06.038.*

- *Lizana J, Ortiz C, Soltero VM, Chacartegui R.* ***District heating systems based on low-carbon energy technologies in Mediterranean areas****. Energy 2017;120:397–416. doi:10.1016/j.energy.2016.11.096.*

- *Lizana J, Chacartegui R, Barrios-Padura A, Ortiz C.* ***Advanced low-carbon energy measures based on thermal energy storage in buildings: A review****. Renew Sustain Energy Rev 2018;82:3705–49. doi:10.1016/j.rsder.2017.10.093.*

- *Soltero V, Chacartegui R, Ortiz C, Lizana J, Quirosa G.* ***Biomass District Heating Systems Based on Agriculture Residues****. Appl Sci 2018;8:476. doi:10.3390/app8040476.*

- *Soltero VM, Chacartegui R, Ortiz C, Velázquez R.* ***Potential of biomass district heating systems in rural areas****. Energy 2018;156:132–43. doi:10.1016/j.energy.2018.05.051.*

Participation in conferences

1) *Soltero VM, Chacartegui R, Ortiz C, Velázquez Vila R, Becerra Villanueva JA.* ***Evaluation of the potential for Natural Gas District Heating Cogeneration in Spain as a tool for economy decarbonization****. 10th Conf. Sustain. Dev. Energy, Water Environ. Syst., Dubrovnik (Croacia): 2015.*

2) *Ortiz C, Chacartegui R, Valverde JM, Alovisio A, Becerra JA.* ***Calcium looping process for Thermochemical Energy Storage in CSP plants. Integration assessment of direct and indirect power cycles.*** *11th Conf. Sustain. Dev. Energy, Water Environ. Syst., 2016, p. 1–29.*

3) *Lizana J, Chacartegui R, Barrios-Padura Á, Ortiz C, Vilches A.* ***Evaluation of thermal energy storage technologies for heating, cooling and hot water applications road to zero energy buildings****. 11th Conf. Sustain. Dev. Energy, Water Environ. Syst., Lisbon: 2016.*

4) *Lizana J, Serrano A, Ortiz C, Becerra Villanueva JA, Chacartegui R.* ***Energy assessment methodology towards low-carbon energy schools applied to Mediterranean buildings.*** *Conf. Sustain. Dev. Energy, Water Environ. Syst., Dubrovnik , Croatia: 2017.*

5) *Ortiz C, Fernandez R, Chacartegui R, Valverde JM, Becerra JA.* ***Almacenamiento termoquímico en plantas CSP basado en calcium-looping: retos y oportunidades.*** *XVI Congr. Ibérico y XII Congr. Iberoam. Energía Sol., Madrid: 2018.*

6) *Soltero VM, Chacartegui R, Ortiz C, Quirosa G.* ***Renewable biomass low temperature heating networks for rural locations.*** *ECOS 2018 - 31ST International. Conference on Efficiency, cost, optimization, simulation and Environmental impact of Energy Systems, Guimaraes (Portugal): 2018.*

7) *Ortiz C, Valverde JM, Chacartegui R, Romeo LM, Perez-Maqueda LA.* ***The mOxy-CaL process: integration of membrane separation, partial oxy-combustion and Calcium Looping for CO_2 capture.*** *21st Conf. Process Integr. Model. Optim. Energy Sav. Pollut. Reduct., 2018.*

8) *Fernandez R, Ortiz C, Chacartegui R, Valverde JM, Becerra JA.* ***Thermochemical Energy Storage for enhancing the dispatchability in PV plants.*** *13th Conf. Sustain. Dev. Energy, Water Environ. Syst. - SDEWES Conf., 2018.*

Patents

1) *Chacartegui R, Becerra JA, Valverde JM, Ortiz C, Alovisio A.* ***Sistema integrado de calcinación-carbonatación y ciclo de lazo cerrado de CO_2 para almacenamiento de energía termoquímica y generación de energía eléctrica.*** *ES201500493A, 2015.Patent*

2) *Ortiz C, Chacartegui R, Valverde JM, Becerra JA.* ***Instalación y procedimiento de captura de CO_2 mediante integración de membranas, oxi-combistión parcial y calcinación-carbonatación.*** *Pending application.*

Awards

Two of the publications that make up this thesis have been awarded with both international and local awards:

1) Award for **Best paper** in 11th Conference on Sustainable Development of Energy, Water and Environment systems (Lisbon, 2016).

Ortiz C, Chacartegui R, Valverde JM, Alovisio A, Becerra JA. ***Calcium looping process for Thermochemical Energy Storage in CSP plants. Integration assessment of direct and indirect power cycles.****"*

2) Award for **Best paper** of the month in the Physics Faculty of the University of Seville

Ortiz C, Valverde JM, Chacartegui R, Benítez-Guerrero M, Perejón A, Romeo LM. ***The Oxy-CaL process: A novel CO_2 capture system by integrating partial oxy-combustion with the Calcium-Looping process.*** *Appl Energy 2017; 196:1–17. doi:10.1016/j.apenergy. 2017.03.120.*

This thesis has been supported by the Spanish Ministry of Economy and Competitivity and FEDER Funds within the contract CTQ2014-52763-C2-2-R (SOLARTEQH project) through a predoctoral grant (BES-2015-073149). Furthermore, part of the research leading to this thesis has received funding from the European Union's Horizon 2020 research and innovation programme under grant agreement No 727348 (SOCRATCES project).

Contents

List of tables

List of figures

Notation

$[CO_2]$	average CO_2 concentration, mol/m^3	t_K	time of the kinetic controlled phase
$[CO_2]_{eq}$	equilibrium concentration of CO_2, mol/m^3	T	Temperature, ºC
D^*_{eff}	equivalent diffusion constant, m^3/ (mol ·s)	T_{carb}	carbonator temperature, ºC
E	emissions ratio after CO2 capture, kg CO_2/kWhe	T_{calc}	calciner temperature, ºC
E_1	activation energy for chemical decomposition, kJ/mol	T_{eq}	equilibrium temperature, ºC
E_{CO2}	carbon capture efficiency	$V_{M_{CaO}}$	molar volume, m3/mol
E_{max}	maximum capture efficiency	W_s	solid inventory in the carbonator, kg
E_{ref}	emissions ratio before CaL, kg CO_2/kWhe	X	CaO conversion
f_0	inlet molar fraction of CO2	X_{ave}	average conversion of the sorbent
f_a	volumetric fraction of CaO that reacts in the kinetic reaction regime	$X_{ave,K}$	average conversion of the sorbent in the kinetic phase
f_{carb}	average carbonation level	$X_{ave,D}$	average conversion of the sorbent in the diffusion phase
f_e	equilibrium molar fraction of CO2	$X_{max,ave}$	Average maximum conversion of the sorbent
F_{CO2}	mole flow rate of CO_2 in flue gas entering the carbonator, kmol/h	X_N	maximum carbonation degree of CaO in the N cycle
F_O	mole flow rate of fresh makeup limestone, kmol/h	X_{ND}	maximum carbonation degree of CaO in the N cycle in the diffusion phase
F_R	mole flow rate of CO_2 in flue gas entering the carbonator, kmol/h	X_{NK}	maximum carbonation degree of CaO in the N cycle in the kinetic phase
F_{fg}	flue gas molar flow rate, kmol/s	X_r	residual conversion capacity of a sorbent particle
h_i	Enthalpy, kJ/kmol	x_{CO2}	CO_2 Molar fraction exiting the plant
k_i	reaction rate constants	x_{O2}	O_2 Molar fraction exiting the plant
k_s	intrinsic kinetic constant m^4/ (mol ·s)	$y_{CO2,in}$	CO2 molar fraction at carbonator inlet
$\dot{m}$	mass flow rate, kg/s	$y_{CO2,eq}$	CO2 molar fraction at carbonation equilibrium
N	calcination–carbonation cycles	W_s	solid inventory in the carbonator, kg
N_{Ca}	mol of Ca in the carbonator, mol	$\dot{W}_{net}$	average electrical power, MWe
P	Pressure, bar	$\dot{W}_{net,night}$	net electrical power for the night mode, MWe
P_{carb}	Carbonator pressure, bar	$\dot{W}_{net,sun}$	net electrical power for the sun mode, MWe
P_{eq}	CO_2 partial pressure at equilibrium, bar	$\dot{W}_{M-TURB}$	power produced by the main CO2 turbine, MWe
PR	pressure ratio	$\dot{W}_{M-COMP}$	power consumed by the main CO2 compressor, MWe
$\dot{Q}_{input}$	solar power input	$\dot{W}_{HPS-TURB}$	power produced by the high-pressure CO2 turbine, MWe
r	reaction rate, s^{-1}	$\dot{W}_{ASU}$	power consumption in the ASU, MW
r_a	rate of adsorption, s^{-1}	$\dot{W}_{sec}$	net power production in secondary steam cycle, MW
r_2	chemical reaction rate, s^{-1}	$\dot{W}_{comp,CO2}$	power consumption in CO_2 compression, MW
$r_{ave,D}$	average reaction rate in the diffusion regime, s^{-1}	$\dot{W}_{comp,fg}$	power consumption in flue gas compression, MW
$r_{ave,K}$	average reaction rate in the kinetic regime, s^{-1}	$\dot{W}_{sólid}$	power consumption in solids transport, MW
S_{ave_K}	average surface area available for reaction, m^{-1}	$\dot{W}_{HPS-COMP}$	power consumption of high pressure intercooled CO2 compressor for the storage system, MWe

$\dot{W}_{ST}$	power produced in the steam turbine cycle, MWe	ρ_g	density of gas phase, g/m3
$\dot{W}_P$	power consumed in the steam turbine cycle, MWe	η	overall net efficiency
$\dot{W}_{PSOLCAL}$	Power consumptions for solids transport in the calciner side, MWe	η_{boiler}	boiler efficiency
$\dot{W}_{PSOLCAR}$	Power consumptions for solids transport in the carbonator side, MWe	η_{CFPP}	coal fire power plant efficiency
$\dot{W}_{AUXPOWCA}$	auxiliary power consumptions in the calciner side, MWe	η_{ref}	reference plant efficiency
$\dot{W}_{AUXPOWCR}$	auxiliary power consumptions in the carbonator side, MWe	η_{int}	new global efficiency (CFPP-capture system)
ϕ_N	particle fraction in the N cycle	$\Delta H_R(T_{react})$	reaction enthalpy at the reactor temperature, kJ/mol
τ	average residence time in the carbonator, s	$\Delta {H_R}^0$	standard reaction enthalpy kJ/mol
ρ_{CaO}	CaO density, g/m3	ΔS_2^0	carbonation entropy change, J/(mol·K)

CaL	Calcium-Looping	SPECCA	Energy consumption per kilogram of CO2 avoided
CSP	Concentrating Solar Power	CAPEX	Capital Expenditures
TCES	Thermochemical Energy Storage	PCC	Post-Combustion Capture
CFPP	Coal fired power plants	CCS	CO_2 Capture and Storage
CFB	Circulating Fluidized Bed	TES	Thermal Energy Storage
PCM	Phase Change Material	SM	Solar Multiple

1. Introduction

$CaCO_3$ is the second most abundant material on Earth after water. The Calcium-Looping (CaL) process is based on the multicyclic calcination-carbonation of $CaCO_3$ according Eq. (1). Calcination is a well-known reaction which is at the basis of the cement industry [1] while the CaL process has many other applications. As early as 1933, the use of CaO-based materials was patented for CO_2 capture to enhance H_2 production from methane reforming [2]. Later on, the CaL process began to be considered as a potential Thermochemical Energy Storage (TCES) system in the late 1970s [3–5]. More recently, the CaL process has been widely studied for post-combustion CO_2 Capture (PCC) in fossil power plants [6–8].

$$CaCO_{3(s)} \rightleftarrows CaO_{(s)} + CO_2 \qquad \Delta H_r^0 = 178 \frac{kJ}{mol} \tag{1}$$

The CaL the process is fully aligned with some of the most important challenges in the energy scenario. Thus, the CaL process can be applied in both renewable and fossil-fuel based power plants as energy storage and CO_2 capture systems, respectively. In the former case, a promising option is the integration of the CaL process in Concentrating Solar Power (CSP) plants to improve the dispatchability of the system. CSP plants, as well as other plants based on renewable resources, are characterized by a variable energy input depending on the non-continuous nature of the solar resource and, when the solar resource is available, variability of the weather conditions. By integrating the CaL process as TCES system, direct solar radiation is used to carry out the calcination reaction (endothermic), releasing CO_2 and CaO as products that are stored separately. Storage conditions and time are flexible and could be accommodated to the energy demand [9]. When energy is needed, the stored products are brought together to carry out the carbonation reaction (exothermic), by which the stored energy is released. In comparison with currently commercial energy storage systems, such as solar molten salts, the CaL process presents several benefits such as its feasibility to work at significantly higher power cycle temperatures, a high energy storage density and the possibility to store energy in the medium-long term.

Regarding CO_2 capture, the CaL process is highlighted as one with higher potential for post-combustion capture. The standard cycle for CO_2 capture from flue gas streams uses lime (CaO), which can be derived from limestone calcination, to produce $CaCO_3$ by carbonation at high temperature (~650ºC). Typical CaL conditions for CO_2 capture involve carbonation at relatively low CO_2 partial pressure (about 0.15 atm) and calcination at very high temperatures (around 950ºC) under high CO_2 partial pressure with short residence times at both stages. Once CO_2 is captured in the carbonator and heat from the exothermic reaction is recovered, the almost CO_2 free flue gas is released into the atmosphere. Pilot plants (of size on the order of 1-2 MWth) have

recently demonstrated the achievement of CO_2 capture efficiencies around 90% [10,11] whereas model simulations predict an efficiency penalty on power generation around 3-9% when scaling up the technology to a commercial level [12].

Because of the huge potential scope for the CaL process within the future energy system, in both renewable and non-renewable power plants, and in new or retrofitted facilities, a fast technology development with a relevant cost reduction is expected. Moreover, it must be highlighted the very favorable characteristics of the CaO precursors such as limestone or dolomite: low cost, wide availability and non-toxicity [13–15], which are necessary conditions for the massive integration on a large scale of any CO_2 capture or energy storage technology.

1.1. Calcium-Looping process for post-combustion CO_2 capture

Finding competitive and sustainable solutions for capturing and sequestering the CO_2 released from fossil fuel combustion processes is a key issue to mitigate global warming [16]. Despite the necessary increase in energy production share from renewable sources, power plants based on natural gas or coal currently generate most of the energy consumed in the world [17]. Currently, 76.5% of the electricity generation in the world is produced by non-renewable sources [18]. It is expected that the commercial deployment of CO_2 capture and storage (CCS) technologies plays a main role within the portfolio of urgent measures to limit global warming below 2°C from preindustrial levels [19,20]. On this decarbonization purpose, future fuel-based power plants must be near to CO_2 emissions free. Coal fired power plants (CFPP) are prime candidates to be retrofitted with CCS. The main R&D challenge for the viability of CFPPs and other fossil fuel-based facilities is to capture CO_2 by means of feasible, sustainable and affordable technologies while, at the same time, the penalties of integrating these technologies on power production and efficiency are minimized. For a real deployment of CO_2 capture technologies, it must be reduced both the energy consumption associated to the CO_2 capture process and the CO_2 capture system size. The former is directly related to the electricity production cost. Typical values reported on energy consumption per kilogram of CO_2 avoided (SPECCA) are around 4 MJ/kg CO_2 [21] using the already mature amines based technology. On the other hand, the CO_2 capture system size affects to capital expenditures (CAPEX).

Post-combustion capture (PCC) refers to CO_2 removal from the flue gas of fossil fuel-based power plants, which can be accomplished by using chemical solvents, solid sorbents or electrochemical processes. Despite post-combustion capture processes are being widely investigated in the last years, Boundary Dam (100MWe) in Canada and Petra Nova (240MWe) in USA are currently the only commercial CFPP that applies CCS by using a chemical absorption process based on amines.

In chemical absorption, the solvent (typically an amine solution such as MEA) binds chemically with the CO_2. Amine absorption and stripping consists of passing the post-combustion flue gas through an aqueous amine solvent, which absorbs CO_2 by chemical reaction [22]. Then, the solvent loaded with CO_2 (the "rich" solvent) is heated up above typically 120 °C in the regenerator reactor wherein the CO_2-amine chemical reaction is reversed to release nearly pure CO_2 and regenerate the amine. The so-called "lean" solvent is recycled back to the absorber to restart the process while the released relatively pure CO_2 is compressed to a suitable pressure for an efficient transportation and storage [23]. After regeneration, the solvent is cooled to be reused [24]. Amine-based PCC can efficiently remove around 90% of the CO_2 emissions.

A main issue of systems based on amine absorption is the large amount of heat required to regenerate the solvent [25–27]. This heat, which is usually obtained from the steam cycle, penalizes significantly (8-12%) the power plant efficiency. Moreover, the commercial expansion of amine-based systems for CO_2 capture at large scale is hindered by amines toxicity [28], degradation [29] and equipment corrosion [30]. Thus, there is a need for developing novel large-scale capture technologies with reduced energy penalty and capture cost, which should rely on environmentally friendly and abundantly available cheap materials.

Another option for PCC is based on membrane separation, which uses the pressure difference between the flue gas and the removed CO_2. The membrane technology is generally useful to treat high-pressure gases [31,32] in spite of which a large number of researches have adapted it for post-combustion capture [33–35]. Regarding efficiency penalty associated to membranes use for PCC, it is estimated in the range of 4.9-8.5% [31]. Membrane separation is a promising solution to reduce the costs of PCC. However, the maximum pressure ratio attainable by feed compression and/or permeate vacuum is limited to approximately 10, due to cost and energy considerations [33].

The development of dry CO_2 capture processes based on cheap materials operating at relatively low temperatures, which would require relatively low energy for sorbent regeneration, is considered as a promising pathway to advance in the deployment of CO_2 capture technologies [36,37]. Na_2CO_3 is the sorbent employed in the Dry Carbonate Process (DCP) early proposed in [38,39] and currently being demonstrated at the pilot-scale stage [40]. An important advantage of the DCP is that sorbent regeneration would be carried out at 100-200ºC and therefore the process could be efficiently assisted by medium temperature solar thermal power. Another proposed technology for PCC is the use of electrochemical processes in Molten Carbonate fuel cells. Some studies show that electricity generation in the fuel cell partially compensates the penalty on the original cycle in wastewater treatment plants [41] and power plants [42–44].

The CaL process is at the root of a promising 2nd generation technology for post-combustion CO_2 capture at coal fired power plants. The potential application of the CaL process is increasingly gaining momentum in the last years mainly due to the possibility of implementing it in already existing power plants and the relatively low penalty on plant performance as compared to other already mature capture technologies such as conventional amine-based capture systems (penalty around 8-12 %) [7,13,45]. Figure 1 shows a conceptual scheme of the CaL process applied for post-combustion CO_2 capture.

The CaL process consists of the capture of CO_2 in the post-combustion flue gas by carbonation in a high temperature fluidized bed reactor of CaO solids derived from the calcination of natural limestone ($CaCO_3$). The process would be carried out in two interconnected circulating fluidized bed (CFB) reactors, both operated under atmospheric pressure at gas velocities of about 5 m/s [46,47] wherein gas-solid contact and heat/mass transfer are promoted. Another CaO precursor could be natural dolomite. According to recent lab-scale studies [48], dolomite-derived CaO would exhibit a greater capture capacity than limestone-derived CaO at CaL conditions for CO_2 capture. On the other hand, several synthetic sorbents have been developed with enhanced capture behavior [49,50]. Nevertheless, the use of these synthetic sorbents usually leads to an important increase of the cost of the system operation [12]. Taking into account that flue gases exiting from coal-fired power plants generally contain a mole fraction of CO_2 in the range 10-15% [51,52], optimum carbonation temperatures are around 650°C in order to achieve significant efficiencies of CO_2 capture (around 80-90%) in short residence times, typically on the order of minutes [53].

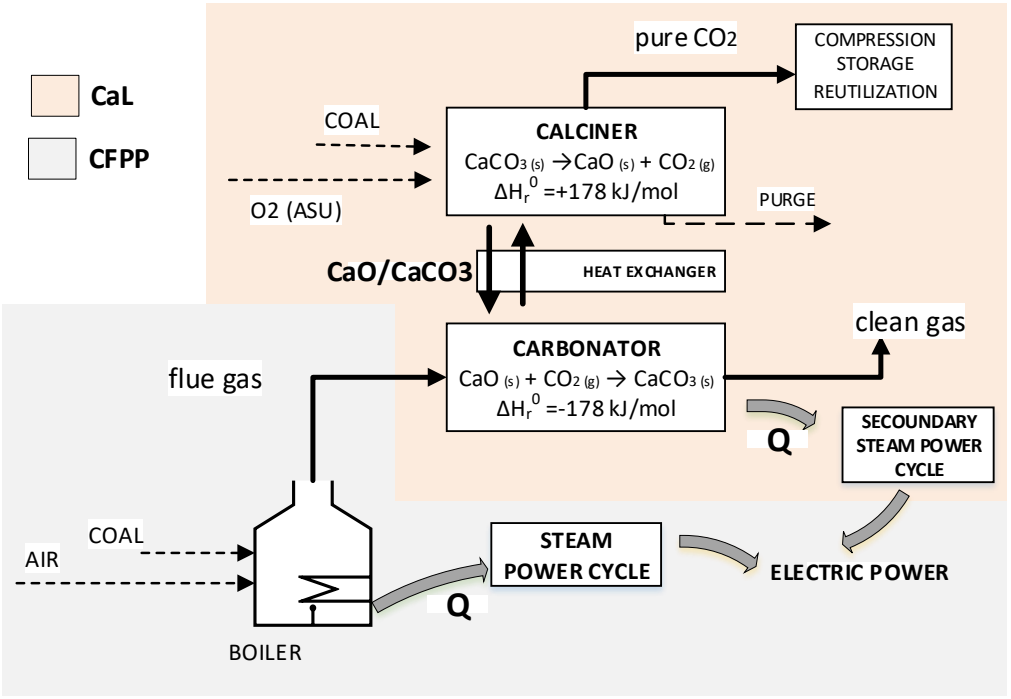

Figure 1: Conceptual scheme of the CaL process for post-combustion CO_2 capture. Modified from [54]

Once CO_2 is captured in the carbonator and heat from the exothermic reaction is recovered, the decarbonized flue gas is vented into the atmosphere. The carbonated solids are calcined in a second fluidized bed reactor (calciner) at higher temperatures, which regenerates CaO for a new cycle and produces a highly concentrated CO_2 stream ready for compression and sequestration. CaO is regenerated in the calciner by calcination under necessarily high CO_2 partial pressure, which requires the use of rather high temperatures (> 930ºC) for efficient calcination in a short residence time [10,55–57].

The endothermic calcination reaction and the drop of temperatures between the sorbent streams entering and leaving the calciner involves the need of providing a high-energy input to the calciner. The most feasible method to generate the heat required in the calciner and avoid CO_2 dilution at the same time is the burning of fuel by oxy-combustion [10,14,55–57]. Thus, calcination is carried out in an environment containing between 70% and 90% vol. concentration of CO_2 at atmospheric pressure [55,58–61]. After calcination, CO_2 is retrieved from the calciner for compression, transport and geological storage or other uses. Under these operating conditions, calcination temperatures above 930ºC are necessary to regenerate the sorbent in short residence times [62–64]. These conditions promote sintering of CaO which compromises the multicyclic CO_2 capture capacity [65].

CaO deactivation is one of main issues to be addressed in the CaL process [66]. It is well-known that carbonation occurs in two consecutive phases. The first stage takes place on the free surface

of the solid through the nucleation and growth of a $CaCO_3$ layer and it is governed by the kinetics of the reaction between CaO and CO_2. The end of the fast stage takes place when a 40–60 nm thickness product layer is formed, which makes inaccessible a large fraction of CaO in the interior of the particles [67]. Then it takes places a second stage controlled by the solid-state diffusion CO_3^{2-} and O^{2-} ions through the product layer, which is a much slower process. TGA tests carried out under calcination at high CO_2 partial pressure show that solid-state diffusion plays an important role in the total CaO conversion since capture in the fast reaction controlled regime is greatly reduced with the number of cycles [48,63]. By using limestone under typical CaL conditions for post-combustion CO_2 capture, the multicyclic CaO conversion decays with the cycle number up to reach a residual value 0.07-0.08 for residence times of about 5 min [68,69].

CaO deactivation is partially compensated by the periodic introduction of a fresh limestone makeup in the calciner while the purged CaO is particularly well suited for cement production [70,71]. CaO deactivation is further enhanced by irreversible CaO sulphation and ashes due to in-situ coal oxy-combustion [6,63,66,72]. To reduce the make-up flow, lab- scale tests suggest that a possibility to enhance the CO_2 capture efficiency could be the recarbonation of the partially carbonated particles in another reactor before the calcination step by using the pure CO_2 stream exiting the calciner [73,74].

Regarding the CFPP-CaL integration, several models have been proposed in the literature aimed at predicting the efficiency penalty that arises from integrating the CaL technology in commercial power plants [75]. These models consider integration of CO_2 capture into coal fired power plants (CFPP) [6,14,76,77], lignite fired power plants (LFPP) [56], natural gas combined cycle power plants (NGCC) [78] and integrated gasification combined cycle power plants (IGCC) [79–82]. Depending on the power plant type, most results show efficiency penalties in the range 3-9% [83], which is lower than in the MEA-based process. Minimizing energy penalties is a key point for the industrial competitiveness of the CaL process. A number of process schemes and configurations to enhance the energy integration have been proposed in the literature [83].

CaL integration studies are generally built upon equilibrium models for the calciner reactor [6,76,84]. As regards the carbonator, previous works have considered equilibrium models [79,85], semi-predictive models using the Kunii-Levenspiel formulation for the fluidized bed hydrodynamics [6,64] or an average conversion model [84]. Several carbonator reactor models have been already proposed to predict the CO_2 capture efficiency under CaL conditions for CO_2 capture [47,77,86,87]. These models have been inferred from thermogravimetric analysis (TGA) results in which calcination is usually carried out under low CO_2 partial pressure, which does not conform to the expected operation conditions in the real system. Experimental results show that

the multicyclic capture capacity of limestone is strongly influenced by the conditions under which calcination is performed [58,88,89].

There are several pilot-scale facilities testing the CaL process for post combustion CO_2 capture. The larger plants are La Pereda (1.7 MWth) [10,90], Darmstadt (1 MWth) [11] and Hualien (1.9 MWth) [91], with the rest of pilot plants in the range of 1-120 KWth [75]. Most of the reactors are based on Fluidized Bed technology, either Circulating or Bubbling Fluidized Bed.

1.1.1. Challenges in the road to the deployment of CO_2 capture technologies

Each one of the above reviewed PCC technologies show specific advantages but also challenges to overcome at their different R&D development stages. Remarkably, PCC is considered as the most appropriate technique to be applied in the short-term for its relatively easy integration in existing fossil fuel power plants [26]. PCC integration penalizes power plant performance, and this hampers indirectly the global CO_2 emissions reduction.

Main drawbacks that hinder the deployment of the CaL process are the high cost of the full CCS chain and the high efficiency penalty imposed on the power plant. As discussed above, diverse alternatives have been analyzed for mitigating the efficiency penalty. A main inconvenient is that sorbent regeneration requires a large amount of heat at high temperatures (900–950°C), which must be properly recovered to increase the process efficiency. Improving heat integration in the CaL process to reduce energy requirements requires from the two main strategies: recovering energy in the CaL loop and modifying the CaL configuration to avoid (or reduce) oxyfuel combustion in the calciner [12].

CaO deactivation is also an important issue, leading to a large amount of inert solids being recirculated through the plant well above the stochiometric needs. Moreover, there are engineering challenges related to circulating solids at high temperature.

Further barriers are the financing of CO_2 transport infrastructure, legal and regulatory frameworks and insurance for safe permanent CO_2 storage or utilization [36].

A part of this introduction to CO_2 capture was published in [92]*, where the author of the thesis was in charge of the review sections. The full manuscript including complete information about a number of CO_2 capture technologies is presented in* ***Annex 8.***

1.1.2 Recently finished and on-going projects

An intense R&D activity is being carried out to assess the feasibility of the CaL process for post-combustion CO_2 capture. Some of the recently finished and on-going relevant projects are:

1. **SCARLET: Scale-up of Calcium Carbonate Looping Technology for Efficient CO_2 Capture from Power and Industrial Plants (2014-2017)**

The SCARLET project[1], funded by the European Union's Horizon 2020 research and innovation programme and recently finished, aimed at validating the feasibility of the CaL technology in an upgraded 1 MWth pilot plant. Successful operation of the pilot plant and the optimization of the process parameters will provide essential information for scaling-up the process to a future 20 MWth pilot plant. The project provided a techno-economic and environmental assessment of the CaL process potential for CO_2 capture from power plants as well cement and steel production plants. Several works have been published within this project [11,93].

2. **CEMCAP: CO_2 capture from cement production (2015-2018)**

CEMCAP is a project funded by the European Union's Horizon 2020 addressing CO_2 capture from cement production by integrating the CaL process. The primary objective of CEMCAP is to prepare the ground for large-scale implementation of CO_2 capture in the cement industry[2]. CEMCAP aims to leverage to Technology Reediness Level (TRL) 6 for cement plants with a targeted capture rate of 90% and develop techno-economic decision-basis for CO_2 capture implementation in the cement industry.

3. **CLEANKER: Clean clinker production by Calcium Looping process (2017-2021)**

This project is funded by the European Union's Horizon 2020 research and innovation programme. In the same line that CEMCAP project, CLEANKER project aims at demonstrating at TRL7 the CaL concept in a configuration highly integrated with the cement production process, making use of entrained flow reactors. The core activity of the project is the design, construction and operation of a CaL demonstration system in the cement plant operated by Buzzi Unicem sited in Vernasca (Piacenza, Italy)[3].

4. **FLEXICAL: Development of flexible coal power plants with CO_2 capture by Calcium Looping (2016-2019)**

FLEXICAL project, funded by the European Research Fund for Coal and Steel, aims to develop novel Calcium looping systems able to respond to a wide range of flue gas load

[1] http://www.project-scarlet.eu
[2] https://www.sintef.no/projectweb/cemcap/
[3] http://www.cleanker.eu/home-page-it

changes [4]. For this, two process options are tested at pilot-scale: a highly load flexible plant concept and an energy storage using $CaO/CaCO_3$ silos. A recent publication about this project can be found in [94].

5. LEILAC: Low Emissions Intensity Lime & Cement (2016-2020)

This project is funded by the European Union's Horizon 2020 research and innovation programme. The LEILAC project is based on a technology called Direct Separation, which aims to enable the efficient capture of the unavoidable process emissions from lime and cement production[5].

1.2 Calcium-Looping as thermochemical energy storage process

The commercial expansion of renewable energy technologies is an urgent need to limit global warming below 2.0°C by 2100 and pursue 1.5°C above pre-industrial levels as agreed at Paris COP21 Conference [20]. Among renewable energy technologies, Concentrated Solar Power (CSP) has a great potential for a full commercial expansion [95]. However, for renewable energies to achieve full autonomy from fossil fuels and to increase their feasibility, a main hurdle to overcome is their inherent variability in production. Thus, efficient and low cost energy storage stands as one of the main technological challenge for large deployment of renewable energies [96–98]. Moreover, large-scale energy storage is essential for a global system with high penetration of solar energy in order to increase the electric grid flexibility and to avoid risks derived from transient peaks [99]. Regarding the necessary dispatchability of renewable power facilities, CSP plants show several advantages over solar PV and wind due to the relatively low cost and feasible integration of thermal energy storage technologies in large-scale facilities compared to battery storage systems [100–102]. Efficient, cheap and non-toxic thermal energy storage (TES) is a key issue for Concentrating Solar Power (CSP) plants to provide a significant share of electricity generation.

In recent years, a number of thermal storage technologies for medium to high temperature CSP systems have been developed based upon three main concepts: sensible thermal energy storage (TES), latent heat storage and thermochemical energy storage (TCES) [103,104]. Sensible heat storage systems are the most mature technologies [105] and they involve the use of different materials with high heat capacity such as water [103], molten salts [106–109], mineral oils [110] or ceramic materials [111]. Commercial plants of considerable size (above 100 MWt) do already

[4] https://www.flexical.eu/
[5] https://www.project-leilac.eu/

exist where heat is stored in molten salts and it is used overnight to generate electricity [112]. Another type of storage system currently at pilot scale level is based on the use of phase change materials to use the latent heat for energy storage [113–116]. Phase change materials (PCM) allow attaining higher storage capacities compared to sensible heat storage [105,117].

A third possibility consists of thermochemical energy storage (TCES), which is being increasingly investigated [105,118,119]. A large number of potential systems [105], experimental research under practical conditions [120] and TCES reactor designs [119] can be found in literature. TCES consists of using the heat obtained from an external source to drive an endothermic reaction. When energy is needed, the separately stored products of the reaction are brought together at the necessary conditions for the reverse exothermic reaction to occur, which releases the previously used heat for power production. The main advantages of TCES as compared to TES and PCMs are a relatively higher energy density as well as the possibility of storing energy in the long term or transport it without significant losses [9,105]. An extended review on long-term solar heat storage can be found in [9].

1.2.1 Energy storage in concentrating solar power plants

CSP technology concentrates solar irradiation to transform it in thermal energy. According to how the solar irradiation is concentrated, CSP systems can be divided into point focusing (tower systems) and line-concentrating (parabolic trough and Fresnel) systems. Solar tower facilities allow achieving very high solar concentration ratios which leads to a higher temperature (and efficiency) than parabolic trough facilities. Today, the installed CSP capacity throughout the world is 5 GWe, while approximately another 7 GW are under construction or planned to be commissioned from 2020 [121,122].

Currently, over 40% of commercial CSP plants around the world incorporate TES systems while this percentage rises up to 83% for those planned and under development [121]. Energy storage systems are typically based on a two-tank TES system to use the sensible heat stored in molten salts, which allows CSP plants to operate up to 15 hours in the absence of solar radiation [121]. Figure 2 shows an overview on cost, storage capacity and type of CSP facilities. As can be seen, the highest capacity factor[6] is around 0.55-0.65. However, molten salts-based systems have several drawbacks that penalize the performance of CSP plants. On one hand, the maximum working temperature is limited to 560ºC to avoid salt degradation, which reduces the power cycle efficiency [106]. On the other, there is a minimum working temperature of 200ºC to avoid salt

[6] Energy production in a year divided by the total energy than could be produced if the CSP plant works 8760 h/year at nominal capacity.

solidification [123], which demands a significant amount of energy to keep the molten salts from solidification when the plant is not under operation. Salt corrosiveness is also a serious issue that requires the use of expensive highly resistant materials for transport and storage [124,125].

Most of the commercial CSP tower plants currently under operation are based on Rankine cycle process [126]. Peak solar to electricity conversion efficiencies in these commercial CSP tower plants are around 25-30%, with an annual solar-to-electricity conversion efficiency lower than 20% [127] and a power cycle efficiency usually lower than 38% [121].

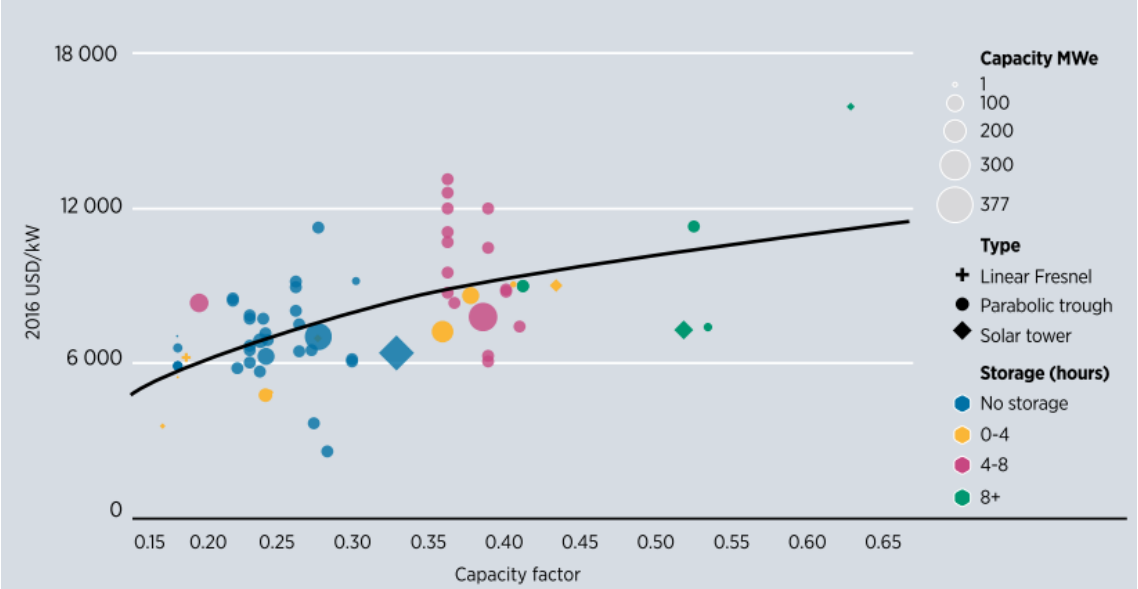

Figure 2: Installed costs and capacity factors of CSP projects. Reproduced with permission from [122]

The global weighted average LCOE of CSP projects commissioned in 2017 was USD 0.22/kWh. However, a huge reduction of LCOE is expected in the coming years. Thus, future CSP projects in South Australia (to be commissioned from 2020) and Dubai (2022) will have a cost of USD 0.06/kWh and USD 0.07/kWh respectively [122].

1.2.2 Thermochemical energy storage in concentrating solar power plants

In the last years, research on Thermochemical Energy Storage (TCES) systems as an alternative to molten salts has gained a considerable momentum [105]. TCES applied to CSP uses the heat available in the solar receiver to drive an endothermic reaction. When energy is needed, the by-products of the reaction are brought together at the required conditions for the reverse exothermic reaction to occur, which releases the previously stored chemical energy for power production. Main advantages of TCES over TES and PCMs are the long term energy storage capacity [9] and

the high energy density potentially achievable [98]. Many TCES systems are being analyzed as candidates for energy storage in CSP plants [105]. Table 1 shows the main reactions for TCES, which are classified as: hydrogen systems, carbonate systems, hydroxide systems, REDOX system, ammonia system, organic systems, metal oxides and sulfur based cycles. A proper selection of the TCES system is critical. In this regard, a general criterion based on the thermodynamics and kinetics of the reaction and the physical properties of the components of the reaction was established by Wentworth et al. [128], which should be sought when selecting a chemical reaction for storing concentrated solar energy.

Table 1: Main reactions for TCES

Group	Example	Reference
Hydrogen systems $MH_n + \Delta H_r \leftrightarrow M + \left(\frac{n}{2}\right) H_2$	$MgH_{2\,(s)} + \Delta H_r \leftrightarrow Mg_{(s)} + H_{2\,(g)}$	[129]
Carbonate systems $MCO_{3\,(s)} + \Delta H_r \leftrightarrow MO_{(s)} + CO_{2\,(g)}$	$CaCO_{3\,(s)} + \Delta H_r \leftrightarrow CaO_{(s)} + CO_{2\,(g)}$	[3]
	$SrCO_{3\,(s)} + \Delta H_r \leftrightarrow SrO_{(s)} + CO_{2\,(g)}$	[130,131]
Hydroxide systems $M(OH)_{2\,(s)} + \Delta H_r \leftrightarrow MO_{(s)} + H_2O_{\,(g)}$	$Mg(OH)_{2\,(s)} + \Delta H_r \leftrightarrow MgO_{(s)} + H_2O_{\,(g)}$	[132]
	$Ca(OH)_{2\,(s)} + \Delta H_r \leftrightarrow CaO_{(s)} + H_2O_{\,(g)}$	[133]
Redox systems $M_xO_{y\,(s)} + \Delta H_r \leftrightarrow xM_{(s)} + \left(\frac{y}{2}\right) O_{2\,(g)}$	$2BaO_{2\,(s)} + \Delta H_r \leftrightarrow 2BaO_{(s)} + O_{2\,(g)}$	[134]
	$2Co_3O_{4\,(s)} + \Delta H_r \leftrightarrow 6CoO_{(s)} + O_{2\,(g)}$	[135]
Ammonia systems	$2NH_{3\,(g)} + \Delta H_r \leftrightarrow N_{2\,(g)} + 3H_{2\,(g)}$	[136]
Organic systems	$CH_{4(g)} + H_2O_{(l)} + \Delta H_r \leftrightarrow CO_{(g)} + 3H_{2\,(g)}$ With a side reaction: $CO_{(g)} + H_2O_{(l)} \leftrightarrow CO_{2\,(g)} + H_{2\,(g)} + \Delta H_r$	[137]
	$CH_{4(g)} + CO_{2\,(g)} + \Delta H_r \leftrightarrow 2CO_{(g)} + 2H_{2\,(g)}$ With a side reaction: $CO_{2(g)} + H_{2(g)} + \Delta H_r \leftrightarrow CO_{(g)} + H_2O_{\,(g)}$	[138]
Sulfur systems	$H_2SO_{4(g)} + \Delta H_r \leftrightarrow SO_{2(g)} + H_2O_{\,(g)} + \frac{1}{2} O_{2\,(g)}$	[139]

1.2.3 Opportunities and challenges

The CaL process is a promising thermochemical energy storage method to be used in concentrated solar power plants [3,140–143]. Figure 3 shows a conceptual scheme of the CaL process integration in a CSP plant as TCES system. The CaL process begins with the decomposition of $CaCO_3$ in the calcination reactor (calciner) yielding CaO and CO_2 as reaction byproducts. A high energy input is necessary to increase the input stream temperature up to the value required for the endothermic calcination reaction to occur at a sufficiently fast rate, which is essentially determined by the composition of the gas in the calcination environment [14,144]. Once sensible heat from the CaO and CO_2 streams at the calciner outlet is recovered, these products are stored

at ambient temperature for their use afterwards as a function of demand. Storage of the products could be prolonged to weeks or even months as depending on storage conditions and energy demand [9]. In the power production mode, the reactants are circulated into a carbonator reactor, where the energy stored in chemical form is released through the reverse reaction (carbonation).

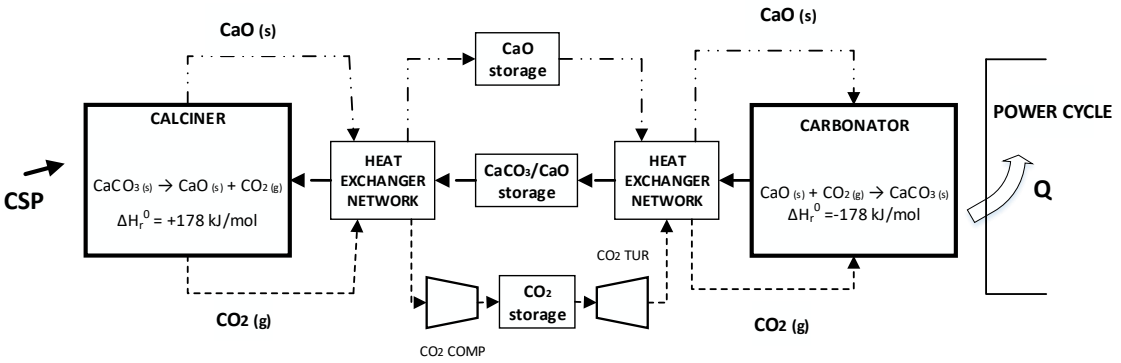

Figure 3: CCP-CaL conceptual scheme. Adapted from [145].

The CSP-CaL integration, although already suggested as a concept in the late 1970s [3–5], has not been analyzed in detail until quite recently. Several solar calcination reactors have been proposed and tested [146–149]. Moreover, a number of studies have been reported regarding Ca-based materials behavior for TCES [124,143,150]. In order to achieve an efficient and cost-effective thermochemical storage process, an adequate selection of the reversible reaction is a key issue. In this section we analyze the potential of the CaL process for thermochemical energy storage by considering a series of chemical, physical and engineering aspects. Based on a particularization of the general criterion established by Wentworth et al. [128], which considers a series of chemical, physical and engineering aspects, the potential feasibility of the CaL process for TCES is analyzed below.

First, the CaL process present the huge advantage of the low price, wide availability and harmlessness towards the environment of natural CaO precursors such as limestone or dolomite [13–15], which is crucial for a massive sustainable development of energy storage systems at large scale. Another of the most interesting advantages of the TCES systems is a high energy density which allows maximize storage capacity. As can be seen in Figure 4, the energy density of the CaO/CO_2 system (around 3.2 GJ/m^3) is one of the largest among the TCES systems considered in literature. An alternative choice with larger energy density and based also on a calcination/carbonation reaction would be to use the SrO/CO_2 system (see Figure 4) [131]. Nevertheless, the too high turning temperature of this system and the high cost of the sorbent precursor (SrCO3) (as compared to a price around $10/tonne or less for natural limestone) makes this alternative less attractive from a practical point of view in a first approach.

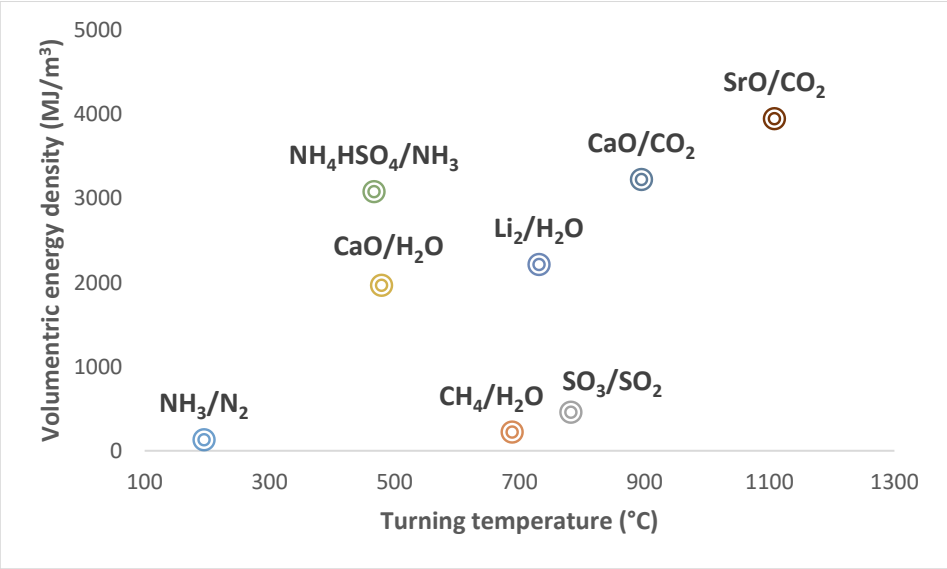

Figure 4: Energy density and turning temperature of various thermochemical energy storage systems. Adapted from [142].

Other works [132,151,152] give values for the energy density of the CaL system in the range of 0.9-2 GJ/m^3 by considering gas and solids vessels and/or that carbonation is not complete. From a practical point of view, it is interesting to address the size of the vessels needed for solids storage (i.e. considering the particles porosity and the packing density of solids), which is more closely connected with the capital costs of the energy storage system. To this end we propose Eq.(2) [153], which can be applied to gas-solid TCES systems with the structure $AB_{(s)} \rightleftarrows A_{(s)} + B_{(g)}$ (for the CaL case: $AB = CaCO_3$; A=CaO; B=CO_2):

$$E_{den}\left[\frac{GJ}{m^3}\right] = \frac{X \cdot \left(\Delta H_R + \int_{T_{B,vessel}}^{T_{reactor}} c_{p,B}\, dT + \int_{T_{AB,vessel}}^{T_{A,vessel}} c_{p,AB} dT\right) + (1-X) \cdot \int_{T_{AB,vessel}}^{T_{A,vessel}} c_{p,A} dT}{\left(\frac{v_{AB}}{(1-\varepsilon_{AB})} + \frac{v_A}{(1-\varepsilon_A)}\right)\frac{1}{\emptyset} + X \cdot v_B} \qquad (2)$$

Where ΔH_R is the reaction enthalpy (GJ/kmol), $c_{p,i}$ is the specific heat of the component i (MJ/kmol·K), $T_{reactor}$ is the decomposition reaction temperature (K), $T_{i,vessel}$ is the storage temperature for of the component i (K), v_i is the specific volume (m^3/kmol) of the component i at storage conditions, ε_i is the internal porosity of the component i and $\emptyset$ is the particle packing density, whose value is set to 0.6 as a typical value for the random loose packing fraction of irregularly shaped particles under gravity [154]. The CO_2 tank volume is a critical factor depending on the gas temperature and pressure. As reference value for the CSP-CaL integration scheme, CO_2 should be stored at high pressure (75 bar) and atmospheric temperature (25ºC) to guarantee supercritical conditions and therefore minimize vessel size. The solids vessels capacity is highly influenced by CaO conversion, since a high CaO reactivity reduces storage volume

needs. Thus, the volumetric energy density of the entire CaL system is mainly dependent on CO_2 storage conditions (pressure and temperature) and CaO conversion. According to CSP-CaL process simulations under typical conditions, the energy density of the entire system varies in a range of 0.39-0.9 GJ/m^3 depending on CaO conversion [153], which is higher than energy storage density of a molten salt system by considering a two-tank configuration [155] with typical values of the temperature change (DT) in CSP plants [121].

Moreover, the CaL process presents the great advantage that reactants and products can be stored long term at ambient temperature in contrast with the need of keeping molten salts at temperatures above ~100-220°C to avoid solidification [123]. However, CaO is highly reactive with ambient H_2O to produce calcium hydroxide ($Ca(OH)_2$). This is an important issue to consider since the formation of $Ca(OH)_2$ can modify the carbonation behavior [51,156]. On the other hand, it must be remarked that $Ca(OH)_2$ presents a higher reactivity towards carbonation as compared to CaO. In fact, the introduction of an intermediate CaO hydroxylation reactor has been proposed to enhance the CaO reactivity in the CaL process for CO_2 capture [51,157]. It is required to avoid any presence of CO_2 in the CaO storage tank to avoid carbonation.

In addition to high energy density, the CaL process applied as TCES has the advantage of a high reaction turning temperature (defined as the temperature for the reaction to be at equilibrium under a CO_2 partial pressure of 1 bar) of T~895°C. Thus, carbonation for generating heat may occur fast in the range of 650-1000°C depending on the CO_2 partial pressure [158]. This would allow a high efficient generation of electricity and it would overcome the current CSP temperature limitation of T~550-600°C mainly imposed by degradation of molten salts at higher temperatures [106,107,159]. Higher efficiencies could be achieved by increasing the maximum temperature allowed in the CSP plants [160].

The calcination reaction must be fast for the absorption of solar energy and CaO regeneration to be carried out rapidly. According to the chemical equilibrium [161], calcination only occurs fast under a pure CO_2 atmosphere at temperatures above T~950°C [65]. At these conditions, a high energy input is required to increase the input stream temperature up to the value required for the endothermic calcination reaction to be carried out at a sufficiently fast rate. On the other hand, a feasible choice to carry out calcination for TCES would be to perform it in an environment of an easily separable gas from CO_2, e.g. superheated steam. Calcination of MgCO3 under superheated steam is an already available technology [162] at the commercial level (Catalytic Flash Calcination, CFC) while the LEILAC project[7] aims to integrate CFC from $CaCO_3$ for cement production with the important benefit that it occurs at a rather fast rate and releases pure CO_2 ready for compression and storage after condensation of H_2O [105]. Moreover, calcination

[7] https://www.project-leilac.eu/

temperatures under superheated steam are considerably decreased down to ~700-750°C [163], which could be a further advantage for a quick integration of the CaL technology in CSP plants. Furthermore, the reactivity of CaO regenerated by calcination under superheated steam is notably enhanced [164], which would expectedly serve to boost the efficiency of the CSP-CaL integration. In addition, superheated steam for calcination in the solar reactor would be directly available from already possible in-situ generation of superheated steam in solar receivers [165]. Nevertheless, a higher energy penalty is expected by carrying out the calcination under superheated steam because of the solar energy consumption to bring the water (after separation) up to the calcination conditions. Another possibility to reduce the calcination temperature is by reducing the CO_2 partial pressure introducing Helium in the calciner, which allows that calcination occurs at 725ºC [166] because of the high thermal conductivity and CO_2 diffusivity in He. Nevertheless, Helium/CO_2 separation brings a new challenge that must be further analyzed. Remarkably, the reduction of calcination temperature could highly reduce the reradiation losses in the solar receiver.

While the particle receiver and high-temperature solids conveying represent a design challenge for the development of the CSP-CaL integration, many other equipment of the plant are currently widely developed on an industrial scale, mainly from the cement and lime industry [1,7,70]. This is the case of the cyclonic gas-solid heat exchangers [167], which could be used in the CSP-CaL integration to preheat the $CaCO_3$ entering the calciner. Efficient gas-solid contact and heat/mass transfer in the calciner and carbonator reactors could be ensured by the use of circulating fluidized-beds (CFB), which are typically operated under the fast fluidization regime with gas velocities of the order of 5-10 m/s [46,168]. CFB reactors are characterized by their contrasted efficiency and durability and their suitability to the CaL process is already proven in CO_2 capture pilot plants [10,11]. Separation of the calcination products prior to storage is feasible using commercially available devices such as gas coolers and cyclones to separate the solids from the CO_2. The CO_2 released in the calcination reaction must be compressed at high pressure to minimize the storage volume [169–171]. This brings about a remarkable loss of efficiency in the global power cycle. In this regard, the option of performing intercooling compression to minimize the energy penalty must be assessed.

One of the main drawbacks of the CaL process is the progressive loss of activity towards carbonation in short residence times of the regenerated CaO as the number of cycles increases depending on the carbonation/calcination operating conditions [12,68,172]. Thus, only a fraction *X* of the total flow of CaO entering the carbonator reacts to produce $CaCO_3$, while *1-X* remains as unreacted CaO. The average CaO conversion X is thus a critical material property for the simulations. CaO conversion is highly dependent on the carbonation-calcination conditions as well as on the CaO precursor [173]. The CaL process applied to post-combustion CO_2 capture,

where most of the CaL research has been focused on in recent years, involves carbonation under low CO_2 partial pressure whereas calcination is carried out under high CO_2 concentration at temperatures around 950ºC. On the other hand, the CO_2 concentration in the gas stream entering the carbonator is imposed (15% v/v of CO_2 in the flue gas from a coal fired power plant). These conditions lead to a severe drop of CaO conversion with the number of cycles, reaching a residual value of just around X=0.07-0.08 [48]. However, CaL conditions for TCES in CSP must not be necessarily the same as those employed for CO_2 capture. Since the concentration of CO_2 entering the carbonator is not imposed, carbonation conditions can be chosen to minimize the negative impact of CaO deactivation while at the same time the thermoelectric efficiency is enhanced.

1.2.4 Research lines and on-going projects

Thermochemical energy storage, solar calcination and high-temperature solar receivers are gaining the attention of many research projects. As described above, the CSP-CaL process has a number of advantages which are fully aligned with the current research lines about CSP plants, namely: i) increasing the plant efficiency; ii) LCOE reduction; iii) increasing the dispatchability in CSP plants and iv) improving the sustainability and the environmental impact [174]. Several projects (recently finished or on-going) related with the CSP-CaL integration are:

1. **SOCRATCES: Solar calcium-looping integration for thermo-chemical energy storage (2018-2020)**

The SOCRATCES project, funded by the European Union's Horizon 2020 research and innovation programme, aims at demonstrating the suitability of this integration by erecting a pilot-scale plant that will reduce the core risks of scaling up the technology as well as allow further understanding of the process integration. The longer-term goal is enabling highly competitive and sustainable CSP plants. The SOCRATCES concept stems from laboratory results Technology Readiness Level (TRL) of 4 to test the concept in a relevant environment (TRL5). Main expected results are: i) prototype demonstration of capacity for energy storage; ii) successful carbonator design with possibility to scale-up and iii) successful calcination at prototype scale by means of flash calcination technology.

2. **Carbon Dioxide Shuttling Thermochemical Storage Using Strontium (2014-2015)**

The project was awarded within the ELEMENTS (Efficiently Leveraging Equilibrium Mechanisms for Engineering New Thermochemical Storage) program, supported by the SunShot Initiative (DOE). The project uses safe, and non-corrosive strontium-based carbonates and high temperatures from concentrated sunlight to break chemical bonds and store energy during the day time. The use of strontium carbonate allows the system to be charged via the reversible

decarbonation reaction at solar energy input temperatures of 1300°C, allowing discharge of the stored solar energy at very high temperatures of over 1000°C.

The project explored sintering inhibitors. Relatively stable materials supported by Yttria-Stabilized Zirconia (YSZ) or SrZO3 were identified as the leading candidates.

3. **Regenerative Carbonate-Based Thermochemical Energy Storage System for Concentrating Solar Power (2014-2016)**

Within the ELEMENTS program, the Regenerative Carbonate-Based Thermochemical Energy Storage System for Concentrating Solar Power project aims to develop a TCES for CSP based on reversible gas-solids reactions of carbonate and silicate sorbent-based at bench-scale.

The modified calcium carbonate sorbents under investigation by SRI for solar TCES performed hundreds of cycles in simultaneous TGA/DSC equipment to measure both mass and heat change as the material undergoes repeatedly high temperature carbonation/decarbonation reactions. Results showed that the highly-refined and tailored reinforced CaO sorbent developed exhibits a very stable multicycle behavior with a stable sorbent capacity around 0.3, although maybe conditioned by the expense of a considerable increase of material costs and technical issues in the Ca-based synthetic material fabrication.

4. **Demonstration of High-Temperature Calcium-Based Thermochemical Storage System for use with Concentrating Solar Power Facilities (2014-2018)**

This project, funded by the APOLLO program (DOE), aims to demonstrate a novel high-temperature calcium-based thermochemical storage system for use with CSP facilities, which is directly related to the CSP-CaL system described throughout the present thesis. The system uses a highly refined and tailored reinforced CaO sorbent undergoing a reversible carbonation reaction in a parallel-plate heat exchanger reactor. Main objectives of the project are [175]: i) to optimize the CaO sorbent composition and to demonstrate the required high capacity and negligible degradation over a large number of cycles at temperatures around 750ºC; ii) to design, build and test bench-scale heat exchanger reactor system to demonstrate the sorbent capacity; iii) to carry out a techno-economic evaluation to optimize heat exchanger reactor system and balance of plant design; iv) to build and validate heat exchanger reactor design multiphysics mathematical models and v) to design, build and demonstrate field scale systems (1MWh).

5. **CSP2: Concentrated solar power in particles (2011-2015)**

The CSP2 project, funded by the European Union's Horizon 2020 research and innovation programme, proposes to use dense gas-particle suspensions (around 50% of solids) in tubes irradiated by CSP as HTF. The dense phase is composed of a granular solid that resists temperatures up to 750ºC, which overcomes the limit imposed by molten salts systems, with a

70-90 % efficiency. It was developed and operated successfully a pilot solar receiver with 100-150 kW thermal capacity placed on the focus of the 1 MW solar furnace of the CNRS. The solar loop was tested for 8 hours, with a flow rate of about 0.7 to 1.8 tonnes per hour. The solar receiver consisted of 16 1m long vertical tubes in which the dense gas-particle suspension (DPS) flowed vertically upward.

6. TCSPower: Thermochemical Energy Storage for CSP Plants (2011-2015)

The overall objective of the TCSPower project, funded by the European Union's Horizon 2020 research and innovation programme, is to build a new, efficient, reliable and economic thermochemical energy storage (TCS) for concentrated solar power plants based on the decomposition of calcium hydroxide, which allows storing energy in a temperature range between 450 and 550°C. For the higher temperatures CSP plants the redox reaction of manganese oxide is evaluated. A simulation tool for the design of TCS reactors with improved heat and mass transfer characteristics is used to identify suitable reactor concepts for the hydroxide and the redox reaction system. Both concepts are being experimentally evaluated at laboratory scale. Additionally, an up-scaling to 10kW will be realized for the more promising reaction system to evaluate the performance of a pilot-scale TCS reactor.

7. SOLPART: High temperature Solar-Heated Reactors for Industrials Production of Reactive Particulates (2016-2019)

This project is also funded by the European Union's Horizon 2020 research and innovation programme. The main objective of the SOLPART project is to develop, at the pilot scale, a high temperature (950°C) 24h/day solar process suitable for supply totally or partially the thermal energy requirement for $CaCO_3$ calcination by high temperature solar heat. The system will operate at 950°C and will include a 30 kWth solar reactor producing 30 kg/h CaO and a 16h hot CaO storage [176]. The project develops and merges three advanced technologies: high temperature solar reactor, transport of high-temperature solid materials and high temperature thermal storage.

8. NEXT-CSP: High Temperature concentrated solar thermal power plan with particle receiver and direct thermal storage (2016-2020).

This project is also funded by the European Union's Horizon 2020 research and innovation programme. The project proposes a fluidized particle-in-tube concept. It aims to further develop the technology to make it rapidly cost-efficient and ready to be introduced in the market. A cost reduction by 38% is expected with respect to current CSP electricity cost. A 4-MWth tubular solar receiver able to heat particles up to 800°C will be constructed and tested. The rest of the loop, a two-tank particle heat storage and a particle-to-pressurized air heat exchanger coupled to a 1.2 MWe gas turbine, will also be tested [177].

1.3 Motivation of the thesis and research opportunities

The motivation of the thesis is to advance in the knowledge on the CaL process for both applications: post-combustion CO_2 capture (PCC) and thermochemical energy storage (TCES). As discussed throughout the previous sections, the CaL process has potential advantages regarding the state-of-the-art of the technology, i.e. amines-based CO_2 capture system and molten salt-based CSP plants, respectively.

The CaL process is already widely studied for CO_2 capture in fossil fuel power plants, as TCES system in renewable power plants and to enhance H_2 production from methane reforming. Either one of these applications requires particular reaction conditions to which the sorbent performance (reaction kinetics and multicycle conversion) is extremely sensitive [12]. Therefore, specific models based on the conditions of any application are needed.

For post-combustion CO_2 capture, promising preliminary results have led to the proliferation of a large number of studies in recent years about the CaL integration in non-renewable power plants being remarkable the successful operation of 1-2 MW pilot plants for a large number of hours, such as La Pereda [10] or Darmstadt [93]. However, several challenges must be solved for a large-scale deployment of the CaL technology. Nowadays, research is mainly focused on enhancing the CaO multicyclic activity, improving the reactors design, improving heat integration in the plant and reducing both CAPEX and OPEX to increase the process profitability. A proper understanding of the reaction mechanisms is a key point for designing the reactors, whose operating conditions (pressure, temperature, size, gas velocity, etc.) will determine the CO_2 capture efficiency. It requires specific accurate models.

The multicyclic calcination/carbonation behavior of CaO used in models found in literature [47,77,86,87] has usually been inferred from thermogravimetric analysis (TGA) results in which calcination is often carried out under low CO_2 partial pressure due to technical limitations related to insufficiently fast heating/cooling rates of conventional ovens. Under these conditions, most of the carbonation reaction in short residence times occurs on the surface of the solids through a reaction controlled fast phase whereas the subsequent solid-state diffusion-controlled phase is comparatively negligible. Recent TGA studies demonstrate that carbonation on the surface of the particles in the reaction controlled fast phase is extraordinarily hampered when the solids are regenerated under high CO_2 pressure in accordance to realistic conditions. On the other hand, carbonation in the subsequent solid-state diffusion phase gains a substantial relevance [173,178].

The integration of CaL process as post-combustion CO_2 capture system in CFPP would involve energy penalty ranges between 4 and 7% points over the reference plant efficiency, which is less

than using MEA-based systems. Nevertheless, CaO deactivation with the number of cycles remains as a shortcoming of the CaL system, which causes an energy consumption that could be reduced if CaO rapid deactivation is mitigated. An important effect of CaO deactivation is that a larger equipment size is required because of the massive presence of non-reacting solids in the system. Improving the CaO multicycle conversion and process integration could reduce the equipment size and therefore the capital cost, which currently hinder the deployment of CO_2 capture technologies.

Thus, further knowledge is needed to:

a) Evaluate the CaL process efficiency under realistic conditions, similar to those that would be obtained when applying the CaL process in a power plant at a commercial scale. It includes the development of models for the reactions to estimate the capture efficiency taking into account the carbonation in the solid-state diffusion carbonation stage. Results from these novel models can affect considerably the optimal conditions that until now have been considered for the operation of the CaL process, namely, calcination and carbonation temperatures of 900ºC and 650ºC respectively with a particles residence time in both reactors of around 5 minutes.
b) Develop new integration schemes. Thus, if the reactor design changes by considering more realistic conditions, the carbon capture process scheme should also vary to be adapted to the optimal operating conditions. Therefore, not only novel reactor models are needed but also new CFPP-Cal integration process schemes.
c) Moreover, from the analysis of the penalties in the power plant performance when incorporating the CCS system, synergies between main CO_2 capture technologies, namely, oxy-combustion, membranes and post-combustion (either CaL or amines) can be detected, which makes interesting the analysis of hybrid processes. This requires the study of each one of these processes to identify the optimum integration and operation conditions to improve the global process. To this end, lab-scale test and modelling are needed to identify the synergies and impact.

Regarding the integration of the CaL process in CSP plants, Section 1.2 discusses the huge potential of the CaL process as TCES system. The number of Concentrating Solar Power (CSP) plants is notably increasing throughout the world in the last 10 years, reaching a total installed capacity worldwide 5 GWe [121]. However, for a massive deployment of CSP facilities several challenges need to be addressed. The CSP-CaL process is fully aligned with the priority research lines in CSP technology, namely, enhancing dispatchability, increasing plant efficiency and cost reduction [174]. Dispatchability can be improved taking advantage of the high storage energy

density of the $CaCO_3$/CaO system. Because the carbonation reaction occurs at temperatures as high as 890ºC in a pure CO_2 atmosphere at ambient pressure (and even higher by increasing the reactor pressure) a higher temperature of heat introduced in the thermodynamic cycle and therefore a higher cycle efficiency than in molten salt-based plants can be achieved. Moreover, cost and sustainability of CSP plants can be enhanced due to low cost, wide availability and non-toxicity of natural CaO precursors (i.e. limestone or dolomite).

The interesting opportunities for the integration of the CaL process as TCES system require new knowledge focused on:

d) Analysis of the feasibility of the process equipment and systems to be integrated at industrial scale.

e) Reactors modelling under TCES realistic operation conditions. CaL process conditions for thermochemical energy storage are not identical to those in CO_2 capture. Thus, optimum reactors temperature and pressure or atmosphere composition varies from one application to another and therefore kinetics, sorbent multicyclic conversion, and physical properties must be analyzed from specific lab-scale tests.

f) Process schemes to optimize the energy integration. A large number of feasible schemes for integrating the CaL process in CSP plants are possible. This includes configurations considering low temperature tanks for long-term energy storage but also high temperature storage in configurations similar to commercial ones with daily storage.

g) Power cycles integration assessment. The CaL process allows operating at higher temperatures than in current CSP plants. To take advantage of this, a proper selection and configuration of the power cycle must be addressed.

h) Finally, it is remarkable that most of the current research on integrating the CaL process for both CO_2 capture and TCES considers limestone as CaO precursor because of the important advantages of using this natural compound. However, the use of other materials with interesting characteristic should be analyzed.

These research opportunities are addressed through the present thesis. The next section describes in detail specific objectives according to the research lines described above.

2. Objectives

In the previous section the context, framework and opportunity for the development of this thesis has been presented. Following, the specific objectives addressed along the thesis are described.

The present thesis aims to contribute to the CFPP-CaL integration research with the following objectives:

1) Developing models based on lab-scale tests using realistic process conditions. From the analysis of full-scale plant operation, a set of operation conditions should be defined to be later reproduced at lab-scale. Results of lab-scale tests can be used in the development of a novel carbonator model which considers realistic CaO regeneration conditions. The new model would allow a more accurate evaluation and prediction of the carbonator performance, which is relevant for the development of process configurations and reactors design for the integration in real power plants. *This objective intends to respond to the research opportunity (a) discussed in the previous section.*

2) Improving the process scheme to reduce the energy consumption in realistic CaL operation. CO_2 capture efficiency and heat integration within the CFPP-CaL plant should be designed by considering the important role of the diffusion-controlled carbonation phase, which becomes relevant when CaO regeneration is carried out under high CO_2 partial pressure as is the case in the CaL process for CO_2 capture. *This objective intends to respond to the research opportunity (b) discussed in the previous section.*

3) Evaluating the performance of several natural CaO precursors, such as limestone, dolomite, and steel slag. Even though there is a large number of synthetic sorbents that are being currently analyzed within the CaL process, the present thesis is focused on the study of sustainable, environmental-friendly, low cost and widely available precursors as required to make possible the CaL large scale deployment. Experimental results on their multicycle capture capacity behavior at realistic CaL conditions are needed to evaluate the feasibility of using these CaO precursors. Furthermore, the energy penalty that arises from the integration of the CaL process into a coal fired power plant using these CaO precursors should be addressed. *This objective intends to respond to the research opportunity (h) discussed in the previous section.*

4) Developing a new hybrid process based on the CaL technology which could improve state-of-the-art configurations. Hybrid processes, which take advantage of synergies

between different CO_2 capture systems (such as CaL, oxy-combustion or membranes technology), could reduce the energy consumption and the equipment size associated to integrate CO_2 capture in fossil-based power plants. *This objective intends to respond to the research opportunity (c) discussed in the previous section.*

Regarding the development of the CaL process as TCES system, the present thesis aims to contribute to the CSP-CaL integration research through the following objectives:

5) Developing models based on realistic operation and multicyclic behavior of CaO within TCES schemes. Thus, a specific carbonation model for TCES should consider optimal integration conditions of the CaL process within CSP facilities, such as reducing the receiver temperature and increasing, as much as possible, the carbonation temperature. Moreover, carbonation under high pressure is an interesting option to improve the power cycle efficiency in TCES schemes, which requires the analysis of how the carbonation (kinetics, sorbent deactivation, etc.) is affected by increasing the reactor pressure. *This objective intends to respond to the research opportunity (e) discussed in the previous section.*

6) Performing a critical assessment about the advantages and challenges of developing the CaL process for high temperature thermochemical energy storage. *This objective intends to respond to the research opportunity (d) discussed in the previous section.*

7) Gaining knowledge about the possibilities of integrating the CaL process in both new and operating CSP plants. Power production from the stored energy by means of a Brayton CO_2 closed cycle could improve both the reliability and the power plant efficiency regarding previously proposed schemes, which are based on air open schemes. *This objective intends to respond to the research opportunity (d) discussed in the previous section.*

8) Exploring the integration with the TCES core system of alternative direct and indirect cycles (steam turbine, closed Brayton CO_2 and indirect-supercritical CO_2) for relevant CSP-CaL integration conditions. *This objective intends to respond to the research opportunity (g) discussed in the previous section.*

9) Enhancing the CSP-CaL plant efficiency by improving heat integration. An interesting possibility of the CaL process is to store energy at ambient temperature for long term energy storage. However, due to the high temperatures in both the calciner and carbonator reactors, a low temperature storage involves a large streams temperature change along the entire cycle, which makes crucial an optimized heat integration to achieve an adequate system efficiency. *This objective intends to respond to the research opportunity (f) discussed in the previous section.*

10) Another possibility is to store the solids at high temperature. In this case the process scheme is simplified by requiring fewer heat exchangers due to a lower temperature difference between the reactors and storage. On the other hand, long term storage cannot be considered because of the temperature losses. However, the CSP-CaL system could be operated under a solar multiple (defined as the ratio of the solar thermal power to the power block design thermal input) in a similar way than in currently CSP plants. The development of specific schemes for this configuration could reach a compromise between the overall plant efficiency and heat integration complexity. *This objective intends to respond to the research opportunity (f) discussed in the previous section.*

11) Assessing the technologies to be used within the CSP-CaL scheme, with special focus on solar receiver and solids management. *This objective intends to respond to the research opportunity (d) discussed in the previous section.*

3. Summary of main results and discussion

Following the objectives presented in the previous section, an intense research activity has led to a number of results which are summarized and discussed below. These results have been published within a set of research papers that show the multidisciplinary work carried out within this thesis. The full manuscripts are included in the Annexes 1-10.

3.1. Carbonation model for CO_2 capture

This section summarizes the main results obtained by the research activity according to the ***objective (1)***, Section 2. As a result of the research activity, in this thesis it is proposed a novel carbonator reactor model for CO_2 capture based on lab-scale multicyclic CaO conversion results which consider realistic CaO operation conditions. These results were published in [179].

3.1.1 Carbonation model development

As shown by the data originally reported in [180], the contribution of the diffusion-controlled phase to CaO conversion is quite relevant being of the same order than CaO conversion in the reaction controlled phase for 5 min overall carbonation periods. Moreover, an increase of the carbonation phase above 5 min would lead to higher conversion in the diffusive phase since carbonation in this stage grows roughly linearly with time until carbonation is completed. Thus, the average conversion of the CaO particles present in the reactor (X_{ave}) is given by the sum of conversion in the kinetic fast phase ($X_{ave,K}$) plus conversion in the diffusive phase ($X_{ave,D}$).

Unlike other capture models found in the literature, which assume that carbonation reaches maximum conversion at a constant rate (proportional to the free surface available of CaO and the thickness of the $CaCO_3$ layer formed) in a time after which the reaction rate drops to zero, the new model proposed in this thesis assumes that the time evolution of CaO conversion can be approximated by two lines of constant slope, one corresponding to the reaction controlled carbonation stage and another for the diffusive phase. According to experimental measurements, conversion would be increased linearly with time in the diffusion controlled stage [180].

The flow rate of CaO solids entering the carbonator (F_R) as well as the CaO present in the reactor bed (N_{Ca}) react with the pure CO_2 stream (flow rate F_{CO2}) to produce $CaCO_3$. Assuming perfectly mixed solids in the reactor, the average maximum conversion ($X_{max,ave}$) can be calculated as the weighted sum of conversions after N cycles:

$$X_{max,ave} = X_{max,ave,K} + X_{max,ave,D} = \sum_{N=1}^{N=\infty} \phi_N X_{NK} + \sum_{N=1}^{N=\infty} \phi_N X_{ND} \quad (3)$$

where ϕ_N is the fraction of particles subjected to a given number of cycles N [66] and X_{NK} and X_{ND} is the CaO conversion in cycle N in the kinetically and diffusion controlled stages respectively.

The average reaction rate can be expressed as a function of the phase in which particles are reacting (Eq. 4):

$$r_{ave_i} = \begin{cases} r_{ave,K} = \dfrac{X_{max,ave,K}}{t_K} \; si \; t \leq t_K \\ r_{ave,D} = \dfrac{X_{max,ave,D}}{T_0 - t_k} \; si \; t_K < t \leq \tau \end{cases} \quad (4)$$

where r_{N_i} is the reaction rate in the i-phase (either kinetic or diffusion), t_K is the time of the kinetic phase, τ is the average residence time of the particles in the carbonator ($\tau = \frac{N_{Ca}}{F_R}$) and $\frac{X_{max,ave,D}}{T_0 - t_k}$ is the rate of diffusive conversion that is derived from experimental data reported in [180].

The average conversion of the particles leaving the carbonator can be obtained from the sum of the average particle conversion reacting in the fast carbonation phase ($X_{ave,K}$) and the average particle conversion reacting in the diffusive phase ($X_{ave,D}$):

$$X_{ave} = X_{ave,K} + X_{ave,D} = f_a X|_{\leq t_K} + (1 - f_a) X|_{> t_K} \quad (5)$$

$$X|_{\leq t_K} = \frac{\int_0^{t_K} r_{ave,K} \; t \left(\frac{1}{\tau}\right) e^{-\frac{t}{\tau}} \, dt}{1 - e^{-\frac{t_K}{\tau}}} \quad (6)$$

$$X|_{> t_K} = X_{max,ave,K} + \frac{\int_{t_K}^{\tau} r_{ave,D} \; t \left(\frac{1}{\tau}\right) e^{-\frac{t}{\tau}} \, dt}{1 - e^{-\frac{t_K}{\tau}}} \quad (7)$$

where f_a is the fraction of particles reacting in the kinetic phase, which is given by [87]:

$$f_a = \left(1 - e^{-\frac{t_K}{\tau}}\right) \quad (8)$$

Since conversion is typically low except for the first cycles, the kinetic expression proposed by Bhatia et al. [181] can be simplified by dismissing the dependence on conversion as done in [87]. Thus, it is possible to express the average reaction rate in each carbonation phase as:

$$r_{ave_K} = k_s S_{ave_K} \left(C_{CO2} - C_{CO2_{eq}} \right) \tag{9}$$

$$r_{ave_D} = D^*_{eff} \left(C_{CO2} - C_{CO2_{eq}} \right) \tag{10}$$

Where S_{ave_K} is the average area surface for a particle reaction in the kinetic phase [182], D^*_{eff} is an effective diffusion constant obtained by fitting experimental kinetics results and C_{CO2} and $C_{CO2_{eq}}$ are the average and equilibrium CO_2 concentration respectively.

Assuming that the gas passes in plug flow through a bed of perfectly mixed solids, the carbon mass balance in the gas phase in a differential element of the carbonator reactor can be written as:

$$F_{CO2} \frac{dE_{CO_2}}{dz} = A \frac{\rho_{CaO}}{V_{M_{CaO}}} (f_a r_{ave_K} + (1 - f_a) r_{ave_D}) \tag{12}$$

Integrating Eq. (12) along the carbonation reactor, it results

$$z = \frac{F_{CO2} \cdot M_{CaO}}{W_s \cdot \rho_g \cdot (S_{ave_K} \cdot f_a \cdot k_s + D^*_{eff} \cdot (1 - f_a)} \psi \tag{13}$$

where,

$$\psi = \left[- \frac{f_0}{f_0 f_e - f_0} E_{CO_2} + \frac{f_0 (f_0 - 1)}{(f_0 f_e - f_0)^2} \ln \left(\frac{(f_0 - f_e) + (f_0 f_e - f_0) E_{CO_2}}{f_0 - f_e} \right) \right] \tag{14}$$

and f_e and f_0 are the equilibrium and inlet molar fraction of CO_2, respectively.

Finally, the capture efficiency in the carbonator E_{CO2} can be calculated as:

$$E_{CO2} = \frac{F_R}{F_{CO2}} X_{ave} \tag{15}$$

3.1.2 Model results and discussion

A series of parametric calculations were carried out to determine the CO_2 capture efficiency of the carbonator under different operating conditions to compare the proposed model and a similar model that dismissed the CO_2 capture in the diffusion stage [87]. Figure 5 shows that, neglecting the CO_2 capture capacity in the diffusion stage, the capture efficiency is not improved further after

a residence time of about 300 s since the fraction of active particles (considered as only those able to react in the fast phase) diminishes with time quickly. On the other hand, the capture efficiency is further improved by taking into account the enhanced conversion in the diffusive phase as shown by the results obtained from the model proposed. As can be seen in the right axis of Figure 5, the capture efficiency in the diffusive phase ($E_{CO_2,D}$) represents most of the contribution to the total carbonation efficiency just after tens of seconds. Consequently, the capture efficiency continues to increase with the residence time and may reach a high value at residence times above 500 s.

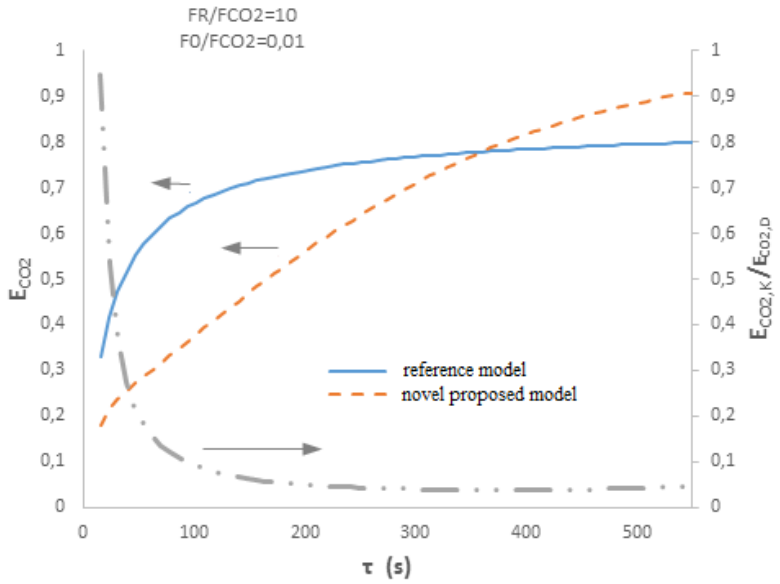

Figure 5: -Left axis- Carbonation efficiency as a function of the residence time in the reactor. –Right axis- Ratio of CO_2 capture efficiency by in the reaction controlled phase to carbonation efficiency in the diffusion controlled phase as a function of residence time [179].

Figure 6 shows the effect on the capture efficiency (E_{CO2}) of increasing the residence time (horizontal bottom axis) by decreasing the flow rate of recirculated solids between the reactors (FR, horizontal top axis) while maintaining fixed a value for the solids inventory.

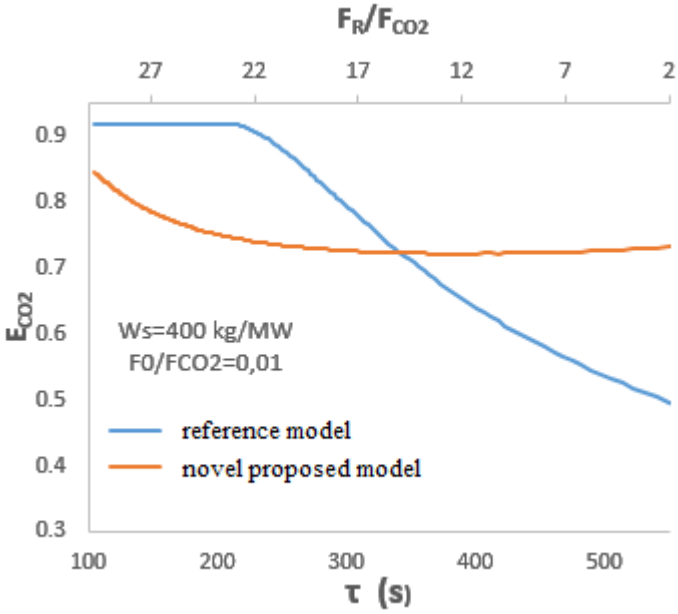

Figure 6: Carbonation efficiency as a function of the residence time in the carbonator. The blue line represents the CO_2 capture efficiency according the reference model proposed in [87] while the orange line is obtained from the novel carbonator model [179].

As may be observed, by considering CaO conversion in the diffusive phase, the capture efficiency is notably increased by increasing the value of the average residence time of the particles (τ) while the solids recirculation flow rate is decreased (with a constant value of solids inventory in the carbonator). This plays a crucial role in the CaL process design, affecting not only to reactors design but also the stream flows along the plant. An additional benefit of reducing the recirculation flow rate can be that the solids activity would be extended for longer times since the frequency of calcinations is reduced, which would serve to minimize the makeup flow of fresh limestone needed.

These results were published in [179]. *The full manuscript including complete information about the proposed carbonation model for CO_2 capture is presented in* ***Annex 1.***

3.2. Carbonation model for TCES

This section summarizes the main results of the work according to the specific ***objective (5)***, which is described in Section 2. In this regard, the analysis carried out in this thesis to model the carbonation reaction for its specific application as TCES system is discussed below. The novel carbonation kinetics model, which was developed by **Professor Jose Manuel Valverde**, is focused on the conditions that lead to an efficient energy integration of CSP-CaL plants for TCES.

A new analytic expression is proposed to estimate the carbonation reaction rate as a function of temperature and pressure. These results were published in [183].

3.2.1 Kinetics analysis and carbonator model

The model considers an ideally plane surface of a perfectly crystalline CaO solid where carbonation takes places in a full CO_2 atmosphere. As usually observed in heterogeneous gas/solid reactions [184], carbonation consists of two consecutive stages: i) CO_2 molecules become physically adsorbed on the CaO surface, after which ii) chemical reaction takes place producing $CaCO_3$. According to the pseudo-steady state hypothesis [185], the rate of increase of the fraction of active sites filled with CO_2 by adsorption must balance the rate of decrease of filled active sites by chemical reaction in order not to have a net accumulation of reactive intermediates. Thus, the rates of adsorption r_a and chemical reaction r_2:

$$r_a = k_a\,\theta\,P - k_d\,(1-\theta) \tag{16}$$

$$r_2 = k_2\,(1-\theta) - k_1\theta \tag{17}$$

Where θ is the fraction of active empty sites, P is the CO_2 partial pressure and k_i are the reaction rate constants.

The microscopic reversibility principle, which has been successfully applied to the kinetics description of a number of reversible processes [186], determines that for the overall reaction to reach equilibrium ($\theta = \theta_{eq},\ P = P_{eq}$), the rate of any process in each elementary step must be equal to the rate of its reverse process ($r_a = r_2 = 0$) [88]. Assuming, as in most gas–solid heterogeneous reactions [184], that the rate-limiting step is the chemical reaction stage ($k_1, k_2 \ll k_aP, k_d$) and rearranging, we arrive at:

$$r \approx a_2\, e^{-\frac{E_2}{RT}} \left(\frac{P}{P_{eq}} - 1\right) \left(\frac{1}{\frac{P}{P_{eq}} + e^{\frac{\Delta S_2^0}{R}}\, e^{-\frac{\Delta H_2^0}{RT}}}\right) \tag{18}$$

where E_2 is the carbonation activation energy, a_2 is a preexponential factor and R the gas constant ($k_2 = a_2\, e^{-E_2/RT}$). The Van't Hoff equation [184] has been used for the equilibrium constant $K_2 = k_2/k_1 = e^{-\Delta G_2^0/RT}$ being $\Delta G_2^0 = \Delta H_2^0 - T\,\Delta S_2^0$ the standard free energy change of carbonation. Equilibrium pressure (P_{eq}) is calculated according thermochemical data [161,187,188].

As the reaction evolves, the carbonation rate is determined as a function of conversion degree X, and reaction temperature T and pressure P. Experimental results on the time evolution of conversion show the typical sigmoidal shape of autocatalytic processes and are well fitted by a Prout−Tompkins model function [189] modified by introducing as conversion limit the CaO conversion at the end of the reaction controlled phase:

$$\frac{dX}{dt} = X\left(1 - \frac{X}{X_k}\right) r(T,P) \;\leftrightarrow X(t) = \frac{X_k}{1 + e^{-r(t-t_0)}} \tag{19}$$

The new reaction kinetics expression shows a good agreement with experimental data and previous works [158]. As may be seen in Figure 7a, a rather good agreement can be found between experiments and theory by only adjusting the pre-factor a_2 in Eq. 18 as a free parameter in the theoretical curve. In view of these results, and even though technical limitations prevented us from carrying out carbonation experiments at pressures greater than atmospheric, Eq. 18 can be used to estimate the reaction rate under CO_2 at pressurized conditions. Table 2 summarizes the values used for the reaction enthalpies, entropies, and activation energies that will be employed for the theoretical reaction rate in the modelling analysis ahead.

Table 2: CO_2 partial pressure at equilibrium, reaction rate and values of enthalpy-entropy changes in the chemical decomposition and desorption stages, and activation energies [183].

ΔH_r^0	180 kJ/mol	E_2	20 kJ/mol
ΔH_1^0	160 kJ/mol	ΔS_r^0	0.16 kJ/(mol·K)
ΔH_d^0	20 kJ/mol	ΔS_1^0	0.068 kJ/(mol·K)
E_d	20 kJ/mol	ΔS_d^0	0.092 kJ/(mol·K)
E_1	180 kJ/mol	a_2	1160 (1/s)

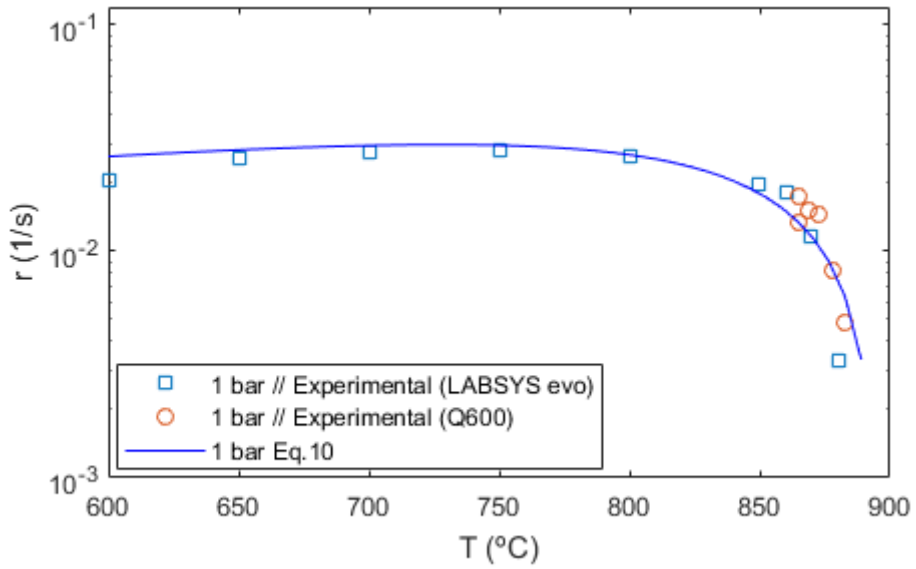

Figure 7: Reaction rate obtained from experimental tests (using different TG analyzers as indicated) and theoretically predicted (Eq. 10, with a2=1160 1/s) for carbonation under pure CO_2 at atmospheric pressure as a function of the temperature [183].

Using the proposed model together with experimental thermogravimetric analysis results found in the literature [141,173,190], a carbonator model, which was previously employed to analyze the CaL process for CO_2 capture [87], has been adapted to analyze the carbonation behavior after a long number of cycles in the industrial process for its integration in CSP plants.

As discussed above in the kinetics study, CaO conversion for a single particle in a certain residence time is dependent on carbonation temperature. Moreover, CaO conversion after several cycles decays to a residual value, which is also dependent on process conditions. By means of a mass balance, the maximum average conversion of the CaO particles in the carbonator can be expressed according Eq. (3). Unlike in the CO_2 capture application, after calcination at 725ºC, most of the carbonation in short residence times on the regenerated CaO skeleton occurs in the fast stage due to the high CO_2 concentration and carbonation temperature [190]. Thus, carbonation in the diffusion-controlled phase can be neglected in this case and therefore $X_r = X_k$. Accordingly, the present carbonator model assumes that carbonation occurs at a given rate until it reaches the maximum carbonation allowed in the fast carbonation stage, after which the particles remain inactive. Thus, only a fraction of particles, f_a , are active in the carbonator with the capacity to react in the fast stage (Eq. 8). Considering a perfect mixing model, the average conversion of the particles leaving the carbonator (X) can be calculated using the followed equations [87]:

$$X = \frac{\int_0^{t_K} r_{ave}\, t\, \left(\frac{1}{\tau}\right) e^{-\frac{t}{\tau}}\, dt}{1 - e^{-\frac{t_K}{\tau}}} = X_{max,ave}\, \frac{f_a}{\ln\left(\frac{1}{1-f_a}\right)} \tag{20}$$

$$f_{carb} = \frac{X}{X_{max,ave}} \tag{21}$$

$$E_{CO2} = \frac{F_R}{F_{CO2}} X = \frac{N_{Ca} f_a r_{ave}}{F_{CO2}} \tag{22}$$

where f_{carb} is the average carbonation level in the carbonator and r_{ave} is the average reaction rate in the fast carbonation stage, which is calculated from the kinetics model theoretical prediction (Eq. 18).

3.2.2 Modelling results

The carbonator model allows us to carry out a sensitivity analysis to assess the effect of pressure, temperature and solids inventory in the carbonator on the average carbonation level (f_{carb}). As can be seen in Figure 8, the average carbonation level (f_{carb}) is enhanced by increasing the carbonator pressure due to faster reaction kinetics. After a few of seconds in the carbonator, most of the CaO reaches the maximum conversion due to the very fast kinetics achieved in these CaL conditions. This is basically because of the high amount of CO_2 entering the carbonator (which exceeds the stoichiometric amount in order to use the effluent excess as heat carrier).

According to the kinetics model, by increasing the carbonator temperature, the average carbonation level is slightly enhanced up to a temperature T(r max) is reached from which kinetics is penalized with the consequent curtailment of the average carbonation level. As shown in Figure 8, this effect is mitigated when the carbonator pressure is increased, which is beneficial in practice since working at higher carbonator temperatures will promote the power cycle efficiency.

These results were published in [183]. *The full manuscript including complete information about the proposed carbonation model for TCES is presented in* ***Annex 9.***

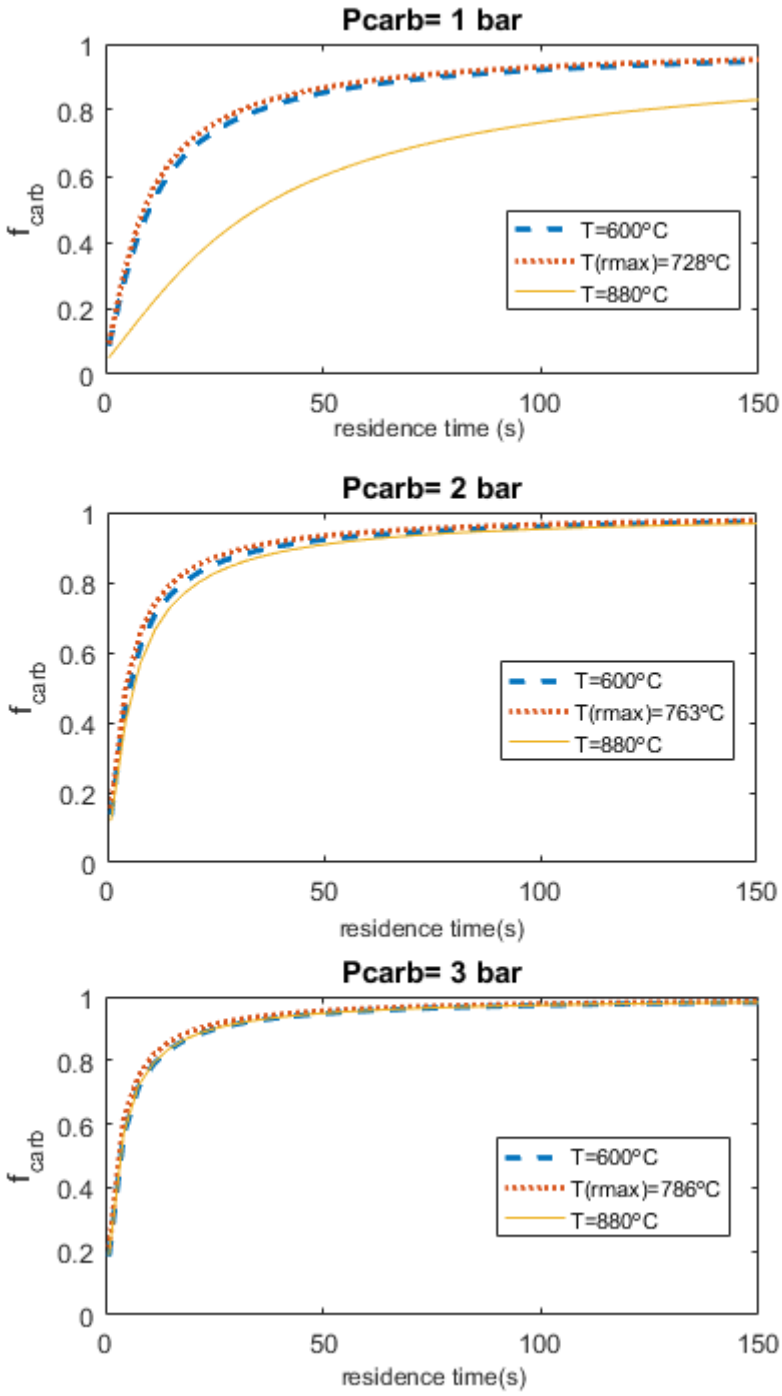

Figure 8: Carbonator model results. Average carbonation level (f_{carb}) for several carbonation conditions (P, T). T(rmax) is the temperature at which the reaction rate reaches a maximum (Fig. 3) [183].

3.3. CaL integration in Coal-Fired Power plants

This section summarizes the main results of the work according to ***objectives (2-3)*** of the present thesis. A principal feature of the CaL process at CO_2 capture conditions is that it produces a large amount of energy and therefore an optimized integration of the systems energy flows is essential

for the feasibility of the integration at the commercial level. The proposed integration model aims to analyze the process under realistic conditions for CO_2 capture so the model proposed in Section 3.1 is used to estimate the carbonation efficiency. This involves considering the important role of the diffusion-controlled carbonation phase, which becomes relevant when CaO regeneration is carried out under high CO_2 partial pressure as it is the case with the CaL process for CO_2 capture. These results were published in [191].

3.3.1 Integration scheme development

A reference 505 MWe coal fired power plant (CFPP) is used in this work for analyzing the energy penalty arising from the CaL integration [51]. Combustion of 205 tonnes per hour of coal takes place in the steam boiler to generate 1,335.7 MWth with an 88.6% efficiency. For the steam cycle, a 42% thermal to electric steam turbine efficiency is assumed based on results reported for similar plants [77,192]. For the CaL-CFPP integration analysis, mass and energy balances in the process have been calculated by using the commercial software ASPEN PLUS^{TM}. Figure 9 shows the schematic CFPP-CaL integration scheme.

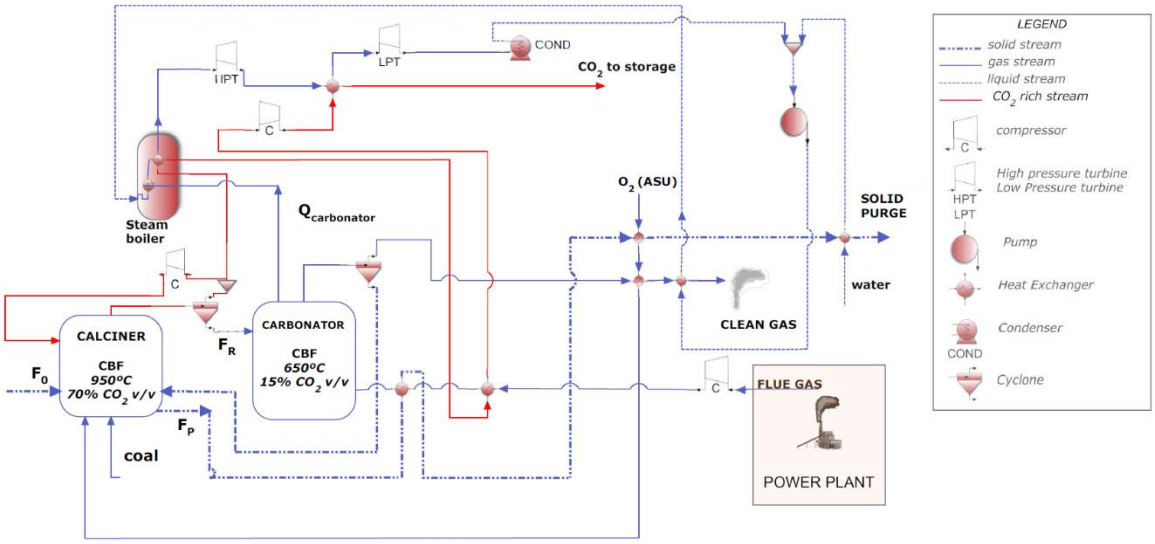

Figure 9: CFPP-CaL integration scheme [191].

The CaL process is started by calcination of the CaO precursor in the CFB calciner, where the heat necessary to increase the temperature of the solids to carry out the endothermic calcination reaction is provided by in-situ oxy-combustion of coal. For simulating the oxy-combustion of coal in the calciner reactor a model based on chemical and phase equilibrium through Gibbs' free energy minimization methods is used. In the model, the energy penalty caused by The Air Unit Separation (ASU) is taken as 200 kWh per tonne of O_2 produced according to results from previous reports [86,193] while the energy consumption derived from solids transportation has

been set at 20 MJ per tonne of solids [194]. A make-up flow of the CaO precursor is introduced into the calciner to compensate for sorbent deactivation.

CO_2 capture takes place in the CFB carbonator reactor. A solids stream (F_R) composed by CaO enters the carbonator to react with the CO_2 loaded flue gas stream ($F_{CO2} = 10{,}388\ \text{kmol/h}$) coming from CFPP main boiler. The operating carbonator temperature is set to 650°C and it works at atmospheric pressure. An inventory of solids in the carbonator bed (W_s) of 200 tonnes of solids (400 kg/MWel) is considered as a typical value used in carbonator models [47,87,179]. Gas pressure loss across the carbonator reactor, which is operated in the continuous fluidized bed (CFB) regime, is calculated from the Kunii-Levenspiel (K-L) fluid dynamic model [195,196].

The heat produced in the CaL cycle is used in a secondary superheated steam cycle for electricity generation. Steam operational parameters have been chosen from data of similar real power plants [197]. The steam boiler is modelled as: i) a preheater where the sensible heat from the flue gas stream is used; ii) an evaporator, which takes advantage of the energy released in the exothermic carbonation reaction and iii) a steam super-heater, which uses the sensible heat of the CO_2 exiting the calciner. A possible strategy to minimize the global energy penalty is to exchange heat between the solids leaving the calciner and the solids entering it that must be heated up to the calcination temperature. Different systems have been proposed to this end such as a mixing valve [198] or a cyclonic preheater [199]. In order to simplify the model, a simple solid–solid heat exchanger is assumed with an approach temperature of 20 ºC. At the carbonator exit, the flue gas (after recovering 70-90% of CO_2) is sent to a series of heat exchangers in order to recover sensible heat from the exhaust gases stream before being vented to the atmosphere.

3.3.2 CFPP-CaL simulation results

Parametric tests have been carried out in order to evaluate the CaL integration potential in a real power plant. Percentage of penalty points was calculated over the plant efficiency. As may be seen in Figure 10, the efficiency penalty is notably decreased as the solids residence time in the carbonator is increased. Moreover, the lower the flow rate of fresh limestone makeup the larger the reduction of efficiency penalty. Thus, it can be concluded that a lower flow of solids recirculation between the reactors would lead to a remarkable improvement of the integrated cycle efficiency. This is a relevant result to be highlighted that arises from the new carbonator model in which the importance of carbonation of the CaO solids in the diffusion controlled phase is considered.

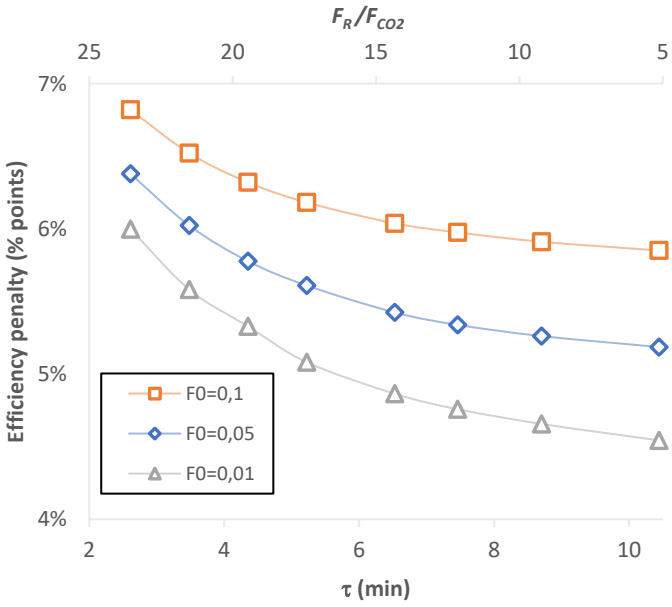

Figure 10: Efficiency penalty for the integration of the CaL technology in a coal combustion power plant as a function of the solids residence time in the carbonator [191].

An interesting parameter to assess the tradeoff between the achieved CO_2 capture efficiency and energy penalty is the specific energy consumption per kg of CO_2 captured (SPECCA). Thus, SPECCA represents the additional fuel consumption (in MJ) necessary to avoid the emission of 1 kg of CO_2 into the atmosphere [56,200,201]. Most of the studies assessing SPECCA for conventional amine based capture systems lead to typical values of about 4 MJ/kg CO_2 [21,35,202]. Figure 11 shows the results of the values obtained for SPECCA in the proposed CFPP-CaL integration model to obtain a CO_2 capture efficiency of 80% and 90%, respectively, as depending on the solids recirculation flow rate. As can be seen, for a given value of the solids recirculation flow rate (FR/F0 fixed), it is necessary to increase the amount of energy required to obtain a higher capture efficiency since the makeup flow rate of fresh limestone introduced into the system F0 must be increased. Furthermore, it is observed that a lower SPECCA is attained as the solids recirculation flow rate if decreased for a given capture efficiency. Thus, the additional energy consumption necessary to achieve a given capture efficiency is lowered as FR/F0 is diminished.

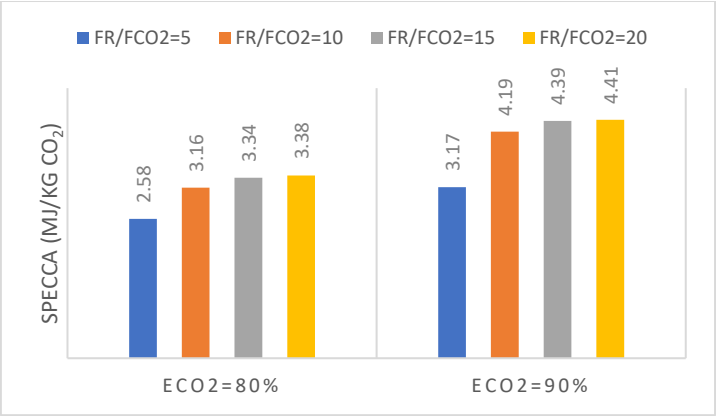

Figure 11: SPECCA value as a function of the ratio of solids recirculation flow rate to CO_2 flow rate (FR/FCO_2) to get a fixed CO_2 capture efficiency (ECO_2) value of 80% (left) and 90% (right) [191].

3.3.3 Comparison between natural CaO precursors

Previous sections are based on limestone as CaO precursor. According to ***objective (3)*** alternative Ca-based precursors have been studied. Although there is a large number of synthetic sorbents being currently analyzed within the CaL process, the present thesis is focused on the study of environmental-friendly, low cost and widely available precursors because of the importance of these factors for the CaL large scale deployment. Thus, this section summarizes results achieved by comparing limestone, dolomite and steel slag as CaO precursors over the CFPP-CaL scheme summarized in the previous section. These results were published in [203].

Dolomite (MgCa(CO3)2) is also a cheap and abundant natural CaO precursor, which upon calcination under the presence of CO_2 is decomposed into MgO and CaO by a two stages process [48,204,205]. The use of dolomite in the CaL process for CO_2 capture would allow reducing the calcination temperature to about 900ºC to attain full calcination of the makeup flow in short residence times [48]. Moreover, the presence of inert MgO grains in the dolomitic lime hinders aggregation and thus sintering of the CaO grains, which mitigates the drop of CO_2 capture capacity with the number for cycles [48,206].

In the same line, the use of steel slag as alternative CaO precursor in the CaL process is also gaining the attention of researchers [207,208]. Steel slag is produced in large amounts by the metallurgical industry, remaining an important part as final waste without valorization. By a previous treatment with acetic acid, calcium acetate as CaO precursor is obtained [209]. Results from TGA tests show that decomposition of calcium acetate occurs mainly in three steps [209–211]: i) an initial dehydration, which occurs from ambient temperature to approximately 250ºC; ii) calcium acetate decomposition from 300ºC to 450ºC to release acetone and $CaCO_3$ and iii) calcination of $CaCO_3$ from 620ºC to 700ºC. According to TGA results [209], the CaO-based

sorbent derived from steel slag presents a low deactivation rate at realistic CaL conditions, which would expectedly improve the CO_2 capture efficiency of the process. A comparison of capture capacity (CC) in both fast and diffusive-controlled carbonation stages between limestone, dolomite and steel slag is shown in Figure 12.

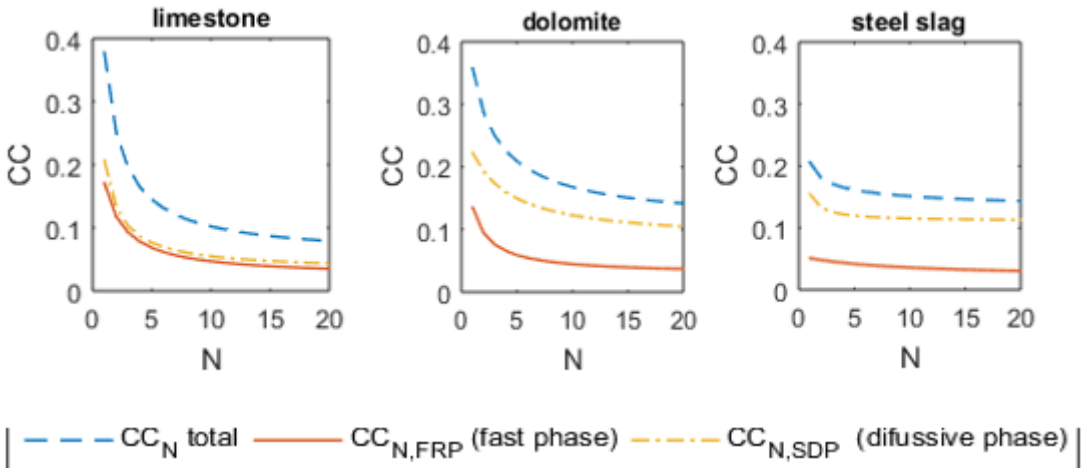

Figure 12: Total CO_2 capture capacity, capture capacity in the fast reaction controlled phase (FRP) and solid-sate diffusion controlled phase (SDP) as a function of the cycle number for limestone, dolomite and steel slag [63] [48] [209]. Reproduced from [203].

As can be seen in Figure 12 in the case of limestone derived CaO, the contribution of the diffusion controlled phase to the overall CO_2 capture capacity in each cycle is similar to the capture capacity in the fast reaction controlled phase (for 5 min overall carbonation periods). Carbonation in the SDP becomes even more relevant for dolomite and steel slag, which suggests that the capture performance may be further improved if the solids residence time in the carbonator is prolonged beyond a few minutes. SPECCA results plotted in Figure 13 show that increasing the solids residence time leads to a decrease of energy consumption for all the CaO precursors.

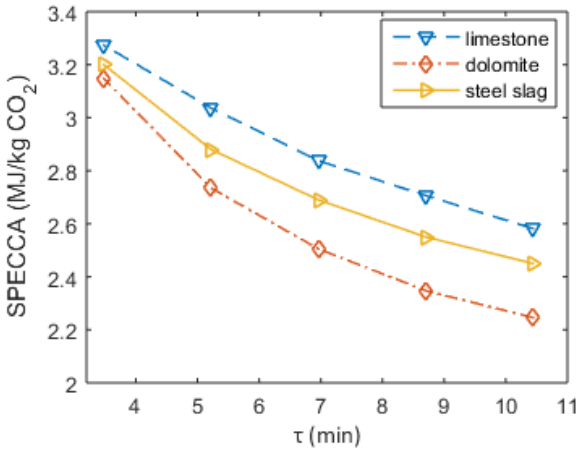

Figure 13: SPECCA values as a function of solids residence time in the carbonator for different CaO precursors [203].

As shown in Figure 13, under the simulated conditions, a SPECCA as low as 2.2 MJ/Kg CO_2 is obtained for dolomite at carbonation residence times of 10 minutes (corresponding to a solids recirculation flow rate of $F_R = 40{,}500$ kmol/h) as compared to 2.6 MJ/Kg CO_2 for limestone.

These results were published in [191,203]. *The full manuscripts including further information about the CFPP-CaL integration modelling are presented in* ***Annexes 2*** *and* ***4.***

3.4. The novel Oxy-CaL process for CO_2 capture

This section summarizes the main results of the work according to ***objective (4)*** of the present thesis. Thus, a novel CO_2 capture system (Oxy-CaL) is proposed from the integration of partial oxy-combustion and the CaL process based on the multicycle carbonation/calcination of limestone derived CaO. Basically, Oxy-CaL consists of carrying out a partial oxy-combustion process to produce a flue gas with a CO_2 concentration in the range 30-60% vol, which is then sent to the CaL capture process. The new process development is supported by experimental results from TGA analysis on the multicycle conversion of limestone derived CaO under realistic calcination conditions (high temperature and high CO_2 concentration). These TGA results are used in the Oxy-CaL integration model to calculate the CO_2 capture efficiency from process simulations. The energy penalty arising from the diverse CO_2 capture technologies considered (total oxy-combustion, CaL and Oxy-CaL) is analyzed and compared with those of other CO_2 capture systems. These results were published in [54].

3.4.1 Thermogravimetric analysis

TGA tests were carried out by **Dra. Mónica Benítez** and **Dr. Antonio Perejón**, recognized specialists in TGA techniques, within a fruitful collaboration among our working groups [54]. In these TGA tests, the CO_2 concentration in the carbonation environment was varied in the range 15-60% vol to address the effect of an excess of CO_2 in the carbonator over the typical vol% in the flue gas at typical combustion conditions (~15%). Moreover, the carbonation temperature was varied in the range 625-680ºC, which affects critically the carbonation kinetics in the solid-state diffusion-controlled stage as will be seen. Figure 14 shows the different sorbent behaviors in both configurations. As may be seen, carbonation in the fast phase is markedly enhanced as the CO_2 concentration is increased, whereas, on the contrary, diffusion-controlled carbonation is markedly

hindered. Thus, carbonation in the diffusion-controlled stage loses relevancy as the CO_2 vol% is increased.

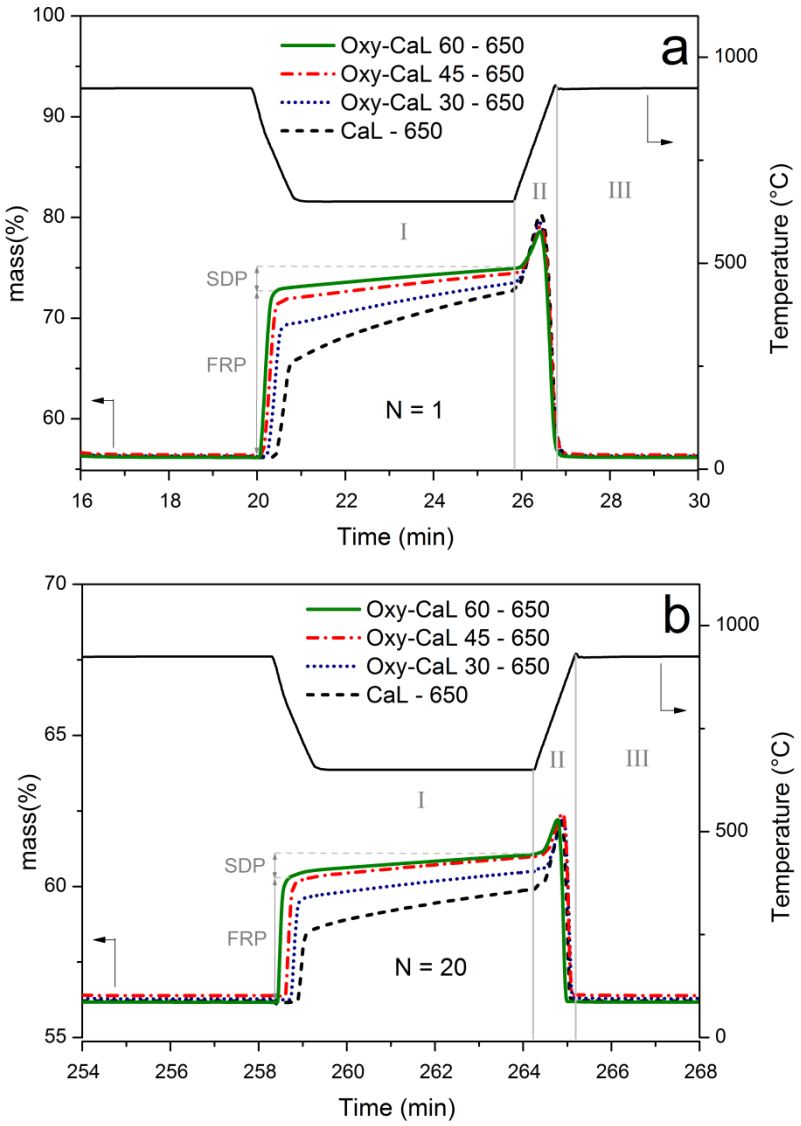

Figure 14: Time evolution of the sorbent mass % during the carbonation and calcination stages in the a) 1st cycle (N=1) and b) 20th cycle (N=20) for limestone tested under CaL (15% vol CO_2 carbonation) and Oxy-CaL (30%, 45%, 60% vol CO_2 carbonation) conditions. I indicates the carbonation stage, II the transition stage and III the calcination stage. Mass gain in the two phases of carbonation (fast reaction-controlled phase FRP and solid-state diffusion controlled phase SDP) are indicated [54].

Figure 15a shows the thermograms corresponding to the 1st cycle obtained from TGA tests performed at different carbonation temperatures (625, 650 and 680ºC) under CaL conditions (15% vol CO_2 carbonation). As may be observed, a variation of just about 25ºC around the typical carbonation temperature used in pilot-scale plants (~650ºC) has a significant effect on the CO_2 uptake in the diffusion-controlled stage, which notably affects the overall capture capacity. Thus,

carbonation in this phase is enhanced with temperature while a decrease of the carbonation temperature yields a rapid decay of the carbonation rate in this solid-state diffusion-controlled stage. A similar behavior has been observed for the samples tested under Oxy-CaL conditions (Figure 15b).

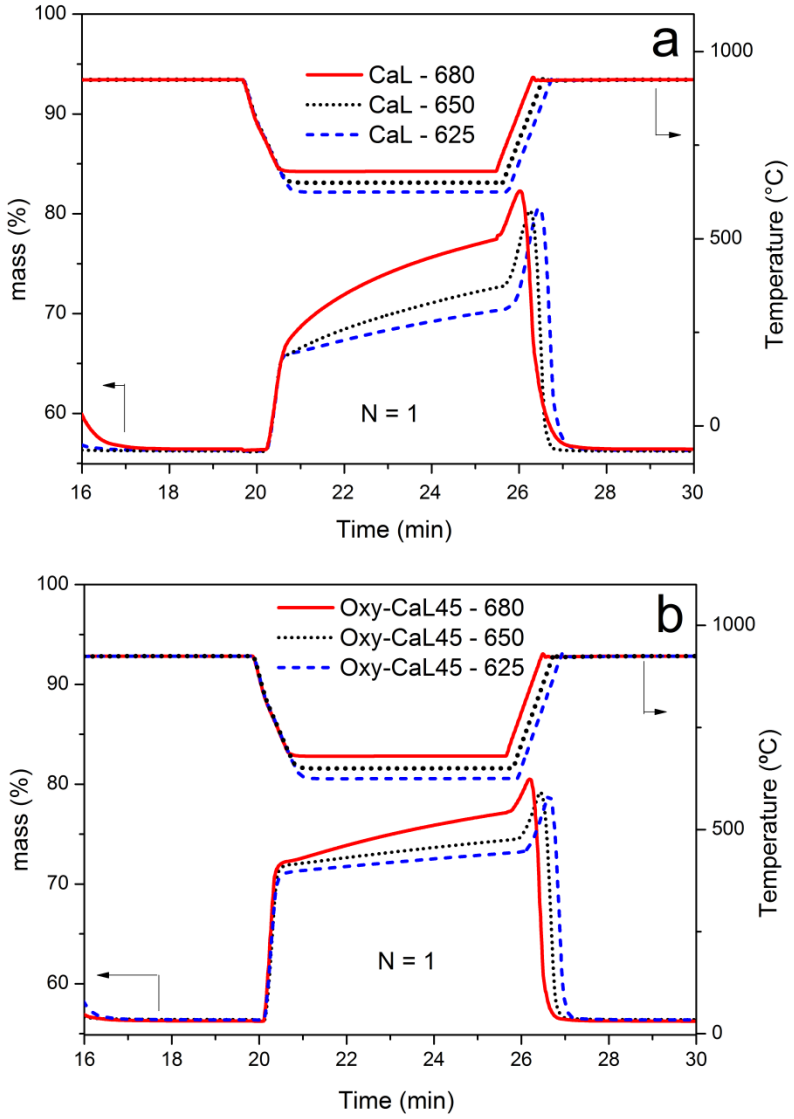

Figure 15: Time evolution of the sorbent mass % during the 1st cycle (N=1) for limestone under (a) CaL (15% vol CO_2 carbonation) and (b) Oxy-CaL 45 (45% vol CO_2 carbonation) conditions for different carbonation temperatures (625ºC, 650ºC and 680ºC) as indicated [54].

3.4.2 The Oxy-CaL process

Figure 16 shows a schematic representation of the process, which has been simulated for several values of the CO_2 vol % in the flue gas effluent from partial oxy-combustion. Partial oxy-combustion is carried out to obtain a CO_2 vol% in the range of 45% in the flue gas at the boiler exit. To this end, a mixture of air and O_2 is used in the boiler for combustion. As in the case of

total oxy-combustion, recirculation of the flue gas serves to control the flame temperature in the boiler, whose value is kept the same for all the simulations. Since the amount of pure O_2 for partial oxy-combustion is substantially decreased (99.3 kg/s to achieve a 45% vol CO_2 concentration instead of 138 kg/s for total oxy-combustion), power consumption in the ASU is notably reduced. Furthermore, the CPU unit for CO_2 purification is not needed since this step is carried out after the CaL process. Altogether, the energy penalty for partial oxy-combustion is significantly reduced to 3.40% in the Oxy-CaL 45 system (9.05% for total oxy-combustion).

After partial oxy-combustion, the CO_2 rich flue gas is sent to the carbonator reactor to follow up with the CaL process. The CO_2 capture efficiency in the CaL process will be analyses by means of the carbonator model described in Section 3.1. Figure 17 shows the evolution of the CO_2 capture efficiency (E_{CO2}) as the solids recirculation flow rate between reactors is decreased or, equivalently, the solids residence time in the carbonator ($\tau = N_{Ca}/F_R$) is increased. As may be seen, a significantly higher capture efficiency is achieved by increasing the CO_2 concentration in the carbonator in the Oxy-CaL systems. Note the differences on the maximum capture efficiency ($E_{max} = (y_{CO2,in} - y_{eq})/y_{CO2,in}$)) for the different systems (obtained for very short residence times) as a consequence of the variation of the CO_2 vol % in the carbonator.

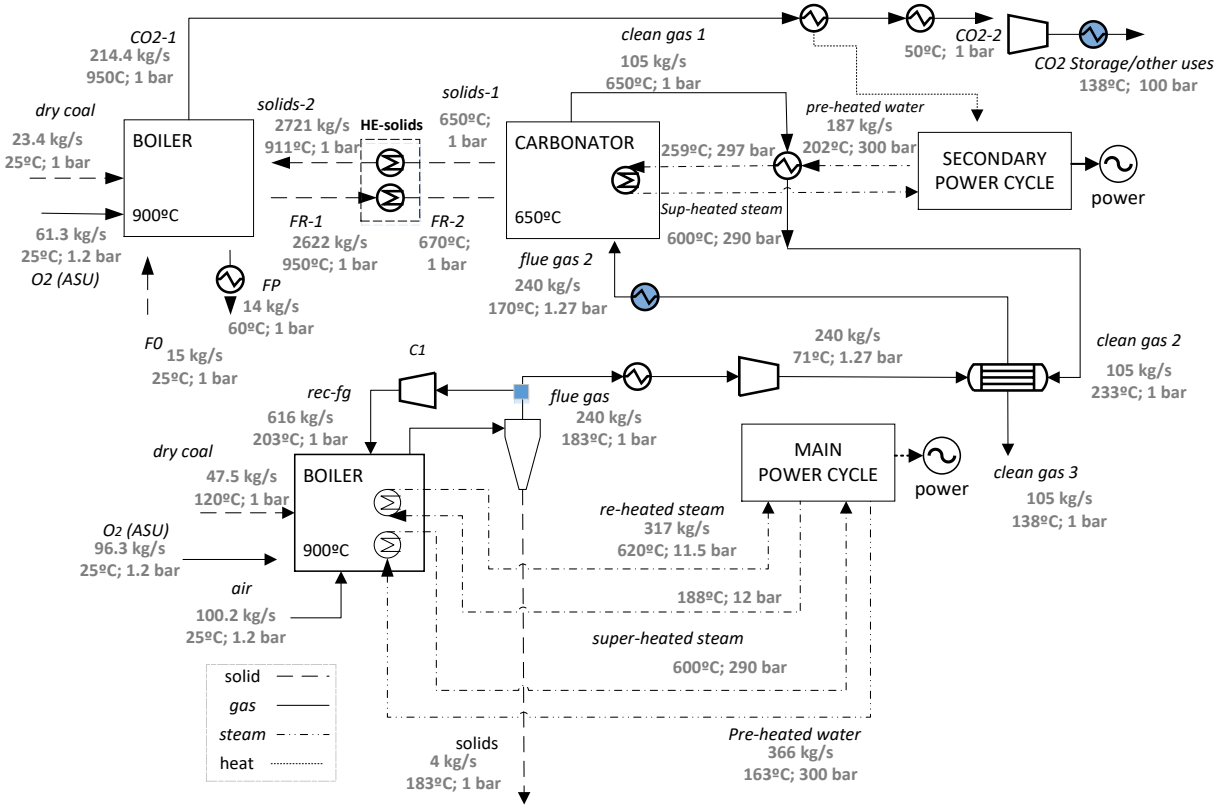

Figure 16: General Oxy-CaL-45 (45% vol CO_2 concentration in the flue gas by partial oxy-combustion) integration scheme [54].

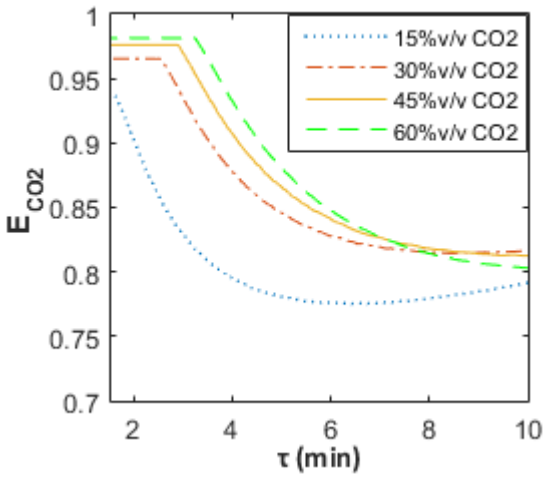

Figure 17: CO_2 capture efficiency as a function of the residence time in the carbonator, which is varied by changing the F_R/F_{CO2} ratio. Calculations are made for fixed values of the solids inventory $W_s = 400\ ton$ and $F_0/F_{CO2} = 0.05$. A carbonation temperature of 650ºC is assumed. [54].

As shown in Figure 17, the capture efficiency is decreased as the solids residence time in the carbonator is prolonged albeit at a minor rate for the CaL process in comparison with the Oxy-CaL systems. This is due to the relatively higher conversion in the solid-state diffusion controlled phase for the CaL process (as seen above from the TGA tests). Thus, the Oxy-CaL-45 system has a CO_2 capture efficiency of 97.6% in the base case as compared to 82.7% in the base case of the CaL system. Despite the need of additional coal and O_2 for oxy-combustion in the calciner, the increase in CO_2 capture efficiency obtained by increasing the CO_2 concentration in the flue gas leads to a reduction of energy consumption in the CaL cycle. Thus, a SPECCA value of 2.37 MJ/kg CO_2 is obtained for the Oxy-CaL-45 system, which is 28% below the SPECCA obtained for the conventional CaL system. Nevertheless, the SPECCA for the complete Oxy-CaL process is 3.62 MJ/kg CO_2, which is 10% higher than in the CaL base case. On the other hand, the Oxy-CaL system allows for a reduction by 11% of energy consumption in comparison with the total oxy-combustion case as shown in Table 3.

Table 3: Main inputs and results for the base case of diverse CO_2 capture systems [54].

	parameter	Reference CFFP (air combustion)	Case a	Case b	Case c		
			oxy-combustion	CaL	Oxy-CaL 30	Oxy-CaL 45	Oxy-CaL 60
CFPP	$\dot{m}_{coal}\ (kg/s)$	42.20	55.05	42.20	46.10	47.50	48.15
	$\dot{m}_{air}\ (kg/s)$	475	-	475	208.90	100.20	43.54
	$\dot{m}_{O2}\ (kg/s)$	-	136.91	-	68.85	96.35	110.503
	v_{CO2}	0.15	0.89	0.15	0.30	0.45	0.60
	η_{CFPP}	0.3777	0.2872	0.3777	0.3517	0.3437	0.3374
	$net\ work\ (MW)$	490.47	488.80	490.47	498.30	502.30	499.75
	$Penalty$	-	**9.05%**	-	**2.60%**	**3.40%**	**4.03%**
	$SPECCA$ (MJ /kg_{CO2})	-	**4.06**	-	**0.94**	**1.25**	**1.50**
CaL	$T_{calc}\ (^{o}C)$	-	-	950	950	950	950
	$T_{carb}\ (^{o}C)$	-	-	650	650	650	650
	E_{CO2}	-		0.827	0.950	0.976	0.981
	$\dot{m}_{coal}\ (kg/s)$	-	-	18.48	22.34	23.40	23.84
	$\dot{m}_{O2}\ (kg/s)$	-	-	48.00	58.41	61.00	62.49
	$\dot{W}_{sec}\ (MW)$	-	-	75.80	113.90	126.46	130.88
	η_{int}	-	-	0.3030	0.2909	0.2882	0.2853
	$Penalty$	-	-	**7.47%**	**6.08%**	**5.55%**	**5.21%**
	$SPECCA$ (MJ /kg_{CO2})	-	-	**3.28**	**2.63**	**2.37**	**2.29**
Total	$\dot{m}_{coal,total}$	-	-	60.68	68.44	70.90	71.99
	$Penalty_{total}$	-	**9.05%**	**7.47%**	**8.68%**	**8.95%**	**9.24%**
	$SPECCA_{total}$ (MJ/kg_{CO2})	-	**4.06**	**3.28**	**3.56**	**3.62**	**3.79**

Figure 18 shows data on SPECCA and solids inventory for the CaL and Oxy-CaL (carbonator temperatures of 625ºC, 650ºC and 680ºC) systems for a fixed capture efficiency (E_{CO2}= 90%. As may be seen, for operation under short residence times (2 min), the Oxy-CaL systems (especially Oxy-CaL-30 and 45) lead to a considerable reduction of the solids inventory (from 400 tons for the CaL-650 system to 286 tons for Oxy-CaL-45-650) and therefore to a reduction of the CaL system size whereas the SPECCA is only slightly increased (from 3.59 MJ/kg for the CaL-650 system to 3.7 MJ/kg for the Oxy-CaL-45-650). Regarding the effect of the carbonator temperature on the CaL and Oxy-Cal systems for a given solids residence time of 2 min, there is not a clear evidence on the optimum system choice (lower SPECCA).

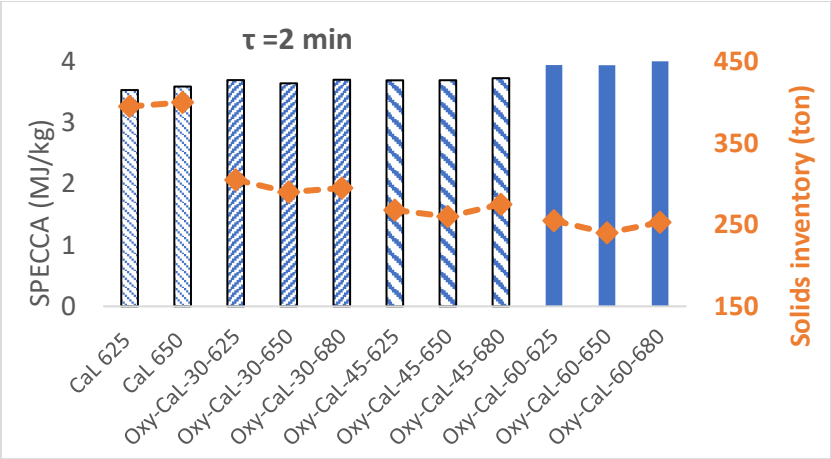

Figure 18: SPECCA and solids inventory for the CaL and Oxy-CaL systems operating under short (2 min) solids residence times. The effect of changing the carbonator temperature (between 625ºC to 680ºC) is also shown. Capture efficiency is fixed to 90% [54].

Results show that the Oxy-CaL system is a promising hybrid concept to be applicable in new power plants, allowing for a substantial reduction of energy penalty as compared to total oxy-fuel combustion. Moreover, the Oxy-CaL system leads to a high CO_2 capture efficiency in comparison with the CaL process, which would serve to reduce significantly the carbonator reactor size.

These results were published in [54]. *The full manuscript including further information about the Oxy-CaL process is presented in* ***Annex 7.***

3.4.3 The mOxy-CaL process

This section proposes a modification over the Oxy-CaL system by integrating membrane separation technology. In the so-called mOxy-CaL process, an oxygen-enriched air stream, which is obtained from air separation by using polymeric membranes, is needed to carry out the partial oxy-combustion. The flue gas exiting the partial oxy-combustion system presents a CO_2 concentration of 30% v/v (higher than 15% v/v typical in coal power plants). After that, the flue gas it is passed to the CaL process where the CO_2 reacts with CaO solids according the carbonation reaction.

Cryogenic distillation for air separation is the most extended technology worldwide and the only one that is currently developed for high purity O_2 production (>99%) at large scale [212]. However, cryogenic distillation has a high energy consumption that penalizes the O_2 production and consequently partial oxy-combustion [213]. However, by considering that a lower O_2 purity

(~20-40% v/v) is sufficient in the case of partial oxy-combustion, air separation can be carried out by means of membranes, which highly reduce the energy consumption associated with the oxy-combustion. In fact, membranes are economically suitable for O_2 purities in the range 25-50% [214].

Membranes are used in a huge amount of industrial applications among which we find air separation [215]. Polymeric membranes are today the most developed membranes for gas separation although other possibilities are gaining attention in the last years such as ion transport membranes. Polymeric membranes are generally non-porous and separate gases from the solution-diffusion transport mechanism by applying a transmembrane partial pressure difference. In a typical membrane-based gas separation process the feed gas is put into contact with the membrane surface under a certain pressure, which is the driving force of the process. The most permeable gas crosses the membrane and leaves the system as permeate stream (at lower pressure that the feed gas), whereas the remaining gas exits at high pressure as the retentate stream without crossing the membrane. Membranes for gas separation are usually analysed in terms of permeability and selectivity, which highly influence the efficiency and cost of a membrane-based gas separation process. As pointed out by [216], in polymeric membranes there is usually a trade-off between permeability and selectivity. The O_2/N_2 separation factor for the best commercially available polymer membranes is 6–8 [217]. In the same work, data can be found for permeability and selectivity of many polymeric membranes.

The pressure ratio (PR) between the upstream and downstream membrane sides is a key operating parameter in the separation process. In order to reach a O_2 purity 40% it would be enough a pressure ratio across the membrane of 0.1 by using a single-stage process for a membrane selectivity 3 [214]. Nevertheless, it is remarkable that the higher pressure ratio the higher permeability of polymeric membranes [216]. Thus, in order to increase the permeability and therefore reduce the membrane area needed, a higher PR must be imposed. The energy consumption associated to a separation process can be calculated from the adiabatic compression work of a perfect gas, which gives a realistic estimation of energy consumption [218]. The pressure ratio can be imposed either by increasing pressure on the upstream side (i.e. compressing the gas entering the membrane system) or by creating vacuum on the downstream side, which is the selected technique in the present work. Since a vacuum strategy is considered, the pressure must be increased again in the permeate (OEA) before entering the boiler. Thus, energy consumption (E_{sep}) can be calculated as [219]:

$$E_{sep} = m_p \frac{\gamma RT}{\gamma - 1}\left[\left(\left(\frac{P_{in}}{P_p}\right)^{\frac{\gamma-1}{\gamma}} - 1\right) + \left(\left(\frac{P_b}{P_p}\right)^{\frac{\gamma-1}{\gamma}} - 1\right)\right] \quad (23)$$

where m_p is the mass of gas permeating though the membrane, γ is the adiabatic expansion factor of the gas, T is the temperature of the system and P_{in}, P_p and P_b are the pressures at the upstream side, downstream side and boiler inlet, respectively.

Membrane separation is simulated within the whole mOxy-CaL process from the energy consumption as given by Eq (1). Thus, by considering a gas pressure at the permeate side of 0.235 bar (similarly to previous works such as [220]), the energy requirement for separation is 90 kwh/tonne O_2. A stage cut, defined as the ratio of permeate flowrate to feed flowrate of 0.1 is assumed [221].

The mOxy-CaL process has been modelled by means of ASPEN PLUS™ with the same assumptions than in the Oxy-CaL simulation case presented in the previous section. Table 4 shows the main results.

Table 4: Main inputs and results for the mOxy-CaL30 process

Coal-Fired Power Plant		**CaL**	
Parameter	Value	Parameter	Value
$\dot{m}_{coal}\ (kg/s)$	46.1	F_R/F_{CO2}	15
$\dot{m}_{air}\ (kg/s)$	0	F_0/F_{CO2}	0.05
$\dot{m}_{O2}(x_{O2} = 0.95)\ (kg/s)$	0	$\tau\ (min)$	2.79
$\dot{m}_{OEA}(x_{O2} = 0.38)\ (kg/s)$	281.02	$T_{calc}\ (ºC)$	950
γ_{fg}	0.63	$T_{carb}\ (ºC)$	650
$F_{fg}\ (kmol/s)$	10.25	E_{CO2}	0.950
$F_{CO2}\ (kmol/s)$	2.84	$\dot{W}_{sec}\ (MW)$	118.14
v_{CO2}	0.3	$\dot{W}_{solids}\ (MW)$	49.73
v_{O2}	0.025	$\dot{W}_{ASU}\ (MW)$	42.13
η_{boiler}	0.89	$\dot{W}_{comp,CO2}\ (MW)$	70.94
η_{CFPP}	0.362	$\dot{W}_{comp,FG}\ (MW)$	7.37
$net\ work\ (MW)$	513.59	η_{int}	0.301
$Penalty$	**1.63%**	$Penalty$	**6.12%**
$SPECCA$ (MJ/kg CO2)	**0.55**	$SPECCA$ (MJ/kg CO2)	**2.49**
$Penalty_{total}$	**7.75%**		
$SPECCA_{total}$ (MJ/kg CO2)	**3.05**		

As can be seen in Table 4, a notable reduction of energy consumption for CO_2 capture is achieved by means of the mOxy-CaL (3.05 MJ/kg CO_2) process in comparison with the Oxy-CaL system (3.56 MJ/kg CO_2 achieved in the previous section). This energy reduction is directly attributable to the membrane separation, which saves power to produce O_2 enriched air as compared with cryogenic distillation.

3.5. Calcium-Looping integration in concentrating power plants

This section summarizes the main results of the thesis according to ***objectives (5,7,9)***. Concentrated Solar Power (CSP) should play a leading role within the new energy landscape as it lends itself to potentially cheap storage of energy in the form of heat [9,95]. Thus, efficient and affordable thermal energy storage systems must be developed in order to decouple production and demand [97,98], which would allow a deep penetration of solar energy power generation into the grid. Among the possibilities explored for TCES in CSP tower plants at large scale, one of the most promising systems is the CaL process. These results were published in [145,222].

3.5.1 CSP-CaL plant description

Process integration is fundamental for the introduction of the CaL process within the solar power plant. Despite that the CaL process was considered as solar energy storage systems in the late 1970s [3,128] and solar calcination has been tested since the 80s [4,5], process integration schemes have not been proposed until a few years ago.

In our scheme, solar energy is used to carry out the calcination at high temperature to achieve sufficiently fast calcination under a pure CO_2 atmosphere. According to equilibrium conditions [161] and reaction kinetics, high temperatures are necessary when operating under high CO_2 partial pressure (above 900°C) for sufficiently fast calcination to achieve completion in short residence times [10,11,223]. A number of solar calciner prototypes have been already developed based on fluidized beds [5,147], rotary kilns [224,225] and cyclone atmospheric reactors [226]. A potentially cheap and simple option consists of falling particle receivers [227]. Further assessment of solar calciners is shown in Section 3.8.1. Since the CSP-CaL integration scheme proposed in this thesis relies on a closed CO_2 cycle, a pure CO_2 stream must be retrieved as output from the calciner. Two options are feasible to this end: i) performing calcination under a 100% CO_2 atmosphere or ii) under an easily separable gas from CO_2. The first choice would make it necessary to operate the calciner under low absolute pressure in order to reduce the calcination temperature and to avoid hampering the reactivity of the regenerated CaO due to excessive sintering as observed when calcination is carried out under high CO_2 partial pressure for CO_2 capture [88].

Among CSP power technologies, solar tower systems are the most appropriate for $CaCO_3$ calcination because of the required temperature. Thus, the total solar energy entering into the system is used to heat the reactants and to drive the endothermic chemical reaction, which serves to store the solar energy as both sensible and chemical and form. The CaO and CO_2 streams released within the calcination are stored separately. Products can be stored at ambient

temperature, which is an important advantage of the CSP-CaL integration over current state of the art sensible heat storage using molten salts, whose temperature must be kept above ~200°C to avoid solidification [123]. In order to use reasonably sized CO_2 storage volumes a minimum pressure of 75 bar is needed to store CO_2 storage under supercritical conditions (considering storage at ambient temperature) [222]. The high compression ratio from calciner to storage conditions (1:75) requires the use of intercooling compression to minimize the efficiency penalty. Note that compression-expansion process of CO_2 before and after than storage resembles a Compressed Air Energy Storage (CAES) system [228] and therefore the process incorporates energy storage not just in chemical form but also as sensible heat and mechanical energy. When power is needed, both calcination products are brought together to another reactor (carbonator) where energy is released through carbonation. Pressurized carbonation is desirable for the power-cycle direct integration and allows carbonation at high temperatures and at a fast rate [229].

The energy discharge phase takes place in the carbonator, which is a pressurized fluidized bed reactor wherein carbonation takes place under pure CO_2 at the highest possible temperature in order to achieve a high thermal to electric efficiency. According to thermodynamic equilibrium, carbonation can be carried out at high temperature (>850ºC) under a pure CO_2 atmosphere at ambient pressure [161]. This would allow a highly efficient generation of electricity thus overcoming temperature limits (T~550-600°C) in currently commercial CSP plants with thermal storage in molten salts. Solids exiting the carbonator are passed through another heat exchanger network to preheat the CaO and CO_2 streams entering the carbonator. In order to achieve a higher integration efficiency an optimized heat exchanger network is necessary.

Solids conveying can be carried out by means of the mature pneumatic technology that guarantees rapid transport of granular solids, routing flexibility, as well as the possibility of streams splitting, and it is suitable to successfully convey high temperature materials. Other possibilities for solids conveying are discussed in Section 3.8.3.

Plant performance is determined as an average over a 24 hours period. An average daytime period Δt_{sun} is considered during which the solar thermal power entering the calciner is constant. Different operations in “sun” and “night” modes were considered. A Solar Multiple (SM) equal to 3 was assumed, which means that, when solar energy is available, the CO_2 mass flow entering the carbonator side is 1/3 the amount produced in the calciner whereas the 2/3 remaining are sent to a CO_2 storage vessel which is discharged during the “night” mode operation (estimated as 2/3 of the day). Therefore, the plant efficiency is determined as a weighted average of the performances in “sun” and “night” modes by means of Eq. 24:

$$\eta = \frac{\int_{24h} \dot{W}_{net}\, dt}{\int_{24h} \dot{Q}_{input}\, dt} = \frac{\dot{W}_{net,sun}\, \Delta t_{sun} + \dot{W}_{net,night}\, (24 - \Delta t_{sun})}{\dot{Q}_{input}\, \Delta t_{sun}} \quad (24)$$

Where $\dot{W}_{net,sun}$ and $\dot{W}_{net,night}$ are the net power produced in "sun" and "night" modes, respectively and $\dot{Q}_{input}$ is the net solar power entering the calciner.

3.5.2 Process scheme: base case

Regarding the integration of the power cycle in the carbonator zone, previous works have proposed the use of an air stream as heat transfer fluid in an open Brayton cycle (Figure 19) [194]. According to this scheme, the CO_2 stream entering the carbonator is wrongly assumed to react completely with the CaO solids to produce $CaCO_3$. Thus, it is assumed that a pure air stream can exit the carbonator to enter the gas turbine for power production in an open Brayton cycle. The outflowing air from the turbine passes through a heat exchanger network, releasing sensible heat further used to preheat the solids directed into the carbonator.

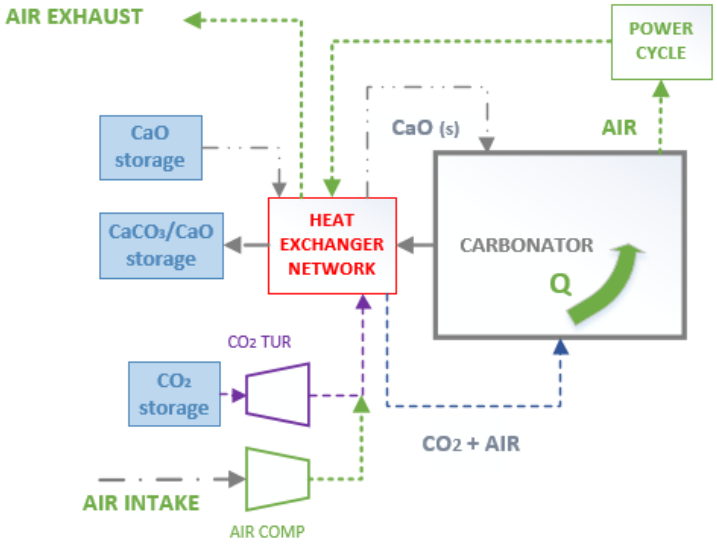

Figure 19: Air/CO_2 open cycle integration in the carbonator zone. Originally proposed by Edwards et al. [194]. Reproduced from [145]

However, reaction equilibrium poses a fundamental limitation to this scheme since the reaction will reach equilibrium and carbonation will stop as soon as the CO_2 partial pressure in the carbonator reactor is decreased to the equilibrium partial pressure as depending on the carbonator temperature. Thus, the effluent gas from the carbonator to be sent to exhaust cannot be free of CO_2. For example, when a 50% v/v CO_2 stream is introduced into a carbonator at atmospheric pressure (P=1 bar) and T=800ºC, the minimum CO_2 concentration in the gas stream exiting the carbonator is around 21% [161].

A possible solution to avoid the inconveniences of an open Brayton cycle is to use a closed CO_2 Brayton cycle [222]. In this configuration, solids in the carbonator (CaO) are fluidized by a pure CO_2 gas flow with a molar rate well above the stoichiometric value. The CO_2 fraction not participating in the reaction is employed to remove heat from the carbonation and is delivered to a gas turbine for the power cycle. This section shows the global integration model and process design to transform an air-open power cycle into a closed-CO_2 power cycle as a first step for improving the CSP-CaL integration. Figure 20 shows a first possible approach for the proposed integration. As can be seen, solids entering the calciner are preheated using the sensible heat released by the hot streams leaving this reactor in a gas-solid heat exchanger (HXB in Figure 20) and in a solid-solid heat exchanger (HXA). The CO_2 power cycle is a closed and regenerative cycle in which the heat removed by the reactants in the carbonator is recovered in a solid-gas heat exchanger (HXF). The additional CO_2 storage vessel (CO_2 inventory storage) is included in the scheme as an inventory control strategy for the gas turbine. On the other hand, the residual heat from the solids at the carbonator output is extracted to pre-heat the CO_2 stream entering the carbonator by means of another gas-solid heat exchanger (HXE). As shown in Figure 20, part of the power needed in the compression stage of the Brayton cycle is provided by the expansion of the pressurized CO_2 coming from the storage vessel [222].

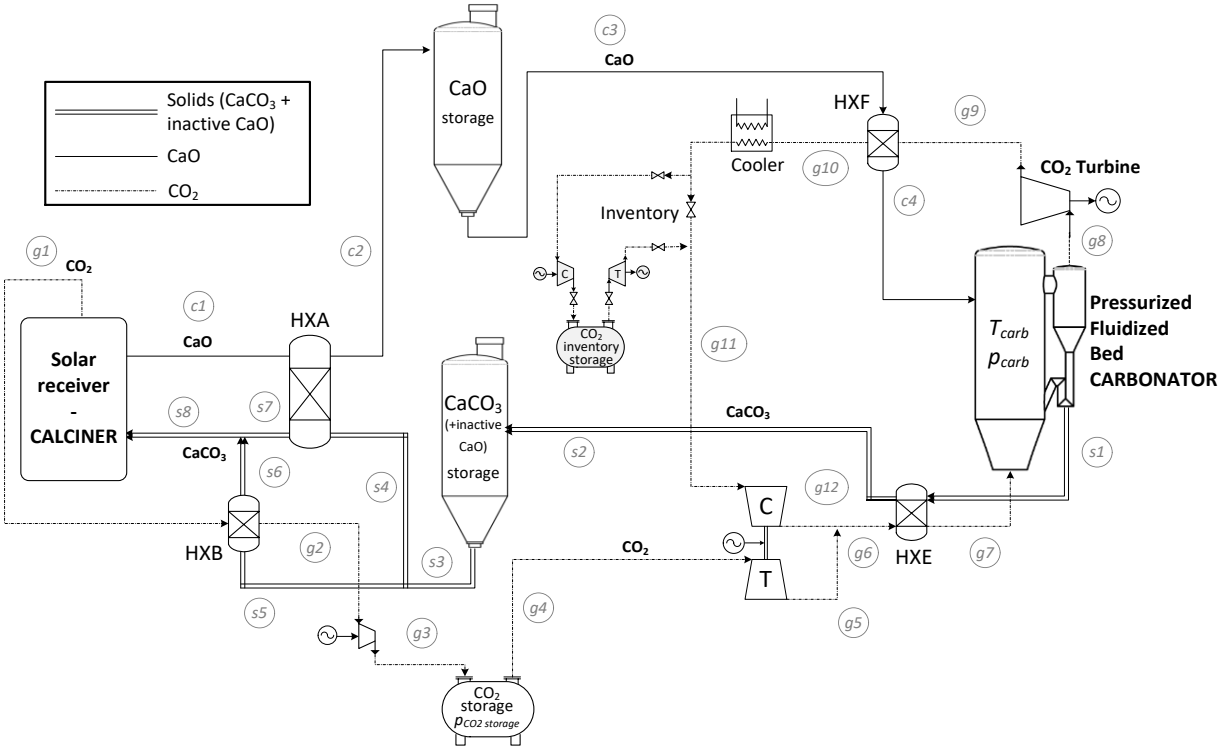

Figure 20: Base case for the CO_2 closed Brayton cycle integration in the CSP-CaL plant. Further information about the stream data can be found in [145].

The CSP-CaL base case was simulated by using the main parameters showed in Table 5. Further information about the simulation is available in **Annex 5.**

Table 5: Main parameters used for simulating the scheme proposed in Figure 20 [145]

Net absorbed solar flux in calciner	100 MW	Approach temperature CO_2 cooler	10 °C
Thermal dispersions in carbonator	10%	Intercoolings in CO_2 storage compression	5
Calciner temperature	900 ºC	Intercoolings in CO_2 cycle compression	4
Ambient temperature	20 ºC	CO_2 storage temperature	25 ºC
Average CaO conversion	0.20	CO_2 storage pressure	75 bar
Carbonator temperature (T)	875 ºC	Solid phase conveying energy consumption	20 MJ/ton
Carbonator pressure (P)	6 bar	Daylight hours	12h
Turbine outlet pressure (TIT)	0.2 bar	Solar Multiple	2
Approach temperature solid-solid HX	20 °C	Isentropic efficiencies (compression/expansion)	0.89
Approach temperature solid-gas HX	15 °C		

Figure 21 shows a contour plot of the system efficiency as a function of both carbonator pressure and turbine outlet pressure, which serves to infer the optimum pressure choice.

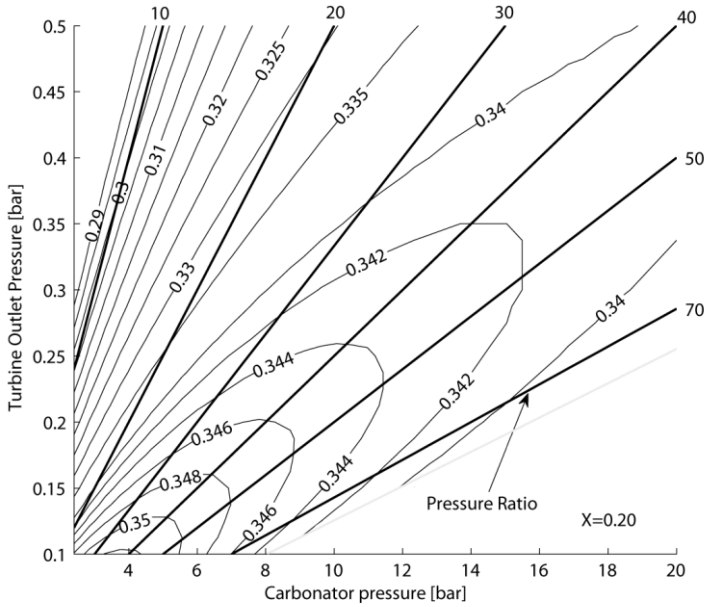

Figure 21: Efficiency as a function of carbonator and turbine outlet pressure. Dashed white lines indicate iso-efficiency cycle values [145].

As shown in Figure 21, maximum efficiency occurs at pressure ratios around 40-50. However, it is important to note that for pressure ratios over 30 the efficiency does not change considerably. From pressure ratios of 30 up to 70, efficiency increases less than 0.5%. Since such high values of pressure ratios are difficult to achieve in practice, a pressure ratio of 30 represents a good trade-off. Moreover, higher efficiency can be achieved by decreasing the turbine outlet pressure.

3.5.3 Improving the CSP-CaL heat integration

From the base case (Figure 20), a CO_2 regenerator (HXG) is incorporated in the heat exchanger train in order to heat up a fraction of the gas stream entering the HXE exchanger (and then in the carbonator) using the sensible heat of a portion of the CO_2 turbine output flow. The two CO_2 streams, which are separately heated through heat exchangers HXF and HXG, are rejoined to evolve in the closed loop power-cycle. By regulating the CO_2 split ratios (i.e. the fractions of the CO_2 stream respectively sent to HXG and HXF), the internal overall heat exchange can be optimized by means of a pinch-analysis [230] of the carbonator side. The pinch-analysis were mainly carried out by **Alessandro Alovisio** and **Professor Ricardo Chacartegui** [145,222] with the collaboration of the author of the present thesis. Full information about the pinch analysis developed is available in **annex 5**.

As result of the pinch-analysis, the energy-optimized process scheme is shown in Figure 22. Remarkably, this energy-optimized scheme is realized by considering low-temperature energy storage conditions. Temperature in the storage vessels highly conditions the configuration of the process scheme and the efficiency of it. Due to the high temperatures in both calciner and carbonator reactors, a low temperature storage involves a large streams temperature change along the entire cycle which makes crucial an optimized heat integration to achieve an adequate system efficiency. Another possibility, which is investigated throughout the Section 3.7, is to storage the solids at high temperature. In this case the process scheme is simplified by requiring fewer heat exchangers due to a lower temperature difference between the reactors and the storage.

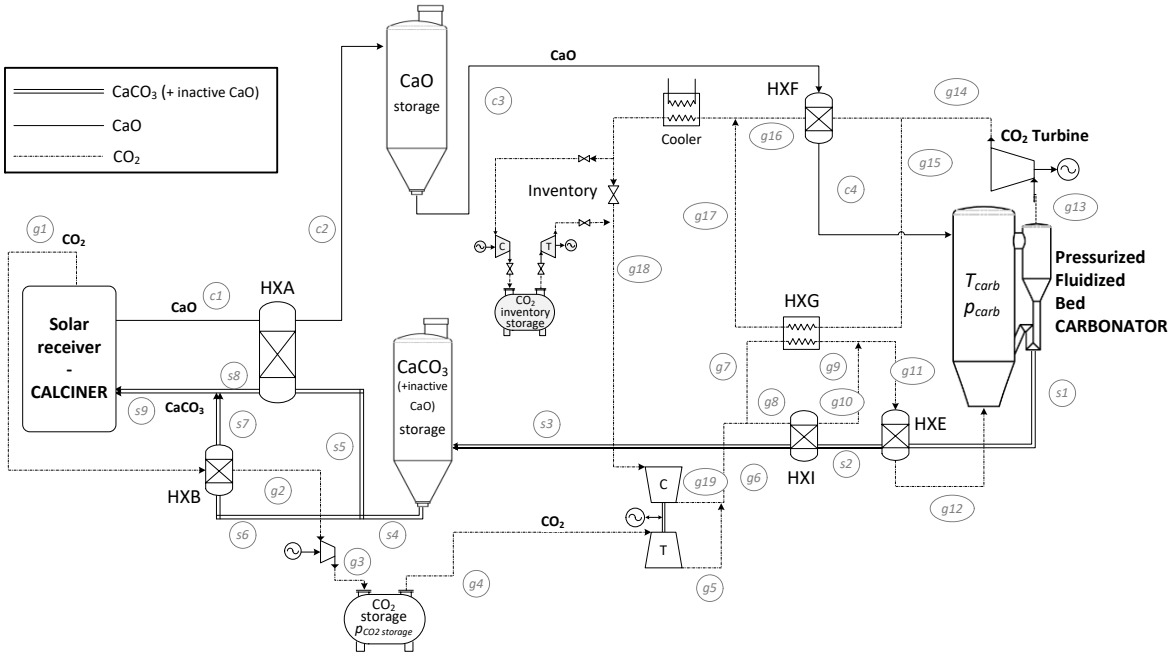

Figure 22: Plant diagram of the energy-optimized integration layout for the CSP-CaL plant with low-temperature storage. Full information about the stream data is given in [145].

According to the pinch analysis results, the proposed final plant configuration is equipped with a solid-solid heat exchanger (HXA), four gas-solid heat exchangers (HXB, HXF, HXE, HXI) and with a gas-gas regenerator (HXG). The CO_2 stream from storage (produced in the calciner side operation) and the CO_2 stream coming from the power loop are mixed, flowing through a heat exchangers train (HXG and HXI) which optimize heat recovery at low temperature. On the other hand, the CO_2 stream flowing out from the turbine is divided into two sub-streams through HXF and HXG to preheat the CaO stream and a fraction of CO_2 entering the carbonator, respectively. In HXE, the high-temperature sensible heat from the $CaCO_3$ stream is used in the final stage of CO_2 stream preheating above the pinch, which serves to maximize the gas temperature at the carbonator inlet and therefore the cycle performance. Table 6 shows a comparison of the main data according to an energy balance for each configuration. At a fixed CaO conversion of 0.2, the global net efficiency increases of about 5% with respect to the base case.

Table 6: Energy balance of for the two CSP-CaL configurations [145].

	Parameter	Layout 1 (Figure 20)	Layout 2 (Figure 22)
	Solar thermal power (MWth) -12h-	100	100
Heat exchangers Thermal Power (MWth)	HXA	120.0	120.0
	HXB	23.2	23.2
	HXF	26.8	46.0
	HXG	-	78.6
	HXI	-	53.7
	HXE	70.4	15.5
	Auxiliary cooler	3.9	6.9
Power outlet (MWe)	compressor calciner (storage)	7.0	7.0
	compressor carbonator (power cycle)	16.7	14.0
	Solids conveying (average)	1.8	1.8
Power inlet (MWe)	turbine (storage)	1.2	2.2
	main turbine (power cycle)	38.6	37.3
	Global net efficiency	**0.356**	**0.403**

The high overall efficiencies achieved indicate a potential interest for the integration of the CaL process in Concentrating Solar Power Plants, although major technological challenges related to the design of the solar receiver and of the high temperature solid handling devices will need to be faced.

These results were published in [145,222]. *The full manuscripts including further information about the CSP-CaL integration modelling are presented in* ***Annex 3*** *and* ***5.***

3.6. Indirect integration of power cycles

This section summarizes the main results of the work according to ***objective (8)*** of the present thesis. Previous results are based on the integration of a CO_2 closed Brayton cycle with direct integration in which the heat transfer fluid used in the carbonator is sent directly into a gas turbine. Main results of the analyses carried out for several power cycle configurations with the main goal of increasing the performance of the overall system integration are summarized below. Possible integration schemes are proposed in which power production is carried out indirectly, by means of a steam reheat Rankine cycle or a supercritical carbon dioxide Brayton cycle. These results were published in [231].

First, the indirect integration of a reheat Rankine cycle is considered, which is the typical power cycle in commercial CSP tower plants [165]. In this configuration, the preheat water of the Rankine cycle is heated by the exhaust CO_2 stream from the carbonator in a heat recovery steam generator (HRSG) until super-heated status is reached. Maximum efficiency (around 35.5%) was obtained at 875ºC operating under atmospheric pressure. From a sensitivity analysis it was shown that the global integration efficiency is enhanced up to 37.5% by increasing the live steam and the reheat temperature. An indirect integration of a recompression supercritical CO_2 (sCO_2) Brayton cycle was also proposed, which led to a global efficiency close to 32% that was limited by the large amount of non-used energy linked to the cooling process before the compression stage. The analysis showed that hot and cold sides in the regenerator are strongly unbalanced, what allows predicting a certain improvement after optimization. Moreover, the low global efficiency value achieved is a consequence of the moderated turbomachinery efficiency values assumed since this technology is yet under development.

The integration of a Combined Cycle (CC) in the CSP-CaL process was also analyzed in [231]. The CC is considered by a hybrid direct-indirect power cycle integration with the CSP-CaL system (Figure 23). The CO_2 stream exiting the carbonator is expanded in a gas turbine as a previous step for transferring heat to steam cycle through a HRSG. Results showed that the highest performance is obtained by decreasing the outlet turbine pressure up to reach a maximum value of 40.4% for operation under an inlet/outlet turbine pressure ratio of 3.6/1.

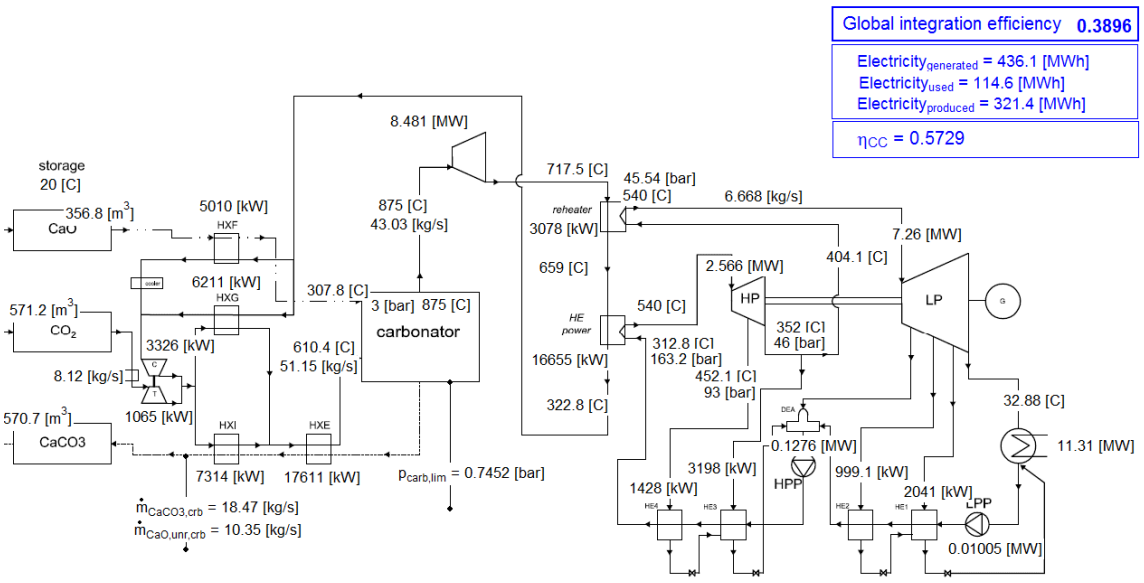

Figure 23: CSP-CaL- CC integration scheme and main simulation results [231]

As a summary, the Combined Cycle yields the higher efficiency, although smaller than in the case of CO_2 closed Brayton direct integration. Nevertheless, additional considerations regarding costs must be addressed to further assess the applicability of these power cycle integrations in the CSP-CaL. Moreover, new configurations in which the CO_2 entering the carbonator is reduced (the minimum amount would be the stochiometric) could improve the CSP-CaL plant efficiency, which is proposed as future work.

These results were published in [231]. The full manuscript including further details about the simulation us presented in ***Annex 6.***

3.7. New process schemes with high temperature solids storage

This section summarizes the main results of the work according to ***objective (10)*** of the present thesis through main results from novel CSP-CaL schemes simulations. These new configurations are based on storing the solids at high temperature. In this case the process scheme is simplified by requiring fewer heat exchangers due to a lower temperature difference between the reactors and the storage. On the other hand, seasonal storage cannot be considered because of the temperature losses. However, the CSP-CaL plant could be operated under a solar multiple (defined as the ratio of the solar thermal power to the power block design thermal input) similar than in currently CSP plants (SM~2-3) [232], and taking into account the higher energy storage density of CaL system in comparison with molten salts [153], a high-temperature CaL storage

system could allow storing energy during several days, instead of up to 16 hours as in molten salts-based CSP plants [121]. These results were published in [153].

A simpler heat integration allows to use novel integration schemes with a design similar to state-of-the-art equipment. Starting from a simplified base case each modified layout seeks to increase the overall plant efficiency at the expense of introducing an additional degree of complexity and therefore a higher investment cost. Figure 24 shows the simplest configuration proposed for the CSP-CaL integration with high-temperature solids storage. CO_2 produced in the calcination is sent to a heat recovery steam generator (HRSG) in order to use its sensible heat for power production by means of a simple superheated steam Rankine cycle. The cooled CO_2 stream (g3) is then compressed up to 3 bar in the main CO_2 compressor (M-COMP) and is split in two streams. A fraction of the CO_2 (1/3 of total) is sent directly to the carbonator (g7a), whereas the rest (g4) is further compressed up to 75 bar (HPS-COMP) and stored (CO_2 storage) for its use during the "night" operation mode. The CaO produced in the calciner (c1) is directly stored in the high temperature CaO storage vessel. Solids are stored at ambient pressure and therefore lock hoppers are needed for decoupling the pressure of the atmospheric solar receiver and of the storage vessel from the pressurized carbonator.

On the carbonator side, electric power is produced by means of a CO_2 closed Brayton cycle wherein a heat exchanger HXG is used as recuperator. For this base case, CO_2 is expanded from carbonator pressure to atmospheric pressure in the turbine with a pressure ratio of 3 (PR). Carbonation has been modelled in the base case by considering a residual value of CaO conversion X=0.15. As can be seen in Figure 24 only gas-gas heat exchangers (HRSG, HXG) and coolers are considered in this base case, which simplifies the plant as compared to previously proposed CSP-CaL integrations in Section 3.5. This new configuration is therefore advantageous from the point of view of plant engineering, construction and operation. Simulation results shows an overall plant efficiency of 32.1%. Modelling assumptions, stream data and energy balance results are available in **Annex 10,** where the detailed study is presented.

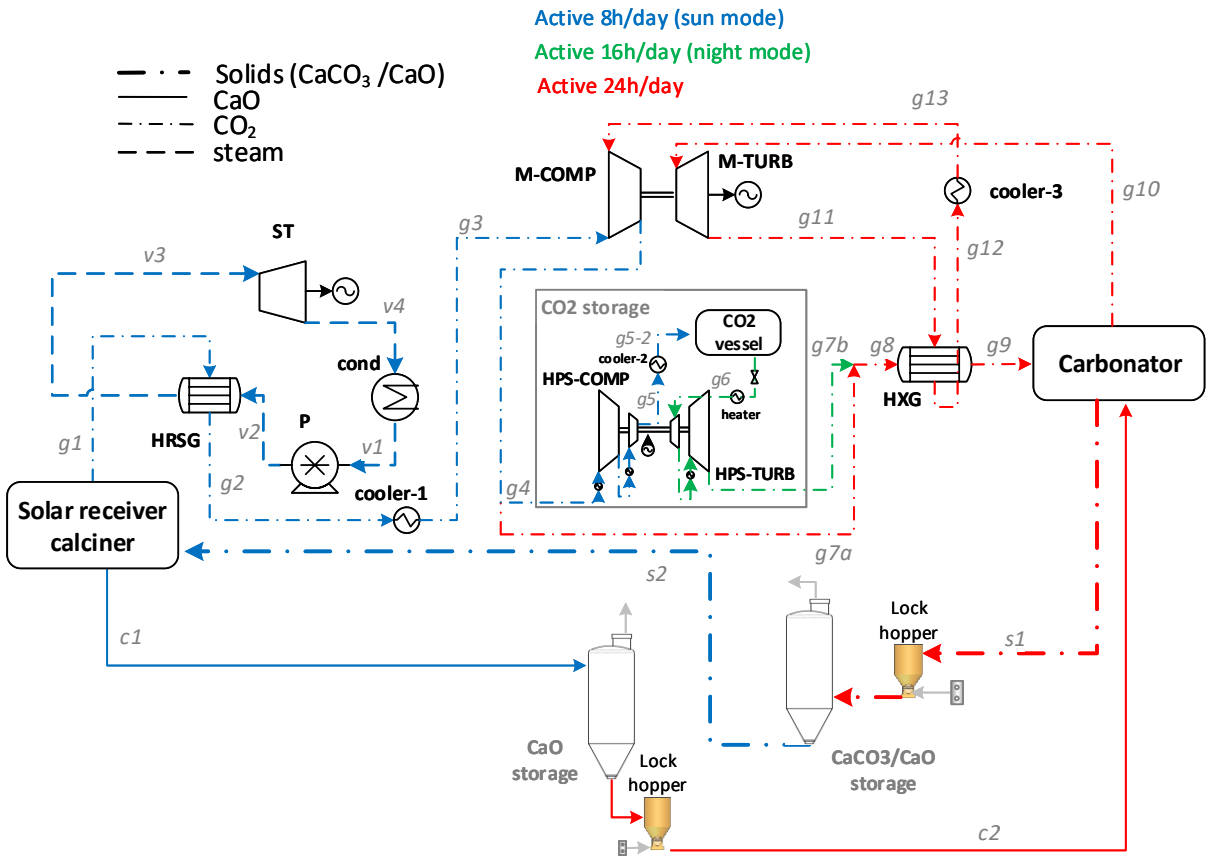

Figure 24: Base case for the CSP-CaL integration with high-temperature solids storage [153].

Once analyzed the base case (Figure 24), more complex high-temperature storage CSP-CaL schemes are considered, which are summarized below:

- Case 2: Addition of solid-gas heat exchangers

Compared to the base configuration, case 2 incorporates the use of solid-gas heat exchangers on both the calciner and carbonator sides. In this way, it is possible to make a more profitable use of the high temperature heat stored in the streams exiting the reactors, which leads to an improved thermal integration. Solids heating could be performed in a suspension preheater where gas and solids are sequentially contacted in risers and separated by cyclones as usually performed in raw meal preheaters of cement plants [1]. Regarding energy balance, an overall plant efficiency of 34.7% has been obtained, i.e. 2.6% points higher than the base case efficiency.

- Case 3: Introduction of solid-gas heat exchangers and intercooled compression

Compared with the previous scheme, case 3 contemplates the use of an intercooled main CO_2 compressor, which allows reducing the consumption for CO_2 compression and achieving a higher cycle efficiency thanks to the presence of the regenerator. The low-pressure intercooled

compressor is used to compress around 140 kg/s of CO_2 from atmospheric pressure to the carbonator pressure. In this case, two intercoolers are assumed with an intercooled temperature of 40ºC, leading to compressor outlet temperatures of 73°C from each stage. This leads to a reduction of the CO_2 stream temperature at the compressor outlet (g8) compared to case 2 (73ºC instead 143ºC). By using a 2 intercooled-stages main compressor (M-comp), electric consumption is reduced by 6.8% and 8.8% in the "sun" and "night" modes, respectively, which implies an overall plant efficiency increase of 3.4%.

- Case 4: Carbonator at ambient pressure

Case 4 allows operating the carbonator at ambient pressure. As a benefit, high temperature lock hoppers for solids pressurization would not be necessary. On the other hand, hermetic machines and heat exchangers to avoid air in-leakages as well as larger turbomachines (to handle the higher volume flow rate), larger carbonator and larger heat exchangers (to compensate the decrease of heat transfer coefficient with gas density) must be employed. Moreover, it is expected to achieve a lower reaction rate in the carbonator, which is favored by high CO_2 pressure [158]. Simulations results show that there are no big differences in terms of efficiency between cases 3 and 4. Therefore, the most advantageous configuration between pressurized and atmospheric pressure carbonator must be chosen based on techno-economic considerations depending on the technical challenge and cost of a high temperature lock hopper system or the sealed components for a specific facility.

The reader is referred to **Annex 10** for further information on the analysis of each CSP-CaL scheme proposed in this section.

Figure 25 shows the resulting overall plant efficiency as a function of the pressure ratio for the different cases and assuming a different number of intercooling stages in the main CO_2 compressor (for cases 3 and 4 only). As can be seen, cases 3 and 4 clearly show a higher efficiency than cases 1 and 2, particularly for higher pressure ratios. This illustrates the benefits of using the multi-stage intercooled compression combined with the gas cycle regenerator HXG.

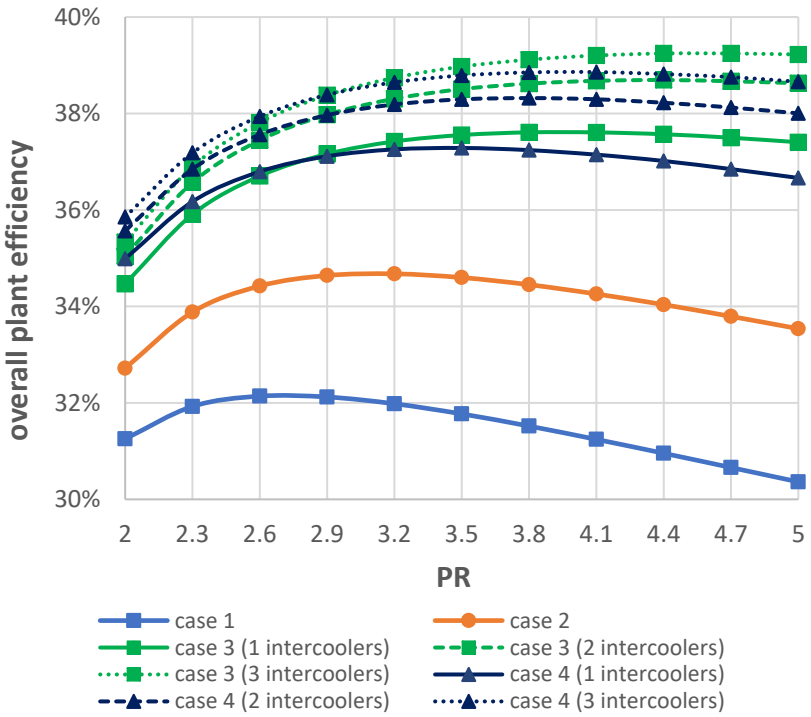

Figure 25: Sensitivity analysis on pressure ratio (PR) for the proposed high-temperature storage schemes.

Considering case 3, a sensitivity analysis is carried out to assess how the overall efficiency is affected by the average CaO value. Figure 26 shows the global CSP-CaL efficiency as a function of CaO conversion (X) and Turbine Inlet Temperature (TIT). The different trends followed by the overall efficiency with X in the cases of TIT=850ºC and 950ºC may be explained by an analysis of the CaO temperature entering the carbonator from the calciner at 900ºC. In the case of TIT=950ºC, a part of the energy released in the carbonator must be used to bring the solids up to the carbonator temperature, being this effect more important when X is reduced. In the case of TIT=850ºC, it is not necessary to heat up the solids since these come from the calciner at higher temperature, and therefore the loss of efficiency by reducing CaO conversion is mitigated.

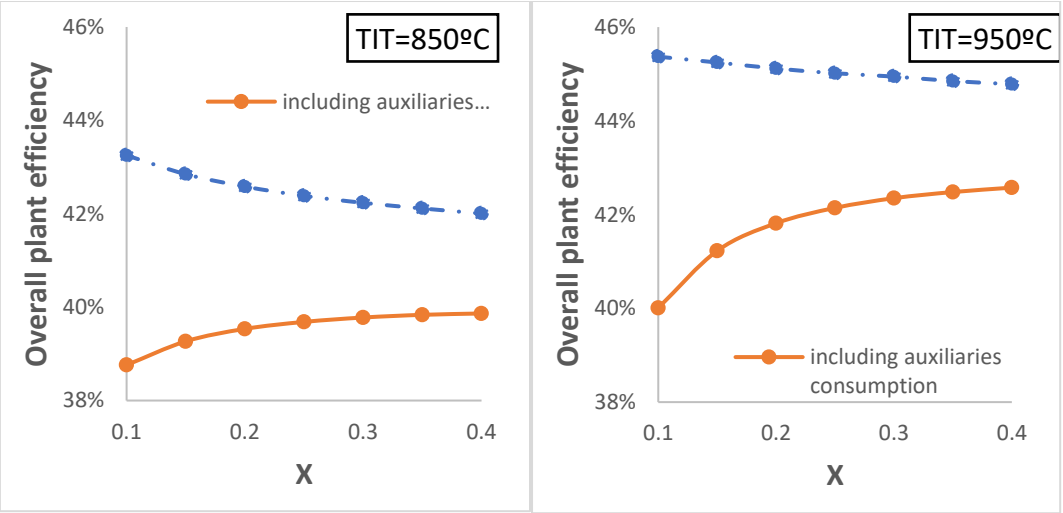

Figure 26: Overall plant efficiency as a function of CaO conversion (X) for two different Turbine Temperature Inlet (TIT). Note that no storage is considered: SM=1 [153].

Figure 26 shows also efficiency results obtained by including or not auxiliaries' consumption. About increasing CaO conversion, energy consumption linked to solids conveying is decreased, which serves to enhance the overall net efficiency. These trends are also appreciated when the overall average daily performance is considered.

These results were published in [153]. *The full manuscript including further information about the schemes simulations are presented in* ***Annex 10.***

3.8. CSP-CaL integration: technology assessment

This section summarizes the main results of the work according to ***objectives (6, 11)*** of the present thesis. Technology is assessed for the CSP-CaL plant, which includes information about both industrial and prototype-scale components to be integrated within the CSP-CaL scheme. The analysis is focused on the technologies with the greatest risks of scaling up within the CSP-CaL scheme, such as: solar calciner, heat exchangers, material conveying and solid-gas separation.

3.8.1 Solar calcination

The global efficiency of a CSP plant is highly dependent on the receiver performance and therefore a proper selection, configuration and sizing of the solar calciner is critical to achieve high overall efficiencies in the CSP-CaL process. Even though first calciner designs and prototypes were assessed as early as 1980 [4,5] solar particle receiver technology is yet under

development. In recent years, research on solar particle receivers has been notably intensified to increase both efficiency and dispatchability in CSP plants. Heat transfer losses is a critical issue for the solar receiver design, especially when high temperatures in the receiver are considered as would be the case of solar calcination under CO_2. Radiation losses are mainly dependent on the receiver temperature although they may be mitigated by a proper design [233]. Conduction losses can be reduced by improving thermal insulation. Thus, increasing the solar absorptance, decreasing the thermal emittance and/or reducing conduction/convective heat losses can yield an important enhancement of thermal efficiency in the receiver [125].

In general, solar particle receivers can be classified by the way particles are irradiated by solar energy, either in a direct or indirect configuration, using in the second case tubes or other receptors to convey and heat the particles. Selection of the solar particle receiver to carry out the calcination of $CaCO_3$ particles is dependent on a multitude of factors, mainly related to how the reaction is produced (kinetics, temperature, atmosphere composition, particle size) but also dependent on solar receiver characteristics (thermal emittance, solar absorptance, etc.) and physical properties of $CaCO_3$ and CaO particles entering the solar calciner relevant to solar. Thus, $CaCO_3$ has a poor solar absorptance [4] and therefore indirect heating in tubes may be more suitable as absorptance is not a determinant factor in this case [125].

Important factors that must be faced for the development of solar particle receivers are: i) enough residence time of the particles to reach the target temperature and allow for reaction completion; ii) adequate particle size; iii) proper management of elevated gas flow-rates used for particles transport (specially in fluidized beds); iv) possible deposition of particles in the optical window causing damage; v) continue operation preferable for scaling-up; vi) minimization of high thermal gradients and non-homogeneous conversion; and vi) particles attrition and agglomeration.

Particles residence time and mass flow are crucial parameters when designing the receiver for solar calcination. In the CSP-CaL integration, solar radiation is used to heat the particles up to calcination temperature. The residence time to achieve full calcination must be long enough for full calcination to be achieved. The temperature at which the particles enter the solar receiver is dependent on the CSP-CaL scheme. Since carbonation does not occur completely, typically a mixture of $CaCO_3$ and CaO solids enters the solar calciner.

3.8.1.1. Falling particle receivers

Falling particle receivers are based on direct heating of solid particles that are falling while irradiated by a beam of concentrated solar energy flux. According to [125], the most interesting features of falling particle receivers are: i) unlimited maximum solar irradiance (>2000 kW/m^2); ii) maximum temperature >1000ºC; iii) thermal efficiency between 50-90% and iv) estimated cost

of about 125$/kWt, which could be lower than molten salt receivers [125,234]. On the other hand, particle attrition is a critical issue that can be promoted in falling particle receivers.

Figure 27 shows a conceptual scheme of the falling particle receiver system where a curtain of particles (produced by a slot at the base of a hopper) is being irradiated within a cavity receiver. This technology seems to be scalable to 10-100 MWe power tower systems [125].

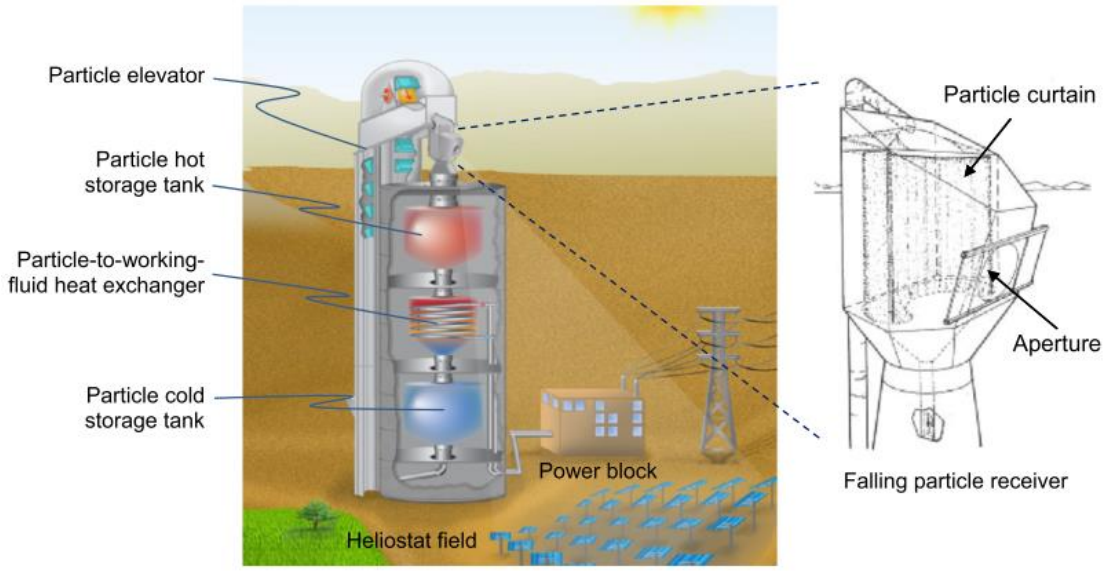

Figure 27: Falling particle receiver system. Reproduced from [235].

A number of previous works have analyzed the main characteristics of falling particle solar receivers [125]. Siegel et al. developed a 2MWt on-sun test of a falling particle receiver, which is useful for validating computational models. The performance model indicated that an 80 W/cm^2 average flux will be required to achieve 900°C given an inlet temperature of 600°C [236]. When the particle mass flow is increased the output temperature is decreased albeit thermal efficiency is improved. A possibility to increase the particles residence time is to recirculate the hot particles into the curtain [235,237]. Another possible strategy to raise the particles outlet temperature is to hinder the flow of falling particles by using chevron-like meshes. Ho et al. [238] studied the performance of a 1 MWth high-temperature falling particle receiver in an on-sun test with continuous recirculation. Ceramic particles were used in the test were and peak particle temperatures reached over 700 °C. They observed significant differences between the temperature in the center of the receiver and along the sides due to a non-uniform irradiance distribution. At an average irradiance of 211 kW/m^2, the particles temperature increase was 57.1 °C per meter of drop length, and the thermal efficiency was ~65% [238].

3.8.1.2. Centrifugal particle receivers

The rotary kiln is a well-known technology for calcination in the cement industry. Since 1895 it has been the central part of all modern clinker producing installations [1]. The rotary kiln consists of a steel tube with a length to diameter ratio of in the range 10-38:1. Some characteristics of conventional rotary kilns are a maximum working temperature up to 2000ºC and scalability (> 200m long) able to produce around 3600 tonnes/day [1]. Usually, rotary kilns are coupled with particles preheaters where the gas effluent from the calciner at 1000ºC preheats the solids entering the kiln up to 700-800ºC. This would be interesting for the CSP-CaL integration. Nevertheless, for its use as solar receiver, the rotary kiln must be properly adapted to be heated at high-temperature by concentrated solar irradiation.

Main advantages of rotary kilns for solar calcination are [149]: i) adjustable residence time of particles by controlling the tube rotational speed and tilting angle; ii) high temperatures achievable in the cavity; iii) solids conversion in continuous mode and in a controlled atmosphere; iv) the rotating tube enables uniform radial heating of the tube; vi) good heat transfer thanks to the direct contact of the rotating bed of particles with the hot tube walls; vii) possible operation in co-current or counter- current flow, allowing solids preheating by the exhaust gas.

A calciner based on a solar rotary kiln technology was proposed in 1980 by Flamant, Badie et al. [4,5]. The reactor is almost horizontal, with an inclination of 5º to facilitate particles transport. Both works highlighted the relevance of the radiative properties of the solar reactor. A thermal efficiency of 0.1-0.3 was achieved with a maximum calcination degree of 0.6 by using a 2 kWt solar furnace reactor with a total absorptance of about 0.9-1 due to the cavity effect. Excellent transfer coefficients between the bed and the internal wall were reported. Meier et al. developed two 10 kWth solar reactors to study calcination, one directly irradiated [224] and one indirectly irradiated [225]. For directly and indirectly heated solar reactors, maximum conversion efficiencies of 20% and 38%, respectively, were achieved for solar flux inputs of 2000 kW/m^2. The typical reactor efficiency achieved from several tests reached 13% while the maximum efficiency reached 20% [224]. Main reactor energy losses were due to re-radiation (16.5%), conduction (9.5%), and sensible heat of products (10%), whereas the remaining losses (50.5%) were mainly due to convection heat losses and un-recovered calcined powder. It is expected that a further improved reactor design incorporating a recovering thermal energy system, and reduced heat losses by convection and conduction would lead to efficiencies up to 83% [224]. The indirectly heated reactor proposed by Meier at al. [225] consists of a tilted cylindrical steel drum with ceramic insulation (Figure 28). The indirectly heated reactor design seems especially interesting for the CSP-CaL integration since CO_2 losses are avoided. In this case, an adequate gas conveying system is needed to ensure a proper gas circulation along the receiver. Typical

reactor overall efficiency varies between 25.2 and 34.8% depending on the rotational speed (8–18 rpm), mass flow rate (2–8 kg/h), and particle size (2–3 mm) [225].

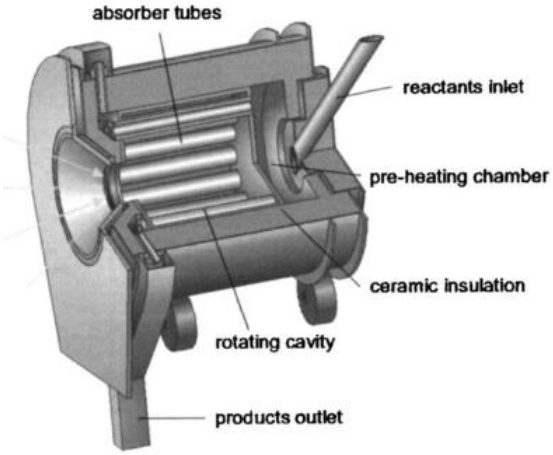

Figure 28: Schematics of the indirect heating multitube rotary kiln. Reproduced from [225].

Main reactor energy losses are caused by re-radiation (13.6%), conduction (20.5%), and sensible heat of products (20.2%), whereas the remaining losses (14.2%) were mainly due to loss of material and convection heat losses. In this case, an improved reactor design incorporating a recovering thermal energy system, and a reduced heat loss by convection and conduction would raise efficiencies up to 70%.

3.8.1.3. Fluidized bed receiver and comparison

Fluidized Bed Reactors (FBRs) present higher thermal inertia than rotary kilns. Therefore continuous operation is improved in the former as the thermal regime can be maintained in the case of short fluctuations of solar radiation [4]. Both rotary kilns and FBRs have the potential for rapid deployment since the technologies on which they are based are already mature in the cement industry and FB-boiler manufacturing, respectively.

Flamant, Badie et al. [4,5] proposed a FBR to carry out the $CaCO_3$ decomposition. The total absorptance of the fluidized bed depends both on particle's emittance and bed characteristics (porosity, particles size, fluidization regime) [4]. Salatino et al. [239] analysed the thermal performance of a bubbling fluidized bed of sand particles to store energy from CSP in sensible form. To evaluate the hydrodynamics of the process a near-2D fluidized bed prototype was constructed [240]. The use of compartmented dense gas fluidized beds was proposed by Chirone et al. [241] (Figure 29). The compartments are: i) the receiver, located around the cavity through which concentrating solar rays enter by means of a Beam-Down technology; ii) the heat exchanger section, where the sensible heat of solids is released to a steam cycle; and iii) storage. Dynamic simulation results showed an overall thermal efficiency (defined as the ratio of the

power transferred to the steam cycle to the incident radiative power) up to 71%. This study was the base for the construction of a 100kWt solar FBR prototype within the SOLTESS project [241].

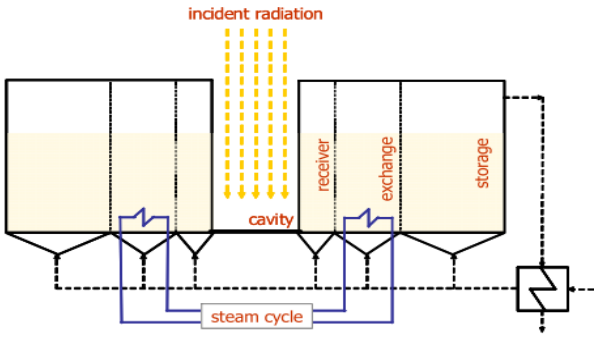

Figure 29: Conceptual scheme of a compartmented dense gas fluidized beds. Reproduced from [241].

Since temperatures achievable in this pilot-scale plant were around 900ºC, it could be suitable to attain calcination of limestone, which could be used instead of sand thus storing energy both in sensible and thermochemical form as proposed in [242].

Finally, a comparison between the main receiver technologies applicable to CSP-CaL integration is shown in Table 7.

Table 7: Receiver technology comparison.

		Particle receiver technology		
		Falling particle receiver	**Rotary kiln**	**FBR**
CSP-CaL integration issues	Benefits	-High solar irradiance - High thermal efficiency - Highly tested in the last years (MWth scale) -Tmax >1000ºC - Good scalability - Geometry similar than solar tower - Improved continuous operation mode - co-current or counter- current flow	-Core technology for calcination in cement industry -Tmax >1000ºC -Well-known preheaters coupling -adjustable residence time of particles - Improved continuous operation mode -good heat transfers - co-current or counter- current flow	- high thermal inertia improving the thermal regimen under short variations of solar radiation - Well-known technology at industry - high transfer coefficients - Direct and indirect heating configuration
	Challenges	- Window integration -Increasing the residence time (especially problematic for particles >200um) - Particle attrition	- Scalability must be addressed because the focalized solar heating - Window integration -Thermal losses in rotary kiln mainly occurs by conduction →improve thermal insulation	-total absorptance of the fluidized bed depends both of particle's emittance and bed configuration - Beam-down technology development - Energy consumption for fluidization -Gas-solid separation
	Restrictions	- Low solar absorptance of $CaCO_3$ particles for direct irradiation - Direct heating is not possible because avoiding CO_2 losses	- Horizontal design which makes difficult is integration in solar tower at large scale.	- Geometry incompatibilities with solar towers
	Tested for calcination	No	[4,5] [224] [225] [243]	[4,5]

3.8.2 Heat exchangers

An optimized heat integration is crucial for achieving high efficiencies in the CSP-CaL scheme due to the high temperature difference between the calciner, storage vessels and carbonator. Because of the system characteristics, a gas-gas heat exchanger as regenerator would be needed by considering a CO_2 close-loop for power production [145]. Thus, CO_2 exiting the turbine is used to preheat the CO_2 stream entering the carbonator. The higher temperature of CO_2 arriving at the carbonator the higher amount of carbonation energy used for power production, with the consequent increase in plant efficiency. On the other hand, the CO_2 exiting the calciner at high temperature (>900ºC) must be cooled previously to be compressed and stored if storage at ambient temperature is the option chosen. To take advantage of the hot CO_2 stream a gas-gas heat exchanger could be used as heat recovery steam generator (HRGS) within a secondary steam cycle, which could produce enough power to carry out CO_2 compression [153]. Another possibility is to use solid-gas heat exchangers to release energy from the hot CO_2 stream to preheat the $CaCO_3$ particles entering the calciner [222]. Similarly, solid-gas preheaters allow increasing the CO_2 temperature entering the carbonator -from the storage in which CO_2 is at low temperature- using heat from the $CaCO_3$ particles exiting the fluidized bed reactor after carbonation. Finally, solid-solid heat exchangers would further improve heat integration.

Gas–solid heat exchange can be carried out in either the open or closed configuration. Direct contact within an open configuration is a well-known technology [1]. Solids heating could be performed in a suspension preheater where gas and solids enter into contact sequentially in risers and are separated by cyclones, as commonly used in cement plants for raw material preheating [167]. In suspension preheaters raw particles are maintained in suspension by the hot gas from the calciner.

Figure 30 shows a schematic of the suspension preheater. Suspension preheaters usually have between four and six cyclone stages, which are arranged one above the other in a 50 –120 m height tower [1]. The exhaust gases from the calciner flow through the cyclone stages from bottom to top. Particles are added to the exhaust gas before the uppermost cyclone stage. They are separated from the gas in the cyclones and re-join it before the next cyclone stage [1]. By using this solid-gas heat exchanger, a same exit temperature of the gas and solids streams are achieved from a co-flow arrangement with a considerably high contact surface. Due to high level of maturity of this technology, it seems an optimum option to carry out both the $CaCO_3$ particles preheating in the calciner side and particles cooling in the carbonator side.

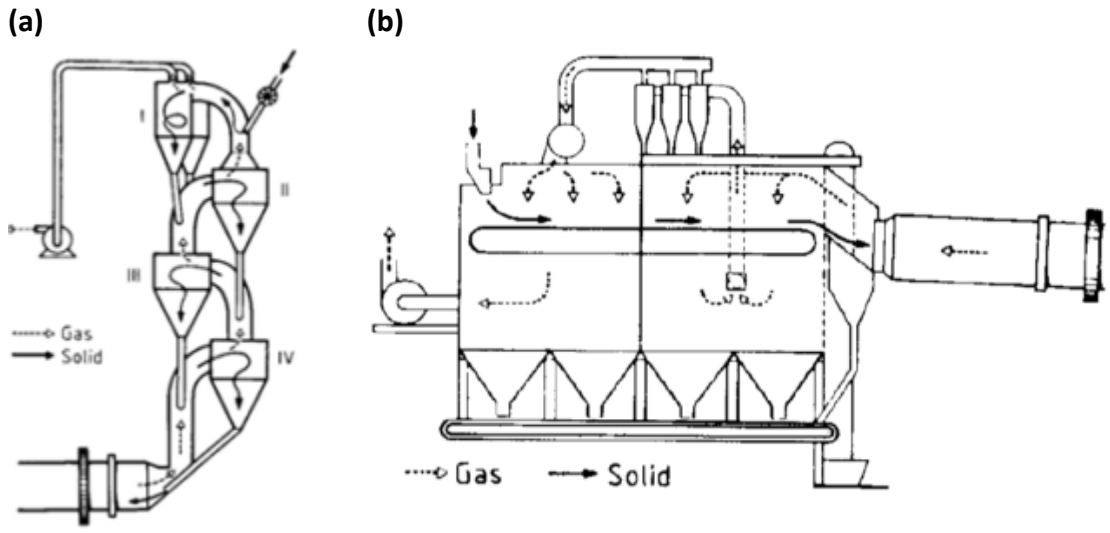

Figure 30: Suspension preheater; b) Grate preheater. Reproduced from [87,113]

The grate preheater is another well-known technique in the cement industry (Figure 30: -b). Particles are fed onto a horizontal grate which travels through a closed tunnel. A fan draws the exhaust gas from the calciner into the top of the preheater. The temperature of the gas could be reduced from >1000ºC to 150ºC while solids would be heated up to 700-800ºC [1]. Another possible solid-gas direct heat exchanger was proposed by Shimizu et al. [244]. This heat exchanger is an axial flow cyclone in which a quasi-counter-flow heat exchange is realized to achieve an effective recovery of the heat carried by particles. By using this design an outlet gas temperature much higher than the particle outlet temperature could be attained. Fluidized-bed designs are also a possibility to perform the solid-gas heating with high heat transfer coefficients (up to ~600 W/m^2-K) but with higher parasitic power consumption and heat loss associated to particles fluidization [245].

In the case of the CSP-CaL integration in which CaO particles are preheated before entering the carbonator with the CO_2 exhaust stream [145,194], an indirect gas-solid heat exchanger is needed in the carbonator side to avoid direct contact between CaO and CO_2, which could lead to partial carbonation with the consequent reduction in the carbonation heat transfer to the power cycle. Indirect solid gas heat exchange could be performed by using multiple heat transfer plates conveniently spaced to allow the flow of material to be heated inside [246]. Another high-temperature solid-gas heat exchanger was proposed by Al-Ansary et al. [247] in which particles circulate on the shell side through tubes arrangements while the CO_2 passes inside the tubes. Moving packed-bed heat exchangers implementing shell-and-tube and finned shell-and-tube designs were investigated by Ho et al. [245]. Tests showed that the particle-side heat transfer

coefficient could reach values up to ~100 W/m^2-K. Regarding the solid-solid heat exchanger, a possible system would use two solid-gas indirect heat exchangers with one intermediate heat-transfer fluid recirculated within the bulk of both solids. Because of the high temperature needs, liquid-metals could be used as fluid transfer to this end.

3.8.3 Solids conveying and gas separation

Available technologies to transport high temperature particles up-down the receiver include: mine hoist, bucket elevator, pocket elevator, screw conveyor, OLDS elevator, pneumatic conveyors, conveyor belts, cleated conveyor belts, metallic belted conveyors, masses elevators, bucket wheels, linear induction motor powered elevators, and electromagnetic field conveyors [235]. De la Verne [248] analyzed a basic skip at the end of a wire rope which showed an overall efficiency of 0.748. The OLDS elevator employs a circular casing rotating around a stationary screw or helix with a small parasitic power consumption [235].

The type of solar receiver technology determines the method employed for solid conveyance. Some commercial technology applicable to the CSP-CaL integration are:

- OLDs elevator, which efficiency of is around 8% [235].

- Conventional Bucket lift. A commercial design for a bucket lift with 120 m transport height at ~2.4x105 kg/hour (260 tons/hour) and 200°C with a 171 kWe motor results in a 50% efficiency [235].

- Mine hoist with an insulated container (skip). Mine hoist consists of a skip at the end of a wire rope which is wrapped around a large motor-powered drum. The material is loaded into the skip at the bottom of a shaft, the skip is raised, and the material is discharged at the top. Mine hoist efficiency is largely determined by the weight of material hoisted and the speed at which it is hoisted. De la Vergne [248] shows an overall lift efficiency of 0.748 for two skips hoisting in balance on a single drum.

- Pocket elevator. This system consists of a series of specially shaped containers (pockets) that travel along a loop of steel cable between two pulleys. The solids fall into the pockets at the bottom pulley and is discharged at the top pulley when the pocket is inverted [235]. Pocket elevators are reported to handle materials up to 500 °C and 930 °C.

- Belt conveyors. Belt conveyors are cost effective only when there is a relatively high production rate and the transport distance is significant [248]. Many types of feeders exist for belt conveyors, but the most popular is the vibrating feeder. It is not recommended

to use belt conveyors to transport dry concentrate. In this case the recommended option is using screw conveyors.

- Screw conveyors. This technology has been considered as suitable for Calcium-Looping applications [249]. In a commercial-scale, with large volumes of solids circulating through the calciner side, the solid loads will vary due to changes in the solar irradiation making the screw conveyors mechanically inefficient [75]. Screw conveyors were used in the Carina European project [93,250] to fed $CaCO_3$ into the calciner. The flow rate of solids through the calciner was properly controlled by using the screw conveyors but the temperature range is a challenge for this system [250].

Since CO_2 and CaO are stored separately, solid-gas separation after calcination is fundamental within the CSP-CaL integration. The same occurs in the power production side, where CO_2 exiting the carbonator and headed to the turbine has to be free of particles.

The most common method to separate particles from a gas stream is by means of cyclones, which are based on centrifugal separation. Thus, particles are forced out against the outer wall and then eliminated through an aperture at the bottom of the unit. Cyclones allow a high separation efficiency (95-100%), they are robust and allow operating under high-temperature with low energy requirement. However, the use of cyclones for small size particles [14], typically lower than 20 μm, is limited. A post-cyclone was proposed by Ray et al. [69] to improve the efficiency when working with fines. The post cyclone consists of a cylindrical annular shell located on top of the vortex finder. Both experiments and simulations indicate a 50% decrease in emission of <5 μm size particles.

4. Discussion

After the summary and discussion of main results achieved along the present thesis, this section further discusses about the fulfillment of the objectives set out in Section 2.

4.1. Calcium-Looping for CO_2 capture

The multicycle CaO behavior, and therefore the calcination and carbonation reactions, are highly dependent on the process conditions, mainly temperature, pressure, particle size and atmosphere composition in the reactors. Carbonator models formulated until now for simulating post-combustion CO_2 capture are based on lab-scale multicyclic CaO conversion results carried out by regenerating CaO under low CO_2 partial pressure. From the analysis of realistic lab-scale results, the novel carbonator model proposed in this thesis incorporates in the calculation of the capture efficiency the conversion in the diffusion-controlled stage of carbonation, which was found as relevant according TGA tests at realistic operation conditions. In this way, ***objective 1*** proposed at the beginning of the thesis is tackled, allowing a more accurate evaluation and prediction of carbonator's performance. Simulations show that the capture efficiency is improved by increasing the residence time in the carbonator, which is a novel find. Thus, for typical inventories of solids in the carbonator used in previous models, the molar flow rate of CaO recirculated can be substantially decreased while a high capture efficiency is obtained. This reduces energy penalty in the operation of power plants since the amount of heat required for calcination would be lowered and the energy necessary for material transport would be also reduced.

Taking into account the important effect of solids residence time in the carbonator on the CO_2 capture efficiency, a novel CFPP-CaL process scheme has been developed. This satisfies ***objective 2*** proposed to adapt the integration schemes to the conditions that improve the process performance considering industrial scale operation. Simulations over the proposed CFPP-CaL scheme show that the integration energy penalty is significantly reduced as the solids residence time is increased within the practical operation range of a few minutes, reaching values as low as 4 and 7% points over the reference plant efficiency. By optimizing the heat exchangers network in the CaL scheme and integrating heat with the retrofitted plant, the large size associated to the secondary power cycle would be significantly reduced. The size of the CaL system is one of the main reasons hindering it for post-combustion CO_2 capture. The large amount of heat required in the calciner entails the production of a large amount of energy in the secondary power cycle, which results in a CaL system of size on the same order than the actual reference power plant (without the CaL cycle) as obtained in previous works, thus hampering investments prospective.

As alternative to limestone, other cheap and abundant CaO precursors such as dolomite or steel slag show an improved performance characterized by less CaO deactivation with the number of cycles than limestone. Despite that the use of either dolomite or steel slag causes a higher energy consumption derived from the solid inert transport, the capture efficiency is also improved for these sorbents, which leads to a further reduction of energy consumption per kg of CO_2 avoided. The high capture capacity of dolomite and steel slag is mainly due to enhanced carbonation in the diffusion-controlled carbonation (SDP) stage, thus it would be advantageous to increase the particles residence time in the carbonator when using these materials. As the carbonation time lag is increased the benefit of using dolomite and steel slag is further promoted due to the higher rate of carbonation in the SDP for the sorbents derived from these precursors as compared to limestone. As the solids residence time in the carbonator is increased the number of solids circulating between reactors is reduced, which mitigates also the amount of additional heat required in the calciner due to the presence of inert solids. By using other natural CaO precursor, such as dolomite instead of limestone, could lead to a decrease of energy consumption around 15% for carbonation residence times of about 10 minutes due to the higher conversion in the diffusion-controlled stage in the case of dolomite. These results have been obtained from the research line corresponding to ***objective 3*** of the thesis.

The new Oxy-CaL process has been proposed as an interesting hybrid system for CO_2 capture. Synergies between oxy-combustion, CaL and membrane systems would lead to several advantages in comparison with these processes separately. According to ***objective 4*** of this thesis, the basic idea behind Oxy-CaL is to exploit the enhancement of CO_2 capture capacity in the CaL process as the CO_2 concentration in the carbonation environment is increased (as seen from TGA tests) whereas the energy penalty for partial oxy-combustion to increase the CO_2 concentration in the flue gas is notably reduced as compared to total oxy-combustion.

A higher CO_2 capture efficiency is achieved by means of the Oxy-CaL hybrid system while the specific energy consumption per kg of CO_2 avoided (SPECCA) is kept below 4 MJ/kg, which is a typical value usually reported for oxy-combustion or amine-based CO_2 capture systems. The higher CO_2 capture efficiency using Oxy-CaL allows to reduce the fresh limestone makeup flow, which leads to a reduction of energy consumption when operating under solids residence times below 7 minutes. In spite that SPECCA in the CaL process could be somewhat smaller than for the Oxy-CaL system when operating under prolonged solids residence times, the latter shows potentially important benefits regarding plant operation flexibility. Substantially smaller amounts of solids inventory are needed in the Oxy-CaL system, which would allow a more efficient response to load changes in coal fired power plants. In addition, TGA results show that the variation with the temperature of the CO_2 capture capacity in the diffusion-controlled stage plays a relatively minor role on the overall capture capacity under Oxy-CaL conditions as compared to

CaL conditions. This means that by applying the Oxy-CaL process a more stable CO_2 capture could be achieved because of the lower sensitivity to eventual temperature changes or thermal gradients as a consequence of irregular heat transfers.

By integrating a membrane system in the so-called mOxy-CaL process, energy consumption for CO_2 capture can be further reduced down to 3 MJ/kg CO_2, which is an outstanding value and shows the high interest of the hybrid CCS technology. Currently commercial polymeric membranes could be employed to achieve the desired O_2 concentration range for partial oxy-combustion. The main barrier for the deployment of the mOxy-Cal process is the need to treat large gas flow rates for producing the power of a typical-size coal power plant, which requires highly permeable membranes. Further techno-economic analysis needs to be done to establish the profitability of both the Oxy-CaL and mOxy-CaL technologies.

4.2. Calcium-Looping for TCES in CSP plants

As shown through this thesis, the CaL process is a promising option to integrate thermochemical energy storage in solar plants. A number of advantages and challenges discussed in section 1.3.3 are linked to ***objective 6***. CaL conditions to achieve high overall efficiency for TCES and electricity generation in CSP plants are not the same than in CFPP integration for CO_2 capture. In the CSP-CaL integration, the carbonation atmosphere is not conditioned by the flue gas composition (as occurs in the post combustion CO_2 capture application) and therefore carbonation conditions can be selected to maximize the process efficiency. Thus, carbonation would be carried out at high CO_2 partial pressure and high temperature (above 850ºC) to increase the maximum temperature at power cycle inlet and therefore the thermal to electric efficiency. On the other hand, calcination could be performed at both relatively low temperature (~700ºC) using a gas easily separable from CO_2 or under CO_2 pure atmosphere, which requires calciner temperatures around 950ºC. The diverse CaL conditions used for PCC and TCES lead also to different multicycle CaO performances and reaction kinetics characteristics. The development of a novel specific carbonator model for TCES application addresses ***objective 5*** in section 2.

As expected from the novel carbonation model described in Section 3.2, the carbonation behavior is different when integrating the CaL process in CSP plants as thermochemical energy storage system compared to post-combustion capture. The carbonation study carried out by considering calcination under helium shows that the carbonation stage controlled by diffusion is negligible and therefore the carbonator model in this case can be simplified. The kinetics model is supported by TGA tests performed under these specific conditions. A new expression to estimate the carbonation conversion rate as a function of the carbonator pressure and temperature has been derived and integrated within the carbonator model. Accordingly, the carbonation rate is enhanced

with the carbonator temperature up to reach a maximum, from which a further increase of temperature is detrimental as the thermodynamic equilibrium temperature is approached. On the other hand, an increase in the carbonator pressure promotes significantly the conversion rate and therefore the average carbonation level in short residence times. Thus, an increase of the carbonator pressure yields an improved performance not only from a reaction kinetics perspective but also because a higher carbonator pressure allows for a higher carbonator temperature, which enhances the power cycle efficiency when stored energy is released.

The CSP-CaL integration schemes have been optimized energetically for low-temperature storage (and therefore allowing long term storage). The enhancement of heat recovery derived from the pinch analysis yields a relevant increase of the cycle performance, which is improved as CaO conversion is increased. Results show that for a ratio of carbonator pressure to outlet turbine pressure of 3.2 bars, and a carbonator temperature of 875 ºC, plant efficiencies above 45% may be reached by directly integrating the carbonator and the power cycle through using CO_2 as heat carrier fluid. These results are part of the work developed in this thesis to cover ***objectives 7-9***. The main parameters to improve the proposed cycle are similar to other power cycles, namely, turbine inlet temperature, pressure ratio in the Brayton turbine, boiler/reactor/heat exchangers efficiency or pressure losses taking into account the particularities linked to calcination/carbonation chemical equilibrium, i.e. considering equilibrium limits concerning partial pressure/concentration or solids reactivity. A number of power cycles and integration possibilities have been analyzed in this thesis to address ***objective 8***. Compared to the air Brayton open cycle proposed elsewhere, the CO_2 Brayton cycle avoids the potential emission of CO_2, which is a necessary requirement for the development of these systems. In regards to direct-indirect cycle integrations, simulation results show that higher performance is achieved for direct integration. Nevertheless, enhancing the energy integration in an indirect way of highly efficient power cycles could make this possibility interesting, especially in the case of integrating combined cycle technology, in which the CO_2 mass flow entering the carbonator can be optimized.

By considering high-temperature solids storage as proposed in ***objective 10***, the process scheme complexity can be significantly reduced. This leads to disregarding long term storage, which is just a design criterion. Then, the CSP-CaL could works with similar Solar Multiple than in currently commercial CSP plants (SM 2.5-3). The storage number of hours could be increased by taking into account the higher energy density of CaL in comparison with molten salts. In this regard, by using the new expression developed in this thesis for the energy density, which takes into account the size of the infrastructure (including all vessels and the packing density of solids), lower values of energy density are achieved. Thus, for the simulated cases, the energy storage

density, mainly dependent on CO_2 pressure, CO_2 temperature and CaO conversion, it varies between 0.2-0.9 GJ/m^3.

The simplest scheme simulated, which considers high-temperature storage and just the regenerator as heat exchanger in the carbonator side presents an overall efficiency of 32%. By adding gas-solid heat exchangers on both the calciner and carbonator sides the overall plant efficiency reaches a 34.7%. Furthermore, if a 2-intercooled stage compression is used in the low-pressure compressor (which is the equipment with greater energy consumption in the plant) efficiency is enhanced up to 38.1%. The optimum configuration for a specific plant will depend on techno-economic considerations. Results from sensitivity analysis on pressure ratio (PR) in the Brayton cycle shows that, similarly to the case of low-temperature storage configuration, the highest efficiency is achieved for PR values around 3-4.5 in all cases. The overall efficiency is also enhanced as CaO conversion is increased (reaching values about 43% at X=0.4), mainly because of the significant reduction of auxiliaries power consumption. One of the main power consumption process within the CSP-CaL integration is related to the high-pressure compressor needed to reduce the CO_2 volume storage size, which has an efficiency penalty over the process around 1.8% points. Note that a part of the energy used for compressing CO_2 is stored similarly than in CAES systems.

Several mature technologies already available at commercial scale can be applied in the CSP-CaL integration. A review of the state of the art of the process has been carried out as according to ***objective 11***. Major technological challenges found are related to the design of the solar receiver/calciner and to the high-temperature solids pressurization and depressurization system.

5. Conclusions and future work

The present thesis is based on a multidisciplinary approach that combines reaction kinetics theory, reactors modelling and process scheme development in order to advance in the knowledge of the applying the CaL process to both CO_2 capture and TCES systems. Thanks to the fruitful collaboration between different research groups the CaL process has been analyzed from the behavior of materials at the local scale to industrial process equipment.

This thesis is composed of two main research areas, such as reactions-reactor modelling and engineering process development, which are developed simultaneously in the analysis of each the challenges and objectives identified for the development of this thesis. They have been developed to each one of the applications of the CaL process under study, namely, post-combustion CO_2 capture and thermochemical storage of solar energy. Thus, from the analysis of up-scale process conditions, lab-scale test has been performance to assess the system within a down-scale process, which in turn provides the basis for processes simulation in a bottom – up approach for large scale application in an iterative process of improving design conditions.

The results obtained along the present thesis show not only the importance of simulating the process by considering industrial realistic conditions but also the need for accurate data under real conditions at the lab-scale. As shown throughout the section 3, changes in temperature, atmosphere composition and pressure in the reactors lead to important differences in the multicyclic CaO conversion which must be properly estimated before moving on to the next stages of scaling the technology.

From the research opportunities discussed and the establishment of objectives, the main contributions of the present thesis over the current state-of-the-art process are summarized below:

- Detailed assessment of process development as well as advantages and challenges for the possible application of the CaL process within the future energy scenario.
- Novel carbonator model from realistic lab-scale conditions for post-combustion CO_2 capture, which allows evaluate the CaO conversion in the diffusive-controlled carbonation stage.
- Novel carbonator model from realistic lab-scale conditions to be applied within thermochemical energy storage assessment in CSP plants.
- Adapted novel high-performance process schemes for each specific application, namely: i) post-combustion CO_2 capture using several CaO precursors and ii) thermochemical storage of solar energy by considering low and high temperature in solids vessels, which allows flexibility when facing the process design.

- Novel hybrid CO_2 capture concept with the aim to reduce the energy penalty related to the integration process.

5.1. On-going and future work

The promising results achieved during the development of the thesis, together with the participation in related research projects, ensure the continuity of the studies here set along the next years. It enables the development of new research lines that have been left out of the scope of this thesis. In this way, related work to be developed in the near future following this research line will try to answer the following issues:

- Solar particle receiver design and assessment. It will involve the analysis of receiver geometry and specific operation conditions from CFD and ray-tracing modeling.
- Off-design models of concentrating solar power plant with TCES based on CaL process. This work will include the analysis of the solar field and the receiver based on the sun position to calculate the hourly optical efficiency. Moreover, other equipment of the plant such as turbomachinery, heat exchangers and storage vessels behavior will be analyzed in an hourly-basis simulation, which will allow a deeper analysis of the CSP-CaL integration.
- Economic assessment for the integration of CaL process in CSP plants. Once the solar receiver, the storage vessels and the solar field necessary for the CSP-CaL integration are known in greater detail, an economic assessment will allow evaluating the integration profitability with an adequate level of detail at the current Technology Readiness Level (TRL 5).
- Novel process schemes for the CSP-CaL integration will be developed, with special focus on the indirect-integration of a combined power cycle. A new configuration in which the CO_2 entering the carbonator will be optimized could improve the CSP-CaL integrations efficiency.
- Validation of models at prototype scale. Our coordination in the SOCRATCES[8] H2020 project will require the development of a number of task related to a CSP-CaL prototype construction. The prototype will allow to study different phenomena in components (solar receiver, reactors, heat exchangers, pipes) and granular media managing. It will allow to adjust models for scaling up studies and the identification of new challenges.

[8] https://socratces.eu/

References

[1] Schorcht F, Kourti I, Scalet BM, Roudier S, Sancho LD. Best Available Techniques (BAT). Reference Document for the Production of Cement, Lime and Magnesium Oxide. 2015. doi:10.2788/12850.

[2] Williams R. Hydrogen Production. US 1938202 A, 1933.

[3] Barker R. The reactivity of calcium oxide towards carbon dioxide and its use for energy storage. J Appl Chem Biotechnol 1974;24:221–7. doi:10.1002/jctb.2720240405.

[4] Flamant G, Hernandez D, Bonet C, Traverse J-P. Experimental aspects of the thermochemical conversion of solar energy; Decarbonation of $CaCO_3$. Sol Energy 1980;24:385–95. doi:10.1016/0038-092X(80)90301-1.

[5] Badie JM, Bonet C, Faure M, Flamant G, Foro R, Hernandez D. Decarbonation of calcite and phosphate rock in solar chemical reactors. Chem Eng Sci 1980;35:413–20. doi:10.1016/0009-2509(80)80114-X.

[6] Shimizu T, Hirama T, Hosoda H, Kitano K, Inagaki M, Tejima K. A Twin Fluid-Bed Reactor for Removal of CO_2 from Combustion Processes. Chem Eng Res Des 1999;77:62–8. doi:10.1205/026387699525882.

[7] Dean CC, Blamey J, Florin NH, Al-Jeboori MJ, Fennell PS. The calcium looping cycle for CO_2 capture from power generation, cement manufacture and hydrogen production. Chem Eng Res Des 2011;89:836–55. doi:10.1016/j.cherd.2010.10.013.

[8] Charitos a., Hawthorne C, Bidwe AR, Sivalingam S, Schuster A, Spliethoff H, et al. Parametric investigation of the calcium looping process for CO_2 capture in a 10kWth dual fluidized bed. Int J Greenh Gas Control 2010;4:776–84. doi:10.1016/j.ijggc.2010.04.009.

[9] N'Tsoukpoe KE, Liu H, Le Pierrès N, Luo L. A review on long-term sorption solar energy storage. Renew Sustain Energy Rev 2009;13:2385–96. doi:10.1016/j.rser.2009.05.008.

[10] Arias B, Diego ME, Abanades JC, Lorenzo M, Diaz L, Martínez D, et al. Demonstration of steady state CO_2 capture in a 1.7MWth calcium looping pilot. Int J Greenh Gas Control 2013;18:237–45. doi:10.1016/j.ijggc.2013.07.014.

[11] Ströhle J, Junk M, Kremer J, Galloy A, Epple B. Carbonate looping experiments in a 1 MWth pilot plant and model validation. Fuel 2014;127:13–22. doi:10.1016/j.fuel.2013.12.043.

[12] Perejon A, Romeo LM, Lara Y, Lisbona P, Valverde JM, Perejón A, et al. The Calcium-Looping technology for CO_2 capture: On the important roles of energy integration and sorbent behavior. Appl Energy 2016;162:787–807. doi:10.1016/j.apenergy.2015.10.121.

[13] Romeo LM, Lara Y, Lisbona P, Martínez A. Economical assessment of competitive enhanced limestones for CO_2 capture cycles in power plants. Fuel Process Technol 2009;90:803–11. doi:10.1016/j.fuproc.2009.03.014.

[14] Martínez A, Lara Y, Lisbona P, Romeo LM. Energy penalty reduction in the calcium looping cycle. Int J Greenh Gas Control 2012;7:74–81. doi:10.1016/j.ijggc.2011.12.005.

[15] Cormos C-C. Economic evaluations of coal-based combustion and gasification power plants with post-combustion CO 2 capture using calcium looping cycle. Energy 2014;78:665–73. doi:10.1016/j.energy.2014.10.054.

[16] IPCC. Special Report on CARBON DIOXIDE CAPTURE AND STORAGE. 2005.

[17] EIA. International Energy Outlook 2016. vol. 0484(2016). 2016. doi:www.eia.gov/forecasts/ieo/pdf/0484(2016).pdf.

[18] International Renewable Energy Agency (IRENA). REthinking Energy 2017: Acelarating the global energy transformation. 2017.

[19] IEA. Energy and Climate Change. 2015. doi:10.1038/479267b.

[20] Framework Convention on Climate Change. Adoption of the Paris Agreement. vol. 21932. 2015.

[21] Politecnico di Milano – Alstom UK (CAESAR project). European best practice guidelines for assessment of CO_2 capture technologies. 2011.

[22] El Hadri N, Quang DV, Goetheer EL V, Abu Zahra MRM. Aqueous amine solution characterization for post-combustion CO_2 capture process. Appl Energy 2015;185:1433–49. doi:10.1016/j.apenergy.2016.03.043.

[23] Cohen SM, Webber ME, Rochelle GT. Utilizing Solar Thermal Energy for Post-Combustion CO_2 Capture. J Energy Power Eng 2011;3:195–208. doi:10.1115/ES2010-90147.

[24] Zhang X, Singh B, He X, Gundersen T, Deng L, Zhang S. Post-combustion carbon capture technologies: Energetic analysis and life cycle assessment. Int J Greenh Gas Control 2014;27:289–98. doi:10.1016/j.ijggc.2014.06.016.

[25] Liang Z, Fu K, Idem R, Tontiwachwuthikul P. Review on current advances, future challenges and consideration issues for post-combustion CO_2 capture using amine-based absorbents. Chinese J Chem Eng 2016;24:278–88. doi:10.1016/j.cjche.2015.06.013.

[26] Wang M, Lawal A, Stephenson P, Sidders J, Ramshaw C, Hill W, et al. Post-combustion CO_2 capture with chemical absorption: A state-of-the-art review. Chem Eng Res Des 2011;89:1609–24. doi:10.1016/j.cherd.2010.11.005.

[27] Spigarelli BP, Kawatra SK. Opportunities and challenges in carbon dioxide capture. J CO_2 Util 2013;1:69–87. doi:10.1016/j.jcou.2013.03.002.

[28] Luis P. Use of monoethanolamine (MEA) for CO_2 capture in a global scenario: Consequences and alternatives. Desalination 2016;380:93–9. doi:10.1016/j.desal.2015.08.004.

[29] Rey A, Gouedard C, Ledirac N, Cohen M, Dugay J, Vial J, et al. Amine degradation in CO_2 capture. 2. New degradation products of MEA. Pyrazine and alkylpyrazines: Analysis, mechanism of formation and toxicity. Int J Greenh Gas Control 2013;19:576–83. doi:10.1016/j.ijggc.2013.10.018.

[30] Fytianos G, Ucar S, Grimstvedt A, Hyldbakk A, Svendsen HF, Knuutila HK. Corrosion and degradation in MEA based post-combustion CO_2 capture. Int J Greenh Gas Control 2016;46:48–56. doi:10.1016/j.ijggc.2015.12.028.

[31] Goto K, Yogo K, Higashii T. A review of efficiency penalty in a coal-fired power plant with post-combustion CO_2 capture. Appl Energy 2013;111:710–20. doi:10.1016/j.apenergy.2013.05.020.

[32] Baker RW, Lokhandwala K. Natural Gas Processing with Membranes : An Overview 2008:2109–21.

[33] Merkel TC, Lin H, Wei X, Baker R. Power plant post-combustion carbon dioxide capture: An opportunity for membranes. J Memb Sci 2010;359:126–39. doi:10.1016/j.memsci.2009.10.041.

[34] Favre E. Membrane processes and postcombustion carbon dioxide capture : Challenges and prospects. Chem Eng J 2011;171:782–93. doi:10.1016/j.cej.2011.01.010.

[35] Aaron D, Tsouris C. Separation of CO_2 from Flue Gas: A Review. Sep Sci Technol 2005;40:321–48. doi:10.1081/SS-200042244.

[36] Nataly Echevarria Huaman R, Xiu Jun T. Energy related CO_2 emissions and the progress on CCS projects: A review. Renew Sustain Energy Rev 2014;31:368–85. doi:10.1016/j.rser.2013.12.002.

[37] Arnette AN. Renewable energy and carbon capture and sequestration for a reduced carbon energy plan: An optimization model. Renew Sustain Energy Rev 2016;70:254–65. doi:10.1016/j.rser.2016.11.218.

[38] Krieg JP, Winston AE. Dry carbonation process. United States Patent. US 06/487114 (US4459272 A), 1984.

[39] Falotico AJ. Dry carbonation of trona. PCT Application. PCT/US1992/006321 (WO1993/011070 A1), 1993.

[40] Nelson TO, Green DA, Box P, Gupta RP, Henningsen G, Turk BS. Carbon dioxide capture from flue gas using dry regenerable sorbents (Final Report). DOE Cooperative Agreement No. DE-FC26-00NT40923, RTI Project No. 0207887. 2009.

[41] Chacartegui R, Monje B, Sánchez D, Becerra J a., Campanari S. Molten carbonate fuel cell: Towards negative emissions in wastewater treatment CHP plants. Int J Greenh Gas Control 2013;19:453–61. doi:10.1016/j.ijggc.2013.10.007.

[42] Discepoli G, Milewski J, Desideri U. Off-design operation of coal power plant integrated with natural gas fueled molten carbonate fuel cell as CO_2 reducer. Int J Hydrogen Energy 2016;41:4773–83. doi:10.1016/j.ijhydene.2016.01.065.

[43] Milewski J, Bujalski W, Wołowicz M, Futyma K, Kucowski J, Bernat R. Experimental investigation of CO_2 separation from lignite flue gases by 100 cm2 single Molten Carbonate Fuel Cell. Int J Hydrogen Energy 2014;39:1558–63. doi:10.1016/j.ijhydene.2013.08.144.

[44] Barelli L, Bidini G, Campanari S, Discepoli G, Spinelli M. Performance assessment of natural gas and biogas fueled molten carbonate fuel cells in carbon capture configuration. J Power Sources 2016;320:332–42. doi:10.1016/j.jpowsour.2016.04.071.

[45] MacKenzie A, Granatstein DL, Anthony EJ, Abanades JC. Economics of CO 2 Capture Using the Calcium Cycle with a Pressurized Fluidized Bed Combustor. Energy & Fuels 2007;21:920–6. doi:10.1021/ef0603378.

[46] Ylätalo J, Ritvanen J, Tynjälä T, Hyppänen T. Model based scale-up study of the calcium looping process. Fuel 2014;115:329–37. doi:10.1016/j.fuel.2013.07.036.

[47] Romano MC. Modeling the carbonator of a Ca-looping process for CO_2 capture from power plant flue gas. Chem Eng Sci 2012;69:257–69. doi:10.1016/j.ces.2011.10.041.

[48] Valverde JM, Sanchez-Jimenez PE, Perez-Maqueda L. Ca-looping for postcombustion CO_2 capture: A comparative analysis on the performances of dolomite and limestone. Appl Energy 2015;138:202–15. doi:10.1016/j.apenergy.2014.10.087.

[49] Wang K, Hu X, Zhao P, Yin Z. Natural dolomite modified with carbon coating for cyclic high-temperature CO_2 capture. Appl Energy 2016;165:14–21. doi:10.1016/j.apenergy.2015.12.071.

[50] Sun R, Li Y, Liu H, Wu S, Lu C. CO_2 capture performance of calcium-based sorbent doped with manganese salts during calcium looping cycle. Appl Energy 2012;89:368–73.

doi:10.1016/j.apenergy.2011.07.051.

[51] Wang W, Ramkumar S, Wong D, Fan LS. Simulations and process analysis of the carbonation-calcination reaction process with intermediate hydration. Fuel 2012;92:94–106. doi:10.1016/j.fuel.2011.06.059.

[52] Manovic V, Anthony EJ. Competition of sulphation and carbonation reactions during looping cycles for CO_2 capture by cao-based sorbents. J Phys Chem A 2010;114:3997–4002. doi:10.1021/jp910536w.

[53] Romano MC, Martínez I, Murillo R, Arstad B, Blom R, Ozcan DC, et al. Process simulation of Ca-looping processes: Review and guidelines. Energy Procedia 2013;37:142–50. doi:10.1016/j.egypro.2013.05.095.

[54] Ortiz C, Valverde JM, Chacartegui R, Benítez-Guerrero M, Perejón A, Romeo LM. The Oxy-CaL process: A novel CO_2 capture system by integrating partial oxy-combustion with the Calcium-Looping process. Appl Energy 2017;196:1–17. doi:10.1016/j.apenergy.2017.03.120.

[55] Ylätalo J, Parkkinen J, Ritvanen J, Tynjälä T, Hyppänen T. Modeling of the oxy-combustion calciner in the post-combustion calcium looping process. Fuel 2013;113:770–9. doi:10.1016/j.fuel.2012.11.041.

[56] Vorrias I, Atsonios K, Nikolopoulos A, Nikolopoulos N, Grammelis P, Kakaras E. Calcium looping for CO_2 capture from a lignite fired power plant. Fuel 2013;113:826–36. doi:10.1016/j.fuel.2012.12.087.

[57] Dieter H, Bidwe AR, Varela-duelli G, Charitos A, Hawthorne C. Development of the calcium looping CO_2 capture technology from lab to pilot scale at IFK , University of Stuttgart. Fuel 2014;127:23–37. doi:10.1016/j.fuel.2014.01.063.

[58] Coppola A, Scala F, Salatino P, Montagnaro F. Fluidized bed calcium looping cycles for CO_2 capture under oxy-firing calcination conditions: Part 1. Assessment of six limestones. Chem Eng J 2013;231:537–43. doi:10.1016/j.cej.2013.07.113.

[59] J.M. Cordero MA. Modelling of the kinetics of sulphation of CaO particles under CaL reactor conditions. Fuel 2015;150:501–11. doi:10.1016/j.fuel.2015.02.075.

[60] Valverde JM, Sanchez-Jimenez PE, Perez-Maqueda LA. Relevant Influence of Limestone Crystallinity on CO 2 Capture in The Ca-Looping Technology at Realistic Calcination Conditions. Environ Sci Technol 2014;48:9882–9. doi:10.1021/es5014505.

[61] Martínez I, Grasa G, Murillo R, Arias B, Abanades JC. Modelling the continuous calcination of $CaCO_3$ in a Ca-looping system. Chem Eng J 2013;215–216:174–81. doi:10.1016/j.cej.2012.09.134.

[62] Manovic V, Anthony EJ. Carbonation of CaO-Based Sorbents Enhanced by Steam Addition. Ind Eng Chem Res 2010;49:9105–10. doi:10.1021/ie101352s.

[63] Valverde JM, Sanchez-Jimenez PE, Perez-Maqueda L. Calcium-looping for post-combustion CO_2 capture. On the adverse effect of sorbent regeneration under CO_2. Appl Energy 2014;126:161–71. doi:10.1016/j.apenergy.2014.03.081.

[64] Martínez I, Murillo R, Grasa G, Rodríguez N, Abanades JC. Conceptual design of a three fluidised beds combustion system capturing CO_2 with CaO. Int J Greenh Gas Control 2011;5:498–504. doi:10.1016/j.ijggc.2010.04.017.

[65] Valverde JM, Medina S. Crystallographic transformation of limestone during calcination under CO_2. Phys Chem Chem Phys 2015;17:21912–26. doi:10.1039/C5CP02715B.

[66] Abanades JC. The maximum capture efficiency of CO_2 using a carbonation/calcination

cycle of $CaO/CaCO_3$. Chem Eng J 2002;90:303–6. doi:10.1016/S1385-8947(02)00126-2.

[67] Alvarez D, Abanades JC. Determination of the Critical Product Layer Thickness in the Reaction of CaO with CO_2. Ind Eng Chem Res 2005;44:5608–15. doi:10.1021/ie050305s.

[68] Grasa GS, Abanades JC. CO 2 Capture Capacity of CaO in Long Series of Carbonation/Calcination Cycles. Ind Eng Chem Res 2006;45:8846–51. doi:10.1021/ie0606946.

[69] Valverde JM, Sanchez-Jimenez PE, Perejon A, Perez-Maqueda L a. CO_2 multicyclic capture of pretreated/doped CaO in the Ca-looping process. Theory and experiments. Phys Chem Chem Phys 2013;15:11775–93. doi:10.1039/c3cp50480h.

[70] Dean CC, Dugwell D, Fennell PS. Investigation into potential synergy between power generation, cement manufacture and CO_2 abatement using the calcium looping cycle. Energy Environ Sci 2011;4:2050. doi:10.1039/c1ee01282g.

[71] Telesca A, Calabrese D, Marroccoli M, Tomasulo M, Valenti GL, Duelli G, et al. Spent limestone sorbent from calcium looping cycle as a raw material for the cement industry. Fuel 2014;118:202–5. doi:10.1016/j.fuel.2013.10.060.

[72] Borgwardt RH. Calcium oxide sintering in atmospheres containing water and carbon dioxide. Ind Eng Chem Res 1989;28:493–500. doi:10.1021/ie00088a019.

[73] Arias B, Grasa GS, Alonso M, Abanades JC. Post-combustion calcium looping process with a highly stable sorbent activity by recarbonation. Energy Environ Sci 2012;5:7353–9. doi:10.1039/c2ee03008j.

[74] Grasa G, Martínez I, Diego ME, Abanades JC. Determination of CaO carbonation kinetics under recarbonation conditions. Energy and Fuels 2014;28:4033–42. doi:10.1021/ef500331t.

[75] Hanak DP, Anthony EJ, Manovic V. A review of developments in pilot-plant testing and modelling of calcium looping process for CO 2 capture from power generation systems. Energy Environ Sci 2015;8:2199–249. doi:10.1039/C5EE01228G.

[76] Yang Y, Zhai R, Duan L, Kavosh M, Patchigolla K, Oakey J. Integration and evaluation of a power plant with a CaO-based CO_2 capture system. Int J Greenh Gas Control 2010;4:603–12. doi:10.1016/j.ijggc.2010.01.004.

[77] Lasheras A, Ströhle J, Galloy A, Epple B. Carbonate looping process simulation using a 1D fluidized bed model for the carbonator. Int J Greenh Gas Control 2011;5:686–93. doi:10.1016/j.ijggc.2011.01.005.

[78] Berstad D, Anantharaman R, Jordal K. Post-combustion CO_2 capture from a natural gas combined cycle by $CaO/CaCO_3$ looping. Int J Greenh Gas Control 2012;11:25–33. doi:10.1016/j.ijggc.2012.07.021.

[79] Wang D, Chen S, Xu C, Xiang W. Energy and exergy analysis of a new hydrogen-fueled power plant based on calcium looping process. Int J Hydrogen Energy 2013;38:5389–400. doi:10.1016/j.ijhydene.2013.02.060.

[80] Connell DP, Lewandowski D a., Ramkumar S, Phalak N, Statnick RM, Fan LS. Process simulation and economic analysis of the Calcium Looping Process (CLP) for hydrogen and electricity production from coal and natural gas. Fuel 2013;105:383–96. doi:10.1016/j.fuel.2012.07.006.

[81] Kunze C, De S, Spliethoff H. A novel IGCC plant with membrane oxygen separation and carbon capture by carbonation-calcinations loop. Int J Greenh Gas Control 2011;5:1176–83. doi:10.1016/j.ijggc.2011.05.038.

[82] Kunze C, Spliethoff H. Assessment of oxy-fuel, pre- and post-combustion-based carbon capture for future IGCC plants. Appl Energy 2012;94:109–16. doi:10.1016/j.apenergy.2012.01.013.

[83] Perejon A, Romeo LM, Lara Y, Lisbona P, Valverde JM. The Calcium-Looping technology for CO_2 capture: On the important roles of energy integration and sorbent behavior. Appl Energy 2015. doi:10.1016/j.apenergy.2015.10.121.

[84] Abanades JC, Anthony EJ, Wang J, Oakey JE. Fluidized Bed Combustion Systems Integrating CO_2 Capture with CaO. Environ Sci Technol 2005;39:2861–6. doi:10.1021/es0496221.

[85] Cormos CC, Cormos AM. Assessment of calcium-based chemical looping options for gasification power plants. Int J Hydrogen Energy 2013;38:2306–17. doi:10.1016/j.ijhydene.2012.11.128.

[86] Romano M, Martínez I, Murillo R, Arstad B. Guidelines for modeling and simulation of Ca-looping processes. 2012.

[87] Alonso M, Rodríguez N, Grasa G, Abanades JC. Modelling of a fluidized bed carbonator reactor to capture CO_2 from a combustion flue gas. Chem Eng Sci 2009;64:883–91. doi:10.1016/j.ces.2008.10.044.

[88] Valverde JM, Sanchez-Jimenez PE, Perez-Maqueda L. Limestone Calcination Nearby Equilibrium: Kinetics, CaO Crystal Structure, Sintering and Reactivity. J Phys Chem C 2015;119:1623–41. doi:10.1021/jp508745u.

[89] Manovic V, Charland JP, Blamey J, Fennell PS, Lu DY, Anthony EJ. Influence of calcination conditions on carrying capacity of CaO-based sorbent in CO_2 looping cycles. Fuel 2009;88:1893–900. doi:10.1016/j.fuel.2009.04.012.

[90] Diego ME, Arias B, Méndez A, Lorenzo M, Díaz L, Sánchez-Biezma A, et al. Experimental testing of a sorbent reactivation process in La Pereda 1.7 MWth calcium looping pilot plant. Int J Greenh Gas Control 2016;50:14–22. doi:10.1016/j.ijggc.2016.04.008.

[91] Chang MH, Chen WC, Huang CM, Liu WH, Chou YC, Chang WC, et al. Design and Experimental Testing of a 1.9MWth Calcium Looping Pilot Plant. Energy Procedia 2014;63:2100–8. doi:10.1016/j.egypro.2014.11.226.

[92] Bonaventura D, Chacartegui R, Valverde JM, Becerra JA, Ortiz C, Lizana J. Dry carbonate process for CO 2 capture and storage: Integration with solar thermal power. Renew Sustain Energy Rev 2018;82:1796–812. doi:10.1016/j.rser.2017.06.061.

[93] Hilz J, Helbig M, Haaf M, Daikeler A, Ströhle J, Epple B. Long-term pilot testing of the carbonate looping process in 1 MW th scale. Fuel 2017:1–8. doi:10.1016/j.fuel.2017.08.105.

[94] Criado YA, Arias B, Abanades JC. Calcium looping CO_2 capture system for back-up power plants. Energy Environ Sci 2017;10:1994–2004. doi:10.1039/C7EE01505D.

[95] International Energy Agency. Technology Roadmap Solar Thermal Electricity 2014:52. doi:10.1007/SpringerReference_7300.

[96] Panwar NL, Kaushik SC, Kothari S. Role of renewable energy sources in environmental protection: A review. Renew Sustain Energy Rev 2011;15:1513–24. doi:10.1016/j.rser.2010.11.037.

[97] Arce P, Medrano M, Gil A, Oró E, Cabeza LF. Overview of thermal energy storage (TES) potential energy savings and climate change mitigation in Spain and Europe. Appl Energy

2011;88:2764–74. doi:10.1016/j.apenergy.2011.01.067.

[98] Kuravi S, Trahan J, Goswami DY, Rahman MM, Stefanakos EK. Thermal energy storage technologies and systems for concentrating solar power plants. Prog Energy Combust Sci 2013;39:285–319. doi:10.1016/j.pecs.2013.02.001.

[99] Denholm P, O'Connell M, Brinkman G, Jorgenson J. Overgeneration from Solar Energy in California: A Field Guide to the Duck Chart (NREL/TP-6A20-65023) 2015:46.

[100] Gil A, Medrano M, Martorell I, Lázaro A, Dolado P, Zalba B, et al. State of the art on high temperature thermal energy storage for power generation. Part 1—Concepts, materials and modellization. Renew Sustain Energy Rev 2010;14:31–55. doi:10.1016/j.rser.2009.07.035.

[101] Wagner SJ, Rubin ES. Economic implications of thermal energy storage for concentrated solar thermal power. Renew Energy 2014;61:81–95. doi:10.1016/j.renene.2012.08.013.

[102] Denholm P, Wan YYH, Hummon M, Mehos M. An Analysis of Concentrating Solar Power with Thermal Energy Storage in a California 33 % Renewable Scenario (Technical Report NREL/TP-6A20-58186). 2013.

[103] Paksoy HÖ. Thermal Energy Storage for Sustainable Energy Consumption. 2007.

[104] Mahlia TMIMI, Saktisahdan TJJ, Jannifar A, Hasan MHH, Matseelar HSCSC. A review of available methods and development on energy storage; Technology update. Renew Sustain Energy Rev 2014;33:532–45. doi:10.1016/j.rser.2014.01.068.

[105] Pardo P, Deydier A, Anxionnaz-Minvielle Z, Rougé S, Cabassud M, Cognet P. A review on high temperature thermochemical heat energy storage. Renew Sustain Energy Rev 2014;32:591–610. doi:10.1016/j.rser.2013.12.014.

[106] Kearney D, Kelly B, Herrmann U, Cable R, Pacheco J, Mahoney R, et al. Engineering aspects of a molten salt heat transfer fluid in a trough solar field. Energy 2004;29:861–70. doi:10.1016/S0360-5442(03)00191-9.

[107] Fernández AG, Ushak S, Galleguillos H, Pérez FJ. Development of new molten salts with LiNO3 and Ca(NO3)2 for energy storage in CSP plants. Appl Energy 2014;119:131–40. doi:10.1016/j.apenergy.2013.12.061.

[108] Rodríguez I, Pérez-Segarra CD, Lehmkuhl O, Oliva A. Modular object-oriented methodology for the resolution of molten salt storage tanks for CSP plants. Appl Energy 2013;109:402–14. doi:10.1016/j.apenergy.2012.11.008.

[109] Chacartegui R, Vigna L, Becerra JA, Verda V. Analysis of two heat storage integrations for an Organic Rankine Cycle Parabolic trough solar power plant. Energy Convers Manag 2016. doi:10.1016/j.enconman.2016.03.067.

[110] Kuravi S, Goswami DY, Stefanakos EK, Ram M, Jotshi C, Trahan J, et al. THERMAL ENERGY STORAGE FOR CONCENTRATING SOLAR POWER PLANTS n.d.

[111] Karagiannakis G, Pagkoura C, Zygogianni A, Lorentzou S, Konstandopoulos AG. Monolithic Ceramic Redox Materials for Thermochemical Heat Storage Applications in CSP Plants. Energy Procedia 2014;49:820–9. doi:10.1016/j.egypro.2014.03.089.

[112] Medrano M, Gil A, Martorell I, Potau X, Cabeza LF. State of the art on high-temperature thermal energy storage for power generation. Part 2-Case studies. Renew Sustain Energy Rev 2010;14:56–72. doi:10.1016/j.rser.2009.07.036.

[113] Zalba B, Marín JM, Cabeza LF, Mehling H. Review on thermal energy storage with phase change: materials, heat transfer analysis and applications. vol. 23. 2003. doi:10.1016/S1359-4311(02)00192-8.

[114] Tian Y, Zhao CY. A review of solar collectors and thermal energy storage in solar thermal applications. Appl Energy 2013;104:538–53. doi:10.1016/j.apenergy.2012.11.051.

[115] Nithyanandam K, Pitchumani R. Design of a latent thermal energy storage system with embedded heat pipes. Appl Energy 2014;126:266–80. doi:10.1016/j.apenergy.2014.03.025.

[116] Nithyanandam K, Pitchumani R. Cost and performance analysis of concentrating solar power systems with integrated latent thermal energy storage. Energy 2014;64:793–810. doi:10.1016/j.energy.2013.10.095.

[117] Sharma A, Tyagi VV, Chen CR, Buddhi D. Review on thermal energy storage with phase change materials and applications. Renew Sustain Energy Rev 2009;13:318–45. doi:10.1016/j.rser.2007.10.005.

[118] Li TX, Wu S, Yan T, Xu JX, Wang RZ. A novel solid–gas thermochemical multilevel sorption thermal battery for cascaded solar thermal energy storage. Appl Energy 2016;161:1–10. doi:10.1016/j.apenergy.2015.09.084.

[119] Neveu P, Tescari S, Aussel D, Mazet N. Combined constructal and exergy optimization of thermochemical reactors for high temperature heat storage. Energy Convers Manag 2013;71:186–98. doi:10.1016/j.enconman.2013.03.035.

[120] Cot-Gores J, Castell A, Cabeza LF. Thermochemical energy storage and conversion: A-state-of-the-art review of the experimental research under practical conditions. Renew Sustain Energy Rev 2012;16:5207–24. doi:10.1016/j.rser.2012.04.007.

[121] National Renewable energy laboratory (NREL). Concentrating Solar Power Projects 2017. https://www.nrel.gov/csp/solarpaces/ (accessed April 2, 2017).

[122] International Renewable Energy Agency. Renewable Power Generation Costs in 2017. Int Renew Energy Agency 2018.

[123] Vignarooban K, Xu X, Arvay A, Hsu K, Kannan AM. Heat transfer fluids for concentrating solar power systems – A review. Appl Energy 2015;146:383–96. doi:10.1016/j.apenergy.2015.01.125.

[124] Valverde JM, Barea-López M, Perejón A, Sánchez-Jiménez PE, Pérez-Maqueda LA. Effect of Thermal Pretreatment and Nanosilica Addition on Limestone Performance at Calcium-Looping Conditions for Thermochemical Energy Storage of Concentrated Solar Power. Energy & Fuels 2017;31:4226–36. doi:10.1021/acs.energyfuels.6b03364.

[125] Ho CK. A review of high-temperature particle receivers for concentrating solar power. Appl Therm Eng 2016;109:958–69. doi:10.1016/j.applthermaleng.2016.04.103.

[126] Siva Reddy V, Kaushik SC, Ranjan KR, Tyagi SK. State-of-the-art of solar thermal power plants - A review. Renew Sustain Energy Rev 2013;27:258–73. doi:10.1016/j.rser.2013.06.037.

[127] Yogi Goswami D. Solar Thermal Power Technology: Present Status and Ideas for the Future. Energy Sources 1998;20:137–45. doi:10.1080/00908319808970052.

[128] Wentworth WE, Chen E. Simple Thermal Decomposition Reactions for Storage of Solar Thermal Energy. Sol Energy 1976;18:205–14. doi:10.1016/0038-092X(76)90019-0.

[129] Qu X, Li Y, Li P, Wan Q, Zhai F. The development of metal hydrides using as concentrating solar thermal storage materials. Front Mater Sci 2015;9:317–31. doi:10.1007/s11706-015-0311-y.

[130] Bagherisereshki E, Tran J, Lei F, AuYeung N. Investigation into SrO/SrCO 3 for high temperature thermochemical energy storage. Sol Energy 2018;160:85–93.

doi:10.1016/j.solener.2017.11.073.

[131] Rhodes NR, Barde A, Randhir K, Li L, Hahn DW, Mei R, et al. Solar Thermochemical Energy Storage Through Carbonation Cycles of SrCO3/SrO Supported on SrZrO3. ChemSusChem 2015:n/a-n/a. doi:10.1002/cssc.201501023.

[132] Guy E. Solar Heat Storage Using Chemical Reactions. J Solid State Chem 1977;22:51–61.

[133] Schmidt M, Linder M. Power generation based on the Ca(OH)2/ CaO thermochemical storage system – Experimental investigation of discharge operation modes in lab scale and corresponding conceptual process design. Appl Energy 2017;203:594–607. doi:10.1016/j.apenergy.2017.06.063.

[134] Fahim MA, Ford JD. Energy storage using the BaO2/ BaO reaction cycle. Chem Eng J 1983;27:21–8.

[135] Singh A, Tescari S, Lantin G, Agrafiotis C, Roeb M, Sattler C. Solar thermochemical heat storage via the Co 3 O 4 /CoO looping cycle: Storage reactor modelling and experimental validation. Sol Energy 2017;144:453–65. doi:10.1016/j.solener.2017.01.052.

[136] Chen C, Aryafar H, Lovegrove KM, Lavine AS. Modeling of ammonia synthesis to produce supercritical steam for solar thermochemical energy storage. Sol Energy 2017;155:363–71. doi:10.1016/j.solener.2017.06.049.

[137] Kugeler K, Niessen HF, Theis KA. TRANSPORT OF NUCLEAR HEAT BY MEANS OF CHEMICAL ENERGY (NUCLEAR LONG-DISTANCE ENERGY). Nucl Eng Des 1975;34.

[138] Edwards JH, Do KT, Maitra AM, Schuck S, Fok W, Stein W. The use if solar-based CO_2/CH_4 reforming for reducing greenhouse gas emissions ruding the generation of electricity and process heat. Energy Convers Manag 1996;37(6-8):1339–44.

[139] Sattler C, Roeb M, Agrafiotis C, Thomey D. Solar hydrogen production via sulphur based thermochemical water-splitting. Sol Energy 2017;156:30–47. doi:10.1016/j.solener.2017.05.060.

[140] Obermeier J, Sakellariou KG, Tsongidis NI, Baciu D, Charalambopoulou G, Steriotis T, et al. Material development and assessment of an energy storage concept based on the CaO-looping process. Sol Energy 2017;150:298–309. doi:10.1016/j.solener.2017.04.058.

[141] Benitez-Guerrero M, Sarrion B, Perejon A, Sanchez-Jimenez PE, Perez-Maqueda LA, Manuel Valverde J. Large-scale high-temperature solar energy storage using natural minerals. Sol Energy Mater Sol Cells 2017;168:14–21. doi:10.1016/j.solmat.2017.04.013.

[142] Kyaw K, Matsuda H, Hasatani M. Applicability of Carbonation/Decarbonation Reactions to High-Temperature Thermal Energy Storage and Temperature Upgrading. J Chem Eng JAPAN 1996;29:119–25. doi:10.1252/jcej.29.119.

[143] Sakellariou KG, Karagiannakis G, Criado YA, Konstandopoulos AG. Calcium oxide based materials for thermochemical heat storage in concentrated solar power plants. Sol Energy 2015;122:215–30. doi:10.1016/j.solener.2015.08.011.

[144] Rodriguez N, Alonso M, Grasa G, Abanades JC. Heat requirements in a calciner of $CaCO_3$ integrated in a CO_2 capture system using CaO. Chem Eng J 2008;138:148–54. doi:10.1016/j.cej.2007.06.005.

[145] Alovisio A, Chacartegui R, Ortiz C, Valverde JM, Verda V. Optimizing the CSP-Calcium Looping integration for Thermochemical Energy Storage. Energy Convers Manag 2017;136:85–98. doi:10.1016/j.enconman.2016.12.093.

[146] Fidaros DK, Baxevanou C a., Vlachos NS. A parametric study of a solar calcinator using computational fluid dynamics. Energy Convers Manag 2007;48:2784–91. doi:10.1016/j.enconman.2007.07.025.

[147] Meier A, Bonaldi E, Cella GM, Lipinski W, Wuillemin D. Solar chemical reactor technology for industrial production of lime. Sol Energy 2006;80:1355–62. doi:10.1016/j.solener.2005.05.017.

[148] Reich L. Towards Solar Thermochemical Carbon Dioxide Capture via Calcium Oxide Looping: A Review. Aerosol Air Qual Res 2014;14:500–14. doi:10.4209/aaqr.2013.05.0169.

[149] Abanades S, André L. Design and demonstration of a high temperature solar-heated rotary tube reactor for continuous particles calcination. Appl Energy 2018;212:1310–20. doi:10.1016/j.apenergy.2018.01.019.

[150] Benitez-Guerrero M, Valverde JM, Perejon A, Sanchez-Jimenez PE, Perez-Maqueda LA. Low-cost Ca-based composites synthesized by biotemplate method for thermochemical energy storage of concentrated solar power. Appl Energy 2018;210:108–16. doi:10.1016/j.apenergy.2017.10.109.

[151] Hanak DP, Manovic V. Calcium looping with inherent energy storage for decarbonisation of coal-fired power plant. Energy Environ Sci 2016;9:971–83. doi:10.1016/j.energy.2016.02.079.

[152] Prieto C, Cooper P, Fernandez AI, Cabeza LF. Review of technology: thermochemical energy storage for concentrated solar power plants. Renew Sustain Energy Rev 2016;60:909–29. doi:10.1017/CBO9781107415324.004.

[153] Ortiz C, Romano MC, Valverde JM, Binotti M, Chacartegui R. Process integration of Calcium-Looping thermochemical energy storage system in concentrating solar power plants. Energy 2018;155:535–51. doi:10.1016/j.energy.2018.04.180.

[154] Valverde JM, Castellanos A. Random loose packing of cohesive granular materials. Europhys Lett 2007;75:985–91. doi:10.1209/epl/i2006-10208-4.

[155] Ortega-Fernández I, Calvet N, Gil A, Rodríguez-Aseguinolaza J, Faik A, D'Aguanno B. Thermophysical characterization of a by-product from the steel industry to be used as a sustainable and low-cost thermal energy storage material. Energy 2015;89:601–9. doi:10.1016/j.energy.2015.05.153.

[156] Wang W, Ramkumar S, Li S, Wong D, Iyer M, Sakadjian BB, et al. Subpilot demonstration of the carbonation-Calcination reaction (CCR) process: High-temperature CO_2 and sulfur capture from coal-fired power plants. Ind Eng Chem Res 2010;49:5094–101. doi:10.1021/ie901509k.

[157] Phalak N, Wang W, Fan L-S. Ca(OH) 2 -Based Calcium Looping Process Development at The Ohio State University. Chem Eng Technol 2013;36:1451–9. doi:10.1002/ceat.201200707.

[158] Kyaw K, Kubota M, Watanabe F, Matsuda H, Hasatani M. Study of Carbonation of CaO for High Temperature Thermal Energy Storage. J Chem Eng JAPAN 1998;31:281–4. doi:10.1252/jcej.31.281.

[159] Peng Q, Yang X, Ding J, Wei X, Yang J. Design of new molten salt thermal energy storage material for solar thermal power plant. Appl Energy 2013;112:682–9. doi:10.1016/j.apenergy.2012.10.048.

[160] Ho CK. Advances in central receivers for concentrating solar applications. Sol Energy 2017. doi:10.1016/j.solener.2017.03.048.

[161] Barin I. Thermochemical data of pure substances VCH, Weinheim (1989) 1989.

[162] Sceats G, Horley CJ, Richardson P, Sceats MG. System and method for the calcination of minerals. WO2007112496A1, 2014.

[163] Wang Y, Lin S, Suzuki Y. CO_2/Steam and CO_2/N_2 Atmospheres. Energy 2008:2326–31. doi:10.1021/ef800039k.

[164] Champagne S, Lu DY, MacChi A, Symonds RT, Anthony EJ. Influence of steam injection during calcination on the reactivity of CaO-based sorbent for carbon capture. Ind Eng Chem Res 2013;52:2241–6. doi:10.1021/ie3012787.

[165] Liu M, Steven Tay NH, Bell S, Belusko M, Jacob R, Will G, et al. Review on concentrating solar power plants and new developments in high temperature thermal energy storage technologies. Renew Sustain Energy Rev 2016;53:1411–32. doi:10.1016/j.rser.2015.09.026.

[166] Valverde JM, Medina S. Reduction of Calcination Temperature in the Calcium Looping Process for CO 2 Capture by Using Helium: In Situ XRD Analysis. ACS Sustain Chem Eng 2016;4:7090–7. doi:10.1021/acssuschemeng.6b01966.

[167] Romano MC, Spinelli M, Campanari S, Consonni S, Marchi M, Pimpinelli N, et al. The Calcium Looping Process for Low CO_2 Emission Cement Plants. Energy Procedia 2014;61:500–3. doi:10.1016/j.egypro.2014.11.1158.

[168] Kim K, Kim D, Park Y, Soon K. A solid sorbent-based multi-stage fluidized bed process with inter-stage heat integration as an energy efficient carbon capture process. Int J Greenh Gas Control 2014;26:135–46. doi:10.1016/j.ijggc.2014.03.012.

[169] Jin B, Zhao H, Zheng C. Thermoeconomic cost analysis of CO_2 compression and purification unit in oxy-combustion power plants Bo. Energy 2015;83:416–30. doi:10.1016/j.energy.2015.02.039.

[170] Jin B, Zhao H, Zheng C. Optimization and control for CO_2 compression and purification unit in oxy-combustion power plants. Energy 2015;83:416–30. doi:10.1016/j.energy.2015.02.039.

[171] Chacartegui R, Muñoz De Escalona JM, Sánchez D, Monje B, Sánchez T. Alternative cycles based on carbon dioxide for central receiver solar power plants. Appl Therm Eng 2011;31:872–9. doi:10.1016/j.applthermaleng.2010.11.008.

[172] Abanades JC, Alvarez D. Conversion limits in the reaction of CO_2 with lime. Energy and Fuels 2003;17:308–15. doi:10.1021/ef020152a.

[173] Valverde JM, Sanchez-Jimenez PE, Perez-Maqueda L. Role of precalcination and regeneration conditions on postcombustion CO 2 capture in the Ca-looping technology. Appl Energy 2014;136:347–56. doi:10.1016/j.apenergy.2014.09.052.

[174] European Solar Thermal Electricity Association (ESTELA). Solar Thermal Electricity Strategic research agenda 2020-2025. 2012.

[175] Gangwal S, Muto A. Demonstration of High-Temperature Calcium-Based Thermochemical Energy Storage System for Use with Concentrating Solar Power Facilities. Sunshot Program Summit 2016. U.S. Department of Energy 2016.

[176] SOLPART project. Temperature Solar-heated Reactors for Industrial production of Reactive Particulates n.d. http://www.solpart-project.eu/ (accessed June 1, 2017).

[177] CNRS. NEXT-CSP project n.d. http://next-csp.eu/ (accessed May 15, 2017).

[178] Valverde JM. A model on the CaO multicyclic conversion in the Ca-looping process.

Chem Eng J 2013;228:1195–206. doi:10.1016/j.cej.2013.05.023.

[179] Ortiz C, Chacartegui R, Valverde J, Becerra J, Perez-Maqueda L. A new model of the carbonator reactor in the calcium looping technology for post-combustion CO_2 capture. FUEL 2015;160:328–38. doi:10.1016/j.fuel.2015.07.095.

[180] Sanchez-Jimenez PE, Valverde JM, Perez-Maqueda LA. Multicyclic conversion of limestone at Ca-looping conditions: The role of solid-sate diffusion controlled carbonation. Fuel 2014;127:131–40. doi:10.1016/j.fuel.2013.09.064.

[181] Bhatia SK, Perlmutter DD. Effect of the product layer on the kinetics of the CO_2-lime reaction. AIChE J 1983;29:79–86. doi:10.1002/aic.690290111.

[182] Grasa GS, Abanades JC, Alonso M, González B. Reactivity of highly cycled particles of CaO in a carbonation/calcination loop. Chem Eng J 2008;137:561–7. doi:10.1016/j.cej.2007.05.017.

[183] Ortiz C, Valverde JM, Chacartegui R, Perez-Maqueda LA. Carbonation of Limestone Derived CaO for Thermochemical Energy Storage: From Kinetics to Process Integration in Concentrating Solar Plants. ACS Sustain Chem Eng 2018;6:6404–17. doi:10.1021/acssuschemeng.8b00199.

[184] Moore WJ. Physical Chemistry (5th Edition). Prentice-Hall; 1999.

[185] Pijolat M, Soustelle M. Experimental tests to validate the rate-limiting step assumption used in the kinetic analysis of solid-state reactions. Thermochim Acta 2008;478:34–40. doi:10.1016/j.tca.2008.08.013.

[186] Perejón A, Sánchez-Jiménez PE, Criado JM, Pérez-Maqueda LA. Magnesium hydride for energy storage applications: The kinetics of dehydrogenation under different working conditions. J Alloys Compd 2016;681:571–9. doi:10.1016/j.jallcom.2016.04.191.

[187] Stanmore BR, Gilot P. Review—calcination and carbonation of limestone during thermal cycling for CO_2 sequestration. Fuel Process Technol 2005;86:1707–43. doi:10.1016/j.fuproc.2005.01.023.

[188] García-Labiano F, Abad A, de Diego LF, Gayán P, Adánez J. Calcination of calcium-based sorbents at pressure in a broad range of CO_2 concentrations. Chem Eng Sci 2002;57:2381–93. doi:10.1016/S0009-2509(02)00137-9.

[189] Brown ME. The Prout-Tompkins rate equation in solid-state kinetics. Thermochim Acta 1997;300:93–106. doi:10.1016/S0040-6031(96)03119-X.

[190] Sarrion B, Valverde JM, Perejon A, Perez-maqueda LA, Sanchez-jimenez PE. On the multicycle activity of natural limestone/dolomite for cheap, efficient and non-toxic Thermochemical Energy Storage of Concentrated Solar Power. Energy Technol 2016. doi:10.1002/ente.201600068.

[191] Ortiz C, Chacartegui R, Valverde JM, Becerra JA. A new integration model of the calcium looping technology into coal fired power plants for CO 2 capture. Appl Energy 2016;169:408–20. doi:10.1016/j.apenergy.2016.02.050.

[192] Romeo LM, Abanades JC, Escosa JM, Paño J, Giménez A, Sánchez-Biezma A, et al. Oxyfuel carbonation/calcination cycle for low cost CO_2 capture in existing power plants. Energy Convers Manag 2008;49:2809–14. doi:10.1016/j.enconman.2008.03.022.

[193] Martínez I, Murillo R, Grasa G, Abanades JC. Integration of a Ca-looping system for CO_2 capture in an existing power plant. Energy Procedia 2011;4:1699–706. doi:10.1016/j.egypro.2011.02.043.

[194] Edwards SEB, Materić V. Calcium looping in solar power generation plants. Sol Energy

2012;86:2494–503. doi:10.1016/j.solener.2012.05.019.

[195] Kunii D, Levenspiel O. The K-L reactor model for circulating fluidized beds. Chem Eng Sci 2000;55:4563–70. doi:10.1016/S0009-2509(00)00073-7.

[196] Kunii D, Levenspiel O. Circulating fluidized-bed reactors. Chem Eng Sci 1997;52:2471–82. doi:10.1016/S0009-2509(97)00066-3.

[197] Chacartegui R, Sanchez D, Becerra JA, Muñoz A, Sanchez T. PERFORMANCE ANALYSIS OF A 565 MW STEAM POWER PLANT. Proc ASME Turbo Expo 2011 GT2011 2011:1–10.

[198] Martínez a, Lara Y, Lisbona P, Romeo LM. Operation of a mixing seal valve in calcium looping for CO_2 capture. Energy and Fuels 2014;28:2059–68. doi:10.1021/ef402487e.

[199] Martínez A, Lara Y, Lisbona P, Romeo LM. Operation of a cyclonic preheater in the ca-looping for CO_2 capture. Environ Sci Technol 2013;47:11335–41. doi:10.1021/es401601k.

[200] Kvamsdal HM, Romano MC, van der Ham L, Bonalumi D, van Os P, Goetheer E. Energetic evaluation of a power plant integrated with a piperazine-based CO 2 capture process. Int J Greenh Gas Control 2014;28:343–55. doi:10.1016/j.ijggc.2014.07.004.

[201] Romano MC. Ultra-high CO_2 capture efficiency in CFB oxyfuel power plants by calcium looping process for CO_2 recovery from purification units vent gas. Int J Greenh Gas Control 2013;18:57–67. doi:10.1016/j.ijggc.2013.07.002.

[202] Mangalapally HP, Hasse H. Pilot plant study of post-combustion carbon dioxide capture by reactive absorption: Methodology, comparison of different structured packings, and comprehensive results for monoethanolamine. Chem Eng Res Des 2011;89:1216–28. doi:10.1016/j.cherd.2011.01.013.

[203] Ortiz C, Valverde JM, Chacartegui R. Energy Consumption for CO_2 Capture by means of the Calcium Looping Process: A Comparative Analysis using Limestone, Dolomite, and Steel Slag. Energy Technol 2016:1–12. doi:10.1002/ente.201600390.

[204] Silaban A, Narcida M, Harrison DP. Characteristics of the reversible reaction between CO_2(g) and calcined dolomite. Chem Eng Commun 1996;146:149–62. doi:10.1080/00986449608936487.

[205] de la Calle Martos A, Valverde JM, Sanchez-Jimenez PE, Perejón A, García-Garrido C, Perez-Maqueda LA. Effect of dolomite decomposition under CO_2 on its multicycle CO_2 capture behaviour under calcium looping conditions. Phys Chem Chem Phys 2016;18:16325–36. doi:10.1039/C6CP01149G.

[206] Valverde JM, Perejon A, Medina S, Perez-Maqueda LA. Thermal decomposition of dolomite under CO_2: insights from TGA and in situ XRD analysis. Phys Chem Chem Phys 2015;17:30162–76. doi:10.1039/C5CP05596B.

[207] Tian S, Jiang J, Li K, Yan F, Chen X. Performance of steel slag in carbonation–calcination looping for CO_2 capture from industrial flue gas. RSC Adv 2014;4:6858. doi:10.1039/c3ra47426g.

[208] Pan SY, Chiang PC, Chen YH, Chang EE, Chen C Da, Shen AL. Process intensification of steel slag carbonation via a rotating packed Bed: Reaction kinetics and mass transfer. Energy Procedia 2014;63:2255–60. doi:10.1016/j.egypro.2014.11.244.

[209] Miranda-Pizarro J, Perejón A, Valverde JM, Sánchez-Jiménez PE, Pérez-Maqueda LA. Use of steel slag for CO_2 capture under realistic calcium-looping conditions. RSC Adv 2016;6:37656–63. doi:10.1039/C6RA03210A.

[210] Niu S, Han K, Lu C, Sun R. Thermogravimetric analysis of the relationship among calcium magnesium acetate, calcium acetate and magnesium acetate. Appl Energy 2010;87:2237–42. doi:10.1016/j.apenergy.2010.01.007.

[211] Musumeci AW, Frost RL, Waclawik ER. A spectroscopic study of the mineral paceite (calcium acetate). Spectrochim Acta - Part A Mol Biomol Spectrosc 2007;67:649–61. doi:10.1016/j.saa.2006.07.045.

[212] Ariono D, Wardani AK. Review of Membrane Oxygen Enrichment for Efficient Combustion Effect of Electric Field in the Stabilized Premixed Flame on Combustion Process Emissions Krickis Otto - Premixed CH 4 /O 2 -enriched air combustion: Identification of thermal, chemical and aerodynamic effects Review of Membrane Oxygen Enrichment for Efficient Combustion. J Phys 2017;877. doi:10.1088/1742-6596/877/1/012050.

[213] Kather A, Scheffknecht G. The oxycoal process with cryogenic oxygen supply. Naturwissenschaften 2009;96:993–1010. doi:10.1007/s00114-009-0557-2.

[214] Matson SL, Ward WJ, Kimura SG, Browall WR. Membrane oxygen enrichment. II. Economic assessment. J Memb Sci 1986;29:79–96. doi:10.1016/S0376-7388(00)82020-7.

[215] Chong KC, Lai SO, Thiam HS, Teoh HC, Heng SL. Recent Progress of Oxygen / Nitrogen Separation Using Membrane Technology. J Eng Sci Technol 2016;11:1016–30.

[216] Robeson LM. Correlation of separation factor versus permeability for polymeric membranes. J Memb Sci 1991;62:165–85. doi:10.1016/0376-7388(91)80060-J.

[217] Murali RS, Sankarshana T, Sridhar S. Air separation by polymer-based membrane technology. Sep Purif Rev 2013;42:130–86. doi:10.1080/15422119.2012.686000.

[218] Humphrey JL, Keller GE. Separation Process Technology. McGraw-Hill; 1997.

[219] Bounaceur R, Lape N, Roizard D, Vallieres C, Favre E. Membrane processes for post-combustion carbon dioxide capture: A parametric study. Energy 2006;31:2220–34. doi:10.1016/j.energy.2005.10.038.

[220] Bhide BC, Stern SA. A new evaluation of membrane processes for the oxygen- enrichment of air. II. Effects of economic parameters and membrane properties. J Memb Sci 1991;62:37–58. doi:10.1016/0376-7388(91)85003-N.

[221] Belaissaoui B, Le Moullec Y, Hagi H, Favre E. Energy efficiency of oxygen enriched air production technologies: Cryogeny vs membranes. Energy Procedia, vol. 63, 2014, p. 497–503. doi:10.1016/j.egypro.2014.11.054.

[222] Chacartegui R, Alovisio A, Ortiz C, Valverde JM, Verda V, Becerra JA. Thermochemical energy storage of concentrated solar power by integration of the calcium looping process and a CO_2 power cycle. Appl Energy 2016;173:589–605. doi:10.1016/j.apenergy.2016.04.053.

[223] Charitos A, Rodríguez N, Hawthorne C, Alonso M, Zieba M, Arias B, et al. Experimental Validation of the Calcium Looping CO_2 Capture Process with Two Circulating Fluidized Bed Carbonator Reactors. Ind Eng Chem Res 2011;50:9685–95. doi:10.1021/ie200579f.

[224] Meier A, Bonaldi E, Cella GM, Lipinski W, Wuillemin D, Palumbo R. Design and experimental investigation of a horizontal rotary reactor for the solar thermal production of lime. Energy 2004;29:811–21. doi:10.1016/S0360-5442(03)00187-7.

[225] Meier A, Bonaldi E, Cella GM, Lipinski W. Multitube Rotary Kiln for the Industrial Solar Production of Lime. J Sol Energy Eng 2005;127:386. doi:10.1115/1.1979517.

[226] Imhof a. Decomposition of limestone in a solar reactor. Renew Energy 1996;9:661–3. doi:10.1016/0960-1481(96)88373-X.

[227] Winter CJ, Sizmann RL, Vant-Hull LL. Solar power plants: fundamentals, technology, systems, economics. Springer-Verlag; 1991.

[228] de Bosio F, Verda V. Thermoeconomic analysis of a Compressed Air Energy Storage (CAES) system integrated with a wind power plant in the framework of the IPEX Market. Appl Energy 2015;152:173–82. doi:10.1016/j.apenergy.2015.01.052.

[229] Yu FC, Fan LS. Kinetic Study of High-Pressure Carbonation Reaction of Calcium-Based Sorbents in the Calcium Looping Process (CLP). Ind Eng Chem Res 2011;50:11528–36. doi:Doi 10.1021/Ie200914e.

[230] Linnhoff B, Hindmarsh E. The pinch design method for heat exchanger networks. Chem Eng Sci 1983;38:745–63. doi:10.1016/0009-2509(83)80185-7.

[231] Ortiz C, Chacartegui R, Valverde JM, Alovisio A, Becerra JA. Power cycles integration in concentrated solar power plants with energy storage based on calcium looping. Energy Convers Manag 2017;149:815–29. doi:10.1016/j.enconman.2017.03.029.

[232] Casati E, Casella F, Colonna P. Design of CSP plants with optimally operated thermal storage. Sol Energy 2015;116:371–87. doi:10.1016/j.solener.2015.03.048.

[233] Reich L, Melmoth L, Yue L, Bader R, Gresham R, Simon T, et al. A Solar Reactor Design for Research on Calcium Oxide-Based Carbon Dioxide Capture. J Sol Energy Eng 2017;139:054501. doi:10.1115/1.4037089.

[234] Kolb G, Ho C, Mancini T, Gary J. Power tower technology roadmap and cost reduction plan. SAND2011-2419, Sandia … 2011:38. doi:10.2172/1011644.

[235] Ho C, Christian J, Gill D, Moya A, Jeter S, Abdel-Khalik S, et al. Technology advancements for next generation falling particle receivers. Energy Procedia 2013;49:398–407. doi:10.1016/j.egypro.2014.03.043.

[236] Siegel NP, Ho CK, Khalsa SS, Kolb GJ. Development and Evaluation of a Prototype Solid Particle Receiver: On-Sun Testing and Model Validation. J Sol Energy Eng 2010;132:021008. doi:10.1115/1.4001146.

[237] Christian J, Ho C. Alternative designs of a high efficiency, north-facing, solid particle receiver. Energy Procedia 2013;49:314–23. doi:10.1016/j.egypro.2014.03.034.

[238] Ho CK, Christian JM, Yellowhair J, Siegel N, Jeter S, Golob M, et al. On-sun testing of an advanced falling particle receiver system. AIP Conf Proc 2016;1734. doi:10.1063/1.4949074.

[239] Salatino P, Ammendola P, Bareschino P, Chirone R, Solimene R. Improving the thermal performance of fluidized beds for concentrated solar power and thermal energy storage. Powder Technol 2016;290:97–101. doi:10.1016/j.powtec.2015.07.036.

[240] Migliozzi S, Paulillo A, Chirone R, Salatino P, Solimene R. Hydrodynamics of compartmented fluidized beds under uneven fluidization conditions. Powder Technol 2017;316:476–91. doi:10.1016/j.powtec.2016.12.052.

[241] Chirone R, Salatino P, Ammendola P, Solimene R, Magaldi M, Sorrenti R, et al. Development of a Novel Concept of Solar Receiver/Thermal Energy Storage System Based on Compartmented Dense Gas Fluidized Beds. 14th Int Conf Fluid 2013.

[242] Valverde J. Thermochemical method for the transfer and storage of concentrated solar energy. WO2015197885A1, 2015.

[243] Abanades S, André L. Design and demonstration of a high temperature solar-heated rotary tube reactor for continuous particles calcination. Appl Energy 2018;212:1310–20. doi:10.1016/j.apenergy.2018.01.019.

[244] Shimizu A, Yokomine T, Nagafuchi T. Development of gas-solid direct contact heat exchanger by use of axial flow cyclone. Int J Heat Mass Transf 2004;47:4601–14. doi:10.1016/j.ijheatmasstransfer.2003.10.045.

[245] Ho CK, Christian J, Yellowhair J, Jeter S, Golob M, Nguyen C, et al. Highlights of the high-temperature falling particle receiver project: 2012 - 2016. AIP Conf. Proc., vol. 1850, 2017. doi:10.1063/1.4984370.

[246] Jordison N, Rozendaal NA, Huang PXD. Indirect-heat thermal processing of particulate material, 2007.

[247] Al-Ansary H, El-Leathy A, Al-Suhaibani Z, Jeter S, Sadowski D, Alrished A, et al. Experimental Study of a Sand–Air Heat Exchanger for Use With a High-Temperature Solar Gas Turbine System. J Sol Energy Eng 2012;134:041017. doi:10.1115/1.4007585.

[248] De La Vergne J, Mcintosh S. Hard Rock Miner's Handbook. vol. 4. 2000.

[249] Zhao M, Minett AI, Harris AT. A review of techno-economic models for the retrofitting of conventional pulverised-coal power plants for post-combustion capture (PCC) of CO 2. Energy Environ Sci 2013;6:25–40. doi:10.1039/C2EE22890D.

[250] EUROPEAN COMMISSION. Carbon capture by means of indirectly heated carbonate looping process. 2014.

Annexes (complete copy of publications)

***ANNEX 1**: Ortiz C, Chacartegui R, Valverde J, Becerra J, Perez-Maqueda L. A new model of the carbonator reactor in the calcium looping technology for post*-combustion CO_2 capture. *FUEL 2015;160:328–38. doi:10.1016/j.fuel.2015.07.095.*

Fuel 160 (2015) 328–338

Contents lists available at ScienceDirect

Fuel

journal homepage: www.elsevier.com/locate/fuel

A new model of the carbonator reactor in the calcium looping technology for post-combustion CO_2 capture

C. Ortiz [a], R. Chacartegui [a,*], J.M. Valverde [b], J.A. Becerra [a], L.A. Perez-Maqueda [c]

[a] Energy Engineering Department, University of Seville, Camino de los Descubrimientos s/n, 41092 Sevilla, Spain
[b] Faculty of Physics, University of Seville, Avenida Reina Mercedes s/n, 41012 Sevilla, Spain
[c] Instituto de Ciencia de Materiales de Sevilla (C.S.I.C. – Univ. Sevilla), Americo Vespucio 49, 41092 Sevilla, Spain

HIGHLIGHTS

- A new carbonator model is proposed taking into account realistic CaL conditions.
- Carbonation in the diffusion stage is considered to predict the capture efficiency.
- High capture efficiency may be achieved by operating with high particles residence time.
- New model allows accurate modelling for extended residence's time.
- Results are in good agreement with data from pilot-scale tests.

ARTICLE INFO

Article history:
Received 19 May 2015
Received in revised form 28 July 2015
Accepted 29 July 2015
Available online 4 August 2015

Keywords:
CO_2 capture
Ca-looping
Limestone calcination
Diffusion phase
Calcium looping
Carbon dioxide capture

ABSTRACT

The Ca-Looping (CaL) process is considered as a promising technology for CO_2 post-combustion capture in power generation plants yielding a minor penalty on plant performance as compared with other capture technologies such as conventional amine-based capture systems. This manuscript presents a new carbonator reactor model based on lab-scale multicyclic CaO conversion results, which take into account realistic CaO regeneration conditions that necessarily involve calcination under high CO_2 partial pressure and high temperature. Under these conditions, CaO conversion in the diffusion controlled stage is a relevant contribution to the carbonation degree during typical residence times. The main novelty of the model proposed in the present work is the consideration of the capture efficiency in the diffusion controlled phase of carbonation. It is demonstrated that increasing the residence time by a few minutes in the carbonator yields a significant improvement of the capture efficiency. Model predictions are shown to agree with experimental results retrieved from pilot-scale tests. The new model allows a more accurate evaluation and prediction of carbonator's performance over a wider range of residence times. The results obtained may be relevant for the optimization of CaL operation parameters to be used in real power plants.

1. Introduction

Taking into account the current energy system and its expected evolution, capture and permanent geological storage of CO_2 from fossil fuel power plants is considered as a necessary technology to be developed at commercial scale in the short term for mitigation of global warming. The IPCC [1] has evaluated existing and emerging technologies of CO_2 capture and storage (CCS) and concludes that, in most scenarios, CCS should contribute by a 15–55% to the cumulative global mitigation effort until 2100. Amongst the CO_2 capture technologies potentially foreseeable for commercial development, the Ca-Looping (CaL) process is highlighted as one with good prospects for post-combustion capture, mainly due to the possibility of being implemented in already existing power plants and the minor penalty on plant performance as compared to other capture technologies such as conventional amine-based capture systems [2,3]. A further advantage of the CaL technology is the low price, wide availability and harmlessness towards the environment of the sorbent precursor raw material, namely natural limestone [2,4,5].

The CaL technology for CO_2 post-combustion capture is based on the reversible chemical reaction of carbonation–calcination of CaO. The basic cycle involves CO_2 capture from the flue gas stream of a power plant using lime (CaO) derived from calcination of natural limestone:

* Corresponding author. Tel.: +34 954487615.
E-mail address: ricardoch@us.es (R. Chacartegui).

http://dx.doi.org/10.1016/j.fuel.2015.07.095
0016-2361/

Nomenclature

A	carbonator section, m^2
C_{CO2}	average CO_2 concentration, mol/m^3
$C_{CO2,eq}$	equilibrium concentration of CO_2, mol/m^3
D_{eff}	intrinsic diffusion constant, $m^3/(mol\ s)$
D^*_{eff}	equivalent diffusion constant, $m^3/(mol\ s)$
E_{CO2}	carbon capture efficiency
$E_{CO2,eq}$	maximum carbon capture efficiency
$E_{CO2,D}$	carbon capture efficiency in the diffusion regime
$E_{CO2,K}$	carbon capture efficiency in the kinetic regime
f_0	inlet molar fraction of CO_2
f_a	volumetric fraction of CaO that reacts in the kinetic reaction regime
f_e	equilibrium molar fraction of CO_2
F_0	mole flow of fresh makeup limestone, mol/s
F_{CO2}	mole flow of CO_2 in flue gas entering the carbonator
$F_{CO2,cal}$	mole flow of CO_2 originating in the calciner, mol/s
F_P	mole flow of solids purge in the calciner, mol/s
F_R	mole flow of CaO coming from the calciner, mol/s
h	thickness of the product layer of a sorbent particle, nm
k_s	intrinsic kinetic constant $m^4/(mol\ s)$
T_0	time of TGA multicyclic test, s
M_{CaO}	molar mass of $CaCO_3$, g/mol
m_{CO2}	volume flow rate per MW of a typical power plant of CO_2 in flue gas entering the carbonator, m^3/s
N	calcination–carbonation cycles
N_{Ca}	mol of Ca in the carbonator, mol
P	pressure (bar)
$r_{ave,D}$	average reaction rate in the diffusion regime, s^{-1}
$r_{ave,K}$	average reaction rate in the kinetic regime, s^{-1}
$r_{N,D}$	particle reaction rate in the diffusion regime, s^{-1}
$r_{N,K}$	particle reaction rate in the kinetic regime, s^{-1}
$S_{ave,K}$	average reaction available surface, m^{-1}
S_N	reaction available surface in the N cycle, m^2/m^3
T	temperature (°C)
t	time, s
t_K	characteristic time at which kinetic phase end, s
t_{max}	Particle residence time in carbonator, s
V_{gas}	volume flow rate per MW of a typical power plant in flue gas entering the carbonator, m^3/s
$V_{M,CaCO3}$	molar volume, m^3/mol
W_s	solid inventory in the carbonator per MW of a typical power plant, kg
$W_{s,c}$	solid inventory in the calciner per MW of a typical power plant, kg
X	carbonation degree of a CaO particle
X_{ave}	average conversion of the sorbent
$X_{ave,D}$	average conversion of the sorbent in the diffusion phase
$X_{ave,K}$	average conversion of the sorbent in the kinetic phase
$X_{max,ave}$	maximum average carbonation degree of CaO in the solid population
$X_{max,ave,D}$	maximum average carbonation degree of CaO in the solid population in the diffusion phase
$X_{max,ave,K}$	maximum average carbonation degree of CaO in the solid population in the kinetic phase
X_N	maximum carbonation degree of CaO in the N cycle
X_{ND}	maximum carbonation degree of CaO in the N cycle in the diffusion phase
X_{NK}	maximum carbonation degree of CaO in the N cycle in the kinetic phase
X_r	residual conversion capacity of a sorbent particle
κ	deactivation constant of a sorbent particle
r_N	particle fraction in the N cycle
ρ_{CaO}	CaO density, g/m^3
ρ_g	density of gas phase, g/m^3
τ	average residence time in the carbonator, s
τ_a	active space time of the carbonator, s

$$CaO_{(s)} + CO_2 \rightleftarrows CaCO_{3(s)} \quad \Delta H_r^0 = -178\ \frac{kJ}{mol} \tag{1}$$

Flue gases from coal-fired power plants generally contain a mole fraction of CO_2 in the range of 10–15% [6,7], whereas typical residence times in the carbonator reactor would be on the order of minutes. Taking into account these constraints, optimum carbonation temperatures are around 650 °C for a quick enough reaction kinetics and low value of the equilibrium CO_2 concentration in order to achieve significant efficiencies of CO_2 capture (around 80–90%) [8]. Efficient gas–solid contact and heat/mass transfer would be ensured by the use of circulating fluidized-bed reactors (CBF). CFBs are typically operated at atmospheric pressure under the fast fluidization regime, with gas velocities of the order of 5–10 m/s [9,10]. The partially carbonated particles are driven into a second fluidized bed reactor (calciner), where CaO is regenerated by calcination under high temperatures and necessarily high CO_2 concentration [11–14].

Once CO_2 is captured in the carbonator and heat from the exothermic reaction is recovered, the flue gas almost free of CO_2 is released into the atmosphere. After a residence time in the carbonator of a few minutes, the carbonated solids are circulated into the calciner. Coal is burned into the calciner reactor using pure O_2 (oxy-combustion) to increase the temperature up to the value required for the endothermic calcination reaction to occur fast and avoid CO_2 dilution at the same time. Thus, CO_2 is retrieved from the calciner for compression, transport and geological storage or other uses. The regenerated sorbent produced in the calciner is returned to the carbonator for a new cycle.

In order to predict the efficiency of CO_2 capture by integrating the CaL technology on existing power plants, a number of models have being proposed in the literature [15–18]. Besides, several pilot-medium scale plants (up to 1.7 MWth) demonstrate a high CO_2 capture efficiency, which raises hopes on a successful scale-up of the technology [13,14,19–21]. Interestingly, the CaL technology is also suitable to be integrated with biomass combustion as shown in a pilot-scale plant (300 kWth), which would allow producing power with negative CO_2 emissions [20].

The multicyclic calcination/carbonation behavior of CaO used in current carbonator models has been inferred from thermogravimetric analysis (TGA) results in which calcination is usually carried out under low CO_2 partial pressure mainly due to technical difficulties. Under these conditions, most of the carbonation reaction in short residence times occurs on the surface of the CaO particles through a kinetically controlled fast phase whereas the subsequent solid-state diffusion controlled phase is comparatively negligible as will be seen in detail below. The present manuscript proposes a new carbonator model that does consider the relevant effect of realistic calcination conditions, necessarily involving calcination under high CO_2 pressure, on the multicyclic CaO conversion behavior. In order to stress the relevant role of calcination conditions on the sorbent performance, the next section is devoted to briefly review recent TGA results that will be employed in the formulation of the new carbonator model. We follow up with the development of the carbonator model. Finally, capture efficiency results from the new model are compared with predictions by models reported in the literature and pilot-scale results.

2. A brief review on the role of calcination conditions on the multicyclic CO_2 capture behavior of limestone

Results of TGA tests show that the multicyclic CO_2 capture capacity of limestone derived CaO is strongly influenced by the conditions under which calcination is performed [22–24]. The most feasible method in practice to generate the heat required in the calciner while at the same time avoiding CO_2 dilution is to burn coal by oxy-combustion [4,11–14]. Thus, calcination is carried out in an environment containing between 70% and 90% vol. concentration of CO_2 at atmospheric pressure [11,23,25–27]. Calcination kinetics becomes extremely slow under high CO_2 partial pressures nearby equilibrium ($T \approx 870$–900 °C) [22]. This makes necessary to increase the temperature over 930 °C to rise the CO_2 partial equilibrium pressure well above the CO_2 partial pressure in the calciner and yield sufficiently fast reaction kinetics in short residence times [14,21,28].

2.1. Sorbent deactivation

The combination of high temperature and high concentration of CO_2 during calcination enhances the progressive deactivation of the sorbent as the number of cycles builds up due to enhanced sintering [29–32]. Enhanced sintering of CaO has a strongly negative effect on the active surface of the solids available for the gas–solid reaction in the kinetically driven fast phase. Grasa and Abanades [33] proposed to fit the observed evolution of CaO conversion X_N (ratio of mass of CaO converted to $CaCO_3$ to mass of CaO initial) with the number of cycles by means of the Eq. (2):

$$X_N = \frac{1}{\frac{1}{1-X_r} + \kappa N} + X_r \tag{2}$$

where $\kappa = 0.52$ and $X_r = 0.075$ are the deactivation constant and the residual conversion, respectively. This equation is however based on results from multicyclic calcination/carbonation TGA tests in which the sorbent is regenerated by calcination under low CO_2 partial pressure. Thus, conversion after 1st calcination (X_1) is close to unity. This high value of conversion is due to the relatively high porosity of the CaO particles derived by short-time calcination under low CO_2 partial pressure. Despite that Eq. (2) cannot reflect the effect of calcination under high CO_2 pressure as would be the case in the CaL technology, it has been routinely used in theoretical studies as representative of the sorbent behavior in order to model the carbonator reactor [15–18].

In more recent TGA studies [34,35], a modified equation was proposed using data obtained from multicyclic calcination/carbonation tests under more realistic calcination conditions involving high CO_2 partial pressure (70% v/v CO_2, 30% air) at temperatures of 950 °C as well as fast transitions between the calcination and carbonation stages. The modified equation proposed is:

$$\frac{X_N}{X_1} = \frac{X_r}{X_1} + \left(\frac{1}{\kappa(N-1) + \left(1 - \frac{X_r}{X_1}\right)^{-1}} \right) \tag{3}$$

where $\kappa = 0.776$ and $X_r = 0.077$ and $X_1 = 0.48$ is CaO conversion after 1st calcination. Carbonation/calcination conditions in these tests where 650 °C/5 min for carbonation under 15% CO_2 and 950 °C/5 min for calcination under 70% CO_2.

Eq. (3) looks similar to Eq. (2), but with the main difference that it takes into account the smaller value of conversion in the first cycle after calcination under high CO_2 partial pressure. Besides, the deactivation constant is higher as compared to that derived from tests carried out calcining under low CO_2 partial pressure. In the real process, a makeup flow of fresh limestone must be continuously fed into the calciner in order to compensate for sorbent deactivation. Limestone is therefore first calcined in the stationary state under high CO_2 partial pressure at the same conditions that the partially carbonated solids are calcined for CaO regeneration. Thus, the use of Eq. (3) for modelling the carbonator reactor might help simulating more realistic CaL conditions.

2.2. Fast and slow carbonation stages

Two well differentiated stages can be observed during carbonation of CaO solid particles [30,36–38]. The first stage takes place on the free surface of the solid through the nucleation and growth of $CaCO_3$ and is governed by the kinetics of the reaction between CaO and CO_2. The end of the fast stage takes place when a 40–60 nm thickness product layer is formed, which makes inaccessible a large fraction of CaO in the interior of the particles for fast kinetically controlled carbonation [39]. Once the CaO free surface directly available for fast carbonation has been covered the reaction continues in a second stage which is controlled by the solid-state diffusion of CO_3^{2-} and O^{2-} ions through the product layer, which is a much slower process [40,41].

TGA results show that the solid-state diffusion controlled carbonation is greatly enhanced when CaO is regenerated under high CO_2 partial pressure as compared to calcination under low CO_2 concentration [26,42,43]. Fig. 1 shows the time evolution of

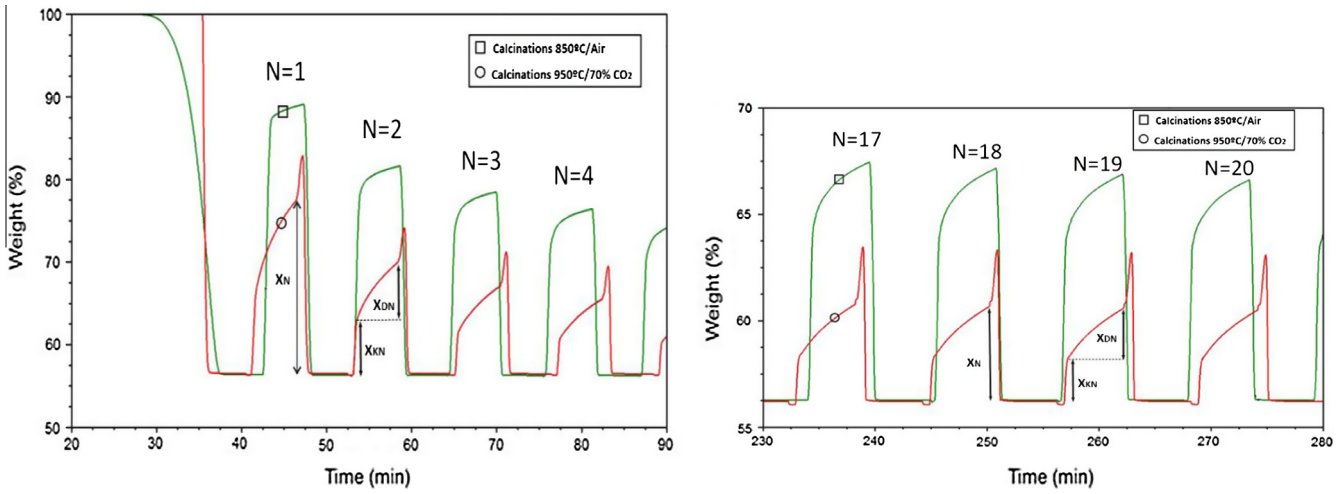

Fig. 1. Time evolution of sorbent weight% during precalcination and subsequent carbonation/calcination cycles. Carbonation at 650 °C for 5 min (15% CO_2/85% air vol/vol). Different calcination conditions are indicated. Reproduced from data reported in [35].

sorbent weight during the first calcination/carbonation cycles of two TGA tests in which calcination was carried out either under high CO_2 partial pressure or air. The results demonstrate that carbonation in the fast initial phase is extraordinarily hindered when the sorbent is regenerated under high CO_2 concentration. Even though the reaction rate is similar for the two tests, the maximum carbonation conversion in the fast phase is significantly hampered for the sorbent regenerated under high CO_2 partial pressure essentially due to severe sintering and drastic reduction of the surface area [22]. On the other hand, carbonation in the diffusion controlled phase is notably enhanced when calcination is carried out under high CO_2 concentration especially in the first cycles.

A close examination of TGA test results reported in the literature for CaO derived from other precursors such as steel slag (Fig. 2a) and results obtained from pilot scale tests (Fig. 2b) reveals also that in those cases the relatively slower solid-state diffusion controlled phase contributes substantially to carbonation for residence times of a few minutes.

Fig. 3 shows the multicyclic evolution of CaO conversion in the kinetically controlled (X_{NK}) and diffusion controlled (X_{ND}) carbonation stages derived from TGA tests reported in [35] in which calcination was carried out under high CO_2 partial pressure. Both X_{NK} and X_{ND} can be pretty well fitted by Eq. (3) using the parameters given in Table 1.

As can be seen in Fig. 3, the contribution of the diffusion controlled phase to CaO conversion is quite relevant being of the same order than CaO conversion in the kinetically controlled phase for 5 min overall carbonation periods. Moreover, an increase of the carbonation phase above 5 min would lead to higher conversion in the diffusive phase since carbonation in this stage grows roughly linearly with time until carbonation is completed [42]. Thus, it seems clear that a carbonator model should consider carbonation in the diffusion stage in order to predict realistic values of efficiency and to draw useful conclusions on the optimum operating parameters in a commercial plant. This is the main goal of the present manuscript.

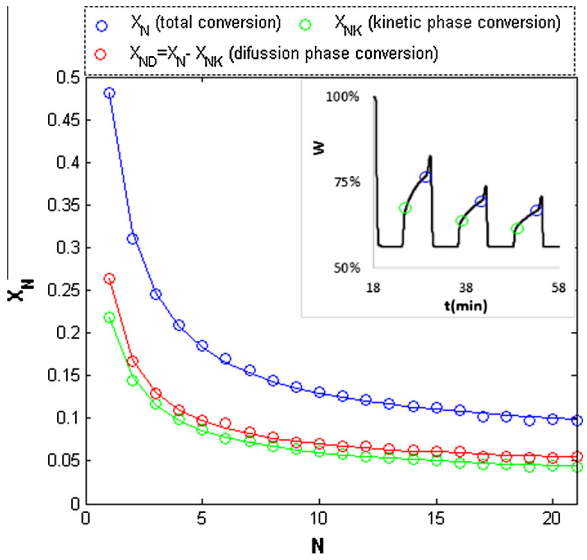

Fig. 3. CaO conversion in the kinetically controlled carbonation stage (X_{NK}) and in the diffusion controlled stage (X_{ND}) as a function of the cycle number. Pre-calcination and calcinations conditions: CO_2 vol% = 70%, t = 5 min, T = 950 °C. Carbonation conditions: CO_2 vol% = 15%, t = 5 min, T = 650 °C. The inset shows the time evolution of sorbent wt% in the first 3 cycles. Obtained from data originally reported in [42].

Table 1
Fitting parameters for sorbent deactivation curves of conversion in the kinetic and diffusion controlled stages (Fig. 3).

Carbonation stage	Kinetic	Diffusion
Time	0.3 min	≈5 min
Deactivation constant	κ_K = 0.676	κ_D = 0.871
Residual conversion	X_{rK} = 0.0296	X_{rD} = 0.0408
1st cycle conversion	$X_{1,K}$ = 0.0218	$X_{1,D}$ = 0.263

3. Carbonator model approach

3.1. Kinetic model

As mentioned in the introduction, in order to predict the CO_2 capture efficiency of the CaL technology, many authors [15–18] propose to simplify the CaO conversion behavior by assuming that it reaches a maximum value, X_N, at a constant rate (proportional to the free surface available of CaO and the thickness of the $CaCO_3$ layer formed) in a time t_{lim}, after which the reaction rate drops to zero (solid lines in Fig. 4a). This simplifying assumption would be reasonable if calcination was performed under low CO_2 partial pressure. However, as pointed out above, the diffusive carbonation

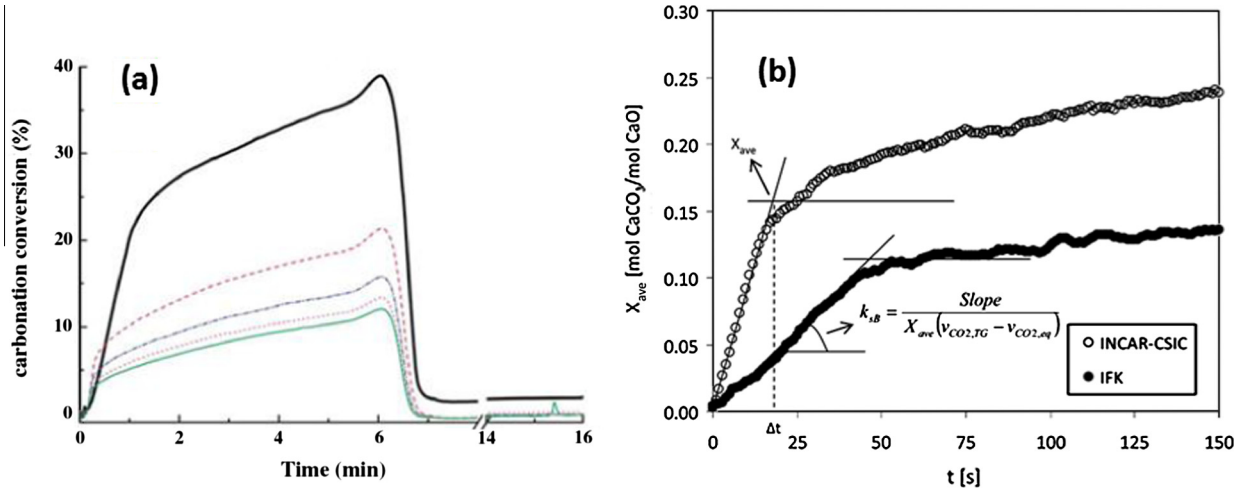

Fig. 2. (a) Time evolution conversion of steel slag during the first, 5th, 10th, 15th, and 20th cycles (reproduced from [48] with permission). (b) Average CO_2 carrying capacity (X_{ave}) vs. time and reaction constant (k_{sB}), derivation for sample removed from the CFB carbonator during operation in pilot-scale test (reproduced from [28] with permission).

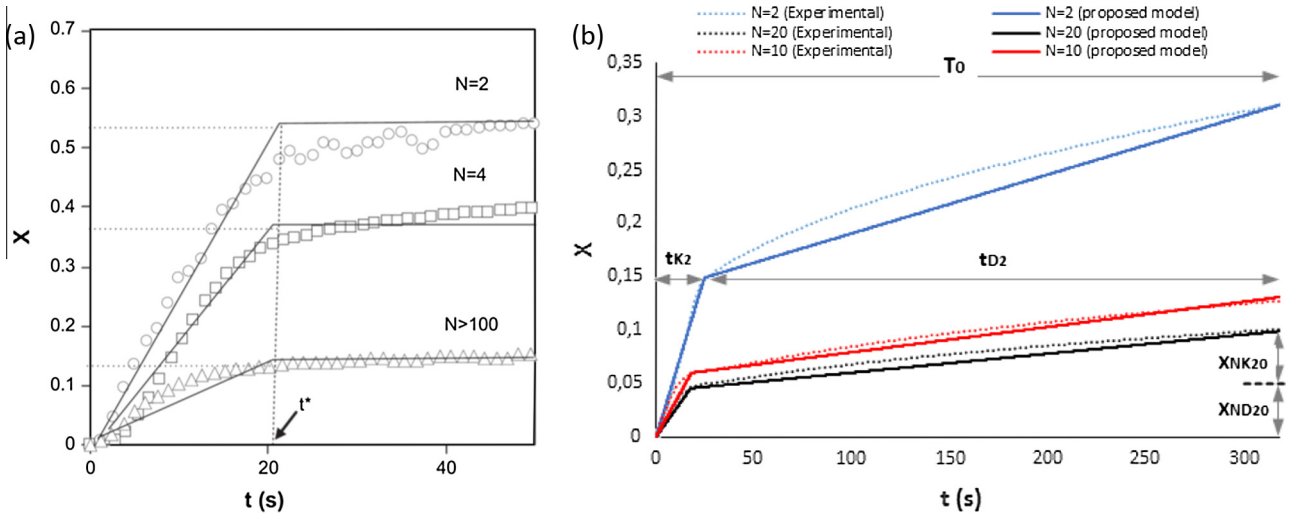

Fig. 4. CaO conversion as a function of time for different cycles showing in (a) the theoretical approximation proposed elsewhere for the kinetic model (solid lines) to describe the progress of the carbonation reaction with time (reproduced from [18] with permission). Data points are experimental results from TGA tests in which calcination was carried under low CO_2 concentration. In (b) the kinetic model curves proposed in the present article (solid lines) are shown superposed to experimental data from TGA tests reported in [49] in which calcination was carried out under high CO_2 concentration (dotted lines). Note the different scales in (a) an (b) for the CaO conversion degree.

phase plays a relevant role for calcination under high CO_2 partial pressure whereas the kinetically controlled carbonation stage is severely hampered. Using the multicyclic TGA results reported in [34,35,42], we develop below a modified carbonator model built upon the model proposed by Alonso et al. [18]. The main novelty of our model is that carbonation in the diffusion controlled phase will be considered to predict the carbonation efficiency.

Fig. 4(a) shows experimental results from TGA tests in which calcinations were carried out under low CO_2 partial pressure. The solid lines are the kinetic curves assumed in the carbonator model described in [18]. As can be seen, the diffusion controlled stage is negligible in the first cycles although as the number of cycles is increased the diffusive conversion becomes more important (see results for cycle $N = 20$ in Fig. 4(a)). As seen in Fig. 4(a) the time for the kinetic stage (t_k) decreases with the number of cycles as conversion in the diffusive phase is enhanced, which is however dismissed in the theoretical model (solid lines). Fig. 4(b) illustrates the kinetic curves proposed in our work as representative of the experimental curves reported in [42] in which calcinations were carried out under high CO_2 partial pressure. It is assumed that the time evolution of CaO conversion can be approximated by two straight lines of constant slope, one corresponding to the kinetically controlled carbonation stage and another one for the diffusive carbonation stage. In this way, the new kinetic model has into account the relevant role of the diffusion controlled phase. According to experimental measurements, conversion would be increased roughly linearly with time during the first minutes in the diffusion controlled stage against the widely accepted conception that once the fast kinetically controlled phase is completed, additional carbonation by solid-state diffusion is negligible. Thus, it may be anticipated that an important parameter influencing the carbonation efficiency would be the residence time of the solids in the carbonator.

According to the kinetic model proposed in this work (solid lines in Fig. 4(b)), the reaction rate can be expressed as a function of residence time in the carbonator by the following expression:

$$r_{N\_i} = \begin{cases} r_{N_K} = \frac{X_{NK}}{t_K} & for\ t \leqslant t_K \\ r_{N_D} = \frac{X_{ND}}{T_0 - t_K} & for\ t_K < t \leqslant t_{max} \end{cases} \quad (4)$$

where r_{N_i} is the reaction rate in the i-phase (either kinetic or diffusion), t_K is the time the kinetic phase takes, t_{max} is the residence time of the particles in the carbonator, and $X_{ND}/(T_0 - t_K)$ is the rate of diffusive conversion that will be derived from experimental results.

Using experimental data reported in [42], the reaction rates in the kinetic phase (r_{Nk}) and diffusive phase (r_{ND}) can be adjusted as a function of the number of cycles N using Eq. (3) as shown in Fig. 5.

According to Bhatia and Perlmutter [38], the rate of CaO conversion in the kinetically controlled fast phase at atmospheric pressure, can be expressed by a first-order kinetic law:

$$\frac{dX}{dt} = r_{NK} = k_s S_N (1 - X)^{\frac{2}{3}} (C_{CO2} - C_{CO2eq}) \quad (5)$$

where C_{CO2} and C_{CO2eq} are the actual and equilibrium CO_2 concentrations, respectively, and k_s is the kinetic constant. S_N is the CaO specific area available for reaction after N cycles, which is proportional to the particle conversion degree. As can be seen in Fig. 5, the reaction

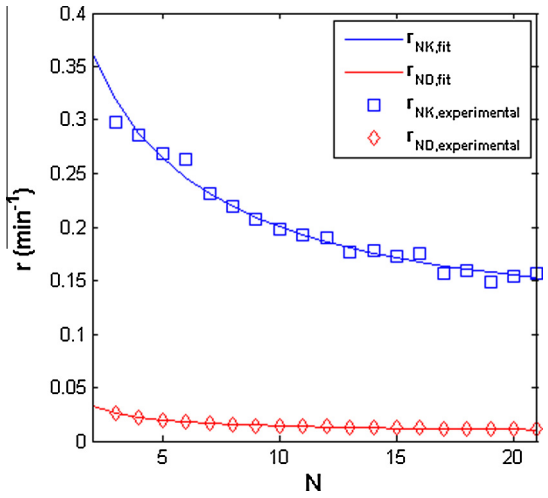

Fig. 5. Rate of kinetic and diffusive carbonation (r_{ND}, r_{NK} respectively) as a function of number of cycles from experimental data reported in [42] obtained by means of TGA tests. The solid lines are best fit curves using Eq. (3) yielding residual values of the kinetic and diffusion rates of 0.096 and 0.0082, respectively and deactivation constants of the kinetic and diffusion rates of 0.315 and 0.917, respectively.

rate in the kinetic phase (r_{Nk}) decays with the number of cycles due to the effect of sintering that leads to a decrease of the available surface S_N).

By integrating Eq. (5) and fitting it to the experimental data reported in [42], we obtain a value of the kinetic constant $k_s = 6.7 \times 10^{-10}$ m^4/(mol s), which is similar to the value reported by other authors [38,44] also for natural limestone but under different operating conditions as regards calcination. This suggests that the kinetics of carbonation in the fast phase is essentially determined by the CaO surface area and does not depend on the calcination conditions. The essential effect of calcination under CO_2 would be thus to enhance sintering, which greatly reduces the available surface area for carbonation and therefore the duration of the kinetic phase.

The rate of conversion in the diffusion controlled phase can be expressed using an effective diffusion constant D_{eff} [40]:

$$\frac{dX}{dt} = r_{ND} = \frac{D_{eff}(C_{CO2} - C_{CO2eq})}{\frac{2}{3}(1-X)^{-\frac{1}{3}} - \frac{2}{3}(Z+(1-Z)(1-X))^{-\frac{1}{3}}} \quad (6)$$

where Z is the ratio of the molar volume of $CaCO_3$ and CaO. Eq. (6) can be adjusted to the experimental data (Fig. 5) to obtain a value for the diffusion constant. As seen from the experimental results (Fig. 5) the rate of carbonation in the diffusive stage remains after 2–3 cycles approximately constant with the number of cycles. In [42], some of the TGA tests presented were made by prolonging the carbonation stage up to 30 min showing that the rate of carbonation in the diffusion controlled phase did not change appreciably over this time interval. Thus, we may neglect as a first approximation the dependence of the diffusive reaction rate on conversion and use the simplified expression:

$$r_{ND} \approx D^*_{eff}(C_{CO2} - C_{CO2eq}) \quad (7)$$

where D^*_{eff} is an effective diffusion constant. By using $r_{ND} \approx 0.01$ min^{-1} (Fig. 5) a value of $D^*_{eff} = 6.5 \times 10^{-5}$ m^3/(mol s) is obtained.

3.2. Capture model

In Fig. 6 we show the global scheme for the CaL system with the definition of main parameters used for defining and evaluating CO_2 capture.

The average conversion of the CaO particles present in the reactor (X_{ave}) is given by the sum of conversion in the kinetic fast phase ($X_{ave,k}$) and conversion in the diffusive phase ($X_{ave,D}$):

$$X_{ave} = X_{ave,K} + X_{ave,D} \quad (8)$$

For a given continuous supply of fresh limestone into the calciner and a given solids purge, the fraction of particles subjected to a given number of cycles N is given by [30]:

$$r_N = \frac{F_0 F_R^{N-1}}{(F_0 + F_R)^N} \quad (9)$$

The average maximum conversion ($X_{max,ave}$) can be calculated as the weighted sum of conversions after N cycles:

$$X_{max,ave} = \sum_{N=1}^{N=\infty} r_N X_N \quad (10)$$

$$X_{max,ave} = X_{max,ave,K} + X_{max,ave,D} = \sum_{N=1}^{N=\infty} r_N X_{NK} + \sum_{N=1}^{N=\infty} r_N X_{ND} \quad (11)$$

The average reaction rate depends on the phase the particles are reacting as:

$$r_{ave\_i} = \begin{cases} r_{ave,K} = \frac{X_{max,ave,K}}{t_K} & si\ t \leqslant t_K \\ r_{ave,D} = \frac{X_{max,ave,D}}{T_0 - t_K} & si\ t_K < t \leqslant \tau \end{cases} \quad (12)$$

where τ is the average residence time of the particles in the carbonator:

$$\tau = \frac{N_{Ca}}{F_R} = \frac{W_s}{56 F_R} \quad (13)$$

The average conversion of the particles leaving the carbonator can be obtained from the sum of the average particle conversion reacting in the fast carbonation phase ($X_{ave,K}$) and the average particle conversion reacting in the diffusive phase ($X_{ave,D}$):

$$X_{ave} = X_{ave,K} + X_{ave,D} = f_a X|_{\leqslant t_K} + (1 - f_a) X|_{>t_K} \quad (14)$$

$$X|_{\leqslant t_K} = \frac{\int_0^{t_K} r_{ave,k}\, t\left(\frac{1}{\tau}\right) e^{-\frac{t}{\tau}} dt}{1 - e^{-\frac{t_K}{\tau}}} \quad (15)$$

$$X|_{>t_K} = X_{max,ave,K} + \frac{\int_{t_K}^{\tau} r_{ave,D}\, t\left(\frac{1}{\tau}\right) e^{-\frac{t}{\tau}} dt}{1 - e^{-\frac{t_K}{\tau}}} \quad (16)$$

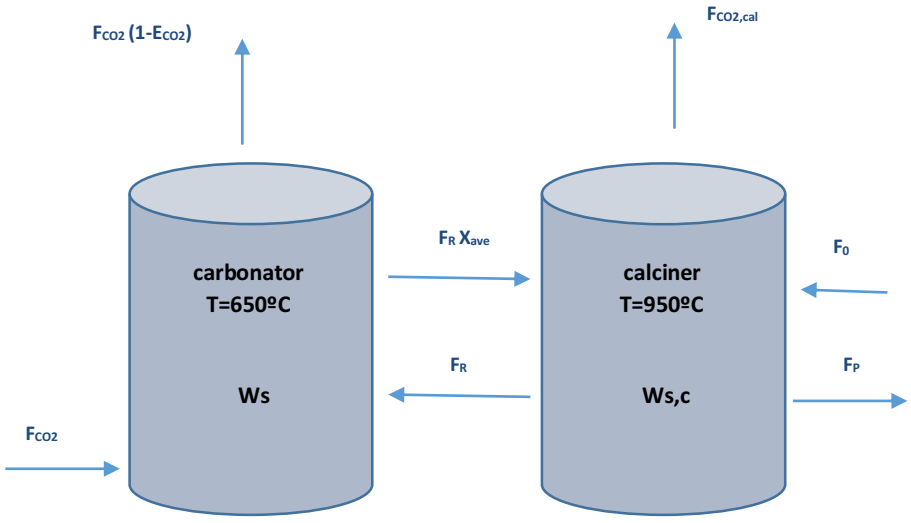

Fig. 6. Scheme of the CaL post-combustion capture model.

where $t_D = \tau - t_K$ and f_a is the fraction of particles reacting in the kinetic phase, which is given by [18]

$$f_a = \left(1 - e^{-\frac{t_K}{\tau}}\right) \tag{17}$$

The average surface area for reaction in the kinetic phase can be expressed by [44]:

$$S_{ave_K} = \frac{V_{M_{CaCO3}} X_{max,ave,K}}{M_{CaO} h} \rho_{CaO} \tag{18}$$

Since conversion is typically low except for the first cycles, Eq. (5) can be simplified by dismissing the dependence of the reaction rate on conversion as done in [18]. Thus, it is possible to express the average reaction rate in each carbonation phase as:

$$r_{ave_K} = k_s S_{ave_K} (C_{CO2} - C_{CO2eq}) \tag{19}$$

$$r_{ave_D} = D^*_{eff} (C_{CO2} - C_{CO2eq}) \tag{20}$$

The capture efficiency in the carbonator E_{CO2} can be calculated as [18]:

$$E_{CO2} = \frac{F_R}{F_{CO2}} X_{ave} \tag{21}$$

$$E_{CO2,K} = \frac{F_R}{F_{CO2}} X_{ave,K} \tag{22}$$

$$E_{CO2,D} = \frac{F_R}{F_{CO2}} X_{ave,D} \tag{23}$$

where the capture efficiency in the fast phase ($E_{CO2,K}$) and the diffusive phase ($E_{CO2,D}$) have been considered as separate contributions in order to evaluate their relative importance.

Assuming that the gas passes in plug flow through a bed of perfectly mixed solids, the carbon mass balance in the gas phase in a differential element of the carbonator reactor can be written as:

$$F_{CO2} \frac{dE_{CO2}}{dz} = A \frac{\rho_{CaO}}{V_{M_{CaO}}} (f_a r_{ave_K} + (1 - f_a) r_{ave_D}) \tag{24}$$

Integrating Eq. (24) along the carbonation reactor, it results

$$\psi = \left[-\frac{f_0}{f_0 f_e - f_0} E_{CO2} + \frac{f_0 (f_0 - 1)}{(f_0 f_e - f_0)^2} \ln \left(\frac{(f_0 - f_e) + (f_0 f_e - f_0) E_{CO2}}{f_0 - f_e} \right) \right] \tag{25}$$

where

$$z = \frac{F_{CO2} \cdot M_{CaO}}{W_s \cdot \rho_g \cdot (S_{ave_K} \cdot f_a \cdot k_s + D_{eff_{sim}} \cdot (1 - f_a))} \psi \tag{26}$$

and f_e and f_0 are the equilibrium and inlet molar fraction of CO_2, respectively.

Table 2
Values of the parameters used for the calculation of capture efficiency.

Parameter	Value	References
m_{CO2}/MW (kg/s)	0.1	[18]
f_0	0.15	[18]
P (bar)	1	[18]
T (°C)	650	[18]
h (nm)	50	[18,40]
K_s (m^4/mol s)	4×10^{-10}	[18]

4. Model results

A series of parametric calculations have been carried out to determine the CO_2 capture efficiency of the carbonator under different operating conditions. The calculations are made for a typical coal combustion power plant using a value of 0.15 for the volumetric fraction of CO_2 in the flue gas entering the carbonator and a flow rate F_{CO2} = 0.1 kg CO_2/s as typical values [18].

In the first run we will use as key input parameters the solid inventory in the carbonator reactor (W_s), the flow rate of fresh limestone makeup (F_0) fed into the calciner and the flow rate of solids entering the carbonator coming from the calciner (F_R). As for the rest of parameters, the same representative values employed in previous works [18] will be used (Table 2). Figs. 7 and 8 show the calculated capture efficiency as function of the total solid inventory in the reactor W (normalized per MWth) for different values of F_R and F_0.

As seen in Figs. 7 and 8, the model proposed in this paper yield results which are less sensitive than those obtained from the reference model [18] to changes in the solids recirculation flow rate (F_R) and the flow rate of fresh limestone introduced in the cycle (F_0). On the other hand, for fixed values of F_0, increasing the solids inventory in the carbonator yields a significant increase of the capture efficiency as a result of having considered the enhanced conversion in the diffusive phase. According to the reference model [18], increasing the solids inventory over a certain value does not lead to an increase of the carbonation efficiency despite it has not reached the maximum attainable value (≈0.92) according to the inlet and equilibrium CO_2 concentration for the carbonation reaction at 650 °C. This would be the maximum capture efficiency

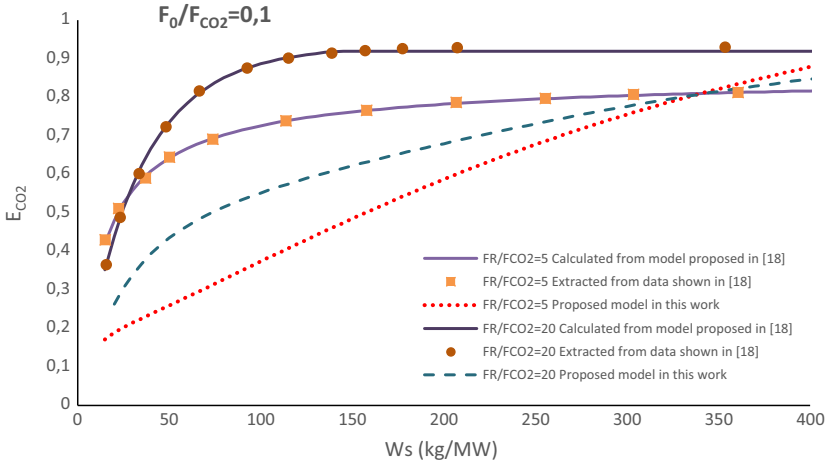

Fig. 7. Capture efficiency calculated as a function of the solids inventory in the carbonator for different F_R/F_{CO2} ratios according to the model presented in [18] and the new model proposed in this work.

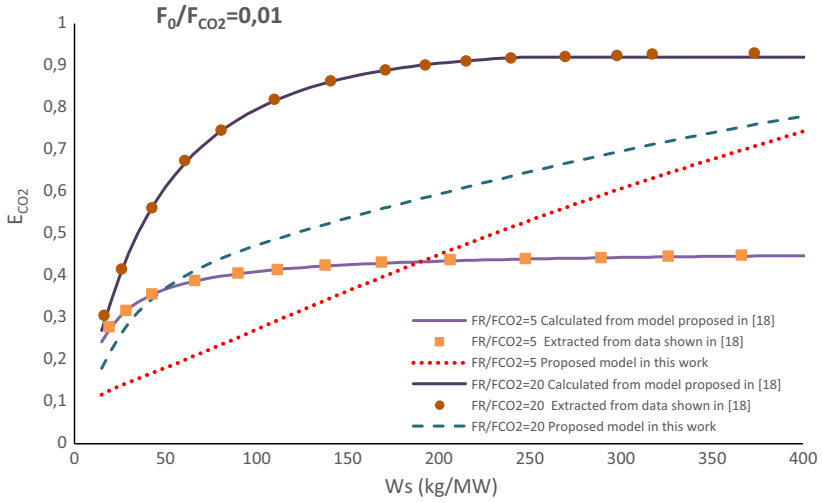

Fig. 8. Carbonation efficiency as a function of the solids inventory in the carbonator at different F_R/F_{CO2} ratios according to the model presented in [18] and the new model proposed in this work.

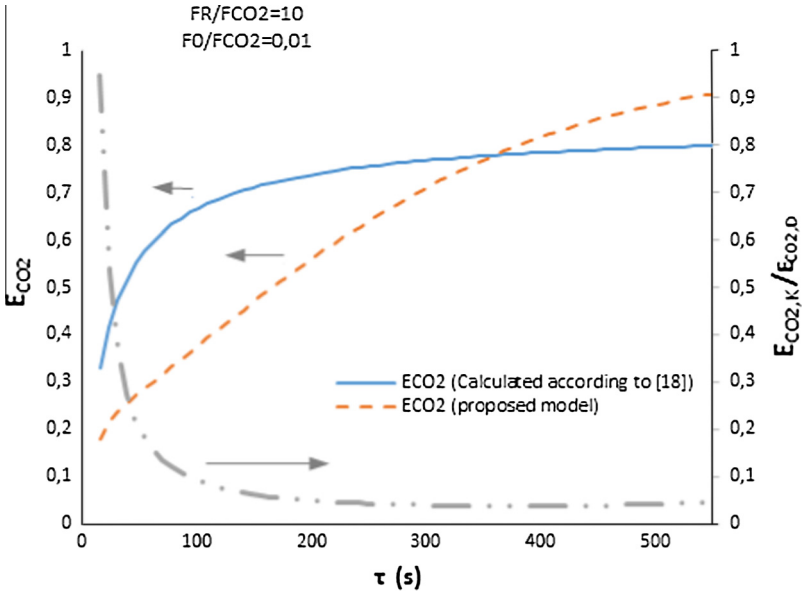

Fig. 9. Left axis: carbonation efficiency as a function of the residence time in the reactor (modifying the solids inventory, Eq. (13)). Right axis: ratio of CO_2 capture efficiency in the kinetic controlled phase to carbonation efficiency in the diffusion controlled phase as a function of residence time. Calculations are made for fixed values of F_R/F_{CO2} and F_0/F_{CO2} as indicated.

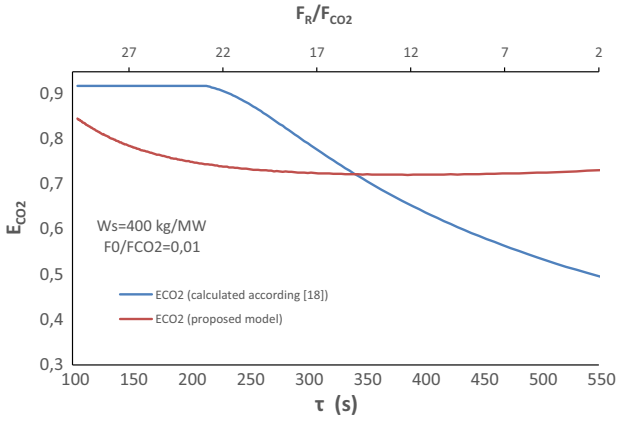

Fig. 10. Carbonation efficiency as a function of the residence time in the carbonator, which is varied by changing the F_R/F_{CO2} ratio (upper horizontal axis). Calculations made for fixed values of W_s and F_0/F_{CO2} as indicated.

achievable if the solids had fully reacted, which is not theoretically allowed if carbonation in the diffusion controlled phase is fully neglected as assumed in previous modelling works [18]. In the reference model [18] the active fraction of solids drops significantly after a short time once the kinetic controlled phase is ended. In contrast, the solids are considered to remain active for a long time in the proposed model in the present work as long as the subsequent carbonation in the diffusion controlled phase is taking place.

Figs. 7 and 8 demonstrate that our model predicts a greater capture efficiency for longer residence times of the particles in the carbonator. For example, Fig. 8 shows that for a ratio $F_R/F_{CO2} = 5$, and a solids inventory of about 200 kg/MW, the proposed model predicts a higher capture efficiency than the reference model [18]. Fig. 9 shows the capture efficiency calculated as a function of the residence time in the carbonator using $F_R/F_{CO2} = 5$ and $F_0/F_{CO2} = 0.01$ and varying the value of solids inventory, which changes the residence time τ (Eq. (13)). This figure shows also the ratio of the carbonation efficiency in the kinetic controlled phase to that in the diffusion controlled phase (right axis).

Fig. 9 shows that, according to the reference model [18], the capture efficiency is not improved further after a residence time of about 300 s since the fraction of active particles (considered as only those able to react in the fast phase) diminishes with time quickly. On the other hand, the capture efficiency is further improved by taking into account enhanced conversion in the diffusive phase as shown by the results obtained from the model proposed. As can be seen in Fig. 9 the capture efficiency in the diffusive phase ($E_{CO2,D}$) becomes the major contribution to the total carbonation efficiency just after tens of seconds. Besides, the capture efficiency continues to increase with the residence time and may reach a rather high value at residence times above 500 s.

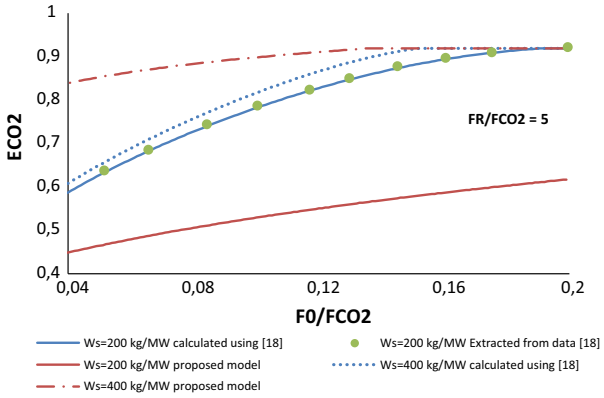

Fig. 11. Capture efficiency as a function of the ratio of makeup flow rate to CO_2 flow rate (F_0/F_{CO2}) at different solid inventories (W_s) and ratios of the recirculation flow rate to CO_2 flow rate (F_R/F_{CO2}). Results from the proposed model in this work are compared with results from the model presented in a previous work [18].

Table 3
Operating conditions used in the simulations whose results are plotted in Fig. 12.

V_{gas} = 1.15 (m^3/s)/MW				
f_0 = 0.15				
W_s (kg/MW) = 100–800				
	Condition 1	Condition 2	Condition 3	Condition 4
F_R/F_{CO2}	5	10	5	10
F_0/F_{CO2}	0.1	0.1	0.01	0.01

Fig. 10 shows the effect on the capture efficiency of increasing the residence time (horizontal bottom axis) by decreasing the flow rate of recirculated solids between the reactors (F_R, horizontal top axis) while maintaining fixed a value for the solids inventory. As may be observed, by taking into account conversion in the diffusive phase, the capture efficiency is notably increased by increasing the value of the average residence time of the particles (τ) while the solids recirculation flow rate is decreased (with a constant value of solids inventory in the carbonator). An additional benefit of reducing the recirculation flow rate can be that the solids activity would be extended for longer times since the frequency of calcinations is reduced, which would serve to minimize the makeup flow of fresh limestone needed.

The results plotted in Fig. 11 correspond to simulations in which the solids recirculation flow rate F_R is kept fixed while the flow rate of limestone makeup into the calciner (F_0) is varied. Interestingly, it is seen that high capture efficiency may be achieved by operating with low values of F_0 when W_s is increased as a consequence of having extended the lifetime of the particles that remain active in the carbonator by virtue of diffusive carbonation. We must note, however, that neither sulphation nor ashes, which will reduce the activity of the sorbent, have been considered in the model. An additional makeup flow of fresh limestone will have to be employed in practice due to irreversible sulphation and deactivation by ashes as reported in many studies [7,16,25,45–47].

Let us now compare predicted results by the proposed model with experimental results obtained from pilot-scale tests. Capture efficiency obtained in pilot-scale tests is usually reported as a function of an "active space time" [13,14,28], which is expressed as the product of the residence time times the fraction of active particles reacting in the fast stage and the average conversion in this stage $\tau_a = \tau f_a X_{ave,K}$. Taking into account also carbonation in the diffusive phase, τ_a would be defined in our model as [28]

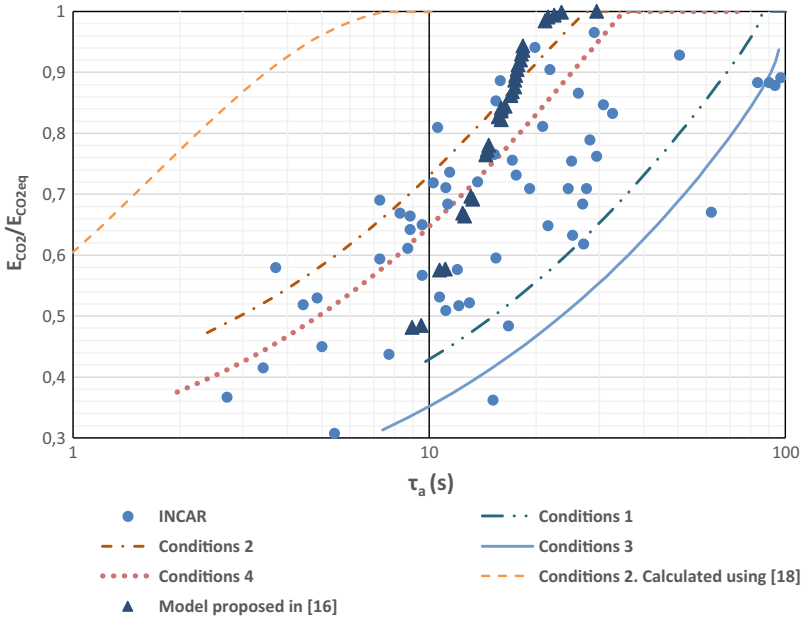

Fig. 12. Normalized capture efficiency as a function of the active space time. Results obtained from the proposed model in this work using diverse operating conditions (displayed in Table 3) are compared with results obtained from previous models [16] [18] and with experimental data reported from pilot-scale INCAR tests [28].

$$\tau_a = \tau(f_a X_{ave,K} + (1 - f_a) X_{ave,D}) \quad (27)$$

Table 3 shows the operating conditions used in the simulations whose results are illustrated in Fig. 12. This figure shows experimental values of the carbonation efficiency obtained from the pilot-scale INCAR plant and reported in [14,19,28]. The operating conditions used in the simulations have been chosen as representatives of those reported at INCAR pilot-scale tests [14,28].

As can be seen in Fig. 12 the model developed in the present work provides results that conform better to experimental results as compared to the results obtained from the previously proposed model by Alonso et al. [18], which predict higher capture efficiencies than the experimental ones. Results extracted from a model proposed by Romano [16], which takes into account the effect of ash, irreversible sulphation, and fluidized bed dynamics have been also plotted in Fig. 12. Romano also neglects carbonation in the diffusion phase and uses CaO multicyclic conversion data derived from tests in which calcination was carried out under low CO_2 partial pressure [33]. Although Romano's model results fit to the experimental results within the data scatter, it may be seen that the carbonation efficiency is predicted to increase with the active residence time at a higher rate than the experimentally observed trend (Fig. 12). Arguably, the key point enabling our model to reproduce the experimental trend is to include CaO conversion in the diffusion phase, which brings about a non-negligible contribution to the carbonation efficiency. As pointed out by Charitos et al. [28], the particle fraction that would be reacting in the diffusion regime can be much higher than the active fraction reacting in the fast regime. Moreover, as reviewed in the introduction of the present work, carbonation in the diffusion regime is greatly enhanced when calcination is carried out under high CO_2 concentration. The new model takes into account these relevant aspects in order to predict more realistic values for the capture efficiency. A subject for further work would be to incorporate into our model the effect of irreversible sulphation, ashes and fluidized bed dynamics.

5. Conclusions

Carbonator models formulated until now are based on lab-scale multicyclic CaO conversion results carried out by regenerating CaO under low CO_2 partial pressure. Under these unrealistic conditions, carbonation in the kinetically controlled fast phase prevails on diffusive carbonation. Thus, these models neglect further carbonation of the particles once the fast carbonation stage is ended. However, calcination under realistic CaO regeneration conditions, involving a high CO_2 partial pressure in the calcination environment, leads to a significant enhancement of CaO carbonation in the diffusion controlled phase as compared to the kinetically controlled fast phase, which is severely hindered. The new model proposed in this work is based on lab-scale multicyclic CaO conversion results in which calcination is carried out under high CO_2 partial pressure as expected in practice. Given the extraordinary relevance of carbonation in the diffusive phase observed under these realistic conditions, the model incorporates in the calculation of the capture efficiency this stage of carbonation. Thus, the particles are considered to remain active in the carbonator beyond the kinetically controlled carbonation phase, which is quite reduced. A main conclusion from the simulation results is that the capture efficiency is improved by increasing the residence time in the carbonator. For typical inventories of solids in the carbonator used in previous models, we see that the molar flow rate of CaO recirculated can be substantially decreased while a high capture efficiency is obtained. By increasing the residence time of the particles in the carbonator, deactivation due to sintering in the calciner would be mitigated. Furthermore, a smaller flow of recirculated solids would allow reducing energy penalties in the operation of power plants since the amount of heat required for calcination would be lowered and the energy necessary for material transport would be also reduced. In addition, a prolonged carbonation during extended residence times in the carbonator will allow extracting more heat from the reaction exothermicity. In a future work we plan to improve the proposed model by taking into account other aspects that will affect the carbonation efficiency at practice such as irreversible sulphation, deactivation by ashes and the effect of fluidization dynamics.

Acknowledgements

This work was supported by the Andalusian Regional Government Junta de Andalucia (contract FQM-5735), Spanish Government Agency Ministerio de Economia y Competitividad (contract CTQ2014-52763-C2-2-R).

References

[1] Change WGI of the IP on C. IPCC 2005: special report on carbon dioxide capture and storage, 2005.
[2] Romeo LM, Lara Y, Lisbona P, Martínez A. Economical assessment of competitive enhanced limestones for CO_2 capture cycles in power plants. Fuel Process Technol 2009;90:803–11. http://dx.doi.org/10.1016/j.fuproc.2009.03.014.
[3] Dean CC, Blamey J, Florin NH, Al-Jeboori MJ, Fennell PS. The calcium looping cycle for CO_2 capture from power generation, cement manufacture and hydrogen production. Chem Eng Res Des 2011;89:836–55. http://dx.doi.org/10.1016/j.cherd.2010.10.013.
[4] Martínez A, Lara Y, Lisbona P, Romeo LM. Energy penalty reduction in the calcium looping cycle. Int J Greenh Gas Control 2012;7:74–81. http://dx.doi.org/10.1016/j.ijggc.2011.12.005.
[5] Cormos C-C. Economic evaluations of coal-based combustion and gasification power plants with post-combustion CO_2 capture using calcium looping cycle. Energy 2014;78:665–73. http://dx.doi.org/10.1016/j.energy.2014.10.054.
[6] Wang W, Ramkumar S, Wong D, Fan LS. Simulations and process analysis of the carbonation–calcination reaction process with intermediate hydration. Fuel 2012;92:94–106. http://dx.doi.org/10.1016/j.fuel.2011.06.059.
[7] Manovic V, Anthony EJ. Competition of sulphation and carbonation reactions during looping cycles for CO_2 capture by cao-based sorbents. J Phys Chem A 2010;114:3997–4002. http://dx.doi.org/10.1021/jp910536w.
[8] Romano MC, Martínez I, Murillo R, Arstad B, Blom R, Ozcan DC, et al. Process simulation of Ca-looping processes: review and guidelines. Energy Proc 2013;37:142–50. http://dx.doi.org/10.1016/j.egypro.2013.05.095.
[9] Kim K, Kim D, Park Y, Soon K. International journal of greenhouse gas control a solid sorbent-based multi-stage fluidized bed process with inter-stage heat integration as an energy efficient carbon capture process. Int J Greenh Gas Control 2014;26:135–46. http://dx.doi.org/10.1016/j.ijggc.2014.03.012.
[10] Ylätalo J, Ritvanen J, Tynjälä T, Hyppänen T. Model based scale-up study of the calcium looping process. Fuel 2014;115:329–37. http://dx.doi.org/10.1016/j.fuel.2013.07.036.
[11] Ylätalo J, Parkkinen J, Ritvanen J, Tynjälä T, Hyppänen T. Modeling of the oxy-combustion calciner in the post-combustion calcium looping process. Fuel 2013;113:770–9. http://dx.doi.org/10.1016/j.fuel.2012.11.041.
[12] Vorrias I, Atsonios K, Nikolopoulos A, Nikolopoulos N, Grammelis P, Kakaras E. Calcium looping for CO_2 capture from a lignite fired power plant. Fuel 2013;113:826–36. http://dx.doi.org/10.1016/j.fuel.2012.12.087.
[13] Dieter H, Bidwe AR, Varela-duelli G, Charitos A, Hawthorne C. Development of the calcium looping CO_2 capture technology from lab to pilot scale at IFK, University of Stuttgart. Fuel 2014;127:23–37. http://dx.doi.org/10.1016/j.fuel.2014.01.063.
[14] Arias B, Diego ME, Abanades JC, Lorenzo M, Diaz L, Martínez D, et al. Demonstration of steady state CO_2 capture in a 1.7MWth calcium looping pilot. Int J Greenh Gas Control 2013;18:237–45. http://dx.doi.org/10.1016/j.ijggc.2013.07.014.
[15] Lasheras A, Ströhle J, Galloy A, Epple B. Carbonate looping process simulation using a 1D fluidized bed model for the carbonator. Int J Greenh Gas Control 2011;5:686–93. http://dx.doi.org/10.1016/j.ijggc.2011.01.005.
[16] Romano MC. Modeling the carbonator of a Ca-looping process for CO_2 capture from power plant flue gas. Chem Eng Sci 2012;69:257–69. http://dx.doi.org/10.1016/j.ces.2011.10.041.
[17] Romano M, Martínez I, Murillo R, Arstad B. Guidelines for modeling and simulation of Ca-looping processes. Prepared for the European Energy Research Alliance. SintefNo, 2012.
[18] Alonso M, Rodríguez N, Grasa G, Abanades JC. Modelling of a fluidized bed carbonator reactor to capture CO_2 from a combustion flue gas. Chem Eng Sci 2009;64:883–91. http://dx.doi.org/10.1016/j.ces.2008.10.044.
[19] Alonso M, Rodríguez N, González B, Grasa G, Murillo R, Abanades JC. Carbon dioxide capture from combustion flue gases with a calcium oxide chemical

loop. Experimental results and process development. Int J Greenh Gas Control 2010;4:167–73. http://dx.doi.org/10.1016/j.ijggc.2009.10.004.
[20] Alonso M, Diego ME, Pérez C, Chamberlain JR, Abanades JC. Biomass combustion with in situ CO_2 capture by CaO in a 300 kWth circulating fluidized bed facility. Int J Greenh Gas Control 2014;29:142–52. http://dx.doi.org/10.1016/j.ijggc.2014.08.002.
[21] Ströhle J, Junk M, Kremer J, Galloy A, Epple B. Carbonate looping experiments in a 1 MWth pilot plant and model validation. Fuel 2014;127:13–22. http://dx.doi.org/10.1016/j.fuel.2013.12.043.
[22] Valverde JM, Sanchez-Jimenez PE, Perez-Maqueda La. Limestone calcination nearby equilibrium: kinetics, CaO crystal structure, sintering and reactivity. J Phys Chem C 2015;119:1623–41. http://dx.doi.org/10.1021/jp508745.
[23] Coppola A, Scala F, Salatino P, Montagnaro F. Fluidized bed calcium looping cycles for CO_2 capture under oxy-firing calcination conditions: part 1. Assessment of six limestones. Chem Eng J 2013;231:537–43. http://dx.doi.org/10.1016/j.cej.2013.07.11.
[24] Manovic V, Charland JP, Blamey J, Fennell PS, Lu DY, Anthony EJ. Influence of calcination conditions on carrying capacity of CaO-based sorbent in CO_2 looping cycles. Fuel 2009;88:1893–900. http://dx.doi.org/10.1016/j.fuel.2009.04.012.
[25] Cordero JM, MA. Modelling of the kinetics of sulphation of CaO particles under CaL reactor conditions. Fuel 2015;150:501–11. http://dx.doi.org/10.1016/j.fuel.2015.02.075.
[26] Valverde JM. Relevant influence of limestone crystallinity on CO_2 Capture in The Ca-Looping technology at realistic calcination conditions, 2014.
[27] Martínez I, Grasa G, Murillo R, Arias B, Abanades JC. Modelling the continuous calcination of $CaCO_3$ in a Ca-looping system. Chem Eng J 2013;215–216:174–81. http://dx.doi.org/10.1016/j.cej.2012.09.134.
[28] Charitos A, Rodríguez N, Hawthorne C, Alonso M, Zieba M, Arias B, et al. Experimental validation of the calcium looping CO_2 capture process with two circulating fluidized bed carbonator reactors. Ind Eng Chem Res 2011;50:9685–95. http://dx.doi.org/10.1021/ie200579f.
[29] Shimizu T, Hirama T, Hosoda H, Kitano K, Inagaki M, Tejima K. A twin fluid-bed reactor for removal of CO_2 from combustion processes. Chem Eng Res Des 1999;77:62–8. http://dx.doi.org/10.1205/026387699525882.
[30] Abanades JC. The maximum capture efficiency of CO_2 using a carbonation/calcination cycle of CaO/ $CaCO_3$. Chem Eng J 2002;90:303–6. http://dx.doi.org/10.1016/S1385-8947(02)00126-2.
[31] Abanades JC, Alvarez D. Conversion limits in the reaction of CO_2 with lime. Energy Fuels 2003;17:308–15. http://dx.doi.org/10.1021/ef020152a.
[32] Borgwardt RH. Calcium oxide sintering in atmospheres containing water and carbon dioxide. Ind Eng Chem Res 1989;28:493–500. http://dx.doi.org/10.1021/ie00088a019.
[33] Grasa GS, Abanades JC. CO_2 capture capacity of CaO in long series of carbonation/calcination cycles. Ind Eng Chem Res 2006;45:8846–51. http://dx.doi.org/10.1021/ie0606946.
[34] Valverde JM. A model on the CaO multicyclic conversion in the Ca-looping process. Chem Eng J 2013;228:1195–206. http://dx.doi.org/10.1016/j.cej.2013.05.023.
[35] Valverde JM, Sanchez-Jimenez PE, Perez-Maqueda La. Role of precalcination and regeneration conditions on post combustion CO_2 capture in the Ca-looping technology. Appl Energy 2014;136:347–56. http://dx.doi.org/10.1016/j.apenergy.2014.09.05.
[36] Arias B, Abanades JC, Grasa GS. An analysis of the effect of carbonation conditions on CaO deactivation curves. Chem Eng J 2011;167:255–61. http://dx.doi.org/10.1016/j.cej.2010.12.052.
[37] Mess D, Sarofim AF, Longwell JP. Product layer diffusion during the reaction of calcium oxide with carbon dioxide. Energy Fuels 1999;13:999–1005. http://dx.doi.org/10.1021/ef980266f.
[38] Bhatia SK, Perlmutter DD. Effect of the product layer on the kinetics of the carbon dioxide-lime reaction. AIChE J 1983;29:79–86. http://dx.doi.org/10.1002/aic.690290111.
[39] Alvarez D, Abanades JC. Determination of the critical product layer thickness in the reaction of CaO with CO_2. Ind Eng Chem Res 2005;44:5608–15. http://dx.doi.org/10.1021/ie050305s.
[40] Li Z, Fang F, Xiao-yu T, Cai N. Effect of temperature on the carbonation reaction of CaO with CO_2. Energy Fuels 2012;26:4607–16. http://dx.doi.org/10.1021/ef300607z.
[41] Sun Z, Luo S, Qi P, Fan LS. Ionic diffusion through Calcite ($CaCO_3$) layer during the reaction of CaO and CO_2. Chem Eng Sci 2012;81:164–8. http://dx.doi.org/10.1016/j.ces.2012.05.042.
[42] Sanchez-Jimenez PE, Valverde JM, Perez-Maqueda La. Multicyclic conversion of limestone at Ca-looping conditions: the role of solid-sate diffusion controlled carbonation. Fuel 2014;127:131–40. http://dx.doi.org/10.1016/j.fuel.2013.09.06.
[43] Valverde JM, Sanchez-Jimenez PE, Perez-Maqueda La. Calcium-looping for post-combustion CO_2 capture. On the adverse effect of sorbent regeneration under CO_2. Appl Energy 2014;126:161–71. http://dx.doi.org/10.1016/j.apenergy.2014.03.08.
[44] Grasa GS, Abanades JC, Alonso M, González B. Reactivity of highly cycled particles of CaO in a carbonation/calcination loop. Chem Eng J 2008;137:561–7. http://dx.doi.org/10.1016/j.cej.2007.05.017.
[45] Symonds RT, Lu DY, Manovic V, Anthony EJ. Pilot-scale study of CO_2 capture by CaO-based sorbents in the presence of steam and SO_2. Ind Eng Chem Res 2012;51:7177–84. http://dx.doi.org/10.1021/ie2030129.
[46] Ryu HJ, Grace JR, Lim CJ. Simultaneous CO_2/SO_2 capture characteristics of three limestones in a fluidized-bed reactor. Energy Fuels 2006;20:1621–8. http://dx.doi.org/10.1021/ef050277q.
[47] Sun P, Grace JR, Lim CJ, Anthony EJ. Removal of CO_2 by calcium-based sorbents in the presence of SO_2. Energy Fuels 2007;21:163–70. http://dx.doi.org/10.1021/ef060329r.
[48] Tian S, Jiang J, Li K, Yan F, Chen X. Performance of steel slag in carbonation–calcination looping for CO_2 capture from industrial flue gas. RSC Adv 2014;4:6858. http://dx.doi.org/10.1039/c3ra47426g.
[49] Valverde JM, Sanchez-Jimenez PE, Perez-Maqueda La. High and stable CO_2 capture capacity of natural limestone at Ca-looping conditions by heat pretreatment and recarbonation synergy. Fuel 2014;123:79–85. http://dx.doi.org/10.1016/j.fuel.2014.01.04.

***ANNEX 2**: Ortiz C, Chacartegui R, Valverde JM, Becerra JA. A new integration model of the calcium looping technology into coal fired power plants for* CO_2 *capture. Appl Energy 2016;169:408–20. doi:10.1016/j.apenergy.2016.02.050.*

Applied Energy 169 (2016) 408–420

Contents lists available at ScienceDirect

Applied Energy

journal homepage: www.elsevier.com/locate/apenergy

A new integration model of the calcium looping technology into coal fired power plants for CO_2 capture

C. Ortiz [a,*], R. Chacartegui [a], J.M. Valverde [b], J.A. Becerra [a]

[a] Energy Engineering Department, University of Seville, Camino de los descubrimientos s/n, 41092 Sevilla, Spain
[b] Faculty of Physics, University of Seville, Avenida Reina Mercedes s/n, 41012 Sevilla, Spain

HIGHLIGHTS

- A CaL-CFPP (coal fired power plant) integration model is proposed and efficiency penalty is estimated.
- Carbonation in the diffusion stage is considered to predict the capture efficiency.
- Low efficiency penalty may be achieved by operating with longer particles' residence time.
- Simulation results show that the energy penalty ranges between 4% and 7% points.

ARTICLE INFO

Article history:
Received 3 November 2015
Received in revised form 15 January 2016
Accepted 6 February 2016
Available online 21 February 2016

Keywords:
CO_2 capture
Ca-looping
Diffusion phase
Calcium looping
Coal power plants
Emissions

ABSTRACT

The Ca-Looping (CaL) process is at the root of a promising 2nd generation technology for post-combustion CO_2 capture at coal fired power plants. The process is based on the reversible and quick carbonation/calcination reaction of $CaO/CaCO_3$ at high temperatures and allows using low cost, widely available and non toxic CaO precursors such as natural limestone. In this work, the efficiency penalty caused by the integration of the Ca-looping technology into a coal fired power plant is analyzed. The results of the simulations based on the proposed integration model show that efficiency penalty varies between 4% and 7% points, which yields lower energy costs than other more mature post-combustion CO_2 capture technologies such as the currently commercial amine scrubbing technology. A principal feature of the CaL process at CO_2 capture conditions is that it produces a large amount of energy and therefore an optimized integration of the systems energy flows is essential for the feasibility of the integration at the commercial level. As a main novel contribution, CO_2 capture efficiency is calculated in our work by considering the important role of the solid-state diffusion controlled carbonation phase, which becomes relevant when CaO regeneration is carried out under high CO_2 partial pressure as is the case with the CaL process for CO_2 capture. The results obtained based on the new model suggest that integration energy efficiency would be significantly improved as the solids residence time in the carbonator reactor is increased.

1. Introduction

The potential application of the recently emerged Ca-Looping (CaL) technology for post-combustion CO_2 capture is increasingly gaining momentum in the last years mainly due to the possibility of implementing it in already existing power plants as a retrofit with a relatively low penalty on plant performance as compared to other already mature capture technologies such as conventional amine-based capture systems (penalty around 8–12.5%) [1,2]. Basically, the CaL process consists of the capture of CO_2 in the post-combustion flue gas by carbonation in a high temperature fluidized bed reactor of CaO solids derived from the calcination of natural limestone ($CaCO_3$). Another CaO precursor could be natural dolomite. According to recent lab-scale studies [3], dolomitic lime would exhibit a greater capture capacity than lime at CaL conditions for CO_2 capture. On the other hand, several synthetics sorbents have been developed with enhanced capture behavior [4,5]. Nevertheless, the use of these synthetic sorbents usually leads to an important increase of the cost of the system operation [6]. Taking into account that flue gases exiting from coal-fired power plants generally contain a mole fraction of CO_2 in the range 10–15% [7,8], optimum carbonation temperatures are about 650 °C in order to achieve significant efficiencies of CO_2 capture (around 80–90%) in short residence times [9]. The carbonated solids are calcined in a second fluidized bed reactor (calciner) at higher

* Corresponding author. Tel.: +34 655783930.
E-mail address: cortiz7@us.es (C. Ortiz).

http://dx.doi.org/10.1016/j.apenergy.2016.02.050
0306-2619/

Notation

E	emissions ratio after CaL, kg CO_2/kWh$_e$
E_{CO2}	carbon capture efficiency
E_{ref}	emissions ratio before CaL, kg CO_2/kWh$_e$
F_{CO2}	mole flow of CO_2 in flue gas entering the carbonator
F_O	mole flow of fresh makeup limestone, mol/s
F_P	mole flow of fresh makeup limestone, mol/s
F_R	mole flow of CO_2 in flue gas entering the carbonator
$\dot{m}_{coal}$	coal mass flow, tonne/h
$\dot{m}_{solids,in}$	solids mass flow entering into the carbonator, tonne/h
$\dot{m}_{vap}$	total steam mass flow, tonne/h
N	calcination–carbonation cycle number
N_{Ca}	number of mols of Ca in the carbonator, mol
P	pressure, bar
P_{CO2}	CO_2 partial pressure
P_{vv}	live steam pressure, bar
Q	general heat flow, MW
$\dot{Q}_{CaL}$	heat consumption in the calciner, MW
$\dot{Q}_{carb}$	heat generated in the carbonator, MW
$\dot{Q}_{CFPP}$	reference plant heat consumption, MW
T	temperature, °C
T_{vv}	live steam temperature, °C
t	time, s
$\dot{W}_{ASU}$	power consumption in the ASU, MW
$\dot{W}_{Bi}$	power consumption in the pump i, MW
$\dot{W}_{ASU}$	power consumption in the ASU, MW
$\dot{W}_{Bi}$	power consumption in the pump i, MW
$\dot{W}_{gen,CaL}$	generated power in the CaL process, MW
$\dot{W}_{COM3}$	CO_2 recycle compressor power, MW
$\dot{W}_{CO2-COMP}$	CO_2 storage compressor power, MW
$\dot{W}_{cons,Cal}$	power consumption in the CaL cycle, MW
$\dot{W}_{FG-COMP}$	flue gas compressor power, MW
$\dot{W}_{CFPP}$	reference plant generated power, MW
Ws	solid inventory in the carbonator per MW of a typical power plant, kg
$\dot{W}_{sólid}$	power consumption in solids transport, MW
$\dot{W}_{steam\,cycle}$	power generate in the steam cycle, MW
$\dot{W}_{tur,i}$	power generate in the turbine i, MW
X	carbonation degree of a CaO particle
$X_{calciner}$	calciner efficiency
$\Delta P_{tur,i}$	pressure change in the turbine i, bar
τ	average residence time in the carbonator, s
η_{ref}	reference plant efficiency
η_{plant}	new global efficiency value in the cycle

Acronyms – Equipment

B2	pump for make-up water flow
B3	pump at secondary steam cycle
BOM1	pump at secondary steam cycle
CALCINER	calciner reactor
CARB	carbonator reactor
COM3	CO_2 stream recycle compressor
CYC1	cyclone linked to calciner
CYC2	cyclone linked to carbonator
DECOMP	auxiliary equipment for simulation model
FG-COMP	flue gas compressor
HEEXT-i	gas–gas heat exchanger
HE-FG	gas–solid heat exchanger
HE5	condenser
HE11	gas–solid heat exchanger
HE20	gas–gas heat exchanger
GASI	degasifier
M1	mixer
MX4	mixer
MXH	mixer
MXL	mixer
PRECAL	gas–liquid heat exchanger
SAT	evaporator
SOBRE	gas–gas heat exchanger
SP	mixer
TUR	high pressure steam turbine
TUR2	low pressure steam turbine
Val-i	expansion valve number i

Acronyms – Streams

CAL-OUT	stream exiting the carbonator
CARB-IN	solids entering into the carbonator
CARB-OUT	stream exiting the carbonator
CO2-INSTO	CO_2 stream exiting the calciner to storage
CO2-STO2	CO_2 stream entering into the HE20 equipment
CO2-STO3	CO_2 stream entering into the re-heater
CO2-STO4	CO_2 stream exiting the re-heater
CO2-COM1	CO_2 stream exiting the HE-FG equipment
CYC1-G	gas stream exiting the CYC1 equipment
CYC1-S	solid stream exiting the CYC1 equipment
CYC2-G	gas stream exiting the CYC2 equipment
CYC2-S	solid stream exiting the CYC2 equipment
DRY-COAL	coal entering into the CaL system
EXT i-j	extraction flow
FG-IN	flue gas entering into the carbonator
FG-PLANT	flue gas exiting the coal power plant
FGPLAN2	compressed flue gas
FGPLAN3	flue gas entering into the HE-FG equipment
FG-OUT2	flue gas entering into the preheater
FG-OUT2	flue gas exiting CaL system
GASI-G	gas stream exiting the GASI equipment
GASI-L	liquid stream exiting the GASI equipment
H2O-1	water stream entering into the condenser
H2O-2	water stream exiting into the condenser
H2O-REP i	water makeup flow
INCALC	auxiliary stream for simulation model
MAKEUP	makeup flow of fresh limestone
O2	O_2 stream entering into the calciner
OUTTUR1	steam flow exiting the TUR equipment
PURGE-i	purge stream flow
Q-CARB	total heat produced in the carbonator
Q-COMB	auxiliary stream for simulation model
REC-CO2	CO_2 stream recirculated into the calciner
REC-CO22	CO_2 stream entering into the calciner
Q-CARB	total heat produced in the carbonator
Q-COMB	auxiliary stream for simulation model
STACARB2	steam flow entering into the evaporator
STACARB3	steam flow exiting the evaporator
SOLIDSIN	solids entering into the calciner
VAP-IN	water stream entering into preheater
VAP2	water stream entering into evaporator
VAP3	steam flow entering into TUR
VAP5	water flow exiting the condenser
VAP6	water flow recirculated to steam production
VAP23	steam flow entering into super-heater
VAP566	water flow exiting the BOM1 equipment

temperatures, which regenerates CaO for a new cycle and produces a highly concentrated CO_2 stream ready for compression and sequestration. Importantly, CaO is regenerated in the calciner by calcination under necessarily high CO_2 partial pressure, which requires the use of rather high temperatures (>930 °C) for efficient calcination in a typically short residence time of a few minutes [10–13]. A number of pilot-scale plants (of size up to ~1–2 MW_{th}) have been erected worldwide in the last years demonstrating the potential suitability of the CaL process for post-combustion CO_2 capture [14].

Several models have been proposed in the literature aimed at predicting the efficiency penalty that arises from integrating the CaL technology in commercial power plants [14]. These models consider integration of CO_2 capture into coal fired power plants (CFPP) [15–18], lignite fired power plants (LFPP) [11], natural gas combined cycle power plants (NGCC) [19] and integrated gasification combined cycle power plants (IGCC) [20–23]. Depending on the power plant type, most results show efficiency penalties in the range 3–9% [6]. CaL integration studies are generally built upon equilibrium models for the calciner reactor [15,16,24]. As regards the carbonator, previous works have considered equilibrium models [20,25], semi-predictive models using the Kunni–Levenspiel formulation for the fluidized bed hydrodynamics [15,26] or an average conversion model [24]. Carbonator models generally use lab-scale experimental results for the multicyclic CaO conversion obtained from thermogravimetric analysis (TGA) whereby a limestone sample is subjected to a large number of carbonation/calcination cycles at controlled conditions of temperature and CO_2 partial pressure. In these tests, calcination is usually carried out under low CO_2 partial pressure due to technical limitations related to insufficiently fast heating/cooling rates of conventional ovens. If CaO solids are regenerated by calcination in a low CO_2 partial pressure environment most of the subsequent carbonation reaction in short residence times occurs on the surface of the CaO particles through a kinetically controlled fast phase [27]. Consequently, the CO_2 capture efficiency predicted by carbonator models based on these lab-scale results is hindered if the residence time of the CaO solids in the carbonator is extended beyond a period of just a few minutes. However, practical conditions to achieve a high CO_2 concentration stream in the calciner outlet generally involve calcination under high CO_2 pressure. Another feasible choice to carry out calcination would be to perform it in an environment of an easily separable gas from CO_2, e.g. superheated steam [28], which is an already available technology [29] at the commercial level (Catalytic Flash Calcination, CFC) for cement production. More recent TGA studies demonstrate that carbonation on the surface of the particles in the kinetically controlled fast phase is extraordinarily hampered when the solids are regenerated under high CO_2 pressure in accordance to realistic conditions. On the other hand, carbonation in the subsequent solid-state diffusion phase gains a substantial relevance [30,31]. A recent study that models the carbonator by using experimental results from TGA tests carried out under realistic calcination conditions shows that the CO_2 capture efficiency can be kept at high values if the residence time of the CaO solids in the carbonator is increased within the practical range of several minutes [32]. The present manuscript shows an integration study of the CaL technology for CO_2 capture in a CFPP using the carbonator model recently developed by Ortiz et al. [32] in which the relevance of the solids residence time in the carbonator as a critical parameter for the CaL capture performance is for the first time demonstrated.

2. Carbonator modeling approach for CaL integration into a CFPP

CO_2 capture efficiency in the present work is assessed by means of the carbonator model proposed by Ortiz et al. [32]. Fig. 1 (reproduced from [32]) shows experimental curves for CaO conversion as a function of time (dotted lines) and obtained from TGA tests whereby CaO is regenerated by calcination under high CO_2 partial pressure [30,31,33]. As can be seen, carbonation occurs through two well differentiated stages. A first fast stage that arises from carbonation on the surface of the CaO particles, and is controlled by the reaction kinetics, is followed by a relatively slower stage which is limited by solid-state diffusion of CO_2 across the product layer. As may be seen in Fig. 1, the contribution of the diffusion controlled phase to CaO conversion, which has been dismissed in previous carbonator models, is quite relevant, being it of the same order than CaO conversion in the kinetically controlled phase for the 5 min overall carbonation periods of the experiments. Thus, a prolongation of the carbonation residence time leads to a substantial increase of CaO conversion since carbonation in the diffusive phase grows roughly linearly with time in the typical range of solids residence time of a few minutes [33]. Remarkably, this is against the widely accepted conception that once the fast kinetically controlled phase is completed, additional carbonation by solid-state diffusion is negligible, which is based on experimental tests in which the sorbent is regenerated by calcination under unrealistically low CO_2 partial pressure [27]. Thus, a main conclusion driven from the carbonator model proposed in [32] is that the CO_2 capture efficiency is maintained at an acceptably high value if the solids recirculation rate between the calciner and carbonator (F_R) is reduced, which yields an increase of the residence time of the solids in the carbonator. In contrast, previous models predicted a marked decrease of CO_2 capture efficiency if F_R was decreased since carbonation was thought to be limited to the short reaction controlled fast stage.

As obtained from the new carbonator model, Fig. 2 (reproduced from [32]) shows the effect on the CO_2 capture efficiency of increasing the solids residence time (horizontal bottom axis) in the carbonator by decreasing the flow rate of recirculated solids between the reactors (F_R, horizontal top axis) while keeping fixed a value for the solids inventory W_s. As may be observed, by taking into account conversion in the diffusive phase, the CO_2 capture efficiency is maintained roughly constant as the average solids residence time (τ) is increased by a reduction of the solids recirculation flow rate. An important benefit derived from reducing the solids recirculation flow rate would be that the lifetime of the particles in the CaL cycle could be prolonged since the frequency of calcinations would be reduced, which would help mitigating deactivation by sintering and irreversible sulfation in the calciner. This would serve to minimize the makeup flow of fresh limestone needed and therefore reduce the cost of the technology. Regarding to CaO deactivation, Zhao et al. [35] proposed to use the spent sorbent for the prior capture of sulfur oxides, which would yield a better resource utilization and a minor capture process cost. Arguably, a lower energy penalty would be achieved by increasing the residence time of the particles in the carbonator. A reduction of the solids recirculation flow rate between the reactors would further allow a reduction of the energy cost and size of the auxiliary equipment for the CaL cycle such as heat exchangers and cyclones, therefore lowering down the capital cost.

3. CaL-CFPP – integration model

3.1. Coal fired power plant (CFPP) description

A reference 505 MW_e coal fired power plant (CFPP) is used in our work for analyzing the energy penalty arising from the CaL integration [7]. Fig. 3 shows a schematic representation of the reference plant. The coal used is called Pittsburgh No. 8 whose composition is shown in Table 1. Data reported by Wang et al. [7] on the operation

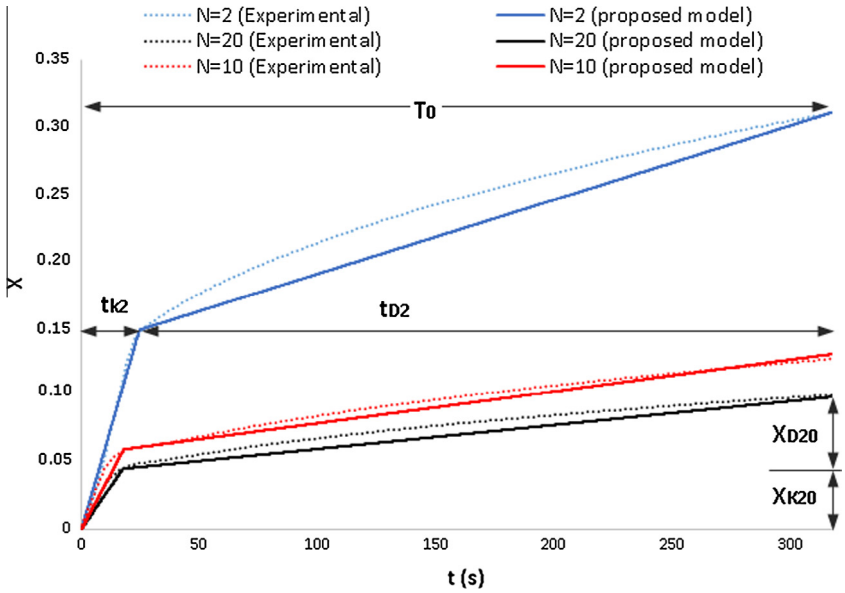

Fig. 1. CaO conversion as a function of carbonation time for different cycles ($N = 2$, 10, and 20) showing the kinetic model curves proposed in [32] (solid lines) and experimental data from TGA tests reported in [34] (dotted lines) in which calcination was carried out under high CO_2 concentration. Conversion (X) and time (t) in the reaction controlled (X_{NK}, t_K) and diffusion controlled (X_{ND}, t_D) carbonation phases are indicated for cycles 20 and 2, respectively. Reproduced from [32] with permission.

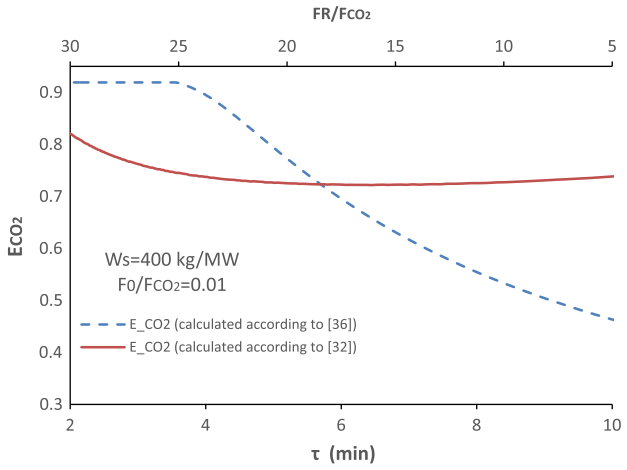

Fig. 2. Carbonation efficiency as a function of the solids residence time in the carbonator τ, which is varied by changing the ratio of the flow rate of recirculated solids between the reactors to the CO_2 flow rate (F_R/F_{CO2}, upper horizontal axis). Calculations made for fixed values of the solids inventory W_s and F_0/F_{CO2} as indicated (F_0 is the flow rate of fresh limestone makeup fed into the calciner). Results from the carbonator model used in the present work (developed in [32]) and a carbonator model previously proposed by other authors [36] are shown for comparison (reproduced from [32]).

parameters of this reference plant are employed. Combustion of 205 tonnes per hour of coal takes place in the steam boiler to generate 1335.7 MW_{th} with an 88.6% efficiency. For the steam cycle, a 42% thermal to electric steam turbine efficiency is assumed based on results reported for similar plants [18,37]. Considering a 10% of global process parasitic electricity consumption, the reference CFPP net power is 505 MW_e. Thus, a 33.5% overall plant efficiency is established [7]. The composition of the flue gas exiting the power plant, which is driven to the CaL cycle, is detailed in Table 2.

3.2. CaL integration

For the CaL-CFPP integration analysis, mass and energy balances in the process have been calculated by using the commercial software ASPEN PLUS™. A schematic view of the integration is shown in Fig. 3.

In order to simplify the model a number of main assumptions are made: (i) steady state operation is assumed, (ii) pressure losses in the heat exchanger equipment are neglected, (iii) solid–solid heat exchange is simulated as a transfer of heat between both solids, (iv) for all gas–solid heat exchangers an approach temperature of 10 °C is established, and (v) gas passes in plug flow through a bed of perfectly mixed solids in the reactors. For the sake of clarity, the integration scheme (Fig. 4) will be analyzed by dividing it into 3 main areas such as the carbonator, calciner and secondary steam cycle.

3.2.1. Carbonator model

In the carbonator reactor, the CaO particles entering it from the calciner (at a flow rate F_R) and those already present in the bed (N_{Ca}) react with the flue gas flowing into it from the coal-fired power plant. CO_2 capture in this reactor is modeled according to an equilibrium reactor following the study reported by Ortiz et al. [32]. The operating carbonator temperature is set to 650 °C and it works at atmospheric pressure. An inventory of solids in the carbonator bed (W_s) of 200 tonnes of solids (400 kg/MW_{el}) is considered as a typical value used in carbonator models [32,36,38]. The heat absorbed by the initial batch of solids to raise its operation temperature for the first time is not taken into account in the analysis since a steady operation regime is considered. Gas pressure loss across the carbonator reactor, which is operated in the continuous fluidized bed (CFB) regime, is calculated from the Kunii–Levenspiel (K–L) fluid dynamics model [39,40]. For the conditions of our simulation, the pressure loss across the carbonator reactor is about 100 mbar, making it necessary to use a compressor for the flue gas entering into it. In the carbonator model simulation carried out in the present work, sulfation of the solids is considered by setting a value of 99% for the SO_2 capture capacity [18,41,42].

According to the carbonator model reported in [32], CO_2 capture efficiency can be expressed as a function of the total solids inventory in the carbonator (W_s), the solids residence time in the carbonator (τ) and the flow rate of fresh limestone makeup fed into

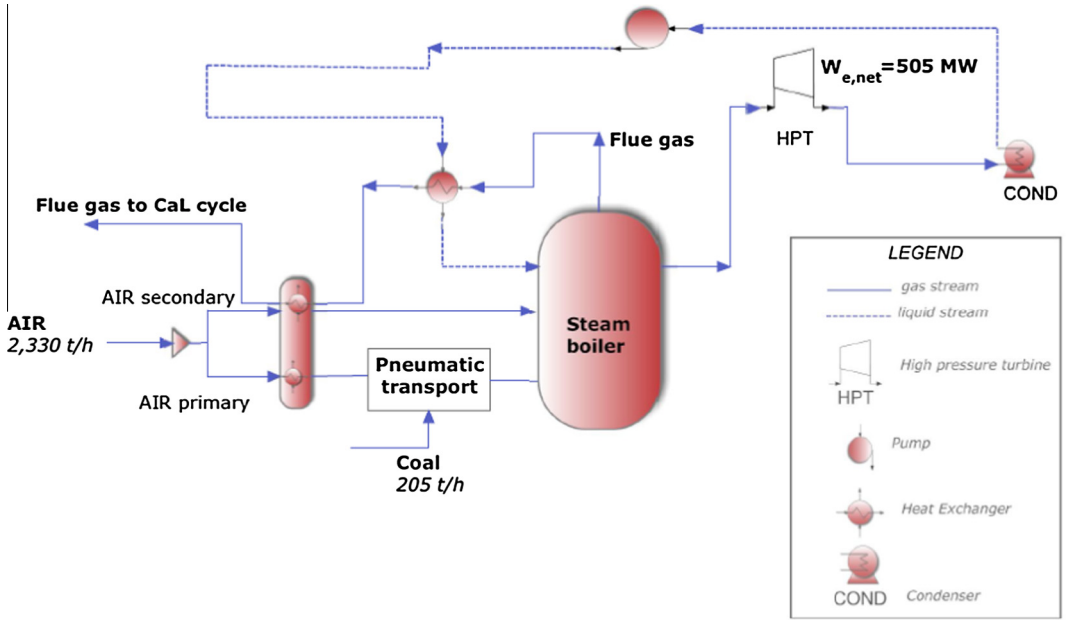

Fig. 3. Schematic representation of the coal fired power plant (CFPP) used as reference for the integration of the CaL cycle.

Table 1
Coal Pittsburgh No. 8 composition [3].

Proximate analysis	%weight (as-received)	%weight (dry)	Ultimate analysis	%weight (as-received)	%weight (dry)
Moisture	5.2	–	Moisture	5.2	–
Fixed carbon	48.1	50.7	Ash	8.6	9.1
Volatile matter	38.1	40.2	Carbon	70.2	74
Ash	8.6	9.1	Hydrogen	4.8	5.1
HHV (BTU/lb)	12.540	13.228	Nitrogen	1.5	1.6
			Chlorine	0	0
			Sulfur	2.2	2.3
			Oxygen	7.5	7.9

Table 2
Flue gas composition of reference CFPP plant [3].

Component	Flow (kmol/h)	Flow (t/h)
N_2	57752.53	1783.37
CO_2	10388.25	503.96
H_2O	4955.28	98.4
O_2	2632.11	92.84
CO	473.68	14.63
NO	455.71	15.07
SO_2	126.39	8.93
H_2	41.81	0.093
NO_2	0.20	0.01
SO_3	0.07	0.06
S	0.01	0.04
Total	76826.03	2517.3
Ash		17.69

the calciner (F_0), among other variables such as the multicyclic CaO conversion used or the calcination conditions. According to carbonator model results, by using limestone derived CaO as sorbent, a CO_2 capture efficiency of about 70–90% can be attained. The almost free CO_2 gas stream that exits the carbonator is sent to a series of heat exchangers (see Fig. 4) in order to recover its sensible heat before the gas is vented into the atmosphere.

As can be seen in Fig. 5, the post-combustion flue gas is preheated before entering into the carbonator reactor (FG-IN) through two heat exchangers (HE-FG and HE20) whereby heat is transferred from the CO_2 gas stream exiting the calciner previous to the storage stage (CO2-STO2) and from the calciner solids purge stream (PURGE3), respectively. The heat produced in the exothermic carbonation reaction, including the sensible heat recovered by the solids from the calciner (Q-CARB) is used in a secondary steam cycle for electricity generation. Given the large flow of solids recirculated between reactors in the CaL cycle, the energy production in the carbonator (and the energy consumption in the calciner) is rather high, which yields a power production in a secondary steam cycle similar to that produced in the reference power plant as obtained also from other previously published models [11,17]. This implies a significant penalty for the integration of the CaL cycle, albeit it could be reduced by inserting a heat exchanger between the solids leaving the calciner (F_R in Fig. 6, with a temperature of about 950 °C) and the solids entering into it that must be heated up to the calcination temperature as detailed in Fig. 6. For this same purpose, Martinez et al. have proposed the insertion of alternative heat exchange systems between the calciner and the carbonator such as a cyclonic preheater [43] or a mixing seal valve [44]. An important consideration is the possibility of recarbonation of the partially carbonated CaO particles when they enter into contact with the gas/solid stream exiting the calciner. According to Valverde et al. [31], recarbonation of the solids would have a relevant effect on their multicyclic conversion behavior that should be considered. A possible solution if recarbonation is to be avoided could be the use of an indirect contact solid–solid heat exchanger, or a coupled pair of efficient gas–solid heat exchangers. In order to simplify the integration model in our work, a simple solid–solid heat exchanger is assumed with an approach temperature of 20 °C. Thus, the energy transferred to the secondary steam cycle

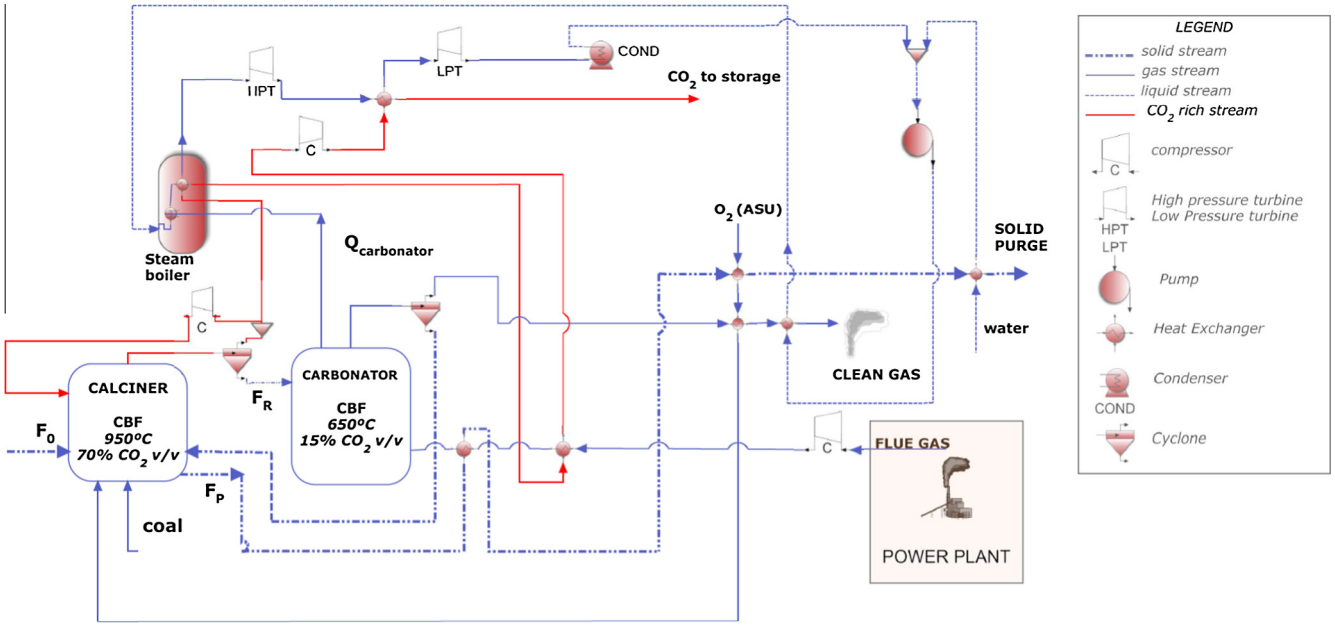

Fig. 4. General CFPP-CaL integration scheme.

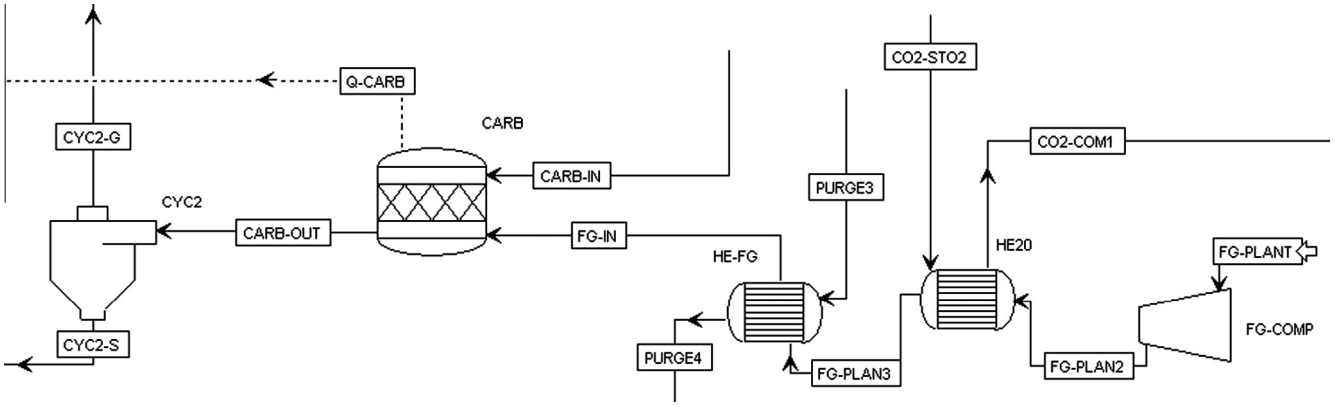

Fig. 5. Schematic representation of the carbonator zone used in the simulations.

is reduced, which lessens power generation from the CaL cycle and therefore allows for a smaller size of equipment and auxiliary systems. Both possible schemes (introducing or not the solids heat exchanger) are shown in Fig. 6. The sensitivity analysis that will be described in Section 4 is devoted to a comparison of the energy penalty that results from both options.

3.2.2. Calciner model

The partially carbonated solids at the carbonator outlet (CYC2-S in Fig. 7) are recirculated into another CFB reactor (the calciner), wherein CaO regeneration takes place through the endothermic calcination reaction at atmospheric pressure. Besides, a fresh makeup flow of limestone (MAKE-UP) that must be periodically introduced into the calciner to compensate for sorbent deactivation has to be also calcined (Fig. 7). As reported in previous works [26,45,46], for the calcination reaction to be fully achieved sufficiently fast in the calciner at atmospheric pressure under high CO_2 partial pressure, it must be operated at temperatures over ~930 °C. At this temperature, which is 30–50 °C above the calcination equilibrium temperature, full calcination of the solids is achieved in short residence times, which yields a sufficiently high calciner efficiency [47]. Increasing the calcination atmosphere pressure promotes sintering of the sorbent and requires the use of higher temperatures [48], which could be detrimental for the plant performance.

The imposition of a high calcination temperature makes it necessary to supply a large amount of heat to the calciner in order to achieve an acceptable calcination efficiency. This is accomplished by in-situ combustion of coal using pure O_2 (O2-IN). Oxy-combustion allows retrieving a CO_2 rich stream at the reactor outlet (70–90% v/v) for subsequent compression and storage (CO-INSTO). As a previous step to oxy-combustion, coal decomposition (DRY-COAL) into its elemental components (IN-CALC) is introduced in the simulation model as may be seen in Fig. 7. For simulating the oxy-combustion of coal in the calciner reactor a model based on chemical and phase equilibrium through Gibbs' free energy minimization methods is used. To obtain the necessary pure stream of O_2 for oxy-combustion in the calciner the most feasible option is to install an air separation unit (ASU). In this work, the energy penalty caused by this equipment is taken as 200 kWh per tonne of O_2 produced according to results from previous reports [42,49].

The necessary drying treatment of the gas stream exiting the calciner (before compression and storage) is not simulated in the

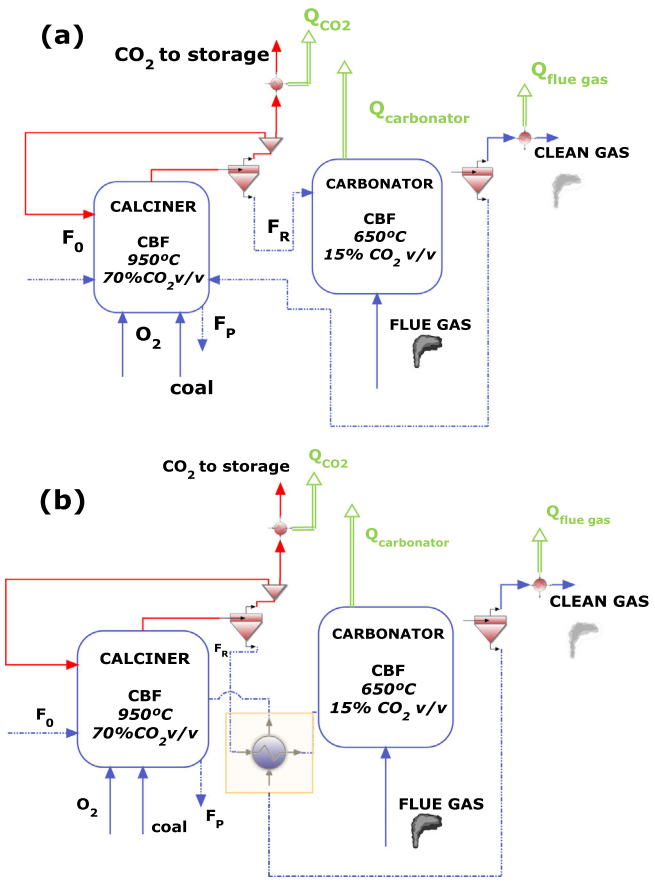

Fig. 6. Schematic CaL cycle without (a) and with (b) solids heat exchanger between the calciner and carbonator.

present work. Thus, only a one-stage compression model is simulated aimed at compressing the gas stream at the calciner outlet to a storage pressure of 100 bar. Before the compression stage, a cooling process is performed in order to improve the compression efficiency. The heat extracted from the CO_2 stream is used for preheating the flue gas entering into the carbonator (Fig. 4).

The regenerated CaO particles are recovered at the exit of the calciner by a cyclone and circulated back into the carbonator for a new cycle. Energy consumption derived from solids transportation has been set at 20 MJ per tonne of solids [50]. Part of the gas stream is recirculated into the calciner (REC-CO22) in order to regulate the composition of gases in the reactor (Fig. 7). Thus, the resulting gas stream at the outlet of the calciner (CO-INSTO) has a high CO_2 content (about 70–90%v/v CO_2). The sensible heat of the calciner's outlet streams (CO_2, CaO and purge stream) is transferred to the secondary steam cycle (Fig. 6a) or to the inlet stream of $CaCO_3$ (Fig. 6b) through heat exchangers. Finally, a purge of solids is carried out in the calciner zone (PURGE3) to eliminate ashes and deactivated solids.

3.2.3. Secondary steam cycle

The third main part in the simulation scheme is the secondary steam cycle zone (Fig. 9). This steam cycle is based on a reheat Rankine cycle with regeneration from five feedwater heaters (HEEXT1:4), one of which are of total mixer exchanger type (GASI). For this reason a series of steam extraction (EXT1:4) is realized. The steam operational parameters have been chosen from data of similar real power plants [51] and taking into account the CaL streams characteristics in order to maximize the integration efficiency without supplying more fuel for steam production. A makeup flow of water is introduced in the system (H2O-REP) to compensate for losses due to condensation in the turbine zone (COND). This water makeup flow is heated using the sensible heat of the solids purged (PURGOUT2). The steam boiler is modeled as a group of three independent zones: (i) the preheater, where the sensible heat flue gas stream (FG-OUT2) is used, (ii) the evaporator, where the heat

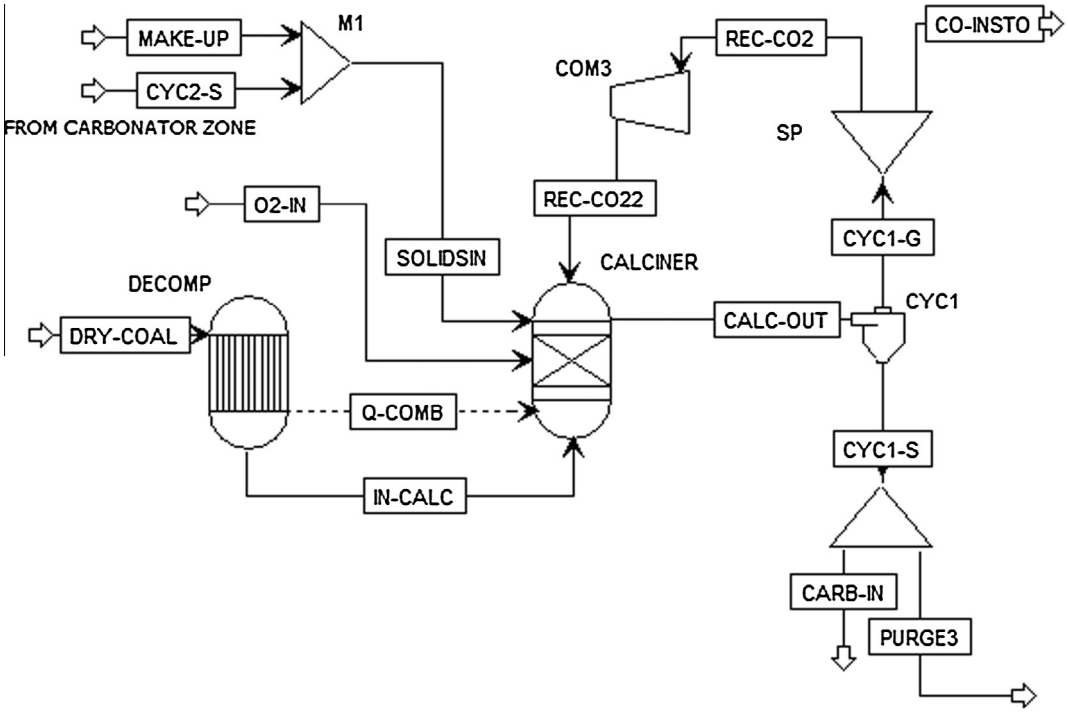

Fig. 7. Schematic representation of the calciner zone used in the simulations.

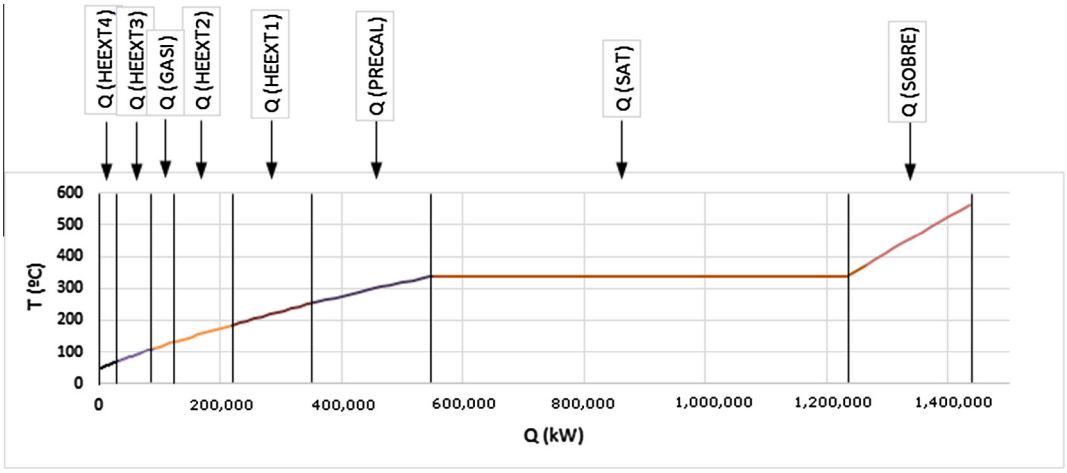

Fig. 8. *T*–*Q* diagram of the main steam heating process to reach the live steam temperature.

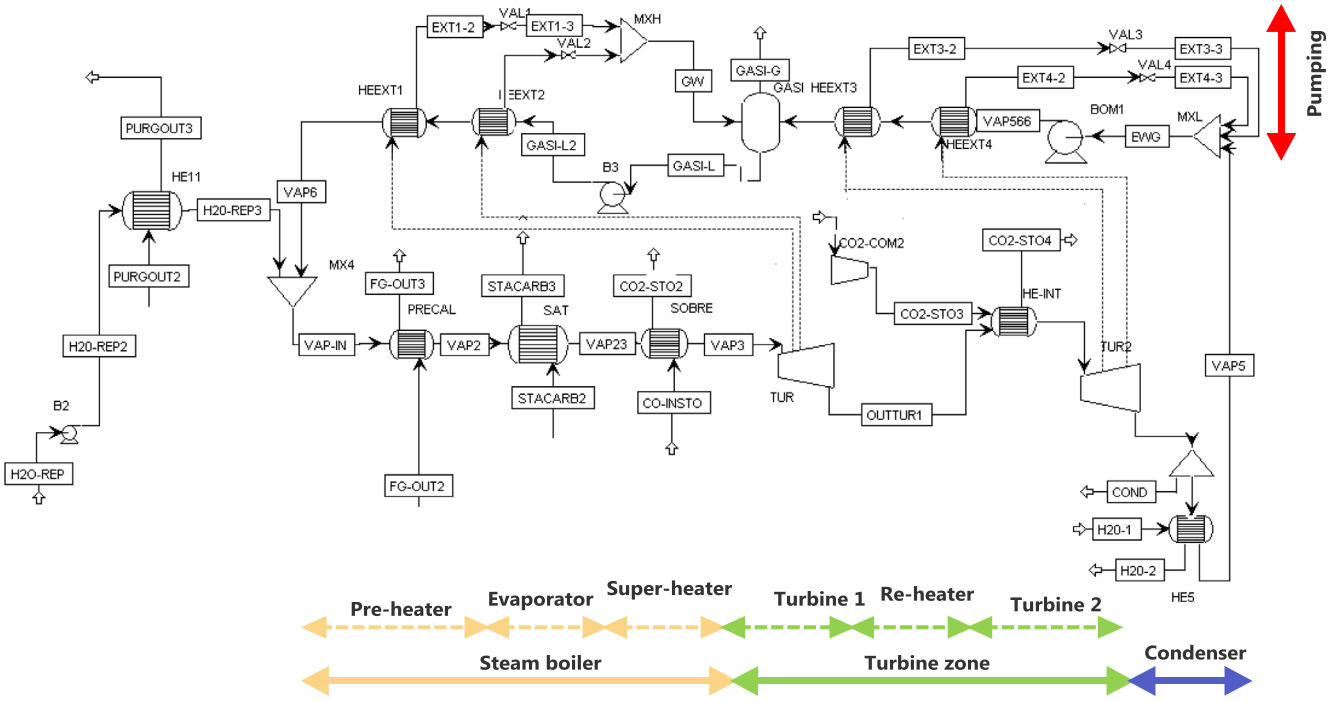

Fig. 9. Schematic representation of the secondary steam cycle zone used in the simulations.

produced by the exothermic carbonation reaction (Q-CARB) is employed for fluid evaporation through a vapor stream from the carbonator (STCARB2), and (iii) the super-heater, where a part of sensible heat of the CO_2 exiting the calciner (CO-INSTO) is used. As can be seen in Figs. 4 and 9, the stream of CO_2 exiting the calciner (at 950 °C) is passed through a series of heat exchangers, being the final stage previous to storage the steam re-heating between turbines facilities (HE-INT). Fig. 8 shows the main steam heating process to reach the live steam temperature. The condenser (HE5) is modeled as a heat exchanger using water as cold stream. Table 3 shows several input parameter of the steam secondary cycle zone.

4. Simulation results

The model described in Section 3 and using the solids heat exchanger between the calciner and the carbonator (Fig. 6a) has been simulated in order to determine the new global efficiency and penalty arising from the CaL cycle integration in the reference coal power plant. The values of the operation parameters used for this purpose are summarized in Table 3.

In order to analyze the effect of integrating the CaL process in the reference plant it is necessary to quantify the cycle efficiency as affected by the new cycle penalty in order to assess whether retrofitting the plant with the CaL process is industrially feasible and competitive against other possible CO_2 capture methods. As specified above, the reference plant efficiency is assumed to be of 33.5%. The new efficiency taking into account the CaL integration is calculated by the following expression (1):

$$\eta_{plant} = \frac{\dot{W}_{CFPP} + \dot{W}_{gen,CaL} - \dot{W}_{cons,CaL}}{\dot{Q}_{CFPP} + \dot{Q}_{CaL}} \quad (1)$$

where η_{plant} is the new global efficiency value after integration, $\dot{W}_{CFPP}$ is the reference plant generated power, $\dot{W}_{gen,CaL}$ is the gener-

Table 3
Main simulation model data.

Equipment/zone	Parameter	Value
	F_{CO2}	10388 kmol/h
	F_0/F_{CO2}	0.05
	τ	313 s
	F_R/F_{CO2}	10
	W_s	200 tonne
Heat exchangers	Approach temperature	10 °C
Compressors, turbines	Isentropic efficiency	0.85
Pumps	Efficiency	0.9
Cyclones	Efficiency	0.99
	Type	Barth 1
	Correlation	Muschelkrautz
Reactor/calciner	T	950 °C
	P	1 atm
	$\dot{m}_{coal}$	137 tonne/h
	P_{CO2}	0.83
	$X_{calciner}$	1
Reactor/carbonator	T	650 °C
	P	1 atm
	E_{CO2}	0.77
ASU	$\dot{W}_{ASU}$	200 kWh/tonne O_2
	$\dot{W}_{solid}$	5.5 kWh/tonne solids

ated power in the CaL process (secondary steam cycle), $\dot{W}_{cons,CaL}$ is the power consumption in the CaL cycle, $\dot{Q}_{CFPP}$ is the reference plant heat consumption and $\dot{Q}_{CaL}$ is the heat consumption in the calciner for oxy-combustion.

The power consumption in the CaL cycle can be expressed according Eq. (2):

$$\dot{W}_{cons,CaL} = \dot{W}_{FG-COMP} + \dot{W}_{CO2-COMP} + \dot{W}_{COM3} + \dot{W}_{ASU} + \dot{W}_{solid} \quad (2)$$

where $\dot{W}_{CO2-COMP}$, $\dot{W}_{COM3}$ and $\dot{W}_{FG-COMP}$ are the power consumed in the CO_2 compressor for storage, CO_2 recycle stream compressor and flue gas compressor, respectively. $\dot{W}_{ASU}$ is the power consumed in the ASU and $\dot{W}_{sólid}$ is the power consumption needed for the transport of solids. Cycle integration and streams simulation results are summarized in Tables 4 and 5, respectively.

Table 4
Main cycle results.

Equipment/zone	Parameter	Value
Reactor/calciner	$\dot{Q}_{cal}$	1150.1 MW
COM3/calciner	Power	9.5 MW
HEO2/calciner	Heat duty	15.6 MW
Reactor/carbonator	$\dot{Q}_{carb}$	711 MW
	E_{CO2}	0.77
FG-comp/carbonator	Power	5.5 MW
HE-FG/carbonator	Heat duty	117.5 MW
CO_2-COM2/CO_2 storage	Power	181 MW
	Pressure	100 bar
Secondary steam cycle	$\dot{W}_{tur,1}$	240.6 MW
	$\Delta_{P_{tur,1}}$	128 bar
	$\dot{W}_{tur,2}$	284.6 MW
	$\Delta_{P_{tur,2}}$	11.9 bar
	$\dot{W}_{B1}$	1.45 MW
	$\dot{W}_{B2}$	0.241
	$\dot{W}_{B3}$	4.86
	η (secondary steam cycle)	0.42
CaL cycle	η (without CO_2 comp)	0.43
	η (with CO_2 comp)	0.28
CFPP + CaL cycle (integration)	η	0.28
	Integration penalty	5.60% points

4.1. Sensitivity analysis

Parametric tests have been carried out in order to evaluate the CaL integration potential in a real power plant. Percentage of penalty points was calculated over the plant efficiency. Firstly, simulation tests were carried out under certain particular conditions imposed on the secondary steam cycle (Table 3). In order to analyze how these conditions affect the efficiency penalty, an analysis changing the cycle conditions was performed by taking into account a 10% relative variation on the values of several parameters such as the live steam pressure (P_{VV}) and live steam temperature (T_{VV}) in the secondary steam cycle, the extraction flow, the rate of consumption of oxygen and coal for oxycombustion in the calciner ($\dot{W}_{ASU}$ and $\dot{W}_{solid}$, respectively), and the pumps and compression efficiencies. As can be seen in Fig. 10, a relative variation of these parameters within a 10% yields a maximum change on the order of 1% in the efficiency penalty. In regards to P_{VV} and T_{VV}, and the compressor efficiencies their increase would yield a remarkable decrease of the efficiency penalty. However, operation at increased P_{VV} and T_{VV} involves a higher equipment cost, making it necessary to carry out an additional sensitivity analysis from the economic standpoint. A variation of the extraction flow and pumps efficiencies does not have a critical effect on the energy penalty. On the other hand, the energy penalty is notably increased by the increase of the flow rate of coal and oxygen used for oxycombustion to raise the calciner temperature as might be expected.

Next a test is performed to analyze the effect of increasing the solids residence time in the carbonator τ by decreasing the recirculation flow rate of solids between the calciner and the carbonator (F_R). As may be seen in Fig. 11, the efficiency penalty is notably decreased as the solids residence time in the carbonator is increased. Moreover, the lower the flow rate of fresh limestone makeup the larger is the reduction of efficiency penalty. Thus, it can be concluded that a lower flow of solids recirculation between the reactors would lead to a remarkable improvement of the integrated cycle efficiency. This is a novel relevant result to be highlighted that arises from the new carbonator model in which the importance of carbonation of the CaO solids in the solid-state diffusion controlled phase is considered.

An interesting parameter to assess the tradeoff between the achieved CO_2 capture efficiency and energy penalty is the specific energy consumption per kg of CO_2 captured (SPECCA). Thus, SPECCA represents the additional fuel consumption (in MJ) necessary to avoid the emission of 1 kg of CO_2 into the atmosphere [11,52,53]. It is calculated according to expression 3:

$$\text{SPECCA} = 3600\frac{\frac{1}{\eta_{plant}} - \frac{1}{\eta_{ref}}}{E_{ref} - E} \quad (3)$$

where η_{ref}, η_{plant} are the power plant efficiency without and with the CaL cycle integrated, and E_{ref}, E are the emissions ratio (in kg CO_2/kWh_e) before and after CaL cycle integration, respectively.

Fig. 12 shows the results of the values obtained for SPECCA in our work to obtain a CO_2 capture efficiency of 80% and 90%, respectively, as depending on the solids recirculation flow rate. As can be seen, for a given value of the solids recirculation flow rate (F_R/F_0 fixed), it is necessary to increase the amount of energy required in order to obtain a higher capture efficiency since the makeup flow rate of fresh limestone introduced into the system F_0 must be increased. Furthermore it is observed that a lower SPECCA is attained as the solids recirculation flow rate if decreased for a given capture efficiency (as was seen in Fig. 9). Thus, the additional energy consumption necessary to achieve a given capture efficiency is lowered as F_R/F_0 is diminished.

Fig. 13 shows the effect of changing the CO_2 compression pressure to storage on the steam cycle efficiency and efficiency penalty.

Table 5
Main streams results.

Streams		Flow rate (kg/s)	Temperature (°C)	Pressure (bar)	Main composition (mole fraction)
Acronyms	Definition				
CARB-IN	Solids entering into the carbonator	1708.32	950	1.01	CaO (0.98)
FG-IN	Flue gas entering into the carbonator	634.35	384.5	1.10	N_2 (0.75) CO_2 (0.14)
CYC2-S	Solid stream exiting the carbonator	1807.29	650	1.01	CaO (0.90) $CaCO_3$ (0.08)
CYC2-G	Gas stream exiting the carbonator	534.21	650	1.01	N_2 (0.84) CO_2 (0.03)
PURGE4	Purge stream flow exiting the system	170.78	88	1.01	CaO (0.98) $CaSO_4$ (0.02) [a]
MAKE-UP	Makeup flow of fresh limestone	170.78	25	1,01	$CaCO_3$ (1.00)
O2-IN	O_2 stream entering into the calciner	87.61	640	1.10	O_2 (1.00)
CYC1-G	Gas stream exiting the calciner	584.01	950	1.01	CO_2 (0.83)
CYC1-S	Solid stream exiting the calciner	1879.03	950	1.01	CaO (0.98)
REC-CO22	CO_2 stream recirculated into the calciner	350.40	970	1.10	CO_2 (0.83)
CO-INSTO	CO_2 stream exiting the calciner zone	233.60	950	1.01	CaO (0.98)
VAP3	Live steam	429.53	560	140.00	H_2O (1.00)
INTUR2	Reheated steam	340.19	472	17.00	H_2O (1.00)
VAP5	Water flow exiting the condenser	293.38	46	0.10	H_2O (1.00)
VAP-IN	Water stream entering into steam boiler	429.53	251	140	H_2O (1.00)
H2O-1	Water stream entering into the condenser	305.50	25	1.00	H_2O (1.00)
H2O-REP	Water makeup flow	15.08	25	1.00	H_2O (1.00)

[a] Does not take into account ash flow (33.06 kg/s).

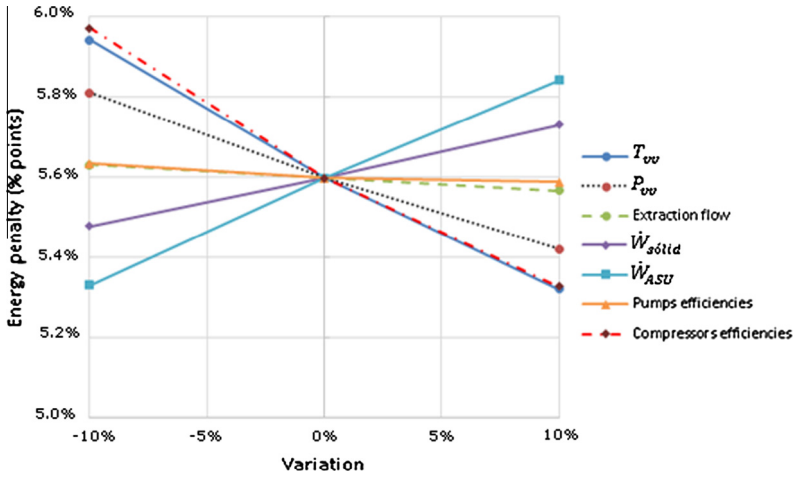

Fig. 10. Efficiency penalty as affected by the variation of several model parameters over the values shown in Table 3. Simulations made using the integration model described in Section 4.

As may be observed, the final value of the CO_2 pressure has a significant role on the integration penalty. A 1% increase of the efficiency penalty is obtained by raising the storage CO_2 pressure from 50 bars to 140 bars. On the other hand, the steam cycle efficiency is enhanced by increasing the storage CO_2 pressure as seen in Fig. 13 since the sensible heat of the CO_2 stream to be compressed is used for steam re-heating between the high and low pressure turbines, which partially mitigates the increase of energy penalty due to higher compression work. Arguably, the efficiency of integration would be enhanced by using a more efficient compression process for the CO_2 produced, such as a multi-stage optimized process, or using the high temperature and pressure CO_2 stream in a secondary cycle, which would allow compression needs to be reduced. In this regard, Fig. 14 shows the CFPP-CaL efficiency penalty by taking into account an intercooled CO_2 multi-stage compression. In the present integration model, a high temperature of CO_2 compressed stream is needed since a part of sensible heat from the CO_2 stream is used for re-heating the steam flow. For this reason, the process is simulated by taking into account a constant inter-stage temperature of 170 °C and avoiding cooling in the last stage, which is followed by heating to the temperature required for the exchange with the steam cycle (around 780 °C). As seen from this analysis, by increasing the stages number it is possible to achieve a reduction of energy penalty of around 0.5%. Recent studies [54,55] have been devoted to a more detailed and optimized heat exchanger analysis aimed at achieving the best heat integration solution. Applying some of the methods proposed in these analyses, an even smaller energy penalty could be attained by operating under a higher solids residence time in the carbonator according to Figs. 11 and 12.

A desirable option to reduce the integration efficiency penalty would be to decrease the calciner reactor temperature with a consequent reduction in fuel and O_2 requirements for oxycombustion. However, as mentioned earlier, fast calcination of the fresh

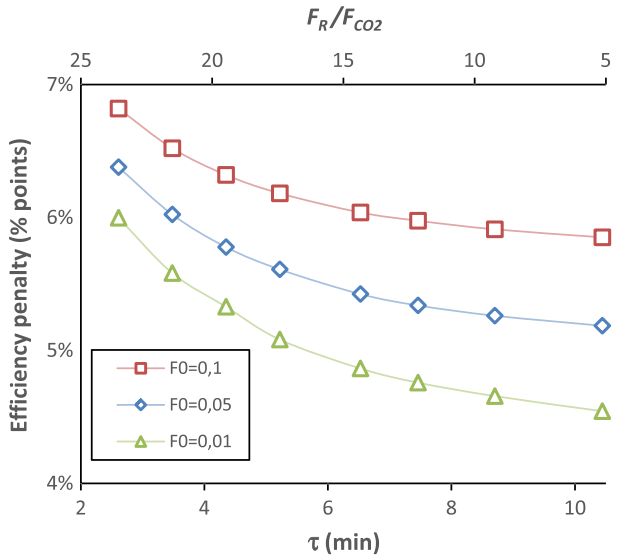

Fig. 11. Efficiency penalty for the integration of the CaL technology in a coal combustion power plant as a function of the solids residence time in the carbonator, which is varied by changing the ratio of solids recirculation to CO_2 flow rates (F_R/F_{CO2}). Calculations were made for several values of the ratio of limestone makeup flow to CO_2 flow rates (F_0/F_{CO2}).

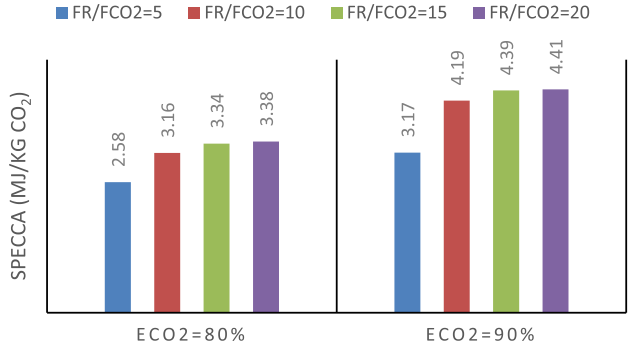

Fig. 12. SPECCA value as a function of the ratio of solids recirculation flow rate to CO_2 flow rate (F_R/F_{CO2}). Calculations made from simulations of the model described in Section 4 by varying the ratio of fresh limestone makeup flow rate to CO_2 flow rate (F_0/F_{CO2}) to get a fixed CO_2 capture efficiency (E_{CO2}) value of 80% (left) and 90% (right).

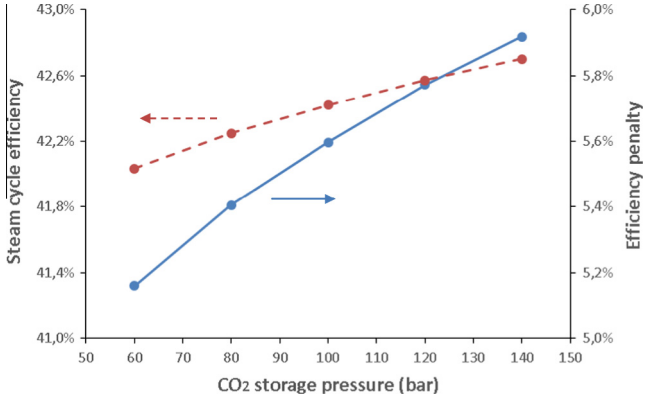

Fig. 13. Steam cycle efficiency (left axis) and integration efficiency penalty (right axis) as a function of CO_2 storage pressure.

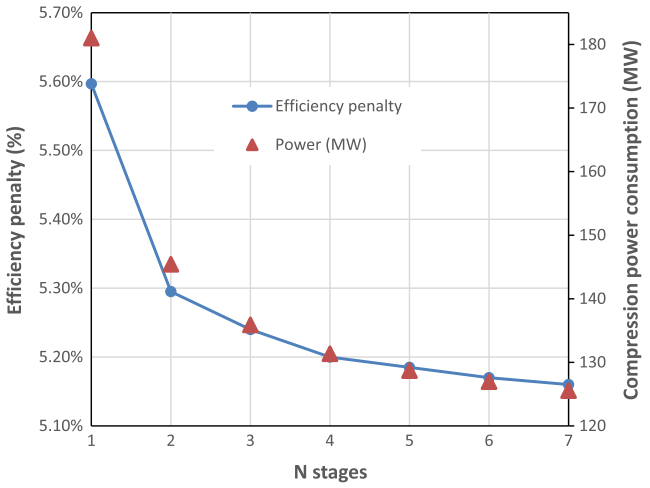

Fig. 14. Efficiency penalty (left axis) and compression power consumption (right axis) as a function of stages number in the CO_2 to storage multi-stage compression.

Table 6
Simulation results for the reference case with/without solid heat exchanger.

	Parameter	Value
Model inputs		
	F_{CO2}	10388 kmol/h
	F_0/F_{CO2}	0.05
	τ	313 s
	F_R/F_{CO2}	10
	W_s	200 tonne
Heat solid exchangers (between calciner–carbonator)	Approach temperature	20 °C
Parameter	Without heat exchanger (reference case)	With heat exchanger
Model outputs		
$\dot{Q}_{calciner}$	1150.1 MW	580.5 MW
$\dot{Q}_{carb}$	711 MW	218 MW
$\dot{W}_{steam\ cycle}$	525.2 MW	291.4 MW
Coal consumption	137 tonne/h	69 tonne/h
Integration penalty	5.6% points	5.35% points

makeup of limestone under high CO_2 partial pressure only takes place at temperatures over ~930 °C. An alternative approach to mitigate the energy penalty would be thus to use a natural CaO precursor showing fast calcination at reduced temperatures as compared to limestone. This can be the case of natural dolomite as suggested by lab-scale TGA tests [3,6].

Let us finally assess the effect of introducing a solids heat exchanger between the calciner and carbonator reactors (Fig. 6). As can be seen in Table 6, the simulation including the heat exchanger yields a significant reduction of coal consumption and the thermal power produced by the CaL cycle (using an approach temperature of 20 °C), which implies a reduction of the efficiency penalty in the global system. Besides, the power production in the steam cycle is decreased and likewise the equipment size and investment cost. Data on the efficiency penalty and coal consumption in the calciner are shown in Fig. 15 as a function of the approach temperature in the solid heat exchanger. As might be expected, both penalty and coal consumption are decreased as the approach temperature is decreased.

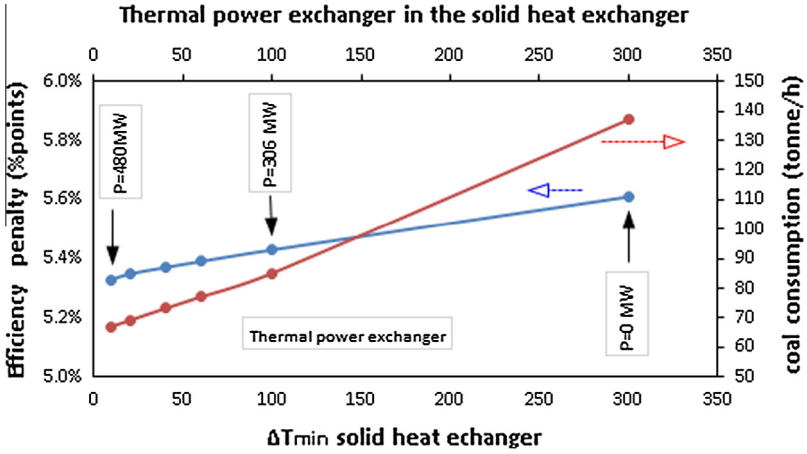

Fig. 15. Efficiency penalty and coal consumption as a function of approach temperature in calciner–carbonator heat exchanger. The insets indicate values of the thermal power exchanger necessary for diverse values of ΔT_{min}.

5. Conclusions

In this work we have analyzed the energy penalty arising from integrating the CaL technology in a coal fired power plant for CO_2 capture. Simulation results show that the energy penalty ranges between 4% and 7% points over the reference plant efficiency (taken as 33.5%). A main novel feature of the integration model proposed is that it uses a carbonator model that considers the critical effect of solids residence time in the carbonator on the CO_2 capture efficiency, as inferred from lab-scale experimental results when the solids are regenerated by calcination under high CO_2 partial pressure in accordance with practical conditions. Thus, the integration energy penalty is significantly reduced as the solids residence time in the carbonator is increased within the practical operation range of a few minutes. The main reason for this result is the lower heat requirement in the calciner reactor as the recirculation flow rate of solids between the calciner and carbonator reactors is decreased. In addition, by increasing the solids residence time, a smaller size of process equipment would be necessary thus reducing investment costs as well as O&M cost.

A further conclusion from the analysis is that optimizing the heat exchangers network and the power system parameters would significantly improve energy penalty results. Nevertheless, the large amount of heat required in the calciner leads to the production of a large amount of energy in a secondary power cycle, which results in a system of size similar to the actual reference power plant size (without the CaL cycle) as obtained in previous works, thus hindering investments prospective. Accordingly, it would be highly convenient to optimize the heat integration of the streams exiting the CaL with the reference power plant flows. Our work suggests that a notably lower energy penalty could be achieved together with a reduction of power production needs by adding s solids heat exchanger system between the calciner and carbonator reactors.

To summarize, operation conditions that would essentially improve the industrial competitiveness of the CaL-CFPP integration would consist of prolonging the residence time in the carbonator reactor and optimizing the integration of heat produced. In a future work an economic feasibility study must be carried out to take into account the reduction of process equipment size possible when the CaL cycle is operated with a lower solids recirculation flow rate as suggested in the present work.

Acknowledgements

This work was supported by the Andalusian Regional Government Junta de Andalucia (contract FQM-5735), and by the Spanish Government Agency Ministerio de Economia y Competitividad (contracts CTQ2014-52763-C2-2-R and CTQ2014-52763-C2-1-R).

References

[1] Hanak DP, Biliyok C, Yeung H, Białecki R. Heat integration and exergy analysis for a supercritical high-ash coal-fired power plant integrated with a post-combustion carbon capture process. Fuel 2014;134:126–39. http://dx.doi.org/10.1016/j.fuel.2014.05.036.

[2] Dean CC, Blamey J, Florin NH, Al-Jeboori MJ, Fennell PS. The calcium looping cycle for CO_2 capture from power generation, cement manufacture and hydrogen production. Chem Eng Res Des 2011;89:836–55. http://dx.doi.org/10.1016/j.cherd.2010.10.013.

[3] Valverde JM, Sanchez-Jimenez PE, Perez-Maqueda L. Ca-looping for postcombustion CO_2 capture: a comparative analysis on the performances of dolomite and limestone. Appl Energy 2015;138:202–15. http://dx.doi.org/10.1016/j.apenergy.2014.10.087.

[4] Wang K, Hu X, Zhao P, Yin Z. Natural dolomite modified with carbon coating for cyclic high-temperature CO_2 capture. Appl Energy 2016;165:14–21. http://dx.doi.org/10.1016/j.apenergy.2015.12.071.

[5] Sun R, Li Y, Liu H, Wu S, Lu C. CO_2 capture performance of calcium-based sorbent doped with manganese salts during calcium looping cycle. Appl Energy 2012;89:368–73. http://dx.doi.org/10.1016/j.apenergy.2011.07.051.

[6] Perejon A, Romeo LM, Lara Y, Lisbona P, Valverde JM. The calcium-looping technology for CO_2 capture: on the important roles of energy integration and sorbent behavior. Appl Energy 2015;162:787–807. http://dx.doi.org/10.1016/j.apenergy.2015.10.121.

[7] Wang W, Ramkumar S, Wong D, Fan LS. Simulations and process analysis of the carbonation–calcination reaction process with intermediate hydration. Fuel 2012;92:94–106. http://dx.doi.org/10.1016/j.fuel.2011.06.059.

[8] Manovic V, Anthony EJ. Competition of sulphation and carbonation reactions during looping cycles for CO_2 capture by CaO-based sorbents. J Phys Chem A 2010;114:3997–4002. http://dx.doi.org/10.1021/jp910536w.

[9] Romano MC, Martínez I, Murillo R, Arstad B, Blom R, Ozcan DC, et al. Process simulation of Ca-looping processes: review and guidelines. Energy Proc 2013;37:142–50. http://dx.doi.org/10.1016/j.egypro.2013.05.095.

[10] Ylätalo J, Parkkinen J, Ritvanen J, Tynjälä T, Hyppänen T. Modeling of the oxy-combustion calciner in the post-combustion calcium looping process. Fuel 2013;113:770–9. http://dx.doi.org/10.1016/j.fuel.2012.11.041.

[11] Vorrias I, Atsonios K, Nikolopoulos A, Nikolopoulos N, Grammelis P, Kakaras E. Calcium looping for CO_2 capture from a lignite fired power plant. Fuel 2013;113:826–36. http://dx.doi.org/10.1016/j.fuel.2012.12.087.

[12] Dieter H, Bidwe AR, Varela-duelli G, Charitos A, Hawthorne C. Development of the calcium looping CO_2 capture technology from lab to pilot scale at IFK, University of Stuttgart. Fuel 2014;127:23–37. http://dx.doi.org/10.1016/j.fuel.2014.01.063.

[13] Arias B, Diego ME, Abanades JC, Lorenzo M, Diaz L, Martínez D, et al. Demonstration of steady state CO_2 capture in a 1.7 MW_{th} calcium looping

pilot. Int J Greenh Gas Control 2013;18:237–45. http://dx.doi.org/10.1016/j.ijggc.2013.07.014.
[14] Hanak DP, Anthony EJ, Manovic V. A review of developments in pilot-plant testing and modelling of calcium looping process for CO_2 capture from power generation systems. Energy Environ Sci 2015. http://dx.doi.org/10.1039/C5EE01228G.
[15] Shimizu T, Hirama T, Hosoda H, Kitano K, Inagaki M, Tejima K. A twin fluid-bed reactor for removal of CO_2 from combustion processes. Chem Eng Res Des 1999;77:62–8. http://dx.doi.org/10.1205/026387699525882.
[16] Yang Y, Zhai R, Duan L, Kavosh M, Patchigolla K, Oakey J. Integration and evaluation of a power plant with a CaO-based CO_2 capture system. Int J Greenh Gas Control 2010;4:603–12. http://dx.doi.org/10.1016/j.ijggc.2010.01.004.
[17] Martínez A, Lara Y, Lisbona P, Romeo LM. Energy penalty reduction in the calcium looping cycle. Int J Greenh Gas Control 2012;7:74–81. http://dx.doi.org/10.1016/j.ijggc.2011.12.005.
[18] Lasheras A, Ströhle J, Galloy A, Epple B. Carbonate looping process simulation using a 1D fluidized bed model for the carbonator. Int J Greenh Gas Control 2011;5:686–93. http://dx.doi.org/10.1016/j.ijggc.2011.01.005.
[19] Berstad D, Anantharaman R, Jordal K. Post-combustion CO_2 capture from a natural gas combined cycle by CaO/$CaCO_3$ looping. Int J Greenh Gas Control 2012;11:25–33. http://dx.doi.org/10.1016/j.ijggc.2012.07.021.
[20] Wang D, Chen S, Xu C, Xiang W. Energy and exergy analysis of a new hydrogen-fueled power plant based on calcium looping process. Int J Hydrogen Energy 2013;38:5389–400. http://dx.doi.org/10.1016/j.ijhydene.2013.02.060.
[21] Connell DP, Lewandowski Da, Ramkumar S, Phalak N, Statnick RM, Fan LS. Process simulation and economic analysis of the calcium looping process (CLP) for hydrogen and electricity production from coal and natural gas. Fuel 2013;105:383–96. http://dx.doi.org/10.1016/j.fuel.2012.07.00.
[22] Kunze C, De S, Spliethoff H. A novel IGCC plant with membrane oxygen separation and carbon capture by carbonation–calcinations loop. Int J Greenh Gas Control 2011;5:1176–83. http://dx.doi.org/10.1016/j.ijggc.2011.05.038.
[23] Kunze C, Spliethoff H. Assessment of oxy-fuel, pre- and post-combustion-based carbon capture for future IGCC plants. Appl Energy 2012;94:109–16. http://dx.doi.org/10.1016/j.apenergy.2012.01.013.
[24] Abanades JC, Anthony EJ, Wang J, Oakey JE. Fluidized bed combustion systems integrating CO_2 capture with CaO. Environ Sci Technol 2005;39:2861–6. http://dx.doi.org/10.1021/es0496221.
[25] Cormos CC, Cormos AM. Assessment of calcium-based chemical looping options for gasification power plants. Int J Hydrogen Energy 2013;38:2306–17. http://dx.doi.org/10.1016/j.ijhydene.2012.11.128.
[26] Martínez I, Murillo R, Grasa G, Rodríguez N, Abanades JC. Conceptual design of a three fluidised beds combustion system capturing CO_2 with CaO. Int J Greenh Gas Control 2011;5:498–504. http://dx.doi.org/10.1016/j.ijggc.2010.04.017.
[27] Grasa GS, Abanades JC. CO_2 capture capacity of CaO in long series of carbonation/calcination cycles. Ind Eng Chem Res 2006;45:8846–51. http://dx.doi.org/10.1021/ie0606946.
[28] Kavosh M, Patchigolla K, Anthony EJ, Oakey JE. Carbonation performance of lime for cyclic CO_2 capture following limestone calcination in steam/CO_2 atmosphere. Appl Energy 2014;131:499–507. http://dx.doi.org/10.1016/j.apenergy.2014.05.020.
[29] Sceats G, Horley CJ, Richardson P. System and method for the calcination of minerals; 2014.
[30] Valverde JM. A model on the CaO multicyclic conversion in the Ca-looping process. Chem Eng J 2013;228:1195–206. http://dx.doi.org/10.1016/j.cej.2013.05.023.
[31] Valverde JM, Sanchez-Jimenez PE, Perez-Maqueda L. Role of precalcination and regeneration conditions on postcombustion CO_2 capture in the Ca-looping technology. Appl Energy 2014;136:347–56. http://dx.doi.org/10.1016/j.apenergy.2014.09.052.
[32] Ortiz C, Chacartegui R, Valverde JM, Becerra J, Perez-Maqueda L. A new model of the carbonator reactor in the calcium looping technology for post-combustion CO_2 capture. Fuel 2015;160:328–38. http://dx.doi.org/10.1016/j.fuel.2015.07.095.
[33] Sanchez-Jimenez PE, Valverde JM, Perez-Maqueda L. Multicyclic conversion of limestone at Ca-looping conditions: the role of solid-sate diffusion controlled carbonation. Fuel 2014;127:131–40. http://dx.doi.org/10.1016/j.fuel.2013.09.064.
[34] Valverde JM, Sanchez-Jimenez PE, Perez-Maqueda L. High and stable CO_2 capture capacity of natural limestone at Ca-looping conditions by heat pretreatment and recarbonation synergy. Fuel 2014;123:79–85. http://dx.doi.org/10.1016/j.fuel.2014.01.045.
[35] Chen H, Zhao Z, Huang X, Patchigolla K, Cotton A, Oakey J. Novel optimized process for utilization of CaO-based sorbent for capturing CO_2 and SO_2 sequentially; 2012.
[36] Alonso M, Rodríguez N, Grasa G, Abanades JC. Modelling of a fluidized bed carbonator reactor to capture CO_2 from a combustion flue gas. Chem Eng Sci 2009;64:883–91. http://dx.doi.org/10.1016/j.ces.2008.10.044.
[37] Romeo LM, Abanades JC, Escosa JM, Paño J, Giménez A, Sánchez-Biezma A, et al. Oxyfuel carbonation/calcination cycle for low cost CO_2 capture in existing power plants. Energy Convers Manage 2008;49:2809–14. http://dx.doi.org/10.1016/j.enconman.2008.03.022.
[38] Romano MC. Modeling the carbonator of a Ca-looping process for CO_2 capture from power plant flue gas. Chem Eng Sci 2012;69:257–69. http://dx.doi.org/10.1016/j.ces.2011.10.041.
[39] Kunii D, Levenspiel O. The K–L reactor model for circulating fluidized beds. Chem Eng Sci 2000;55:4563–70. http://dx.doi.org/10.1016/S0009-2509(00)00073-7.
[40] Kunii D, Levenspiel O. Circulating fluidized-bed reactors. Chem Eng Sci 1997;52:2471–82. http://dx.doi.org/10.1016/S0009-2509(97)00066-3.
[41] Cormos C-C. Economic evaluations of coal-based combustion and gasification power plants with post-combustion CO_2 capture using calcium looping cycle. Energy 2014;78:665–73. http://dx.doi.org/10.1016/j.energy.2014.10.054.
[42] Romano M, Martínez I, Murillo R, Arstad B. Guidelines for modeling and simulation of Ca-looping processes. Prepared for the European energy research alliance. SintefNo; 2012.
[43] Martínez A, Lara Y, Lisbona P, Romeo LM. Operation of a cyclonic preheater in the Ca-looping for CO_2 capture. Environ Sci Technol 2013;47:11335–41. http://dx.doi.org/10.1021/es401601k.
[44] Martínez A, Lara Y, Lisbona P, Romeo LM. Operation of a mixing seal valve in calcium looping for CO_2 capture. Energy Fuels 2014;28:2059–68. http://dx.doi.org/10.1021/ef402487.
[45] Manovic V, Anthony EJ. Carbonation of CaO-based sorbents enhanced by steam addition. Ind Eng Chem Res 2010;49:9105–10. http://dx.doi.org/10.1021/ie101352s.
[46] Valverde JM, Sanchez-Jimenez PE, Perez-Maqueda L. Calcium-looping for post-combustion CO_2 capture. On the adverse effect of sorbent regeneration under CO_2. Appl Energy 2014;126:161–71. http://dx.doi.org/10.1016/j.apenergy.2014.03.081.
[47] Beruto DT, Searcy AW, Kim MG. Microstructure, kinetic, structure, thermodynamic analysis for calcite decomposition: free-surface and powder bed experiments. Thermochim Acta 2004;424:99–109. http://dx.doi.org/10.1016/j.tca.2004.05.027.
[48] Kavosh M, Patchigolla K, Oakey JE, Anthony EJ, Champagne S, Hughes R. Pressurised calcination–atmospheric carbonation of limestone for cyclic CO_2 capture from flue gases. Chem Eng Res Des 2015;102:116–23. http://dx.doi.org/10.1016/j.cherd.2015.06.024.
[49] Martínez I, Murillo R, Grasa G, Abanades JC. Integration of a Ca-looping system for CO_2 capture in an existing power plant. Energy Proc 2011;4:1699–706. http://dx.doi.org/10.1016/j.egypro.2011.02.043.
[50] Edwards SEB, Materić V. Calcium looping in solar power generation plants. Sol Energy 2012;86:2494–503. http://dx.doi.org/10.1016/j.solener.2012.05.019.
[51] Chacartegui R, Sanchez D, Becerra JA, Muñoz A, Sanchez T. Performance analysis of a 565 MW steam power plant. In: Proc ASME turbo expo 2011. GT2011, Vancouver, British Columbia, Canada; 2011. p. 1–10.
[52] Kvamsdal HM, Romano MC, van der Ham L, Bonalumi D, van Os P, Goetheer E. Energetic evaluation of a power plant integrated with a piperazine-based CO_2 capture process. Int J Greenh Gas Control 2014;28:343–55. http://dx.doi.org/10.1016/j.ijggc.2014.07.004.
[53] Romano MC. Ultra-high CO_2 capture efficiency in CFB oxyfuel power plants by calcium looping process for CO_2 recovery from purification units vent gas. Int J Greenh Gas Control 2013;18:57–67. http://dx.doi.org/10.1016/j.ijggc.2013.07.002.
[54] Lara Y, Lisbona P, Martínez A, Romeo LM. Design and analysis of heat exchanger networks for integrated Ca-looping systems. Appl Energy 2013;111:690–700. http://dx.doi.org/10.1016/j.apenergy.2013.05.044.
[55] Lara Y, Lisbona P, Martínez A, Romeo LM. A systematic approach for high temperature looping cycles integration. Fuel 2014;127:4–12. http://dx.doi.org/10.1016/j.fuel.2013.09.062.

***ANNEX 3**: Chacartegui R, Alovisio A, Ortiz C, Valverde JM, Verda V, Becerra JA. Thermochemical energy storage of concentrated solar power by integration of the calcium looping process and a CO_2 power cycle. Appl Energy 2016;173:589–605. doi:10.1016/j.apenergy.2016.04.053.*

Applied Energy 173 (2016) 589–605

Contents lists available at ScienceDirect

Applied Energy

journal homepage: www.elsevier.com/locate/apenergy

Thermochemical energy storage of concentrated solar power by integration of the calcium looping process and a CO_2 power cycle

R. Chacartegui [a,*], A. Alovisio [a,c], C. Ortiz [a,b], J.M. Valverde [b], V. Verda [c], J.A. Becerra [a]

[a] Energy Engineering Department, University of Seville, Camino de los Descubrimientos s/n, 41092 Sevilla, Spain
[b] Faculty of Physics, University of Seville, Avenida Reina Mercedes s/n, 41012 Sevilla, Spain
[c] Politecnico di Torino, Department of Energy Engineering, Corso Duca degli Abruzzi 24, 10129 Torino, Italy

HIGHLIGHTS

- Novel concept for thermochemical energy storage for medium–high temperature CSP.
- Energy storage based on the integration of calcium looping and carbon dioxide power cycle.
- Full system performance analysis at design and off design conditions.
- Global system efficiency including storage above 45%.
- Sensitivity analysis on main design and operation parameters of the cycle.

ARTICLE INFO

Article history:
Received 24 November 2015
Received in revised form 18 March 2016
Accepted 10 April 2016
Available online 22 April 2016

Keywords:
Energy storage
Calcium Looping (CaL)
Concentrated Solar Power (CSP)
CO_2
Thermochemical energy storage (TCES)

ABSTRACT

Energy storage is the main challenge for a deep penetration of renewable energies into the grid to overcome their intrinsic variability. Thus, the commercial expansion of renewable energy, particularly wind and solar, at large scale depends crucially on the development of cheap, efficient and non-toxic energy storage systems enabling to supply more flexibility to the grid. The Ca-Looping (CaL) process, based upon the reversible carbonation/calcination of CaO, is one of the most promising technologies for thermochemical energy storage (TCES), which offers a high potential for the long-term storage of energy with relatively small storage volume. This manuscript explores the use of the CaL process to store Concentrated Solar Power (CSP). A CSP–CaL integration scheme is proposed mainly characterized by the use of a CO_2 closed loop for the CaL cycle and power production, which provides heat decoupled from the solar source and temperatures well above the ~550 °C limit that poses the use of molten salts currently used to store energy as sensible heat. The proposed CSP–CaL integration leads to high values of plant global efficiency (of around 45–46%) with a storage capacity that allows for long time gaps between load and discharge. Moreover, the use of environmentally benign, abundantly available and cheap raw materials such as natural limestone would mark a milestone on the road towards the industrial competitiveness of CSP.

1. Introduction

Efficient and affordable energy storage systems are urgently needed in order to cope with the intrinsic variability of renewable energy sources, which would allow a deep penetration of renewable energy power generation into the grid. In particular, Concentrated Solar Power (CSP) lends itself for the storage of heat as a primary form of energy that could be used for electricity generation on demand. In recent years, a number of thermal storage technologies for medium to high temperature CSP systems have been developed from the use of materials in which energy is stored as sensible heat [1–3]. Diverse materials with high heat capacity are employed in thermal energy storage (TES) systems such as water [4], molten salts [5–7], mineral oils [8] or ceramic materials [9]. Commercial plants of considerable size (>100 MWth) do already operate in which heat is stored in molten salts and used overnight to generate electricity. Another type of storage under investigation is based on the latent heat stored in some materials when they experience a change of phase [10–12]. Phase change materials (PCM) allow attaining higher storage capacities as compared to storage as sensible heat [13]. Nevertheless, both sensible and latent heat storage forms suffer from unavoidable

* Corresponding author.
E-mail address: ricardoch@us.es (R. Chacartegui).

http://dx.doi.org/10.1016/j.apenergy.2016.04.053
0306-2619/

Nomenclature

C1	CO_2 compressor (from T1 outlet to carbonator pressure)
C2	CO_2 compressor (from calciner to storage pressure)
$c_{p,i}$	specific heat, kJ/(kmol K)
E_{eq}	equilibrium CO_2 reaction efficiency
F_i	molar flow rate of component *i*, kmol/s
F_{CaCO_3}	molar flow rate of $CaCO_3$
$F_{CaCO_3,carb}$	molar flow rate of $CaCO_3$ (carbonator side)
$F_{CaCO_3,clc}$	molar flow rate of $CaCO_3$ (calciner side)
$F_{CaO,crb}$	molar flow rate of CaO (carbonator side)
$F_{CaO,clc}$	molar flow rate of regenerated sorbent
$F_{CaO,unr,carb}$	molar flow rate of unreacted CaO (carbonator side)
$F_{CaO,unr,clc}$	molar flow rate of unreacted CaO (calciner side)
$F_{CO_2,clc,out}$	molar flow rate of CO_2 at calciner outlet
$F_{CO_2,s}$	CO_2 looped fraction flowing in the carbonator side
$F_{R,carb}$	recirculating molar flow rate (carbonator side)
$F_{R,clc}$	recirculating molar flow rate (calciner side)
h_i	enthalpy, kJ/kmol
HXA	solid–solid heat exchanger
HXB	gas–solid heat exchanger
HXE	gas–solid heat exchanger
HXF	gas–solid heat exchanger
HXI	gas–solid heat exchanger
k	CaO deactivation constant
HXG	gas–solid heat exchanger
$\dot{m}_{CO_2,crb}$	CO_2 mass flow rate through carbonator
P	absolute carbonator pressure, bar
P_{eq}	CO_2 partial pressure at equilibrium, bar
PR	pressure ratio (between P and TOP)
p_{drop}	pressure drops in CO_2 circuit, bar
$y_{CO_2,carb,in}$	inlet molar fraction of CO_2 in the carbonator
y_{eq}	equilibrium fraction of CO_2 in the carbonator
T	temperature, K
TOP	T1 outlet pressure, bar
T1	CO_2 turbine (at carbonator outlet)
T2	CO_2 turbine (from storage to carbonator pressure)
$\dot{W}$	mechanical power, kW
X	CaO conversion X
X_{lim}	minimum critical value of CaO conversion
X_N	CaO conversion in the N cycle
X_r	residual CaO conversion
Δt_{sun}	average daytime period
$\Delta H_R(T_{react})$	heat of reaction at the reactor temperature
ξ	extent of reaction per unit time
Φ	heat flux
$\Phi_{carbonation}$	available heat of carbonation

energy losses and other issues, which hinder their industrial competitiveness in the short-medium term.

A third possibility to store CSP, currently under research and development, is the thermochemical energy storage (TCES) [14,15]. TCES consists of using the heat obtained from an external source to drive an endothermic reaction. When energy is needed, the separately stored products of the reaction are brought together at the necessary conditions for the reverse exothermic reaction to occur, which releases the previously used heat for power production. The main advantages of TCES as compared to TES and PCMs are a considerably higher energy density as well as the possibility of storing energy in the long term [1,14]. Moreover, in addition to the chemically stored heat, the products of the reaction can be also employed to store sensible heat.

Among the diverse possibilities explored for TCES at large scale, one of the most promising technologies is the Calcium Looping (CaL) process, which relies on the calcination–carbonation reaction of $CaCO_3$ (Eq. (1)) [16–18]:

$$CaCO_{3(s)} \rightleftarrows CaO_{(s)} + CO_{2(g)} \quad \Delta H_r^0 = 178\ \text{kJ/mol} \tag{1}$$

As can be seen in Table 1, the energy density of the CaO/CO_2 system (around 3.2 GJ/m^3) is rather high (for comparison, the energy density of molten salts currently used in commercial plants is about 0.8 GJ/m^3 [20]). On the other hand, it has a turning temperature near to 900 °C (defined as the temperature for the reaction to be at equilibrium under a CO_2 partial pressure of 1 atm) that fits in the desirable range of high temperatures potentially attainable in CSP tower plants. This relevant feature would allow for a more efficient generation of electricity from stored energy, thus overcoming the current limitation of ~550 °C imposed by the degradation of molten salts nowadays employed in commercial CSP plants [21,22]. Furthermore, the reactants and products can be stored at ambient temperature in contrast with the need of keeping molten salts always at temperatures above ~200 °C to avoid solidification [23].

Table 1
Energy density and turning temperature of various thermochemical energy storage systems. Adapted from [19].

Thermochemical energy storage systems	Turning temperature (°C)	Energy density (MJ/m^3)
NH_3/N_2	195	131
CH_4/H_2O	688	223
SO_3/SO_2	782	459
CaO/H_2O	479	1967
Li_2O/H_2O	731	2216
NH_4HSO_4/NH_3	467	3082
CaO/CO_2	895	3226
SrO/CO_2	1108	3948

The CaL process begins with the decomposition of $CaCO_3$ in the calcination reactor (calciner) yielding CaO and CO_2 as reaction byproducts. A high energy input is necessary to increase the input stream temperature up to the value required for the endothermic calcination reaction to occur at a sufficiently fast rate, which is essentially determined by the composition of the gas in the calcination environment [24,25]. Once sensible heat from the CaO and CO_2 streams at the calciner outlet is recovered, these products are stored at ambient temperature for their use afterwards as a function of demand. Storage of the products could be prolonged to weeks or even months as depending on storage conditions and energy demand [1]. Once needed, the reactants are circulated into a carbonator reactor, where the energy stored in chemical form is released through the reverse reaction (carbonation). Efficient gas–solid contact and heat/mass transfer in the calciner and carbonator reactors could be ensured by the use of circulating fluidized-beds (CFB), which are operated under the fast fluidization regime with gas velocities of the order of 5–10 m/s [26,27]. An advantage of this technology ahead of its incorporation into the market is the proven efficiency and durability of such type of fluidized bed reactors.

The CaL process has been widely studied in recent years but mainly for its application to capture CO_2 in fossil fuel power plants [28]. The standard cycle for CO_2 capture from flue gas streams uses lime (CaO), which can be derived from limestone calcination, to produce $CaCO_3$ by quick carbonation at high temperature (~650 °C). Once CO_2 is captured in the carbonator and heat from the exothermic reaction is recovered, the almost CO_2 free flue gas is released into the atmosphere. Several carbonator reactor models have been developed to predict the CO_2 capture efficiency as

depending on operating conditions and CaO multicycle conversion under CaL conditions for CO_2 capture [29–31]. These involve carbonation under relatively low CO_2 partial pressure (about 0.15 atm) and calcination at very high temperatures (around 950 °C) under high CO_2 partial pressure with short residence times at both stages. Under these conditions, limestone derived CaO exhibits a severe drop of conversion in only a few cycles converging towards a residual value of just about 0.07, which makes it necessary to periodically purge the poorly active sorbent and replace it by a makeup flow of fresh limestone. The efficiency of the calciner reactor and the energy penalty efficiency caused by the CaL integration [32,33] into coal fired power plants (CFPP) have been also important subjects of analysis [25,34–36]. Pilot plants (of size on the order of 1–2 MWth) demonstrate the achievement of CO_2 capture efficiencies around 90% [37,38] whereas model simulations predict a penalty on power generation around 5–6% when scaling up the technology to a commercial level [39].

The present manuscript is focused on the development of an integration model to use the CaL process for TCES in CSP plants. Integration models aimed at similar goals have been already analyzed by other authors. Tregambi et al. [40] proposed a scheme whereby calcination in the CaL process is assisted by CSP for CO_2 capture in a coal fired power plant. Edwards and Materić [17] studied a CSP–CaL system in which the heat produced in the carbonator reactor is used for power generation through a CO_2/air open cycle. Remarkably, results from this work indicate that the global plant efficiency would be hampered by a too high CaO reactivity. Nevertheless, a high CaO reactivity leads to a decrease of the fraction of unreacted CaO in the circulating stream of solids thereby allowing for a reduction of the energy penalty. This suggests that the performance of the CSP–CaL integration could be further improved by optimizing the heat recovery exchanger network as will be shown in the present work.

In this manuscript, a novel CSP–CaL integration model is explored from coupling the CaL process to a closed CO_2 power system. Full integration is optimized by means of the pinch-analysis methodology. A global layout is derived and the effects of main parameters on the global cycle performance are studied by a sensitivity analysis. The obtained results demonstrate that a global thermal efficiency above 45% may be attained, which makes the proposed integration model a highly competitive option for TCES. The use of an abundantly available and cheap CaO precursor such as limestone allows achieving the goal of decoupling the storage and delivery phases at low cost, and the process may be carried out with already existing mature technologies to further reduce costs. In the rest of the manuscript, the proposed CSP–CaL integration model is described after which the effects of parameters critically intervening on the cycle are discussed. Finally, a sensitivity analysis of the model response to the variation of main inputs is carried out.

2. CSP–CaL energy storage system

This section is devoted to describe the model developed for the analysis and optimization of the CSP–CaL integration (Engineering Equation Solver Professional software has been used to this end). The integration is built upon models of the different components that play a main role on the technology such as the carbonator reactor, solid streams, heat exchangers, solid reservoirs, CO_2 storage tank, turbines and compressors.

2.1. Description of the CSP–CaL integration

A major benefit of the CSP–CaL integration is that it makes use of natural limestone as CaO precursor. Limestone is an abundant, non-toxic and non-corrosive cheap material (~10$/ton), which is geographically widespread and has adequate physical properties in the desired temperature range for CSP energy storage. As usually reported in the last years by studies on the use of the CaL process for CO_2 capture, limestone derived CaO shows a marked deactivation under the standard CaL conditions specific for CO_2 capture [34,41,42] that necessarily involve calcination at rather high temperatures (~950 °C) under high CO_2 partial pressure and carbonation under low CO_2 partial pressure [28]. Thus, it is usually assumed that a marked drop of CaO conversion will also hinder the efficiency of the CaL process for TCES [43]. However, it is important to remark that the multicycle conversion of CaO under calcination/carbonation conditions that optimize the efficiency of the CSP–CaL integration (radically different from those specific for CO_2 capture as will be seen) could be kept at a stable and high value. This has been confirmed by a recent thermogravimetric analysis study whose results will be summarized in Section 3.5 [44].

Fig. 1 shows a schematic representation of the proposed CSP–CaL integration. The central idea behind this scheme is to separate the heat storage and power generation phases. Heat storage takes place in the solar receiver, where the calcination reaction of $CaCO_3$ occurs at expense of solar energy. Calcination can be performed in a solar reactor, most likely a central tower receiver. A number of solar calciner prototypes have been already developed based on fluidized beds [45,46], rotary kilns [47,48] and cyclone atmospheric reactors [49]. A potentially cheap and simple option consists of falling particle receivers [50]. Since the CSP–CaL integration scheme proposed in the present work relies on a closed CO_2 cycle, a pure CO_2 stream must be retrieved as output from the calciner. Two options are feasible to this end: (i) performing calcination under a 100% CO_2 atmosphere or (ii) under an easily separable gas from CO_2. The first choice would make it necessary to operate the calciner under low absolute pressure in order to reduce the calcination temperature and to avoid hampering the reactivity of the regenerated CaO due to excessive sintering as observed when calcination is carried out under high CO_2 partial pressure for CO_2 capture [51]. In regards to the second option, calcination could be carried out under superheated steam, which is separable from the released CO_2 by condensation. Calcination under superheated steam can be carried out by means of a flash calcination process, whereby limestone particles are quickly calcined in an entrained-flow reactor at short residence times [14] [52]. Moreover, calcination under superheated steam enhances the $CaCO_3$ decomposition rate and considerably decreases the required temperature to attain complete calcination down to ~700–750 °C [53,54]. Thus, calcination under superheated steam in flash calciners is completed in seconds, compared to hours in rotary and shaft kilns [54]. Achieving fast calcination at a moderate temperature would be highly beneficial for the integration of the CaL technology in CSP tower plants. It would allow using mature and inexpensive solar receivers capable of heating the working gas at temperatures up to 800 °C based on metal alloys instead of ceramic materials currently under development that would be needed to achieve higher temperatures [55]. The use of superheated steam for calcination in the solar reactor would be also facilitated by the possibility of in-situ direct generation of superheated steam in solar receivers. Another gas that could be employed for calcination is Helium, which is easily separable from CO_2 by means of membranes and has a catalyzing effect similar to superheated steam due to its high thermal conductivity and the high diffusivity of the released CO_2 [53].

Coming back to the integration scheme (Fig. 1), and once calcination takes place using concentrated solar power, the released CO_2 is sent to a storage tank after being cooled and compressed whereas the CaO stream is transported to the storage

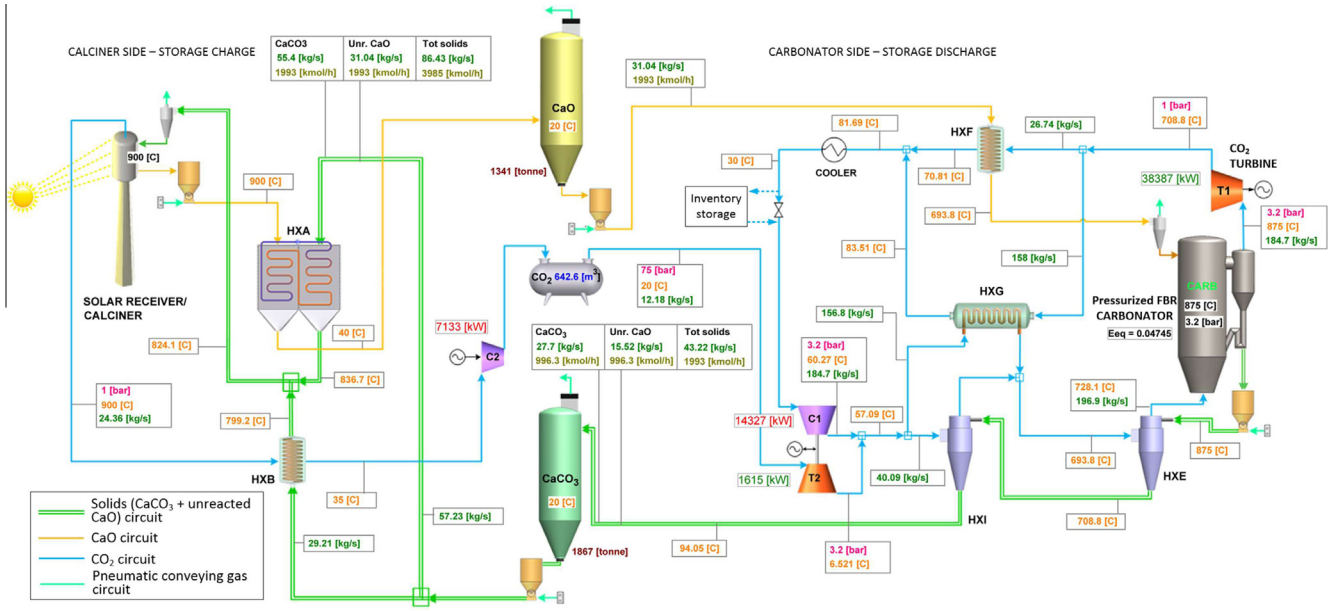

Fig. 1. Schematic representation of the CSP–CaL integration model with values of temperature, pressure, mass flow rate and composition in key stages (a 100 MW_{th} CSP tower plant is considered).

solids reservoir after being brought near to ambient conditions. The solids stream entering into the calciner, and consisting of $CaCO_3$ and unreacted CaO, is preheated in two exchangers (HXA and HXB as detailed in Fig. 1) using the sensible heat released by the hot streams leaving the calciner. Thus, solar energy entering into the system is used to heat the reactants and to drive the endothermic chemical reaction, which serves to store the solar energy as both sensible and chemical and form.

The energy discharge phase takes place in the carbonator, which is a pressurized fluidized bed reactor wherein the carbonation reaction takes place under pure CO_2 at the highest possible temperature in order to achieve a high thermal to electric efficiency. Pressurized carbonation provides a great range of possibilities and thermal applications for a direct integration with a power cycle, and could enhance the long term CaO reactivity in the CaL process [56]. The heat of the carbonation reaction is delivered to a gas turbine by means of the CO_2 as carrier and through a Joule–Brayton cycle, which implies a direct integration between heat released and power cycle. Another possibility could be to implement an indirect integration through a heat exchanger that can be coupled with an externally heated power block (steam turbine, Stirling, Supercritical CO_2 (SCO_2), etc.). The proposed CO_2 power cycle is a closed and regenerative cycle, whereby the heat removed by the reactants in the carbonator is recovered in an open cyclone exchanger (HXF in Fig. 1). Thus, in this heat exchanger (HXF) heat from the exhaust CO_2 stream serves to heat up the CaO solids before entering into the carbonator while in HXE the residual heat from the solids at the carbonator output is extracted to pre-heat the CO_2 stream at the carbonator inlet. Part of the power needed in the compression stage of the Joule–Brayton cycle is provided by the expansion of the pressurized CO_2 used for reaction in the carbonator. Expansion of stored CO_2 yields useful work while, at the same time, provides efficiently cooling power by expanding to low temperatures (up to −30 °C to be used for CO_2 intercooling compression of the stream coming from the carbonator). On the other side, CO_2 may fall under the saturation curve while expanding, thereby some form of heat supply before and during expansion is needed to protect the turbine blades. For these reasons, C1 and T2 (see Fig. 1) are thermally coupled to avoid the use of massive air cooling devices and to further reduce costs. A possible thermal coupling scheme between C1 and T2 is detailed in Fig. 2.

Concerning C2, due to the high compression ratios (about 100:1), intercooling compression is needed in order to lower down the power penalty. Sensible heat available between the compression end temperature at each stage and the dead state is recovered. The possibility of recovering waste CO_2 compression heat has been investigated by means of pinch-analysis and minimum external energy requirement analysis techniques. As a main outcome, only a small fraction of waste compression heat (13–20% depending on the number of stages) is recoverable. By increasing the number of intercooling stages the recovered heat turns to be less valuable while the compression work is reduced thus resulting in increased efficiency. If more than 5 intercooling stages are performed, the inclusion of additional waste heat exchangers yields negligible efficiency gain. Thus, the optimum solution as regards cost, efficiency and technical feasibility is to carry out intercooling compression up to supercritical pressure and then cooling to near ambient temperature by means of simple water/air coolers without heat recovery.

Solids conveying can be carried out by means of the mature pneumatic technology that guarantees rapid transport of granular solids, routing flexibility, as well as the possibility of streams splitting, and it is suitable to successfully convey high temperature materials. Calcium based powders are easily conveyable in the dense phase involving low gas velocity in a non-suspension mode. The very high solids loading ratios (defined as the ratio between material and pneumatic gas mass flow rate) associated with dense phase conveying (around 45 for cement powders [57]) imply relatively low conveying energy consumption (around 3–5 MJ ton^{-1}/100 m [57]) and a limited heat exchange between the conveying gas and conveyed particles that has been dismissed in the model.

In order to achieve higher integration efficiency an optimized heat exchanger network is necessary. In the model, heat exchangers are characterized by a single parameter, namely their minimum temperature difference. Countercurrent flow is assumed in each exchanger. Gas–solid heat exchange can be performed in both open (direct contact) or closed configuration. Open configurations have been experimentally demonstrated to be effective, reaching approach temperatures of 15 °C by means of axial flow cyclones

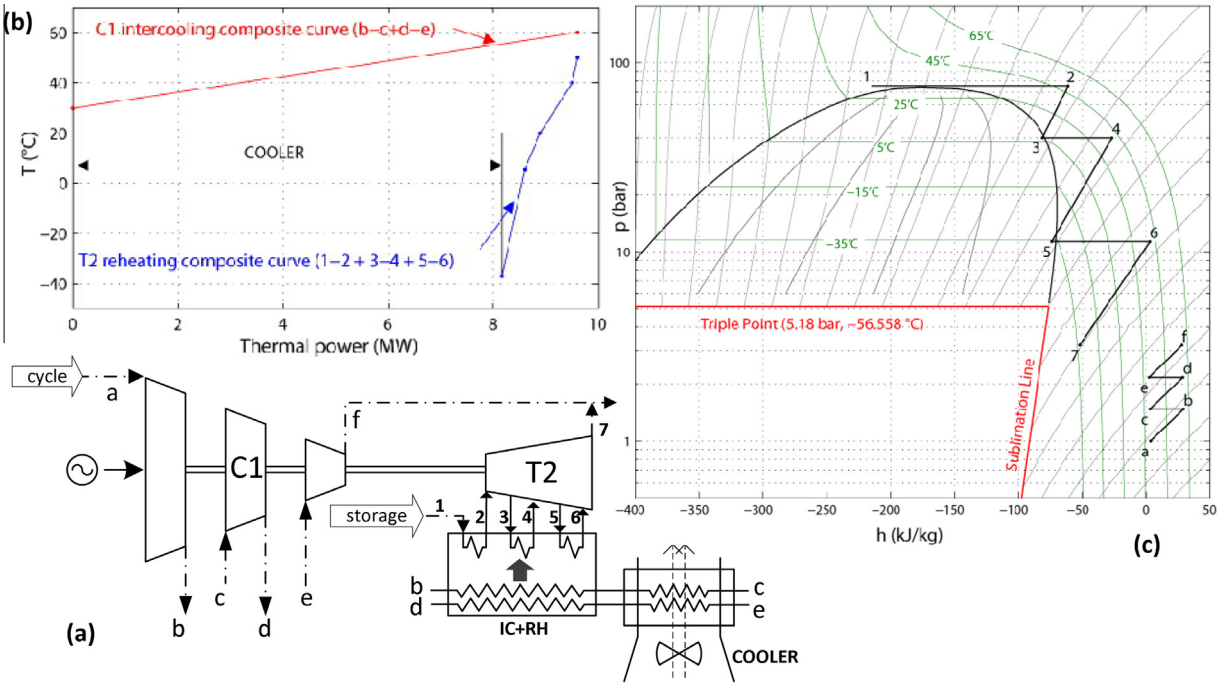

Fig. 2. Possible thermal coupling scheme between C1 and T2 (see Fig. 1) by means of an external IC + RH exchanger. RH: initial pre-heating to 50 °C (1–2) and multistage expansion with re-heating stages up to 40 °C. IC: cooling up to 30 °C. (a) Schematics. (b) Composite curves. (c) Processes on the PH diagram.

operating in a close to counter-flow mode [58]. There exist several closed gas–solid exchangers operating in counter-flow mode commercially available. A favorable choice for our purpose would consist of a series of vertical plates, across which bulk solids slowly flow downwards by gravity exchanging heat by conduction with a fluid circulating inside the plates [59]. This mature technology is characterized by low energy consumption and is almost maintenance-free as it does not include any moving parts. Solid–solid heat exchange can be pursued in practice by adapting conveniently this technology and using one or more intermediate heat-transfer fluids recirculated within the bulk of both solids by means of a small pumping device.

2.1.1. Mass balance

Fig. 3 shows a schematic representation of the mass streams circulating in the loop.

As can be seen in Fig. 3, a fraction $F_{CaO,crb}$ of the total sorbent recirculating flow rate ($F_{R,crb}$) fully reacts in the carbonator, which yields an equal molar flow rate of carbonated solids $F_{CaCO_3,crb}$ while the remaining flow rate is assumed to stay as unreacted CaO ($F_{CaO,unr,crb}$). Their sum gives at the outlet a solid molar rate $F_{R,crb}$. In the model, $F_{CaCO_3,crb}$ and $F_{CaO,unr,crb}$ are considered as two distinct streams, although the powder in reality consists of partially carbonated particles in which a core of unreacted CaO is surrounded by a layer of $CaCO_3$. The average CaO conversion X is a fundamental parameter to quantify the amount of CaO converted to $CaCO_3$ in the calciner, i.e. the amount of $CaCO_3$ produced ($X = F_{CaCO_3}/F_R$). Thus, small values of CaO conversion X lead to the requirement of large amounts of unreacted sorbent recirculating in the loop to keep constant the $CaCO_3$ production.

In the calciner, the partially carbonated particles are assumed to experience complete decomposition, thus each mole of $CaCO_3$ ($F_{CaCO_3,clc}$) gives rise to a mole of CO_2 ($F_{CO_2,clc,out}$) and a mole of regenerated sorbent ($F_{CaO,clc}$). The molar flow rate at the calciner output is therefore the sum of two streams: a solid stream of CaO composed of both regenerated and unreacted sorbent and a gaseous stream ($F_{CO_2,clc,out}$) of CO_2.

As shown in Fig. 3, the molar rate of CO_2 flowing into the carbonator is well above the reacting molar rate, which is given by $E_{eq}F_{CO_2,crb,in}$. Here, E_{eq} is the equilibrium CO_2 reaction efficiency (to be defined in Eq. (9)). The excess CO_2 ($F_{CO_2,S}$) is thus used to remove the heat of carbonation and is looped through the closed power cycle for the generation of electricity.

The molar flows circulating in the two regions of the plant are decoupled. While the solar calciner can work only in presence of solar power (daytime and clear sky conditions), power demand in the carbonator side must be satisfied over a 24 h period. Storage vessels must be thus sized to provide buffer storage to allow the carbonator/turbine group supplying electricity demand over 24 h by adjusting the load as needed. Concerning the CO_2 storage volume (Fig. 4), a minimum pressure of 75 bar is needed in order to guarantee supercritical CO_2 storage conditions (considering storage at ambient temperature). As can be seen in Fig. 4, at lower storage pressures, it would be necessary to liquefy the CO_2 (with the consequent energy penalization) in order to avoid unreasonably large storage volumes. The proportional size of storage tanks can be achieved by integrating several commercially available tanks. They would use a reduced area compared to the large surface area field available in the associated tower CSP plant. Higher CO_2 storage pressures can be considered but, in this case, the cycle efficiency could be lower as will be seen below in Fig. 19.

In order to guarantee steady-state operation, the following mass-balance must be satisfied:

$$\int_{24h} F_{CaCO_3,clc}(t)dt = \int_{24h} F_{CaCO_3,crb}(t)dt \tag{2}$$

In the present model, the plant performance is determined as an average over a 24 h period, in which the molar flows are considered as constant and equal to the integral average value over the daytime curve. Accordingly, an average daytime period Δt_{sun} is considered, in which the sun-solar concentrators provide sufficient energy to run the decomposition reaction in the calciner. In this way, it is possible to derive an averaged ratio between the circulating flow rates in the calciner and carbonator sides of the plant:

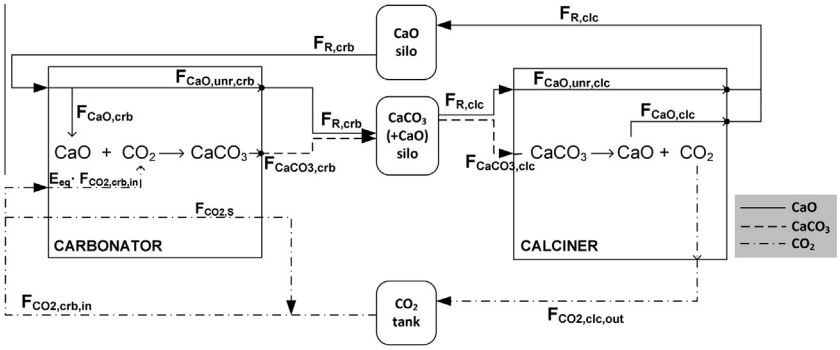

Fig. 3. Mass-balance schematics of the plant showing the flow rates of solids and CO_2 streams between the carbonator and calciner.

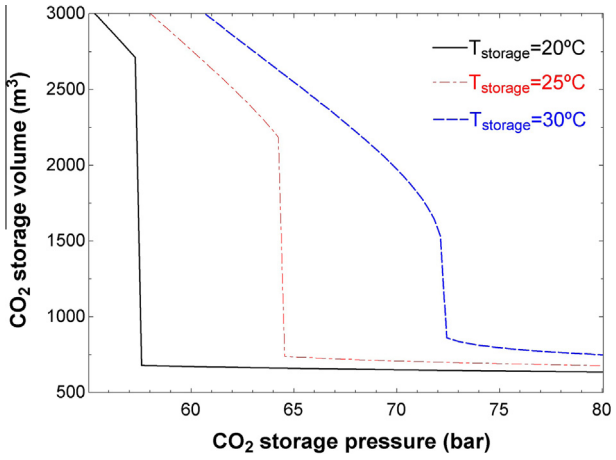

Fig. 4. CO_2 storage conditions by considering a 12 h daytime (100 MW_{th} CSP plant).

$$\overline{F_{CaCO_3,clc}} \cdot \Delta t_{sun} = \overline{F_{CaCO_3,crb}} \cdot 24 \tag{3}$$

If, for instance, we consider a daytime Δt_{sun} of 8 h (clear sky), the ratio between the circulating streams in the calciner and the carbonator will be of 3 over the 24 h, while in case that the daytime is 12 h, the molar flow rates in the calciner side will be twice those in the carbonator side. A more sophisticated model (dynamic model) would be necessary in a framework of long-period control taking into account real data for solar energy input in order to obtain real energy production values along the year. Nevertheless, the scope of this paper is just to estimate the cycle efficiency for a fixed irradiation. A variation in the solar input power (as a function of solar irradiance) modifies mass and energy flows in the cycle, which requires improving the control strategy to maximize the cycle performance, including part-load strategies for the closed Brayton cycle.

2.1.2. Energy balance

The first thermodynamics law applied to a reacting system is used in both the carbonator and calciner reactors for the energy balance:

$$\sum_i F_{i,out} h_{i,out} - \sum_i F_{i,in} h_{i,in} = \Phi - \dot{W} \tag{4}$$

$$F_{i,out} - F_{i,in} = \xi \nu_i \tag{5}$$

where ξ denotes the extent of reaction per unit time. Arranging and considering that output conditions are reactor conditions, it is:

$$\xi \Delta H_R(T_{react}) + \sum_i F_{i,in}(h_{i,react} - h_{i,in}) = \Phi - \dot{W} \tag{6}$$

with

$$\Delta H_R(T_{react}) = \sum_i \nu_i h_{i,T} = \Delta H_R^0 + \sum_i \nu_i \int_{ref}^{T_{react}} c_{p,i} dT \tag{7}$$

being the reaction enthalpy change at the reaction temperature.

Energy change in the control volume consists therefore of the heat of reaction at the reactor temperature $\xi \Delta H_R(T_{react})$ and the heat required to bring the reactants from inlet to reactor's conditions $\sum_i F_{i,in}(h_{i,react} - h_{i,in})$.

Eq. (4), when applied to the carbonator, serves to balance out the amount of CO_2 ($F_{CO_{2,S}}$ in Fig. 3) needed to remove all the heat that is not absorbed by reactants or dispersed through the walls assuming isothermal conditions at the reactor. On the other hand, Eq. (4), when applied to the calciner, balances out the $CaCO_3$ production in accordance with the net energy input of the system, which is the solar heat supply minus the heat losses occurring between the solar receiver and the reactor due to conduction, thermal radiation, absorption, etc.

3. CSP–CaL energy storage cycle analysis

The proposed cycle configuration is the result of an optimization analysis based on the pinch-point method [60,61]. Thus, the heat exchanger network seeks for optimal internal heat-recovery performance in a broad range of operational conditions. In this section, the influence of the main cycle parameters are analyzed in order to determine the most efficient operating conditions. Table 2 shows several parameters used in the cycle simulations whose influence is discussed below.

The proposed plant (Fig. 1) is equipped with a solid–solid heat exchanger HXA, two indirect gas–solid heat exchangers (HXB and HXF), a gas–gas regenerator (HXG) and two cyclone gas–solid direct heat exchangers (HXE and HXI).

The results of the model for the proposed plant configuration will be reported as a function of the CaO conversion X, pressure ratio PR in the CO_2 turbine T1 (see Fig. 1), absolute carbonator pressure (P), T1 turbine outlet pressure (TOP), and carbonator temperature (T), which have been identified as the key operational parameters.

3.1. CaO conversion

Conversion (X) of the CaO solids population recycled in the loop plays a relevant role in the plant performance. Changes in the value of this parameter cause remarkable modifications in the necessary flow rates of the circulating solids, CO_2 generation and $CaCO_3$ consumption in the calciner, heat balance in the calciner and useful carbonation heat and storage size, which have a significant effect on the plant efficiency.

Table 2
Values of the main parameters used in our work to simulate the proposed CSP–CaL integration model.

Net absorbed solar flux in calciner	100 MWt
Daylight hours (constant solar flux)	12
Thermal dispersions in carbonator	10%
Calciner temperature	900 °C
Carbonator temperature	875 °C
Carbonator pressure	3.2 bar
Turbine outlet pressure	1 bar
Ambient temperature	20 °C
Minimum temperature difference solid–solid HX	20 °C
Minimum temperature difference solid–gas HX	15 °C
Minimum temperature difference gas–gas HX	15 °C
Minimum temperature difference CO_2 cooler	10 °C
Intercoolings in CO_2 storage compression	5
Intercoolings in power cycle compression	2
Pressure losses in CO_2 circuit	0 bar
CO_2 storage conditions	75 bar, *T* ambient
Solid phase conveying energy consumption	10 MJ/tonne/100 m
Equivalent length solids conveying carbonator side	100 m
Equivalent length solids conveying calciner side	100 m
Isentropic efficiencies (compression/expansion)	0.89

The results of the model simulations carried out demonstrate that the power balance in the calciner side is favored by high values of *X* that allow decreasing the amounts of circulating solids, thus yielding lower heat-losses in the calciner side exchangers network and more heat available for calcination. $CaCO_3$ decomposition and CO_2 generation in the calciner are consequently enhanced and more heat is available in the discharge phase for carbonation. Carbonation heat is proportional to the amount of CaO and CO_2 produced in the calciner and is partially absorbed by reactants and partially removed by the CO_2 stream for power generation. For values of CaO conversion below a certain lower bound, the heat removed by inactive solids overcomes the heat of carbonation. In this situation, isothermal operation of the carbonator becomes compromised unless heat is provided by an external source. This critical value of conversion, X_{lim}, is mainly dependent on the temperature of the inlet CaO, which is in turn imposed by the temperature at main turbine output through HXF. This means that, in practice, the ratio of carbonator pressure to the T1 turbine outlet pressure (*PR*) is the parameter that mainly determines the minimum value of CaO conversion needed for operation as will be seen ahead.

As can be observed in Fig. 5, the higher CaO conversion the higher fraction of heat can be removed by the power fluid (CO_2 in the present case) given the lower flow rate of solids cycled within the system, which reduces the energy required in the form of sensible heat for the solids to reach the carbonation temperature. In the current cycle configuration, the presence of exchangers HXG and HXI ensure optimal thermal recovery and consequently the CO_2 mass flow rate in the cycle is perfectly proportional to the carbonation heat (as may be seen in Fig. 5).

Fig. 6a shows the thermal capacity rate (defined as the product of the molar flow rate by the specific heat of the fluid of interest Fc_p) of the carbonator-side streams as a function of the CaO conversion. The cooling (CO_2c) and preheating (CO_2p) CO_2 streams' split ratios (see Fig. 1) are determined by means of a pinch-point optimization method.

When the amount of solids is reduced, a larger fraction of heat is regenerated in the heat exchanger HXG. This results in an increased size of the gas–gas regenerator HXG, unlike for HXF and HXI. High values of CO_2 molar flow rates for low pressure ratios *PR* can push up too much the size of the exchanger HXG. For this reason, too low *PR* values should be avoided.

The efficiency curve is represented in Fig. 6b as a function of CaO conversion *X* for a fixed pressure ratio *PR* = 3.2 used as an optimum value. Efficiencies are shown for the cases of a carbonator operating under atmospheric pressure (expansion to sub atmospheric pressure) and a pressurized carbonator (atmospheric turbine output). As may be seen, efficiency increases with CaO conversion and reaches a maximum between 44% and 46% under the conditions considered. Importantly, the energy consumption related to solids conveying diminishes the efficiency especially in the case of low values of CaO conversion.

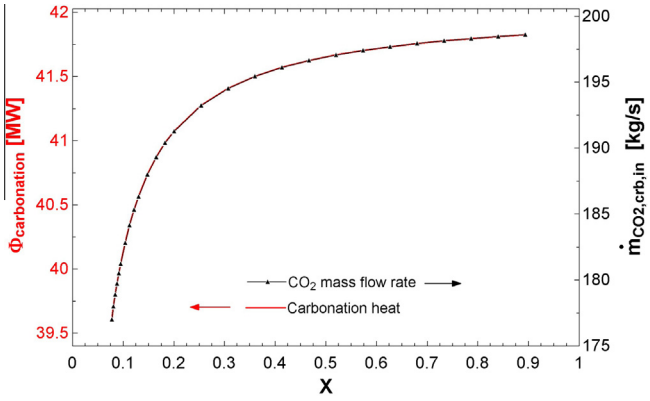

Fig. 5. Available heat of carbonation (left axis) and CO_2 mass flow rate through the carbonator (right axis) vs CaO conversion.

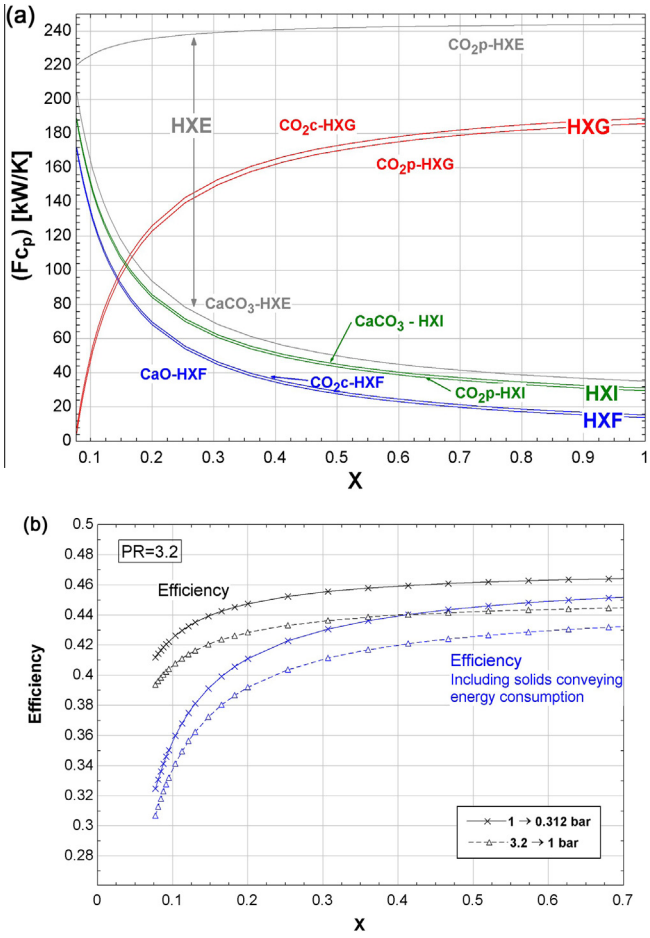

Fig. 6. (a) Thermal capacity of streams (CaO, $CaCO_3$, and CO_2) in the carbonator side heat exchangers (HXE, HXF, HXG, HXI) vs CaO conversion for a pressure ratio *PR* = 3.2. (b) Efficiency vs CaO conversion (using *PR* = 3.2) for selected absolute pressures of the carbonator and turbine outlet, respectively, as indicated.

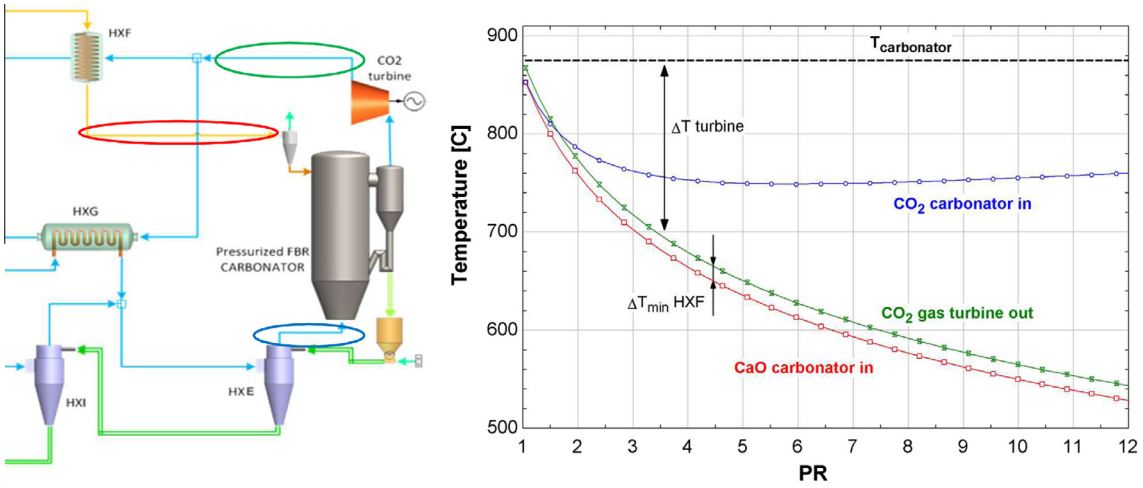

Fig. 7. Variation of temperatures in the regions encircled in the diagram (according to the colors code) with pressure ratio. (For interpretation of the references to color in this figure legend, the reader is referred to the web version of this article.)

3.2. Pressure

The carbonator pressure determines the upper pressure of the Brayton cycle and therefore plays a crucial role in the plant performance. The pressure ratio in the power turbine (T1) influences carbonator side's parameters, mainly temperatures (first of all turbine outlet temperature), flow rates, exchangers' nominal power (and size) and operational parameters. Some system variables show a direct dependence on the pressure ratio *PR* while others depend separately on the absolute values of the carbonator pressure and turbine outlet pressure.

High pressure ratios yield a reduced temperature at the turbine outlet as seen in Fig. 7 where the effect on the temperature of the sorbent (CaO) at the carbonator inlet can be observed too. Note that the optimized heat exchangers configuration adopted in the model yields high and stable values of the CO_2 temperature at the carbonator inlet regardless of the pressure ratio.

The trends of CaO and CO_2 temperatures at the carbonator inlet, both approaching the carbonator temperature in the limit $PR \rightarrow 1$, yield an infinite CO_2 flow rate for removal of the carbonation heat. At higher pressure ratios, CO_2 inlet temperature is quite stable while CaO temperature decreases, absorbing more heat in the reactor and causing the CO_2 flow rate to drop as it is seen in Fig. 9b (green curve)[1]. For this reason, high pressure ratios are desirable in order to reduce costs related to the limited inventory storage capacity and to the plant machinery size.

On the other hand, reduced values of *PR* allow for less strict operational limits regarding the critical value for CaO conversion below which no isothermal carbonator operation is possible. Fig. 8 shows the minimum CaO conversion required X_{lim} in the proposed power cycle as a function of the pressure ratio *PR*. The trend is again justified by the lower CaO temperatures at the carbonator inlet for increasing values of *PR*.

A detailed scheme of the CO_2 reaction turbine T2–CO_2 cycle compression C1 group is shown in Fig. 9a. The specific work of compression increases with the pressure ratio as seen in Fig. 9b. At a fixed pressure ratio, lower absolute pressures are associated with higher specific compression work, thus giving rise to an undesirable increase of compression power. This effect is shown in the blue curve of Fig. 10a where the power (calculated as the product of the CO_2 flow rate, following the trend shown in the green curve of Fig. 9b, by the specific work of compression, blue curve) is plotted vs pressure ratio for different values of turbine outlet pressure (shaded scale).

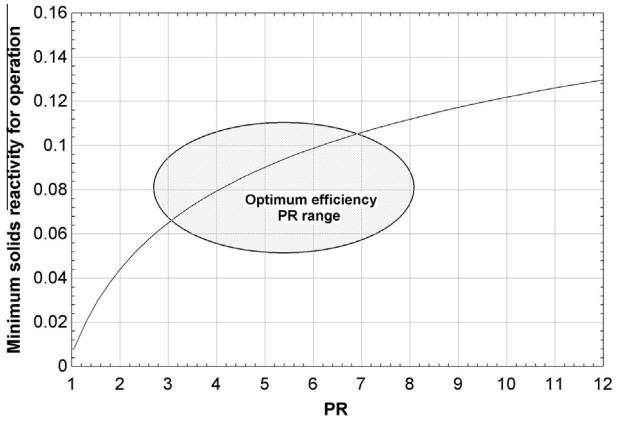

Fig. 8. Minimum value of CaO conversion for carbonator isothermal operation vs pressure ratio.

As may be seen in Fig. 10a, lower carbonator absolute pressures (and TOP) imply a higher expansion ratio in the turbine T2 (from 75 bar to carbonator pressure) and a proportional increase of power generation (see the shaded scaling around the green curve in Fig. 10a). Thus, smaller absolute pressures determine higher compression power but also higher expansion power. The latter beneficial effect prevails over the former detrimental one, thus the net power consumption of the group is decreased in practice by low absolute pressure values. As can be seen in Fig. 10b, the gross power generation in the turbine depends only weakly on the absolute pressures. Hence, better performances are retrieved for lower absolute pressures at a fixed pressure ratio. This explains the global plant efficiency trend with pressures, which is shown in detail in Figs. 11 and 12 (note that the energy consumption in compressor C2 does not depend on *PR*). Fig. 11 demonstrates that, as usually occurs for regenerative Brayton power cycles, there is a maximum in the efficiency-*PR* curve, occurring in the present case at 3.2 bar. A more detailed representation of the global efficiency achievable, as depending on the carbonator pressure *P* and turbine outlet pressure *TOP*, is given in the contour plot of Fig. 12 where a constant value of CaO conversion $X = 0.5$ has been assumed.

[1] For interpretation of color in Fig. 9, the reader is referred to the web version of this article.

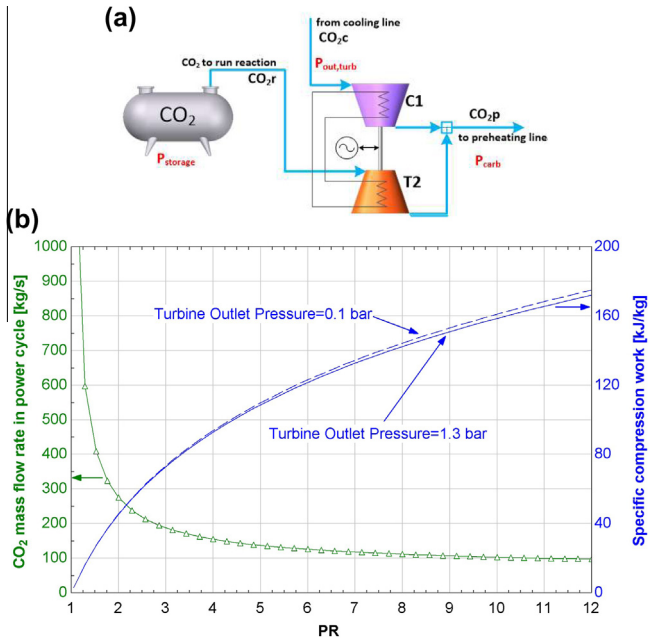

Fig. 9. (a) CO_2 reaction turbine–CO_2 cycle compression group. (b) Left axis: Specific work of compression vs pressure ratio *PR* for several turbine outlet pressures (TOP). TOP = 0.1 bar (dashed line) and 1.3 bar (solid line). Right axis: CO_2 mass flow rate vs *PR*.

The effect of gas pressure drops in the CO_2 power cycle has been also investigated since viscous frictional forces can be enhanced by the use of fluidized bed reactors and open cyclone exchangers. Due to pressure drops, the power consumption of the plant increases and the efficiency decreases. At the same time, the maximum of efficiency is shifted to higher pressure ratios albeit the location of the maximum becomes less marked as the pressure drop is increased (see Fig. 13). The weighted dotted line joins all the maximums for different values of pressure drops in the power cycle (expressed as percentage of the absolute carbonation pressure).

3.3. Temperature

In a Brayton cycle, the increase of turbine inlet temperature (which is, in the present case, the carbonator temperature *T*) naturally enhances the efficiency. It is therefore crucial to envisage which limits are imposed to the maximum carbonator temperature. A main limitation is linked to the equilibrium of the calcination/carbonation reaction. At a given temperature the reaction reaches equilibrium for a CO_2 pressure below which carbonation cannot take place. Equivalently, at a given CO_2 pressure, there is a maximum temperature above which carbonation is not possible. For example, under a pure CO_2 environment at atmospheric pressure, equilibrium is reached at ~895 °C. Carbonation slows down as practical operation conditions approach equilibrium [62]. Thus, the closer to equilibrium conditions the smaller will be the quantity of CO_2 reacting in the carbonator in practice (Fig. 14a).

The equilibrium fraction of CO_2 in the carbonator (molar fraction of CO_2 at maximum capture efficiency) is defined as [63]:

$$y_{eq} = \frac{P_{eq}}{P} = \frac{1}{P}\left[4.137\ 10^{7} \exp\left(-\frac{20474}{T}\right)\right] \quad (8)$$

where P_{eq} (bar) is the CO_2 pressure at equilibrium. According to Eq. (8), at a fixed carbonator pressure *P*, an increase of the carbonator temperature yields an increase of the equilibrium pressure of CO_2, and thus of y_{eq}.

At low temperatures, the CO_2 equilibrium pressure is small, thus the equilibrium molar fraction (y_{eq}) achievable is also very close to 0 and (almost) the entire stoichiometric amount of CO_2 can react even though the reaction kinetics will be hindered at very low temperatures [64]. On the other hand, if the temperature is increased, the equilibrium molar fraction of CO_2 achievable at the output approaches the CO_2 molar fraction at the input since the CO_2 pressure in the inlet gas stream becomes closer to the equilibrium pressure ($P_{CO_2,carb,in} \rightarrow P_{eq}$). When the combination of temperature and CO_2 pressure yields an equilibrium molar fraction of CO_2 equal to the inlet molar fraction ($y_{CO_2,carb,in}$) carbonation is not possible anymore. In the present application, the value of $y_{CO_2,carb,in}$ has been maximized by working with pure CO_2 in the carbonator, with the consequent relevant improvements in reaction kinetics and reactor efficiency. The equilibrium CO_2 reaction efficiency E_{eq}, defined as:

$$E_{eq} = \frac{F_{CO_2,in} - F_{CO_2,eq}}{F_{CO_2,in}} \quad (9)$$

represents the ratio of the CO_2 flow rate that reacts in the carbonator to the total CO_2 flow rate entering into it as limited by the reaction equilibrium. By increasing the carbonator temperature, the equilibrium CO_2 reaction efficiency is decreased (black curve of Fig. 14a). Thus, more CO_2 must be circulated in the loop in order to maintain the desired rate of thermal energy generation in the carbonator (Fig. 14b). It is therefore important not to work too close to the equilibrium limit in order to keep CO_2 flow rates at a feasible value. Moreover, the reaction kinetics would be slowed down as equilibrium is approached [64]. Note that the above means that higher carbonator pressures may yield an increase of efficiency through a carbonation temperature upgrade, as shown in the dotted curves of Fig. 14a.

3.4. Combined effect of temperature, pressure ratio and carbonator pressure

The search for an optimum operation point that might result from a specific combination of temperature, carbonator pressure and pressure ratio is not straightforward. On one side, despite low absolute pressures are beneficial for increasing the efficiency at a fixed carbonator temperature, high pressures allow for further temperature upgrading, which yields higher efficiency. This is shown in Fig. 15 where the red curve, corresponding to low absolute pressures (turbine outlet pressure of 1 bar) shows a maximum efficiency of 42.6% at 875 °C for *PR* = 3.2. If absolute pressures are increased, operation at the optimum pressure ratio may be possible at an increased temperature of 950 °C, thus increasing the efficiency through a temperature upgrade despite the higher absolute pressure.

Note that in Fig. 15 the CO_2 flow rate is calculated by taking into account the real equilibrium limitations (as shown in Fig. 14b). The dashed part of the curves in Fig. 15 represent a constrained operation range on the circulating rates set by an equilibrium molar fraction of CO_2 in the carbonator exceeding 0.3.

Despite the maximum in the efficiency curve occurs at pressure ratios around 3, the molar flow rates (and the size of all exchangers, in particular the exchanger HXG) can be considerably reduced through an increase of the pressure ratio without efficiency penalizations. If the carbonator pressure is increased higher carbonation temperatures are in fact achievable and therefore the same efficiency can be reached through optimizing costs as shown in Fig. 16.

Summarizing, the analysis carried out yields the following main conclusions:

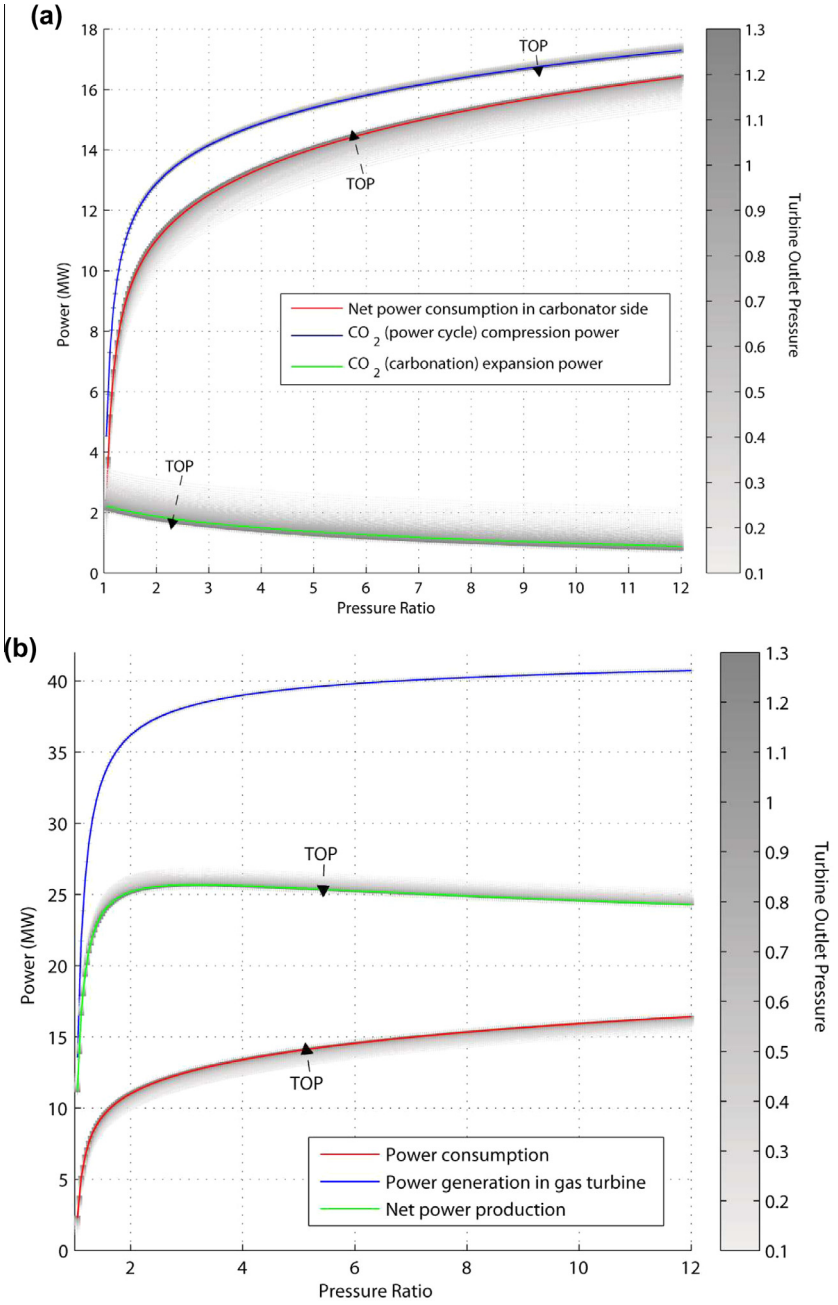

Fig. 10. (a) Power balance in the T2/C1 group. Net power consumption (carbonator side) vs pressure ratio for different values of turbine outlet pressure (shaded scale, where arrows direction represents higher TOP values). Solid curves refer to atmospheric turbine output pressure. (b) Power balance in the carbonator side. Net power consumption, power generation in the turbine and net power production vs pressure ratio for different values of turbine outlet pressure are shown. A constant value of CaO conversion $X = 0.5$ is used.

- Thermal optimization of the power cycle increase the global plant efficiency and invert the negative trend of the efficiency with increasing CaO average conversion in the carbonator (X) that was inferred from a previous work [17]. The optimum configuration with exchangers HXE, HXF, HXG and HXI yield high integration efficiencies.
- Achieving high values of CaO conversion X is beneficial for every aspect: higher efficiency, amount of passive solids reduction, lower size of silos and storage, lower size of exchangers and lower fresh sorbent makeup flow (in the case it was needed). Nevertheless, the nominal power of the regenerator HXG increases with X and this can lead to a disproportionate increase of cost unless pressure ratio is increased.
- The optimal pressure ratio value is found at low values (PR around 3.2) although several issues must be remarked:
  - o Pressure ratios below the maximum must be avoided because they lead to a notable efficiency drop.
  - o Pressure ratios above the maximum only generate a slow decrease in efficiency.
  - o The presence of frictional pressure losses in the CO_2 circuit decreases the maximum efficiency and shifts the maximum to higher PR (around $PR = 4.8$ when pressure losses are 20% of the carbonator pressure P, $PR = 7.1$ when they are 50%P). Besides, it stabilizes the efficiency value for a wide range of pressure ratios (e.g. if 20%P pressure losses occur, the optimum point is at $PR = 5$ but the efficiency variation is below 1% for PR in the range 2.8–10).

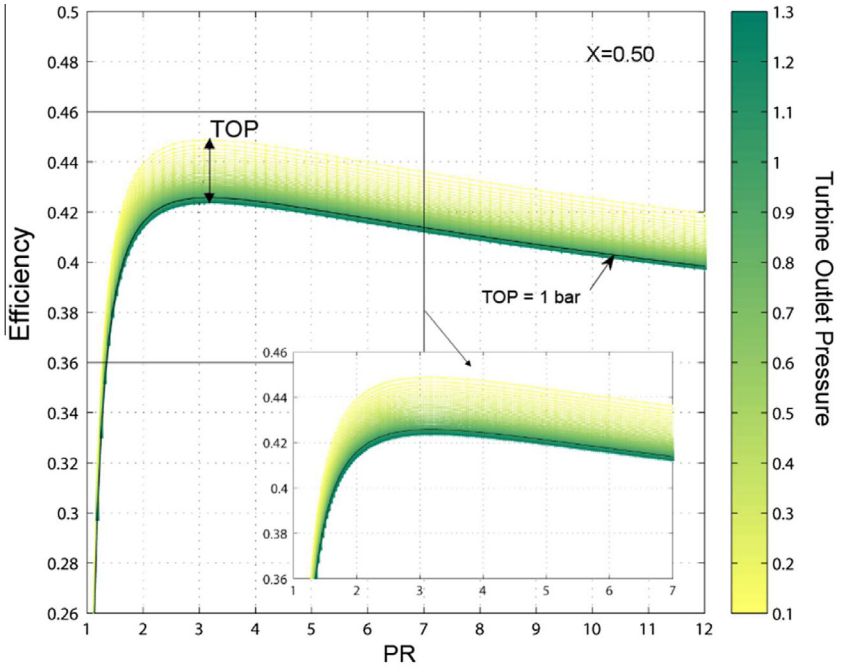

Fig. 11. Plant efficiency as a function of carbonator to turbine outlet pressures ratio (for a fixed CaO conversion $X = 0.5$) and turbine outlet pressure TOP (shaded scaling). The solid line corresponds to TOP = 1 bar.

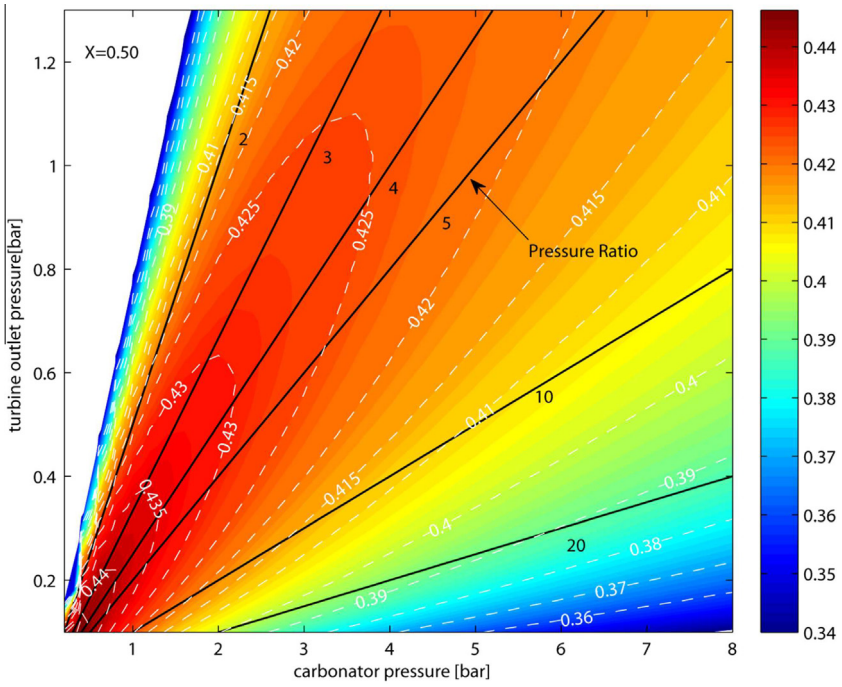

Fig. 12. Contour plot of efficiency (assuming a constant value of CaO conversion $X = 0.5$) as depending on carbonator and turbine outlet pressure. Black lines indicate a constant value of pressure ratio.

- o The CO_2 flow rate needed in the power cycle reaches very high values when pressure ratios are small (At $X = 0.5$ it should be >300 kg/s for $PR < 2$; >200 kg/s for $PR < 2.8$; <100 kg/s for $PR > 10$).
- o Consequently, the nominal power (thus size and cost) of all heat exchangers can be reduced by increasing the pressure ratio. This concerns in particular the regenerator HXG (the most affected one by the CO_2 flow rate) whose size is reduced by 3–4 times when PR is increased from $PR = 3$ to $PR = 9$.

– Despite the (although small) efficiency drop, high pressure ratios are therefore desirable to reduce the circulating CO_2 flow rate and the size of exchanger HXG, in particular if the CaO solids show a high value of conversion X. The unavoidable

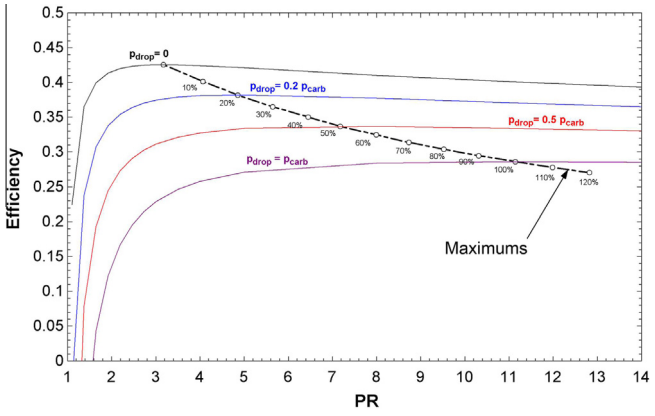

Fig. 13. Influence of pressure drops of CO_2 in the circuit on efficiency as a function of pressure ratio *PR*. Maximum efficiency is decreased and the optimum pressure ratio is increased. Turbine outlet pressure = 1 bar, CaO conversion $X = 0.5$.

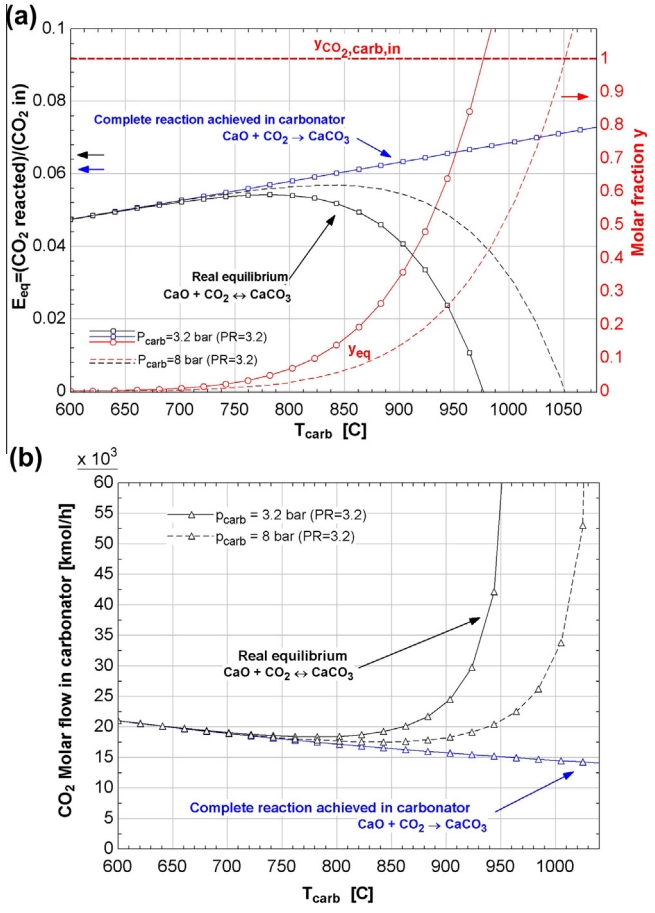

Fig. 14. (a) Left axis: Carbonator capture efficiency vs temperature in the case of fully achieved carbonation (blue curve) and equilibrium capture efficiency (black curve) for carbonator pressures of 3.2 (solid line) and 8 (dotted line) bar (fixed pressure ratio $PR = 3.2$). Right axis: equilibrium and inlet molar fraction of CO_2 vs temperature. (b) CO_2 molar flow rate through the carbonator vs carbonation temperature. Note that pure CO_2 is used in the carbonator as working fluid.

presence of gas pressure losses makes this choice less penalizing from the efficiency point of view.

– The role of absolute carbonator and turbine outlet pressure on the plant efficiency is significant:
  o Lower absolute pressures yield higher performances at fixed carbonator temperature thanks to the higher CO_2 turbine T2 expansion ratio.

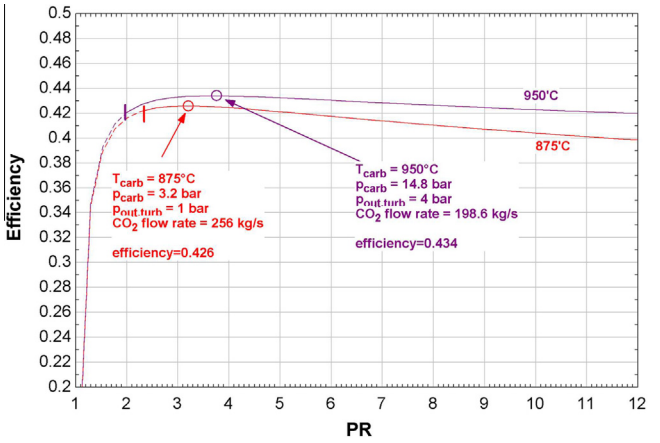

Fig. 15. Efficiency as a function of *PR* for different values of carbonation temperature and turbine outlet pressure. Red curve: turbine outlet pressure = 1 bar, carbonation temperature = 875 °C; operation point (max efficiency): carbonator pressure = 3.2 bar ($PR = 3.2$). Purple curve: turbine outlet pressure = 4 bar, carbonation temperature = 950 °C; operation point: carbonator pressure = 14.8 bar ($PR = 3.7$). The dashed part of the curves corresponds to CO_2 equilibrium molar fraction > 0.3. It can be seen that working at the optimum point with higher absolute pressures enhances efficiency through a temperature upgrade. (For interpretation of the references to color in this figure legend, the reader is referred to the web version of this article.)

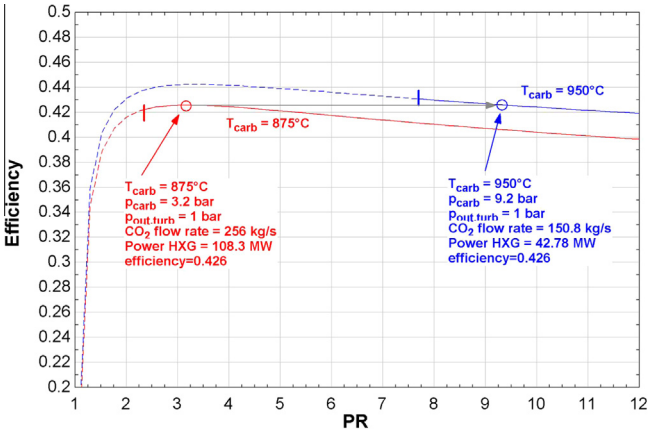

Fig. 16. Efficiency as a function of *PR* for different values of the carbonation temperature. Red curve: turbine outlet pressure = 1 bar, carbonation temperature = 875 °C; operation point: carbonator pressure = 3.2 bar ($PR = 3.2$). Blue curve: turbine outlet pressure = 1 bar, carbonation temperature = 950 °C; operation point: carbonator pressure = 9.2 bar ($PR = 9.2$). The dashed part of the curves corresponds to CO_2 equilibrium molar fraction > 0.3. The horizontal arrow shows that working at higher pressure ratios is possible without penalizing efficiency through a temperature upgrade. (For interpretation of the references to color in this figure legend, the reader is referred to the web version of this article.)

  o Nevertheless, high carbonator pressures ensure from equilibrium considerations higher temperature achievable in the carbonation reaction with the consequent efficiency upgrade.
  o At same time, at low pressures the specific volume of CO_2 may lead to an excessive increase of the size of the gas turbine and pipelines (especially for turbine outlet below atmospheric pressure).

3.5. Limestone derived CaO conversion at CSP–CaL integration conditions

The combined effects of pressure ratio, carbonator pressure and temperature must be carefully re-evaluated once the value of residual CaO conversion achievable under the specific CaL

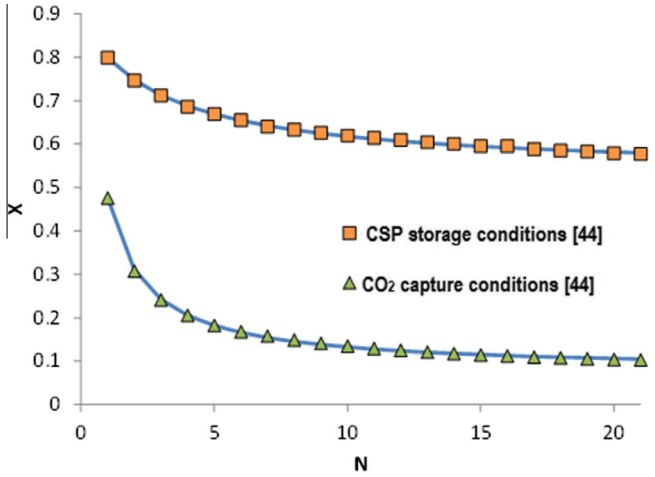

Fig. 17. Multicycle conversion of limestone derived CaO as obtained from thermogravimetric analysis (TGA) tests under different CaL conditions (reported in [44]). CSP storage conditions: carbonation at 850 °C under pure CO_2 and calcination at 700 °C under pure He. CO_2 capture conditions: Carbonation at 650 °C under a 15% CO_2/85% air vol/vol atmosphere and calcination at 950 °C under a 70%CO_2/30% air vol/vol atmosphere. Residence times at both stages were 5 min. The solid lines are best fits from Eq. (10) to data.

operating conditions for the CSP–CaL integration is determined from lab-scale experimental measurements. It is important to remind here that most of previous lab-scale experimental measurements on the multicycle conversion of limestone derived CaO are carried out at the standard conditions corresponding to the CaL process for CO_2 capture [28]. These are rather different from those to be found in the CSP–CaL integration at the optimum efficiency operating conditions inferred from the present work.

The CaL process requires usually a periodic purge of deactivated sorbent, which must be compensated by a makeup flow of fresh limestone in order to keep the mass balance. This is indeed the case of the CaL process for CO_2 capture. The specific CaL conditions for this integration involve calcination under high temperature at high CO_2 partial pressure and carbonation under low CO_2 partial pressure, which give rise to a severe drop of the CaO conversion after only a few cycles. After a large number of cycles CaO conversion converges asymptotically towards a residual value of just about 0.07–0.08 [65,66]. However, the specific conditions for an efficient integration of the CaL process into CSP plants involve, as seen above, carbonation under high CO_2 partial pressure at high temperatures. Fig. 17 shows recently obtained experimental results from thermogravimetric tests on the conversion of limestone derived CaO as a function of the calcination/carbonation

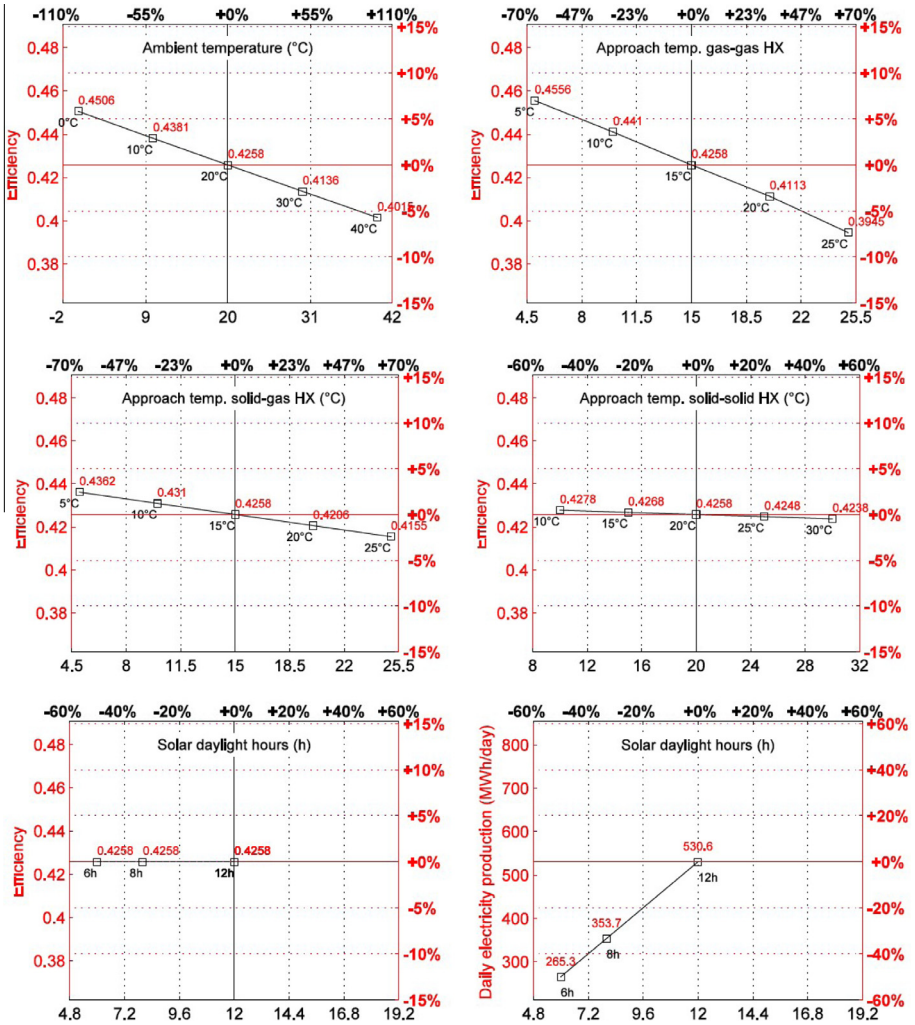

Fig. 18. Efficiency variation derived from a sensitivity analysis on ambient temperature, heat exchangers and solar daylight hours using as reference values those shown in Table 3.

Table 3
Reference values and ranges of variation for the parameters considered in the sensitivity analysis.

Parameter	Sensitivity on	Ref. value	Range of variation		
Ambient temperature	Efficiency, Storage volume	20 °C	0 °C	÷	40 °C
Carbonator thermal dispersions (% of carbonator thermal power production)	Efficiency	10%	2%	÷	15%
CO_2 storage pressure	Efficiency	75 bar	50 bar	÷	120 bar
Minimum temperature difference solid–solid exchangers	Efficiency	20 °C	10 °C	÷	30 °C
Minimum temperature difference gas–solid exchangers	Efficiency	15 °C	5 °C	÷	25 °C
Minimum temperature difference gas–gas exchangers	Efficiency	15 °C	5 °C	÷	25 °C
Pressure drops in carbonator circuit (% of carbonator pressure)	Efficiency	0%	0%	÷	20%
Conveying consumption factor	Efficiency	10 MJ/ 100 m/tonne	3 MJ/ 100 m/tonne	÷	18 MJ/ 100 m/tonne
Total solid conveying equivalent distance	Efficiency	200 m	50 m	÷	350 m
Solar daylight hours	Daily electricity production	12 h	6 h	÷	12 h

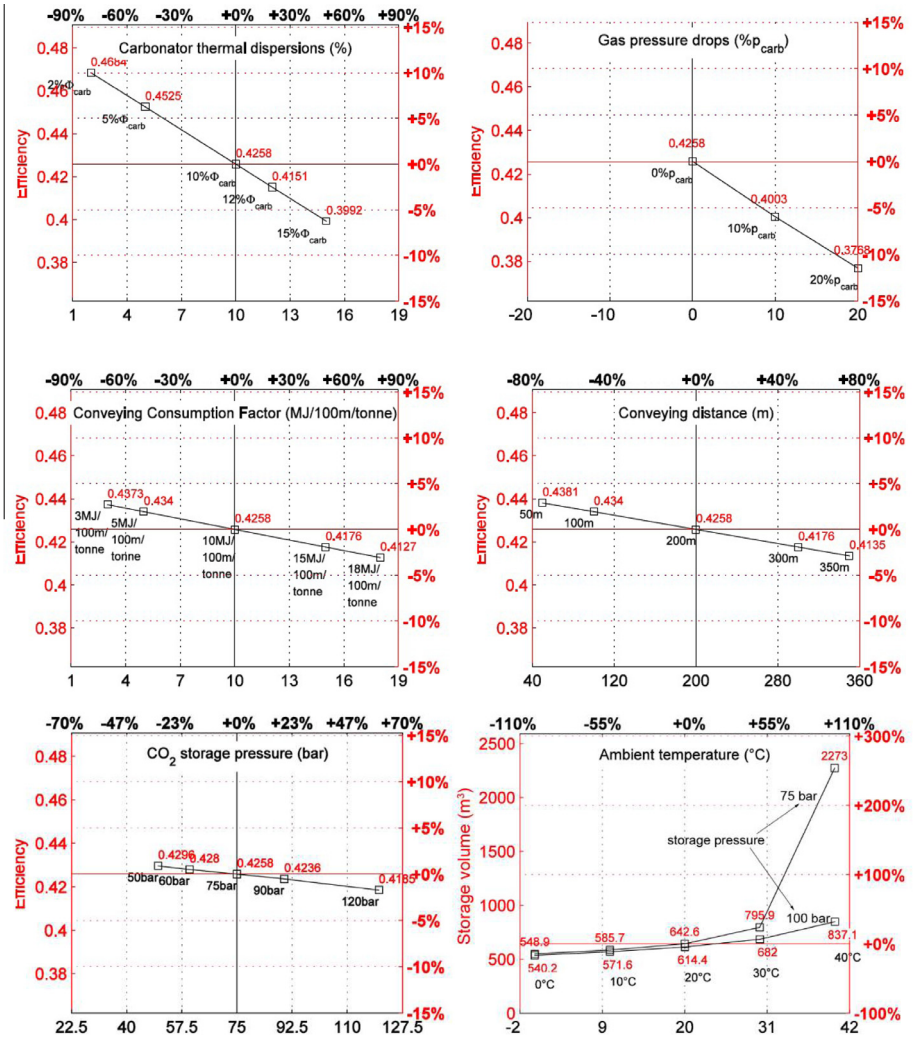

Fig. 19. Efficiency variation derived from a sensitivity analysis on carbonator thermal dispersion, system transport and storage pressure using as reference values those shown in Table 3.

cycle number N under CaL conditions specific for both CO_2 capture and CSP energy storage [44].

The experimental results shown in Fig. 17 highlight the radical different behavior of natural limestone derived CaO as depending on the CaL conditions. In order to find out a value of the residual CaO conversion X_r, the semi-empirical Eq. (10) can be fitted to conversion data [66].

$$\frac{X_N}{X_1} = \frac{X_r}{X_1} + \left(\frac{1}{\kappa(N-1) + \left(1 - \frac{X_r}{X_1}\right)^{-1}} \right) \tag{10}$$

Thus, the obtained residual CaO conversion is just about 0.08 for CO_2 capture conditions whereas it becomes as large as X_r = 0.53 for conditions that correspond to the CSP–CaL integration. Expectedly,

this value will be even higher when the CaO solids are carbonated under CO_2 at over atmospheric pressure, which will enhance the reaction kinetics and increase the equilibrium temperature, thus allowing carbonation at even higher temperatures [62]. Importantly, this high residual CaO conversion is obtained for residence times of just 5 min both in the carbonation and calcination stages [44]. This would allow in practice the use of circulating fluidized bed (CFB) reactors that ensure a highly efficient transfer of mass and heat for solid–gas reactions and whose suitability to the CaL process is already proven in CO_2 capture pilot plants. Note that fast calcination is achieved at a reduced temperature of just 700 °C under a gas which is easily separable from CO_2 (either He as in the TGA experiments or superheated steam as in Catalytic Flash Calcination technology [52]), which would allow the use of already mature and inexpensive metallic solar receivers thus reducing technological risks.

4. Sensitivity analysis

Results from a sensitivity analysis of the intervening parameters on plant efficiency are shown in Figs. 18 and 19 using the data reported in Table 3. In Fig. 18 a sensitivity analysis on the effects of ambient temperature, heat exchangers design and solar daylight hours is presented whereas in Fig. 19 the effects on global plant efficiency of carbonator thermal dispersion, transport losses and storage pressure are shown. Reference values are obtained for $X = 0.5$, carbonator pressure of 3.2 bar, turbine outlet pressure of 1 bar and carbonator temperature of 875 °C.

According to the results obtained from the sensitivity analysis carried out on diverse parameters (Figs. 18 and 19) the following main conclusions may be drawn:

- The sensitivity of efficiency to ambient temperature is high. An ambient temperature variation of 20 °C leads to a 6% relative variation of efficiency. The same increase leads to roughly 250% bigger volumes when storage pressure is 75 bar. By increasing the storage pressure above 100 bar, the volume growth is more restricted (around 36%). Due to the high ambient temperatures typically present in CSP plant emplacements, the addition of gas-cooling devices upstream compression to avoid this effect should be considered.
- A ±70% variation of exchangers' approach temperatures (excluded the gas–gas regenerator) produces a modest efficiency variation, which is below 3% in relative terms.
- Unlike for the other heat exchangers, the approach temperature of the regenerator HXG (gas–gas exchanger) has a critical effect on performance. Reducing the value of ΔT_{min} by 10 °C leads to a relative increase of efficiency greater than 7%, passing from 42.6% to 45.6% in absolute value.
- Thermal dispersions in the carbonator and pipework have a major influence on efficiency: a decrease of thermal dispersion from 10% down to 2% of the reaction heat can lead to over 10% relative higher efficiency. This issue highlights the importance of providing efficient insulation to the hot components.
- A 150 m conveying distance variation produces a relative efficiency variation below 3%. The same variation is caused by an 8 MJ/100 m/ton change of the specific conveying consumption factor.
- Solids conveying energy consumption, as noted in previous paragraphs, can be quite critical if high values of CaO conversion are not achievable due to the higher amounts of solids in the loop.
- The impact of pressure drops in the gas circuit is very relevant, with a 12% relative efficiency decrease when going from 0% pressure losses to 20% losses (% referred to the carbonator pressure).
- The number of solar daylight hours influences the amounts of dissociated products (CaO and CO_2) available at the beginning of the day for energy production in the discharge phase.

5. Conclusions

This paper explores a thermochemical energy storage concept in Concentrated Solar Power plants (CSP) based on the Calcium Looping process (CaL), which allows a fully decoupled operation of charge and discharge phases for long periods. It uses an abundant, geographically widespread, cheap and non-toxic raw material such as limestone. Moreover, the multicycle conversion of limestone derived CaO at specific CaL conditions for integration in CSP plants converges towards a rather high residual value as demonstrated by lab-scale TGA results. Therefore, affordable costs can be expected.

The proposed CSP–CaL integration is technically feasible with mature technologies already available in the market for input heat powers (net heat supply at the calciner) ranging from small to above 100 MW_{th} values. It uses a pressurized fluidized reactor for carbonation, solids pneumatic conveying technology, gas–solid cyclone/closed heat exchangers, gas–gas regenerators, a pressurized storage vessel at 75 bar for CO_2, two atmospheric silos for CaO and $CaCO_3$ storage, and conventional intercooling compressor and turbine systems. A main feature of the integration is that a closed CO_2 circuit is used for operation of both the CaL process and the power cycle.

The analyses presented in the paper shows that for a ratio of carbonator to outlet turbine pressures of 3.2 bars, and a carbonator temperature of 875 °C, plant efficiencies above 45% may be reached. The optimized CSP–CaL integration provides several benefits over previous studies, including complete absence of CO_2 released from the system, improved kinetics in the carbonator at elevated temperatures and high CO_2 pressures, high carbonator temperatures attainable and high thermal efficiency values. First law efficiency of 40–46% and second law efficiency of 43–48% are achievable under realistic conditions and taking into account heat losses, pressure drops and conveying energy consumption. According to our study, the main parameters to improve the proposed cycle are similar to those used in other power cycles, namely, turbine inlet temperature, pressure ratio in the Brayton turbine, boiler/reactor/heat exchangers' efficiency or pressure losses taking into account the particularities linked to chemical equilibrium and reaction kinetics as determined by CO_2 partial pressure and temperature.

The competitiveness of the proposed integration is reinforced by the fact that the obtained efficiency is higher than that of Rankine cycles traditionally employed in CSP plants. A detailed economic assessment is out of the scope of the present manuscript. However, it is estimated elsewhere that an efficient CSP–CaL integration would reduce the cost of Levelized Cost of Electricity (LCOE) below 7c€/kWh (see SUNSHOT program [67]). This estimation takes into account further improvements in the solar field, receiver and power block and considers a thermochemical energy storage cost below \$15/kWh_{th}.

Acknowledgements

This work was supported by the Andalusian Regional Government Junta de Andalucia (contract FQM-5735) and Spanish Government Agency Ministerio de Economia y Competitividad and FEDER Funds (contracts CTQ2014-52763-C2-1-R, CTQ2014-52763-C2-2-R and MAT2013-41233-R). The Functional Characterization service of the Innovation, Technology and Research Center of the University of Seville (CITIUS) is gratefully acknowledged.

References

[1] N'Tsoukpoe KE, Liu H, Le Pierrès N, Luo L. A review on long-term sorption solar energy storage. Renew Sust Energy Rev 2009;13:2385–96. http://dx.doi.org/10.1016/j.rser.2009.05.008.

[2] Mahlia TMI, Saktisahdan TJ, Jannifar A, Hasan MH, Matseelar HSC. A review of available methods and development on energy storage; technology update. Renew Sust Energy Rev 2014;33:532–45. http://dx.doi.org/10.1016/j.rser.2014.01.06.

[3] Medrano M, Gil A, Martorell I, Potau X, Cabeza LF. State of the art on high-temperature thermal energy storage for power generation. Part 2 – Case studies. Renew Sust Energy Rev 2010;14:56–72. http://dx.doi.org/10.1016/j.rser.2009.07.03.

[4] Paksoy HÖ. Thermal energy storage for sustainable energy consumption; 2007.

[5] Kearney D, Kelly B, Herrmann U, Cable R, Pacheco J, Mahoney R, et al. Engineering aspects of a molten salt heat transfer fluid in a trough solar field. Energy 2004;29:861–70. http://dx.doi.org/10.1016/S0360-5442(03)00191-9.

[6] Fernández AG, Ushak S, Galleguillos H, Pérez FJ. Development of new molten salts with $LiNO_3$ and $Ca(NO_3)_2$ for energy storage in CSP plants. Appl Energy 2014;119:131–40. http://dx.doi.org/10.1016/j.apenergy.2013.12.061.

[7] Rodríguez I, Pérez-Segarra CD, Lehmkuhl O, Oliva A. Modular object-oriented methodology for the resolution of molten salt storage tanks for CSP plants. Appl Energy 2013;109:402–14. http://dx.doi.org/10.1016/j.apenergy.2012.11.008.

[8] Kuravi S, Trahan J, Goswami DY, Rahman MM, Stefanakos EK. Thermal energy storage technologies and systems for concentrating solar power plants. Prog Energy Combust Sci 2013;39:285–319. http://dx.doi.org/10.1016/j.pecs.2013.02.001.

[9] Karagiannakis G, Pagkoura C, Zygogianni A, Lorentzou S, Konstandopoulos AG. Monolithic ceramic redox materials for thermochemical heat storage applications in CSP plants. Energy Proc 2014;49:820–9. http://dx.doi.org/10.1016/j.egypro.2014.03.089.

[10] Zalba B, Marín JM, Cabeza LF, Mehling H. Review on thermal energy storage with phase change: materials, heat transfer analysis and applications 2003; 23. http://dx.doi.org/10.1016/S1359-4311(02)00192-8.

[11] Tian Y, Zhao CY. A review of solar collectors and thermal energy storage in solar thermal applications. Appl Energy 2013;104:538–53. http://dx.doi.org/10.1016/j.apenergy.2012.11.051.

[12] Nithyanandam K, Pitchumani R. Design of a latent thermal energy storage system with embedded heat pipes. Appl Energy 2014;126:266–80. http://dx.doi.org/10.1016/j.apenergy.2014.03.025.

[13] Sharma A, Tyagi VV, Chen CR, Buddhi D. Review on thermal energy storage with phase change materials and applications. Renew Sust Energy Rev 2009;13:318–45. http://dx.doi.org/10.1016/j.rser.2007.10.005.

[14] Pardo P, Deydier A, Anxionnaz-Minvielle Z, Rougé S, Cabassud M, Cognet P. A review on high temperature thermochemical heat energy storage. Renew Sust Energy Rev 2014;32:591–610. http://dx.doi.org/10.1016/j.rser.2013.12.01.

[15] Li TX, Wu S, Yan T, Xu JX, Wang RZ. A novel solid–gas thermochemical multilevel sorption thermal battery for cascaded solar thermal energy storage. Appl Energy 2016;161:1–10. http://dx.doi.org/10.1016/j.apenergy.2015.09.084.

[16] Abedin A, Rosen M. A critical review of thermochemical energy storage systems. Open Renew Energy J n.d.:42–6. http://dx.doi.org/10.2174/1876387101004010042.

[17] Edwards SEB, Materić V. Calcium looping in solar power generation plants. Sol Energy 2012;86:2494–503. http://dx.doi.org/10.1016/j.solener.2012.05.019.

[18] Sakellariou KG, Karagiannakis G, Criado YA, Konstandopoulos AG. Calcium oxide based materials for thermochemical heat storage in concentrated solar power plants. Sol Energy 2015;122:215–30. http://dx.doi.org/10.1016/j.solener.2015.08.011.

[19] Kyaw K, Matsuda H, Hasatani M. Applicability of carbonation/decarbonation reactions to high-temperature thermal energy storage and temperature upgrading. J Chem Eng Jpn 1996;29:119–25. http://dx.doi.org/10.1252/jcej.29.119.

[20] Ortega-Fernández I, Calvet N, Gil A, Rodríguez-Aseguinolaza J, Faik A, D'Aguanno B. Thermophysical characterization of a by-product from the steel industry to be used as a sustainable and low-cost thermal energy storage material. Energy 2015;89:601–9. http://dx.doi.org/10.1016/j.energy.2015.05.153.

[21] Peng Q, Yang X, Ding J, Wei X, Yang J. Design of new molten salt thermal energy storage material for solar thermal power plant. Appl Energy 2013;112:682–9. http://dx.doi.org/10.1016/j.apenergy.2012.10.048.

[22] Peng Q, Ding J, Wei X, Yang J, Yang X. The preparation and properties of multi-component molten salts. Appl Energy 2010;87:2812–7. http://dx.doi.org/10.1016/j.apenergy.2009.06.022.

[23] Vignarooban K, Xu X, Arvay A, Hsu K, Kannan AM. Heat transfer fluids for concentrating solar power systems – a review. Appl Energy 2015;146:383–96. http://dx.doi.org/10.1016/j.apenergy.2015.01.125.

[24] Rodriguez N, Alonso M, Grasa G, Abanades JC. Heat requirements in a calciner of $CaCO_3$ integrated in a CO_2 capture system using CaO. Chem Eng J 2008;138:148–54. http://dx.doi.org/10.1016/j.cej.2007.06.005.

[25] Martínez A, Lara Y, Lisbona P, Romeo LM. Energy penalty reduction in the calcium looping cycle. Int J Greenhouse Gas Control 2012;7:74–81. http://dx.doi.org/10.1016/j.ijggc.2011.12.005.

[26] Kim K, Kim D, Park Y, Soon K. A solid sorbent-based multi-stage fluidized bed process with inter-stage heat integration as an energy efficient carbon capture process. Int J Greenhouse Gas Control 2014;26:135–46. http://dx.doi.org/10.1016/j.ijggc.2014.03.012.

[27] Ylätalo J, Ritvanen J, Tynjälä T, Hyppänen T. Model based scale-up study of the calcium looping process. Fuel 2014;115:329–37. http://dx.doi.org/10.1016/j.fuel.2013.07.036.

[28] Perejon A, Romeo LM, Lara Y, Lisbona P, Valverde JM. The calcium-looping technology for CO_2 capture: on the important roles of energy integration and sorbent behavior. Appl Energy 2015;162:787–807. http://dx.doi.org/10.1016/j.apenergy.2015.10.121.

[29] Romano MC. Modeling the carbonator of a Ca-looping process for CO_2 capture from power plant flue gas. Chem Eng Sci 2012;69:257–69. http://dx.doi.org/10.1016/j.ces.2011.10.041.

[30] Ortiz C, Chacartegui R, Valverde J, Becerra J, Perez-Maqueda L. A new model of the carbonator reactor in the calcium looping technology for post-combustion CO_2 capture. Fuel 2015;160:328–38. http://dx.doi.org/10.1016/j.fuel.2015.07.095.

[31] Charitos A, Hawthorne C, Bidwe AR, Sivalingam S, Schuster A, Spliethoff H, et al. Parametric investigation of the calcium looping process for CO2 capture in a 10 kWth dual fluidized bed. Int J Greenhouse Gas Control 2010;4:776–84. http://dx.doi.org/10.1016/j.ijggc.2010.04.00.

[32] Hanak DP, Anthony EJ, Manovic V. A review of developments in pilot-plant testing and modelling of calcium looping process for CO_2 capture from power generation systems. Energy Environ Sci 2015. http://dx.doi.org/10.1039/C5EE01228G.

[33] Lara Y, Lisbona P, Martínez A, Romeo LM. Design and analysis of heat exchanger networks for integrated Ca-looping systems. Appl Energy 2013;111:690–700. http://dx.doi.org/10.1016/j.apenergy.2013.05.044.

[34] Shimizu T, Hirama T, Hosoda H, Kitano K, Inagaki M, Tejima K. A twin fluid-bed reactor for removal of CO_2 from combustion processes. Chem Eng Res Des 1999;77:62–8. http://dx.doi.org/10.1205/026387699525882.

[35] Yang Y, Zhai R, Duan L, Kavosh M, Patchigolla K, Oakey J. Integration and evaluation of a power plant with a CaO-based CO_2 capture system. Int J Greenhouse Gas Control 2010;4:603–12. http://dx.doi.org/10.1016/j.ijggc.2010.01.004.

[36] Lasheras A, Ströhle J, Galloy A, Epple B. Carbonate looping process simulation using a 1D fluidized bed model for the carbonator. Int J Greenhouse Gas Control 2011;5:686–93. http://dx.doi.org/10.1016/j.ijggc.2011.01.005.

[37] Arias B, Diego ME, Abanades JC, Lorenzo M, Diaz L, Martínez D, et al. Demonstration of steady state CO_2 capture in a 1.7 MWth calcium looping pilot. Int J Greenhouse Gas Control 2013;18:237–45. http://dx.doi.org/10.1016/j.ijggc.2013.07.014.

[38] Ströhle J, Junk M, Kremer J, Galloy A, Epple B. Carbonate looping experiments in a 1 MWth pilot plant and model validation. Fuel 2014;127:13–22. http://dx.doi.org/10.1016/j.fuel.2013.12.043.

[39] Ortiz C, Chacartegui R, Valverde JM, Becerra JA. A new integration model of the calcium looping technology into coal fired power plants for CO_2 capture. Appl Energy 2016;169:408–20. http://dx.doi.org/10.1016/j.apenergy.2016.02.050.

[40] Tregambi C, Montagnaro F, Salatino P, Solimene R. A model of integrated calcium looping for CO_2 capture and concentrated solar power. Sol Energy 2015;120:208–20. http://dx.doi.org/10.1016/j.solener.2015.07.017.

[41] Abanades JC. The maximum capture efficiency of CO_2 using a carbonation/calcination cycle of $CaO/CaCO_3$. Chem Eng J 2002;90:303–6. http://dx.doi.org/10.1016/S1385-8947(02)00126-2.

[42] Abanades JC, Alvarez D. Conversion limits in the reaction of CO_2 with lime. Energy Fuels 2003;17:308–15. http://dx.doi.org/10.1021/ef020152a.

[43] Rhodes NR, Barde A, Randhir K, Li L, Hahn DW, Mei R, et al. Solar thermochemical energy storage through carbonation cycles of $SrCO_3/SrO$ supported on $SrZrO_3$. ChemSusChem 2015. http://dx.doi.org/10.1002/cssc.201501023. n/a–n/a.

[44] Sarrion B, Valverde JM, Perejon A, Perez-maqueda LA, Sanchez-jimenez PE. On the multicycle activity of natural limestone/dolomite for cheap, efficient and non-toxic thermochemical energy storage of concentrated solar power. Energy Technol; 2016. http://dx.doi.org/10.1002/ente.201600068.

[45] Meier A, Bonaldi E, Cella GM, Lipinski W, Wuillemin D. Solar chemical reactor technology for industrial production of lime. Sol Energy 2006;80:1355–62. http://dx.doi.org/10.1016/j.solener.2005.05.017.

[46] Badie JM, Bonet C, Faure M, Flamant G, Foro R, Hernandez D. 52 Decarbonation of calcite and phosphate rock in solar chemical reactors. Chem Eng Sci 1980;35:413–20. http://dx.doi.org/10.1016/0009-2509(80)80114-X.

[47] Meier A, Bonaldi E, Cella GM, Lipinski W, Wuillemin D, Palumbo R. Design and experimental investigation of a horizontal rotary reactor for the solar thermal production of lime. Energy 2004;29:811–21. http://dx.doi.org/10.1016/S0360-5442(03)00187-7.

[48] Meier A, Bonaldi E, Cella GM, Lipinski W. Multitube rotary kiln for the industrial solar production of lime. J Sol Energy Eng 2005;127:386. http://dx.doi.org/10.1115/1.1979517.

[49] Imhof A. Decomposition of limestone in a solar reactor. Renew Energy 1996;9:661–3. http://dx.doi.org/10.1016/0960-1481(96)88373-X.

[50] Winter CJ, Sizmann RL, Vant-Hull LL. Solar power plants: fundamentals, technology, systems, economics. Springer-Verlag; 1991.

[51] Valverde JM, Sanchez-Jimenez PE, Perez-Maqueda L. Limestone calcination nearby equilibrium: kinetics, CaO crystal structure, sintering and reactivity. J Phys Chem C 2015;119:1623–41. http://dx.doi.org/10.1021/jp508745u.

[52] Sceats G, Horley CJ, Richardson P, Sceats MG. System and method for the calcination of minerals. WO2007112496A1; 2014.
[53] Berger EE. Effect of steam on the decomposition of limestone. Ind Eng Chem 1927;19:594–6. http://dx.doi.org/10.1021/ie50209a026.
[54] Wang Y, Lin S, Suzuki Y. CO_2/steam and CO_2/N_2 atmospheres. Energy 2008:2326–31.
[55] Ávila-Marín AL. Volumetric receivers in solar thermal power plants with central receiver system technology: a review. Sol Energy 2011;85:891–910. http://dx.doi.org/10.1016/j.solener.2011.02.002.
[56] Yu FC, Fan LS. Kinetic study of high-pressure carbonation reaction of calcium-based sorbents in the calcium looping process (CLP). Ind Eng Chem Res 2011;50:11528–36. http://dx.doi.org/10.1021/Ie200914e.
[57] Mills D. Pneumatic conveying design guide; 2004. p. 80.
[58] Shimizu A, Yokomine T, Nagafuchi T. Development of gas–solid direct contact heat exchanger by use of axial flow cyclone. Int J Heat Mass Transfer 2004;47:4601–14. http://dx.doi.org/10.1016/j.ijheatmasstransfer.2003.10.045.
[59] Jordison N, Rozendaal NA, Huang PXD. Indirect-heat thermal processing of particulate material; 2007.
[60] Marechal F. Process integration and improvement. Exergy, Energy Syst. Anal. Optim. – Vol. I – Process Integr. Improv., vol. I; 2009.
[61] Verda V, Guelpa E. Metodi termodinamici per l'uso efficiente delle risorse energetiche. Società Editrice Esculapio; 2013.
[62] Kyaw K, Kubota M, Watanabe F, Matsuda H, Hasatani M. Study of carbonation of CaO for high temperature thermal energy storage. J Chem Eng Japan 1998;31:281–4. http://dx.doi.org/10.1252/jcej.31.281.
[63] Barin I. Thermochemical data of pure substances. Weinheim: VCH; 1989.
[64] Sun P, Grace JR, Lim CJ, Anthony EJ. Determination of intrinsic rate constants of the CaO–CO_2 reaction. Chem Eng Sci 2008;63:47–56. http://dx.doi.org/10.1016/j.ces.2007.08.055.
[65] Grasa GS, Abanades JC. CO_2 capture capacity of CaO in long series of carbonation/calcination cycles. Ind Eng Chem Res 2006;45:8846–51. http://dx.doi.org/10.1021/ie0606946.
[66] Valverde JM. A model on the CaO multicyclic conversion in the Ca-looping process. Chem Eng J 2013;228:1195–206. http://dx.doi.org/10.1016/j.cej.2013.05.023.
[67] U.S.DOE. SUNSHOT PROGRAM n.d. <http://energy.gov/eere/sunshot/concentrating-solar-power>.

***ANNEX 4**: Ortiz C, Valverde JM, Chacartegui R. Energy Consumption for CO_2 Capture by means of the Calcium Looping Process: A Comparative Analysis using Limestone, Dolomite, and Steel Slag. Energy Technol 2016:1–12. doi:10.1002/ente.201600390.*

Energy Consumption for CO_2 Capture by means of the Calcium Looping Process: A Comparative Analysis using Limestone, Dolomite, and Steel Slag

Carlos Ortiz,*[a] José M. Valverde,[a] and Ricardo Chacartegui[b]

The calcium looping (CaL) process, based upon the dry carbonation/calcination of $CaO/CaCO_3$, is at the center of a potentially low-cost, second-generation technology for CO_2 capture. This manuscript analyzes the energy penalty that arises from the integration of the CaL process into a coal-fired power plant using cheap and abundantly available CaO precursors such as natural limestone, dolomite, and steel slag. Experimental results on their multicycle capture capacity behavior obtained from thermogravimetric analysis (TGA) at realistic CaL conditions for CO_2 capture are used to this end. This work shows that the specific energy consumption for CO_2 avoided (SPECCA) is reduced by using either dolomite or steel slag, whose carbonation kinetics in the diffusive phase are accelerated as compared to limestone. Thus, the use of dolomite as CaO precursor would yield a low SPECCA value of approximately 2 MJ kg^{-1} CO_2 for a residence time of the solids in the carbonator of approximately 10 minutes, which is clearly below the SPECCA value usually reported for conventional amine-based CO_2 capture systems.

Introduction

The commercial deployment of CO_2 capture and storage (CCS) must play a main role within the portfolio of urgently needed measures to limit global warming to +2 °C over pre-industrial levels.[1,2] Coal-fired power plants (CFPP) are prime candidates to be retrofitted with CCS. However, Boundary Dam (100 MWe) in Canada is up to date the only commercial CFPP that applies CCS using chemical absorption by monoethanolamine (MEA). The expansion of this mature technology for CO_2 capture at a large scale is hindered by a number of challenges such as amine toxicity[3] and degradation,[4] equipment corrosion,[5] and the high energy consumption for sorbent regeneration.[6–8] Thus, there is a need for developing new large-scale capture technologies with reduced energy penalty and capture cost, which should rely on environmentally friendly, abundantly available, and inexpensive materials.

The calcium looping (CaL) process is at the basis of a second-generation, post-combustion capture technology, which has already been validated at the pilot level (1–2 MW_{th});[9,10] it uses CaO as dry sorbent, derived from cheap, abundant precursors such as natural limestone. According to recent studies,[11,12] the CaL process yields a reduced penalty over the power plant efficiency as compared to conventional amine-based capture systems, which together with the low price (≈10 €/ton), wide availability, and non-toxicity of the sorbent precursor, makes it an attractive alternative to amines for post-combustion CO_2 capture.[13–15]

The CaL process is based on the dry carbonation and calcination of CaO solid particles:

$$CaO + CO_2 \rightleftharpoons CaCO_3 \qquad \Delta H_r^{-0} = 178\ kJ\ mol^{-1}$$

When applied to post-combustion CO_2 capture, the CaL process is performed using two interconnected circulating-fluidized-bed (CFB) reactors, both operated under atmospheric pressure at gas velocities of approximately 5–10 m s^{-1}.[16,17] wherein gas–solid contact and heat/mass transfer are promoted. CaO particles react in the carbonator reactor at optimum temperatures of approximately 650 °C with the CO_2 present in the flue gas at a volume concentration of ≈15 %. The carbonated particles are then circulated into the calciner reactor in which fast decomposition of $CaCO_3$ occurs to produce CaO and a rich CO_2 stream ready to be compressed and transported for storage or other uses. The regenerated CaO particles are recovered at the calciner exit by a cyclone and sent back to the carbonator for a new cycle. CaO deactivation, mainly caused by sintering during the $CaCO_3$/CaO transformation,[18] is compensated by the periodic introduction of a fresh limestone makeup in the calciner whereas the purged CaO is particularly well suited for cement production.[19,20] For the endothermic calcination reaction to be fully attained in short residence times and under necessarily high CO_2 partial pressure the calciner tempera-

[a] C. Ortiz, Dr. J. M. Valverde
Facultad de Física
Universidad de Sevilla
Avenida Reina Mercedes s/n, 41012 Sevilla (Spain)
E-mail: cortiz7@us.es

[b] Dr. R. Chacartegui
Escuela Técnica Superior de Ingenieros
Universidad de Sevilla
Camino de los Descubrimientos s/n, 41092 Sevilla (Spain)

Part of a Special Issue on "Chemical Looping for Energy Technologies". To view the complete issue, visit:
http://dx.doi.org/10.1002/ente.v4.10/

ture must exceed 900 °C, which is achieved in practice by in situ oxy-combustion of fossil fuel.[21,22]

Besides capital investment and operating and maintenance (O&M) cost, energy consumption is a main factor that determines the viability of a capture technology. The specific energy consumption for CO_2 avoided (SPECCA)[23] is usually employed to quantify the additional fuel consumption (in MJ) needed to avoid the emission of 1 kg of CO_2 into the atmosphere [Equation (2)]:

$$\mathrm{SPECCA}[\mathrm{MJ\,kg_{CO_2}^{-1}}] = 3600\,\frac{\frac{1}{\eta_{\mathrm{plant}}}-\frac{1}{\eta_{\mathrm{ref}}}}{E_{\mathrm{ref}}-E} \qquad (2)$$

where η_{ref} and η_{plant} are the power plant efficiencies, and E_{ref} and E are the emissions ratios (in kg $CO_2\,kWh_e^{-1}$) without and with the CaL process integrated, respectively.

Most of the studies assessing SPECCA for conventional amine-based capture systems lead to typical values of approximately 4 $MJ\,kg^{-1}$ CO_2.[23–25] Regarding the integration of the CaL process into CFPP, reported values of SPECCA are close to those obtained for amines for a 90% CO_2 capture efficiency.[26] The evolution with the number of cycles of the CO_2 capture capacity of limestone-derived CaO, which must be used as input in this analysis, is a critical parameter that affects the overall capture efficiency.[17] CaL–CFPP integration models usually employ results for the multicycle CaO capture capacity obtained from lab-scale thermogravimetric analysis (TGA), which are relevantly affected by the cycling conditions. Thus, recent studies have shown that the kinetics of carbonation at short residence times are importantly influenced by calcination under high-CO_2 partial pressures.[27,28] However, this relevant issue has been mostly dismissed in previous works.[29–31] Moreover, results from TGA tests performed at realistic CaL conditions indicate that the CO_2 capture efficiency could be improved from the use of other CaO precursors such as dolomite[32] and steel slag[33] with more favorable carbonation kinetics as compared to limestone.

This work analyzes the energy consumption of the CFPP–CaL integration using results from TGA tests on limestone, dolomite, and steel slag in which calcination is performed under high CO_2 partial pressure, as would be the case in the practical application for CO_2 capture in power plants. The structure of this paper is the following: first, the multicycle carbonation behavior of CaO derived from natural limestone,[28] dolomite,[32] and steel slag[33] and the CFPP–CaL integration model[34] are briefly summarized. Results from these studies are then used to evaluate the energy consumption and CO_2 capture efficiency. A sensitivity analysis has been performed to assess the influence of the different key parameters involved in the CO_2 capture process using these CaO precursors. The obtained results indicate that better global integration efficiency and lower energy consumption are attained using dolomite and steel slag instead of limestone due to their enhanced carbonation activity in the diffusion-controlled stage, which leads to an improvement of the whole system performance by prolonging the solids residence time in the carbonator reactor beyond a few minutes.

Multicycle CO_2 capture behavior of limestone, dolomite and steel slag

One of the main drawbacks of the CaL process is the progressive loss of activity of CaO particles at short residence times as the number of carbonation/calcination cycles is increased. This is especially true for limestone-derived CaO at CaL conditions corresponding to post-combustion CO_2 capture[17,27,35–37] because of the enhanced sintering of the CaO grains. Enhanced sintering during the $CaCO_3$/CaO transformation drastically reduces the active surface of the solids in the reaction-controlled fast phase that takes place in the first seconds of carbonation.[17,38] As the reaction progresses, this fast reaction-controlled stage is followed by a slower phase that becomes controlled by the solid-state diffusion of CO_3^{2-} and O^{2-} ions across the $CaCO_3$ product layer built upon the surface of the particles.[38] Thus, CaL conditions involving calcination at very high temperatures (≈950 °C) under high CO_2 partial pressures cause a marked loss of surface area due to promoted aggregation and sintering of the CaO grains during calcination,[18] and this leads to a severe drop in CaO conversion at short residence times after just a few cycles.[28,39,40]

Dolomite [$MgCa(CO_3)_2$] is also a cheap, naturally abundant CaO precursor, which upon calcination in the presence of CO_2 is decomposed into MgO and CaO in a two-stage process:[32,41,42]

$$\mathrm{MgCa(CO_3)_2 \rightarrow CaCO_3 + MgO + CO_2} \quad \Delta H_r^0 = 127\,\mathrm{kJ\,mol^{-1}} \qquad (3)$$

$$\mathrm{CaCO_3 + MgO \rightarrow CaO + CO_2 + MgO} \quad \Delta H_r^0 = 178\,\mathrm{kJ\,mol^{-1}}$$

At a temperature of approximately 700 °C, dolomite decomposes directly into MgO and CaO regardless of the CO_2 partial pressure in the calcination environment.[42] If the calcination is performed under high CO_2 partial pressure (as is the case of the CaL process), the nascent CaO nanocrystals become immediately recarbonated, which leads to the formation of poorly crystalline $CaCO_3$ as the intermediate product of decomposition. This nascent $CaCO_3$ decomposes rapidly under high CO_2 partial pressures because of its low crystallinity (as compared to limestone), when the reaction is thermodynamically favorable near 900 °C, which leads to a low crystallinity and therefore highly reactive CaO.[43] Thus, the use of dolomite in the CaL process for CO_2 capture would allow the reduction of the calcination temperature to approximately 900 °C to attain full calcination at short residence times.[32] Moreover, the presence of inert MgO grains in the dolomitic lime hinders aggregation and thus sintering of the CaO grains, which mitigates the drop in CO_2 capture capacity with the number for cycles.[32,43]

The use of steel slag as an alternative CaO precursor in the CaL process is also gaining the attention of researchers.[44,45] Steel slag is produced in large amounts by the metallurgical industry, remaining an important part as final waste without valorization. In 2010 steel slag production increased

up to 21.8 million tons, 13% of which was used as landfill waste.[46] According to Ref. [47], steel slag annual production amounts to approximately 1 Mt in the UK alone. To use it as a CaO precursor, steel slag can be pretreated with acetic acid to obtain calcium acetate [$Ca(CH3COO)_2$].[33] Results from TGA tests show that the decomposition of calcium acetate occurs mainly in three steps:[33,48,49] i) an initial dehydration, which occurs from ambient temperature to approximately 250 °C; ii) calcium acetate decomposition between 300 and 450 °C to release acetone and $CaCO_3$, and iii) calcination of $CaCO_3$ in the range from 620 to 700 °C. According to TGA results,[33] the CaO-based sorbent derived from steel slag presents a low deactivation rate at realistic CaL conditions, which would expectedly improve the CO_2 capture efficiency of the process. Moreover, the sorbent can be regenerated in very short residence times at 900 °C. In addition to CaO, pretreated steel slag also contains other metallic oxides as impurities such as aluminum, magnesium, iron, and silicon oxides,[50,51] which would help mitigating the sintering of CaO grains much in the same way as MgO does in the case of dolomite.

In order to compare the multicycle CO_2 capture behavior of the above three sorbents and to take into account the presence of inert oxides in the case of dolomite and steel slag, the appropriate parameter to be assessed is the capture capacity (CC), defined as the ratio of mass of CO_2 captured to the total mass of sorbent (including the inert oxides) in each cycle. Figure 1 a shows the evolution of the CO_2 capture capacity for limestone, dolomite, and pretreated steel slag with the number of cycles, as reported elsewhere from TGA tests at realistic CaL conditions.[28,32,33] The stoichiometric CO_2 capture capacity for calcined limestone is the highest due to the presence of inert oxides in decomposed dolomite and steel slag, which leads to a higher capture capacity in the first cycle for the still relatively porous CaO derived from limestone, as presented in Figure 1 a. However, the sorbents derived from dolomite and steel slag show a higher capture capacity after just a few cycles, which indicates that CaO deactivation in these sorbents is clearly mitigated.[33,41,44] Thus, the multicycle capture capacity of dolomite- and steel-slag-derived sorbents becomes twice that of lime after just 20 cycles (Figure 1 a).

As shown in Figure 1 a, the capture capacity data can be well fitted to the following semi-empirical equation:[32,52]

$$\frac{CC_N}{CC_1} = \frac{CC_r}{CC_1} + \left(\frac{1}{\kappa(N-1) + \left(1 - \frac{CC_r}{CC_1}\right)^{-1}} \right) \quad (4)$$

in which N is the cycle number, κ is the deactivation rate constant, and CC_r is the residual capture capacity, towards which the capture capacity converges asymptotically after a large number of cycles. The best fitting parameters are summarized in Table 1.

The TGA curves also allow us to separately obtain the capture capacity in the fast reaction-controlled phase (FRP) and solid-state diffusion-controlled phase (SDP) as illustrated in Figure 1 b, where the time evolution of the capture capacity for cycle $N=20$ is plotted for the three sorbents analyzed in our work. Multicycle capture capacity data obtained for both phases are plotted in Figure 2.

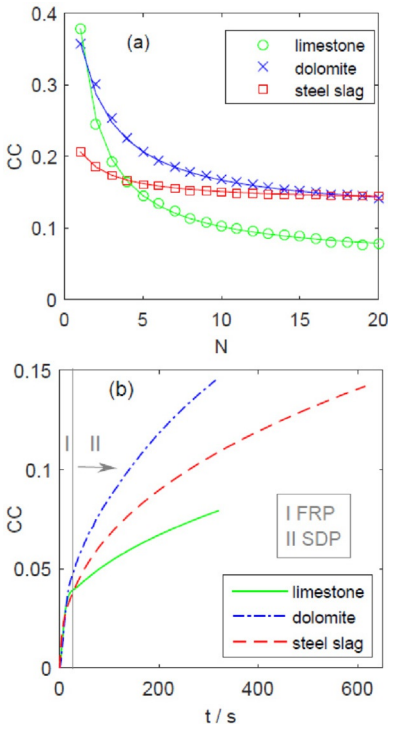

Figure 1. a) CO_2 capture capacity for limestone,[28] dolomite,[32] and steel slag[33] derived sorbents as a function of the number of carbonation/calcination cycles. Solid lines are best-fit curves of Equation (4) to the data (best-fitting parameters are shown in Table 1). b) Time evolution of the capture capacity during cycle number 20 for the three sorbents (the fast reaction-controlled phase FRP and solid-state diffusion-controlled phase SDP are indicated). In these tests, the carbonation is performed for 5 min under 15% CO_2/85% N_2 *v/v* at 650 °C whereas calcination occurs at 900 °C (950 °C in the case of limestone to attain full calcination) under 70% CO_2/30% N_2 *v/v*. The residence time for both stages is 5 min. In the case of steel slag, the carbonation was prolonged to 10 min. See Refs. [28, 32, 33] for further details.

As shown in Figure 2, in the case of limestone-derived CaO, the contribution of the diffusion-controlled phase to the overall CO_2 capture capacity in each cycle is similar to the capture capacity in the fast reaction-controlled phase (for 5 min overall carbonation periods). Carbonation in the SDP becomes even more relevant for dolomite and steel slag, for which it represents a major part of the total CO_2 capture. Accordingly, the efficiency of CO_2 capture would be expectedly kept at a high value by prolonging the carbonation time lag, as carbonation in the diffusive phase grows roughly linearly with time within a time span of a few minutes[27,53] (see also Figure 1 b).

Kinetic model approach

Here we briefly summarize the kinetic model developed elsewhere in which the relevant contribution of carbonation in the SDP, as described above, is explicitly considered.[35] The

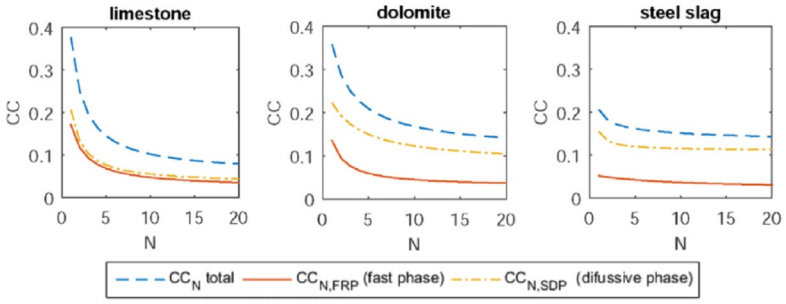

Figure 2. Total CO_2 capture capacity and capture capacities in the fast reaction-controlled phase (FRP) and solid-sate diffusion controlled phase (SDP), respectively, as a function of the cycle number for limestone, dolomite, and steel slag.[28,32,33] In these tests carbonation is performed for 5 min under 15% CO_2/75% N_2 *v/v* at 650 °C whereas calcination occurs at 900 °C (950 °C in the case of limestone) under 70% CO_2/30% N_2 *v/v*. Residence time for both stages is 5 min. In the case of steel slag, the carbonation was prolonged to 10 min.

Table 1. Values of best fitting parameters in Equation (4) to the TGA experimental data.[28,32,33]

		Limestone	Dolomite	Steel slag
capture capacity (total)	time	5.3 min	5.3 min	10.3 min
	CC_1	0.378	0.358	0.206
	κ	0.747	0.621	1.335
	CC_r	0.054	0.116	0.137
	R_{sqr}	0.9993	0.9995	0.9984
capture capacity (fast phase)	time	0.3 min	0.3 min	0.3 min
	CC_1	0.171	0.135	0.051
	κ	0.648	0.791	0.179
	CC_r	0.023	0.029	0.020
	R_{sqr}	0.9993	0.9948	0.9506
	time	5 min	5 min	10 min
capture capacity (diffusive phase)	time	5 min	5 min	10 min
	CC_1	0.207	0.222	0.155
	κ	0.872	0.420	3.518
	CC_r	0.032	0.081	0.111
	R_{sqr}	0.9985	0.9941	0.9896

model is used to describe the multicycle CO_2 capture capacity of limestone-, dolomite-, and steel slag-derived sorbents. Accordingly, the reaction rates in the FRP and SDP are simply expressed as:

$$r_{N_{FRP}} = \frac{CC_{N_{FRP}}}{t_{FRP}} \text{ for } t \le t_{FRP} \quad (5)$$

$$r_{N_{SDP}} = \frac{CC_{N_{SDP}}}{T_0 - t_{FRP}} \text{ for } t_{FRP} < t \le t_{max} \quad (6)$$

in which r_{N_i} is the reaction rate in the *i*-phase (either FRP or SDP), t_{FRP} is the time of the FRP phase, t_{max} is total carbonation time, CC_i is the capture capacity in the *i*-phase, and T_0 is the experimental carbonation time lag.

The rate of capture capacity in the kinetically controlled fast phase ($r_{N_{FRP}}$) at atmospheric pressure can be approximated to a first-order kinetic law:[54]

$$r_{N_{FRP}} = k_s S_N (CC_{max} - CC)^{\frac{2}{3}} ([CO_2] - [CO_2]_{eq}) \quad (7)$$

in which $[CO_2]$ and $[CO_2]_{eq}$ are the actual and equilibrium CO_2 concentrations, respectively, k_s is the kinetic constant, CC_{max} is the maximum CO_2 capture capacity, and S_N is the sorbent specific area available for reaction after N cycles, which is proportional to the capture capacity degree. The rate of capture capacity in the diffusion-controlled phase can be expressed by using an effective diffusion constant (D^*_{eff}).[35]

$$r_{N_{SDP}} \approx D^*_{eff} ([CO_2] - [CO_2]_{eq}) \quad (8)$$

Both Equation (7) and Equation (8) can be fitted to experimental data[27,32,33] to obtain the values of k_s and D^*_{eff} to be used in the kinetic model for limestone, dolomite, and steel slag, respectively. The best-fitting parameters are shown in Table 2. Figure 3a shows the time evolution of the CO_2 capture capacity for several cycles (N) according to the kinetic model for limestone, dolomite, and steel slag. A comparison is shown in Figure 3b between the kinetic model and experimental curves extracted from the TGA tests[28,32,33] (Figure 1b). It has previously been observed that the use of a linear law for carbonation in the kinetic model is actually below the experimental capture capacity curve in the diffu-

Table 2. Kinetic model parameters obtained from the best fits of Equations (7) and (8) to the experimental data.[28,32,33]

	Limestone	Dolomite	Steel slag
$k_s \left[\frac{m^4}{mol \cdot s}\right]$	6.7×10^{-10}	8.8×10^{-10}	11.0×10^{-10}
$D^*_{eff} \left[\frac{m^3}{mol \cdot s}\right]$	6.5×10^{-5}	15.0×10^{-5}	9.6×10^{-5}

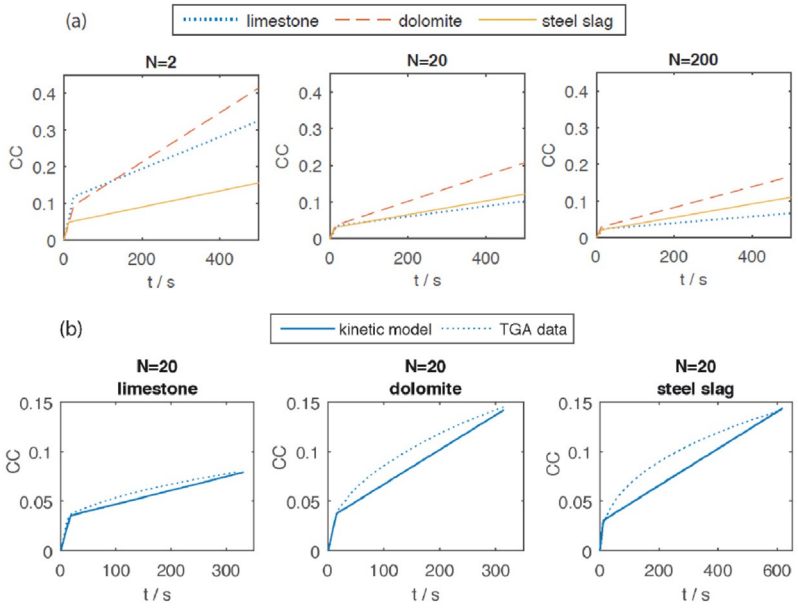

Figure 3. a) CO_2 capture capacity as a function of time for different cycles (N) according to the kinetic model using best-fitting parameters to the experimental data.[28, 32, 33] b) Comparison between the kinetic model and TGA experimental curves for cycle $N = 20$.

sion phase. In this regard, our results on the capture efficiency and energy penalty can be judged as conservative.

CaL–CFPP integration model

In this section, we summarize the main features of the CaL–CFPP integration model (illustrated in Figure 4), which is used to evaluate the capture efficiency and energy penalty in this work. A detailed description of the integration model is given in Ref. [34]. ASPEN PLUS™ has been employed in the analysis. To simplify the model a number of assumptions were made: (i) the system operates at steady-state conditions, (ii) pressure losses in the heat exchange equipment are neglected, (iii) the solid–solid heat exchange is modeled as a transfer of heat between solids, (iv) the approach temperature is 10 °C for all gas–solid heat exchangers, (v) gas passes in plug flow across a bed of perfectly mixed solids in the reactors, and (vi) reactors do not suffer from thermal energy losses.

A 505 MW_e CFPP is taken as a reference to analyze the CO_2 capture efficiency and energy penalty. Data for coal composition (coal Pittsburgh No. 8), flue gas composition, and CFPP operation parameters are extracted from Ref. [55]. In this plant, combustion of 205 tons per hour of coal takes place in the steam boiler to generate 1335.7 MW_{th}, which releases to the atmosphere 2517 $t\,h^{-}$ of flue gas with a CO_2 molar fraction of 0.135. Taking into account parasitic electricity consumption, the reference power plant has a 33.5 % overall efficiency.

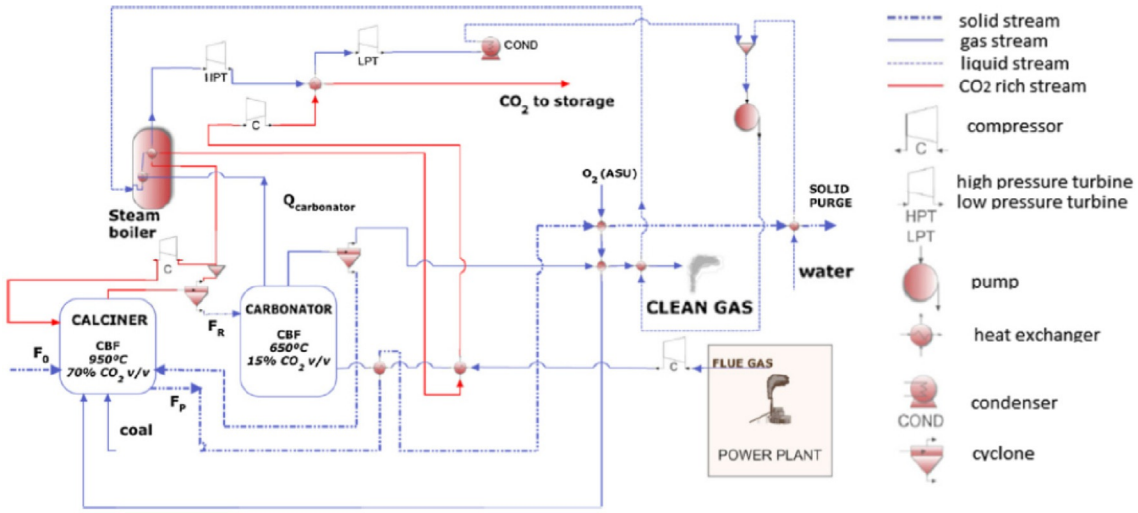

Figure 4. Schematics of the CaL–CFPP integration model (reproduced from Ref. [34] with permission).

The CaL process is started by calcination of the CaO precursor in the CFB calciner, where the heat necessary to increase the temperature of the solids to conduct the endothermic calcination reaction is provided by in situ oxy-combustion of coal. Oxy-combustion allows the retrieval of a CO_2-rich stream at the calciner outlet (70–90 vol% concentration),[21,56] which is sent to a compression and storage process. A make-up flow of the CaO precursor is introduced into the calciner to compensate for sorbent deactivation. The heat extracted from the CO_2 stream is used for pre-heating the flue gas entering into the carbonator (Figure 4). At the exit of the calciner, the regenerated sorbent particles are recovered by a cyclone and circulated into the carbonator after a solids purge stage is performed to eliminate ashes, irreversibly sulphated CaO, and deactivated solids. A minor modification over the general model used for limestone and dolomite has been implemented for steel slag to incorporate the acetic-acid pretreatment. Thus, the process is started from the decomposition of calcium acetate as described in the previous section, which releases $CaCO_3$ and acetone; the latter is separated from the solids stream using a cyclone and sent to a heat exchanger as an initial step towards removal from the cycle to use its sensible heat for preheating the pretreated steel slag stream entering into the system. This acetone has an economic value and could be utilized for other purposes. The $CaCO_3$ resulting from the decomposition is sent to the CaL process, where it follows the same path as limestone and dolomite.

The heat produced in the CaL cycle is used in a secondary superheated steam cycle for electricity generation, whose main parameters are described in Table 3. The steam boiler is modeled as: i) a preheater where the sensible heat from the flue gas stream is used; ii) an evaporator, which takes advantage of the energy released in the exothermic carbonation reaction, and iii) a steam super-heater, which uses the sensible heat of the CO_2 exiting the calciner (see Ref. [34] for more details).

The energies released and consumed in the carbonator and calciner reactors, respectively, are rather high due to the large flow of solids recirculating between both reactors and the high temperature requirements. To minimize the global energy penalty, a possible strategy is to exchange heat between the solids leaving the calciner and the solids entering into it, which must be heated up to the calcination temperature. Different systems have been proposed to this end such as a mixing valve[57] or a cyclonic preheater.[58] To simplify the model, a simple solid–solid heat exchanger is assumed with an approach temperature of 20 °C. At the carbonator exit, the flue gas (after recovering 70–90 % of CO_2) is sent to a series of heat exchangers to recover the sensible heat from the exhaust gases stream before being vented to the atmosphere.

Table 3. Main data used in the model simulations.

Equipment/zone	Parameter	Value
	F_{CO_2}	10388 kmol h^{-1}
	F_0/F_{CO_2}	0.05
	τ	313 s
	F_R/F_{CO_2}	10
	W_s	200 tonne
heat exchangers	approach temperature	10 °C
compressors, turbines	isentropic efficiency	0.85
	CO_2 storage pressure	100 bar
pumps	efficiency	0.9
cyclones	efficiency	0.99
	type	Barth 1
reactor/calciner	T	950 °C (limestone case) 900 °C (dolomite and steel slag cases)
	P	1 atm
	P_{CO_2}	0.83
	$E_{calciner}$	1
reactor/carbonator	T	650 °C
	P	1 atm
ASU	$\dot{W}_{ASU}$	200 kWh tonne^{-1} O_2
	$\dot{W}_{solid}$	5.5 kWh tonne^{-1} solids
secondary steam cycle	T_{vv}	560 °C
	P_{vv}	140 bar
	reheat temperature	476 °C
	$\dot{m}_{vap}$	1.530 tonne h^{-1}
	extraction pressure (1/2/3/4)	42/20/4/1 bar
	extraction flow (1/2/3/4)	183.9/134.9/72.8/45.6 tonne h^{-1}

CO_2 capture occurs in the CFB carbonator reactor. This reactor has been modeled in a recent work.[35] A solids stream (F_R) composed of CaO (and inert solids if present) enters into the carbonator to react with the CO_2-loaded flue gas stream ($F_{CO_2} = 10388$ kmol h^{-1}) coming from the CFPP main boiler. As presented in Figure 4, the flue gas is preheated before entering into the carbonator reactor. According to the model, the average capture capacity of the particles leaving the carbonator can be obtained from the sum of the average capture capacity in the fast and diffusion carbonation phases, and the CO_2 capture efficiency can be calculated as a function of the total solids inventory in the carbonator (W_s), the solids residence time in the carbonator (τ), and the flow rate of fresh sorbent precursor makeup fed into the calciner (F_0). The rates of carbonation in the fast reaction-controlled phase [Eq. (6)] and the solid-state diffusion-controlled phase [Eq. (7)] derived from the experimental data presented above are used to compute the average capture capacity in the carbonator. The model assumes that the gas passes in plug flow through a bed of perfectly mixed solids.

CaL–CFPP Simulation Results

CO_2 capture efficiency

Figure 5 shows the CO_2 capture efficiency results obtained from the model. For fixed values of F_0, an increase of the solids inventory W_s in the carbonator yields a significant im-

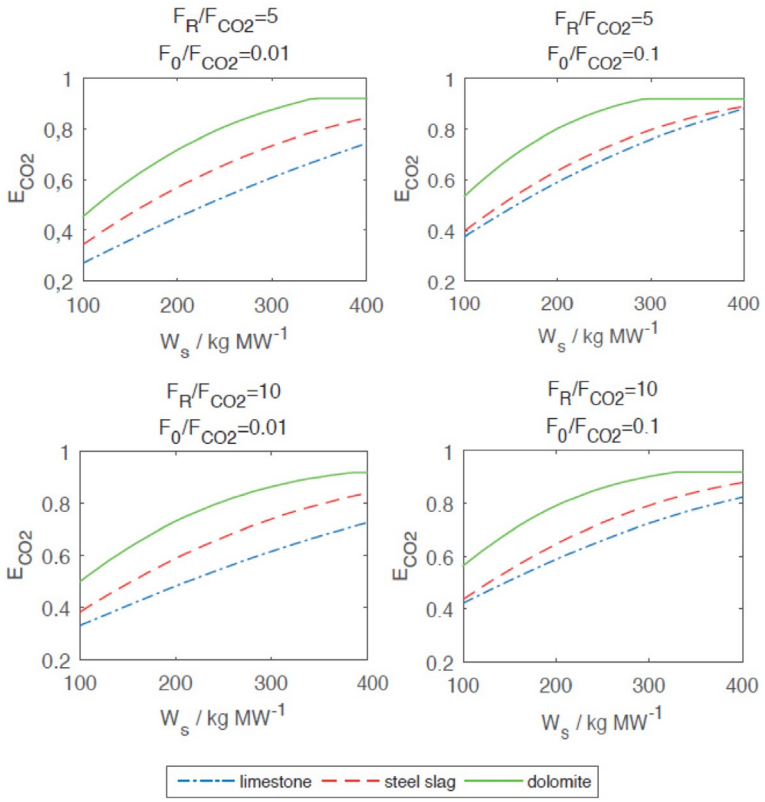

Figure 5. Capture efficiency as a function of the solids inventory in the carbonator for different F_R/F_{CO_2} and F_0/F_{CO_2} ratios. ($F_{CO_2} = 10.39$ kmol h^{-1}) and for the three CaO precursors analyzed in this work.

provement of the capture efficiency for all sorbents analyzed. A higher capture efficiency is achieved also by increasing the makeup flow F_0, which serves to counteract sorbent deactivation. Nevertheless, this leads also to higher energy consumption in the calciner and therefore to an increase in the energy penalty. As shown Figure 5, dolomite is the CaO precursor that provides a higher capture efficiency in the carbonator for all simulated conditions (performed by varying key model parameters such as F_R, F_0, W_s).

On the other hand, Figure 5 shows that decreasing the solids recirculation flow rate between reactors (F_R), or equivalently, increasing the particles residence time in the carbonator ($\tau = N_{Ca}/F_R$), the capture efficiency is not penalized, which underlines the importance of carbonation in the diffusion-controlled phase in the CO_2 capture process. This effect is also illustrated in Figure 6, where the capture efficiency is plotted as a function of the residence time in the carbonator. The capture efficiency can be maintained at a high level by prolonging the carbonation residence time. The results show a relatively high capture efficiency for dolomite and steel slag due to enhanced carbonation in the SDP phase as compared to limestone. Prolonging the carbonation residence time would bring about important benefits to the CaL process, such as a mitigated deactivation due to sintering in the calciner (because the recirculation rate is decreased), lower cost for the transportation of solids, and a reduction in the energy penalty (because the amount of heat required for calcination would be decreased).

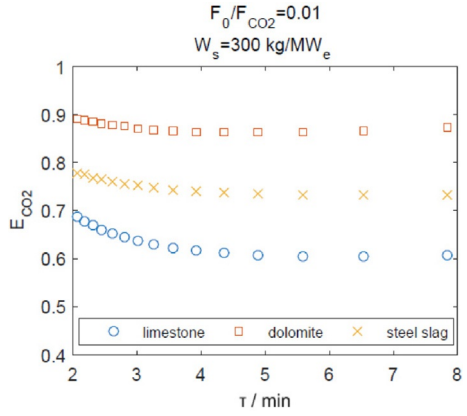

Figure 6. CO_2 capture efficiency as a function of the residence time in the carbonator, which is varied by changing the F_R/F_{CO_2} ratio (keeping fixed $F_{CO_2} = 10.39$ kmol h^{-1} according to reference power plant[55]). Calculations are made for fixed values of W_s and F_R/F_{CO_2} as indicated. Results for the three CaO precursors analyzed in the present work are shown.

Energy consumption

A number of analyses have been performed to determine the penalty in the power plant performance of integrating the CaL process for CO_2 capture using limestone, dolomite, and steel slag as CaO precursors. The values of the main operation parameters used for the simulations are summarized in Table 3. CFPP–CaL integration results are shown in Table 4. The heat required in the calciner ($\dot{Q}_{cal}$) is lower for steel slag than for limestone as the needed temperature to attain full calcination of the makeup flow is decreased (900 °C for steel slag as compared to 950 °C for limestone). The heat released at the carbonator ($\dot{Q}_{carb}$) is the sum of the heat produced by the carbonation reaction and the sensible heat of solids entering into the carbonator at the calciner temperature. A consequence of the presence of inert solids is that a higher energy consumption is needed (than in the case requiring limestone) in the make-up process ($\dot{Q}_{makeup}$) for a given $CaCO_3$ flow rate (F_0) entering into the calciner. Moreover, coal oxy-combustion to a higher extent is needed in the case of dolomite, which leads to a higher power consumption for compression due to an increase in the gas flow rate exiting the calciner. For steel slag, inert oxides are marginally present as impurities which do not affect markedly the energy consumption.

Simulation results from the carbonator model (Figure 5) indicate a lower capture efficiency for limestone as compared to dolomite and steel slag. It is important to take into account that a lower capture efficiency in the carbonator leaves also a lower amount of $CaCO_3$ entering the calciner, which reduces the energy requirements. Nevertheless, as

Table 4. Main CaL–CFPP integration results.

Equipment/zone	Parameter	CaO-based sorbent used Limestone	Dolomite	Steel slag
reactor/calciner	$\dot{Q}_{cal}$ [MW]	1150.1	1550.7	1041.5
	$\dot{Q}_{makeup}$ [MW]	40.5	72.1	47.2
reactor/carbonator	$\dot{Q}_{carb}$ [MW]	711	1177.2	660.5
	E_{CO_2}	0.77	0.92	0.86
flue gas compressor/carb	power [MW]	5.5	5.5	5.5
compressor/CO_2 storage	power [MW]	181	226	178.1
steam cycle	η_{plant}	0.42	0.42	0.42
CaL–CFPP cycle (integration)	η_{plant}	0.279	0.276	0.277
	integration penalty	5.60%	5.91%	5.79%
	SPECCA	3.08	2.77	2.88

shown in Table 4, even though the use of dolomite and steel slag would lead to a higher energy penalty over the plant without capture, the SPECCA values obtained for these sorbents is decreased; that is, less total energy consumption is needed for each kilogram of CO_2 avoided due to the increase in the capture efficiency. Figure 7 shows the thermal characteristics of the main streams in the CaL cycle for each CaO precursor base case. The CO_2 capture values from the flue gas are shown in Table 5.

As shown in Figure 7, the heat delivered by oxy-fuel combustion is used to increase the inlet stream temperature (Q_{sens}), to drive the calcination reaction (Q_{calcin}), and to satisfy other heat demands, linked to boiler combustion and thermal losses, etc. The dolomite case has a higher CO_2 capture, and therefore a higher heat delivery from carbonation is obtained.

As pointed out above, the enhancement of the capture capacity in the SDPs for dolomite and steel slag suggests that the capture performance may be further improved if the solids residence time in the carbonator is prolonged beyond a few minutes. Accordingly, the SPECCA results plotted in Figure 8 show that increasing the solids residence time leads to a decrease of energy consumption for all the CaO precursors. Despite that the use of either dolomite or steel slag

Table 5. Flue gas component flow.

Component	Mass flow [kg s^{-1}] Flue gas inlet Flue gas	Flue gas outlet Limestone	Dolomite	Steel slag
H_2O	24.80	24.80	24.80	24.80
N_2	449.40	449.40	449.40	449.40
O_2	23.40	22.84	22.84	22.84
NO	3.80	3.80	3.80	3.80
SO_2	2.25	0.02	0.02	0.02
H_2	0.02	0.02	0.02	0.02
CO	3.69	3.69	3.69	3.69
CO_2	127.00	27.99	10.26	17.78

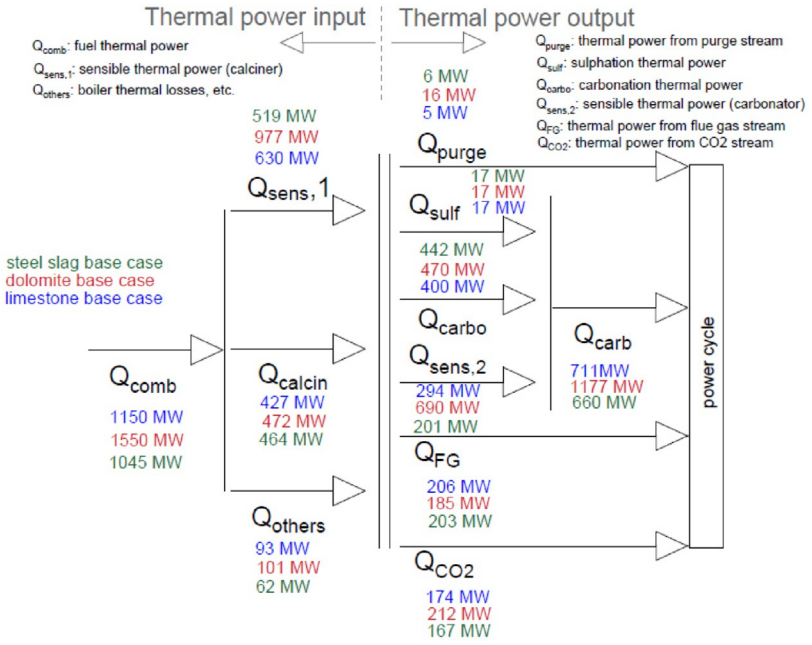

Figure 7. Thermal characteristics of the main streams in the CaL cycle.

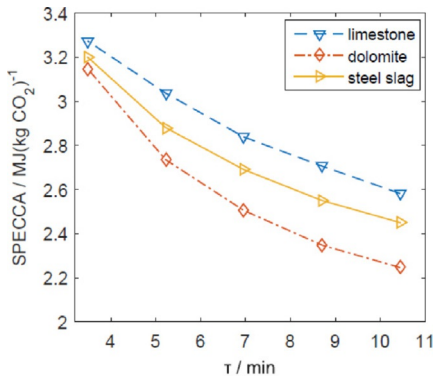

Figure 8. SPECCA values as a function of solids residence time in the carbonator for the different CaO precursors analyzed in this work.

causes a higher energy penalty (Table 4), the capture efficiency is also improved for these sorbents (Figure 6), which leads to a further reduction in energy consumption per kg of CO_2 avoided, as shown in Figure 8. The higher capture capacity of dolomite in the SDP (Figure 3) yields the lowest SPECCA. Moreover, as the carbonation time lag is increased, the advantage of using dolomite and steel slag is further promoted due to the higher rate of carbonation in the SDP for the sorbents derived from these precursors as compared to limestone. As the solids residence time in the carbonator increases, the amount of solids circulating between reactors is reduced, which also mitigates the amount of additional heat required in the calciner due to the presence of inert solids. This together with the enhanced capture efficiency in the SDP for dolomite leads to the lowest SPECCA value when dolomite is used. Thus, a SPECCA value as low as 2.2 MJ kg^{-1} CO_2 is obtained for dolomite at a carbonation residence time of 10 min (corresponding to a solids recirculation flow rate of $F_R = 40.5$ kmol h^{-1}), compared to the higher value of 2.6 MJ kg^{-1} CO_2 for limestone (Figure 8).

Sensitivity analysis

To assess the influence of other key parameters to the CaL–CFPP integration on SPECCA a sensibility analysis was performed in our work. Figure 9 shows the effects of varying the: i) energy consumption related to solids conveying ($\dot{W}_{solids}$); ii) air separation unit (ASU) energy consumption for oxy-combustion ($\dot{W}_{ASU}$); iii) make-up flow into the calciner (F_0); iv) isentropic efficiency in the compressors of the CaL process (η_{comp}); and v) steam power cycle efficiency (η_{steam}).

As seen in Figure 9, the most critical effect is observed for a variation of the power cycle efficiency. As expected, the higher-efficiency power cycles would allow for a more effective use of the vast amount of energy produced in the CaL process. In this regard, Hanak et al.[9] propose to integrate a supercritical CO_2 cycle instead of a steam cycle, which could reduce the energy penalty by more than 1 %. Increasing the solids transport requirements or the $CaCO_3$ make-up flow has a higher influence for dolomite and steel slag than for limestone. On the other hand, within the range of variation of the parameters analyzed (shaded area in Figure 9) the lowest values of SPECCA are achieved for dolomite, with an energy consumption of approximately 2.2 MJ kg^{-1} CO_2. Thus, our simulations suggest that SPECCA values of about 4 MJ kg^{-1} CO_2, which are typical for conventional amine-based capture systems,[23] could be substantially reduced by means of the CaL process.

Conclusions

In this work the energy requirements for integrating a CO_2 capture calcium looping (CaL) process in a coal-fired power plant (CFPP) are analyzed. A study is presented on the performance of the integration for three different CaO precursors, taking into account the relevant role of the solid-state diffusion (SDP)-controlled carbonation phase for carbonation/calcination cycles performed under realistic conditions. These conditions necessarily imply calcination under high CO_2 pressures. The sorbent precursors investigated are limestone, dolomite, and steel slag, which are non-toxic and widely available at very low prices, as they are unavoidably needed for the commercial deployment of CCS at large scale (typically 3 Mt of CO_2 are released by a CFPP per year).

The analysis has been performed using a CaL–CFPP integration model recently reported and based on thermogravimetric analysis (TGA) experimental data available in the lit-

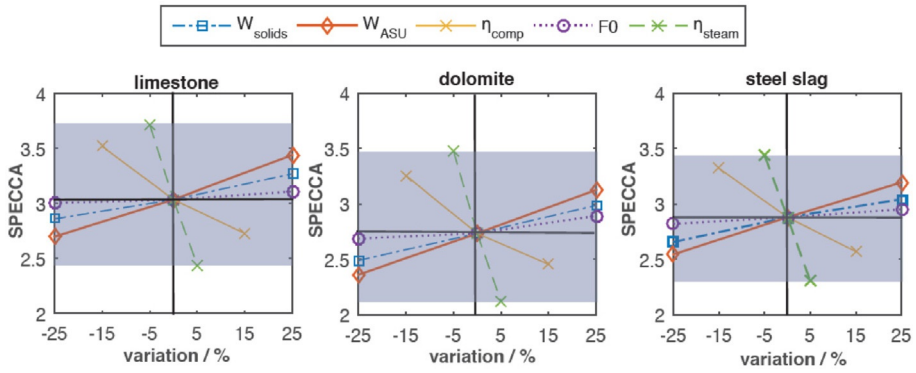

Figure 9. Sensitivity analysis on SPECCA for the different CaO precursors analyzed in this work.

erature. The TGA results show an enhanced carbonation in the solid-state diffusion-controlled phase, which is specially marked for dolomite and steel slag. The enhanced carbonation in the solid-state diffusion-controlled phase leads to a significant reduction in the specific energy consumption for CO_2 avoided (SPECCA) when the solids residence time in the carbonator is prolonged beyond a few minutes. Thus, the use of dolomite as CaO precursor instead of limestone could lead to a decrease of the energy consumption by approximately 15 % for carbonation residence times of approximately 10 min. Thus, SPECCA values as low as 2 MJ kg^{-1} CO_2 could be achieved from the use of low-cost, non-toxic, and abundantly available CaO precursors, which would enhance the competitiveness of the CaL process against conventional amine-based capture systems.

Symbols

CC	CO_2 capture capacity
CC_r	residual CO_2 capture capacity
$CC_{N_{FRP}}$	Sorbent CO_2 capacity capture at N cycle in the carbonation fast phase
$CC_{N_{SDP}}$	sorbent CO_2 capacity capture at N cycle in the carbonation diffusive phase
CC_{max}	maximum capture capacity
$[CO_2]$ [mol m^{-3}]	average CO_2 concentration
$[CO_2]_{eq}$ [mol m^{-3}]	equilibrium concentration of CO_2
D^*_{eff} [m^3/(mol s)]	effective diffusion constant
E [kg CO_2/kWhe]	emissions ratio after CaL
E_{CO_2}	carbon capture efficiency
E_{calc}	calciner conversion efficiency
E_{ref} [kg CO_2/kWhe]	emissions ratio before CaL
F_{CO_2} [kmol h$^-$]	molar flow of CO_2 in flue gas entering the carbonator
F_0 [kmol h$^-$]	molar flow of fresh makeup limestone
F_P [kmol h$^-$]	molar flow of fresh makeup limestone
F_R [kmol h$^-$]	molar flow of CO_2 in flue gas entering the carbonator
FRP	fast reaction-controlled phase
SDP	solid-state diffusion controlled phase
$\dot{m}_{vap}$ [tonne h$^-$]	total steam mass flow
N_{Ca} [mol]	mol of Ca in the carbonator
P [bar]	pressure
P_{vv} [bar]	live steam pressure
$\dot{Q}_{CaL}$ [MW]	heat consumption in the calciner
$\dot{Q}_{carb}$ [MW]	heat generated in the carbonator
$\dot{Q}_{makeup}$ [MW]	make-up heat consumption in the calciner
$r_{N_{FRP}}$ [1 s^{-1}]	reaction rate in the carbonation fast phase
$r_{N_{SDP}}$ [1 s^{-1}]	reaction rate in the carbonation diffusive phase
S_N [m^2/m^3]	reaction available surface in the N cycle
T [°C]	temperature
T_{vv} [°C]	live steam temperature
t_{FRP} [s]	time of the carbonation fast phase
t_{max} [s]	total carbonation time
W_s [kg]	solid inventory in the carbonator per MW of a typical power plant
$\dot{W}_{ASU}$ [MW]	power consumption in the ASU
$\dot{W}_{solid}$ [MW]	power consumption in solids transport
η_{ref}	reference plant efficiency
η_{plant}	new global efficiency (CFPP–CaL)
η_{comp}	compressor efficiency (CFPP–CaL)
η_{steam}	power cycle global efficiency
τ [s]	average residence time in the carbonator

Acknowledgements

This work was supported by the Spanish Government Agency Ministerio de Economia y Competitividad (contract CTQ2014-52763-C2-2-R).

Keywords: calcium looping · carbon capture and storage · carbon dioxide · chemical looping · combustion

[1] IEA, *Energy and Climate Change*, **2015**.
[2] United Nations. Framework Convention on Climate Change, *Adoption of the Paris Agreement*, **2015**.
[3] P. Luis, *Desalination* **2016**, *380*, 93–99.
[4] A. Rey, C. Gouedard, N. Ledirac, M. Cohen, J. Dugay, J. Vial, V. Pichon, L. Bertomeu, D. Picq, D. Bontemps, F. Chopin, P.-L. Carrette, *Int. J. Greenhouse Gas Control* **2013**, *19*, 576–583.
[5] G. Fytianos, S. Ucar, A. Grimstvedt, A. Hyldbakk, H. F. Svendsen, H. K. Knuutila, *Int. J. Greenhouse Gas Control* **2016**, *46*, 48–56.
[6] Z. Liang, K. Fu, R. Idem, P. Tontiwachwuthikul, *Chinese J. Chem. Eng.* **2016**, *24*, 278–288.
[7] M. Wang, A. Lawal, P. Stephenson, J. Sidders, C. Ramshaw, *Chem. Eng. Res. Des.* **2011**, *89*, 1609–1624.
[8] B. P. Spigarelli, S. K. Kawatra, *J. CO2 Util.* **2013**, *1*, 69–87.
[9] D. P. Hanak, E. J. Anthony, V. Manovic, *Energy Environ. Sci.* **2015**, *8*, 2199–2249.
[10] A. Perejón, L. M. Romeo, Y. Lara, P. Lisbona, J. M. Valverde, *Appl. Energy* **2016**, *162*, 787–807.
[11] L. M. Romeo, Y. Lara, P. Lisbona, A. Martínez, *Fuel Process. Technol.* **2009**, *90*, 803–811.
[12] C. C. Dean, J. Blamey, N. H. Florin, M. J. Al-Jeboori, P. S. Fennell, *Chem. Eng. Res. Des.* **2011**, *89*, 836–855.
[13] I. Vorrias, K. Atsonios, A. Nikolopoulos, N. Nikolopoulos, P. Grammelis, E. Kakaras, *Fuel* **2013**, *113*, 826–836.
[14] W. Wang, S. Ramkumar, L. S. Fan, *Fuel* **2013**, *104*, 561–574.
[15] M. Romano, *Energy Procedia* **2009**, *1*, 1099–1106.
[16] J. Ylätalo, J. Ritvanen, T. Tynjälä, T. Hyppänen, *Fuel* **2014**, *115*, 329–337.
[17] M. C. Romano, *Chem. Eng. Sci.* **2012**, *69*, 257–269.
[18] J. M. Valverde, S. Medina, *Phys. Chem. Chem. Phys.* **2015**, *17*, 21912–21926.
[19] C. C. Dean, D. Dugwell, P. S. Fennell, *Energy Environ. Sci.* **2011**, *4*, 2050–2053.
[20] A. Telesca, D. Calabrese, M. Marroccoli, M. Tomasulo, G. L. Valenti, G. Duelli, F. Montagnaro, *Fuel* **2014**, *118*, 202–205.
[21] J. Ylätalo, J. Parkkinen, J. Ritvanen, T. Tynjälä, T. Hyppänen, *Fuel* **2013**, *113*, 770–779.
[22] H. Dieter, A. R. Bidwe, G. Varela-duelli, A. Charitos, C. Hawthorne, *Fuel* **2014**, *127*, 23–37.
[23] Politecnico di Milano—Alstom UK (CAESAR project), *European Best Practice Guidelines for Assessment of CO2 Capture Technologies*, **2011**.
[24] D. Aaron, C. Tsouris, *Sep. Sci. Technol.* **2005**, *40*, 321–348.

[25] H. P. Mangalapally, H. Hasse, *Chem. Eng. Res. Des.* **2011**, *89*, 1216–1228.
[26] K. Atsonios, K. Panopoulos, P. Grammelis, E. Kakaras, *Int. J. Greenhouse Gas Control* **2016**, *45*, 106–117.
[27] P. E. Sanchez-Jimenez, J. M. Valverde, L. Perez-Maqueda, *Fuel* **2014**, *127*, 131–140.
[28] J. M. Valverde, P. E. Sanchez-Jimenez, L. Perez-Maqueda, *Appl. Energy* **2014**, *126*, 161–171.
[29] A. Lasheras, J. Ströhle, A. Galloy, B. Epple, *Int. J. Greenhouse Gas Control* **2011**, *5*, 686–693.
[30] M. Romano, I. Martínez, R. Murillo, B. Arstad, Richard Blom, Dursun Can Ozcan, Hyungwoong Ahn, Stefano Brandani *Guidelines for Modeling and Simulation of Ca-Looping Processes* **2012**, Sintef https://www.sintef.no/globalassets/project/eera-ccs/eera—ca-looping-simulation-guidelines.pdf.
[31] M. Alonso, N. Rodríguez, G. Grasa, J. C. Abanades, *Chem. Eng. Sci.* **2009**, *64*, 883–891.
[32] J. M. Valverde, P. E. Sanchez-Jimenez, L. Perez-Maqueda, *Appl. Energy* **2015**, *138*, 202–215.
[33] J. Miranda-Pizarro, A. Perejón, J. M. Valverde, P. E. Sánchez-Jiménez, L. A. Pérez-Maqueda, *RSC Adv.* **2016**, *6*, 37656–37663.
[34] C. Ortiz, R. Chacartegui, J. M. Valverde, J. A. Becerra, *Appl. Energy* **2016**, *169*, 408–420.
[35] C. Ortiz, R. Chacartegui, J. Valverde, J. Becerra, L. Perez-Maqueda, *Fuel* **2015**, *160*, 328–338.
[36] G. S. Grasa, J. C. Abanades, *Ind. Eng. Chem. Res.* **2006**, *45*, 8846–8851.
[37] B. Sarrion, J. M. Valverde, A. Perejon, L. A. Perez-maqueda, P. E. Sanchez-jimenez, *Energy Technol.* **2016**, *4*, 1013–1019.
[38] D. Alvarez, J. C. Abanades, *Ind. Eng. Chem. Res.* **2005**, *44*, 5608–5615.
[39] M. E. Diego, B. Arias, G. Grasa, J. C. Abanades, *Ind. Eng. Chem. Res.* **2014**, *53*, 10059–10071.
[40] J. C. Abanades, E. J. Anthony, J. Wang, J. E. Oakey, *Environ. Sci. Technol.* **2005**, *39*, 2861–2866.
[41] A. Silaban, M. Narcida, D. P. Harrison, *Chem. Eng. Commun.* **1996**, *146*, 149–162.
[42] A. de la Calle Martos, J. M. Valverde, P. E. Sanchez-Jimenez, A. Perejón, C. García-Garrido, L. A. Perez-Maqueda, *Phys. Chem. Chem. Phys.* **2016**, *18*, 16325–16336.
[43] J. M. Valverde, A. Perejon, S. Medina, L. A. Perez-Maqueda, *Phys. Chem. Chem. Phys.* **2015**, *17*, 30162–30176.
[44] S. Tian, J. Jiang, K. Li, F. Yan, X. Chen, *RSC Adv.* **2014**, *4*, 6858.
[45] S. Y. Pan, P. C. Chiang, Y. H. Chen, E. E. Chang, C. D. Chen, A. L. Shen, *Energy Procedia* **2014**, *63*, 2255–2260.
[46] The European Slag Association, The European Steel Association, *Position Paper on the Status of Ferrous Slag*, **2012**.
[47] P. Renforth, C. L. Washbourne, J. Taylder, D. A. C. Manning, *Environ. Sci. Technol.* **2011**, *45*, 2035–2041.
[48] S. Niu, K. Han, C. Lu, R. Sun, *Appl. Energy* **2010**, *87*, 2237–2242.
[49] A. W. Musumeci, R. L. Frost, E. R. Waclawik, *Spectrochim. Acta, Part A* **2007**, *67*, 649–661.
[50] I. Ortega-Fernández, N. Calvet, A. Gil, J. Rodríguez-Aseguinolaza, A. Faik, B. D'Aguanno, *Energy* **2015**, *89*, 601–609.
[51] J. M. Manso, J. A. Polanco, M. Losañez, J. J. Gonzalez, *Cem. Concr. Compos.* **2006**, *28*, 528–534.
[52] J. M. Valverde, *Chem. Eng. J.* **2013**, *228*, 1195–1206.
[53] R. Barker, *J. Appl. Chem. Biotechnol.* **1973**, *23*, 733–742.
[54] S. K. Bhatia, D. D. Perlmutter, *AIChE J.* **1983**, *29*, 79–86.
[55] W. Wang, S. Ramkumar, D. Wong, L. S. Fan, *Fuel* **2012**, *92*, 94–106.
[56] M. C. Romano, *Int. J. Greenhouse Gas Control* **2013**, *18*, 57–67.
[57] A. Martínez, Y. Lara, P. Lisbona, L. M. Romeo, *Energy Fuels* **2014**, *28*, 2059–2068.
[58] A. Martínez, Y. Lara, P. Lisbona, L. M. Romeo, *Environ. Sci. Technol.* **2013**, *47*, 11335–11341.

Received: June 23, 2016
Revised: July 18, 2016
Published online on August 9, 2016

***ANNEX 5**: Alovisio A, Chacartegui R, Ortiz C, Valverde JM, Verda V. Optimizing the CSP-Calcium Looping integration for Thermochemical Energy Storage. Energy Convers Manag 2017;136:85–98. doi:10.1016/j.enconman.2016.12.093.*

Energy Conversion and Management 136 (2017) 85–98

Contents lists available at ScienceDirect

Energy Conversion and Management

journal homepage: www.elsevier.com/locate/enconman

Optimizing the CSP-Calcium Looping integration for Thermochemical Energy Storage

A. Alovisio [a,b], R. Chacartegui [b], C. Ortiz [c,*], J.M. Valverde [c], V. Verda [a]

[a] Politecnico di Torino, Department of Energy Engineering, Corso Duca degli Abruzzi 24, 10129 Torino, Italy
[b] Energy Engineering Department, University of Seville, Camino de los Descubrimientos s/n, 41092 Sevilla, Spain
[c] Faculty of Physics, University of Seville, Avenida Reina Mercedes s/n, 41012 Sevilla, Spain

ARTICLE INFO

Article history:
Received 11 July 2016
Received in revised form 1 December 2016
Accepted 31 December 2016
Available online 11 January 2017

Keywords:
Calcium looping (CaL)
Energy storage
Concentrated Solar Power (CSP)
CO_2
Thermochemical energy storage (TCES)
CO_2 power cycle

ABSTRACT

Thermochemical energy storage (TCES) is considered a promising technology to overcome the issues of intermittent energy generation in Concentrated Solar Power (CSP) plants and couple them with yearly electricity demand. The development of this technology could favor the commercial deployment of CSP, which is considered as a key factor for new challenges in reducing GHG emissions. Among other possibilities, using the Calcium Looping (CaL) process for TCES is an interesting choice mainly due to the low cost of natural CaO precursors such as limestone (below $10/ton) and the high energy density that can be achieved (around 3.2 GJ/m^3). This manuscript explores several configurations in order to maximize the performance of the CSP-CaL integration with the focus on power cycle integration in the carbonator zone. For this purpose, firstly, a discussion about the possibility of using open and closed power cycles is carried out, which leads to the conclusion that a CO_2 closed cycle is more appropriate. Then, a closed regenerative CO_2 Brayton cycle is analyzed in further detail and optimized by means of the pinch-analysis methodology. A main output is that high plant efficiencies (of about 45%) can be achieved using a simple closed CO_2 Brayton power cycle. The optimized integration layout shows good performances at carbonator to turbine outlet pressure ratios around 3, thus allowing for a feasible integration of the power cycle in the CSP-CaL system.

1. Introduction

The commercial expansion of renewable energy technologies is an urgent need to limit global warming to "well below" 2.0 °C by 2100 and pursue 1.5 °C above pre-industrial levels as agreed at Paris COP21 Conference [1]. Among renewable energy technologies, concentrated solar power (CSP) has a great potential for commercial expansion [2]. However, for CSP to achieve full autonomy from fossil fuels and to increase its feasibility a main hurdle to overcome is its inherent variability in power production. Thus, efficient and low cost energy storage stands as a major technological challenge to mitigate global warming [3–5]. Moreover, large-scale energy storage is essential for a global system with high penetration of solar energy in order to increase the electric grid flexibility and avoid risks derived from transient peaks [6].

In recent years, a number of potential technologies have been proposed to store thermal energy in CSP plants. These are based upon three main concepts: sensible thermal energy storage (TES), latent heat storage and thermochemical energy storage (TCES) [7,8]. Sensible heat storage systems are the most mature [9] and involve the use of various materials with high heat capacity such as water [7], molten salts [10–13], mineral oils [14] or ceramic materials [15]. A number of commercial CSP plants do already exist or are under construction [16] wherein heat is stored in molten salts and used to generate electricity overnight. Another type of storage system currently at the pilot scale level makes use of the latent heat associated with the phase change in some materials [17–20]. Phase change materials (PCM) allow attaining higher storage capacities as compared to sensible heat storage [9,21]. A third possibility relies on thermochemical energy storage (TCES), which is being increasingly investigated [9,22–24]. TCES basically consists of using the heat obtained from an external source such as CSP to drive an endothermic chemical reaction. When energy is needed the stored products from the reaction are brought together at the necessary conditions for the reverse exothermic reaction to occur. This releases the previously used heat for power production. The main advantages of TCES as compared to TES are a considerably higher energy density as well as the possibility of storing energy in the long term or transport it without significant losses

* Corresponding author.
E-mail address: cortiz7@us.es (C. Ortiz).

http://dx.doi.org/10.1016/j.enconman.2016.12.093
0196-8904/

Nomenclature

$c_{p,i}$	specific heat, kJ/(kmol·K)
E	fraction of CO_2 spent in the reaction
F_i	molar flow rate of component i, kmol/s
F_{CaCO_3}	$CaCO_3$ molar flow rate
$F_{CaCO3,carb}$	$CaCO_3$ molar flow rate (calciner side)
$F_{CaCO3,clc}$	$CaCO_3$ molar flow rate (carbonator side)
$F_{CaO,crb}$	molar flow rate of CaO
$F_{CaO,clc}$	mole of regenerated sorbent
$F_{CaO,nr,carb}$	molar flow rate of unreacted CaO (carbonator side)
$F_{CaO,nr,clc}$	molar flow rate of unreacted CaO (calciner side)
$F_{CO_2,clc,out}$	CO_2 molar flow rate at calciner outlet
$F_{CO_2,nr}$	non reacted CO_2 molar flow in the carbonator
$F_{R,carb}$	recirculating molar flow rate (carbonator side)
$F_{R,clc}$	recirculating molar flow rate (calciner side)
$F_{CO_2,stoich}$	stoichiometric CO_2 molar flow
h_i	enthalpy, kJ/kmol
HXA	solid-solid heat exchanger
HXB	gas-solid heat exchanger
HXE	gas-solid heat exchanger
HXF	gas-solid heat exchanger
HXG	gas-gas heat exchanger
HXI	gas-solid heat exchanger
$\dot{m}_{CO2,crb}$	CO_2 mass flow rate through carbonator
P_{carb}	absolute carbonator pressure, bar
P_{eq}	CO_2 partial pressure at equilibrium, bar
PR	pressure ratio
p_{drop}	pressure drops of CO_2, bar
$y_{CO2,carb,in}$	inlet molar fraction of CO_2 in the carbonator
y_{eq}	equilibrium fraction of CO_2 in the carbonator
T	temperature, °C
T_{clc}	calciner temperature, °C
T_{carb}	carbonator temperature, °C
v_i	stoichiometric coefficient of compound i
$\dot{W}$	mechanical power, kW
X	average CaO conversion
Δt_{sun}	average daytime period (h)
$\Delta H_R(T_{react})$	reaction enthalpy at the reactor temperature, kJ/mol
ΔH_R^0	standard enthalpy of reaction, kJ/mol
ξ	extent of reaction per unit time
Φ	thermal power, KW
Φ_{disp}	dissipated heat of carbonation, kW

[9,25]. Moreover, the sensible heat stored in the reaction products is also usable in addition to the chemically stored heat.

An appropriate reversible reaction is necessary in order to achieve an efficient and cost-effective TCES [26]. One of the most promising systems for the development of TCES at large scale is the Calcium Looping (CaL) process, which relies on the carbonation-calcination reaction of CaO (Eq. (1)) [27–30]. The CaL process begins with the decomposition of a bed of $CaCO_3$ particulate solids in a calcination reactor (calciner) yielding CaO and CO_2 as products. Once the sensible heat from the calciner outlet streams (CaO, with a similar heat capacity to molten salts, and CO_2 streams) is recovered, the products are stored. Storage conditions and time are flexible and could be accommodated to the energy demand [25]. When needed, the CaO and CO_2 products would be circulated into a carbonator reactor, where energy is obtained from the carbonation reaction:

$$CaO_{(s)} + CO_{2(g)} \rightleftarrows CaCO_{3(s)} \quad \Delta H_r^0 = -178\ \text{kJ/mol} \tag{1}$$

The CaL process has been extensively investigated as a potentially low energy penalty alternative to the use of the commercial amine based technology for CO_2 capture [31–34].The main drawback is that CaO shows indeed a marked deactivation at the specific conditions of the CaL process for CO_2 capture, which necessary involve regeneration of CaO by calcination at high temperature (around 950 °C) under high CO_2 partial pressure and carbonation under relatively low CO_2 partial pressure [32,35,36]. Nevertheless, thermodynamic conditions to achieve high TCES global efficiency in the CaL process are radically different than those for CO_2 capture. The former involves carbonation at high CO_2 partial pressure at high temperature whereas calcination can be carried out at low CO_2 concentration and therefore relatively low temperatures. According to recently published thermogravimetric analysis (TGA) tests [37], the residual conversion exhibited by CaO derived from calcination of natural limestone can be as high as $X_r = 0.5$ under these CSP conditions in contrast with the very small values obtained for post-combustion CO_2 capture conditions ($X_r = 0.08$). Thus, the use of expensive Ca-based composites that might hinder the short-term commercial development of CSP would not be necessary. A main goal of the present manuscript is to analyze the CaL conditions for an optimum performance of the CSP-CaL integration.

Integration of the CaL process and CSP has been previously analyzed by other authors under several schemes. Tregambi et al. [38] proposed a configuration whereby $CaCO_3$ calcination is assisted by CSP in order to lower the energy penalty associated to CO_2 capture in a coal fired power plant by means of the CaL process. Zhai et al. [39] analyzed several schemes in which CSP served to recover energy in the CO_2 capture system, although the contribution of CSP to the system is lower than 10%. On the other hand, Edwards et al. [29] studied a CSP-CaL integration in which the heat produced in the carbonator reactor is used for power generation through a CO_2/air open cycle albeit with a limited efficiency critically affected by CaO conversion. Muñoz-Anton et al. [40] analyzed the integration of a close to critical regenerative CO_2 Brayton cycle in a CSP power plant without storage, to achieve a higher cycle efficiency. A relative high efficiency CSP-CaL integration was proposed by Chacartegui et al. [23] in which power generation is carried out by means of a closed CO_2 power cycle.

In this work, a deep analysis of the CSP-CaL-power system integration is carried out. Departing from an open loop configuration, several layouts are explored and compared in order to improve the power system integration within the thermochemical storage system. The coupling of the CaL process with a closed CO_2 power system is analyzed in detail to look for an optimal configuration. Full integration is investigated through application of pinch-analysis. Results demonstrate that a global efficiency above 45% may be attained at CaL conditions that favor a stable and high value of the multicycle conversion of CaO derived from natural limestone, which makes the proposed integration model a highly competitive option for TCES.

2. CSP-CaL system for thermochemical energy storage

Fig. 1 shows a conceptual approach of the CSP-CaL integration for thermochemical energy storage. The cycle begins with the $CaCO_3$ decomposition reaction (calcination), which is performed at high temperature from solar heat radiation. According to equilibrium conditions [41] and reaction kinetics, high temperatures are necessary when operating under high CO_2 partial pressure (above 900 °C) for sufficiently fast reaction to achieve completion in short residence time [42–44]. Nevertheless, the use of

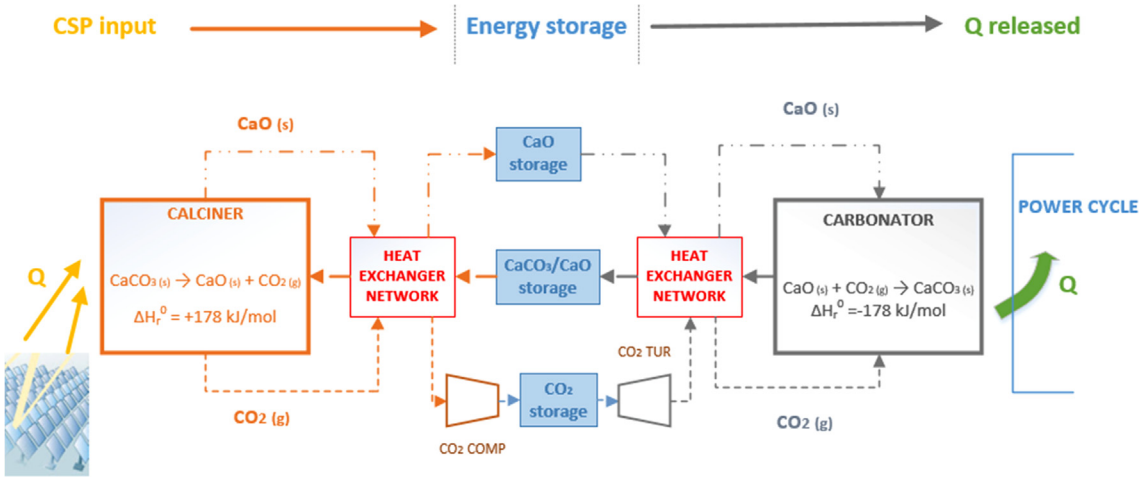

Fig. 1. Conceptual CSP-CaL integration for thermochemical energy storage.

superheated steam in the calciner environment would allow to decrease the calcination temperature down to 700–750 °C whereas the mixture H_2O/CO_2 flowing out from the calciner reactor would be easily separable. Among the CSP power technologies, solar tower systems result the most appropriate for this purpose according to the temperature requirements. Small prototypes of solar calciners have been already developed based on fluidized beds [45,46], rotary kilns [47,48] and cyclone atmospheric reactors [49].

As seen in Fig. 1, the CO_2 released after calcination is sent to a storage tank after being cooled down and compressed, whereas the CaO stream is circulated to a solids storage reservoir after being brought to ambient conditions. The solid stream entering the calciner, composed by $CaCO_3$ and unreacted CaO, is preheated through a heat exchanger network where the sensible heat of the hot streams leaving the calciner is used.

The energy release stage occurs in the carbonator zone, where the heat of the carbonation reaction is delivered at high temperature (650–1000 °C as a function of carbonation conditions) to a power cycle by means of a stream carrier. Limestone derived CaO usually shows a marked deactivation at the specific conditions of the CaL process for post-combustion CO_2 capture although, as said above, the multicycle CaO behavior could be considerably different operating under conditions that would maximize the efficiency of the present integration [37]. Solids exiting the carbonator are passed through a heat exchanger network to preheat CaO and CO_2 streams circulating toward the carbonator. The CO_2 stream exiting the storage is expanded to a selected carbonator pressure lower than the storage pressure, which allows the use of commercial fluidized bed technology. As can be seen in Fig. 1, compression-expansion process of CO_2 before and after than storage resembles a compressed air energy storage (CAES) system [8,50]. Thus, the integration incorporates energy storage not just in chemical form but also as sensible heat and mechanical energy through CO_2 compression.

Regarding the integration of the power cycle in the carbonator zone, previous works have proposed the use of an air stream as heat transfer fluid in an open Brayton cycle (Fig. 2) [29]. According to this scheme, the CO_2 stream entering into the carbonator is assumed to react completely with the CaO solids to produce $CaCO_3$. Thus, it is implicitly assumed that pure air stream exits the carbonator to enter the gas turbine for power production in an open Brayton cycle. The outflowing air from the turbine passes through a heat exchanger network, releasing sensible heat further used to preheat the solids recirculated into the carbonator. However, reaction equilibrium poses a fundamental limitation to this scheme

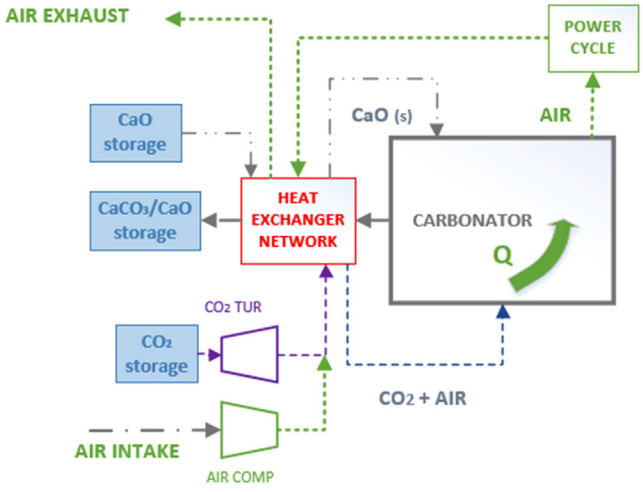

Fig. 2. Air/CO_2 open cycle integration in the carbonator zone. Originally proposed by Edwards et al. [29].

since the reaction will reach equilibrium and carbonation will stop as soon as the CO_2 partial pressure in the carbonator reactor is decreased to the equilibrium partial pressure as depending on the carbonator temperature. Thus, the effluent gas from the carbonator to be sent to exhaust cannot be free of CO_2 because of fundamental thermodynamic reasons.

The equilibrium molar fraction of CO_2 in the carbonator y_{eq} is given by Eq. (2)

$$y_{eq} = \frac{P_{eq}}{P} = \frac{\left[4.137 \cdot 10^7 \exp\left(-\frac{20.474}{T+273}\right)\right]}{P} \quad (2)$$

where P_{eq} (bar) is the CO_2 partial pressure at equilibrium and P (bar), T (°C) are the carbonator pressure and temperature [41].

Thus, when a 15% v/v CO_2 stream is introduced into a carbonator at atmospheric pressure (P = 1 bar) and T = 650 °C, the minimum CO_2 concentration in the gas stream exiting the carbonator is around 1% (Fig. 3a). As can be seen in Fig. 3b, if the carbonator temperature is increased to 850 °C to enhance the thermoelectric efficiency a minimum carbonator pressure of 4 bar is required for carbonation to take place. This becomes even much higher (P = 50 bar) if the required CO_2 concentration in the flue gas is below 1%. In addition, the theoretical maximum of carbonation efficiency is hardly achievable in practice. For these reasons, the

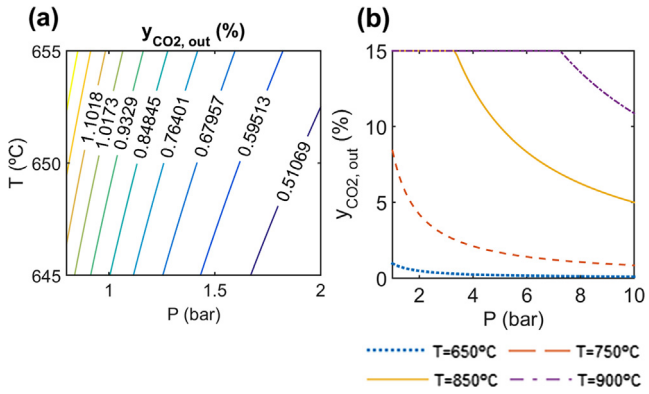

Fig. 3. Minimum CO_2 concentration (% v/v) exiting the carbonator as a function of carbonator pressure P and temperature T for a CO_2 concentration at carbonator inlet of 15 %v/v.

open Brayton cycle does not guarantee a CO_2 emission free CSP-CaL integration.

A possible solution to avoid the inconveniences of an open Brayton cycle is to use a closed CO_2 Brayton cycle [23]. In this configuration, solids in the carbonator (CaO) are fluidized by a pure CO_2 gas flow with a molar rate well above the stoichiometric value. The CO_2 fraction not participating in the reaction is employed to remove heat from the carbonation and is delivered to a gas turbine for the power cycle. In the next section an energy optimized process leading to a global CSP-CaL integration efficiency above 43% with high feasibility index is described in detail.

3. CSP-CaL integration model

This section shows the global integration model and the process design to transform an air-open power cycle (Fig. 2) to a closed-CO_2 power cycle as a first step for optimizing the CSP-CaL integration. Optimal CSP-CaL integration in our work starts from the heat exchanger network proposed in [29] with the necessary adaptations derived from the use of a CO_2 closed Brayton cycle in the carbonator side. Fig. 4 shows a first possible approach for the proposed integration in which the new equipment needed for the closed cycle is marked by the shaded area. As can be seen, solids entering into the calciner are preheated using the sensible heat released by the hot streams leaving this reactor in a gas-solid heat exchanger (HXB in Fig. 4) and in a solid-solid heat exchanger (HXA). The CO_2 power cycle is a closed and regenerative cycle in which the heat removed by the reactants in the carbonator is recovered in a solid-gas heat exchanger (HXF). On the other hand, the residual heat from the solids at the carbonator output is extracted to pre-heat the CO_2 stream entering the carbonator by means of another gas-solid heat exchanger (HXE). Solids can be conveyed by means of the mature pneumatic technology, whose energy consumption is about 3–5 MJ ton^{-1}/100 m [51].

As detailed in Fig. 4, part of the power needed in the compression stage of the Brayton cycle is provided by the expansion of the pressurized CO_2 coming from the storage vessel. The expansion of CO_2 yields useful work while, at the same time, releases very low temperature heat (up to −30 °C to be spent for CO_2 intercooling compression of the stream coming from carbonator).

3.1. Mass and energy balances

In this section the main aspects of the CSP-CaL integration model are described, concerning mass and energy balances in the heat exchangers, reservoirs and reactors. Fig. 5 shows the mass flow scheme in the CaL process. The solids stream ($CaO/CaCO_3$ mixture) entering into the carbonator (flow rate $F_{R,clc}$) reacts with the CO_2 stream coming from calciner side. Due to the possible loss of CaO reactivity with the number of cycles and depending on

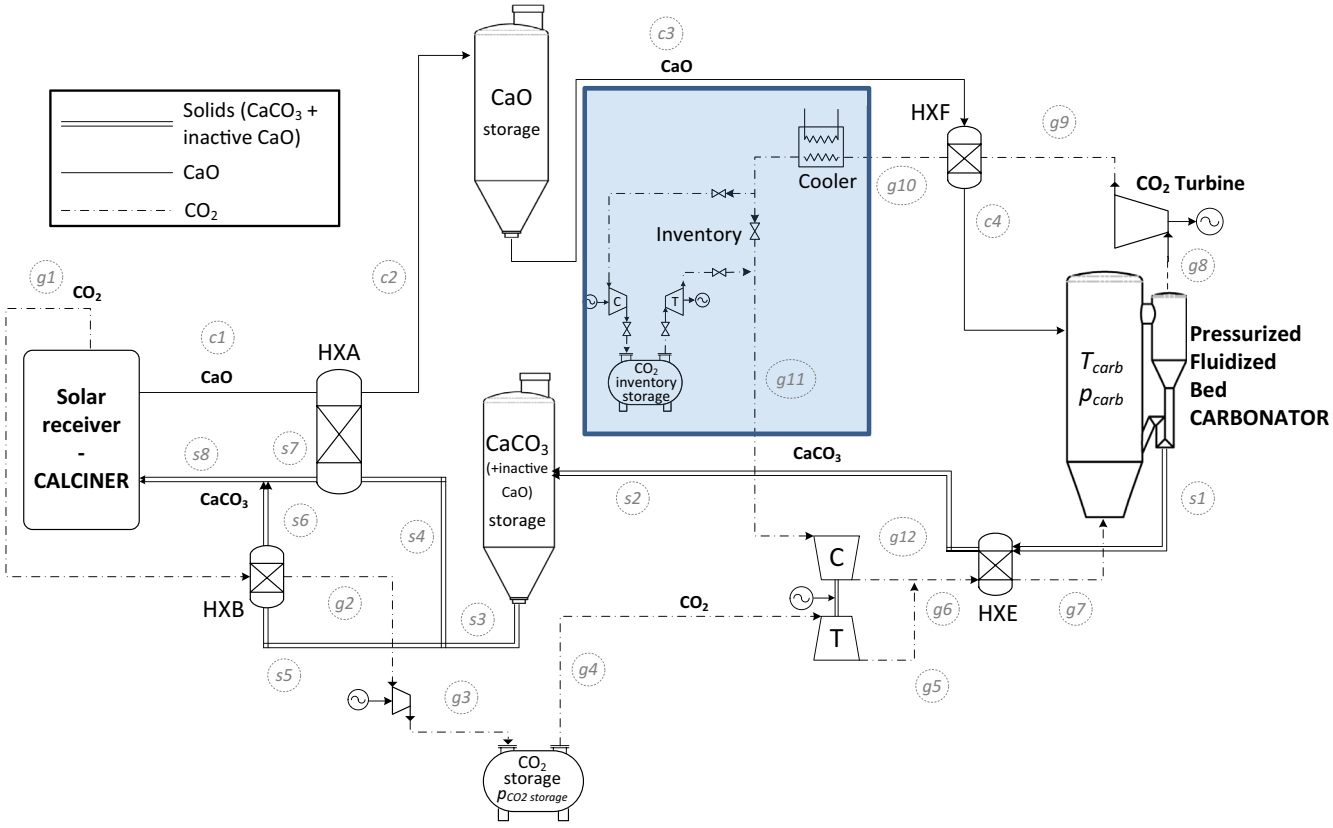

Fig. 4. Preliminary plant diagram using a CO_2 closed loop (layout 1). Stream main data are shown in Appendix A.

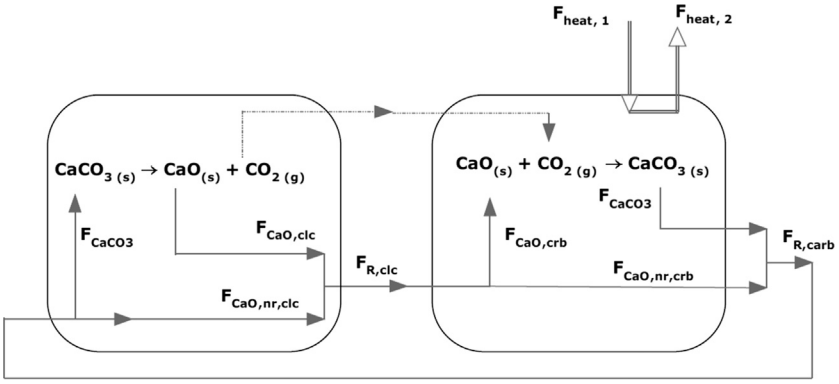

Fig. 5. Mass-balance schematics of the plant.

residence times and mass/heat transfer conditions, only a part of the solids is assumed to react ($F_{CaO,crb}$) to produce $CaCO_3$. Thus, the solids at the carbonator outlet ($F_{R,crb}$) consist of the $CaCO_3$ produced by carbonation (F_{CaCO3}) and the unreacted CaO ($F_{CaO,nr,crb}$). The stream F_{heat} is the CO_2 molar flow used to remove the heat of reaction from the carbonation environment and to perform the power cycle for generation of electricity, which is in this proposed cycle a 100% CO_2 stream. The carbonated particles are assumed to attain complete decomposition in the calciner. Thus, each mole of $CaCO_3$ gives rise to a mole of CO_2 and a mole of regenerated CaO ($F_{CaO,clc}$). The calciner solids output will therefore consist of CaO (partially regenerated CaO and partially unreacted CaO) at a flow rate $F_{R,clc}$.

The storage vessels must be sized to allow for a buffer storage that enables the carbonator/turbine group running over 24 h by an adequate load adjustment. In order to guarantee 24 h steady-state operation, the mass-balance equation that must be satisfied is:

$$\int_{24h} F_{CaCO3,clc}(t)dt = \int_{24h} F_{CaCO3,crb}(t)dt \tag{3}$$

Plant performance is determined as an average over the 24 h period and the molar flow rates are assumed constant and equal to the integral average value over the daytime curve. Accordingly, an average daytime period Δt_{sun} is considered during which the sun-solar concentrators system is able to provide sufficient energy for the decomposition reaction to be fully achieved in the calciner. In this way, it is possible to derive an averaged ratio between the circulating flow rates in the calciner and carbonator side of the plant. For a daytime of 8 h (assuming clear skies), the average ratio over the 24 h between the circulating flow rates of the streams in the calciner and in the carbonator over the 24 h will be equal 3, while in case the daytime is 12 h, the flow rates through the calciner will be twice that through the carbonator. More sophisticated control strategies should be actuated within a framework of long-period control to ensure steady operation over periods larger than 24 h. This control should be based on the meteorological forecasts and according to the power load curve.

Energy balances in the calciner and carbonator are shown in Fig. 6. The energy and mass balances in the carbonator and calciner reactors can be expressed as:

$$\sum_i F_{i,out}h_{i,out} - \sum_i F_{i,in}h_{i,in} = \Phi - \dot{W} \tag{4}$$

$$F_{i,out} - F_{i,in} = \xi \nu_i \tag{5}$$

where F_i is the molar flow and h_i is the molar enthalpy of component i. Φ and $\dot{W}$ represent respectively the thermal and mechanical

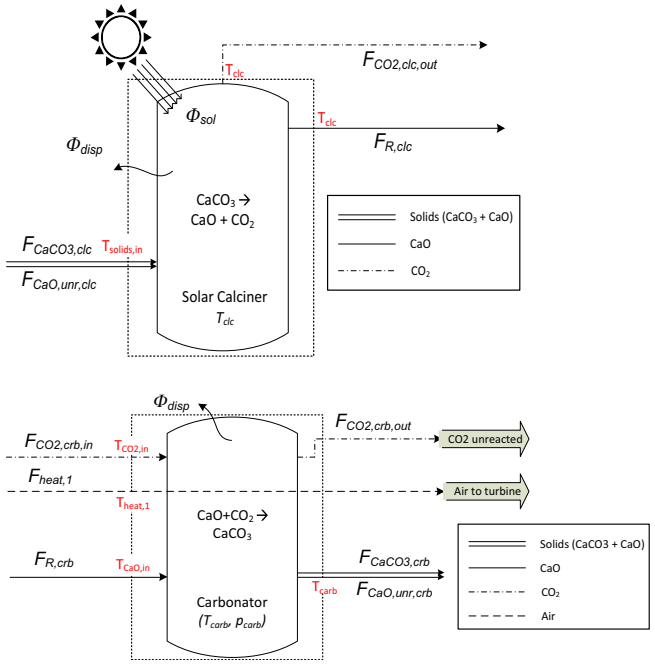

Fig. 6. Energy balance in the calciner (top) and carbonator (bottom) reactors.

power interchange between the system and its surroundings. ξ is the reaction rate of the considered reversible reaction and ν_i is the stoichiometric coefficient of compound i.

Considering the outlet flows in the same conditions of the reactor, eqs. (4) and (5) can be rearranged as:

$$\xi \Delta H_R(T_{react}) + \sum_i F_{i,in}(h_{i,react} - h_{i,in}) = \Phi - \dot{W} \tag{6}$$

where $\Delta H_R(T_{react})$ is the reaction enthalpy change at the reaction temperature.

$$\Delta H_R(T_{react}) = \sum_i \nu_i h_{i,T} = \Delta H_R^0 + \sum_i \nu_i \int_{ref}^{T} c_{p,i}dT \tag{7}$$

Energy change in the control volume consists therefore of the part associated to the heat of reaction at reactor temperature ($\xi \Delta H_R(T_{react})$) and the heat required to bring reactants from inlet to reactor condition ($\sum_i F_{i,in}(h_{i,react} - h_{i,in})$).

Assuming reactor isothermal conditions, Eq. (6) applied to the carbonator serves to balance out the amount of CO_2 needed to remove the heat which is not absorbed by reactants or dispersed through the walls. On the other hand, Eq. (6) applied to the calciner

yields the $CaCO_3$ decomposition in accordance to the net energy input into the system given by the balance of solar heat supply and energy loss occurring between the sun and the reactor (due to undesirable heat transfer, radiation, absorption losses or reflection effects).

The carbonator is a pressurized fluidized bed wherein the carbonation reaction takes place at high temperature. Pressurized carbonation is desirable for the power-cycle direct integration and allows carbonation at high temperatures and at a fast rate [52]. The solids in the carbonator (CaO) are fluidized by a pure CO_2 gas flow. Thus, the molar flow rate of CO_2 flowing into the carbonator is well above the stoichiometric need. The CO_2 fraction which does not intervene in the reaction is used to remove heat from carbonation and deliver it to the gas turbine. Let us define a parameter E to quantify the fraction of CO_2 spent in the reaction (Eq. (8)), so that the non-reacting fraction of CO_2 is just re-circulating in the loop:

$$E = \frac{molCO_2 reacted}{molCO_2 in} = 1 - \frac{F_{CO_2,out}}{F_{CO_2,in}} = 1 - \frac{F_{CO_2,powercycle} + F_{CO_2,nr}}{F_{CO_2,powercycle} + F_{CO_2,stoich}} \quad (8)$$

Here $F_{CO_2,nr}$ is the non-reacting portion of the $F_{CO_2,stoich}$ stoichiometric moles of CO_2 needed for the reaction. The CO_2 cycle is a closed and regenerative cycle, where the heat removed by reactants in the carbonator is recovered in an indirect gas-solid heat exchanger, HXF (see Fig. 4). This avoids the direct contact between CO_2 and CaO streams, which could lead to a partial carbonation reaction with a possible poor utilization of the reaction heat. In the heat exchanger HXF, heat from the exhaust CO_2 stream is used to heat up the solids before entering the carbonator, while in the heat exchanger HXE (see Fig. 4) the residual heat from the solids leaving the carbonator is used to pre-heat the CO_2 at the carbonator inlet. Part of the power needed in the compression stage of the CO_2 Joule-Brayton cycle is provided from the expansion of the pressurized CO_2 needed to run the reaction in the carbonator. Expansion in the gas turbine finally supplies the useful power of the cycle. CO_2 expansion from storage also provides some usable work, and at the same time releases useful energy at very low temperature (up to −30 °C), which can be employed for the CO_2 intercooling compression of the stream coming from carbonator. For this reason, C and T (see Fig. 4) are thermally coupled to avoid the use of massive air cooling devices (and to further reduce costs).

3.2. Layout 1 simulation

The schematics proposed in Fig. 4 was simulated in order to calculate the cycle efficiency with energy storage, defined by the following expression:

$$\eta = \frac{\int_{24h} \dot{W}_{net} dt}{\int_{24h} \dot{Q}_{input} dt} \quad (9)$$

where $\dot{W}_{net}$ is the net power produced in the global cycle and $\dot{Q}_{input}$ is the CSP input in the calciner.

The values of the operation parameters used for design purpose are summarized in Table 1. The cycle performance is analyzed as a function of four key parameters for cycle efficiency, namely CaO conversion X (defined as the ratio of CaO mass converted to $CaCO_3$ to the CaO mass entering the carbonator), the carbonator temperature T_{carb}, the carbonator pressure p_{carb} and the CO_2 main turbine outlet pressure $p_{out,turbine}$.

A key parameter for the cycle performance is the carbonator temperature T_{carb}. The temperature at which carbonation is carried out is the heat-release temperature of the storage system to the power cycle. When the combination of temperature and CO_2 partial pressure yields an equilibrium molar fraction of CO_2 equal to the inlet molar fraction, carbonation is not possible anymore ($F_{CO_2,nr} = F_{CO_2,stoich}$). Thus, increasing the carbonator pressure allows shifting the carbonation temperature to higher values (see Eq. (2)). For example, carbonator temperatures of 950–975 °C are potentially achievable in the case of carbonation under pure CO_2 at a pressure of 7 bar and 1025–1050 °C would be achievable in case of 15 bar.

Table 1
Fixed model conditions in CO_2 closed power cycle configuration.

Net absorbed solar flux in calciner	100	MW
Thermal dispersions in carbonator	10	%
Calciner temperature	900	°C
Ambient temperature	20	°C
CaO conversion (X)	0.20	
Carbonator temperature (T_{carb})	875	°C
Carbonator pressure (p_{carb})	6	bar
Turbine outlet pressure ($p_{out,turbine}$)	0.2	bar
Approach temperature solid-solid HX	20	°C
Approach temperature solid-gas HX	15	°C
Approach temperature CO_2 cooler	10	°C
Intercoolings in CO_2 storage compression	5	
Intercoolings in CO_2 cycle compression	4	
CO_2 storage conditions	75 bar, T ambient	
Solid phase conveying energy consumption	10	MJ/ton/100 m
Equivalent length for solids conveying (carbonator side)	100	m
Equivalent length for solids conveying (calciner side)	100	m
Daylight hours	12	h
Isentropic efficiencies (compression/expansion)	0.89	

The results obtained for the global plant efficiency are plotted in Fig. 7 as a function of the carbonator temperature and for two fixed values of CaO conversion (X = 0.2 and 0.5). As can be seen, the plant efficiency would be hampered by a CaO conversion higher than 0.2. However, a high CaO conversion should help increasing the cycle performance since a minor fraction of unreacted CaO would be present in the circulating stream of solids, therefore allowing for a reduction of the energy penalty. This suggests that the performance of the CSP-CaL integration could be improved by optimizing the heat recovery exchanger network as will be discussed in the next sections.

Another critical parameter for the system performance is the pressure ratio in the main turbine, defined as $PR = p_{carb}/p_{out,turbine}$. On the other hand, the global cycle efficiency has a dependence

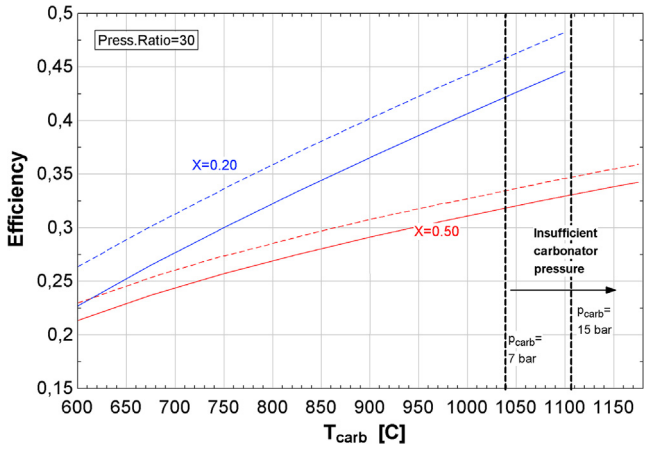

Fig. 7. Efficiency vs carbonator temperature (PR = 30) calculated for fixed values of CaO conversion X = 0.20 and X = 0.50 (solid lines). Dashed lines show efficiency calculated without including energy consumption for solid conveying. Temperature limits due to equilibrium constrains are marked for carbonator pressures of 7 bar and 15 bar.

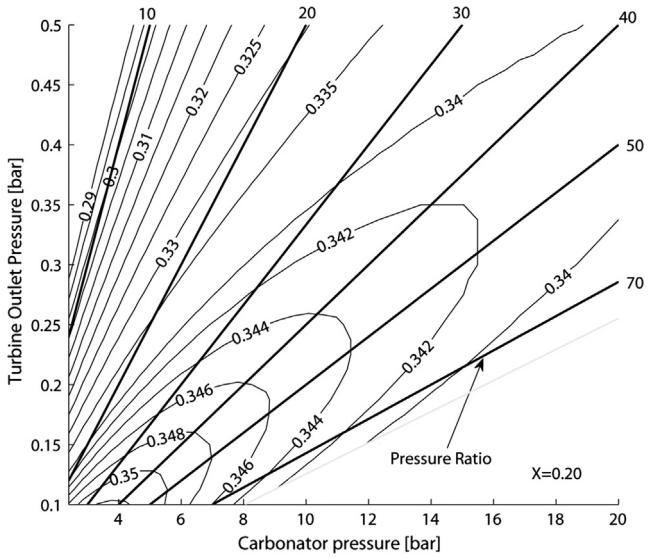

Fig. 8. Efficiency as a function of carbonator and turbine outlet pressure calculated for a fixed value of CaO conversion X = 0.20. Contour lines indicate iso-efficiency cycle values.

also on the absolute carbonator and turbine outlet pressures. Fig. 8 shows a contour plot of the system efficiency as a function of both carbonator pressure and turbine outlet pressure, which serves to infer the optimum pressure choice. In layout 1, CaO conversion (X) has been fixed to 0.2 which gives a close to maximum cycle efficiency.

As shown in Fig. 8, the maximum efficiency occurs at pressure ratios around 40–50. However, it is important to note that for pressure ratios over 30 the efficiency does not change considerably. From pressure ratios of 30 up to 70, efficiency increases less than 0.5%. Since such high values of pressure ratios are difficult to achieve in practice, a pressure ratio of 30 represents a good trade-off.

Fig. 8 shows that higher efficiency can be achieved by decreasing the turbine outlet pressure. There are at least two reasons for which expansion to under-atmospheric pressures should be taken into consideration: (i) If the turbine outlet pressure is atmospheric, the optimum pressure occurs at too high values (around 30 bar) currently unpractical from the pressurized carbonator technology; (ii) Efficiency increases markedly with decreasing the turbine outlet pressure, mainly thanks to the higher power generated by decompressing the stored CO_2. When the turbine outlet pressure is around 0.1 bar, for instance, efficiency is almost 1% higher than when outlet pressure is 0.3 bar. Over-expanding up to under-atmospheric pressures is not a problem by itself although it must be taken into account that too strong vacuums are difficult to manage from the practical point of view and may lead to increased pipelines volume.

As a summary, the analysis of layout 1 shows that:

- The best performances are achieved for pressure ratios in the range 40–50 (if intercooling is performed during compression of the power fluid). Nevertheless, pressure ratios over 30 do not enhance efficiency beyond 0.1–0.2%, thus a good trade-off is to keep the pressure ratio around 30.
- Such high optimum values of the pressure ratio suggest the necessity of over-expanding up to a pressure below atmospheric. Over-expansion also results in better performances (higher efficiency).
- On the other side, the higher the carbonator pressure the higher carbonator temperatures may be, which yields a higher efficiency.
- In this configuration (layout 1), global efficiency is hampered by an increase of CaO conversion due to a non-optimized heat integration as shown in next sections.

4. Improving the heat exchange recovery in the power production stage to optimize the CSP-CaL-power cycle integration performance

Fig. 9 shows a first modification of layout 1 (Fig. 4) oriented toward improving the heat exchange recovery in order to enhance the system performance through an increase of CaO conversion. With respect to the preliminary configuration, a CO_2 regenerator (HXG) is incorporated in the heat exchanger train in order to heat up a fraction of the gas stream entering the HXE exchanger (and then in the carbonator) using the sensible heat of a portion of the CO_2 turbine output flow. The two CO_2 streams, which are separately conditioned through heat exchangers HXF and HXG, are rejoined to evolve in the closed loop power-cycle. By regulating the CO_2 split ratios (i.e. the fractions of the CO_2 stream respectively sent to HXG and HXF), the internal overall heat exchange can be optimized. As a result, layout 2 can offer a wider range of regulating possibilities for efficiency rise. As shown in Fig. 10, Layout 2 shows higher performances as CaO conversion is increased. The additional CO_2 storage vessel (CO_2 inventory storage) is included in the scheme as an inventory control strategy for the gas turbine. Since mass flow rate is one of the parameters that determines the power output of the CO_2 closed-cycle (along with the compressor inlet temperature, turbomachinery efficiencies and the pressure ratio) [53], power generation can be controlled in the CSP-CaL scheme by modifying the circulating mass flow in the cycle (by injecting or removing CO_2 using the CO_2 inventory storage) to respond to a load change [54,55].

Fig. 10 shows the new cycle (layout 2) efficiency with respect to pressure inferred from the simulations using the same inlet parameters as for layout 1. Higher efficiency values are achieved for layout 2 as a result of an enhanced heat recovery at the carbonator outlet. As for layout 1, a fixed value of CaO conversion is set to $X = 0.2$. Further improvement can be achieved by a deeper thermal optimization of the system as discussed below.

4.1. Pinch-analysis

This section presents a pinch-analysis [56] of the carbonator side with the goal of achieving a plant configuration showing minimum energy consumption in a wide range of operational conditions.

4.1.1. Streams identification

Four streams can be identified in the carbonator side as detailed in Table 2 and Fig. 11. Heat transfer will be characterized by the minimum temperature approach (ΔT_{min}), which is set in a first approximation to 10 °C. The hot CO_2 stream flowing out from the turbine (which needs to be cooled) and the cold CO_2 stream in the pre-heating stage are indicated as $CO_{2,c}$ and $CO_{2,p}$ respectively.

The average thermal capacity FC_p of the streams is plotted in Fig. 12 as a function of the value of the CaO conversion X (referring to layout 1). The values are averaged between the heat exchanger input and output temperature. Exchanger HXF couples the CaO cold stream with the $CO_{2,c}$ stream at the turbine output, while a stream of solids is used to preheat the CO_2,p stream. In a counter-current heat exchange process, the best exergy performances are obtained when thermal capacities of the two streams are identical. As can be seen in Fig. 12, the exchange of heat is rather optimized for low values of X while for high values of X there is still room for further improvement.

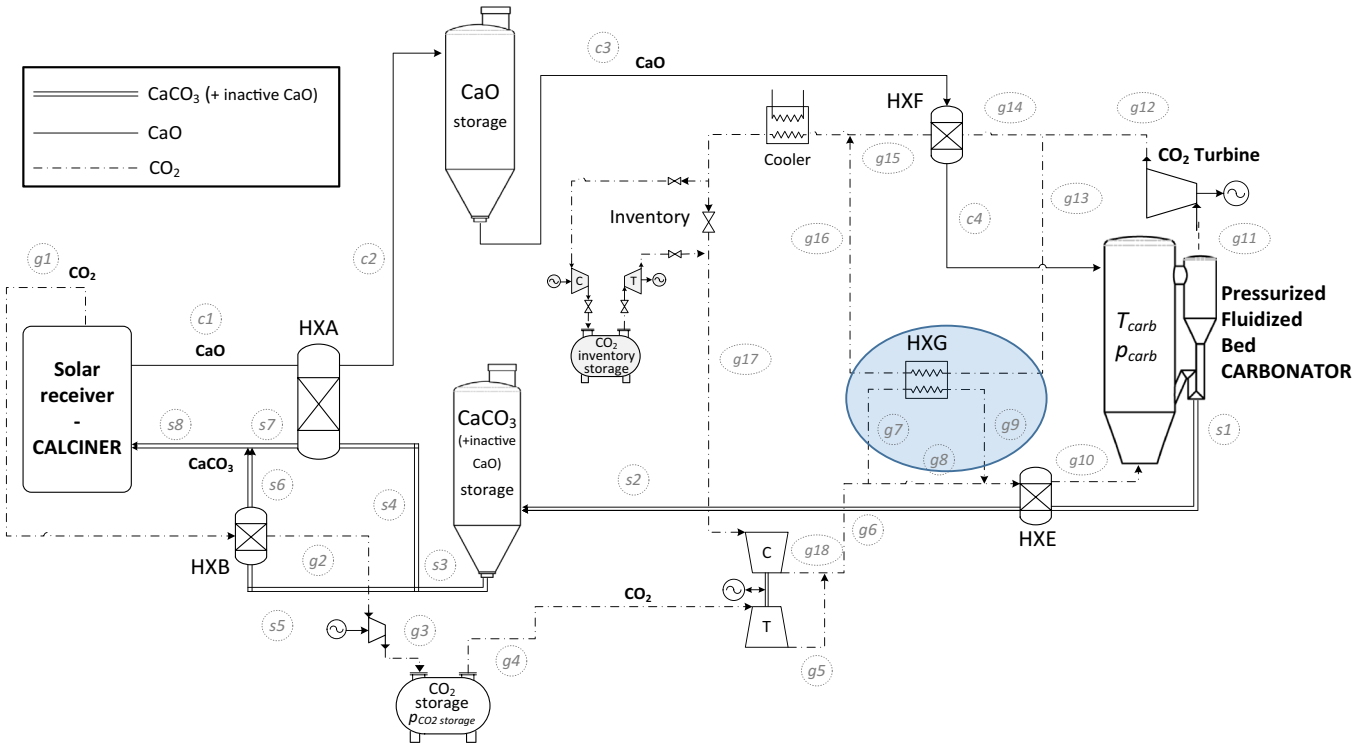

Fig. 9. Proposed plant diagram for better heat recovery in the power production stage (layout 2). Stream main data are shown in Appendix A.

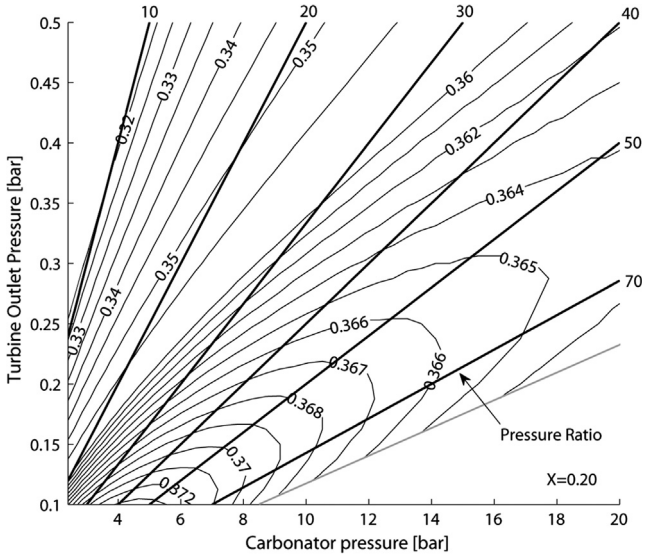

Fig. 10. Efficiency as a function of carbonator and turbine outlet pressure calculated using layout 2 configuration (Fig. 9) and for a fixed value of CaO conversion X = 0.20. Dashed white lines show iso-efficiency curves.

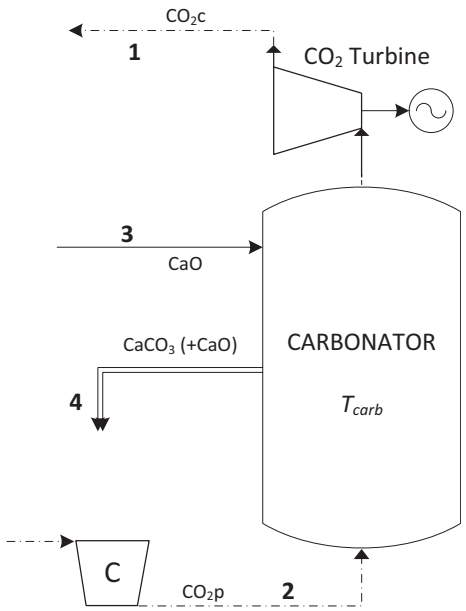

Fig. 11. Identification of the streams in the carbonator side used for the pinch-analysis.

Table 2
Streams identification in the carbonator side.

Stream	Description	*Type*	T_{in}	T_{out}
1	CO_2 at turbine output ($CO_{2,c}$)	Hot	$T_{out,turbine}$	T_{amb}
2	CO_2 at compressor output ($CO_{2,p}$)	Cold	$T_{out,compressor}$	T_{carb}
3	CaO	Cold	T_{amb}	T_{carb}
4	Solids ($CaCO_3$ + CaO)	Hot	T_{carb}	T_{amb}

The targets are set in view of some considerations:

- The cold streams should be preheated at a temperature as high as possible before flowing into the carbonator.
- The heat available from the carbonator effluent streams needs to be recovered. After heat recovery, such streams should be at the lowest temperature achievable.
- The lowest temperature achievable for the hot streams is ambient temperature while the target high temperature for the cold streams is the carbonator temperature. In addition, the CO_2 temperature must be as low as possible at the compressor inlet in order to reduce the compression work.

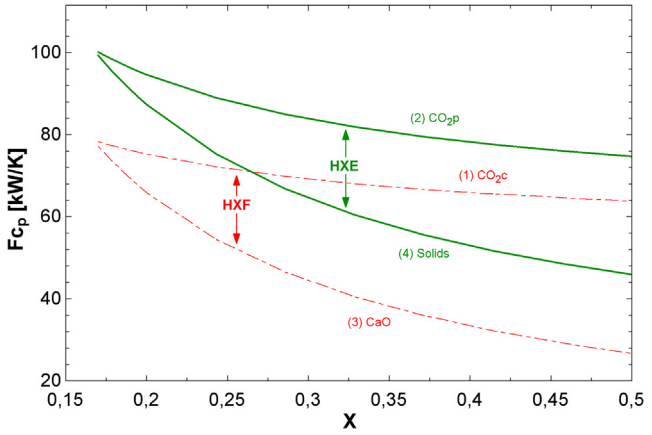

Fig. 12. Average thermal capacity (FC_p) of the streams in the carbonator side as indicated vs CaO conversion (X) for HXE and HXF heat exchangers cases.

Table 3
Streams characterization for X = 0.2.

Stream	Type	Fc_p (kW/K)	T_{in} (°C)	T_{out} (°C)	Φ (MW)
1	Hot	75.3	426	20	−30.6
2	Cold	94.65	20	875	80.9
3	Cold	65.92	20	875	56.4
4	Hot	87.35	875	20	−74.7

The analysis based on the above considerations has been done using an ambient temperature of 20 °C, a carbonator temperature of 875 °C and a turbine outlet temperature of 426 °C which is the expected outlet temperature for a 7–0.2 bar expansion. The compressor output temperature has been set equal to ambient temperature in order to simplify calculations. This choice is justified by the fact that CO_2 compression is performed with intercooling and temperature is brought down by the low-T heat available from the CO_2 expansion. Table 3 shows the values of the stream parameters used in the calculations. A fixed value of CaO conversion ($X = 0.2$) has been employed.

4.1.2. Composite curves

Streams data are combined in the so-called 'composite curves', one for hot streams (defined as the streams releasing heat), one for cold streams (streams requiring heat). From the composite curves, it is possible to get information on the minimum heating and cooling requirements of the system considered. Once the minimum heating and cooling requirements are calculated, the energy targets are achieved through heat exchangers. The composite curves obtained from the pinch analysis and for fixed values of CaO conversion in the carbonator, $X = 0.2$ and $X = 0.5$, are shown in Fig. 13. As can be seen, additional external heat is needed to bring the reactants at the carbonator temperature. On the other side, the minimum cooling requirement can be interpreted as the external power that must be subtracted to the $CO2_c$ stream in order to cool it down to ambient temperature before the compression stage. Both heating and cooling requirements increase with the CaO conversion.

4.1.3. Heat exchangers network. Resulting plant

The heat exchangers' network has been designed following the basic rules of pinch-analysis and including some additional technical constraints:

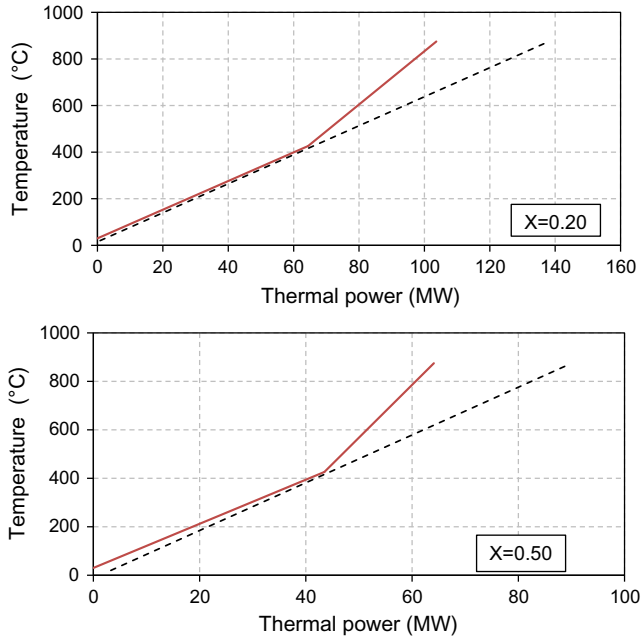

Fig. 13. Composite curve of carbonator-side streams derived from the pinch analysis for hot streams (solid line) and cold streams (dotted line) for different values of a fixed CaO conversion X.

- Coupling between the two solid streams (CaO and $CaCO_3$) are avoided since gas-solid and gas-gas exchangers show better performance and rely on more mature technologies.
- Splitting of the solid streams is technologically much more difficult (although possible by means of pneumatic conveying) than splitting the gas streams. Thus, any splitting involves CO_2 when possible.

The final goal of the analysis is to infer a network configuration that remains valid for a wide range of operating conditions. In particular, the configuration should be able to exchange the entire exchangeable heat (according to the minimum external heat requirement calculation) for any value of CaO conversion X and for any pressure ratio imposed at the turbine (which determines the pinch-point temperature). Fig. 14 shows the network configuration inferred that fulfils these requirements. This configuration provides a good flexibility by splitting the two CO_2 gas streams. In this way it is possible to regulate case-by-case the mass fraction in each branch. This configuration ensures also an optimal internal heat-recovery performance, with a relatively reduced number of heat exchangers and for a broad range of changes of any of the following parameters: carbonator temperature, turbine outlet temperature (or turbine pressure ratio), ambient temperature, CO_2 compressor outlet temperature, CaO conversion and minimum temperature difference in the heat exchangers. The resulting plant is shown in Fig. 15.

5. Optimized CaL- power cycle integration (layout 3)

According to the pinch analysis results, the proposed final plant configuration (shown in Fig. 16) is equipped with a solid-solid heat exchanger (HXA), four gas-solid heat exchangers (HXB, HXF, HXE, HXI) and with a gas-gas regenerator (HXG). The CO_2 stream from storage (produced in the calciner side operation) and the CO_2 stream coming from the power loop are mixed, flowing through a heat exchangers train (HXG and HXI) which optimize heat recovery at low temperature. On the other hand, the CO_2 stream flowing out from the turbine is divided into two sub-streams through HXF

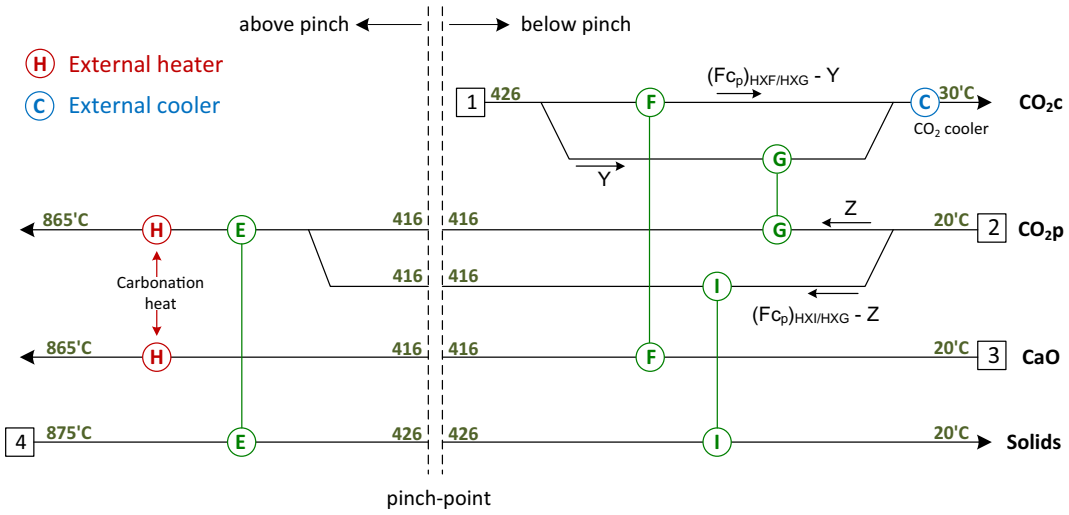

Fig. 14. Minimum energy consumption network inferred from the pinch-analysis.

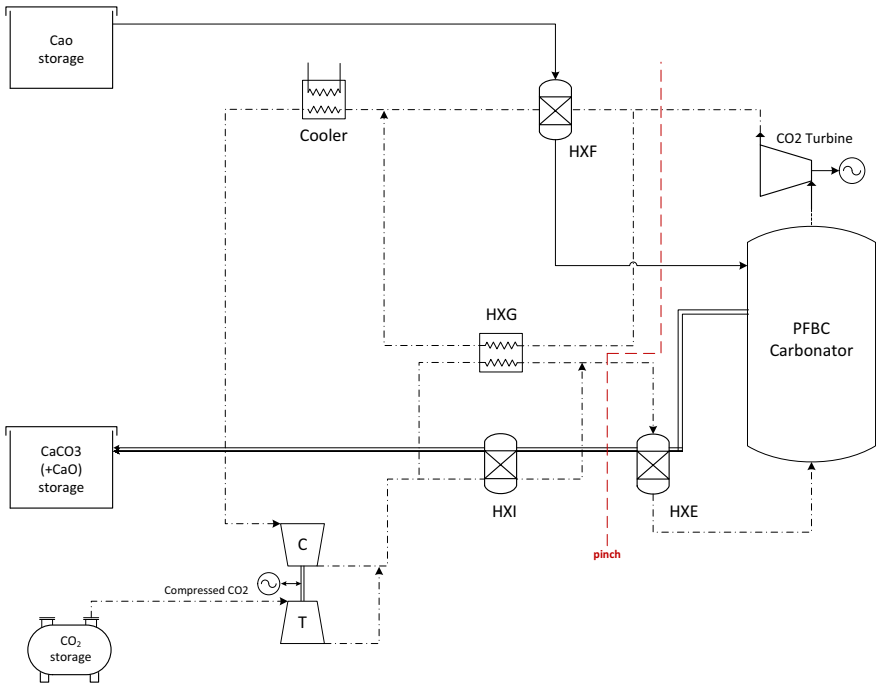

Fig. 15. Plant configuration (carbonator-side) resulting from the pinch analysis.

and HXG to preheat the CaO stream and a fraction of CO_2 entering into the carbonator respectively. In HXE, the high-temperature sensible heat from the $CaCO_3$ stream is used in the final stage of CO_2 stream preheating above the pinch, which serves to maximize the gas temperature at the carbonator inlet and therefore the cycle performance. Table 4 shows a comparison of the main data according to an energy balance for each configuration. At a fixed CaO conversion of 0.2, the global net efficiency increases of about 5% with respect to the base case.

Concerning the storage capacity, the volumetric energy density is usually expressed as the ratio between the stored thermal energy and the reactant storage volume [9]. The amount of solid stored material is highly influenced by the CaO conversion (X). By considering all the tanks in the plant, for the base case of the optimized cycle (Fig. 16), assuming X = 0.2, vessels volumes needed are 989.6 m^3, 633.7 m^3 and 1227 m^3 for CaO, CO_2 and solids ($CaO + CaCO_3$) respectively. On the other hand, thermal energy production during the night from the storage reaches 2124 GJ, which implies a global energy storage density of 1.26 GJ/m^3, still being higher than in the case of molten salts (0.5 GJ/m^3) [57]. Considering power production from the storage stage, from the CaL cycle is possible to store 170.53 kW h_e/m^3. In addition to the chemical storage heat, the sensible heat stored in the reaction by-products is also usable.

The results obtained from the model for the optimized plant configuration (Fig. 16) have been analyzed as a function of CaO conversion (X), pressure ratio (PR) in the power cycle, absolute carbonator pressure (P_{carb}) and carbonator temperature (T_{carb}), which

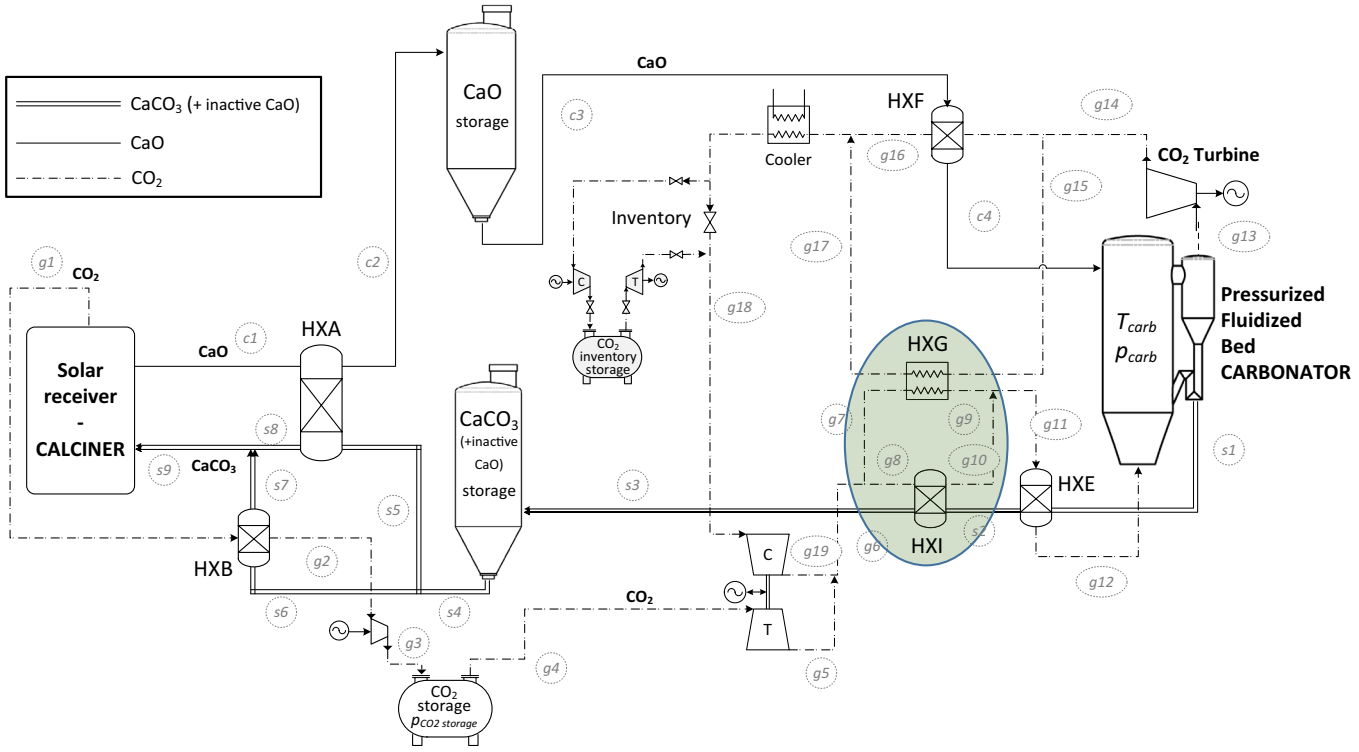

Fig. 16. Plant diagram of the highest efficiency integration layout for Thermochemical Energy Storage in a CSP plant using the CaL process (layout 3). Stream main data are shown in Appendix A.

Table 4
Energy balance of for the three configurations.

	Parameter	Configuration 1 (Fig. 4)	Configuration 2 (Fig. 9)	Configuration 3 (Fig. 16)
	Solar thermal power (MW_{th}) -12 h-	100	100	100
Heat exchangers	HXA	120.0	120.0	120.0
Thermal Power	HXB	23.2	23.2	23.2
(MWth)	HXF	26.8	26.8	46.0
	HXG	–	3.4	78.6
	HXI	–	–	53.7
	HXE	70.4	67.1	15.5
	Auxiliary cooler	3.9	0.6	6.9
Power outlet (MWe)	Compressor calciner (storage)	7.0	7.0	7.0
	Compressor carbonator (power cycle)	16.7	16.8	14.0
	Solids conveying (average)	1.8	1.8	1.8
Power inlet (MWe)	Turbine (storage)	1.2	1.2	2.2
	Main turbine (power cycle)	38.6	38.8	37.3
	Global net efficiency	0.356	0.358	0.403

have been found as the critical operational parameters. Several tests have been carried out to compare the cycle efficiency with the results from the previous layouts (layout 1 in Fig. 4 and layout 2 in Fig. 9). For this purpose, the same model conditions (detailed in Table 1) were used for the three layouts.

Fig. 17 shows a comparison of the efficiency curves obtained for the three proposed configurations as a function of CaO conversion. As can be seen, the enhancement of heat recovery derived from the pinch analysis yields a relevant increase of the cycle performance (layout 3 configuration), which is further improved as CaO conversion is increased. For layouts 1 and 2 the best performance is provided by high values of the pressure ratio, by CaO conversions close to 0.2 and with overexpansion in the gas turbine. In layout 3 an optimum performance is obtained also for much smaller pressure-ratios and both atmospheric turbine outlet pressure (as may be seen in Fig. 18) or atmospheric carbonator (Fig. 17). Considering that rather high CaO conversion is foreseen to be achievable with high-T and high CO_2 partial pressure carbonation [37], efficiency values close to the maximum are expected to be reached.

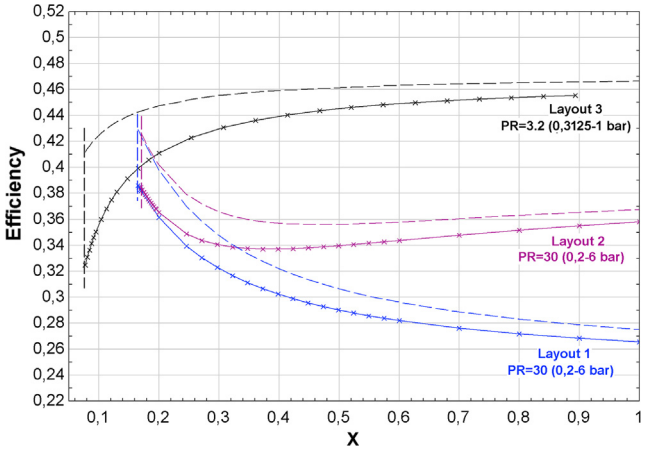

Fig. 17. Efficiency curves obtained for the diverse layout configurations described in the present work at the optimum pressure ratio. Solid lines are derived by including energy consumption due to solids conveying.

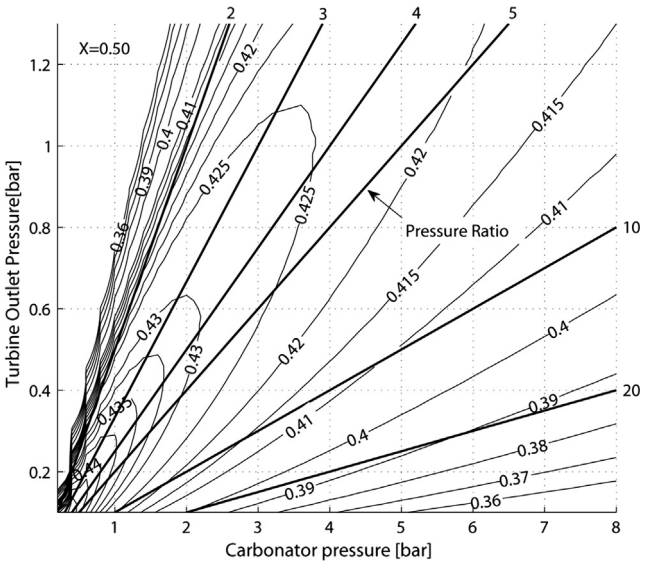

Fig. 18. Contour plot of efficiency vs carbonator and turbine outlet pressure including energy consumption for solids conveying. Black lines: constant pressure ratio. Dashed white lines: iso-efficiency curves. A fixed value of CaO conversion X = 0.50 is used.

6. Conclusions

In this work, several schemes for Thermochemical Energy Storage (TCES) of Concentrated Solar Power (CSP) using the Calcium Looping (CaL) process have been analyzed. High values of global efficiency are achievable by working at high carbonator to turbine outlet pressure ratios according to layouts 1 and 2 based on a closed CO_2 Brayton cycle. High values of the carbonator to turbine outlet pressure ratio are preferably attained by over-expanding up to pressures below 1 atm in order to keep the carbonator absolute pressure at reasonable values (normally not exceeding 15 bar). Moreover, operation under a high carbonator pressure allows to raise the carbonation temperature (according to the reaction equilibrium), which leads consequently to higher efficiencies. In these layouts (1) and (2) higher global integration efficiencies are obtained with CaO conversions (X) close to 0.2. Results from TGA experiments at realistic CSP-CaL conditions reported elsewhere show that conversion of CaO derived from either natural limestone or dolomite could reach residual values even higher. In layout 3, derived from a pinch-analysis thermal optimization, larger performances are predicted using much lower ratios of carbonator to turbine outlet pressures, with a predicted power production efficiency up to 44–46% for X = 0.5 and showing an increasing trend with CaO conversion.

Acknowledgements

This work was supported by the Spanish Government Agency Ministerio de Economia y Competitividad (contract CTQ2014-52763-C2-2-R).

Appendix A. Main stream data for the base case of each CSP-CaL configuration

See Table 5.

Table 5
Main stream data for the base case of each CSP-CaL configuration.

Stream ID	Configuration 1 (Fig. 4) - PR = 30, X = 0.2			Configuration 2 (Fig. 9) - PR = 30, X = 0.2			Configuration 3 (Fig. 16) - PR = 3.2, X = 0.2		
	P (bar)	T (°C)	$\dot{m}$ (kg/s)	P (bar)	T (°C)	$\dot{m}$ (kg/s)	P (bar)	T (°C)	$\dot{m}$ (kg/s)
s1	1.01	875	88.5	1.01	875	88.5	1.01	875	88.5
s2	1.01	68	88.5	1.01	110	88.5	1.01	708.8	88.5
s3	1.01	20	177.0	1.01	20	177.0	1.01	83.0	88.5
s4	1.01	20	146.3	1.01	20	146.3	1.01	20	177.1
s5	1.01	20	30.7	1.01	20	30.7	1.01	20	146.3
s6	1.01	802.9	30.7	1.01	802.9	30.7	1.01	20	30.7
s7	1.01	863	146.3	1.01	863	146.3	1.01	802.9	30.7
s8	1.01	852.6	177.0	1.01	852.6	177.0	1.01	863	146.3
s9	–	–	–	–	–	–	1.01	852.6	177.1
c1	1.01	900	153.0	1.01	900	153.0	1.01	900	153.0
c2	1.01	40	153.0	1.01	40	153.0	1.01	40	153.0
c3	1.01	20	76.5	1.01	20	76.6	1.01	20	76.5
c4	1.01	427.2	76.5	1.01	427.2	76.6	1.01	693.9	76.5
g1	1.01	900	24.0	1.01	900	24.0	1.01	900	24.0
g2	1.01	35	24.0	1.01	35	24.0	1.01	35	24.0
g3	75	40	24.0	75	40	24.0	75	40	24.0
g4	75	20	12.0	75	20	12.0	75	20	12.0
g5	6	10.8	12.0	6	10.8	12.0	1	−1.3	12.0
g6	6	53	85.8	6	53	85.8	1	56.5	191.3
g7	6	795.6	85.8	6	53	9.0	1	56.5	113.6
g8	6	875	73.8	6	53	76.7	1	56.5	77.7
g9	0.2	442.2	73.8	6	427.2	9.0	1	693.8	113.6
g10	0.2	90.1	73.8	6	796	85.8	1	693.8	77.7
g11	0.2	30	73.8	6	875	73.8	1	693.8	191.3
g12	6	59.6	73.8	0.2	442.2	73.8	1	759.7	191.3
g13	–	–	–	0.2	442.2	8.9	1	875	179.3
g14	–	–	–	0.2	442.2	64.9	0.313	708.9	179.3
g15	–	–	–	0.2	35	64.9	0.313	708.9	115.1
g16	–	–	–	0.2	68	8.9	0.313	49.9	64.2
g17	–	–	–	0.2	30	73.8	0.313	87.1	115.1
g18	–	–	–	6	59.61	73.8	0.313	30	179.3
g19	–	–	–	–	–	–	1	60.2	179.3

References

[1] United Nations. Framework Convention on Climate Change. Adoption of the Paris Agreement. vol. 21932; 2015.
[2] International Energy Agency. Technology Roadmap Solar Thermal Electricity; 2014:52. http://dx.doi.org/10.1007/SpringerReference_7300.
[3] Panwar NL, Kaushik SC, Kothari S. Role of renewable energy sources in environmental protection: a review. Renew Sustain Energy Rev 2011;15:1513–24. http://dx.doi.org/10.1016/j.rser.2010.11.037.
[4] Arce P, Medrano M, Gil A, Oró E, Cabeza LF. Overview of thermal energy storage (TES) potential energy savings and climate change mitigation in Spain and Europe. Appl Energy 2011;88:2764–74. http://dx.doi.org/10.1016/j.apenergy.2011.01.067.
[5] Kuravi S, Trahan J, Goswami DY, Rahman MM, Stefanakos EK. Thermal energy storage technologies and systems for concentrating solar power plants. Prog Energy Combust Sci 2013;39:285–319. http://dx.doi.org/10.1016/j.pecs.2013.02.001.
[6] Denholm P, O'Connell M, Brinkman G, Jorgenson J. Overgeneration from Solar Energy in California: A Field Guide to the Duck Chart (NREL/TP-6A20-65023); 2015:46.
[7] Paksoy HÖ. Thermal energy storage for sustainable energy consumption; 2007.
[8] Mahlia TMI, Saktisahdan TJ, Jannifar a, Hasan MH, Matseelar HSC. A review of available methods and development on energy storage; Technology update. Renew Sustain Energy Rev 2014;33:532–45. http://dx.doi.org/10.1016/j.rser.2014.01.06.
[9] Pardo P, Deydier a, Anxionnaz-Minvielle Z, Rougé S, Cabassud M, Cognet P. A review on high temperature thermochemical heat energy storage. Renew Sustain Energy Rev 2014;32:591–610. http://dx.doi.org/10.1016/j.rser.2013.12.01.
[10] Kearney D, Kelly B, Herrmann U, Cable R, Pacheco J, Mahoney R, et al. Engineering aspects of a molten salt heat transfer fluid in a trough solar field. Energy 2004;29:861–70. http://dx.doi.org/10.1016/S0360-5442(03)00191-9.
[11] Fernández AG, Ushak S, Galleguillos H, Pérez FJ. Development of new molten salts with $LiNO_3$ and $Ca(NO_3)_2$ for energy storage in CSP plants. Appl Energy 2014;119:131–40. http://dx.doi.org/10.1016/j.apenergy.2013.12.061.
[12] Rodríguez I, Pérez-Segarra CD, Lehmkuhl O, Oliva A. Modular object-oriented methodology for the resolution of molten salt storage tanks for CSP plants. Appl Energy 2013;109:402–14. http://dx.doi.org/10.1016/j.apenergy.2012.11.008.
[13] Chacartegui R, Vigna L, Becerra JA, Verda V. Analysis of two heat storage integrations for an Organic Rankine Cycle Parabolic trough solar power plant. Energy Convers Manag 2016;125:353–67. http://dx.doi.org/10.1016/j.enconman.2016.03.067.
[14] Kuravi S, Goswami DY, Stefanakos EK, Ram M, Jotshi C, Trahan J, et al. Thermal energy storage for concentrating solar power plants. In: Kuravi Sarada, Goswami D. Yogi, Stefanakos Elias K, Ram Manoj, Jotshi Chand, Pendyala Swetha, Trahan Jamie, Sridharan Prashanth, Rahman Muhammad, Krakow Burton, editors. Clean Energy Research Center, U n.d.
[15] Karagiannakis G, Pagkoura C, Zygogianni A, Lorentzou S, Konstandopoulos AG. Monolithic ceramic redox materials for thermochemical heat storage applications in CSP plants. Energy Procedia 2014;49:820–9. http://dx.doi.org/10.1016/j.egypro.2014.03.089.
[16] Medrano M, Gil A, Martorell I, Potau X, Cabeza LF. State of the art on high-temperature thermal energy storage for power generation. Part 2-Case studies. Renew Sustain Energy Rev 2010;14:56–72. http://dx.doi.org/10.1016/j.rser.2009.07.03.
[17] Zalba B, Marín JM, Cabeza LF, Mehling H. Review on thermal energy storage with phase change: materials, heat transfer analysis and applications. Appl Therm Eng 2003;23. http://dx.doi.org/10.1016/S1359-4311(02)00192-.
[18] Tian Y, Zhao CY. A review of solar collectors and thermal energy storage in solar thermal applications. Appl Energy 2013;104:538–53. http://dx.doi.org/10.1016/j.apenergy.2012.11.051.
[19] Nithyanandam K, Pitchumani R. Design of a latent thermal energy storage system with embedded heat pipes. Appl Energy 2014;126:266–80. http://dx.doi.org/10.1016/j.apenergy.2014.03.025.
[20] Nithyanandam K, Pitchumani R. Cost and performance analysis of concentrating solar power systems with integrated latent thermal energy storage. Energy 2014;64:793–810. http://dx.doi.org/10.1016/j.energy.2013.10.095.
[21] Sharma A, Tyagi VV, Chen CR, Buddhi D. Review on thermal energy storage with phase change materials and applications. Renew Sustain Energy Rev 2009;13:318–45. http://dx.doi.org/10.1016/j.rser.2007.10.005.
[22] Li TX, Wu S, Yan T, Xu JX, Wang RZ. A novel solid-gas thermochemical multilevel sorption thermal battery for cascaded solar thermal energy storage. Appl Energy 2016;161:1–10. http://dx.doi.org/10.1016/j.apenergy.2015.09.084.
[23] Chacartegui R, Alovisio A, Ortiz C, Valverde JM, Verda V, Becerra JA. Thermochemical energy storage of concentrated solar power by integration of the calcium looping process and a CO_2 power cycle. Appl Energy 2016;173:589–605. http://dx.doi.org/10.1016/j.apenergy.2016.04.053.
[24] Neveu P, Tescari S, Aussel D, Mazet N. Combined constructal and exergy optimization of thermochemical reactors for high temperature heat storage. Energy Convers Manag 2013;71:186–98. http://dx.doi.org/10.1016/j.enconman.2013.03.035.
[25] N'Tsoukpoe KE, Liu H, Le Pierrès N, Luo L. A review on long-term sorption solar energy storage. Renew Sustain Energy Rev 2009;13:2385–96. http://dx.doi.org/10.1016/j.rser.2009.05.008.
[26] Wentworth WE, Chen E. Simple thermal decomposition reactions for storage of solar thermal energy. Sol Energy 1976;18:205–14. http://dx.doi.org/10.1016/0038-092X(76)90019-0.
[27] Barker R. The reactivity of calcium oxide towards carbon dioxide and its use for energy storage. J Appl Chem Biotechnol 1974;24:221–7. http://dx.doi.org/10.1002/jctb.2720240405.
[28] Abedin A, Rosen M. A critical review of thermochemical energy storage systems. Open Renew Energy J, n.d.: 42–6. http://dx.doi.org/10.2174/1876387101004010042.
[29] Edwards SEB, Materić V. Calcium looping in solar power generation plants. Sol Energy 2012;86:2494–503. http://dx.doi.org/10.1016/j.solener.2012.05.019.
[30] Sakellariou KG, Karagiannakis G, Criado YA, Konstandopoulos AG. Calcium oxide based materials for thermochemical heat storage in concentrated solar power plants. Sol Energy 2015;122:215–30. http://dx.doi.org/10.1016/j.solener.2015.08.011.
[31] Dunsmore HE. A geological perspective on global warming and the possibility of carbon dioxide removal as calcium carbonate mineral. Energy Convers Manag 1992;33:565–72. http://dx.doi.org/10.1016/0196-8904(92)90057-4.
[32] Ortiz C, Chacartegui R, Valverde J, Becerra J, Perez-Maqueda L. A new model of the carbonator reactor in the calcium looping technology for post-combustion CO_2 capture. Fuel 2015;160:328–38. http://dx.doi.org/10.1016/j.fuel.2015.07.095.
[33] Ylätalo J, Parkkinen J, Ritvanen J, Tynjälä T, Hyppänen T. Modeling of the oxy-combustion calciner in the post-combustion calcium looping process. Fuel 2013;113:770–9. http://dx.doi.org/10.1016/j.fuel.2012.11.041.
[34] Sanchez-Jimenez PE, Valverde JM, Perez-Maqueda L. Multicyclic conversion of limestone at Ca-looping conditions: the role of solid-sate diffusion controlled carbonation. Fuel 2014;127:131–40. http://dx.doi.org/10.1016/j.fuel.2013.09.064.
[35] Valverde JM. Relevant influence of limestone crystallinity on CO_2 capture in the Ca-looping technology at realistic calcination conditions; 2014.
[36] Valverde JM, Sanchez-Jimenez PE, Perez-Maqueda L. Calcium-looping for post-combustion CO_2 capture. On the adverse effect of sorbent regeneration under CO_2. Appl Energy 2014;126:161–71. http://dx.doi.org/10.1016/j.apenergy.2014.03.081.
[37] Sarrion B, Valverde JM, Perejon A, Perez-maqueda LA, Sanchez-jimenez PE. On the multicycle activity of natural limestone/dolomite for cheap, efficient and non-toxic Thermochemical Energy Storage of Concentrated Solar Power. Energy Technol 2016. http://dx.doi.org/10.1002/ente.201600068.
[38] Tregambi C, Montagnaro F, Salatino P, Solimene R. A model of integrated calcium looping for CO_2 capture and concentrated solar power. Sol Energy 2015;120:208–20. http://dx.doi.org/10.1016/j.solener.2015.07.017.
[39] Zhai R, Li C, Qi J, Yang Y. Thermodynamic analysis of CO_2 capture by calcium looping process driven by coal and concentrated solar power. Energy Convers Manag 2016;117:251–63. http://dx.doi.org/10.1016/j.enconman.2016.03.022.
[40] Muñoz-Antón J, Rubbia C, Rovira A, Martínez-Val JM. Performance study of solar power plants with CO_2 as working fluid. A promising design window. Energy Convers Manag 2015;92:36–46. http://dx.doi.org/10.1016/j.enconman.2014.12.03.
[41] Barin I. Thermochemical data of pure substances VCH, Weinheim; 1989.
[42] Charitos A, Rodríguez N, Hawthorne C, Alonso M, Zieba M, Arias B, et al. Experimental validation of the calcium looping CO_2 capture process with two circulating fluidized bed carbonator reactors. Ind Eng Chem Res 2011;50:9685–95. http://dx.doi.org/10.1021/ie200579f.
[43] Arias B, Diego ME, Abanades JC, Lorenzo M, Diaz L, Martínez D, et al. Demonstration of steady state CO_2 capture in a 1.7MWth calcium looping pilot. Int J Greenh Gas Control 2013;18:237–45. http://dx.doi.org/10.1016/j.ijggc.2013.07.014.
[44] Ströhle J, Junk M, Kremer J, Galloy A, Epple B. Carbonate looping experiments in a 1 MWth pilot plant and model validation. Fuel 2014;127:13–22. http://dx.doi.org/10.1016/j.fuel.2013.12.043.
[45] Meier A, Bonaldi E, Cella GM, Lipinski W, Wuillemin D. Solar chemical reactor technology for industrial production of lime. Sol Energy 2006;80:1355–62. http://dx.doi.org/10.1016/j.solener.2005.05.017.
[46] Badie JM, Bonet C, Faure M, Flamant G, Foro R, Hernandez D. 52 Decarbonation of calcite and phosphate rock in solar chemical reactors. Chem Eng Sci 1980;35:413–20. http://dx.doi.org/10.1016/0009-2509(80)80114-X.
[47] Meier A, Bonaldi E, Cella GM, Lipinski W, Wuillemin D, Palumbo R. Design and experimental investigation of a horizontal rotary reactor for the solar thermal production of lime. Energy 2004;29:811–21. http://dx.doi.org/10.1016/S0360-5442(03)00187-7.
[48] Meier A, Bonaldi E, Cella GM, Lipinski W. Multitube rotary kiln for the industrial solar production of lime. J Sol Energy Eng 2005;127:386. http://dx.doi.org/10.1115/1.1979517.
[49] Imhof A. Decomposition of limestone in a solar reactor. Renew Energy 1996;9:661–3. http://dx.doi.org/10.1016/0960-1481(96)88373-.
[50] de Bosio F, Verda V. Thermoeconomic analysis of a Compressed Air Energy Storage (CAES) system integrated with a wind power plant in the framework of the IPEX Market. Appl Energy 2015;152:173–82. http://dx.doi.org/10.1016/j.apenergy.2015.01.052.
[51] Mills D. Pneumatic conveying design guide; 2004:80.

[52] Yu FC, Fan LS. Kinetic study of high-pressure carbonation reaction of calcium-based sorbents in the Calcium Looping Process (CLP). Ind Eng Chem Res 2011;50:11528–36. http://dx.doi.org/10.1021/Ie200914e.
[53] Yan X. Dynamic analysis and control system design for an advanced nuclear gas turbine power plant. Massachusetts Inst Technol 1990.
[54] Sánchez D, Chacartegui R, Muñoz De Escalona JM, Muñoz A, Sánchez T. Performance analysis of a MCFC & supercritical carbon dioxide hybrid cycle under part load operation. Int J Hydrogen Energy 2011;36:10327–36. http://dx.doi.org/10.1016/j.ijhydene.2010.09.072.
[55] Olumayegun O, Wang M, Kelsall G. Closed-cycle gas turbine for power generation: a state-of-the-art review. Fuel 2016;180:694–717. http://dx.doi.org/10.1016/j.fuel.2016.04.074.
[56] Linnhoff B, Hindmarsh E. The pinch design method for heat exchanger networks. Chem Eng Sci 1983;38:745–63. http://dx.doi.org/10.1016/0009-2509(83)80185-7.
[57] Janz GJ, Allen, Carolyn B, Bansal NP, Murphy RM, Tomkins RP. Physical properties data compilations relevant to energy storage. II. Molten salts: data on single and multi-components salt systems. Natl Bur Stand 1979.

***ANNEX 6**: Ortiz C, Chacartegui R, Valverde JM, Alovisio A, Becerra JA. Power cycles integration in concentrated solar power plants with energy storage based on calcium looping. Energy Convers Manag 2017;149:815–29. doi:10.1016/j.enconman.2017.03.029.*

Energy Conversion and Management 149 (2017) 815–829

Contents lists available at ScienceDirect

Energy Conversion and Management

journal homepage: www.elsevier.com/locate/enconman

Power cycles integration in concentrated solar power plants with energy storage based on calcium looping

C. Ortiz [a,*], R. Chacartegui [b], J.M. Valverde [a], A. Alovisio [c], J.A. Becerra [b]

[a] Faculty of Physics, University of Seville, Avenida Reina Mercedes s/n, 41012 Sevilla, Spain
[b] Energy Engineering Department, University of Seville, Camino de los Descubrimientos s/n, 41092 Sevilla, Spain
[c] Politecnico di Torino, Department of Energy Engineering, Corso Duca degli Abruzzi 24, 10129 Torino, Italy

ARTICLE INFO

Article history:
Available online 20 March 2017

Keywords:
Global warming
Renewable energies
Concentrated Solar Power (CSP)
Thermochemical Energy Storage (TCES)
Calcium Looping (CaL)
Power cycles
Supercritical CO_2 power cycle

ABSTRACT

Efficient, low-cost and environmentally friendly storage of thermal energy stands as a main challenge for large scale deployment of solar energy. This work explores the integration into concentrated solar power plants of the calcium looping process based upon the reversible carbonation/calcination of calcium oxide for thermochemical energy storage. An efficient concentrated solar power-calcium looping integration would allow storing energy in the long term by calcination of calcium carbonate thus overcoming the hurdle of variable power generation from solar. After calcination, the stored products of the reaction (calcium oxide and carbon dioxide) are brought together in a carbonator reactor whereby the high temperature exothermic reaction releases the stored energy for efficient power production when needed. This work analyses several power cycle configurations with the main goal of optimizing the performance of the overall system integration. Possible integration schemes are proposed in which power production is carried out directly (using a closed carbon dioxide Brayton power cycle) or indirectly (by means of a steam reheat Rankine cycle or a supercritical carbon dioxide Brayton cycle). The results obtained show that the highest plant efficiencies (up to 45–46%) are achievable using a closed carbon dioxide Brayton power cycle.

1. Introduction

The commercial expansion of renewable energy technologies is an urgent need to limit global warming to "well below" 2.0 °C (by 2100) and pursue 1.5 °C above pre-industrial levels as was agreed at Paris COP21 Conference [1]. In particular, Concentrated Solar Power (CSP) should play a leading role within the new energy landscape as it lends itself to potentially cheap storage of energy in the form of heat [2]. Thus, efficient and affordable thermal energy storage systems must be developed in order to decouple production and demand [3], which would allow a deep penetration of solar energy power generation into the grid.

In recent years a large number of potential thermal storage technologies for medium to high temperature CSP systems have been proposed [4] based upon three main concepts: (i) sensible Thermal Energy Storage (TES), such as direct steam storage [5] or molten salt systems [6]; (ii) latent heat storage using Phase Change Materials (PCMs), on which Zalba et al. [7] published a comprehensive review of materials and applications; and (iii) Thermochemical Energy Storage (TCES). Regarding TCES, a large number of potential systems [8], experimental research under practical conditions [9] and TCES reactor designs [10] can be found in the recent literature. Essentially, TCES consists of using the heat obtained from an external source, such as CSP, to drive an endothermic reaction. When energy is needed, the separately stored by-products of the reaction are brought together at the necessary conditions for the reverse exothermic reaction to occur, which releases the previously used heat for power production. The main advantages of TCES as compared to TES and PCMs are the considerably high energy density attainable, which is well above the energy density of molten salts currently used in commercial plants (~0.5 GJ/m^3) [11], and the possibility of storing energy in the long term [8]. An extended review on long-term solar heat storage can be found in Ref. [12]. Moreover, in addition to the chemically stored heat, sensible heat stored in the reaction by-products is also usable.

The focus of the present manuscript is on TCES in CSP tower plants. In order to achieve an efficient and cost-effective thermochemical storage process, a proper selection of the reversible reaction is a crucial issue. Among the possibilities explored for TCES in CSP tower plants at large scale, one of the most promising systems is the Calcium Looping (CaL) process, which relies on the

* Corresponding author.
E-mail address: cortiz7@us.es (C. Ortiz).

http://dx.doi.org/10.1016/j.enconman.2017.03.029
0196-8904/

Notation

$c_{p,i}$	specific heat (kJ/(kmol K))
dT_min_HE	minimum temperature approach (°C)
F_i	molar flow rate of component i (kmol/s)
F_{CaCO_3}	molar flow rate of $CaCO_3$
$F_{CaCO_3,carb}$	molar flow rate of $CaCO_3$ (carbonator side)
$F_{CaCO_3,clc}$	molar flow rate of $CaCO_3$ (calciner side)
$F_{CaO,crb}$	molar flow rate of CaO (carbonator side)
$F_{CaO,clc}$	molar flow rate of regenerated sorbent
$F_{CaO,unr,carb}$	molar flow rate of unreacted CaO (carbonator side)
$F_{CaO,unr,clc}$	molar flow rate of unreacted CaO (calciner side)
$F_{CO_2,clc,out}$	molar flow rate of CO_2 at calciner outlet
$F_{R,carb}$	recirculating molar flow rate (carbonator side)
$F_{R,clc}$	recirculating molar flow rate (calciner side)
h_i	enthalpy (kJ/kmol)
HXA	solid-solid heat exchanger
HXB	gas-solid heat exchanger
HXE	gas-solid heat exchanger
HXF	gas-solid heat exchanger
HXI	gas-solid heat exchanger
HXG	gas-solid heat exchanger
$\dot{m}_{CO_2,crb}$	CO_2 mass flow rate through carbonator
$\dot{m}_{solids}$	solids mass flow rate (kg/s)
P_{carb}	absolute carbonator pressure (bar)
Q_{input}	thermal power input (MW)
P_{eq}	CO_2 partial pressure at equilibrium (bar)
PR	pressure ratio
p_{drop}	pressure drops in CO_2 circuit, bar
P_{vv}	live steam pressure (bar)
$y_{CO_2,carb,in}$	inlet molar fraction of CO_2 in the carbonator
$P_{out,turb}$	outlet turbine pressure (bar)
y_{eq}	equilibrium fraction of CO_2 in the carbonator
T	temperature (K)
T_{carb}	carbonator temperature (K)
T_{in,CO_2}	CO_2 temperature at carbonator inlet (°C)
$T_{in,CaO}$	CaO temperature at carbonator inlet (°C)
T_{reheat}	reheat temperature (Rankine cycle) (°C)
T_{vv}	live steam temperature (°C)
$W_{comp,1}$	compressor 1 power, sCO_2 (MW)
$W_{comp,2}$	compressor 2 power, sCO_2 (MW)
W_{turb}	turbine power, sCO_2 (MW)
$\dot{W}$	mechanical power (kW)
X	CaO conversion
X_{slp}	split factor, sCO_2
η_c	isentropic compressor efficiency
η_t	isentropic turbine efficiency
$\eta_{integration}$	global integration performance
$\eta_{storage}$	storage performance
η_{cycle}	power cycle performance
η_{cc}	combined cycle performance
ϕ_{cycle}	power cycle practicability
Δt_{sun}	average daytime period
$\Delta H_R(T_{react})$	heat of reaction at the reactor temperature
ξ	extent of reaction per unit time
Φ	heat flux
$\Phi_{carbonation}$	available heat of carbonation
ε_{rec}	recuperator efficiency (%)
$\Delta P_{R,hot}$	pressure drop recuperator- hot side (%)
$\Delta P_{R,cold}$	pressure drop recuperator- coldside (%)
$\Delta P_{R,HE}$	pressure drop heat exchanger- sCO_2 (%)

carbonation-calcination reaction of calcium oxide (CaO) (Eq. (1)) [13]. The use of several CaO precursors for TCES in CSP plants has been analysed in [14].

$$CaO_{(s)} + CO_{2(g)} \rightleftarrows CaCO_{3_{(s)}} \qquad \Delta H_r^0 = -178\ \text{kJ/mol} \tag{1}$$

Generally, the CaL process would begin with the decomposition of calcium carbonate ($CaCO_3$) particulate solids in a calcination reactor (calciner) yielding CaO and CO_2 as by-products. A high energy input is necessary to rise the solids stream temperature up to the value required for the reaction to occur at a sufficiently fast rate and to carry out the endothermic calcination reaction [15]. Thus, the optimum calcination temperature is essentially determined by the composition of the gas in the calcination environment [16]. Once the sensible heat from the calciner outlet streams (CaO and CO_2 streams) is recovered, these products are separately stored. Storage conditions and time are flexible and could be accommodated to energy demand and environmental circumstances. When needed, the CaO and CO_2 products are circulated into a carbonator reactor, where energy is recovered from the carbonation reaction.

A great benefit of the CaL process is the low price (~10 $/ton), wide availability and harmlessness towards the environment of natural limestone or dolomite to be used as CaO precursor [17]. However, a usually claimed drawback of the CaL process is the marked deactivation of CaO derived from these natural minerals with the number of carbonation/calcination cycles. CaO deactivation is indeed particularly relevant when the CaL process is used for CO_2 capture [18] under conditions that necessary involve regeneration of CaO by high temperature (around 950 °C) calcination at high CO_2 partial pressure and carbonation at low CO_2 partial pressure (~0.15 bar). Nevertheless, CaL conditions to achieve a high global efficiency for TCES and electricity generation in CSP plants can be radically different to those corresponding to its application for CO_2 capture [19]. In the CSP-CaL integration, carbonation would be carried out under high CO_2 partial pressure and high temperature (around or above 850 °C) whereas calcination could be ideally performed at relatively low temperature (~700 °C) under a gas easily separable from CO_2 such as Helium [16] or superheated steam [20]. Under these conditions, CaO derived from natural limestone or dolomite may exhibit a high value of the residual conversion [19].

In addition to enhancing solar energy storage capacity, advanced high efficiency CSP-TES-power cycle integrations should be developed exploiting energy storage conditions to achieve a significant improvement of CSP plant performance. Integration of power cycles in commercial CSP tower plants with thermal storage in the form of sensible heat using molten salts is limited by a maximum temperature achievable around 550–600 °C. This limitation is mainly imposed by the degradation of molten salts at higher temperatures [21]. In recent years, molten alkali carbonates salts (MACs) have been investigated for energy storage. According to Frangini et al. [22], temperature stability of additives limits the applicability of oxidizing MAC salts at temperatures below 650 °C. On the other hand, thermal radiation losses at the open focal point [23] adds a further temperature limitation in currently CSP plants. This implies that most of the commercial CSP tower plants currently under operation are based in Rankine cycle process [24]. Peak solar to electricity conversion efficiencies in these commercial CSP tower plants are around 25–30%, with an annual solar-to-electricity conversion efficiency lower than 20% [25]. In

this regard, Liu et al. [26] show current annual efficiencies as a function of solar technology used: 13–15% for parabolic trough, 14–18% for tower ad 9–13% for Fresnel. On the other hand, the European Academies Scientific Advisory Council [27] points out the difference of annual solar to electricity efficiencies between conceptual (around 22–28%) and industrial (around 14–18%) status.

This manuscript analyses several integration schemes to use the CaL process for TCES in CSP plants. Integration models aimed at similar goals have been already investigated by other authors. Tregambi et al. [28] proposed a scheme whereby calcination in the CaL process is assisted by CSP for CO_2 capture in a coal fired power plant. Edwards et al. [29] investigated a CSP-CaL integration in which the heat produced in the carbonator reactor is used for power generation through a CO_2/air open cycle. This configuration assumes that the CO_2 stream entering into the carbonator reacts completely with the CaO solids to produce $CaCO_3$. However, attending to the reaction equilibrium, carbonation will be ceased when the CO_2 partial pressure in the carbonator reactor reaches the equilibrium partial pressure (see Eq. (8)). Thus, a certain amount of CO_2 in the carbonator effluent gas will be unavoidably released to the environment in a CO_2/air open cycle at a concentration depending on the carbonator temperature. In order to guarantee the absence of CO_2 emissions, alternative power cycles must be employed. In this regard, Chacartegui et al. [30] have recently proposed a CSP-CaL integration wherein the TCES system is integrated with a closed CO_2 power cycle directly coupled to the carbonator following a pinch-analysis methodology [31]. In the discharge operation the circulating CO_2 passes directly to the carbonator and power turbine. The present manuscript explores the integration with the TCES core system of alternative direct and indirect cycles (steam turbine, closed Brayton CO_2 and indirect-supercritical CO_2) for relevant CSP-CaL integration conditions. The obtained results show that the highest efficiencies are achieved using direct cycles, potentially reaching global power efficiencies above 44%.

2. Concentrated solar power-calcium looping integration model

In this section the main aspects of the concentrated solar power-calcium looping integration model based on mass and energy balance in heat exchangers, solid reservoirs, CO_2 storage tank and reactors are summarized. The interested reader is referred to [30] where the model is described in detail. Moreover, the main CSP-CaL model simulation results are analysed as a previous step to discuss the power cycle integration.

2.1. Model description

Fig. 1 shows a schematic representation of the CSP-CaL integration model. The process starts in the solar receiver, where solar energy input is used to carry out the calcination of $CaCO_3$ (endothermic reaction). Currently commercial CSP tower systems would allow achieving temperatures in the range of 700–900 °C, which are high enough to drive limestone calcination in short residence times [19] using a solar calciner reactor among those already proposed in the literature [32]. For example, Meier et al. [33] have developed a solar multi-tube rotary kiln prototype for carrying out the calcination reaction at temperatures up to 1100 °C. Once calcination takes place, the released CO_2 is sent to a storage tank after being cooled and compressed whereas the CaO stream is transported to a solids reservoir. Both streams exiting the calciner at high temperature are passed through a heat exchanger network to extract their sensible heat as a previous step to storage at ambient temperature. This is a main advantage of the CSP-CaL integration over current state of the art sensible heat storage using molten salts, whose temperature must be kept above ~200 °C to avoid solidification [34]. In order to use reasonably sized CO_2 storage volumes a minimum pressure of 75 bar is needed to store CO_2 under supercritical conditions (considering storage at ambient temperature) [30]. The high compression ratio from calciner to storage conditions (1:75) requires the use of intercooling compression to minimize the efficiency penalty. Solids transport can be carried out by means of pneumatic conveying, an already mature technology to transport high temperature granular solids [35]. For Ca based particles and a typical transport length of 200 m, an energy consumption of 20 MJ/ton has been used in the CSP-CaL integration model [30].

When power is needed the energy stored is released in the carbonator through the exothermic carbonation reaction. According to thermodynamic reaction equilibrium carbonation can be carried out at high temperature (>850 °C) under high CO_2 partial pressure [36]. This would allow a highly efficient generation of electricity thus overcoming temperature limits (T ~ 550–600 °C) in currently commercial CSP plants with thermal storage in molten salts. Solids exiting the carbonator are passed through another heat exchanger network to preheat the CaO and CO_2 streams entering the carbonator. After the storage step, the CO_2 stream is expanded to the selected carbonator pressure, which must be below the storage pressure in order to use the commercial fluidized bed technology. As can be seen in Fig. 1, compression-expansion process of CO_2 before and after the storage step resembles a compressed air energy storage (CAES) system [4]. Thus, besides of sensible and thermochemical energy storage, the integration energy storage

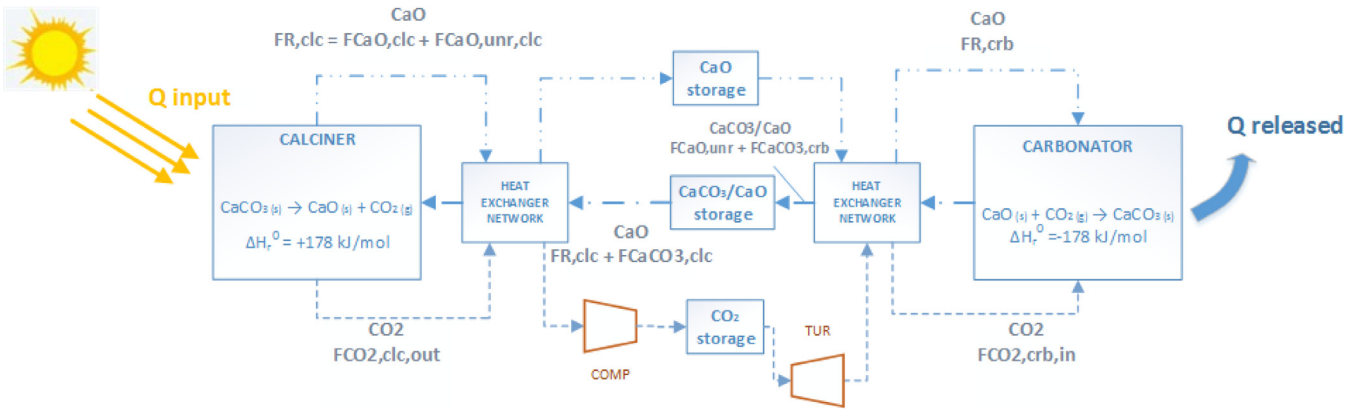

Fig. 1. CSP-CaL integration scheme.

also in the form of compressed gas with a round trip efficiency of about 67% using a compression-expansion train (see [30] for further details).

As can be seen in Fig. 1, only a fraction of the total flow rate of the CaO entering into the carbonator ($F_{R,crb}$) reacts with CO_2 to produce $CaCO_3$ ($F_{CaCO_3,crb}$), remaining the rest as unreacted CaO ($F_{CaO,unr}$). The average CaO conversion (or activity) X determines the amount of CaO converted to $CaCO_3$ in the carbonator ($X = F_{CaCO_3,crb}/F_{R,crb}$). On the other hand, the carbonated particles entering into the calciner reactor are assumed to achieve a complete decomposition, yielding one mole of CO_2 ($F_{CO_2,clc,out}$) and one mole of regenerated CaO ($F_{CaO,clc}$) for each mole of $CaCO_3$ ($F_{CaCO_3,clc}$) according to Eq. (1).

The streams circulating in either the calciner or carbonator sides are decoupled. Thus, the solar calciner only works in the daytime and under clear sky conditions whereas the carbonator reactor must operate on demand during a 24 h period, which requires a properly storage vessel sizing. More sophisticated control strategies should be devised within a framework of long-period control to ensure steady operation over time lags beyond 24 h. Such control should rely on meteorological forecasts and the power load curve. Thus, in order to guarantee a steady-state operation, the mass-balance equation:

$$\int_{24h} F_{CaCO_3,clc}(t)\,dt = \int_{24h} F_{CaCO_3,crb}(t)\,dt \tag{2}$$

must be satisfied. An average daytime period (Δt_{sun}) is assumed during which solar irradiation is sufficiently intense to attain full calcination. In this case Eq. (2) can be derived to obtain:

$$\overline{F_{CaCO_3,clc}} \cdot \Delta t_{sun} = \overline{F_{CaCO_3,crb}} \cdot 24 \tag{3}$$

For energy balance, the first thermodynamics law is applied to the carbonator and calciner reactors:

$$\sum_i F_{i,out} h_{i,out} - \sum_i F_{i,in} h_{i,in} = \Phi - \dot{W} \tag{4}$$

$$F_{i,out} - F_{i,in} = \xi \nu_i \tag{5}$$

where ξ denotes the extent of reaction per unit time. Arranging and considering that output conditions are reactor conditions, it is:

$$\xi \Delta H_R(T_{react}) + \sum_i F_{i,in}(h_{i,react} - h_{i,in}) = \Phi - \dot{W} \tag{6}$$

with

$$\Delta H_R(T_{react}) = \sum_i \nu_i h_{i,T} = \Delta H_R^0 + \sum_i \nu_i \int_{ref}^{T_{react}} c_{p,i} dT \tag{7}$$

being the reaction enthalpy change at the reaction temperature.

2.2. Model results

The proposed CSP-CaL integration model has been simulated to assess the integration efficiency. A sensitivity analysis has been carried out on relevant CaL cycle parameters such as CaO conversion X and carbonation equilibrium conditions [37]. Data used for the reference case are reported in Table 1.

CaO conversion has a significant influence on the solids flow rates, storage vessels, power production and consumption, and heat exchangers network configuration. Thus, a high CaO conversion leads to a low fraction of unreacted CaO left, which affects relevantly the plant's performance. Also, as the CaO conversion increases the solids mass flow rate is decreased (Fig. 2), therefore energy consumption due to solids conveying is reduced.

Fig. 3 shows the effect of the CaO conversion on the thermal power effectively used for energy storage. Keeping fixed a

Table 1
CSP-CaL reference case simulation data.

Net absorbed solar heat flux in calciner	100	MWt
Thermal dispersions in carbonator	10	%
Calciner temperature	900	°C
Calciner pressure	1	bar
Ambient temperature	20	°C
CaO average conversion (X)	0.5	
Carbonator temperature	875	°C
Carbonator pressure	7	bar
CO_2 storage conditions	75 bar, T ambient	
Solid phase conveying energy consumption	20	MJ/ton
Daylight hours (constant solar flux)	8 h	
Isentropic efficiencies (compression/expansion)	0.89	

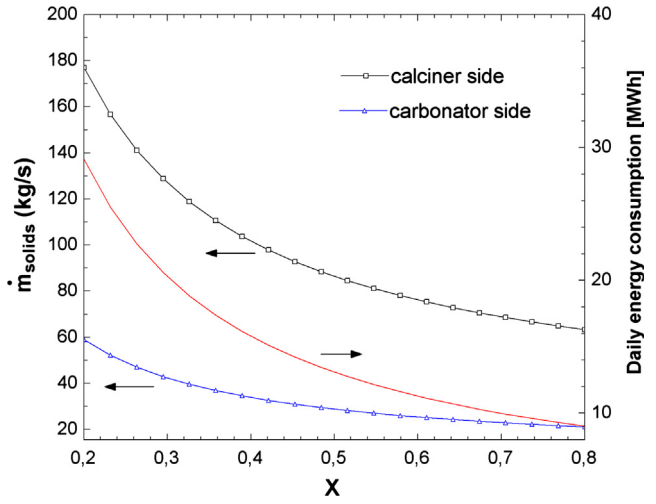

Fig. 2. Solids mass flow rate (left axis) and daily energy consumption (right axis) due to solids conveying as a function of average CaO conversion (X).

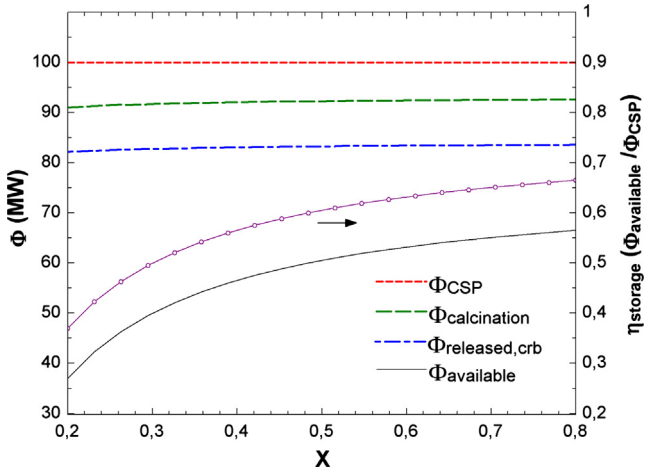

Fig. 3. Thermal power fluxes (left axis) and energy storage efficiency (right axis) as a function of average CaO conversion in the carbonator.

100 MW_{th} of CSP input (ϕ_{CSP}) into the system, the thermal power used to carry out the calcination reaction ($\phi_{calcination} = 92$ MWth) does not depend on the solids conversion in the carbonator while the rest (8 MWth) is employed to raise the solids temperature before entering into the calciner. A part of the released power in the carbonator $\phi_{released,crb}$ is used to increase the temperature of the inlet streams up to the carbonation temperature, which leaves the rest of thermal energy available $\phi_{available}$ to be used in the power

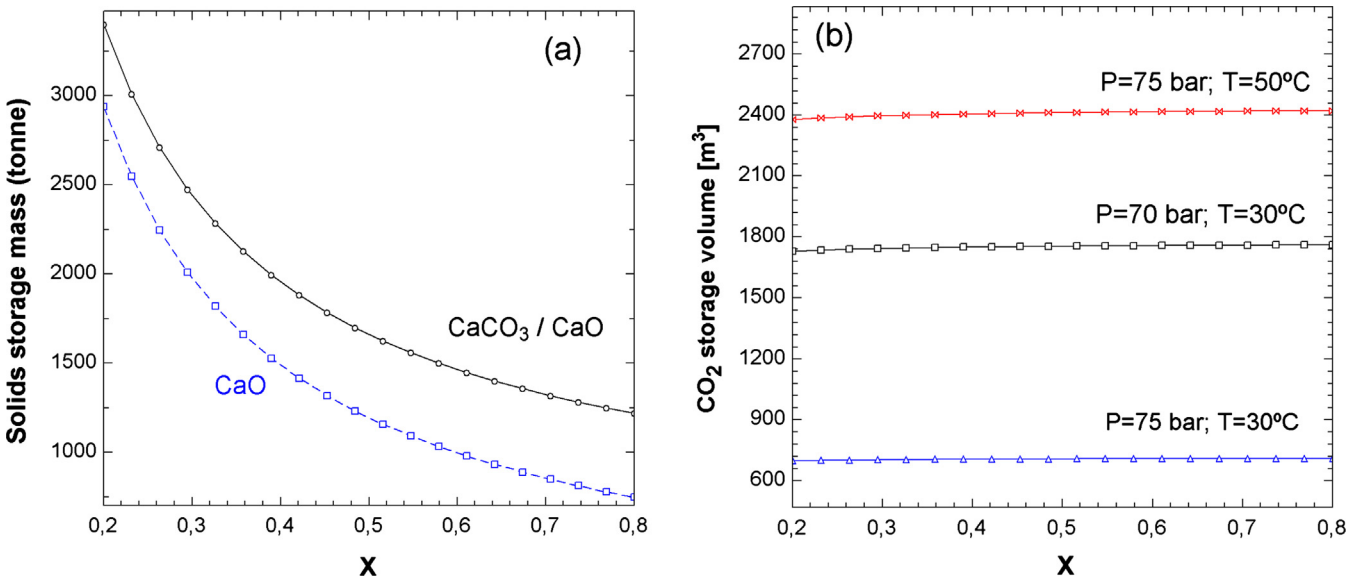

Fig. 4. (a) Solids storage mass as a function of average CaO conversion. (b) CO_2 storage volume as a function of average CaO conversion for several storage conditions.

cycle for electricity production. The difference between calcination and carbonation power is due to thermal energy dispersions in the carbonator (10%).

Another relevant issue to be considered is that increasing the average CaO conversion allows for an important reduction of the solids storage volumes as can be seen in Fig. 4a. On the other hand, a change in X does not yield a significant variation of the CO_2 storage volume, which is however quite sensitive to CO_2 density as determined by storage pressure and temperature (Fig. 4b).

Previous works on the CaO multicycle conversion in the CaL process have been mostly focused on Post-Combustion CO_2 Capture (PCCC) conditions, either on laboratory-scale analysis [38], reactor modelling [39] or process integration models [40], involving in all cases carbonation under relatively low CO_2 partial pressure (~0.15 bar) and calcination at very high temperatures (~950 °C) under high CO_2 partial pressure. Under these conditions the CO_2 sorbent (CaO) presents a severe drop of conversion after a few cycles converging towards a residual value of just about 0.07–0.08 [41]. Nevertheless, it is important to remark that the CSP-CaL integration for thermochemical energy storage involves CaL conditions radically diverse from those in the case of PCCC. Thus, thermogravimetric analysis (TGA) tests show that the residual conversion of limestone derived CaO can be as large as $X_r = 0.5$ for conditions that correspond to the optimum CSP-CaL integration shown in the present work that involve carbonation at high temperature under high CO_2 partial pressure [19]. Moreover, according to TGA results fast calcination may be achieved at a reduced temperature of just 700–725 °C under a gas which is easily separable from CO_2 (either He as in the TGA experiments described in [19] or superheated steam [20]). Attaining such a low calcination temperature would allow the use of already mature and inexpensive metallic solar receivers thus reducing technological risks. Nevertheless, the work of He/CO_2 or H_2O/CO_2 separation should be also included in an extended techno-economic energy analysis.

Carbonator conditions (pressure and temperature) are highly relevant for the global CSP-CaL power cycle integration. Carbonator pressure is selected by considering the most favourable conditions for the CaL-power cycle integration, i.e. a fluidized bed reactor operated under atmospheric pressure if an indirect power cycle is integrated and a pressurized fluidized bed reactor for direct integration with a power cycle, in order to achieve the higher integration performance. Increasing the carbonator temperature (T_{carb}) leads to higher power cycle efficiencies and therefore enhances the CSP-CaL-power cycle integration performance. However, the maximum temperature in the carbonator is limited by the thermodynamic equilibrium of the carbonation/calcination reaction. Thus, for a given CO_2 partial pressure in the carbonator there is a maximum carbonator temperature above which the carbonation reaction is not thermodynamically favourable. According to thermochemical data [36], the CO_2 partial pressure for the reaction to be at equilibrium at a given temperature T(K) is given by:

$$P_{eq}\ (\text{bar}) = P \cdot y_{eq} = \left[4.137 \cdot 10^7 \exp\left(-\frac{20,474}{T}\right)\right] \quad (8)$$

In Eq. (8), y_{eq} is the molar fraction of CO_2 in the carbonation environment. For a fixed carbonator temperature, there is a minimum carbonator pressure below which the CO_2 partial pressure is insufficient for carbonation to occur. Fig. 5 shows the minimum carbonator pressure as a function of reactor temperature to carry out

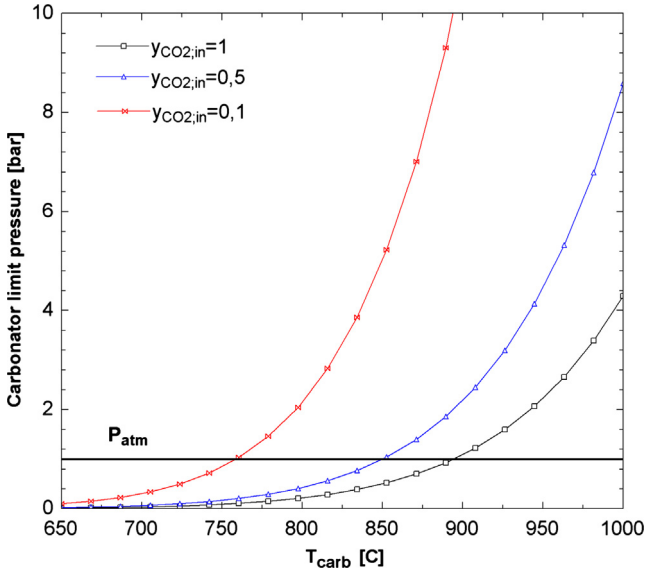

Fig. 5. Minimum carbonator pressure as a function of carbonator temperature T_{carb} for several CO_2 molar fractions at the carbonator inlet ($y_{CO_2,in}$).

carbonation and for different CO_2 molar fractions (Eq. (8)). It is clear that operating under pure CO_2 ($y_{CO_2,in} = 1$) allows working under higher temperatures and low carbonator total pressures.

3. Power cycle integration

This section is devoted to the study of several power cycle integrations into the CaL based CSP storage system. Power cycles are classified in two categories: power cycles with direct integration (CO_2 regenerative Brayton cycle) and power cycles with indirect integration (Rankine reheat cycle and supercritical CO_2 recompression cycle).

3.1. Direct integration

In power cycles with direct integration the heat transfer fluid used in the carbonator is sent directly into a gas turbine. In the following a CO_2 closed Brayton cycle is analysed.

3.1.1. CO_2 closed Brayton cycle

In this integration scheme (Fig. 6), the heat released by the carbonation reaction is delivered to a gas turbine by the excess CO_2 that does not participate in the reaction and is used as carrier through a Joule-Brayton cycle. This is therefore a direct integration between the heat released and power cycle, which has been recently studied in [30].

Fig. 6 shows the CO_2 closed Brayton cycle scheme. This CO_2 power cycle is a closed and regenerative cycle, whereby the heat removed by the reaction products in the carbonator is recovered in an open cyclone exchanger (HXF in Fig. 6). Thus, in this heat exchanger (HXF) heat from the exhaust CO_2 stream serves to heat the CaO solids before entering the carbonator while in HXE the residual heat from the solids at the carbonator output is extracted to pre-heat the CO_2 stream at the carbonator inlet. Part of the power needed in the compression stage of the Joule-Brayton cycle is provided by the expansion of the pressurized CO_2 used for reaction in the carbonator. In the CO_2 closed configuration the carbonator operates under a 100% CO_2 environment. Therefore, the molar flow rate of CO_2 flowing into the carbonator is by large in excess over the stoichiometric need. The CO_2 stream in the carbonator side is balanced out to use the non-reacting excess CO_2 to deliver heat of the carbonation reaction to the gas turbine for power production. Main data set used in the simulations is shown in Fig. 6 as well as results obtained.

The CO_2 closed Brayton cycle presents the following characteristics:

- Regarding to chemical equilibrium considerations, by operating in a pure CO_2 atmosphere, the minimum carbonator pressure coincides with the CO_2 partial pressure, making it possible to attain carbonation temperatures of around 950 °C for carbonator absolute pressures above 2.2 bar and until around 890 °C for carbonator pressures above atmospheric pressure (Fig. 5).

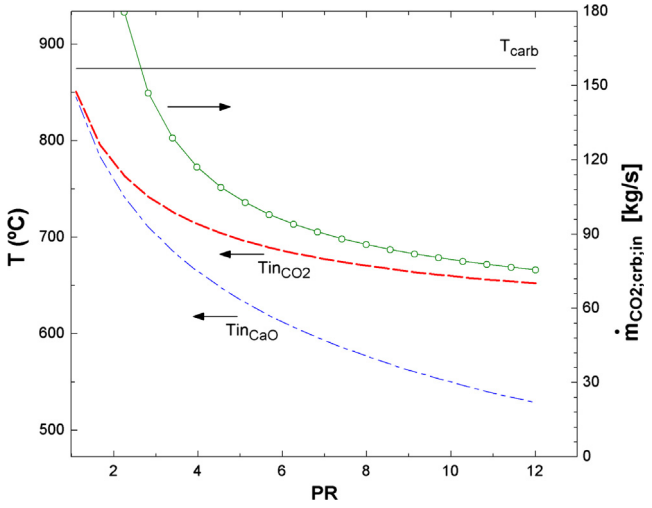

Fig. 7. Left axis: Temperature of CaO (Tin_{CaO}) and CO_2 (Tin_{CO_2}) streams entering into the carbonator reactor as a function of Pressure Ratio (PR). Right axis: CO_2 mass flow rate entering into the carbonator. The carbonator temperature (T_{carb}) is fixed to 875 °C.

Net absorbed solar flux in calciner	100	MW
Thermal dispersions in carbonator	10	%
Ambient temperature	20	°C
CaO conversion	0.5	
Approach temperature solid-solid HX	20	°C
Approach temperature solid-gas HX	15	°C
Approach temperature CO_2 cooler	10	°C
Intercoolings in CO_2 storage compression	5	
Interheatings in CO_2 power cycle compression	8	
Interheatings in CO_2 expansion from storage	7	
Solid phase conveying energy consumption	20	MJ/tonne
Daylight hours (constant solar flux)	8h	
Isentropic efficiencies (compression/expansion)	0.89	

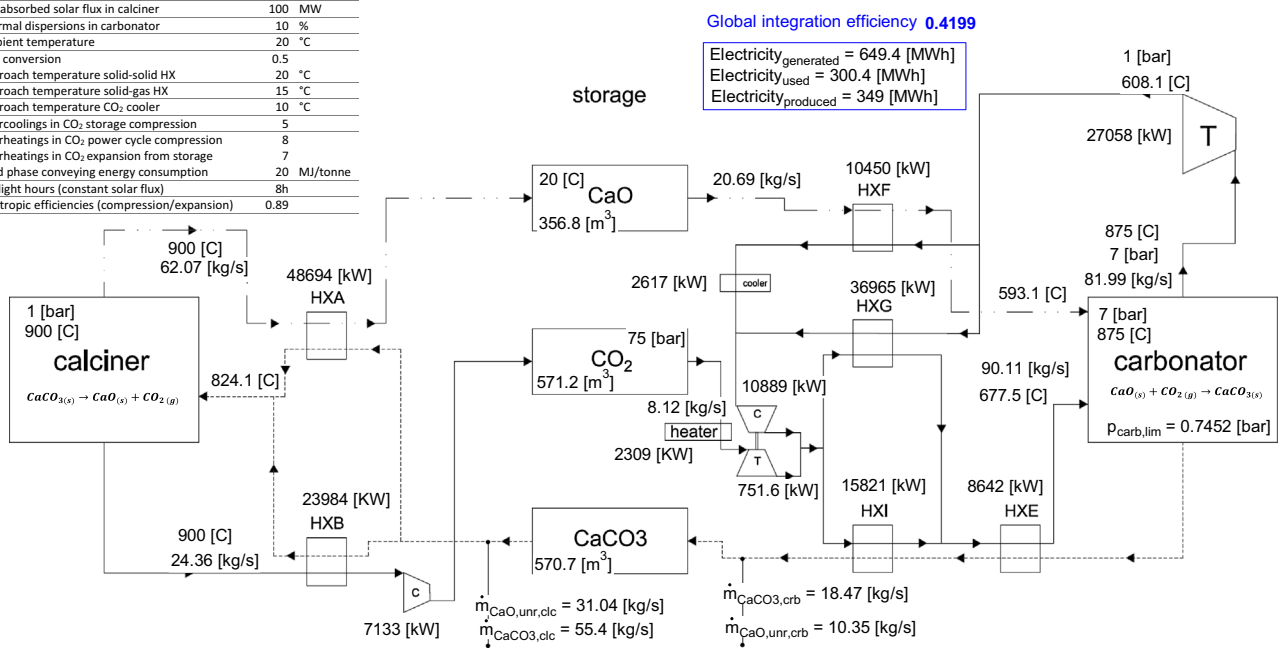

Fig. 6. CSP-CaL- CO_2 closed Brayton integration scheme.

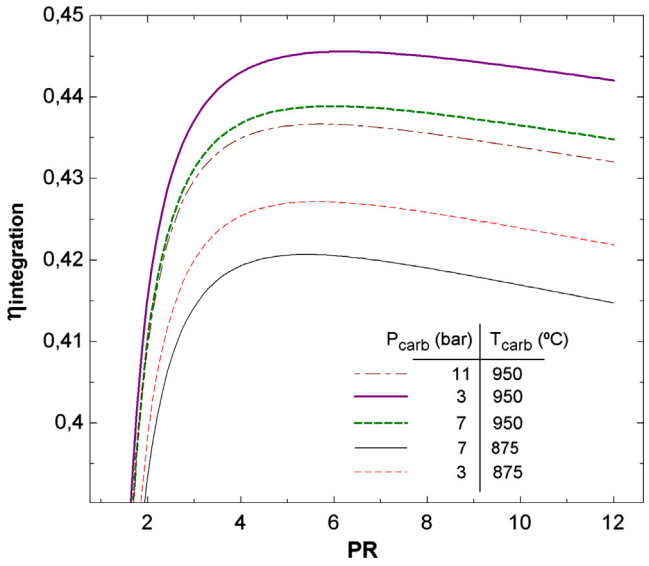

Fig. 8. Global integration efficiency (CO_2 closed Brayton cycle) as a function of pressure ratio for several carbonator operation points as indicated.

- CO_2 is characterized by lower values of both compression and expansion work compared to air.
- The CO_2 Brayton cycle provides a higher useful to expansion work ratio than an air Brayton cycle. Therefore, for a given useful work produced, the CO_2 at the turbine output presents a higher enthalpy. This is beneficial from the point of view of thermal energy recovery to preheat the streams entering into the carbonator (Fig. 6), which enhances the plant efficiency.
- Regarding to isentropic efficiency of compressor and turbine, CO_2 is less sensitive than air, especially at the compressor [42].
- Being a closed cycle, a more flexible operation is possible as compared to open cycles since possible CO_2 emissions to the atmosphere are avoided. Thus, the closed Brayton cycle could use a mix of several components as carrier fluid.

A sensitivity analysis has been carried out in order to assess the global cycle performance under several Brayton cycle conditions. The cycle behaviour is analysed as affected by the pressure ratio (PR) value. PR is defined as the ratio between pressure at turbine inlet to pressure at outlet, which in this integration is given by the ratio of the carbonator pressure to the turbine outlet pressure. Fig. 7 shows the relationship between PR and the carbonator inlet stream (CaO and CO_2) temperatures by keeping a fixed value of the carbonator pressure at 7 bar. As PR is increased, the turbine outlet temperature is decreased (lower value of enthalpy), which implies a lower heating capacity on the carbonator inlet streams (by means of the heat exchangers HXG, HXI and HXE in Fig. 6) and therefore more carbonation heat must be used to bring the CaO and CO_2 streams to the carbonation temperature. Thus, on one hand, a high value of PR yields a higher power production in the Brayton turbine, which increases the global cycle performance. On the other, it reduces the heat available for power production, which implies a lower CO_2 mass flow rate entering into the carbonator as heat transfer fluid (left side of Fig. 6). The effect of increasing PR and temperature on the global plant efficiency is shown in Fig. 8. As can be seen, an increase of the carbonator temperature leads always to a higher global efficiency whereas efficiency at a given temperature has a maximum at a given value of PR.

3.2. Indirect integration

In indirect power cycle integration, heat from the carbonator is transferred to the power cycle through a heat exchanger network. In this section a Rankine Reheat cycle and a supercritical CO_2 recompression cycle are analysed. Moreover, a special case based on a combined cycle is investigated.

3.2.1. Reheat Rankine cycle

Currently commercial CSP tower plants incorporate the steam Rankine power cycle technology for power production [26]. As a previous step to integration within the CSP-CaL cycle, a simple reheat Rankine cycle has been modelled to analyse the power cycle efficiency. Fig. 9 shows a schematic of the cycle model, which is based on a reheat Rankine cycle with regeneration from five

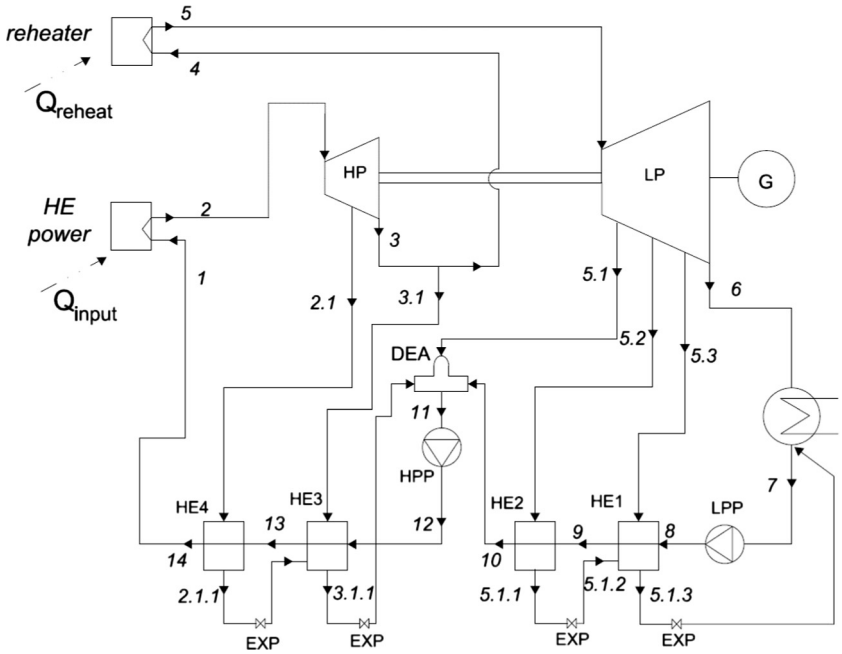

Fig. 9. Base reheat Rankine cycle layout.

Table 2
Main simulation Rankine cycle results for a 50MWth steam power cycle (P_{vv} = 160 bar, T_{vv} = 540/540 °C).

Q_{input}	50 MW_{th}
Q_{reheat}	9.1 MW_{th}
$W_{pump,HPP}$	0.35 MW_e
$W_{pump,LPP}$	0.03 MW_e
$W_{turb,HP}$	6.99 MW_e
$W_{turb,LP}$	18.82 MW_e
P_{HE1}	5.46 MW_{th}
P_{HE2}	2.68 MW_{th}
P_{HE3}	8.64 MW_{th}
P_{HE4}	3.88 MW_{th}
η_{cycle}	43.07%

Table 3
Stream data for a 50MWth steam power cycle (P_{vv} = 160 bar, T_{vv} = 540/540 °C).

Stream	$\dot{m}$ (kg/s)	T (C)	P (bar)	*Stream*	$\dot{m}$ (kg/s)	T (C)	P (bar)
1	22.67	315.9	204	5.2.1	1.16	132	4.95
2	22.67	540	200	5.3	1.08	99.63	1
2.1	2.45	452.1	93	5.3.1	2.23	58.6	0.99
2.1.1	2.45	294.8	92.1	6	14.29	43.77	0.09
3	20.18	352	46	7	16.53	43.58	0.09
3.1	2.02	352	46	8	16.53	43.59	18.4
3.1.1	4.51	215	45.5	9	16.53	122	18.2
4	18.16	352	46	10	16.53	159.8	18
5	18.16	540	45.5	11	22.67	202.9	18
5.1	1.63	403.7	18	12	22.67	205	208
5.2	1.16	248.5	5	13	22.67	284.8	205.9

feed-water heaters (HE1:4), one of which is a total mixer exchanger type (DEA). For this reason, a series of steam extractions (Fig. 9) are implemented. The steam operational parameters and benchmarking have been chosen from data of similar real power plants [43]. Turbine and pump efficiencies values of 0.9 have been considered, as well as a heat exchangers minimum temperature difference of 10 °C. On the other hand, a 1% pressure drop is assumed in all heat exchangers. Tables 2 and 3 show the main simulation results obtained for the system schematized in Fig. 9.

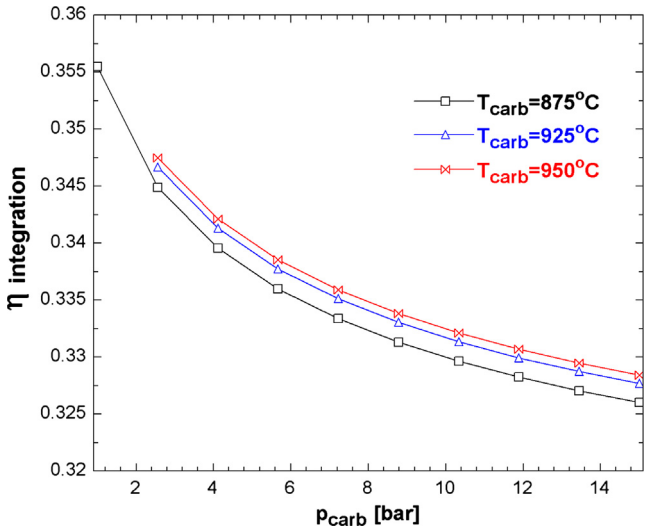

Fig. 11. Efficiency of the CaL-Rankine integration as a function of carbonator pressure and for diverse temperatures. Note that a minimum carbonator pressure is required according to thermochemical equilibrium as temperature is increased.

Once the power cycle block model is developed, it is integrated into the CSP-CaL scheme. CSP-CaL main operation parameters are the same as in previous schemes (Fig 6). Pure CO_2 is used for carbonation, which allows operating at high carbonator temperatures.

Fig. 10 shows a schematic representation of the CSP-CaL-Rankine integration and main simulation results considering carbonation at 875 °C under atmospheric pressure. The integration efficiency is shown in Fig. 11 as a function of the carbonator pressure for diverse temperatures. As can be seen, the maximum effi-

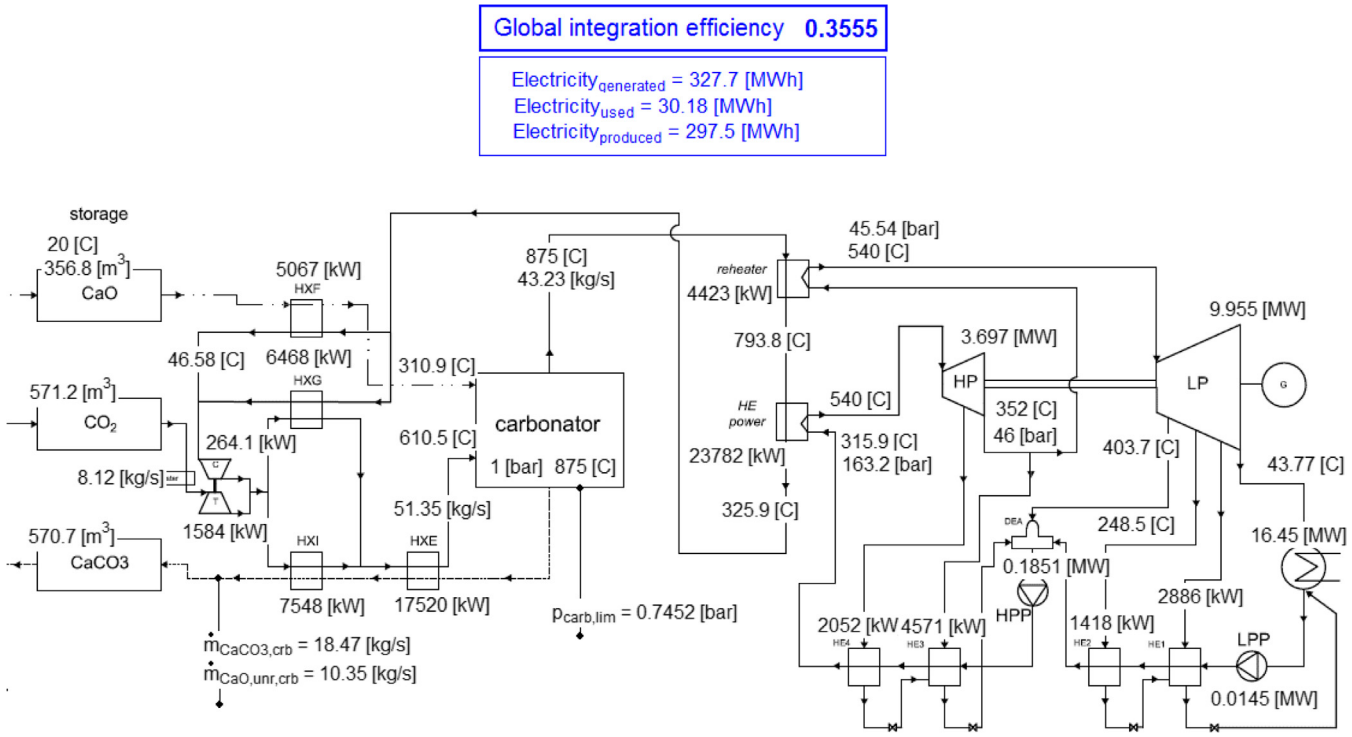

Fig. 10. CSP-CaL- Regenerative Rankine integration scheme and main simulation results for carbonation under 1 bar at 875 °C.

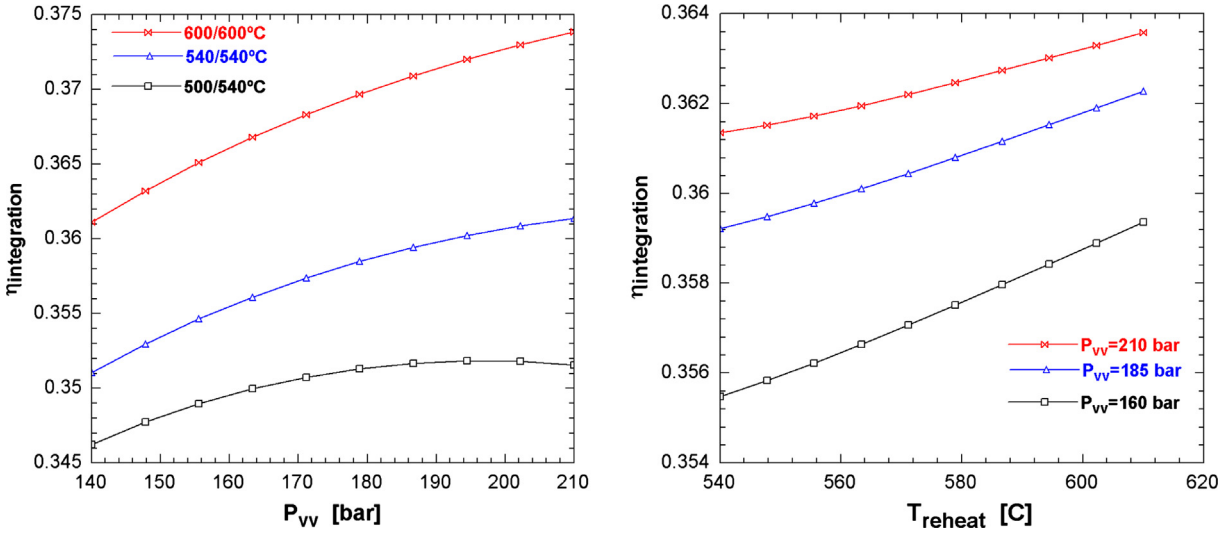

Fig. 12. Global integration efficiency as a function of (LEFT) steam turbine inlet and (RIGHT) reheat temperature conditions.

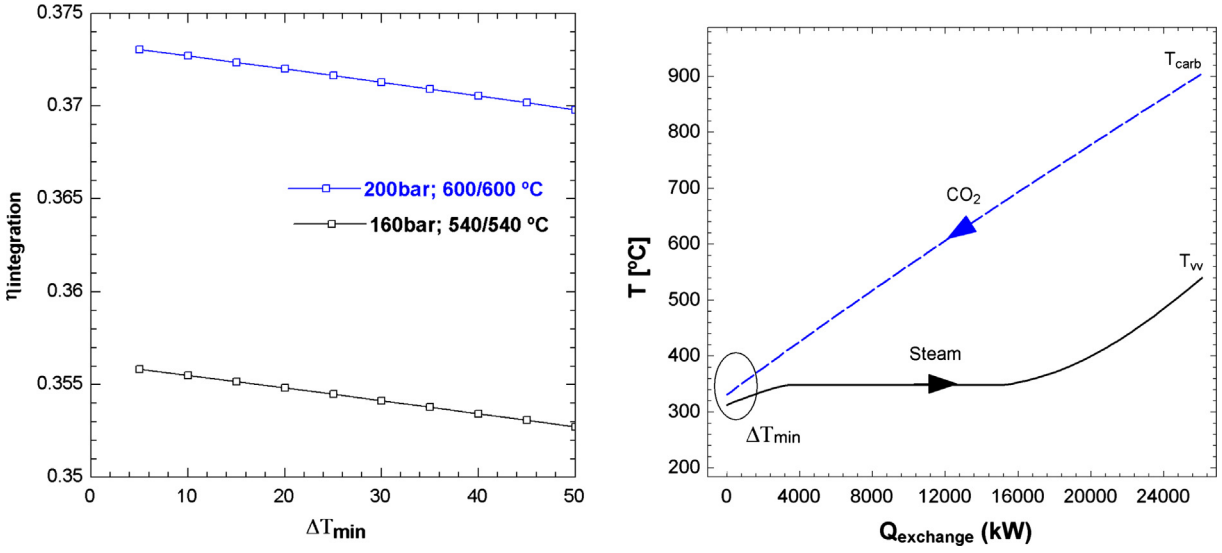

Fig. 13. Global integration efficiency as a function of minimum temperature approach in HRSG.

ciency (around 35.5%) is obtained at 875 °C operating under atmospheric pressure, which is well over conventional CSP plant performances. Higher temperatures in the carbonator would require higher minimum carbonator pressures for carbonation to be thermodynamically favourable at which efficiency is decreased.

A sensitivity analysis has been carried out in which the main Rankine cycle parameters have been tuned. As can be seen in Fig. 12, the global integration efficiency is promoted by increasing live steam conditions (pressure (P_{vv}) and temperature (T_{vv})). It may be also seen that efficiency is enhanced as the reheat temperature is increased.

As seen in Fig. 10, the preheat water of the Rankine cycle is heated by the exhaust CO_2 stream from the carbonator in a heat recovery steam generator (HRSG) until the super-heated regime is reached. One key parameters in Rankine power cycles is the HRSG efficiency, which can be analysed from the pinch point value across the steam production process. Fig. 13 shows that lower values of the pinch point (higher HRSG efficiency) causes an increase in the global cycle efficiency.

3.2.2. Supercritical carbon dioxide (sCO_2) recompression cycle

The supercritical CO_2 (sCO_2) Brayton cycle, which was originally introduced by Feher [44], has emerged in the last years as a promising technique for high-efficiency power production. It basically consists of a closed-loop Brayton cycle that operates entirely above CO_2 critical pressure (73.77 bar and 30.98 °C) and presents a high drop in compressibility, which brings about a similar reduction in compression work while the turbine operates with CO_2 in a close to ideal behaviour. Among different layouts proposed for sCO_2 cycles, a recompression scheme seems to be the highest efficiency cycle [45], which is thus the one used in the present study. Fig. 14 shows the recompression cycle model. An important feature of the regeneration process in the sCO_2 Brayton cycle is that the specific heat of the cold side is 2–3 times higher than the hot side. Thus, the CO_2 stream is split (stream 5b in Fig. 14a) to compensate for the specific heat difference in the low temperature recuperator, which maximizes the heat recuperation.

CSP-sCO_2 integration models have been already developed to increase the CSP power plant performance. Thus, Chacartegui et al. [46] compared the integration of supercritical and transcriti-

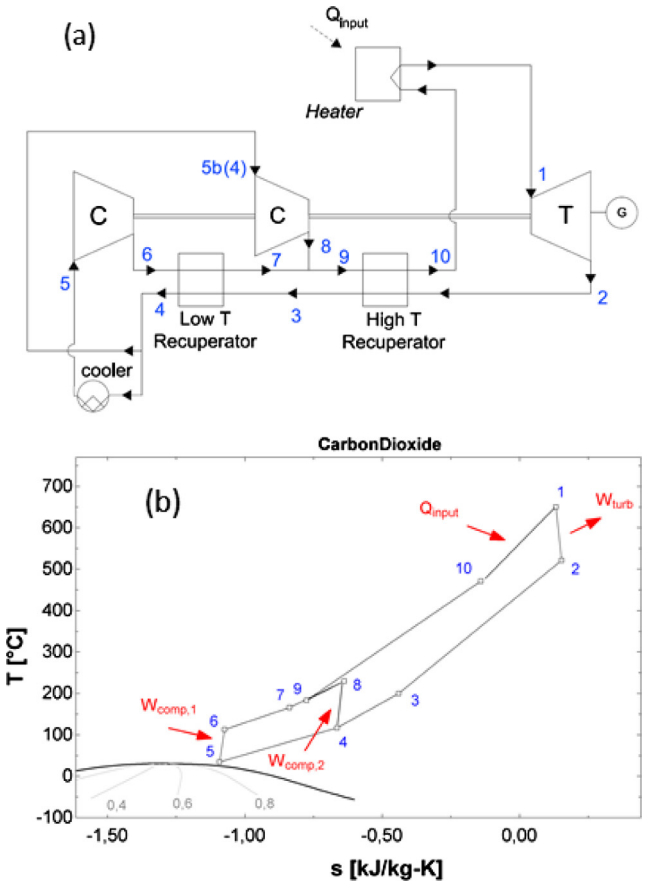

Fig. 14. (a) Base recompression - sCO_2 Brayton cycle layout. (b) Temperature-entropy diagram.

Table 4
Input data parameters for the sCO_2 cycle [52].

η_c (%)	85
η_t (%)	90
ε_{rec} (%)	95
$\Delta P_{R,hot}$ (%)	0.5
$\Delta P_{R,cold}$ (%)	1.5
$\Delta P_{R,HE}$ (%)	0.5

Table 5
Main sCO_2 cycle simulation results .

Q_{input}	50 MW_{th}
$W_{comp,1}$	7.14 MW_e
$W_{comp,2}$	5.74 MW_e
W_{turb}	33.38 MW_e
η_{cycle}	41.01%
ϕ_{cycle}	69%

Table 6
Stream data for sCO_2 recompression cycle.

Stream	$\dot{m}$ (kg/s)	T (C)	P (bar)
1	223.6	650	213.9
2	223.6	521.1	78
3	223.6	200.2	77.61
4	223.6	117.2	77.22
5	158.8	35	75
5b	64.85	117.2	77.22
6	158.8	113.1	225
7	158.8	166.0	223.9
8	64.85	229.8	221.6
9	223.6	183.1	221.6
10	223.6	471	218.3

cal carbon dioxide cycles as well as a combined cycle composed by a topping Brayton CO_2 cycle and a bottoming Organic Rankine Cycle. Iverson et al. [47] presents the behaviour of Brayton cycle turbomachinery including a data set for stable supercritical CO_2 Brayton cycle operation. Moreover, Ma et al. [48] analyses the integration of sCO_2 power cycles by considering sensible heat storage (thermocline system). One of the most important advantages of the sCO_2 Brayton cycle is its compact turbomachinery, albeit it is still under development [49]. A sCO_2 technology review is presented in [42], from which values on turbomachinery efficiency and pressure drops are taken in the present work. Thus, the recompression sCO_2 cycle has been simulated using data specified in Table 4.

Fig. 14a shows the recompression sCO_2 Brayton scheme proposed. Thermodynamic parameters of the streams involved in the cycle are shown in Fig. 14b in a temperature (T)-entropy (S) diagram. Main sCO_2 cycle simulation results are shown in Tables 5 and 6. A cycle efficiency of around 41% is obtained from this configuration, which is in agreement with results from previous works [50].

Once the recompression sCO_2 cycle is analysed and benchmarked it is integrated in the CSP-CaL configuration as shown in Fig. 15. A global integration efficiency close to 32% is achieved, although it must be taken into account that a large amount of energy, linked to the cooling process before the compression stage, is not used. This suggests that a bottoming cycle could serve to improve the cycle performance [46].

Results from a sensitivity analysis are shown in Fig. 16. It is observed that the recuperation process in the sCO_2 Brayton cycle greatly influences the thermal efficiency since CO_2 properties are very sensitive to pressure and temperature near the critical point. Therefore, the hot and cold sides in the regenerator are strongly unbalanced. As can be seen in Fig. 16, by increasing the turbomachinery efficiency (which depends upon further technology development) the global cycle performance is significantly enhanced.

3.2.3. Combined cycle

The combined cycle is based on the integration of two subsystems consisting of a gas turbine (Brayton cycle) and a steam turbine (Rankine cycle), which leads to an improvement of efficiency due to the synergy between both cycles [51].

A number of integrated solar combined cycle (ISCC) systems have been proposed to improve the power plant efficiency [52]. ISCCS power plants currently in operation employ the parabolic trough concentrator technology. Further work is still needed to advance in the technological readiness of solar tower – ISCC power plants [53]. ISCC cycles operate using a solar-fuel combination [54], with the gas turbine being fuelled by a non-solar source (based on fossil or renewable fuel) due to the temperature limitation in CSP power plants imposed by degradation of molten salts and thermal radiation losses at the focal point. Solar power share in ISCC power plants is on average below 34% [53]. Compared with the solar-only power plants, ISCC plants exhibit several advantages such as higher solar-to-electricity conversion performance. Moreover, thermal inefficiency associated with the daily start-up and shutdown of the steam turbine can be avoided [55]. Another configuration proposed in a recent work [56] evaluates a combined cycle based on a closed Brayton and organic Rankine cycle for solar power tower plants by means of energy and exergy analysis, showing that higher performance than using steam and supercritical CO_2 cycles can be achieved.

Fig. 17 shows the global cycle integration proposed by considering a combined cycle for power production. The combined cycle involves a hybrid direct-indirect power cycle integration with the CSP-CaL system. The CO_2 stream exiting the carbonator is expanded in a gas turbine as a previous step for transferring heat

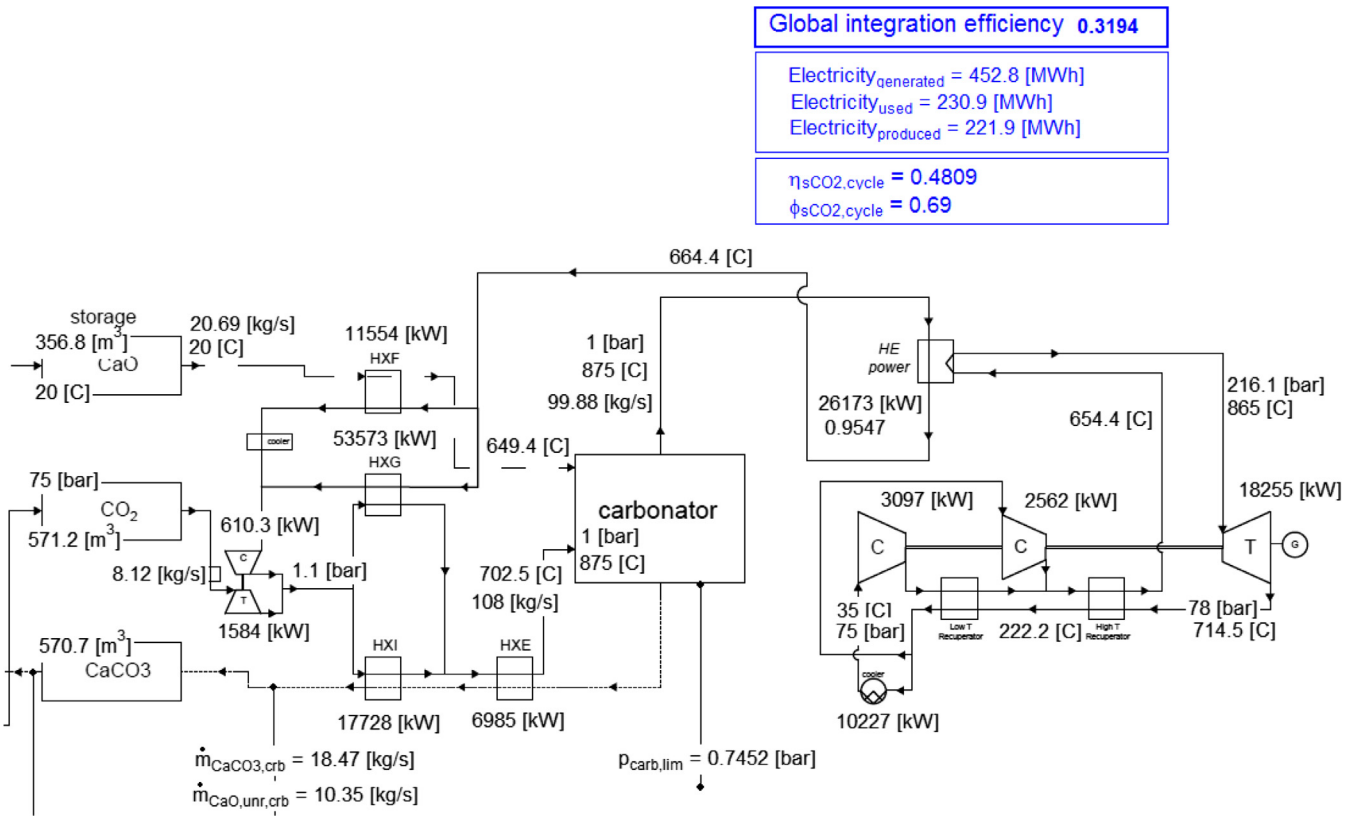

Fig. 15. CSP-CaL- sCO_2 integration scheme and main simulation results.

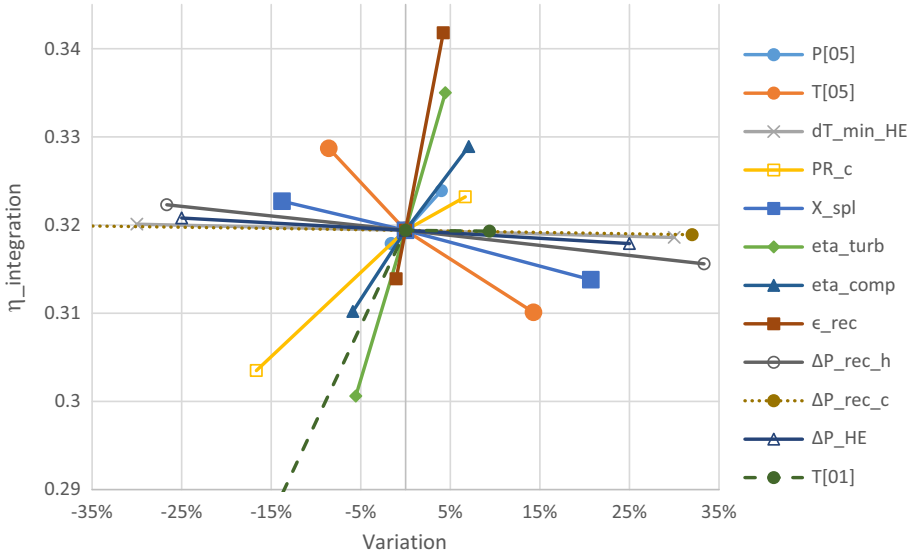

Fig. 16. Sensitivity analysis results of the CSP-CaL- sCO_2 integration.

to steam cycle through a HRSG. Main simulation results are shown also in Fig. 17.

Fig. 18 shows the global cycle performance as a function of the carbonator pressure (or, equivalently, the inlet turbine pressure) for different values of the turbine outlet pressure. As can be seen, a higher performance is obtained by decreasing the outlet turbine pressure, reaching a maximum value of 40.4% for operation under an inlet/outlet turbine pressure ratio of 3.6/1. In order to simplify the heat exchanger network, an atmospheric outlet turbine pressure will be next considered.

4. Comparative analysis on the power cycles integration

In order to compare the performances of the diverse CSP-CaL-power cycle integrations a sensitivity analysis has been carried out using reference parameters for which the efficiency of these integrations is optimized. Main power cycle parameters for each integration scheme are given in Table 7. A carbonator temperature of 875 °C has been selected, which guarantees carbonation under the different carbonator pressures of each cycle. Unless otherwise

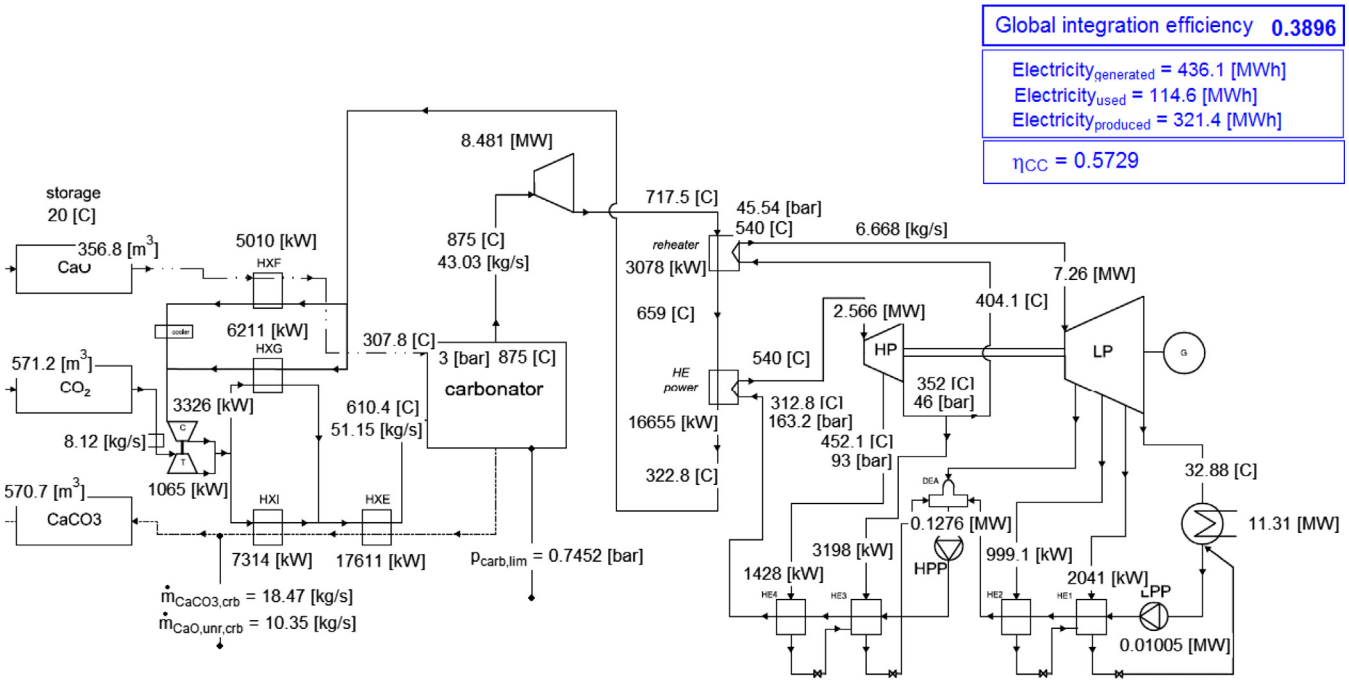

Fig. 17. CSP-CaL- CC integration scheme and main simulation results.

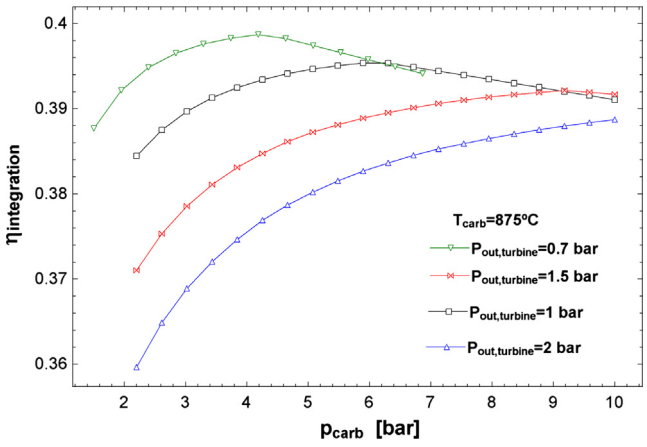

Fig. 18. Efficiency of the CSP-CaL-CC integration as a function of the carbonator pressure for several values of the Brayton turbine outlet pressure.

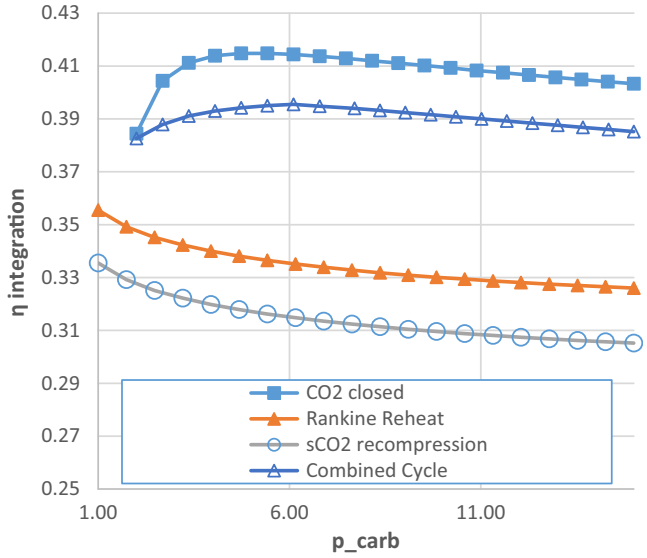

Fig. 19. Global cycle integration efficiency as a function of carbonator pressure for the different power cycles coupled to the CSP-CaL system (using data showed in Table 7).

indicated, the values of the parameters employed for the CaL cycle are those previously specified in Table 1. Note that temperatures for the steam turbine in the case of the combined cycle are conditioned by the Brayton turbine exit and therefore the values shown in this table correspond to the maximum temperatures achievable.

Fig. 19 shows the global integration efficiency obtained for the different power cycles analysed in this work as a function of the carbonator pressure. As can be seen, the CO_2 closed cycle direct integration yields the best efficiency results. Only by means of the indirect integration is possible to operate the carbonator under atmospheric pressure, being the efficiency hampered in this integration as the carbonator pressure is increased further. The opposite trend occurs in the CO_2 closed and CC power cycles. Using these power cycles, the global efficiency is promoted as the carbonator pressure is increased up to a certain optimum value, which is around 4.2 bar for the CO_2 closed cycle and 5.1 bar for the CC cycle (atmospheric turbine outlet pressure). Results show also that despite the sCO_2 recompression cycle could be a potentially attractive choice from a thermodynamic point of view, the conservative values used for the turbomachinery efficiencies (in accordance with the current state of art [42]) prevents the CSP-CaL-sCO_2 cycle integration from reaching very high global efficiencies. Efficiency results are plotted in Fig. 20 as a function of the CaO average conversion. Generally, the enhancement of CaO conversion promotes efficiency as would be expected.

Additional considerations regarding costs must be addressed to further assess the applicability of these power cycle integrations in the CSP-CaL. As this technology is in an early concept stage, data from prototypes or experimental installations are not available for the TCES core. A detailed economic prospective analysis is under development and will be presented in future works. How-

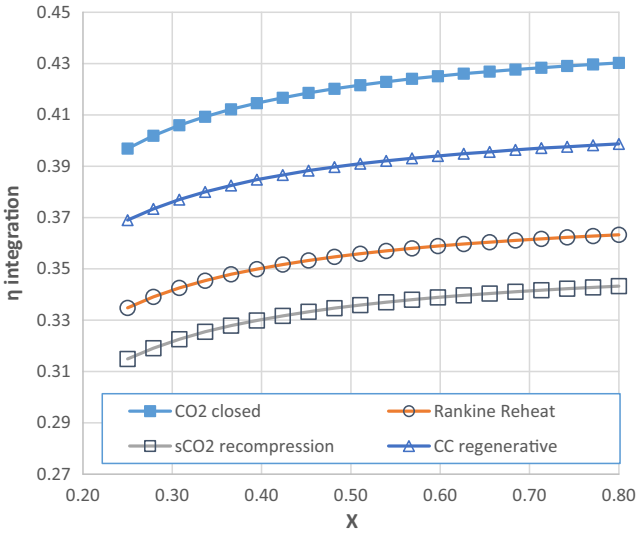

Fig. 20. Global cycle integration efficiency as a function of average CaO conversion for the different power cycles coupled to the CSP-CaL system (using data showed in Table 7).

Table 7
Main power cycle parameters for each integration scheme.

	Closed CO_2 Brayton	Reheat Rankine	sCO_2 recompression	Combined cycle
$P_{out,turb}$ (bar)	1	–	–	1
P_{carb} (bar)	3.2	1	1	3.2
P_{vv} (bar)	–	160	–	160
T_{carb} (C)	875	875	875	875
T_{vv} (C)	–	540	–	540
T_{reheat} (C)	–	540	–	540
ΔT_{min}	–	10	10	10
P[05] (bar)	–	–	75	–
T[05] (C)	–	–	32	–
PR	3.2	–	3	3.2
X	0.5	0.5	0.5	0.5

ever, some preliminary considerations can be already made by extrapolating components information from other technologies. In commercial CSP plants, the power block cost percentage is estimated around 32% [57] and power cycle integration has a critical influence on capital investment. Some considerations may be made also on the maturity of the power technologies analysed in this work. These include one full mature technology (steam power cycle), two fully feasible power technologies with already available commercial components (real gas CO_2 closed cycle and the derived combined cycle) and a promising power technology with great advances expected (supercritical CO_2 cycle).

Steam power cycles fulfilling specific conditions for their integration in CSP plants (optimized for complex and challenging cycle conditions) are at the commercial level [58]. For conventional steam power cycles, capital and O&M costs can be estimated as 1280 $/kW and 5.7$CO_2$ $/MW h, respectively [59]. For the CO_2 closed-cycle gas turbine, although not fully available, main components are already usable or can be integrated from different applications. Thermal turbomachinery, compressors and turbines are already in use at commercial scale using as working fluid air, e.g. the Gelsenkirchen plant [60] and Oberhausen I [61], or Helium, e.g. Oberhausen II [61]. In the case of CO_2 as working fluid, compressors are being widely analysed and tested in recent years as fundamental equipment within the Carbon Capture and Storage (CCS) technology [62]. Thermal machinery characteristics for the pressure ratios and temperatures presented in this work will be quite similar to the ones operating with air and combustion gases, as shown by Najjar et al. [63] for compressor pressure ratios of 5, compressor temperature inlet of 310 K and turbine temperature inlet of 1100 K. Therefore, already available technologies for turbines and compressors could be employed. In the case of closed-Brayton cycles, the introduction of additional heat exchangers increases capital investment [46]. Therefore, technologies for the conditions presented in this work are already available, and costs for the fully developed technology could be expected as similar to the ones in the range between current gas turbines and combined cycles. For a 100 MWe power block estimated capital and total O&M costs for an open gas turbine combined cycle (considering only the power block) are around 660 $/kW and 2.2 $/MW h, respectively [59] whereas for an air-open Brayton cycle they can be estimated as 1026 $/kW and 3.42 $/MW h respectively [64]. Finally, in the case of supercritical CO_2 technology, in spite of that sCO_2 cycle is a non-mature technology, in a project under development granted by US DOE through the Sunshot initiative [65] a power plant investment cost of 1200 $/kW at the commercial stage is assumed [66].

Regarding the CaL thermochemical energy storage system, it implies an intrinsic benefit regarding life cycle cost and system sustainability as it is based on the use of low price, non-toxic and widely available natural CaO precursors such as limestone and dolomite. According to [67], the use of the CaL process for TCES would make it possible to achieve a thermal storage cost lower than 15$/kWh$_t$. This preliminary approach shows the potential of these integrations. Detailed and fully developed life cycle and economic analysis are under development and will be the subject of future works.

5. Conclusions

This manuscript analyses several CSP tower plant integration schemes with thermochemical energy storage (TCES) using the Calcium-Looping (CaL) cycle. The work is focused on assessing the power production cycle. The CSP-CaL integration yields high temperatures (above 850 °C) at the power cycle inlet, which allows using high efficiency power cycles employed in fuel based power plants (or combined CSP-fuel power plants). Thus, the CSP-CaL integration achieves high density/long term storage capacity and lends itself for the integration of higher performance power cycles as compared with the current state of the art in commercial CSP plants.

In regards to direct-indirect cycles integration, results show that the highest performance is achieved for direct integration. On the other hand, higher efficiencies are attained as the CaO conversion is increased. Among the power cycles analysed in the present work, the CO_2 closed Brayton cycle shows the best overall performance, reaching efficiencies potentially above 44–45% (including penalty for solids conveying) if the carbonator is operated at temperatures around 950 °C and under pressures about 3.5 bar for atmospheric pressure at the Brayton turbine outlet. Importantly, carbonation conditions in this integration allows for high values of the residual conversion of CaO derived from natural minerals such as limestone and dolomite as recently demonstrated by thermogravimetric studies. The wide availability, abundance, lack of corrosiveness, non-toxicity and cheapness (~10 $/ton) of these natural minerals makes the proposed integration an attractive technology for large-scale storage of solar energy and highly efficient grid-level power production.

Acknowledgments

This work was supported by the Spanish Government Agency Ministerio de Economia y Competitividad and FEDER Funds (con-

tracts CTQ2014-52763-C2-1-R, CTQ2014- 52763-C2-2-R and MAT2013-41233-R).

References

[1] United Nations. Framework convention on climate change. Adoption of the Paris agreement, vol. 21932. 2015.

[2] International Energy Agency. Technology roadmap solar thermal electricity 2014:52, doi:http://dx.doi.org/10.1007/SpringerReference_7300.

[3] Kuravi S, Trahan J, Goswami DY, Rahman MM, Stefanakos EK. Thermal energy storage technologies and systems for concentrating solar power plants. Prog Energy Combust Sci 2013;39:285–319. http://dx.doi.org/10.1016/j.pecs.2013.02.001.

[4] Mahlia TMIMI, Saktisahdan TJJ, Jannifar A, Hasan MHH, Matseelar HSCSC. A review of available methods and development on energy storage; Technology update.. Renew Sustain Energy Rev 2014;33:532–45. http://dx.doi.org/10.1016/j.rser.2014.01.068.

[5] Medrano M, Gil A, Martorell I, Potau X, Cabeza LF. State of the art on high-temperature thermal energy storage for power generation. Part 2-Case studies.. Renew Sustain Energy Rev 2010;14:56–72. http://dx.doi.org/10.1016/j.rser.2009.07.036.

[6] Fernández AG, Ushak S, Galleguillos H, Pérez FJ. Development of new molten salts with $LiNO_3$ and $Ca(NO_3)_2$ for energy storage in CSP plants. Appl Energy 2014;119:131–40. http://dx.doi.org/10.1016/j.apenergy.2013.12.061.

[7] Zalba B, Marín JM, Cabeza LF, Mehling H. Review on thermal energy storage with phase change: materials. Heat Transfer Anal Appl 2003;23. http://dx.doi.org/10.1016/S1359-4311(02)00192-8.

[8] Pardo P, Deydier a, Anxionnaz-Minvielle Z, Rougé S, Cabassud M, Cognet P. A review on high temperature thermochemical heat energy storage. Renew Sustain Energy Rev 2014;32:591–610. http://dx.doi.org/10.1016/j.rser.2013.12.014.

[9] Cot-Gores J, Castell A, Cabeza LF. Thermochemical energy storage and conversion: A-state-of-the-art review of the experimental research under practical conditions. Renew Sustain Energy Rev 2012;16:5207–24. http://dx.doi.org/10.1016/j.rser.2012.04.007.

[10] Neveu P, Tescari S, Aussel D, Mazet N. Combined constructal and exergy optimization of thermochemical reactors for high temperature heat storage. Energy Convers Manage 2013;71:186–98. http://dx.doi.org/10.1016/j.enconman.2013.03.035.

[11] Janz GJ, Allen, Carolyn B, Bansal NP, Murphy RM, Tomkins RP. Physical properties data compilations relevant to energy storage. II. Molten salts: data on single and multi-components salt systems. Natl Bur Stand; 1979.

[12] N'Tsoukpoe KE, Liu H, Le Pierrès N, Luo L. A review on long-term sorption solar energy storage. Renew Sustain Energy Rev 2009;13:2385–96. http://dx.doi.org/10.1016/j.rser.2009.05.008.

[13] Abedin A, Rosen M. A critical review of thermochemical energy storage systems. Open Renew Energy J n.d.;42–6. doi:http://dx.doi.org/10.2174/1876387101004010042.

[14] Sakellariou KG, Karagiannakis G, Criado YA, Konstandopoulos AG. Calcium oxide based materials for thermochemical heat storage in concentrated solar power plants. Sol Energy 2015;122:215–30. http://dx.doi.org/10.1016/j.solener.2015.08.011.

[15] Rodriguez N, Alonso M, Grasa G, Abanades JC. Heat requirements in a calciner of $CaCO_3$ integrated in a CO_2 capture system using CaO. Chem Eng J 2008;138:148–54. http://dx.doi.org/10.1016/j.cej.2007.06.005.

[16] Valverde JM, Medina S. Reduction of calcination temperature in the calcium looping process for CO_2 capture by using helium: in situ XRD analysis. ACS Sustain Chem Eng 2016. http://dx.doi.org/10.1021/acssuschemeng.6b01966.

[17] Romeo LM, Lara Y, Lisbona P, Martínez A. Economical assessment of competitive enhanced limestones for CO_2 capture cycles in power plants. Fuel Process Technol 2009;90:803–11. http://dx.doi.org/10.1016/j.fuproc.2009.03.014.

[18] Perejon A, Romeo LM, Lara Y, Lisbona P, Valverde JM. The calcium-looping technology for CO_2 capture: on the important roles of energy integration and sorbent behavior. Appl Energy 2015;162:787–807. http://dx.doi.org/10.1016/j.apenergy.2015.10.121.

[19] Sarrion B, Valverde JM, Perejon A, Perez-maqueda LA, Sanchez-jimenez PE. On the multicycle activity of natural limestone/dolomite for cheap, efficient and non-toxic thermochemical energy storage of concentrated solar power. Energy Technol 2016. http://dx.doi.org/10.1002/ente.201600068.

[20] Berger EE. Effect of steam on the decomposition of limestone. Ind Eng Chem 1927;19:594–6. http://dx.doi.org/10.1021/ie50209a026.

[21] Kearney D, Kelly B, Herrmann U, Cable R, Pacheco J, Mahoney R, et al. Engineering aspects of a molten salt heat transfer fluid in a trough solar field. Energy 2004;29:861–70. http://dx.doi.org/10.1016/S0360-5442(03)00191-9.

[22] Frangini S, Masi A. Molten carbonates for advanced and sustainable energy applications: part I. Revisiting molten carbonate properties from a sustainable viewpoint. Int J Hydrogen Energy 2016;41:18739–46. http://dx.doi.org/10.1016/j.ijhydene.2015.12.073.

[23] Fletcher EA, Moen RL. Hydrogen and oxygen from water. Science 1977;197(80):1050–6.

[24] Siva Reddy V, Kaushik SC, Ranjan KR, Tyagi SK. State-of-the-art of solar thermal power plants - a review. Renew Sustain Energy Rev 2013;27:258–73. http://dx.doi.org/10.1016/j.rser.2013.06.037.

[25] Yogi Goswami D. Solar thermal power technology: present status and ideas for the future. Energy Sources 1998;20:137–45. http://dx.doi.org/10.1080/00908319808970052.

[26] Liu M, Steven Tay NH, Bell S, Belusko M, Jacob R, Will G, et al. Review on concentrating solar power plants and new developments in high temperature thermal energy storage technologies. Renew Sustain Energy Rev 2016;53:1411–32. http://dx.doi.org/10.1016/j.rser.2015.09.026.

[27] European Academies Scientific Advisory Council. Concentrating solar power: its potential contribution to a sustainable energy future; 2011.

[28] Tregambi C, Montagnaro F, Salatino P, Solimene R. A model of integrated calcium looping for CO_2 capture and concentrated solar power. Sol Energy 2015;120:208–20. http://dx.doi.org/10.1016/j.solener.2015.07.017.

[29] Edwards SEB, Materić V. Calcium looping in solar power generation plants. Sol Energy 2012;86:2494–503. http://dx.doi.org/10.1016/j.solener.2012.05.019.

[30] Chacartegui R, Alovisio A, Ortiz C, Valverde JM, Verda V, Becerra JA. Thermochemical energy storage of concentrated solar power by integration of the calcium looping process and a CO_2 power cycle. Appl Energy 2015. http://dx.doi.org/10.1016/j.apenergy.2016.04.053.

[31] Alovisio A, Chacartegui R, Ortiz C, Valverde JM, Verda V. Optimizing the CSP-calcium looping integration for thermochemical energy storage. Energy Convers Manage 2017;136:85–98.

[32] Fidaros DK, Baxevanou CA, Vlachos NS. A parametric study of a solar calcinator using computational fluid dynamics. Energy Convers Manage 2007;48:2784–91. http://dx.doi.org/10.1016/j.enconman.2007.07.025.

[33] Meier A, Bonaldi E, Cella GM, Lipinski W, Wuillemin D. Solar chemical reactor technology for industrial production of lime. Sol Energy 2006;80:1355–62. http://dx.doi.org/10.1016/j.solener.2005.05.017.

[34] Vignarooban K, Xu X, Arvay A, Hsu K, Kannan AM. Heat transfer fluids for concentrating solar power systems – a review. Appl Energy 2015;146:383–96. http://dx.doi.org/10.1016/j.apenergy.2015.01.125.

[35] Mills D. Pneumatic conveying design guide 2004;80.

[36] Barin I. Thermochemical data of pure substances. VCH, Weinheim; 1989.

[37] Hanak DP, Anthony EJ, Manovic V. A review of developments in pilot-plant testing and modelling of calcium looping process for CO_2 capture from power generation systems. Energy Environ Sci 2015;8:2199–249. http://dx.doi.org/10.1039/C5EE01228G.

[38] Grasa GS, Abanades JC. CO_2 capture capacity of CaO in long series of carbonation/calcination cycles. Ind Eng Chem Res 2006;45:8846–51. http://dx.doi.org/10.1021/ie0606946.

[39] Romano MC. Modeling the carbonator of a Ca-looping process for CO_2 capture from power plant flue gas. Chem Eng Sci 2012;69:257–69. http://dx.doi.org/10.1016/j.ces.2011.10.041.

[40] Ortiz C, Chacartegui R, Valverde JM, Becerra JA. A new integration model of the calcium looping technology into coal fired power plants for CO_2 capture. Appl Energy 2016;169:408–20. http://dx.doi.org/10.1016/j.apenergy.2016.02.050.

[41] Valverde JM, Sanchez-Jimenez PE, Perez-Maqueda L. Ca-looping for postcombustion CO_2 capture: a comparative analysis on the performances of dolomite and limestone. Appl Energy 2015;138:202–15. http://dx.doi.org/10.1016/j.apenergy.2014.10.087.

[42] Sánchez D, Muñoz de Escalona JM, Chacartegui R, Muñoz A, Sánchez T. A comparison between molten carbonate fuel cells based hybrid systems using air and supercritical carbon dioxide Brayton cycles with state of the art technology. J Power Sour 2011;196:4347–54. http://dx.doi.org/10.1016/j.jpowsour.2010.09.091.

[43] Cheang VT, Hedderwick Ra, McGregor C. Benchmarking supercritical carbon dioxide cycles against steam Rankine cycles for Concentrated Solar Power. Sol Energy 2015;113:199–211. http://dx.doi.org/10.1016/j.solener.2014.12.016.

[44] Feher EG. The supercritical thermodynamic power cycle. Energy Convers 1968;8:85–90. http://dx.doi.org/10.1016/0013-7480(68)90105-8.

[45] Ahn Y, Bae SJ, Kim M, Cho SK, Baik S, Lee JI, et al. Review of supercritical CO_2 power cycle technology and current status of research and development. Nucl Eng Technol 2015;47:647–61. http://dx.doi.org/10.1016/j.net.2015.06.009.

[46] Chacartegui R, Muñoz De Escalona JM, Sánchez D, Monje B, Sánchez T. Alternative cycles based on carbon dioxide for central receiver solar power plants. Appl Therm Eng 2011;31:872–9. http://dx.doi.org/10.1016/j.applthermaleng.2010.11.008.

[47] Iverson BD, Conboy TM, Pasch JJ, Kruizenga AM. Supercritical CO_2 Brayton cycles for solar-thermal energy. Appl Energy 2013;111:957–70. http://dx.doi.org/10.1016/j.apenergy.2013.06.020.

[48] Ma Z, Turchi CS. Advanced supercritical carbon dioxide power cycle configurations for use in concentrating solar power systems. In: Supercritical CO_2 power cycle symposium; 2011. p. 1–4, doi:http://dx.doi.org/10.1115/GT2012-68932.

[49] Wright SA, Conboy TM, Rochau GE. High-temperature split-flow recompression Brayton cycle initial test results. Nucl Energy 2012.

[50] Moisseytsev A, Sienicki JJ. Investigation of alternative layouts for the supercritical carbon dioxide Brayton cycle for a sodium-cooled fast reactor. Nucl Eng Des 2009;239:1362–71. http://dx.doi.org/10.1016/j.nucengdes.2009.03.017.

[51] Sabouhi H, Abbaspour A, Fotuhi-Firuzabad M, Dehghanian P. Reliability modeling and availability analysis of combined cycle power plants. Int J Electr Power Energy Syst 2016;79:108–19. http://dx.doi.org/10.1016/j.ijepes.2016.01.007.

[52] Alqahtani BJ, Patiño-Echeverri D. Integrated solar combined cycle power plants: paving the way for thermal solar. Appl Energy 2016;169:927–36. http://dx.doi.org/10.1016/j.apenergy.2016.02.083.
[53] Okoroigwe E, Madhlopa A. An integrated combined cycle system driven by a solar tower: a review. Renew Sustain Energy Rev 2016;57:337–50. http://dx.doi.org/10.1016/j.rser.2015.12.092.
[54] Manente G. High performance integrated solar combined cycles with minimum modifications to the combined cycle power plant design. Energy Convers Manage 2016;111:186–97. http://dx.doi.org/10.1016/j.enconman.2015.12.079.
[55] Li Y, Yang Y. Thermodynamic analysis of a novel integrated solar combined cycle. Appl Energy 2014;122:133–42. http://dx.doi.org/10.1016/j.apenergy.2014.02.017.
[56] Zare V, Hasanzadeh M. Energy and exergy analysis of a closed Brayton cycle-based combined cycle for solar power tower plants. Energy Convers Manage 2016;128:227–37. http://dx.doi.org/10.1016/j.enconman.2016.09.080.
[57] Zarza E, Romero-Alvarez M. Concentrating solar thermal power. Handbook of energy efficient renewable energy. CRC Press; 2007. p. 21–98. http://dx.doi.org/10.1201/9781420003482.ch21.
[58] Siemens. Steam turbines for CSP plants. Siemens AG - Rep 2010;1–16.
[59] Rubin ES, Yeh S, Antes M, Berkenpas M, Davison J. Use of experience curves to estimate the future cost of power plants with CO_2 capture. Int J Greenh Gas Control 2007;1:188–97. http://dx.doi.org/10.1016/S1750-5836(07)00016-3.
[60] BAMMERT K, BOHNENKAMP W, REHWINKEL H. Results of acceptance tests on the blast furnace gas and oil fired Gelsenkirchen gas turbine. Stahl Und Eisen 1971:91.
[61] Bentivoglio F, Tauveron N, Geffraye G, Gentner H. Validation of the CATHARE2 code against experimental data from Brayton-cycle plants. Nucl Eng Des 2008;238:3145–59. http://dx.doi.org/10.1016/j.nucengdes.2007.12.026.
[62] Martynov SB, Daud NK, Mahgerefteh H, Brown S, Porter RTJ. Impact of stream impurities on compressor power requirements for CO_2 pipeline transportation. Int J Greenh Gas Control 2016;54:652–61. http://dx.doi.org/10.1016/j.ijggc.2016.08.010.
[63] Najjar YSH, Zaamout MS. Comparative performance of closed cycle gas turbine engine with heat recovery using different gases. Heat Recover Syst CHP 1992;12:489–95. http://dx.doi.org/10.1016/0890-4332(92)90017-C.
[64] U.S. Energy Information Administration. Cost and performance characteristics of new generating technologies. Annual Energy Outlook; 2016
[65] U.S. Departement of Energy. 2014 SunShot initiative portfolio 2014;232.
[66] Moore J. Development of a high efficiency hot gas turbo-expander and low cost heat exchangers for optimized CSP SCO_2 operation; 2016.
[67] Gangwal S, Muto A. Demonstration of high-temperature calcium-based thermochemical energy storage system for use with concentrating solar power facilities. Sunshot Program Summit 2016. U.S. Department of Energy; 2016.

***ANNEX 7**: Ortiz C, Valverde JM, Chacartegui R, Benítez-Guerrero M, Perejón A, Romeo LM. The Oxy-CaL process: A novel CO_2 capture system by integrating partial oxy-combustion with the Calcium-Looping process. Appl Energy 2017;196:1–17. doi:10.1016/j.apenergy.2017.03.120.*

Applied Energy 196 (2017) 1–17

Contents lists available at ScienceDirect

Applied Energy

journal homepage: www.elsevier.com/locate/apenergy

The Oxy-CaL process: A novel CO_2 capture system by integrating partial oxy-combustion with the Calcium-Looping process

C. Ortiz [a,*], J.M. Valverde [a], R. Chacartegui [b], M. Benítez-Guerrero [a,c], A. Perejón [c,d], L.M. Romeo [e]

[a] Facultad de Física, Universidad de Sevilla, Sevilla, Spain
[b] Escuela Técnica Superior de Ingeniería, Universidad de Sevilla, Sevilla, Spain
[c] Instituto de Ciencia de Materiales de Sevilla (C.S.I.C. – Univ. Sevilla), Sevilla, Spain
[d] Departamento de Química Inorgánica, Facultad de Química, Universidad de Sevilla, Sevilla, Spain
[e] Escuela de Ingeniería y Arquitectura, Departamento de Ingeniería Mecánica, Universidad de Zaragoza, Spain

HIGHLIGHTS

- A novel CO_2 capture process (Oxy-CaL) is proposed.
- Carbonation in the diffusion stage is analyzed by varying the CO_2 concentration.
- Simulation results show that energy consumption in the Oxy-CaL is below of 4 MJ/kg.
- Smaller amounts of solids inventory are needed in the Oxy-CaL system.

ARTICLE INFO

Article history:
Received 12 December 2016
Received in revised form 3 March 2017
Accepted 24 March 2017
Available online 3 April 2017

Keywords:
Calcium-Looping
Oxy-combustion
CCS
SPECCA

ABSTRACT

This paper proposes a novel CO_2 capture technology from the integration of partial oxy-combustion and the Calcium-Looping capture process based on the multicycle carbonation/calcination of limestone derived CaO. The concentration of CO_2 in the carbonator reactor is increased by means of partial oxy-combustion, which enhances the multicycle CaO conversion according to thermogravimetric analysis results carried out in our work, thus improving the CO_2 capture efficiency. On the other hand, energy consumption for partial oxy-combustion is substantially reduced as compared to total oxy-combustion. All in all, process simulations indicate that the integration of both processes has potential advantages mainly regarding power plant flexibility whereas the overall energy penalty is not increased. Thus, the resulting energy consumption per kilogram of CO_2 avoided is kept smaller than 4 MJ/kg CO_2, which remains below the typical values reported for total oxy-combustion and amine based CO_2 capture systems whereas CO_2 capture efficiency is enhanced in comparison with the Calcium-Looping process.

1. Introduction

Carbon Capture and Storage (CCS) is considered as one key short to médium-term measure to mitigate global warming [1,2]. In order to achieve a commercial deployment of post-combustion CO_2 capture in fossil fuel power plants, several technologies are being analyzed aimed mainly at maximizing the capture efficiency while energy penalty and capital cost are minimized [3,4]. Among diverse possibilities, already commercial amine-based capture systems and the Calcium-Looping (CaL) process, currently under pilot-scale stage, have attracted a great deal of attention in the last years [5,6]. Although CO_2 capture by using MEA (monoethanolamine) is an industrial mature process, its commercial deployment as post-combustion CO_2 capture technology is hampered by the high energy penalty (8–12%) mainly due to sorbent regeneration [7–9], amine toxicity [10] and degradation [11].

The CaL process is based on the carbonation/calcination reaction of solid CaO particles, which is carried out in two interconnected circulating fluidized bed (CFB) reactors [12]. This second generation capture technology has several potential advantages when compared with amine-based process such as a lower energy penalty over the power plant (4–9%) [6], higher CO_2 capture efficiency (above 90%) and the use of low cost, widely available and non-toxic natural minerals as CaO precursors such as limestone or dolomite [13]. Even though several pilot scale plants ($\sim$1–2 MW_{th}) are already showing promising results [14,15] the CaL technology has not reached a demonstration stage yet. The

* Corresponding author.
E-mail address: cortiz7@us.es (C. Ortiz).

http://dx.doi.org/10.1016/j.apenergy.2017.03.120
0306-2619/

Nomenclature

$[CO_2]$	average CO_2 concentration, mol/m^3
$[CO_2]_{eq}$	equilibrium concentration of CO_2, mol/m^3
D^*_{eff}	equivalent diffusion constant, m^3/(mol·s)
E	emissions ratio after CO2 capture, kg CO_2/kW he
E_{CO2}	carbon capture efficiency
E_{ref}	emissions ratio before CaL, kg CO_2/kW he
E_{max}	maximum capture efficiency
F_{CO2}	mole flow rate of CO_2 in flue gas entering the carbonator, kmol/h
F_O	mole flow rate of fresh makeup limestone, kmol/h
F_R	mole flow rate of CO_2 in flue gas entering the carbonator, kmol/h
F_{fg}	flue gas molar flow rate, kmol/s
FRP	fast reaction controlled phase
SDP	solid-state diffusion controlled phase
k_s	intrinsic kinetic constant m^4/(mol·s)
k	deactivation constant of a sorbent particle
$\dot{m}$	mass flow, kg/s
$\dot{m}_{CO2,calc}$	CO_2 mass flow exiting the calciner, kg/s
$\dot{m}_{gas,calc}$	total gas mass flow exiting the calciner, kg/s
N_{Ca}	mol of Ca in the carbonator, mol
P	pressure, bar
P_{vv}	live steam pressure, bar
$P_{HE,solids}$	solid-solid thermal power exchanged, MW
$SPECCA$	energy consumption for kg CO_2 avoided, MJ/kg CO_2
$r_{ave,SDP}$	average reaction rate in the diffusion regime, s^{-1}
$r_{ave,FRP}$	average reaction rate in the kinetic regime, s^{-1}
S_{ave}	average surface area available for reaction, m^{-1}
t	time, s
T_{calc}	calciner temperature, °C
T_{carb}	carbonator temperature, °C
T_{vv}	live steam temperature, °C
t_0	time lag of TGA multicycle test, s
t_{FRP}	time of the carbonation fast phase, s
t_{max}	total carbonation time, s
v_{CO2}	CO_2 v/v concentration at CFPP outlet
v_{O2}	O_2 v/v concentration at CFPP outlet
W_s	solid inventory in the carbonator per MW of a typical power plant, kg
$\dot{W}_{ASU}$	power consumption in the ASU, MW
$\dot{W}_{sec}$	net power production in secondary steam cycle, MW
$\dot{W}_{comp,CO2}$	power consumption in CO_2 compression, MW
$\dot{W}_{comp,fg}$	power consumption in flue gas compression, MW
$\dot{W}_{solid}$	power consumption in solids transport, MW
X	carbonation degree of CaO
X_{ave}	average conversion of the sorbent
$X_{ave,SDP}$	average conversion of the sorbent in the diffusion phase
$X_{ave,FRP}$	average conversion of the sorbent in the kinetic phase
W_s	solid inventory in the carbonator per MW of a typical power plant, kg
x_{CO2}	CO_2 molar fraction exiting the plant
x_{O2}	O_2 molar fraction exiting the plant
$y_{CO2,in}$	CO_2 molar fraction at carbonator inlet
$y_{CO2,eq}$	CO_2 molar fraction at carbonation equilibrium
η_{boiler}	boiler efficiency
η_{CFPP}	coal fire power plant efficiency
η_{ref}	reference plant efficiency
η_{int}	new global efficiency (CFPP-capture system)
τ	average residence time in the carbonator, s

main causes that hinder such step forward are linked to the excessively large size of the capture system (carbonator reactor height ~40 m; carbonator solids inventory ~400 ton; additional coal consumption for CO_2 capture ~45–55%), which increases significantly both capital and operating costs (CAPEX and OPEX) for power generation [16,17].

Another interesting possibility to mitigate CO_2 emissions from power plants is the oxy-combustion technology, which has been successfully demonstrated in large-scale pilot projects (30 MW_e) [18–20]. Essentially, oxy-combustion consists of replacing air by pure O_2 (mixed with CO_2-rich flue gas recycled) as combustion gas, which yields a highly-concentrated CO_2 flue gas stream. After purification, the CO_2 stream (~95% vol) is suitable for compression and storage or utilization [21]. The main drawback for the large-scale deployment of oxy-combustion is the high energy consumption for pure O_2 production in the cryogenic Air Separation Unit (ASU), which causes an energy penalty in the range of 7–13% [22,23] or, equivalently, over 20% additional fuel consumption for power production.

In this paper a novel system (Oxy-CaL) for CO_2 capture is investigated based on the combination of partial oxy-combustion and the CaL process with the goal of exploiting the synergies between such technologies. Basically, Oxy-CaL consists of carrying out a partial oxy-combustion process to produce a flue gas with a CO_2 concentration in the range 30–60% vol, which is then sent to the CaL capture process. In a similar way, other authors have analyzed the integration of partial oxy-combustion and MEA [24], which is expected to help mitigating MEA degradation and energy consumption.

The manuscript starts by showing experimental results from a thermo-gravimetric analysis (TGA) on the multicycle conversion of limestone derived CaO under realistic calcination conditions (high temperature and high CO_2 concentration). In these TGA tests, the CO_2 concentration in the carbonation environment was varied in the range 15–60% vol in order to address the effect of an excess of CO_2 in the carbonator over the typical vol% in the flue gas at typical combustion conditions (~15%). Moreover, the carbonation temperature was varied in the range 625–680 °C, which affects critically the carbonation kinetics in the solid-state diffusion-controlled stage as will be seen. These TGA results are used afterwards in the Oxy-CaL integration model to calculate the CO_2 capture efficiency from process simulations. The energy penalty arising from the diverse CO_2 capture technologies considered (total oxy-combustion, CaL and Oxy-CaL) is analyzed. Finally, the oxy-CaL performance is assessed and compared with those of other CO_2 capture systems.

Our results show that the Oxy-CaL system is a promising hybrid concept to be implemented in new power plants, allowing for a substantial reduction of energy penalty as compared to total oxy-fuel combustion. Moreover, the Oxy-CaL system leads to a high CO_2 capture efficiency in comparison with the CaL process, which would serve to reduce significantly the carbonator reactor size.

2. Thermogravimetric analysis

2.1. Materials and methods

The material employed in this work was natural limestone of high purity (99.6%wt $CaCO_3$), received from Segura S.L (Matagallar quarry, Pedrera, Spain). Carbonation/calcination multicycle tests were carried out using a thermogravimetric analyzer TGA Discovery (TA Instruments 2011) equipped with an infrared halogen lamp

furnace wherein the lamps are placed symmetrically with respect to a SiC enclosure to minimize undesired heat transfer phenomena. This setup allows for high heating/cooling rates (300 °C/min), which is a necessary requirement to mimic realistic conditions in the CaL process where the solids are rapidly circulated between the reactors. The TGA instrument is also equipped with a high sensitivity balance (<0.1 μg) characterized by a small baseline dynamic drift (<10 μg). A thermocouple is located close to the sample and underneath it for a reliable measurement and control of temperature in the sample.

TGA experiments consisted of 20 carbonation/calcination cycles preceded by a calcination of the sample at 950 °C for 5 min under a 30% air/70% CO_2 vol/vol. atmosphere. Then, the temperature was decreased at 300 °C/min to introduce the carbonation stage at the desired temperature and under a given CO_2/air mixture. After that, the sample was calcined for CaO regeneration by quickly increasing the temperature at 300 °C/min to 950 °C under a high CO_2 concentration environment (30% air/70% CO_2 vol/vol.) as representative in the calciner environment [25,26]. Short residence times of 5 min for both calcination and carbonation stages have been employed as corresponds to realistic conditions. In order to mimic the integration of the CaL process with oxy-fuel combustion (Oxy-CaL), four different CO_2/air mixtures were tested for the carbonation stage: 15% CO_2/85% air, 30% CO_2/70% air, 45% CO_2/55% air and 60% CO_2/40% air (vol/vol). Three different carbonation temperatures (625 °C, 650 °C and 680 °C) were used. Tests are labeled as CaL-T for those in which carbonation was performed under 15% CO_2, where T stands for the carbonation temperature, and Oxy-CaL-vol-T, where vol is the vol% of CO_2 in the CO_2/air mixture and T is the carbonation temperature. Samples of small and fixed mass (~10 mg) were employed to avoid mass transfer resistance within the sample. Intraparticle pore diffusion limitations on the reaction rate were mitigated by using particles of size below 100 μm [27,28].

2.2. Experimental results and discussion

Fig. 1 shows examples of thermograms obtained for the 1st (Fig. 1a) and 20th (Fig. 1b) carbonation/calcination cycles under CaL (15% vol CO_2 carbonation) and Oxy-CaL (30%, 45% and 60%

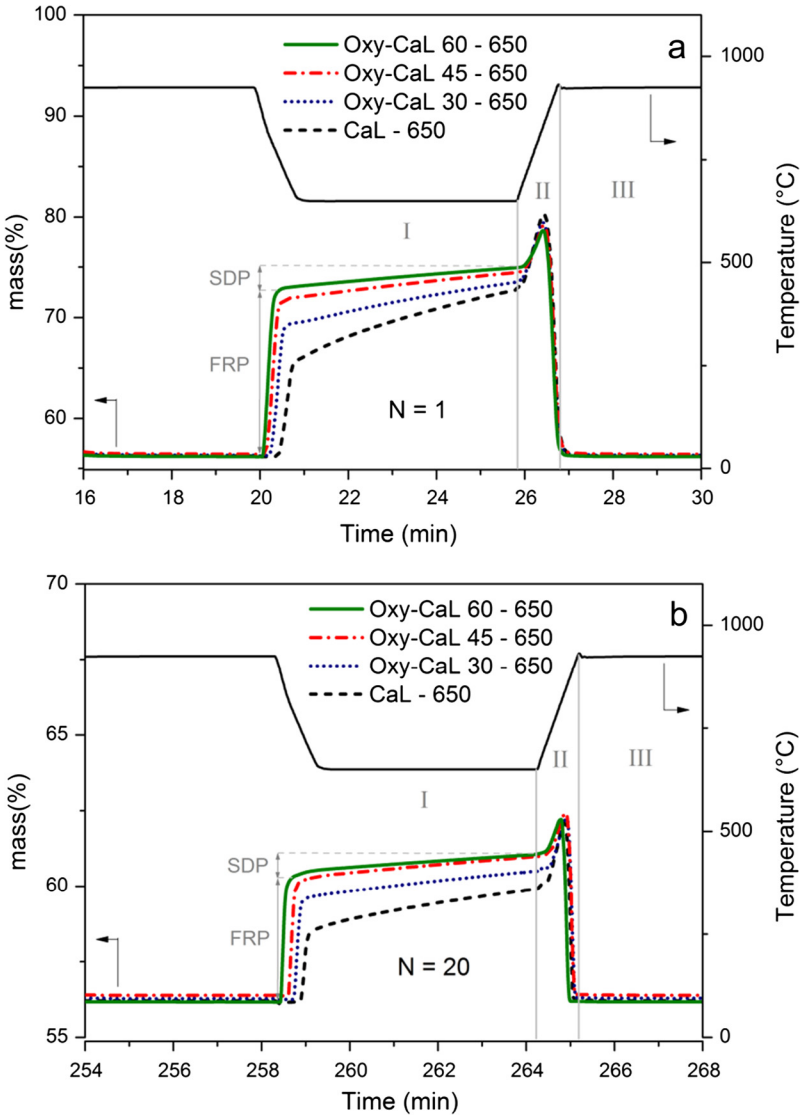

Fig. 1. Time evolution of the sorbent mass % during the carbonation and calcination stages in the (a) 1st cycle (N = 1) and (b) 20th cycle (N = 20) for limestone tested under CaL (15% vol CO_2 carbonation) and Oxy-CaL (30%, 45%, 60% vol CO_2 carbonation) conditions. Carbonation temperature is fixed to 650 °C. I indicates the carbonation stage, II the transition stage and III the calcination stage. Mass gain in the two phases of carbonation (fast reaction-controlled phase FRP and solid-state diffusion controlled phase SDP) are indicated.

vol CO_2 carbonation) conditions. These thermograms show the time evolution of temperature and sample mass% along the cycles and demonstrate an important effect of raising the carbonation CO_2 vol concentration on the reaction kinetics. As well-known from previous studies CaO carbonation is seen to take place along two well-differentiated stages [29–31]. The first stage consists of a reaction-controlled fast phase on the surface of the particles that ends up when a 30–50 nm thick carbonate layer is built up on the CaO surface [29]. This first phase is followed up by a second slower phase limited by the solid-state diffusion of CO_3^{2-} mobile ions and counter-current diffusion of O^{2-} anions across the $CaCO_3$ product layer [31,32].

As may be seen in Fig. 1, carbonation in the fast phase is markedly enhanced as the CO_2 concentration is increased, whereas, on the contrary, solid-state diffusion-controlled carbonation is markedly hindered. Thus, carbonation in the diffusion-controlled stage contributes significantly to the overall capture capacity under CaL conditions but loses relevancy as the CO_2 vol% is increased. As will be seen from process simulations this effect on the carbonation kinetics has remarkable implications on the role of key process operation parameters such as the solids residence time in the carbonator.

Fig. 2a shows the thermograms corresponding to the 1st cycle obtained from TGA tests performed at different carbonation temperatures (625, 650 and 680 °C) under CaL conditions (15% vol CO_2 carbonation). As may be observed, a variation of just about 25 °C around the typical carbonation temperature used in pilot-scale plants (~650 °C) has a significant effect on the CO_2 uptake in the diffusion-controlled stage, which notably affects the overall capture capacity. Thus, carbonation in this phase is enhanced with temperature while a decrease of the carbonation temperature yields a rapid decay of the carbonation rate in this solid-state diffusion-controlled stage. This result is consistent with the strong dependence on temperature measured elsewhere for C^{14} isotope diffusivity in CaO and for the effective product layer diffusivity of CO_3^{2-} mobile ions in the range of carbonation temperatures used in our work [30,33]. A similar behavior has been observed for the samples tested under Oxy-CaL conditions. Nonetheless, the variation with the temperature of the CO_2 capture capacity in the diffusion-controlled stage plays a relatively minor role on the overall capture capacity under Oxy-CaL conditions as compared to CaL conditions. This may be seen in Fig. 2b, which shows the 1st cycle of the thermograms obtained under different carbonation temperatures for the sample tested under Oxy-CaL 45 conditions.

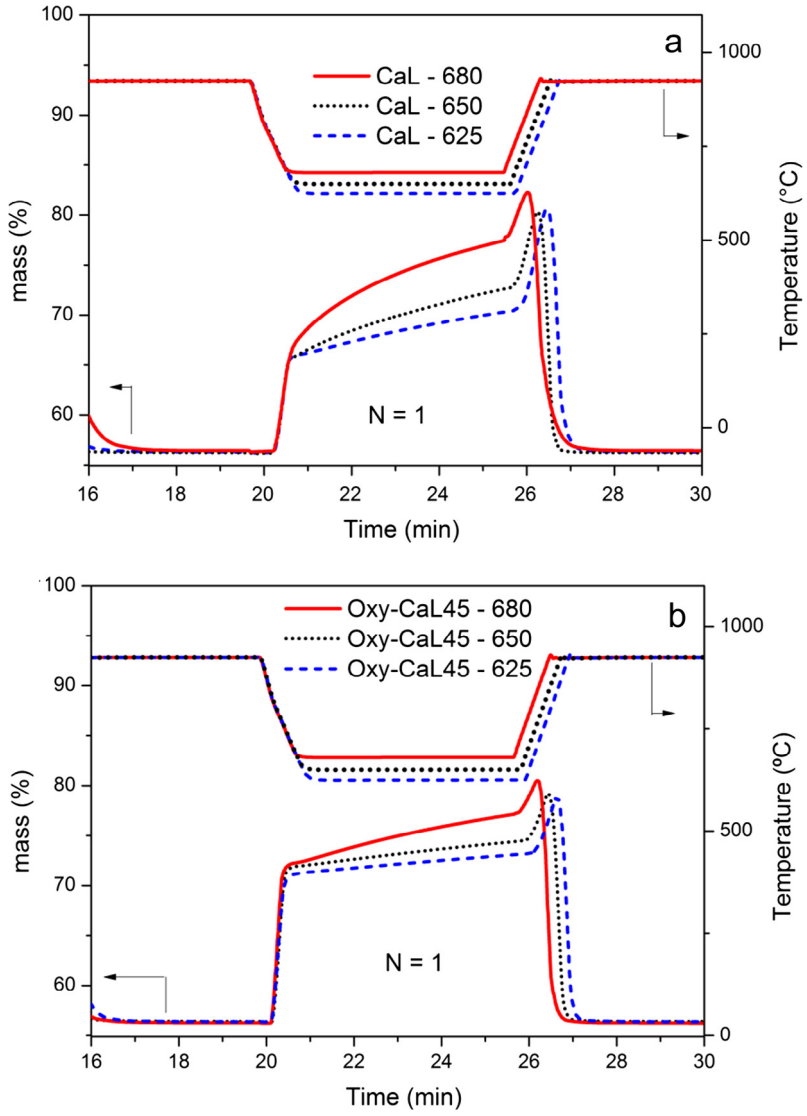

Fig. 2. Time evolution of the sorbent mass % during the 1st cycle (N = 1) for limestone under (a) CaL (15% vol CO_2 carbonation) and (b) Oxy-CaL 45 (45% vol CO_2 carbonation) conditions for different carbonation temperatures (625 °C, 650 °C and 680 °C) as indicated.

The parameter used to compare the multicycle capture performance of limestone under CaL and Oxy-CaL conditions is CaO conversion, defined as the ratio of CaO mass converted to $CaCO_3$ in the carbonation stage of each cycle to the sorbent mass before carbonation. Multicycle CaO conversion data can be generally well fitted by the following semi-empirical equation [6,34,35]:

$$X_N = X_r + \frac{X_1}{k(N-1) + \left(1 - \frac{X_r}{X_1}\right)^{-1}}; \quad (N = 1, 2, \ldots.) \tag{1}$$

where N is the cycle number, X_1 is CaO conversion at the first cycle, k is the deactivation rate constant and X_r is the residual CaO conversion. Fig. 3a shows multicycle CaO conversion data and best fit curves from Eq. (1) for the samples tested under CaL and Oxy-CaL conditions for a carbonation temperature of 650 °C. Best fitting parameters are summarized in Table 1. As well known, CaO conversion decreases progressively with the cycle number due to enhanced grain sintering in the calcination stage at high temperature and under high CO_2 partial pressure [6,36,37], which reduces the CaO surface area available for fast carbonation in each cycle. Note however, that the deactivation rate is decreased as the CO_2 concentration in the carbonation stage is increased. Thus, the residual conversion X_r takes values of 0.062, 0.070, 0.076 and 0.081 for the samples tested under CaL-650, Oxy-CaL 30-650, Oxy-CaL 45-650 and Oxy-CaL 60-650 conditions, respectively.

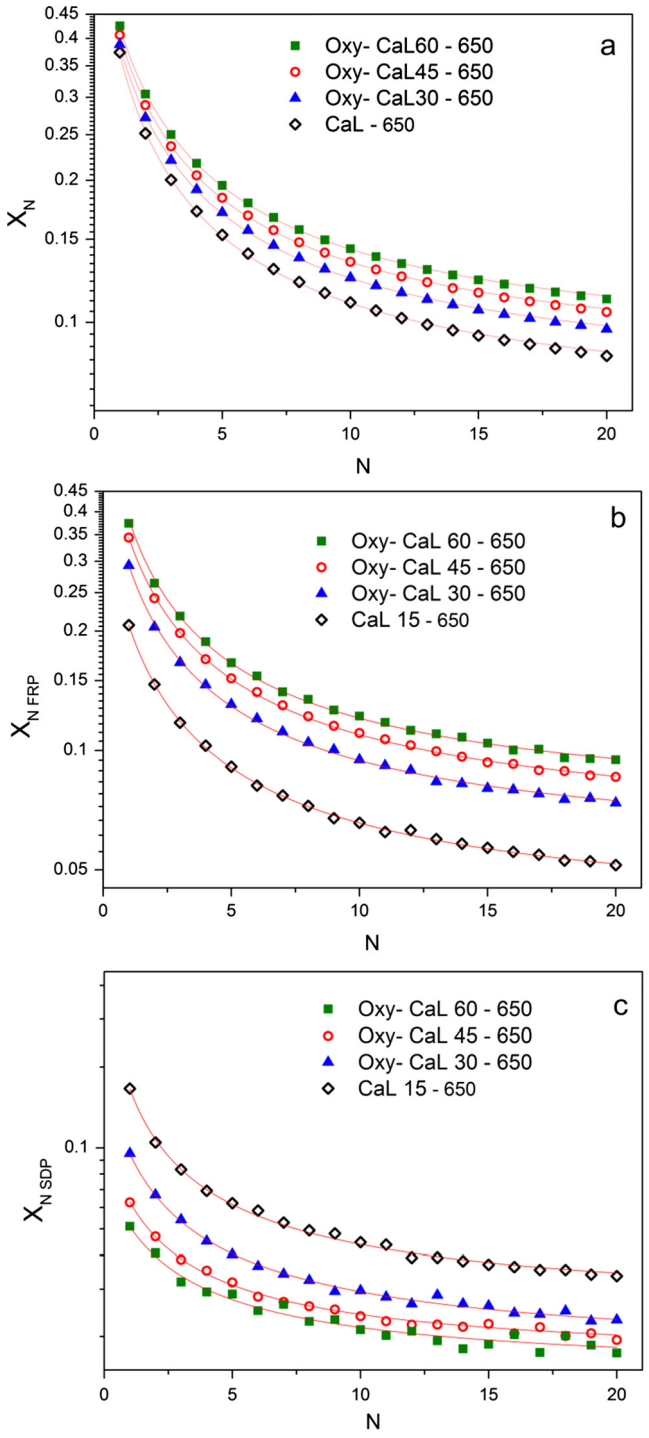

Fig. 3. (a) CaO conversion versus cycle number for carbonation/calcination tests carried out under CaL and Oxy-CaL conditions. (b) Conversion in the fast reaction controlled phase. (c) Conversion in the solid-state diffusion controlled phase. Carbonation is carried out at 650 °C under 15% vol CO_2 (CaL) and 30% vol, 45%CO_2 and 60% vol CO_2 for the Oxy-CaL tests as indicated. Calcination in all the tests is performed at 950 °C (70% CO_2/30% air vol/vol). Solids lines are the best fits of equation 1 to data.

The relative contributions to the overall CaO conversion of carbonation in the fast reaction controlled phase (FRP) and in the solid-state diffusion controlled phase (SDP) have been analyzed by extracting from the thermograms the values of CaO conversion in each one of these phases (X_{FRP} and X_{SDP}, respectively, see Fig. 1a). Data on X_{FRP} and X_{SDP} are shown in Fig. 3b and c, respectively. As was inferred from Fig. 2, it is seen that X_{FRP} becomes increasingly relevant while X_{SDP} is decreased as the CO_2 concentration in the carbonation environment is increased.

The effect of varying the carbonation temperature around 650 °C on the multicycle CaO conversion performance for the different CaL and Oxy-CaL conditions was also investigated in our work. Data on the multicycle CaO conversion (X_N, X_{FRP} and X_{SDP}) for the tests carried out under CaL and Oxy-CaL-45 conditions at 625, 650 and 680 °C are given in Appendix A. The results show that the overall conversion increases with the carbonation temperature while conversion in the fast reaction controlled phase is essentially independent of the carbonation temperature in the range of temperatures tested. The main effect of varying the carbonation temperature in that range is therefore observed on conversion in the solid-state diffusion controlled phase, which is significantly enhanced with the carbonation temperature (see Fig. 15c and f in Appendix A).

3. The Oxy-CaL process

3.1. Description

The Oxy-CaL process newly proposed in the present manuscript is a CO_2 capture hybrid system based on the combined use of partial oxy-combustion and the CaL capture process. The basic idea behind Oxy-CaL is to exploit the enhancement of CO_2 capture capacity in the CaL process as the CO_2 concentration in the carbonation environment is increased (as seen above from the TGA tests) whereas the energy penalty for partial oxy-combustion to increase the CO_2 concentration in the flue gas is notably reduced as compared to total oxy-combustion. Fig. 4 shows a schematic representation of this integration as applied to CO_2 capture in a coal fired power plant (CFPP).

As can be seen in Fig. 4, the Oxy-CaL process is initiated by partial oxy-combustion of coal using to this end a mixture of air, nearly pure oxygen (purity ≥95%) and CO_2-enriched recycled flue gas at combustor temperatures between 850 °C and 950 °C. As a result, the flue gas stream exiting the boiler reaches a CO_2 vol concentration in the range 30–60% (depending on the air/O_2/CO_2 mixture composition) instead of the typical 15% vol concentration obtained from combustion with just air. The heat released by

Table 1
Values of the deactivation rate constant κ and residual conversion X_r obtained from the best fits of Eq. (1) to TGA experimental data for carbonation at different CO_2 concentrations (15% vol in the CaL tests; 30%, 45%, and 60% vol in the Oxy-CaL tests).

		CaL-650	Oxy-CaL30-650	Oxy-CaL45-650	Oxy-CaL60-650
X_N	X_1	0.373	0.388	0.407	0.425
	κ	0.731	0.667	0.651	0.633
	X_r	0.061	0.070	0.076	0.081
	R_{sqr}	0.999	0.999	0.999	0.999
X_{FRP}	X_1	0.207	0.293	0.344	0.374
	κ	0.660	0.661	0.641	0.674
	X_r	0.037	0.053	0.060	0.068
	R_{sqr}	0.999	0.999	0.999	0.998
X_{SDP}	X_1	0.166	0.095	0.063	0.051
	κ	0.828	0.686	0.711	0.633
	X_r	0.025	0.016	0.016	0.014
	R_{sqr}	0.998	0.998	0.993	0.980

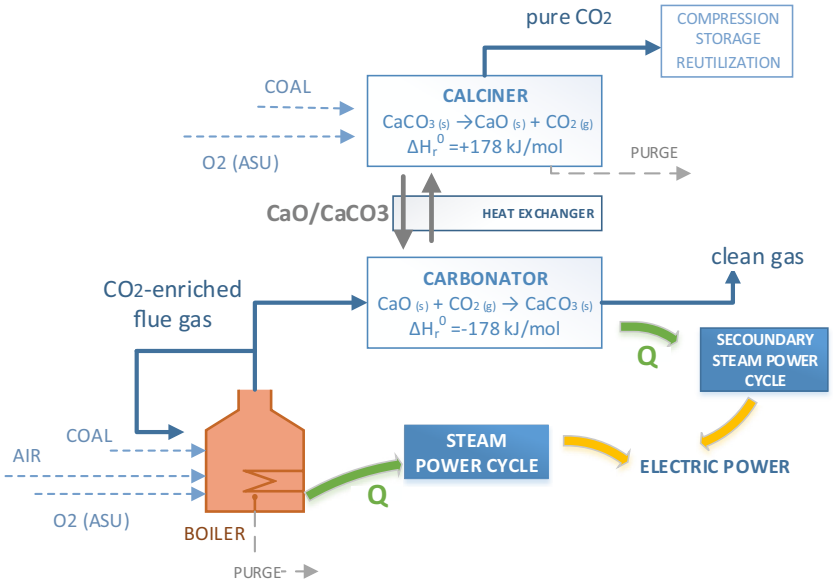

Fig. 4. Oxy-CaL process schematics.

combustion is used for electric power production by means of a steam power cycle. Once partial oxy-combustion is carried out, the CO_2-enriched flue gas is sent to the CaL process. The CO_2 present in the flue gas reacts in the carbonator with a fluidized bed of CaO particles at temperatures around 650 °C. The carbonated particles are then circulated to the calciner reactor in which fast decomposition of $CaCO_3$ occurs to regenerate the CaO solids and produce a rich CO_2 stream ready to be compressed and transported for storage or other uses.

3.2. CO_2 capture efficiency (carbonator model)

The CO_2 capture efficiency in the CaL process will be analysed by means of the carbonator model described in detail elsewhere [38]. Accordingly, the CO_2 capture efficiency can be expressed as a function of the total solids inventory in the carbonator (W_s), or the moles number of Ca-based solids (N_{Ca}), the CaO/$CaCO_3$ particles residence time in the carbonator (τ) and the makeup flow of fresh limestone fed into the system (F_0). In this model an average CaO conversion (X_{ave}) is defined by the sum of the average conversion in the fast reaction-controlled phase ($X_{ave,FRP}$) and conversion in the solid-state diffusion controlled phase ($X_{ave,SDP}$), where both $X_{ave,FRP}$ and $X_{ave,SDP}$ are calculated by assuming that the gas passes in plug flow across a bed of perfectly mixed solids in the carbonator. The interested reader may see the work of Ortiz et al. [38] for an extended description on the carbonator model.

According to this carbonator model, the average reaction rates in the FRP and SDP phases are expressed as:

$$r_{ave_{FRP}} = \frac{X_{ave_{FRP}}}{t_{FRP}} \; for \; t \leqslant t_{FRP} \tag{2}$$

$$r_{ave_{SDP}} = \frac{X_{ave_{SDP}}}{t_0 - t_{FRP}} \; for \; t_{FRP} < t \leqslant t_{max} \tag{3}$$

where $r_{ave,_i}$ is the average reaction rate in the i-phase (either FRP or SDP), t_{FRP} is the time lag of the FRP phase, t_{max} is total carbonation time, $X_{ave,i}$ is the average capture capacity in the i-phase, and t_0 is the overall carbonation time lag in the carbonation TGA test (Section 2).

The average rate of CaO conversion in the kinetically controlled fast phase ($r_{ave_{FRP}}$) at atmospheric pressure can be approximated by a first-order kinetic law [30]:

$$r_{ave_{FRP}} = k_s S_{ave} (1 - X)^{\frac{2}{3}} ([CO_2] - [CO_2]_{eq}) \tag{4}$$

where $[CO_2]$ and $[CO_2]_{eq}$ are the actual and equilibrium CO_2 concentrations, respectively, k_s is the kinetic constant and S_{ave} is the average CaO specific surface area available for reaction after N cycles.

Table 2
Kinetic model parameters obtained from the best fits of Eqs. (4) and (5) to experimental TGA data.

	k_s $(\times 10^{10})$ $\left[\frac{m^4}{mol \cdot s}\right]$	D^*_{eff} $(\times 10^{5})$ $\left[\frac{m^3}{mol \cdot s}\right]$
CaL-625	8.87	2.70
CaL-650	10.00	4.63
CaL-680	12.27	8.09
Oxy-CaL30-625	4.429	1.07
Oxy-CaL30-650	6.08	1.61
Oxy-CaL30-680	4.51	2.75
Oxy-CaL45-625	3.21	0.61
Oxy-CaL45-650	3.60	1.02
Oxy-CaL45-680	2.75	1.68
Oxy-CaL60-625	2.00	0.61
Oxy-CaL60-650	2.38	0.71
Oxy-CaL60-680	1.98	1.10

On the other hand, the average rate of CaO conversion in the diffusion controlled phase can be expressed by means of an effective diffusion constant (D^*_{eff}) [38].

$$r_{ave_{SDP}} \approx D^*_{eff}([CO_2] - [CO_2]_{eq}) \quad (5)$$

Both Eqs. (4) and (5) can be well fitted to the experimental TGA data shown above, which allows us obtaining the values of k_s and D^*_{eff} to be used in the kinetic model for each one of the CaL and oxy-CaL systems considered. Values of best fitting parameters are shown in Table 2.

Once the average CaO conversion is calculated, the capture efficiency in the carbonator (E_{CO2}) can be obtained as:

$$E_{CO2} = \frac{F_R}{F_{CO2}} X_{ave} \quad (6)$$

where F_R is the solids recirculation flow rate between the carbonator and calciner reactors, which is given by $F_R = W_s/N_{Ca}$.

Fig. 5 shows the evolution of the CO_2 capture efficiency (E_{CO2}) as the solids recirculation flow rate between reactors is decreased or, equivalently, the solids residence time in the carbonator $(\tau = N_{Ca}/F_R)$ is increased. As may be seen, a significantly higher capture efficiency is achieved by increasing the CO_2 concentration in the carbonator in the Oxy-CaL systems. Note the differences on the maximum capture efficiency $(E_{max} = (y_{CO2,in} - y_{eq})/y_{CO2,in})$ for the different systems (obtained for very short residence times) as a consequence of the variation of the CO_2 vol% in the carbonator. Even though the use of short residence times leads to relatively high capture efficiencies it must be kept in mind that short residence times would rise the cost for solids transportation. The sensible heat needed to increase the temperature of the solids stream entering the calciner would be also raised as the solids recirculation rate is increased to achieve short residence times.

A shown in Fig. 5, the capture efficiency is decreased as the solids residence time in the carbonator is prolonged albeit at a minor rate for the CaL process in comparison with the Oxy-CaL systems. This is due to the relatively higher conversion in the solid-state diffusion controlled phase for the CaL process (as seen above from the TGA tests). This result becomes more marked as the carbonator temperature is increased (compare Fig. 5a and c) as a consequence of the enhancement of solid-state diffusivity with temperature. The results obtained up to this point show already some hints concerning the CFPP-CO_2 capture integration. An increase in the solids residence time in the carbonator would arguably allow for a reduction of the energy penalty although the capture efficiency would be hampered depending on the capture system. Thus, a comparative assessment of the diverse capture systems and their integration into CFFP must necessarily include an evaluation of the energy penalty. This will be the subject of the next section.

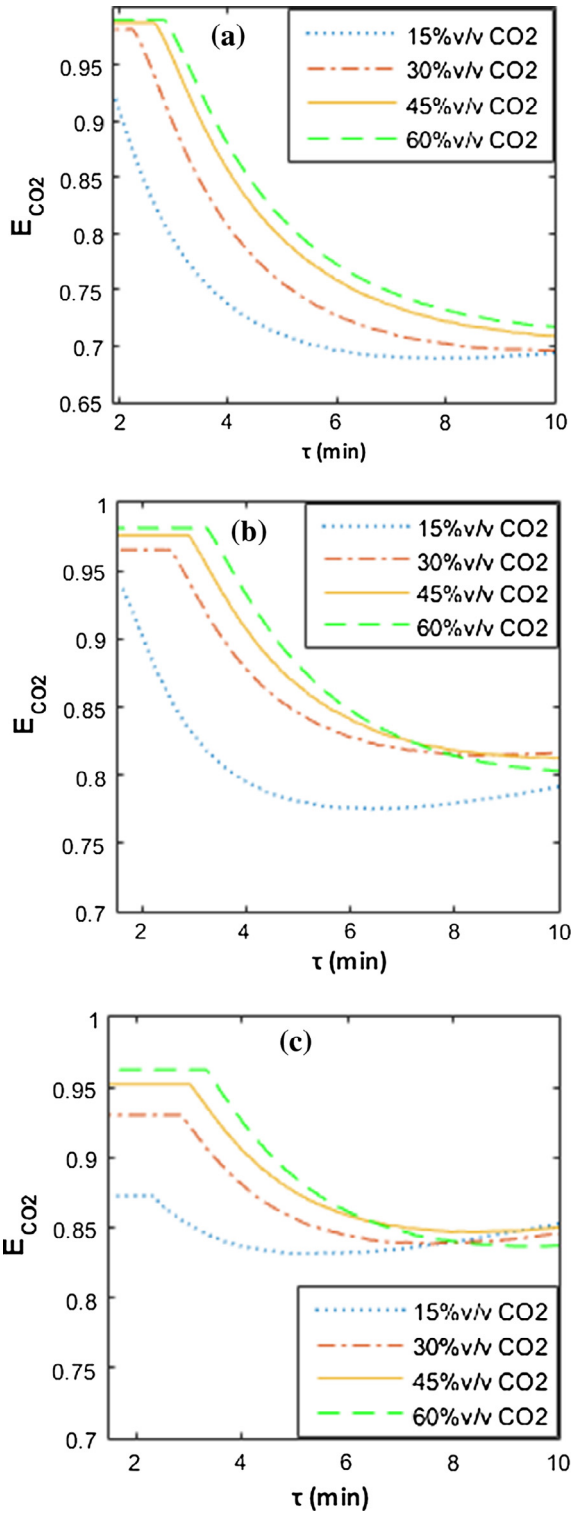

Fig. 5. CO_2 capture efficiency as a function of the residence time in the carbonator, which is varied by changing the F_R/F_{CO2} ratio. Calculations are made for fixed values of the solids inventory $W_s = 400$ ton and $F_0/F_{CO2} = 0.05$ and different carbonation temperatures. (a) $T_{carb} = 625$ °C; (b) $T_{carb} = 650$ °C and (c) $T_{carb} = 680$ °C.

4. CFPP-CO_2 capture integration models

This section is devoted to a comparative assessment of several CO_2 capture technologies, namely oxy-combustion, CaL and Oxy-CaL, and their integration into a Coal Fired Power Plant (CFPP). Regarding energy penalty, the parameter usually employed in the

Table 3
Main inputs and results for the base case of diverse CO_2 capture systems.

	Parameter	Reference CFFP (air combustion)	Case a	Case b	Case c		
			Oxy-combustion	CaL	Oxy-CaL 30	Oxy-CaL 45	Oxy-CaL 60
CFPP	$\dot{m}_{coal}$ (kg/s)	42.20	55.05	42.20	46.10	47.50	48.15
	$\dot{m}_{air}$ (kg/s)	475	–	475	208.90	100.20	43.54
	$\dot{m}_{O2}$ (kg/s)	–	136.91	–	68.85	96.35	110.503
	v_{CO2}	0.15	0.89	0.15	0.30	0.45	0.60
	η_{CFPP}	0.3777	0.2872	0.3777	0.3517	0.3437	0.3374
	network (MW)	490.47	488.80	490.47	498.30	502.30	499.75
	Penalty	–	**9.05%**	**–**	**2.60%**	**3.40%**	**4.03%**
	SPECCA (MJ/kg$_{CO2}$)	–	**4.06**	**–**	**0.94**	**1.25**	**1.50**
CaL	T_{calc} (°C)	–	–	950	950	950	950
	T_{carb} (°C)	–	–	650	650	650	650
	E_{CO2}	–		0.827	0.950	0.976	0.981
	$\dot{m}_{coal}$ (kg/s)	–	–	18.48	22.34	23.40	23.84
	$\dot{m}_{O2}$ (kg/s)	–	–	48.00	58.41	61.00	62.49
	$\dot{W}_{sec}$ (MW)	–	–	75.80	113.90	126.46	130.88
	η_{int}	–	–	0.3030	0.2909	0.2882	0.2853
	Penalty	–	–	**7.47%**	**6.08%**	**5.55%**	**5.21%**
	SPECCA (MJ/kg$_{CO2}$)	–	–	**3.28**	**2.63**	**2.37**	**2.29**
Total	$\dot{m}_{coal.total}$	–	–	60.68	68.44	70.90	71.99
	$Penalty_{total}$	–	**9.05%**	**7.47%**	**8.68%**	**8.95%**	**9.24%**
	$SPECCA_{total}$ (MJ/kg$_{CO2}$)	–	**4.06**	**3.28**	**3.56**	**3.62**	**3.79**

Bold indicate the most relevant values.

literature is the specific energy consumption for CO_2 avoided (SPECCA) [7], which quantifies the additional fuel consumption (in MJ) needed to avoid the emission of 1 kg of CO_2 into the atmosphere (Eq. (6)).

$$\text{SPECCA } [\text{MJ/kg}_{CO_2}] = 3600\frac{\frac{1}{\eta_{plant}} - \frac{1}{\eta_{ref}}}{E_{ref} - E} \tag{7}$$

where η_{ref}, η_{plant} are the CFPP efficiency, and E_{ref}, E are the emissions ratio (in kg CO_2/kW h_e) without and with the capture system integrated, respectively.

A 490 MW_e CFPP has been chosen in our work as reference plant, which is modelled using the commercial software ASPEN PLUS™. The main model assumptions are summarized as follows: (i) the system operates at steady conditions; (ii) minimum temperature difference is 20 °C for all heat exchangers; (iii) ideal behavior of cyclones; (iv) solid–solid heat exchange is simulated as a transfer of heat between solids; (v) 89% isentropic efficiencies are assumed as constant for all turbomachinery. In this CFPP, air-combustion of 42.2 kg/s of coal Pittsburgh No. 8 (see [39] for coal type details) takes place in the steam boiler (operating at an average temperature of 900 °C) to generate 1297 MW_{th}, which releases to the atmosphere 513.4 kg/s of flue gas with a CO_2 vol concentration of 15% at atmospheric pressure. Electric power is produced by means of a reheat supercritical steam cycle (P_{vv} = 290 bar, T_{vv} = 600/620 °C), wherein the steam regenerative process is carried out from four feed-water heaters, one of which is a total mixer exchanger type (degasifier). Selected conditions lead to a 44% thermal to electric net efficiency. Taking into account parasitic electricity, the overall net efficiency drops to 37.77%. This value will be used as a reference to calculate the penalty arising from the integration in this plant of the diverse CO_2 capture systems. Main inputs and results from the reference plant model are summarized in Table 3. An extended table showing additional parameters is given in Appendix B. Table 3 shows main inputs and derived outputs for the three cases analyzed in this section: oxy-combustion (case a), calcium looping (case b) and hybrid combinations of both (case c) with different values of CO_2 in vol%. A detailed description is given below.

4.1. Total Oxy-combustion

Firstly, an oxy-fuel combustion process will be analyzed in order to assess the CO_2 capture efficiency and the energy consumption in comparison with the above-mentioned reference plant. The CFPP oxy-combustion model has been developed using ASPEN PLUS™ and the same coal (Pittsburgh No. 8). Fig. 6 shows a flow diagram of the oxy-combustion model that highlights the differences with respect to the reference air-combustion plant. For simulating coal oxy-combustion a reactor model based on Gibbs' free energy minimization method is used.

In this CFPP oxy-combustion case, combustion of 55.3 kg/s of coal Pittsburgh No. 8 with 137.6 kg/s of a high purity (95%) O_2 stream from ASU releases 187.8 kg/s of flue gas with a CO_2 vol concentration (dry-basis) of 89% at atmospheric pressure, which, after purification and compression, is ready to be stored [40] or used in other industrial processes [41,42]. A flue gas recirculation with a recycle ratio of 0.78 is carried out in order to control the flame temperature in the boiler [43]. A compressor (C1 in the figure) is used to overcome the pressure drop in the reactor. ASU energy consumption has been estimated as 200 kW h per kg of pure O_2 [44,45]. CO_2 purification unit (CPU) specific energy consumption has been fixed to 143 kW h/tCO_2 [22] in order to simplify the model. Power is produced using the same reheat supercritical steam cycle (P_{vv} = 290 bar, T_{vv} = 600/620 °C) as in the reference air-combustion CFPP case. Main inputs and results from the model are summarized in Table 3. From the simulations, the resulting specific CO_2 emissions are 86.2 g/kW h corresponding to 90% CO_2 capture efficiency. Remaining CO_2 emissions result from the nearly 8% of CO_2 lost in the purification process, which is consistent with results from previous works [40]. A net thermal to electric efficiency of 28.8% is achieved yielding an energy penalty of 9.1% points, which is within the range of previously reported results (8–12%) [18,46].

4.2. Calcium-Looping

In this section, the CaL integration model for post-combustion CO_2 capture used in the present work is summarized. The reader interested in further details may see the work of Ortiz et al. [47]

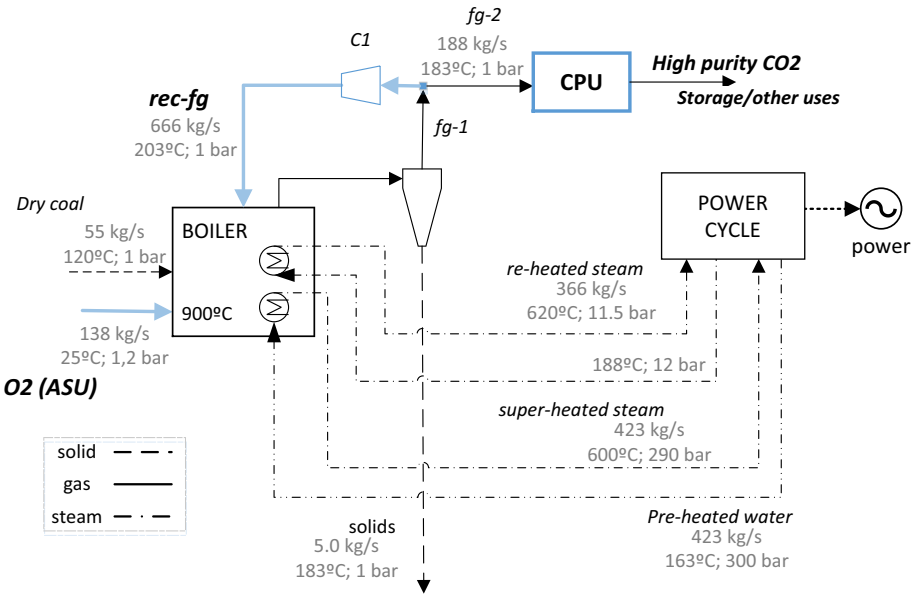

Fig. 6. Schematics of the total oxy-combustion CFPP. Differences with air-combustion CFPP are highlighted in blue color (for interpretation of the references to color in this figure, the reader is referred to the web version of this article.)

where a similar model is thoroughly described. The CaL process is accomplished by using two interconnected circulating- fluidized-bed (CFB) reactors, both operated under atmospheric pressure at gas velocities of approximately 5 m/s [48,49]. CaO particles react in the carbonator according to the carbonation reaction (Eq. (7)) at temperatures between 625 and 680 °C with the CO_2 present in the flue gas stream coming from the CFPP plant. The partially carbonated particles are then circulated into the calciner reactor in which fast decomposition of $CaCO_3$ occurs at 950 °C [15,25,50,51] to regenerate the sorbent and produce a rich CO_2 stream to be compressed and transported for storage or other uses. At the calciner exit, CaO particles are recovered by a cyclone and sent back to the carbonator for a new cycle. CO_2 capture in this reactor is modelled according to an equilibrium reactor following the model described in Section 3.2:

$$CaO + CO_2 \rightleftarrows CaCO_3 \quad \Delta H_r^0 = -178\ \frac{kJ}{mol} \tag{8}$$

Fig. 7 shows a schematic representation of the CaL process. Steam is used as heat carrier fluid to take advantage of heat produced in the exothermic carbonation reaction for electricity generation by means of a secondary steam cycle. Moreover, the sensible heat from the CO_2 stream exiting the calciner is also used to increase the steam production. Since a large flow rate of solids are recirculated in the CaL cycle, a heat exchanger (simplified as a heat transfer between solids with a temperature approach of 20 °C) is incorporated for transferring sensible heat between the CaO particles leaving the calciner (F_R in Fig. 7, with a temperature of about 950 °C) and the solids ($CaCO_3$ and unreacted CaO particles) entering into it to be heated up to the calcination temperature.

In order to attain full calcination in short residence times of the limestone makeup fed into the calciner, the temperature in the calciner reactor must be 930° o even higher [14,52]. This makes necessary to supply a large amount of heat to the calciner, which is accomplished by in-situ oxy-fuel combustion in order not to dilute CO_2 in this reactor. CO_2 compression is modelled as a multi-stage compression to 100 bar refrigerated with water from the low-pressure section of the steam cycle. Pressure drop of the flue gas across the carbonator is calculated from the Kunii–Levenspiel (K–L) fluid dynamics model [53,54]. A compressor is used to counteract this pressure drop. Energy consumption derived from solids transportation has been set at 20 MJ per ton of solids [55]. Main inputs and results from the model are summarized in Table 3. The base case for the CFPP-CaL integration leads to a CO_2 capture efficiency of 82.7% for an overall plant efficiency of 30.3%, which implies an energy penalty of 7.4% points in the range of previous values reported in literature [6,56,57]. As regards specific energy consumption (Eq. (6)), a SPECCA value of 3.3 MJ/kg CO_2 is achieved.

4.3. Oxy-CaL

This section describes the novel Oxy-CaL hybrid system proposed in the present work. Fig. 8 shows a schematic representation of the process, which has been simulated for several values of the CO_2 vol% in the flue gas effluent from partial oxy-combustion. As can be seen in Fig. 8, the process is initiated by an oxy-fuel combustion similar to that described in Section 4.1. Partial oxy-combustion is carried out to obtain a CO_2 vol% in the range of 30–60% in the flue gas at the boiler exit. To this end, a mixture of air and O_2 is used in the boiler for combustion. The air/O_2 ratio is calculated to achieve a given CO_2 vol% in the flue gas (45% in the case illustrated in Fig. 8). As in the case of total oxy-combustion, recirculation of the flue gas serves to control the flame temperature in the boiler, whose value is kept the same for all the simulations.

Since the amount of pure O_2 for partial oxy-combustion is substantially decreased (99.3 kg/s to achieve a 45% vol CO_2 concentration instead of 138 kg/s for total oxy-combustion), power consumption in the ASU is notably reduced. Furthermore, the CPU unit for CO_2 purification is not needed since this step is carried out after the CaL process. Altogether, the energy penalty for partial oxy-combustion is significantly reduced. Thus, energy penalty is 3.40% in the Oxy-CaL 45 system as compared to 9.05% for total oxy-combustion.

After partial oxy-combustion, the CO_2 rich flue gas is sent to the carbonator reactor to follow up with the CaL process, being before slightly compressed (to overcome the pressure drop in the carbonator) and preheated with the hot gas streams exiting the CaL cycle. In contrast with the CaL scheme (Fig. 7), flue gas preheating is car-

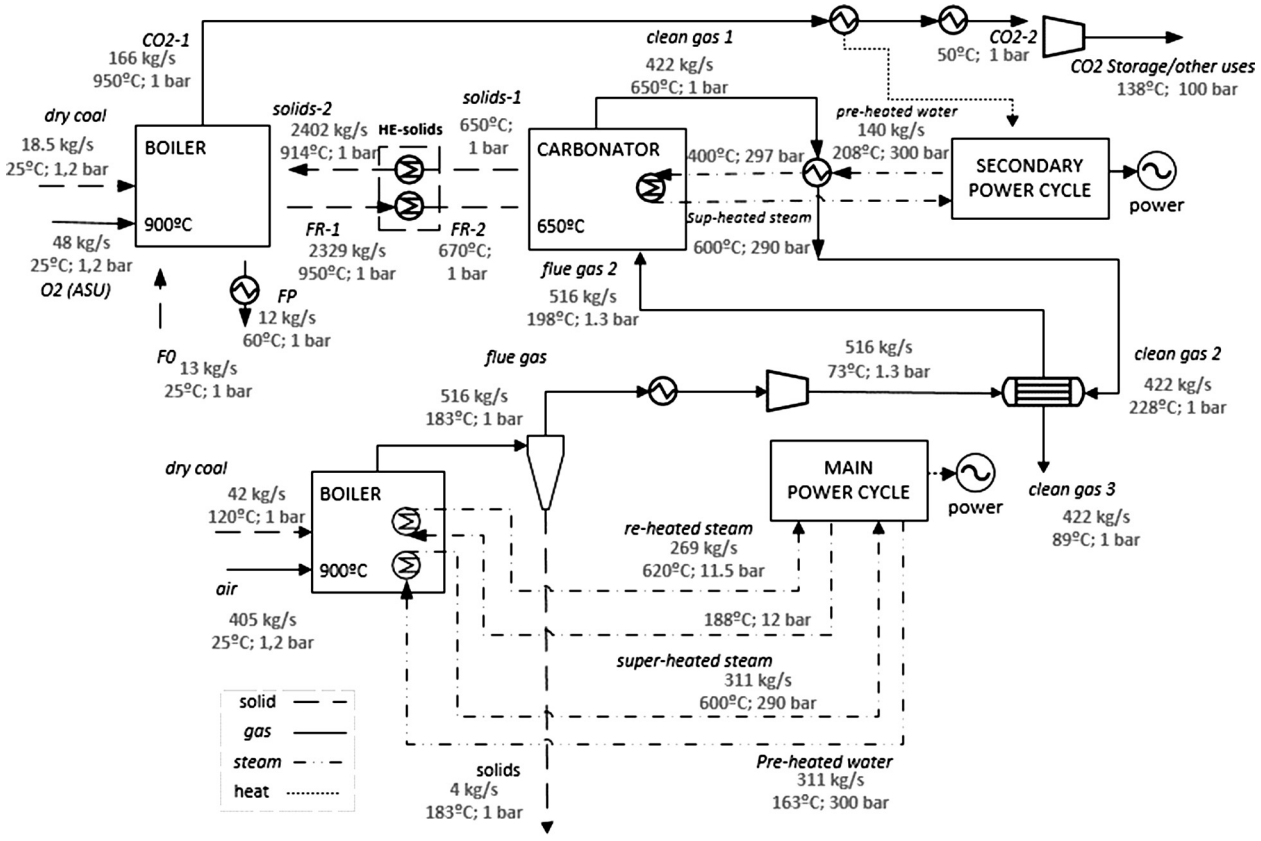

Fig. 7. CFPP-CaL integration scheme.

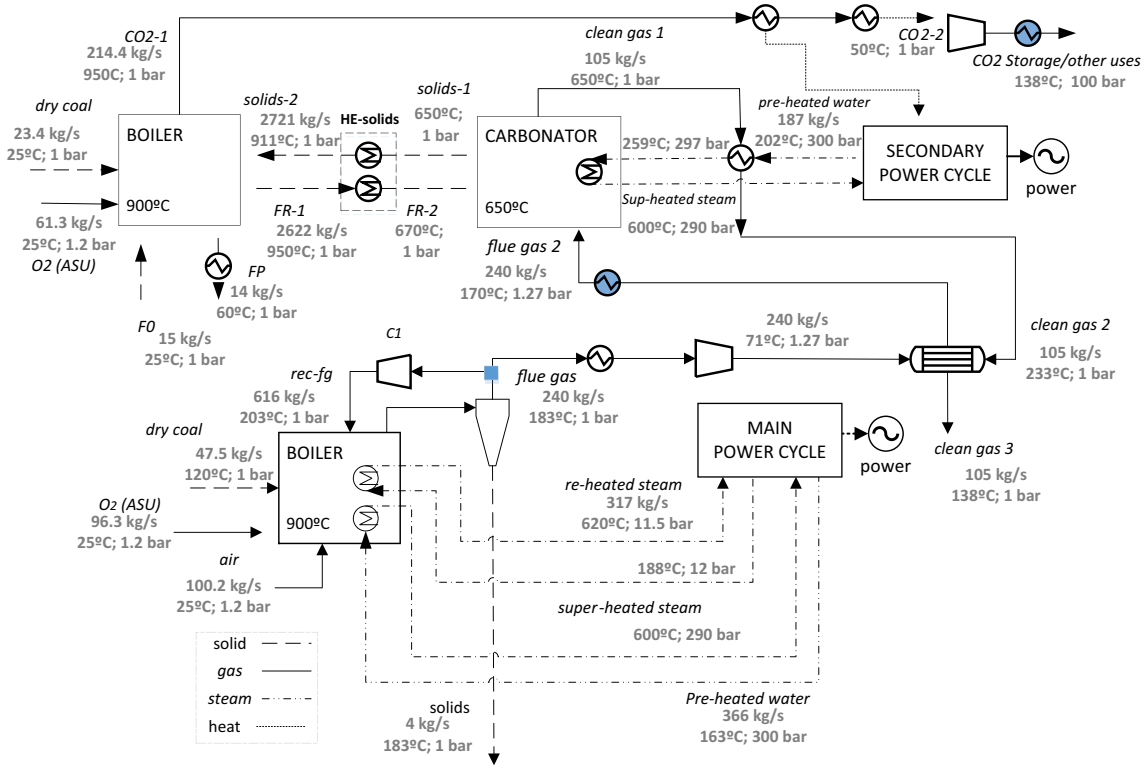

Fig. 8. General Oxy-CaL-45 (45% vol CO_2 concentration in the flue gas by partial oxy-combustion) integration scheme.

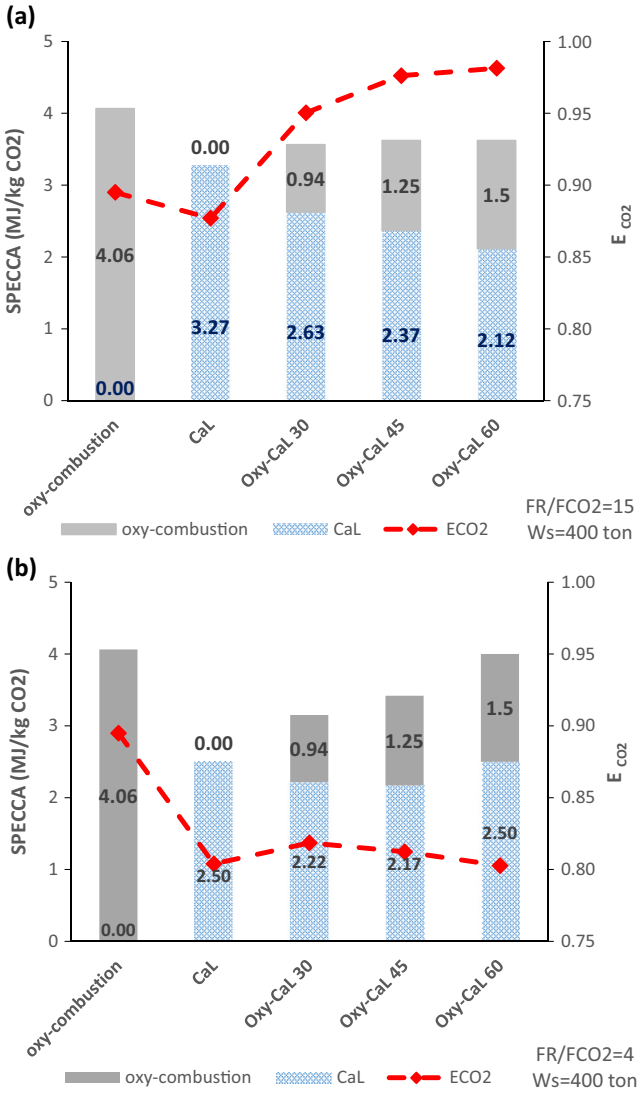

Fig. 9. SPECCA values and CO_2 capture efficiencies for the CO_2 capture systems analyzed in this work and using reference parameters shown in Table 3. Figures (a) and (b) correspond to different values of the solids residence time τ in the carbonator for the CaL process. (a) $FR/FCO_2 = 15$ (τ = 2 min) and (b) $FR/FCO_2 = 4$ (τ = 10 min).

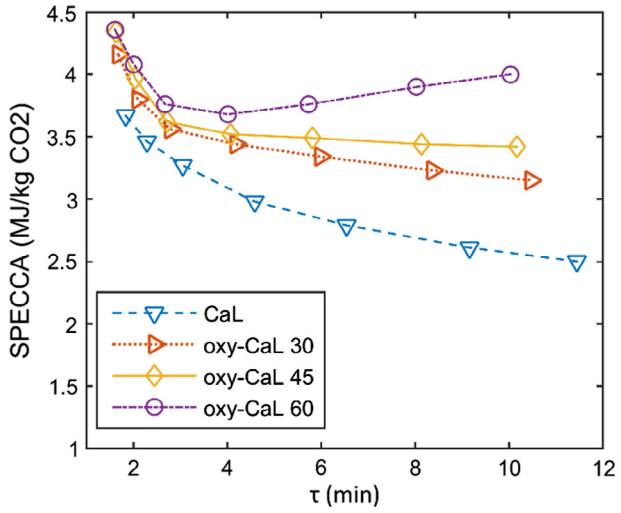

Fig. 10. SPECCA values as a function of solids residence time in the carbonator for CaL and Oxy-CaL systems operating at T_{carb} = 650 °C (solids inventory fixed at Ws = 400 ton).

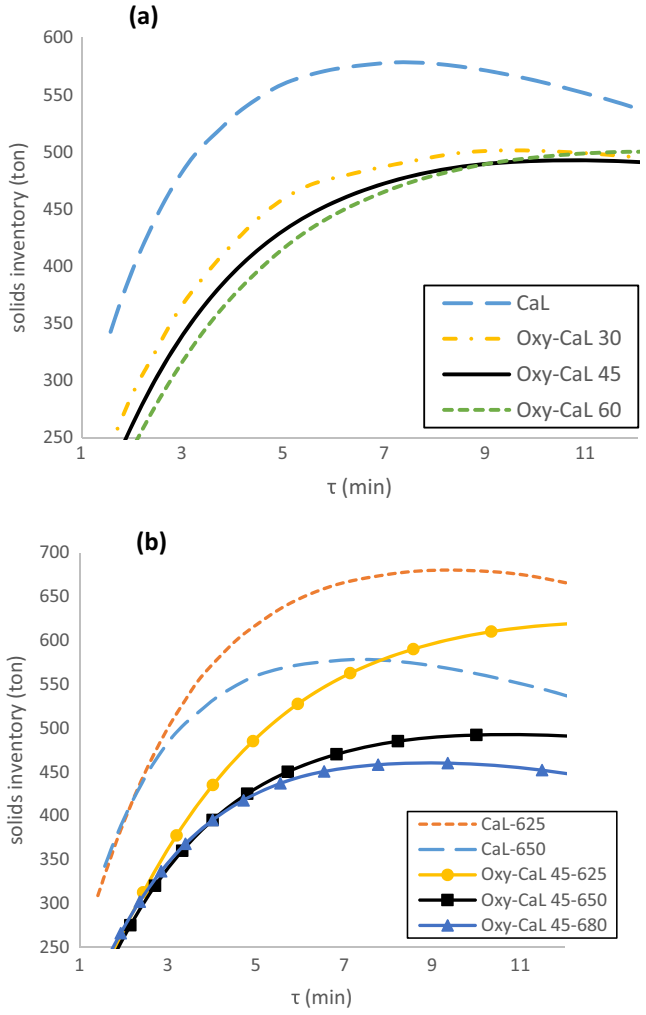

Fig. 11. 90% capture iso-efficiency lines as a function of solids inventory and solids residence time in the carbonator for CaL and Oxy-CaL systems at a carbonator temperature Tcarb = 650 °C (a) and for the CaL and Oxy-CaL-45 systems at carbonation temperatures of 625, 650, and 680 °C (b).

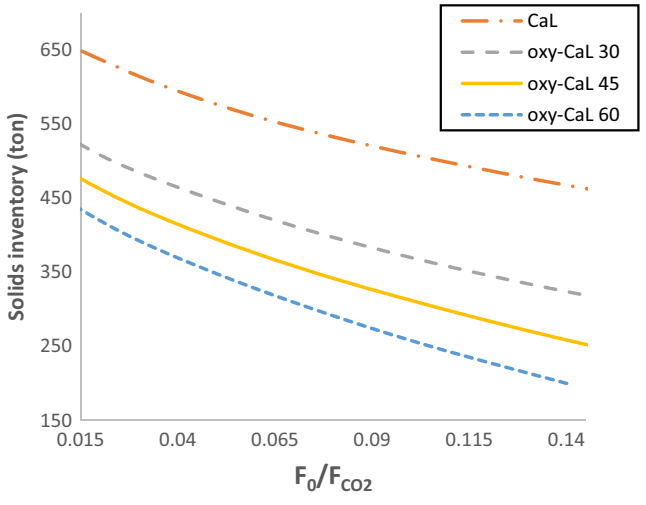

Fig. 12. Solids inventory as a function of makeup flow for CaL and Oxy-CaL systems at a carbonator temperature Tcarb = 650 °C and at capture efficiency of 90%. Solids recirculation flow rate is fixed to F_R/F_{CO2} = 15.

ried out in the Oxy-CaL system by using firstly the compressed CO_2 stream since the thermal capacity of the flue gas at the carbonator exit is lower than in the case of the CaL. The CO_2 entering into the carbonator reacts with the CaO solids coming from the calciner as in the conventional CaL model (Section 4.2) according to the carbonation reaction (Eq. (7)). As discussed in Section 3, the capture efficiency is significantly enhanced when the CO_2 concentration in the flue gas is increased (Fig. 5). Thus, the Oxy-CaL-45 system has a CO_2 capture efficiency of 97.6% in the base case (see Fig. 5a) as compared to 82.7% in the base case of the CaL system. Such increase in the capture capacity implies also the handling of a larger amount of $CaCO_3$, which leads to higher heat needs in the calciner for CaO regeneration, and therefore to a higher consumption of coal and O_2 as can be seen by comparison of Figs. 7–9. Nonetheless, the amount of CO_2 captured in this Oxy-CaL-45 system is 29% over that captured by means of CaL (Section 4.2) and 14% above the CO_2 captured by total oxy-combustion (Section 4.1).

Despite the need of additional coal and O_2 for oxy-combustion in the calciner, the increase in CO_2 capture efficiency obtained by increasing the CO_2 concentration in the flue gas leads to a reduction of energy consumption in the CaL cycle. Thus, a SPECCA value of 2.37 MJ/kg CO_2 is obtained for the Oxy-CaL-45 system, which is 28% below the SPECCA obtained for the conventional CaL system. Nevertheless, the SPECCA for the complete oxy-CaL process is 3.62 MJ/kg CO_2, which is 10% higher than in the CaL base case. On the other hand, the Oxy-CaL system allows for a reduction by 11% of energy consumption in comparison with the total oxy-combustion case. The next sections are devoted to a deeper comparative analysis of both capture efficiency and energy penalty resulting from the diverse capture systems with the goal of finding the most feasible choice to be implemented in practice.

5. CO_2 capture efficiency and energy consumption

As was shown in Sections 2.2 (TGA results) and 3.2 (carbonator model), the CO_2 capture efficiency in the CaL process is remarkably enhanced by increasing the CO_2 concentration in the flue gas stream entering into the carbonator. This is reflected also in the SPECCA, which is decreased due to the higher efficiency of the CO_2 capture process. On the other hand, partial oxy-combustion carried out to increase the CO_2 concentration at the inlet of the carbonator in the CaL process contributes also to an additional energy penalty. The use of the CaL process, total oxy-combustion or a hybrid Oxy-CaL process for CO_2 capture in CFPP is carefully assessed below on the basis of the benefits and drawbacks of each one of these systems.

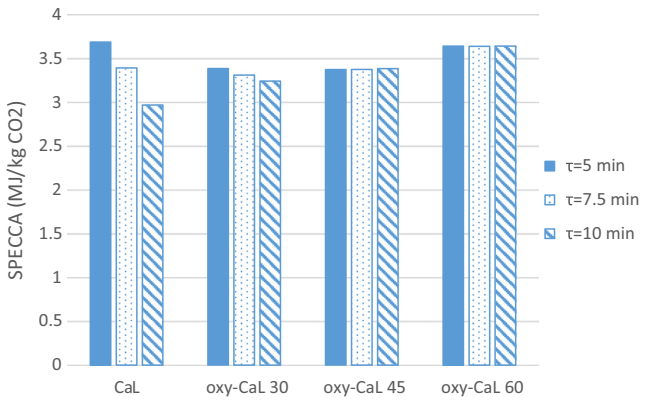

Fig. 13. SPECCA values for the CaL and Oxy-CaL systems obtained by considering a fixed solids inventory of Ws = 450 tons and capture efficiency to 90%.

Fig. 9 shows the CO_2 capture efficiency and SPECCA values for total oxy-combustion, CaL, and Oxy-CaL systems obtained for the base cases analyzed in Section 4. As seen in Fig. 9a, the part of SPECCA that corresponds to the CaL process in the Oxy-CaL systems is decreased as the carbonation CO_2 vol% is increased if the oxy-CaL process is operated with a high solids recirculation flow rate (F_R/F_0 = 15 corresponding to τ = 2 min for the solids residence time and fixing Ws = 400 tons as solids inventory). Nevertheless, energy consumption in the partial oxy-combustion part of the process leads to global oxy-CaL SPECCA values somewhat higher than for the purely CaL process. On the other hand, the oxy-CaL 30, 45 and 60 systems have a SPECCA smaller than total oxy-combustion. Note also that the CO_2 capture efficiency is notably increased for the oxy-CaL systems as compared to oxy-combustion and is especially increased over the CaL process. Fig. 9b shows however that under prolonged solids residence times of τ = 10 min (corresponding to a reduced solids recirculation flow F_R/F_0 = 4 and fixing Ws = 400 tons as solids inventory) the capture efficiency of the oxy-CaL systems is hindered since carbonation in the solid-state diffusion controlled stage is not significant for carbonation under relatively high CO_2 vol% as was seen from the TGA tests (Section 3.2).

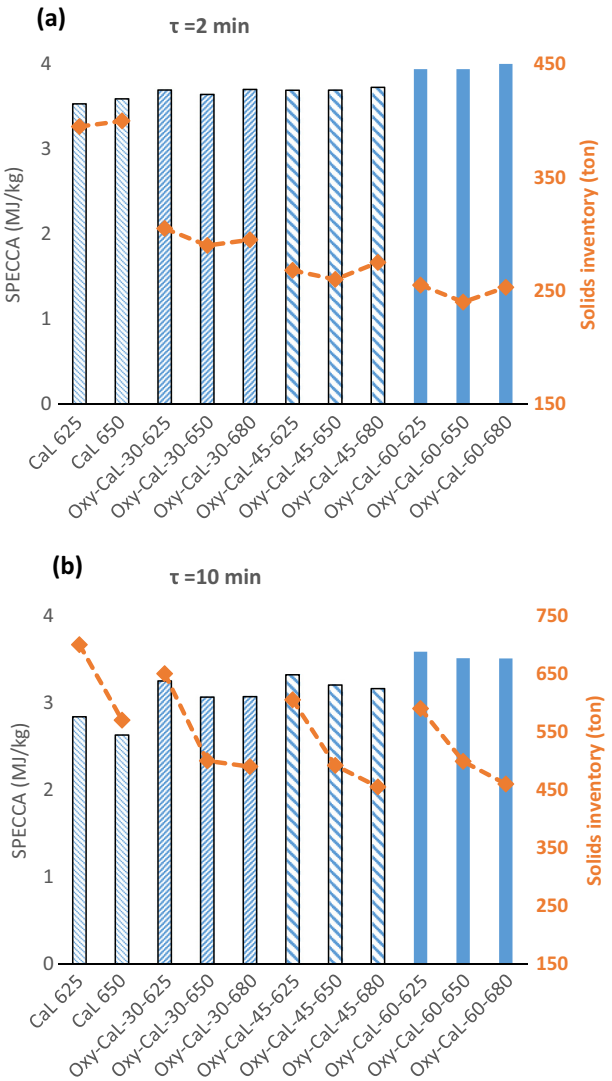

Fig. 14. SPECCA and solids inventory for the CaL and Oxy-CaL systems operating under (a) short (2 min) and (b) prolonged (10 min) solids residence times. The effect of changing the carbonator temperature (between 625 °C and 680 °C) is also shown. Capture efficiency is fixed to 90%.

As discussed above and according to recent works [13,47], energy consumption in the CaL process is highly dependent on the carbonation rate in the solid-state diffusion controlled phase (SDP), which determines the role of the solids residence time τ in the carbonator. Fig. 10 shows how SPECCA evolves as τ is increased for the CaL and hybrid oxy-CaL processes. In the case of the CaL process, the rate of carbonation in the solid-state diffusion controlled phase is not negligible as compared to the carbonation rate in the fast reaction controlled phase, which leads to a considerable reduction of the energy consumption as τ is increased [13,47]. On the other hand, the rate of carbonation in the solid-state diffusion controlled phase is decreased by increasing the CO_2 concentration in the flue gas as occurs in the oxy-CaL systems (see Fig. 1), which hinders a further reduction of SPECCA as τ is increased. For the Oxy-CaL-60 case, the SPECCA is even raised as τ is prolonged beyond ~4 min. On the other hand, the SPECCA values for the CaL and oxy-CaL systems are similar for short solids residence time (of about 2 min). Thus, it may be concluded that optimum operation of the oxy-CaL system is under short residence times.

5.1. Role of solids inventory

A straightforward consequence of the improvement of CO_2 capture efficiency in the CaL process as the CO_2 vol% in the carbonator

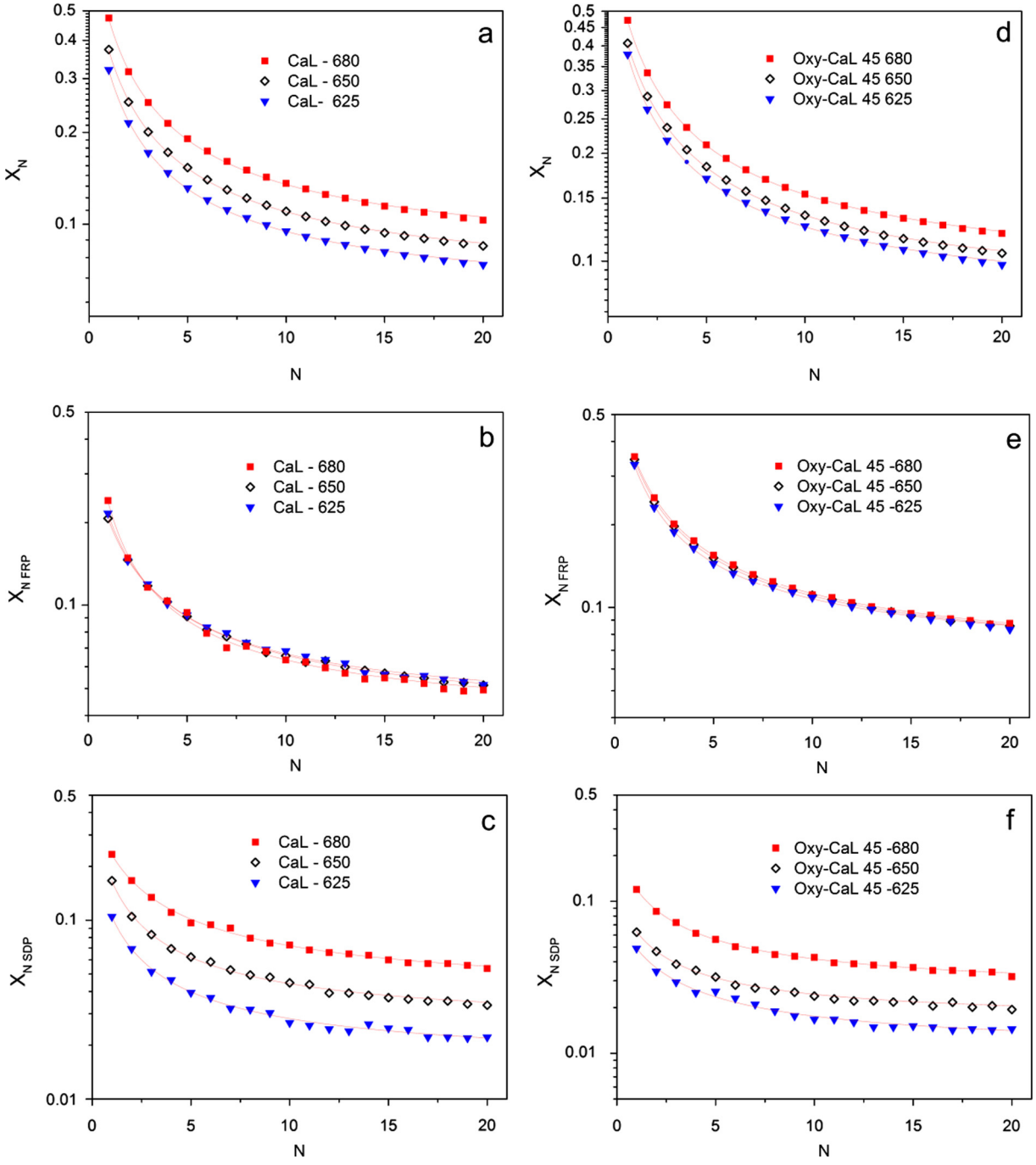

Fig. 15. (a and d) Overall CaO conversion versus the cycle number for carbonation/calcination cycles carried out under CaL and Oxy-CaL-45 conditions. (b and e) Conversion in the fast reaction controlled phase. (c and f) Conversion in the solid-state diffusion controlled phase. Carbonation is carried out under 15% vol CO_2 (CaL conditions) and 45% vol CO_2 (Oxy-CaL-45 conditions) at 625 °C, 650 °C and 680 °C as indicated. Calcination is performed at 950 °C (70% CO_2/30% air vol/vol) in all the tests.

is increased (Oxy-CaL) is the possibility of reducing the solids inventory (W_s) and the limestone makeup flow (F_0), which could lead to a potentially relevant capital and operational cost cutback. Fig. 12a shows the variation of the solids inventory (W_s) in the CaL and oxy-CaL processes with the solids residence time for a fixed value of the capture efficiency (E_{CO2} = 90%). As can be seen, significantly lower solids inventories are needed in the Oxy-CaL processes under carbonation residence times below ~12 min that would conform to usual operation conditions in CFB reactors. This result implies an important potential for reducing the CaL size in the hybrid oxy-CaL systems. It must be reminded that system size is currently one of the main limitations for the CaL process to reach a demonstration stage [4,16]. Moreover, a lower solids inventory, as would be possible in the Oxy-CaL system, leads to a reduction of power consumption to overcome the gas pressure drop across the reactor. The oxygen production and coal input needed for heating-up the additional quantity of solids in calciner are also diminished.

Fig. 11b shows the evolution of W_s with the solids residence time in the carbonator for carbonation temperatures T = 625 °C, 650 °C and 680 °C and a fixed capture efficiency (E_{CO2} = 90%). As may be observed, the relative decrease of the carbonation rate in the solid-state diffusion controlled stage when T is decreased to 625 °C leads to a remarkable increase of W_s for solids residence times beyond ~3 min. Thus, the CaL process operated under long residence times, which would allow decreasing notably SPECCA [13,47], can be hampered by a small decrease of the carbonator temperature that could be expected locally under practical conditions [14,48] due to inefficient mass and/or energy transfer. Note that chemical equilibrium prevents in the case of the CaL process to achieve a 90% capture efficiency when operating at 680 °C (see the maximum capture value possible in Fig. 5a). On the other hand, since the Oxy-CaL system would be ideally operated under short residence times, its performance would not be essentially affected by temperature changes.

As seen in the results obtained from our TGA experiments (Fig. 2), the rate of carbonation in the solid-state diffusion controlled phase depends critically on the carbonator temperature. Thus, carbonation in this phase is hindered if the temperature is decreased just from 650 °C to 625 °C whereas it becomes enhanced by an increase of temperature up to 680 °C. It is therefore interesting to assess the sensitivity of SPECCA and solids inventory needed in the CaL process to this small change of carbonation temperature that might occur in practice.

Despite the potential for reducing the CaL size in the Oxy-CaL process, the additional energy consumption due to partial oxy-combustion, and therefore O&M costs, must be also considered to assess the Oxy-CaL feasibility. In this regard, a further benefit of the Oxy-CaL hybrid system is that the higher capture efficiency achieved allows to reduce the fresh limestone makeup, which yields a decrease of energy penalty. Fig. 12 shows the relationship between the solids inventory and make-up flow for the diverse systems analyzed at a fixed capture efficiency of 90%.

As can be seen in Fig. 12, by using the Oxy-CaL hybrid system it is possible to reduce considerably the fresh limestone makeup in comparison with the CaL process. For example, if we consider the Oxy-CaL 45 system with a solids inventory of 450 tons, the ratio of limestone makeup to CO_2 flow rates (F_0/F_{CO2}) is just around 0.015, which is quite below the amount needed for the CaL process under the same operation conditions and capture efficiency (F_0/F_{CO2} = 0.12). Fig. 13 shows the SPECCA values obtained by fixing the solids inventory at 450 tons and varying the makeup flow to attain with each system a capture efficiency of 90%.

As shown in Fig. 13, using a given solids inventory of 450 tons in the carbonator, SPECCA values for Oxy-CaL systems are lower than for the CaL process when operating under solids residence times below 7.5 min due to the lower makeup flow needed to reach a 90% capture efficiency. Thus, the use of the Oxy-CaL systems would allow also for a reduction of O&M costs associated to the capture process using typical reactor sizes. On the other hand, if the solids residence time is prolonged to 10 min, the CaL process yields a lower SPECCA due to promoted carbonation in the solid-state diffusion controlled phase.

Fig. 14 shows data on SPECCA and solids inventory for the CaL and Oxy-CaL (carbonator temperatures of 625 °C, 650 °C and 680 °C) systems for a fixed capture efficiency (E_{CO2} = 90%), and short (2 min) and prolonged (10 min) solids residence times. A may be seen, for operation under short residence times, the Oxy-CaL systems (especially Oxy-CaL-30 and 45) lead to a considerable reduction of the solids inventory (from 400 tons for the CaL-650 system to 286 tons for Oxy-CaL-45-650) and therefore to a reduction of the CaL system size whereas the SPECCA is only slightly increased (from 3.59 MJ/kg for the CaL-650 system to 3.7 MJ/kg for the Oxy-CaL-45-650). Regarding the effect of carbonator temperature on the CaL and Oxy-Cal systems for a given solids residence time of 2 min, there is not a clear evidence on the optimum system choice (lower SPECCA). On the other hand, for longer residence times (Fig. 14b), the CaL-625 system shows a better performance in terms of efficiency albeit a considerable higher solids inventory is required in this case. Thus, the CaL process advantage is lost by a modest decrease of the carbonator temperature, which would require a considerable increase of the solids inventory to ensure a high capture efficiency. At this point, it is important to note that both the CaL and Oxy-CaL systems yield a lower energy consumption than the conventional oxy-fuel combustion process regardless of the carbonator temperature and carbonator CO_2 concentration.

Concerning the Oxy-CaL-30 system operated under short residence times, it would allow reducing the solids inventory from 400 tons (CaL-625) system to 300 tons (−33% relative reduction) and thus the reactors (carbonator and calciner) size could be decreased, which should be quantitatively assessed in future works. Thermal inertia and flexible operation of the installation must be also carefully addressed in further analysis. These effects are amplified when the residence time is increased to 10 min for the CaL process. The efficiency penalty is then reduced by around 1 MJ/kg CO_2 but the solids inventory is increased over a 200% up to near 700 ton. Care should be taken in this case to design and operate a system with such a large thermal inertia due to solids heat capacity. Starts-up and shuts-down would be also risky. This could be a suitable option if the CO_2 capture system is to be used in base load power plants. When power plant flexibility is required, the smaller inventory allowed by the Oxy-CaL hybrid system is preferred to better accommodate the installation to load changes.

6. Conclusions

This work analyzes a novel CO_2 capture system (Oxy-CaL) based on the integration of the CaL process with partial oxy-combustion, the latter used to raise the CO_2 concentration in the flue gas thus enhancing the CaL capture efficiency. Results from thermogravimetric analysis experiments are used to simulate the hybrid capture system when integrated into a coal fired power plant (CFPP). Energy penalty and capture efficiency are analyzed for diverse Oxy-CaL systems to reach a CO_2 vol% in the flue gas in the range 30–60% and the results are compared with those obtained for the pure CaL and oxy-combustion processes.

Main highlights concluded from the study are:

- A higher CO_2 capture efficiency is achieved by means of the Oxy-CaL hybrid system while the specific energy consumption per kg of CO_2 avoided (SPECCA) is kept below 4 MJ/kg, which

is a typical value usually reported for oxy-combustion or amine-based CO_2 capture systems. Thus, CO_2 capture using an Oxy-CaL system could be a potentially attractive alternative to total oxy-combustion for newly erected CFPPs.
- The CaL process seems to be the most advantageous CO_2 capture process when operating under relative long solids residence time in the carbonator. However, its performance has a strong sensitivity to the carbonation rate in the solid-state diffusion controlled stage, which depends critically on temperature within the range of temperatures practically attainable in the carbonator.
- The effect of varying the carbonation temperature is more relevant when operating under long residence times due to the strong sensitivity of CaO carbonation to temperature in the solid-state diffusion controlled stage, especially for the pure CaL process.
- The higher CO_2 capture efficiency using Oxy-CaL systems allows to reduce the fresh limestone makeup flow, which leads to a reduction of energy consumption when operating under solids residence times below 7.5 min.
- In spite that SPECCA in the CaL process could be somewhat smaller than for the Oxy-CaL system when operating under prolonged solids residence times, the latter shows potentially important benefits regarding plant operation flexibility. Substantially smaller amounts of solids inventory are needed in the Oxy-CaL system, which would allow a more efficient response to load changes in coal fired power plants.

In a future work, a detailed techno-economic study must be developed in order to assess quantitatively the cost of CO_2 capture by means of the Oxy-CaL system as compared to CaL and oxy-combustion and for same values of SPECCA and capture efficiency.

Acknowledgements

This work was supported by the Spanish Government Agency Ministerio de Economia y Competitividad and FEDER Funds (contracts CTQ2014-52763-C2-1-R, CTQ2014-52763-C2-2-R and MAT2013-41233-R). We gratefully acknowledge the Functional Characterization Services of the Innovation, Technology and Research Centre of the University of Seville (CITIUS). The authors also thank VPPI-US for the AP current contract.

Appendix A

Fig. 15 shows data on the multicycle overall CaO conversion (X_N, X_{FRP} and X_{SDP} as a function of the cycle number for the tests carried out under CaL and Oxy-CaL-45 conditions and for the

Table 4
Values of the deactivation rate constant κ and residual conversion X_r obtained from the best fits of Eq. (1) to TGA experimental data for carbonation at different temperatures (625, 650, and 680 °C) and CO_2 concentrations (15% vol in the CaL tests; 30%, 45%, and 60% vol in the Oxy-CaL tests).

T carb = 625 °C		CaL-625	Oxy-CaL30-625	Oxy-CaL45-625	Oxy-CaL60-625
$X_{overall}$	X_1	0.321	0.338	0.378	0.400
	κ	0.753	0.665	0.675	0.623
	X_r	0.053	0.067	0.072	0.077
	R_{sqr}	0.999	0.999	0.999	0.999
X_{FRP}	X_1	0.216	0.260	0.329	0.350
	κ	0.737	0.697	0.683	0.647
	X_r	0.038	0.056	0.062	0.067
	R_{sqr}	0.999	0.998	0.999	0.999
X_{SDP}	X_1	0.105	0.078	0.049	0.050
	κ	0.792	0.573	0.615	0.464
	X_r	0.015	0.011	0.010	0.0103
	R_{sqr}	0.997	0.996	0.990	0.994
T carb = 650 °C		CaL-650	Oxy-CaL30-650	Oxy-CaL45-650	Oxy-CaL60-650
$X_{overall}$	X_1	0.373	0.388	0.407	0.425
	κ	0.731	0.667	0.651	0.633
	X_r	0.061	0.070	0.076	0.081
	R_{sqr}	0.999	0.999	0.999	0.999
X_{FRP}	X_1	0.207	0.293	0.344	0.374
	κ	0.660	0.661	0.641	0.674
	X_r	0.037	0.053	0.060	0.068
	R_{sqr}	0.999	0.999	0.999	0.998
X_{SDP}	X_1	0.166	0.095	0.063	0.051
	κ	0.828	0.686	0.711	0.633
	X_r	0.025	0.016	0.016	0.014
	R_{sqr}	0.998	0.998	0.993	0.980
T carb = 680 °C		CaL-680	Oxy-CaL30-680	Oxy-CaL45-680	Oxy-CaL60-680
$X_{overall}$	X_1	0.474	0.472	0.472	0.474
	κ	0.737	0.681	0.636	0.636
	X_r	0.074	0.081	0.085	0.086
	R_{sqr}	0.999	0.999	0.999	0.999
X_{FRP}	X_1	0.240	0.299	0.352	0.391
	κ	0.876	0.716	0.630	0.673
	X_r	0.037	0.057	0.060	0.066
	R_{sqr}	0.997	0.999	0.999	0.999
X_{SDP}	X_1	0.233	0.173	0.120	0.083
	κ	0.609	0.627	0.655	0.478
	X_r	0.037	0.025	0.025	0.020
	R_{sqr}	0.998	0.999	0.999	0.990

Table 5
Inputs and results of diverse CO_2 capture systems for the base case.

	Parameter	Reference CFFP (air combustion)	Oxy-combustion	CaL	Oxy-CaL 30	Oxy-CaL 45	Oxy-CaL 60
CFPP	$\dot{m}_{coal}$ (kg/s)	42.20	55.05	42.20	46.10	47.50	48.15
	$\dot{m}_{air}$ (kg/s)	475	–	475	208.90	100.20	43.54
	$\dot{m}_{O2}$(kg/s)	–	136.91	–	68.85	96.35	110.503
	γ_{fg}	–	0.78	–	0.63	0.72	0.75
	F_{fg} (kmol/s	17.12	3.85	17.12	10.13	7.25	5.74
	F_{CO2} (kmol/s)	2.60	3.39	2.60	2.84	2.93	2.96
	υ_{CO2}	0.15	0.89	0.15	0.30	0.45	0.60
	υ_{O2}	0.023	0.025	0.023	0.025	0.025	0.025
	η_{boiler}	0.90	0.90	0.90	0.90	0.90	0.90
	η_{CFPP}	0.3777	0.2872	0.3777	0.3517	0.3437	0.3374
	network (MW)	490.47	488.80	490.47	498.30	502.30	499.75
	Penalty	–	**9.05%**	**–**	**2.60%**	**3.40%**	**4.03%**
	SPECCA (MJ/kg_{CO2})	–	**4.06**	**–**	**0.94**	**1.25**	**1.50**
CaL	F_R/F_{CO2}	–	–	15	15	15	15
	F_0/F_{CO2}	–	–	0.05	0.05	0.05	0.05
	$\tau(min)$	–	–	3.05	2.79	2.71	2.68
	T_{calc} (°C)	–	–	950	950	950	950
	T_{carb} (°C)	–	–	650	650	650	650
	E_{CO2}	–		0.827	0.950	0.976	0.981
	$\dot{m}_{coal}$ (kg/s)	–	–	18.48	22.34	23.40	23.84
	$\dot{m}_{O2}$ (kg/s)	–	–	48.00	58.41	61.00	62.49
	γ_{fg}	–	–	0.7	0.7	0.7	0.7
	$\dot{m}_{gas,calc}$ (kg/s)	–	–	165.07	203.6	214	218.34
	$\dot{m}_{CO2,calc}$ (kg/s)	–	–	150.45	185.70	195.40	199.19
	x_{CO2}	–	–	0.030	0.019	0.017	0.026
	x_{O2}	–	–	0.028	0.032	0.042	0.058
	$P_{HE,solids}$	–	–	640.92	697.60	717.80	727.29
	$\dot{W}_{sec}$ (MW)	–	–	75.80	113.90	126.46	130.88
	$\dot{W}_{solids}$ (MW)	–	–	45.70	49.72	51.16	51.82
	$\dot{W}_{ASU}$ (MW)	–	–	34.56	42.05	43.92	44.99
	$\dot{W}_{comp,CO2}$ (MW)	–	–	57.55	71.01	74.59	75.20
	$\dot{W}_{comp,FG}$ (MW)	–	–	12.53	7.27	4.90	3.66
	η_{int}	–	–	0.3030	0.2909	0.2882	0.2853
	Penalty	–	–	**7.43%**	**6.04%**	**5.48%**	**5.27%**
	SPECCA (MJ/kg_{CO2})	–	–	**3.28**	**2.63**	**2.37**	**2.29**
Total	$\dot{m}_{coal,total}$	–	–	60.68	68.44	70.90	71.99
	$Penalty_{total}$	–	**9.05%**	**7.47%**	**8.68%**	**8.95%**	**9.24%**
	$SPECCA_{total}$ (MJ/kg_{CO2})	–	**4.06**	**3.28**	**3.56**	**3.62**	**3.79**

Bold indicate the most relevant values.

diverse carbonation temperatures employed (625, 650 °C and 680 °C). Values of the deactivation rate constant and residual conversion obtained from the fittings of Eq. (1) to experimental data are also shown in Table 4.

Appendix B

See Table 5.

References

[1] IEA. Energy technology perspectives 2012; 2012. http://dx.doi.org/10.1787/energy_tech-2012-en.

[2] Tokimatsu K, Konishi S, Ishihara K, Tezuka T, Yasuoka R, Nishio M. Role of innovative technologies under the global zero emissions scenarios. Appl Energy 2016;162:1483–93. http://dx.doi.org/10.1016/j.apenergy.2015.02.051.

[3] Goto K, Yogo K, Higashii T. A review of efficiency penalty in a coal-fired power plant with post-combustion CO_2 capture. Appl Energy 2013;111:710–20. http://dx.doi.org/10.1016/ j.apenergy.2013.05.020.

[4] Bevan N, Boston A. CCS forum report; 2016.

[5] Wang M, Lawal A, Stephenson P, Sidders J, Ramshaw C, Hill W, et al. Post-combustion CO_2 capture with chemical absorption: a state-of-the-art review. Chem Eng Res Des 2011;89:1609–24. http://dx.doi.org/10.1016/j.cherd.2010.11.005.

[6] Perejon A, Romeo LM, Lara Y, Lisbona P, Valverde JM. The Calcium-Looping technology for CO_2 capture: on the important roles of energy integration and sorbent behavior. Appl Energy 2015;162:787–807. http://dx.doi.org/10.1016/j.apenergy.2015.10.121.

[7] Politecnico di Milano – Alstom UK (CAESAR project). European best practice guidelines for assessment of CO_2 capture technologies; 2011.

[8] Aaron D, Tsouris C. Separation of CO_2 from flue gas: a review. Sep Sci Technol 2005;40:321–48. http://dx.doi.org/10.1081/SS-200042244.

[9] Wang M, Joel AS, Ramshaw C, Eimer D, Musa NM. Process intensification for post-combustion CO_2 capture with chemical absorption: a critical review. Appl Energy 2015;158:275–91. http://dx.doi.org/10.1016/j.apenergy.2015.08.083.

[10] Luis P. Use of monoethanolamine (MEA) for CO_2 capture in a global scenario: consequences and alternatives. Desalination 2016;380:93–9. http://dx.doi.org/10.1016/ j.desal.2015.08.004.

[11] Rey A, Gouedard C, Ledirac N, Cohen M, Dugay J, Vial J, et al. Amine degradation in CO_2 capture. 2. New degradation products of MEA. Pyrazine and alkylpyrazines: analysis, mechanism of formation and toxicity. Int J Greenh Gas Control 2013;19:576–83. http://dx.doi.org/10.1016/j.ijggc.2013.10.018.

[12] Shimizu T, Hirama T, Hosoda H, Kitano K, Inagaki M, Tejima K. A twin fluid-bed reactor for removal of CO_2 from combustion processes. Chem Eng Res Des 1999;77:62–8. http://dx.doi.org/10.1205/026387699525882.

[13] Ortiz C, Valverde JM, Chacartegui R. Energy consumption for CO_2 capture by means of the calcium looping process: a comparative analysis using limestone, dolomite, and steel slag. Energy Technol 2016:1–12. http://dx.doi.org/10.1002/ente.201600390.

[14] Ströhle J, Junk M, Kremer J, Galloy A, Epple B. Carbonate looping experiments in a 1 MWth pilot plant and model validation. Fuel 2014;127:13–22. http://dx.doi.org/10.1016/ j.fuel.2013.12.043.

[15] Arias B, Diego ME, Abanades JC, Lorenzo M, Diaz L, Martínez D, et al. Demonstration of steady state CO_2 capture in a 1.7 MWth calcium looping pilot. Int J Greenh Gas Control 2013;18:237–45. http://dx.doi.org/10.1016/j.ijggc.2013.07.014.

[16] Hanak DP, Anthony EJ, Manovic V. A review of developments in pilot-plant testing and modelling of calcium looping process for CO_2 capture from power generation systems. Energy Environ Sci 2015;8:2199–249. http://dx.doi.org/10.1039/C5EE01228G.

[17] Abanades JC, Grasa G, Alonso M, Rodriguez N, Anthony EJ, Romeo LM. Cost structure of a postcombustion CO_2 capture system using CaO. Environ Sci Technol 2007;41:5523–7. http://dx.doi.org/10.1021/es070099a.

[18] Scheffknecht G, Al-Makhadmeh L, Schnell U, Maier J. Oxy-fuel coal combustion – a review of the current state-of-the-art. Int J Greenh Gas Control 2011;5:16–35. http://dx.doi.org/10.1016/j.ijggc.2011.05.020.

[19] Escudero AI, Espatolero S, Romeo LM, Lara Y, Paufique C, Lesort A-L, et al. Minimization of CO_2 capture energy penalty in second generation oxy-fuel power plants. Appl Therm Eng 2016;103:274–81. http://dx.doi.org/10.1016/j.applthermaleng.2016.04.116.

[20] Jin B, Zhao H, Zheng C. Thermoeconomic cost analysis of CO_2 compression and purification unit in oxy-combustion power plants. Energy Convers Manage 2015;83:416–30. http://dx.doi.org/10.1016/j.energy.2015.02.039.

[21] Posch S, Haider M. Optimization of CO_2 compression and purification units (CO_2CPU) for CCS power plants. Fuel 2012;101:254–63. http://dx.doi.org/10.1016/j.fuel.2011.07.039.

[22] Escudero AI, Espatolero S, Romeo LM. Oxy-combustion power plant integration in an oil refinery to reduce CO_2 emissions. Int J Greenh Gas Control 2016;45:118–29. http://dx.doi.org/10.1016/j.ijggc.2015.12.018.

[23] Kather A, Scheffknecht G. The oxycoal process with cryogenic oxygen supply. Naturwissenschaften 2009;96:993–1010. http://dx.doi.org/10.1007/s00114-009-0557-2.

[24] Vega F, Sanna A, Maroto-Valer MM, Navarrete B, Abad-Correa D. Study of the MEA degradation in a CO_2 capture process based on partial oxy-combustion approach. Int J Greenh Gas Control 2016;54:160–7. http://dx.doi.org/10.1016/j.ijggc.2016.09.007.

[25] Ylätalo J, Parkkinen J, Ritvanen J, Tynjälä T, Hyppänen T. Modeling of the oxy-combustion calciner in the post-combustion calcium looping process. Fuel 2013;113:770–9. http://dx.doi.org/10.1016/j.fuel.2012.11.041.

[26] Martínez I, Grasa G, Murillo R, Arias B, Abanades JC. Modelling the continuous calcination of $CaCO_3$ in a Ca-looping system. Chem Eng J 2013;215–216:174–81. http://dx.doi.org/10.1016/j.cej.2012.09.134.

[27] Koga N, Criado JM. The influence of mass transfer phenomena on the kinetic analysis for the thermal decomposition of calcium carbonate by constant rate thermal analysis (CRTA) under vacuum. Int J Chem Kinet 1998;30:737–44. http://dx.doi.org/10.1002/(SICI)1097-4601(1998)30:10<737::AID-KIN6>3.0.CO;2-W.

[28] Alonso M, Criado Ya, Abanades JC, Grasa G. Undesired effects in the determination of CO_2 carrying capacities of CaO during TG testing. Fuel 2014;127:52–61. http://dx.doi.org/10.1016/j.fuel.2013.08.005.

[29] Grasa G, Murillo R, Alonso M, Abanades JC. Application of the random pore model to the carbonation cyclic reaction. AIChE J 2009;55:1246–55. http://dx.doi.org/10.1002/aic.11746.

[30] Bhatia SK, Perlmutter DD. Effect of the product layer on the kinetics of the carbon dioxide-lime reaction. AIChE J 1983;29:79–86. http://dx.doi.org/10.1002/aic.690290111.

[31] Sun Z, Luo S, Qi P, Fan LS. Ionic diffusion through Calcite ($CaCO_3$) layer during the reaction of CaO and CO_2. Chem Eng Sci 2012;81:164–8. http://dx.doi.org/10.1016/ j.ces.2012.05.042.

[32] Bhatia SK, Perlmutter DD. Effect of the product layer on the kinetics of the CO_2-lime reaction. AIChE J 1983;29:79–86. http://dx.doi.org/10.1002/aic.690290111.

[33] Anderson TF. Self-diffusion of carbon and oxygen in calcite by isotope exchange with carbon dioxide. J Geophys Res 1969;74:3918–32. http://dx.doi.org/10.1029/JB074i015p03918.

[34] Grasa GS, Abanades JC. CO_2 capture capacity of CaO in long series of carbonation/calcination cycles. Ind Eng Chem Res 2006;45:8846–51. http://dx.doi.org/10.1021/ ie0606946.

[35] Valverde JM. A model on the CaO multicyclic conversion in the Ca-looping process. Chem Eng J 2013;228:1195–206. http://dx.doi.org/10.1016/j.cej.2013.05.023.

[36] Blamey J, Anthony EJ, Wang J, Fennell PS. The calcium looping cycle for large-scale CO_2 capture. Prog Energy Combust Sci 2010;36:260–79. http://dx.doi.org/10.1016/ j.pecs.2009.10.001.

[37] Zhu Y, Wu S, Wang X. Nano CaO grain characteristics and growth model under calcination. Chem Eng J 2011;175:512–8. http://dx.doi.org/10.1016/j.cej.2011.09.084.

[38] Ortiz C, Chacartegui R, Valverde J, Becerra J, Perez-Maqueda L. A new model of the carbonator reactor in the calcium looping technology for post-combustion CO_2 capture. Fuel 2015;160:328–38. http://dx.doi.org/10.1016/j.fuel.2015.07.095.

[39] USA National Energy Technology Laboratory. Detailed coal specifications quality guidelines for energy system. Studies 2012.

[40] Romano MC. Ultra-high CO_2 capture efficiency in CFB oxyfuel power plants by calcium looping process for CO_2 recovery from purification units vent gas. Int J Greenh Gas Control 2013;18:57–67. http://dx.doi.org/10.1016/j.ijggc.2013.07.002.

[41] Zhang X, Bauer C, Mutel CL, Volkart K. Life cycle assessment of power-to-gas: approaches, system variations and their environmental implications. Appl Energy 2017;190:326–38. http://dx.doi.org/10.1016/j.apenergy.2016.12.098.

[42] Perez-Fortes M, Schoneberger JC, Boulamanti A, Tzimas E. Methanol synthesis using captured CO_2 as raw material: techno-economic and environmental assessment. Appl Energy 2016;161:718–32. http://dx.doi.org/10.1016/j.apenergy.2015.07.067.

[43] Pei X, He B, Yan L, Wang C, Song W, Song J. Process simulation of oxy-fuel combustion for a 300 MW pulverized coal-fired power plant using Aspen Plus. Energy Convers Manage 2013;76:581–7. http://dx.doi.org/10.1016/j.enconman.2013.08.007.

[44] Romano M, Martínez I, Murillo R, Arstad B. Guidelines for modeling and simulation of Ca-looping processes; 2012.

[45] Martínez I, Murillo R, Grasa G, Abanades JC. Integration of a Ca-looping system for CO_2 capture in an existing power plant. Energy Procedia 2011;4:1699–706. http://dx.doi.org/10.1016/j.egypro.2011.02.043.

[46] Hanak DP, Powell D, Manovic V. Techno-economic analysis of oxy-combustion coal-fired power plant with cryogenic oxygen storage. Appl Energy 2017;191:193–203. http://dx.doi.org/10.1016/j.apenergy.2017.01.049.

[47] Ortiz C, Chacartegui R, Valverde JM, Becerra JA. A new integration model of the calcium looping technology into coal fired power plants for CO_2 capture. Appl Energy 2016;169:408–20. http://dx.doi.org/10.1016/j.apenergy.2016.02.050.

[48] Ylätalo J, Ritvanen J, Tynjälä T, Hyppänen T. Model based scale-up study of the calcium looping process. Fuel 2014;115:329–37. http://dx.doi.org/10.1016/j.fuel.2013.07.036.

[49] Romano MC. Modeling the carbonator of a Ca-looping process for CO_2 capture from power plant flue gas. Chem Eng Sci 2012;69:257–69. http://dx.doi.org/10.1016/j.ces.2011.10.041.

[50] Vorrias I, Atsonios K, Nikolopoulos A, Nikolopoulos N, Grammelis P, Kakaras E. Calcium looping for CO_2 capture from a lignite fired power plant. Fuel 2013;113:826–36. http://dx.doi.org/10.1016/j.fuel.2012.12.087.

[51] Dieter H, Bidwe AR, Varela-duelli G, Charitos A, Hawthorne C. Development of the calcium looping CO_2 capture technology from lab to pilot scale at IFK, University of Stuttgart. Fuel 2014;127:23–37. http://dx.doi.org/10.1016/j.fuel.2014.01.063.

[52] Charitos A, Rodríguez N, Hawthorne C, Alonso M, Zieba M, Arias B, et al. Experimental validation of the calcium looping CO_2 capture process with two circulating fluidized bed carbonator reactors. Ind Eng Chem Res 2011;50:9685–95. http://dx.doi.org/10.1021/ie200579f.

[53] Kunii D, Levenspiel O. The K-L reactor model for circulating fluidized beds. Chem Eng Sci 2000;55:4563–70. http://dx.doi.org/10.1016/S0009-2509(00)00073-7.

[54] Kunii D, Levenspiel O. Circulating fluidized-bed reactors. Chem Eng Sci 1997;52:2471–82. http://dx.doi.org/10.1016/S0009-2509(97)00066-3.

[55] Edwards SEB, Materić V. Calcium looping in solar power generation plants. Sol Energy 2012;86:2494–503. http://dx.doi.org/10.1016/j.solener.2012.05.019.

[56] Martínez I, Grasa G, Parkkinen J, Tynjälä T, Hyppänen T, Murillo R, et al. Review and research needs of Ca-Looping systems modelling for post-combustion CO_2 capture applications. Int J Greenh Gas Control 2016;50:271–304. http://dx.doi.org/10.1016/ j.ijggc.2016.04.002.

[57] Hanak DP, Kolios AJ, Manovic V. Comparison of probabilistic performance of calcium looping and chemical solvent scrubbing retrofits for CO_2 capture from coal-fired power plant. Appl Energy 2016;172:323–36. http://dx.doi.org/10.1016/j.apenergy.2016.03.102.

***ANNEX 8**: Bonaventura, D., Chacartegui, R., Valverde, J.M., Becerra, J.A., Ortiz, C., Lizana, J., 2018. Dry carbonate process for CO 2 capture and storage: Integration with solar thermal power. Renew. Sustain. Energy Rev. 82, 1796–1812. https://doi.org/10.1016/j.rser.2017.06.061*

Renewable and Sustainable Energy Reviews 82 (2018) 1796–1812

Contents lists available at ScienceDirect

Renewable and Sustainable Energy Reviews

journal homepage: www.elsevier.com/locate/rser

Dry carbonate process for CO_2 capture and storage: Integration with solar thermal power

D. Bonaventura[a,b], R. Chacartegui[b,*], J.M. Valverde[c], J.A. Becerra[b], C. Ortiz[c], J. Lizana[d]

[a] Politecnico di Torino, Corso Duca degli Abruzzi, 24, 10129 Torino, Italy
[b] Departamento de Ingeniería Energética, Universidad de Sevilla, Camino de los Descubrimientos s/n, 41092 Seville, Spain
[c] Facultad de Física, Universidad de Sevilla, Avda. Reina Mercedes s/n, 41012 Seville, Spain
[d] Departamento de Construcciones Arquitectónicas, Universidad de Sevilla, Avda. Reina Mercedes 2, 41012 Seville, Spain

ARTICLE INFO

Keywords:
Carbon capture
Post-combustion carbon capture
Coal fired power plant
Dry carbonate process
CCS economy
Solar thermal power

ABSTRACT

Capture and sequestration of CO_2 released by conventional fossil fuel combustion is an urgent need to mitigate global warming. In this work, main CO_2 capture and sequestration (CCS) systems are reviewed, with the focus on their integration with renewables in order to achieve power plants with nearly zero CO_2 emissions. Among these technologies under development, the Dry Carbonate Process shows several advantages. This manuscript analyses the integration of a CO_2 sorption-desorption cycle based on $Na_2CO_3/NaHCO_3$ into a coal fired power plant (CFPP) for CO_2 capture with solar support for sorbent regeneration. The Dry Carbonate Process relies on the use of a dry regenerable sorbent such as sodium carbonate (Na_2CO_3) to remove CO_2 from flue gases. Na_2CO_3 is converted to sodium bicarbonate ($NaHCO_3$) through reaction with CO_2 and water steam. Na_2CO_3 is regenerated when $NaHCO_3$ is heated, which yields a gas stream mostly containing CO_2 and H_2O. Condensation of H_2O produces a pure CO_2 stream suitable for its subsequent use or compression and sequestration. In this paper, the application of the Dry Carbonate CO_2 capture process in a coal-based power plant is studied with the goal of optimizing CO_2 capture efficiency, heat and power requirements. Integration of this CO_2 capture process requires an additional heat supply which would reduce the global power plant efficiency by around 9–10%. Dry Carbonate Process has the advantage compared with other CCS technologies that requires a relatively low temperature for sorbent regeneration (< 200 °C). It allows an effective integration of medium temperature solar thermal power to assist $NaHCO_3$ decarbonation. This integration reduces the global system efficiency drop to the consumption associated with mechanical parasitic consumption, resulting in a fossil fuel energy penalty of 3–4% (including CO_2 compression). The paper shows the viability of the concept through economic analyses under different scenarios. The results suggest the interest of advancing in this Solar-CCS integrated concept, which shows favourable outputs compared to other CCS technologies.

1. Introduction

There is a worldwide interest in finding competitive solutions for capturing and sequestering the carbon dioxide (CO_2) released from fossil fuel combustion processes to mitigate global warming. In the 2015 Paris Climate Conference (COP21), a universal agreement signed by the consensus of 195 countries was reached, which has been ratified in 2016, to drastically reduce CO_2 emissions in order to keep global warming below 2 °C from preindustrial levels [1]. To this end future coal-fired power plants (CFPPs) must be near to CO_2 emissions free. Currently, 76.5% of the electricity generation in the world is produced by non-renewable sources [2]. The main R&D challenge for the viability of CFPPs and other fossil fuel based facilities is to capture CO_2 by means of feasible and affordable technologies while, at the same time, penalties on power production and efficiency are minimized.

Carbon capture and storage (CCS) technologies can be classified into three main groups: pre-combustion, post-combustion and oxy-fuel combustion processes [3]. Despite post-combustion capture (PCC) processes are being widely investigated in the last years, Boundary Dam (100MWe) in Canada is currently the only commercial CFPP that applies CCS by using a chemical absorption process based on mono-ethanolamine (MEA). In amine-based systems the CO_2 loaded solvent is separated from the rest of the exhaust gas and heated, which yields relatively pure CO_2 ready for compression and sequestration. After regeneration, the solvent is cooled to be reused [4]. A main issue of systems based on amine absorption is the large amount of heat

* Corresponding author.
E-mail address: ricardoch@us.es (R. Chacartegui).

http://dx.doi.org/10.1016/j.rser.2017.06.061
Received 22 December 2016; Received in revised form 15 June 2017; Accepted 18 June 2017
Available online 01 July 2017
1364-0321/

Nomenclature

AC avoiding CO_2 cost
ASU air separation unit
BAC biomass annual cost
BFB bubbling fluidized bed
CaL calcium-looping process
CARB carbonation
CCS carbon capture and storage
CFB circulating fluidized bed
CFPP: coal-fired power plant
COE cost of electricity
COECCS cost of electricity associated to CCS system
c_{CO2} carbon tax
COP21 2015 Paris Climate Conference
CPU CO2 purification unit
CSP concentrated solar power
DCP dry carbonate process
DECARB: decarbonation
ECCS emission ratio with dry carbonate process integrated
ECO2 AVOIDED avoided cost due to the avoided emission of CO2,
EDRYCARBONATE carbon capture system installation cost
ENET, GAIN, year annual benefit due to avoided emissions.
EO&M operation and maintenance cost
EINCR revenues due to electricity incremented cost
Eref reference plant emission ratio
ESOLAR solar plant installation cost
ETOT, REV total annual revenues
ETOT total investment cost
FB fluidized bed
FC fuel cost
FCF fixed charge factor
FGD flue gas desulfurization
FGPLAN4 cooled flue gas
FGPLANT CO_2 input flow to the carbonator
GHG greenhouse gases
IPCC Intergovernmental Panel on Climate Change
IRR internal rate of return (%)
$m_{CO2,\ FGPLANT}$ CO_2 mass flows of flue gas exits the CFPP
$m_{CO2,\ CARB.OUT}$ CO_2 mass flows of flue gas exits the carbonator
MEA monoethanolamine solvent
NGCC natural gas combined cycles
NPV net present value
O&M operation and maintenance
PCC post-combustion capture
$P_{NET,\ year}$ total electric energy per year produced by the plant.
Q_{CFPP} CFPP thermal power consumptions
Q_{DC} dry carbonate thermal power consumption
SE-SMR sorption-enhanced steam methane reforming
SMR steam methane reforming
SPB simple payback
SPECCA specific energy consumption for CO_2 avoided
TCR capital cost
$ton_{CO2,\ ref}$ reference plant CO_2 emissions
$ton_{CO2,\ CCS}$ CO_2 emissions with the dry carbonate process integrated
VOM variable cost
W_{CFPP} CFPP net power production
W_{COMP} electric consumption for CO_2 compression
$W_{cons,\ DC}$ dry carbonate electric power consumption
W_{solid} electric consumption for solids conveying
WGS water gas shift
WHATHOT water inlet stream
YR yearly revenues
ε_{ABS} absorption efficiency
η_{plant} plant efficiency
η_{CCS} plant efficiency with the dry carbonate process integrated

required to regenerate the solvent. This heat, which is usually obtained from the steam cycle, penalizes significantly the power plant efficiency. Moreover, amine-based systems have serious problems related to toxicity and corrosion [5]. In addition, additional power is required to compress the captured CO_2 for transporting it through the pipeline network to the storage site.

Among the new generation of CCS technologies under R & D the Dry Carbonate Process stands as one of the most interesting options. This process uses Na_2CO_3 solid particles as dry sorbent to separate CO_2 from other flue gases through the gas-solid carbonation reaction. An important advantage of this approach is that sorption can occur at relatively low temperature (below 100 °C) to achieve a high capture capacity whereas regeneration is also carried out at relatively low temperatures (around 200 °C). Such temperatures do not cause significant degradation of the sorbent besides of not requiring high amounts of energy supply [6]. Other advantages of the Dry Carbonate Process are the low cost of the sorbent as well as the high CO_2 sorption capacity [7]. Due to the high interest attracted by this technology, CO_2 capture pilot plants have been integrated in CFPP in USA and Korea [8]. Recent studies have analyzed also its potential integration with the production of chemical products [9].

In this paper, a novel integration of the Dry Carbonate Process for CO_2 capture with solar thermal power is analyzed. The relative low temperature in the regeneration reactor allows for an effective integra-

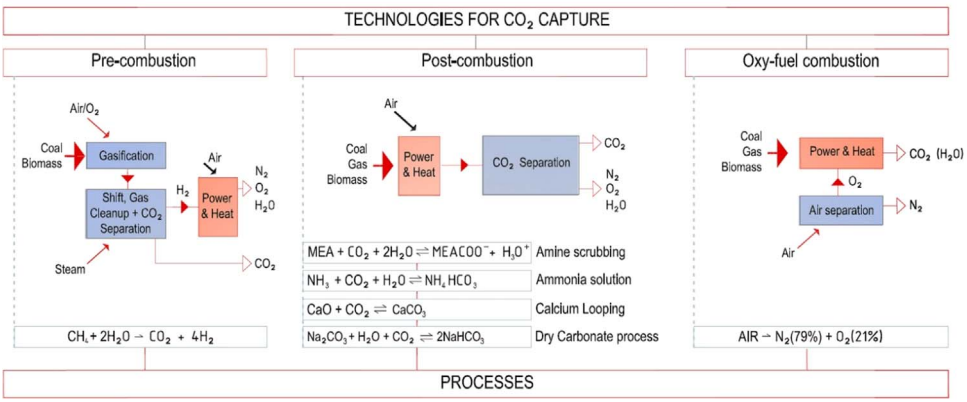

Fig. 1. Overview of technologies for CO_2 capture.

tion with solar thermal power, which supplies medium temperature heat at relatively reduced cost. This combination yields a significantly reduced penalty in the global efficiency compared with other technologies. Therefore, the Dry Carbonate Process has the potential for a real breakthrough as CO_2 capture system integrated in CFPP with a reduced penalty on the global process and a high CO_2 capture efficiency, which would help achieving a near to zero CO_2 emissions power plant. The deployment of the Dry Carbonate process could represent an enormous step forward to efficiently retrofit power plants based on no-renewable fossil fuels. Such ambitious goal is fully aligned with both the IPCC projections (CCS should contribute by about 55% to the cumulative global mitigation effort until 2100 [10]) and the IEA roadmap (1000 GW of installed Concentrated Solar power capacity by 2050 [11]).

The present paper has the following structure. Firstly, an overview of CO_2 capture technologies is given. Different alternatives are discussed, highlighting advantages and challenges of the Dry Carbonate Process as compared to other techniques. Secondly, a case study based on the integration of a CFPP with the Dry Carbonate Process is described (layout, processes and chemistry). Based on these analyses an economic study is carried out to assess the proposed plant viability and sensitivity to different relevant parameters (price of electricity, cost of technologies, fuel cost variability, energy penalty, carbon taxes). The results obtained suggest the high interest of the proposed integration under some particular scenarios.

2. CO_2 capture technologies. A brief review

This section is devoted to an overview of the state of art regarding CO_2 capture technologies. It is structured around the three main CCS technologies (Fig. 1), namely pre-combustion, post-combustion and oxy-fuel combustion processes [3].

2.1. Pre-combustion CO_2 capture

Pre-combustion CO_2 capture is based on the reaction of a fuel with oxygen or air with or without the presence of steam to produce a gaseous fuel, synthesis gas or syngas, which mainly consists of hydrogen and carbon monoxide. Carbon monoxide reacts afterwards with steam in a catalytic reactor (or shift converter) to produce CO_2 and more hydrogen. Finally, CO_2 is separated by means of physical or chemical absorption processes to obtain a hydrogen-rich fuel [10].

Syngas is usually generated from coal, biomass or natural gas by adding steam to the fuel (steam reforming) or by fuel partial oxidation. When natural gas is used as primary fuel in the conventional steam methane reforming (SMR) method the main reaction takes place in reformer tubes filled with catalyst [12]. In the case coal or biomass are used as fuel, gasification is the main conversion technology used to produce syngas. After syngas production, the water gas shift (WGS) reaction (Eq. (1)), involves the reaction between CO and steam to yield CO_2 and H_2 as products.

$$CO_{(g)} + H_2O_{(g)} \rightleftharpoons CO_{2(g)} + H_2 \qquad \Delta H_{298K} = -41\frac{kJ}{mol} \tag{1}$$

The high pressure (15–40 bar) of the produced gas stream (with a CO_2 content in the range of 15–60% in dry basis) facilitates the removal of CO_2 [13]. The captured CO_2 is ready to be compressed and stored whereas the rich H_2-product can be used for power production through a gas turbine [14], combined cycles [15] or in fuel cells [16].

The main advantage of pre-combustion capture is the production of CO_2 at elevated pressure, which reduces energy consumption for compression, and the production of a carbon-free fuel [10]. According to the IEA GHG program [17], an efficiency penalty of 16% is expected for natural gas combined cycles (NGCC) with pre-combustion CO_2 capture. This efficiency drop is caused by syngas production (6%), H_2/CO_2 separation (5%), the WGS process (3%), and CO_2 compression (2%) [12].

Due to the expected efficiency drop, current research is focussed on reducing energy losses and investment costs associated with CO_2 capture equipment. The most promising solution under study is based on the combination of reforming and the WGS reactions with CO_2 removal in one single stage, which shifts the reaction equilibrium towards the production of hydrogen. Thus, several H_2/CO_2 separation technologies have emerged in the last years based on membranes and solid sorbents [12]. In this regard, an modification of this process is the sorption-enhanced steam methane reforming (SE-SMR), where the process is enhanced by using a CO_2 sorbent in the reactor, which promotes the WGS reaction and achieves in situ CO_2 separation [18].

An option widely investigated in recent years is to integrate pre-combustion and post-combustion technologies, which allows exploiting potential synergies between both technologies [19]. Thus, SE-SMR-CaL and CaL enhanced gasification are being investigated. SE-SMR-CaL integration is based on CO_2 capture by CaO solids, which is thermodynamically favourable at the process conditions [20]. According to Martinez et al. [21], the SE-SMR-CaL integration achieves much higher H_2 production efficiencies (above 77%) in comparison with a conventional steam methane reforming (SMR) based plant using commercially available amines for CO_2 capture.

In the case of solid fuel gasification, it is also interesting to integrate the CaL process for increasing the hydrogen content in the syngas. According to Ramkumar and Fan thermodynamic analysis [22], the addition of CaO as sorbent allows to attain a hydrogen purity over 99% in the absence of a water-gas shift catalyst at near-stoichiometric steam to carbon (S:C) ratios, especially when operating at high pressures (> 21 atm) [22].

2.2. Oxy-fuel combustion

In oxy-fuel combustion a fuel is burned using pure oxygen rather than air as the primary oxidant. As a result, fuel consumption is diminished and flame temperature is higher as compared to air combustion, where part of the released heat is absorbed by nitrogen. Oxy-combustion requires an air separation process to remove nitrogen from the intake air to obtain an enriched oxygen stream with an oxygen concentration as high as 95%. To avoid a too high flame temperature by directly firing the fuel with pure oxygen, the mixture is diluted with CO_2 rich recycled flue gas [23,24]. In this way combustion temperature and heat transfer rate are controlled, and conventional equipment designed for conventional fuel/air combustion can be used in the coal power plant retrofitting process [25]. According to Kather et al. [26] the flue gas recirculation ratio appropriate to yield a mixture in the boiler with combustion temperatures and heat transfer fluxes similar to those obtained with conventional coal/air-combustion is in the range of 0.65–0.75 [27]. An alternative method to control flame temperature is the use of steam injection [28]. Although oxy-fuel combustion allows reducing CO_2 emissions quite efficiently, oxygen separation from air is a high energy demanding and costly process. Thus, the main drawback for the commercial deployment of oxy-combustion is the high energy consumption for pure O_2 production in the air separation unit (ASU). Cryogenic distillation is the common technique for this purpose, which requires an energy consumption of about 200 kWh per kg of pure O_2 [29,30].

After a purification process, the almost pure CO_2 stream (~ 95 vol%) is suitable for compression and storage or utilization [31,32]. According to Escudero et al. [33], CO_2 purification unit (CPU) specific energy consumption can be estimated as 143 kWh/tCO_2. The energy penalty associated to the integration of oxy-fuel combustion is in the range 7–13% [26,33,34].

Oxy-combustion has been successfully demonstrated in large-scale pilot projects (30 MW_e) [27,35,36]. Currently, most of the research activities on oxy-combustion are focused on pulverized coal combustion. However, Fluidized Bed (FB) combustion seems to be also an interesting alternative technology for oxy-combustion [37]. FB oxy-combustion was employed in CIUDEN project [38] with a thermal power of 30 MW_{th} obtained from burning diverse fuels (petroleum

coke, subbituminous coal and biomass among others) in a Circulating Fluidized Bed (CFB) boiler. Oxy-combustion using bubbling fluidized beds (BFB) has been also tested at the pilot scale [39]. A detailed review on current and proposed large scale oxy-coal combustion demonstration projects is presented in [25].

2.3. Post-combustion CO_2 capture

Post-combustion capture refers to CO_2 removal from the exhaust gas of fossil fuel power plants, which can be accomplished by using chemical solvents, solid sorbents or electrochemical processes.

In the currently mature chemical absorption technology, the solvent (typically an amine solution such as MEA) binds chemically with the CO_2. Amine absorption and stripping consists of passing the post-combustion flue gas through an aqueous amine solvent, which absorbs CO_2 by chemical reaction [40]. Then, the solvent loaded with CO_2 (the "rich" solvent) is heated up above typically 120 °C in the regenerator reactor wherein the CO_2-amine chemical reaction is reversed to release nearly pure CO_2 and regenerate the amine. The so-called "lean" solvent is recycled back to the absorber to restart the process while the released CO_2 is compressed to a suitable pressure for an efficient transportation and storage [41]. Amine-based PCC can efficiently remove around 90% of the CO_2 emissions.

In spite that CO_2 capture by chemical absorption using MEA is a well-established process in industry, the commercial deployment of this technology for post-combustion CO_2 capture at large scale is hindered by a combination of factors such as high energy penalty (8–12%) due to regeneration of the solvent [42,43], amine toxicity [44], solvent degradation [45] and equipment corrosion [46].

Sorption of CO_2 by solids (either by chemical reaction or physical adsorption) is an alternative method to chemical absorption with potential advantages linked to the arguably lower energy requirement for regeneration and easier operation and maintenance. Suitable sorbents for CO_2 removal should meet several requirements including high sorption capacity, high selectivity towards CO_2, fast kinetics, mild conditions for desorption, and high multicycle stability [47].

The calcium looping (CaL) process [48] is at the basis of a 2nd generation PCC technology [47] that uses CaO, typically derived from natural limestone, to capture CO_2 from flue gases by means of the reversible carbonation/calcination reaction (Eq. (2)):

$$CaO_{(s)} + CO_{2(g)} \rightleftharpoons CaCO_{3(s)} \quad \Delta H_{298K} = -178\frac{kJ}{mol} \tag{2}$$

The sorbent is repeatedly cycled between two CFB reactors. In the carbonator, CO_2 from the flue gas is captured by carbonation of the CaO particles. Taking into account that flue gases exiting from CFPP generally contain a mole fraction of CO_2 in the range 10– 15% [48,49], carbonation proceeds at a satisfactory high rate at temperatures in the range 625–700 °C while the reverse reaction to regenerate the sorbent is carried out in the calciner under high CO_2 partial pressure, thereby at much higher temperatures (900–950 °C) in order to achieve complete decarbonation in a typically short residence time of a few minutes [50–53]. The regenerated CaO particles are returned to the carbonator while a concentrated stream of CO_2 is released from the calciner ready for compression, transport and sequestration. A drawback of the process is the progressive deactivation of the regenerated CaO with the number of cycles due to the harsh calcination conditions leading to marked grain sintering. Thus, the CaO residual conversion at these CaL conditions is just around 0.07–0.08 [54,55], which requires a periodic feed of fresh limestone (make-up) to replace the poorly active sorbent. The endothermicity of the calcination reaction and the temperature difference between sorbent streams entering and leaving the calciner make it necessary to provide a high-energy input to the calciner. In order to achieve the required calcination temperature without CO_2 dilution, Shimizu and co-workers [56] proposed to oxy-fire coal (auxiliary fuel) in the calciner with O_2 provided by an external air separation unit, whose estimated size would be approximately one third of that required for an oxy-fuel power plant. This option serves to reach the high temperatures in the calciner typical of oxy-firing while CO_2 is not diluted, albeit CaO deactivation is further enhanced by irreversible CaO sulphation and ashes due to in-situ coal oxycombustion [55–58]. Recently, a combination of Oxy-combustion and CaL technologies has been proposed for coal power plants with some expected benefits such as the reduction of the CaL system size [59].

The CaL technology has several potential advantages when compared to amine scrubbing including a higher CO_2 capture efficiency (above 90%) with minor energy penalty over the power plant (4–9%) [19,60] and the low cost, wide availability and non-toxicity of natural CaO precursors such as natural limestone or dolomite [61]. Even though several pilot plant projects (~ 1–2 MW_{th}) are already showing promising results [52,62] the CaL technology has not yet reached a demonstration stage.

Another option for PCC is based on membrane separation, which uses the pressure difference between the flue gas and the removed CO_2. The membrane technology is generally useful to treat high-pressure gases [63,64] in spite of which a large number of researches have adapted it for post-combustion capture [43,65,66]. Regarding efficiency penalty associated to membranes use for PCC, it is estimated in the range of 4.9–8.5% [63]. Membrane separation is a promising solution to reduce the costs of PCC. However, the maximum pressure ratio attainable by feed compression and/or permeate vacuum is limited to approximately 10, due to cost and energy considerations [65].

A recently proposed option for PCC is the use of electrochemical processes in Molten Carbonate fuel cells. Some studies show that electricity generation in the fuel cell partially compensates the penalty on the original cycle in wastewater treatment plants [67] and power plants [68–70].

The development of dry CO_2 capture processes based on cheap materials operating at relatively low temperatures, which would require relatively low energy for sorbent regeneration, is considered as a promising pathway to advance in the deployment of CO_2 capture technologies [3,71]. In the present manuscript, the use of an abundant and cheap material such as sodium carbonate (Na_2CO_3) with a high dry CO_2 sorption capacity at relatively low temperatures is studied. Na_2CO_3 is the sorbent employed in the Dry Carbonate Process (DCP) early proposed in [72,73] and currently being demonstrated at the pilot-scale stage [74]. As Nelson et al. report [6], this capture process exhibits many potential advantages. First, sorbent regeneration is achieved at relatively low temperatures (100–200 °C) and it uses a dry sorbent. This helps decreasing considerably the energy required for sorbent regeneration as compared to amine based absorption, wherein much energy is lost due to the requirement of heating the large amounts of water in which the amine is dissolved. The DCP does not require any flue gas pretreatment and the reactor materials are not subjected to high thermal stresses or corrosive issues at the temperatures of operation. A further important advantage, as proposed in this work, is that dry sorbent regeneration in the range of working temperatures can be efficiently assisted by medium temperature solar thermal power, which significantly reduces energy penalty at affordable costs.

2.4. Challenges in the road to the deployment of CO_2 capture technologies

Each one of the above reviewed PCC technologies show specific advantages but also challenges to overcome at their different R & D development stages. Nonetheless, PCC is considered as the most appropriate technique to be applied in the short-term for its relatively easy integration in existing fossil fuel power plants [75]. PCC integration penalizes power plant performance and this hampers indirectly the global CO_2 emissions reduction. The use of renewable sources such as

solar thermal energy or biomass to aid the process is a possibility for mitigating this penalty. An intense R & D activity is being carried out to assess the feasibility of PCC-solar integration with the focus on reducing solar installation costs and providing a significant fraction of the heat required for sorbent regeneration [76].

The main drawbacks that hinder the deployment of PCC technologies are the high cost of the full CCS chain and the high efficiency penalty imposed on the power plant. Further obstacles are the financing of CO_2 transport infrastructure, legal and regulatory frameworks and insurance for safe permanent CO_2 storage or utilization [71]. As discussed below, diverse alternatives have been analyzed for mitigating the efficiency penalty through the assistance of solar thermal energy mainly focussed on amines and CaL based PCC systems. However, these studies fail generally to demonstrate net benefits from the solar-PCC integration in the absence of external incentives [77]. A main inconvenient for the integration of solar in the CaL process is that sorbent regeneration is rather energy intensive requiring calcination of large flow rates of solids at very high temperatures (900–950 °C) [50]. On the other hand, sorbent regeneration in amine-based capture systems is carried out at relatively much lower temperatures (slightly above 120 °C) [41]. Yet, regeneration of the aqueous amine solution involves heating a large amount of water which requires a high energy supply [78]. In this sense, the Dry Carbonate Process stands as a promising alternative since it demands a relatively small amount of energy supply for sorbent regeneration. In this process the dry sorbent (Na_2CO_3) is regenerated at much lower temperatures (150–200 °C) as compared to the CaL system [6,72,74]. Thus, solar thermal energy requirements for sorbent regeneration would be significantly reduced, which would favour the flexibility and economic viability of the solar-PCC integration.

3. Integration of renewables on post-combustion carbon capture systems

A main objective of R & D activities on PCC is to significantly reduce CO_2 emissions from fossil fuel plants with a reduced penalty on the power plant efficiency due to the high amount of energy required by the CO_2 capture processes. One way on the road to facilitate demonstration and deployment of PCC technologies is the use of renewable energy sources such as solar or biomass. The energy supplied by these renewable sources does not contribute to additional CO_2 emissions and is thus CO_2 neutral in the global process.

The integration of solar thermal energy in PCC technologies can be achieved through two different strategies: i) by assisting sorbent regeneration, and ii) by contributing to power production to minimize the efficiency penalty. Main research activities regarding solar-assisted PCC are focused on amine-based CO_2 capture and the recently emerged CaL process. In order to mitigate the high penalty associated to amine-based capture systems, a number of R & D activities have been carried out to assess the use of solar thermal technologies:

- Parvareh et al. [76] analyzed the use of different solar thermal technologies to support amine-based PCC for retrofitting CFPPs. They concluded that the large amount of thermal energy required for solar integration in this PCC technology would need a huge thermal storage and considerably high solar capital costs, which raises doubts on the feasibility of solar integration in amine based CO_2 capture systems. In addition, the huge solar thermal energy requirement for such integration to be effective is not available in most geographical locations globally.
- Mokhtar et al. [79] reported a study to reduce the energy intensity of the CO_2 separation process for retrofitting existing fossil fuel power plants. Partial solar thermal energy integration was assessed to reduce the penalty derived from amine-based PCC energy input in a CFPP case study of 300 MW_e. A main conclusion of this work is that the proposed integration could be economically viable for solar collector costs of USD100/m^2 and if more than 22% of the required solvent regeneration energy is provided by solar thermal energy.
- A techno-economic analysis of solar-assisted PCC applied to different locations in Australia has been recently reported by Qadir et al. [77]. The application was divided into three subsystems: the power plant (660 MW_e), the amine-based PCC plant and the solar collector field. Different solar technologies were compared under scenarios without and with heat integration between the three subsystems. Regarding solar collectors, the integration based on evacuated tube collectors performed better when heat integration between the three subsystems is properly accomplished, whereas parabolic trough collectors were more effective in the case without heat integration. The study concludes that process design (heat integration) and climatic constraints are important considerations for the effectiveness of solar-assisted PCC. However, the cases under study did not yield net benefits of using any of the solar collector technologies analyzed in the absence of incentives.
- Li et al. [80] studied the feasibility of integrating solar thermal energy into amine-based PCC for a 520 MW_e CFPP. They concluded that, in order to have an improvement on electricity and CO_2 avoidance costs with the solar integration, the prices of solar thermal collectors and vacuum tubes should be lower than 150 USD/m^2 and 90 USD/m^2 respectively. Also, the viability of solar-assisted PCC was highly dependent on climate conditions.
- Cohen et al. [41] have reviewed the use of high temperature solar thermal technologies to assist amine-based PCC. As a main outcome, it is concluded that using high temperature solar thermal energy for direct electricity generation is more efficient than using solar energy for assisting sorbent regeneration.
- A small-scale pilot study has been carried out by Wang et al. [81,82] on amine-based PCC coupled with a solar thermal sub-system. Two types of solar collectors were used to gain the required thermal energy of the reboiler (parabolic trough collectors and linear Fresnel reflectors). Both of them could provide the required temperature heat source at the small-scale of the test. The results suggested that the efficiency of parabolic trough collectors was higher and less dependent on solar radiation.

- Carapellucci et al. [83] analyzed two options for integrating renewable energies into a CFPP with CO_2 post-combustion capture either using an auxiliary biomass boiler or a concentrating solar power (CSP) system. The obtained results for the biomass boiler integration showed that the power plant capacity was increased by approximately 14% whereas the energy penalty (– 8%) was weakly reduced as compared to the reference case (with an efficiency of 42%). Regarding the CSP system it was shown that its integration causes a net efficiency decrease to 31%.
- Sharma et al. [84] proposed a highly integrated amine-based CO_2 capture power plant in which a solar thermal plant provides heat in order to avoid steam extraction from HP and IP turbines, which increases power production. By means of a Heat Exchanger Network (HEN) analysis, where the compressed gas energy is also utilized in the integration process, a significant reduction of power plant output penalty is achieved (efficiency is increased up to 34.9% from 29.4% for the base case).

In the case of CaL process, recent works have assessed the use of CSP to support CaL-based PCC for retrofitting fossil fuel power plants:

- Zhang et al. [85] evaluated the energy efficiency of the CaL system when the calciner is driven by a combination of oxy-fuel combustion and CSP, which provides 101 MW_{th} (a 7.4% of the total energy input in the calciner). An integration of the CCR process into an ultra-supercritical 1019 MW_{th} power plant was proposed. In this scheme, part of the CO_2 leaving the calciner was heated in the solar collectors after which it was returned to the calciner. Fossil fuel consumption

in the calciner was reduced by 6.9 g/kWh compared to the coal-driven case, which entails a decrease of the additional CO_2 generated and a decrease of the mass flow rate of fresh limestone makeup. This scheme leads to an overall efficiency penalty of 9.63% points associated to the CO_2 capture process. The thermal efficiency of co-driven case is just 0.28% points below that of the conventional coal-driven case (without CSP) due to the big losses of solar radiation to thermal conversion, which hinders the CSP efficiency. Accordingly, the increase of the CSP capacity reduces fuel consumption, but thermal efficiency is penalized due to the decrease of CSP efficiency.

- Zhai et al. [86] analyzed the CaL-PCC integration partially assisted by CSP for retrofitting existing CFPPs in order to recover the energy of the capture system. The work analyzes the integration through two different strategies, i) CFPP with solar aided CO_2 capture system ((solar + CC) + PP), which uses solar energy to reduce the fuel consumption in the calciner (a similar case than in [85]), and ii) solar aided CFPP plant with CO_2 capture system ((solar + PP) + CC) where solar energy is used in the main cycle for increasing power production. In both cases the solar thermal power available for the cycle is 88.58 MW_{th}. Results show that the second case is more beneficial regarding technical and environmental aspects, whereas the first case ((solar + CC) + PP) achieve a thermal efficiency slightly higher than in the ((solar + PP) + CC) case (31.20% against 31.09%).
- Tregambi et al. [87] assessed the performance of coupling the CaL system to CSP for a 100 MW_{th} CFPP with the goal of using renewable energy for providing all the thermal energy required in the calciner. The maximum thermal energy needed in the calciner to be provided entirely by CSP was 135 MW_{th}. As a novelty, the plant allows storing the excess power produced during the daytime as CaO resulting from the endothermic $CaCO_3$ calcination reaction, which could be recovered from the exothermic CaO carbonation reaction during the nighttime. They concluded that the CO_2 capture efficiency reaches a value close to 90% whereas 80% of the thermal input from the CSP system to the calciner can be recovered.

4. Detailed analysis on dry-carbonate process

In the rest of this work the use of an abundant and cheap material such as sodium carbonate (Na_2CO_3) with a high dry CO_2 sorption capacity at relatively low temperatures is analyzed.

4.1. Description

CO_2 is captured in the Dry Carbonate Process through the chemical binding of CO_2 to Na_2CO_3 in the carbonator reactor at operating temperatures below 100 °C. Na_2CO_3 is converted to $NaHCO_3$ through the chemical reaction with CO_2 in the presence of steam. The sorbent is regenerated back to its carbonate form when heated at temperatures above 100 °C, thus releasing a nearly pure CO_2 stream after steam condensation. The design of the Dry Carbonate Process takes into account the need to periodically replenish a certain amount of sorbent makeup due to particle attrition and the loss of sorbent activity by the irreversible reaction with SO_2 and HCl. It should be noted however that in post- wet flue gas desulfurization, SO_2 and HCl are present in the flue gas at very low concentrations (less than 20 ppm for SO_2 and 1 ppm for HCl), which would require a lower amount of fresh sorbent makeup flow. Fig. 2 shows a schematic flow diagram of the Dry Carbonate process.

The Dry Carbonate Process is particularly well suited for being retrofitted into CFPPs with wet flue gas desulfurization and for natural gas–fired power plants. In the work conducted by Nelson et al. [74] it was estimated that a commercial-scale Dry Carbonate Process (a 500 MW_e nominal power plant fed with natural gas and carbon) would require an initial sorbent loading of roughly 387 t and a makeup rate of fresh sorbent of about 0.2 t/h. After integration of the Dry Carbonate Process, the net efficiency of the plant would suffer a drop from 40.5% to 33.4% (7.1% penalty). In the case of power plants fed only with coal, there is a larger concentration of CO_2 in the flue gas and a larger amount of sorbent for CO_2 capture is needed whereas a similar loss of efficiency is expected.

The reactions involved in the capture of CO_2 using Na_2CO_3 result in the reversible formation of $NaHCO_3$ and Wegscheider's salt ($Na_2CO_3 \cdot 3NaHCO_3$) according to Eqs. (3) and (4) [74]:

$$Na_2CO_{3(s)} + CO_{2(g)} + H_2O_{(g)} \rightleftharpoons 2NaHCO_3 \quad \Delta H = -135.56 \frac{kJ}{mol} \tag{3}$$

$$Na_2CO_{3\,(s)} + 0,6CO_{2\,(g)} + 0,6H_2O_{(g)} \rightleftharpoons 0,4[Na_2CO_3 3NaHCO_{3\,(s)}] \quad \Delta H = -135.98 \frac{kJ}{mol} \tag{4}$$

Other possible reaction byproducts, such as sodium sesquicarbonate ($Na_2CO_3 \cdot NaHCO_3 \cdot 2H_2O$) and sodium bicarbonate hydrate ($NaHCO_3 \cdot 2H_2O$) are negligible at the reaction conditions of interest. Both forward reactions are exothermic. Therefore, heat integration is important for an efficient implementation of the process in a commercial system. Thermodynamically, the formation of Wegscheider's salt is favored under practical H_2O and CO_2 partial pressures at reaction temperatures of 70 °C and above. For regeneration of the sorbent, $NaHCO_3$ decomposes to Na_2CO_3, H_2O and CO_2 in the temperature range of 100–200 °C [88] although ideally fast conversion is reached at 200 °C [89].

Multicycle carbonation/regeneration tests reported in [74] show the results plotted in Fig. 3 for Na_2CO_3 conversion as a function of the cycle number (carbonation at 60 °C and regeneration at 160 °C). Even though further thermogravimetric analysis tests should be carried out including a larger number of cycles and analyzing also the reaction kinetics, these results suggest that conversion is kept stable at a relatively high level (around 0.9), which may be explained by the relatively low temperatures used for sorbent regeneration.

Potential contaminants present in the flue gas, such as SO_2 and

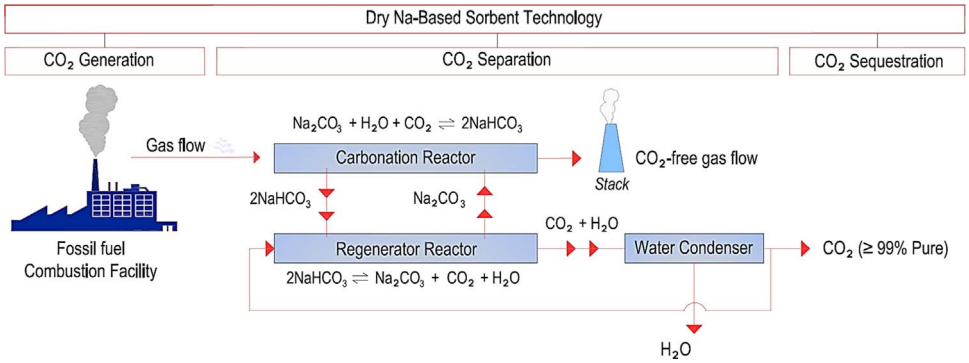

Fig. 2. General scheme of the dry carbonate process.

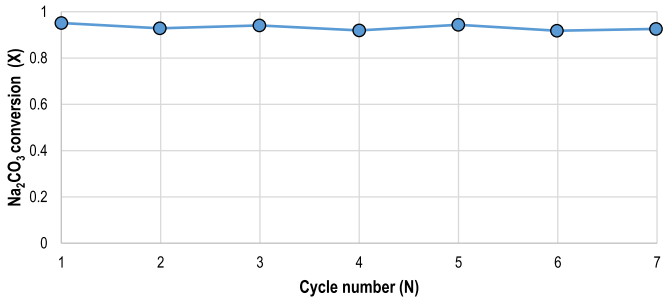

Fig. 3. Na_2CO_3 conversion as a function of the cycle number (data extracted from [74]).

HCl, could react irreversibly with Na_2CO_3 at process conditions according to the following reactions (Eqs. (5) and (6)):

$$Na_2CO_3 + 2HCl \rightleftharpoons 2NaCl + CO_2 + H_2O \quad (5)$$

$$Na_2CO_{3(s)} + SO_{2(g)} + \frac{1}{2}O_{2(g)} \rightleftharpoons Na_2SO_4 + CO_2 \quad (6)$$

Formation of NaCl and Na_2SO_4 reduces the capacity of the sorbent for CO_2 capture in subsequent cycles. However, the relative concentrations of HCl and SO_2 are one order of magnitude lower than the CO_2 concentration present in the flue gas following wet FGD (flue gas desulfurization) treatment, which mitigates the irreversible loss of conversion due to this issue.

4.2. Chemistry of the process

In order to gain further understanding of the dry carbonation process, the reaction mechanisms of Na_2CO_3 carbonation are detailed in this section. A possible mechanism by which Na_2CO_3 reacts with CO_2 is (Eqs. (7)–(10)) [90]:

$$CO_2 + 2H_2O \rightarrow H_3O^+ + HCO_3^- \quad (7)$$

$$HCO_3^- + H_2O \rightarrow H_3O^+ + CO_3^{--} \quad (8)$$

$$Na_2CO_3 \rightarrow 2Na^+ + CO_3^{--} \quad (9)$$

$$Na^+ + HCO_3^- \rightarrow NaHCO_3 \quad (10)$$

If the gas contains SO_2 other reactions would occur in the carbonation process. SO_2 can dissolve into water yielding sulfurous acid (H_2SO_3), and then the sulfurous acid dissociates, forming H^+ and HSO_3^- (Eq. (11)):

$$SO_{2(g)} + H_2O \rightarrow H_2SO_3 \rightarrow H^+ + HSO_3^- \quad (11)$$

Meanwhile, before the gas is dissolved into water, part of the SO_2 can react with O_2 to form SO_3, after which the SO_3 gas may dissolve into water to form sulfuric acid, which dissociates to H^+ and SO_4^{2-} ions leading to a reduction of the solution pH value. In addition, sulfurous acid (H_2SO_3) can also react with O_2 to form sulfuric acid. These reactions are given by Eqs. (12)–(14):

$$2SO_{2(g)} + O_{2(g)} \rightarrow 2SO_{3(g)} \quad (12)$$

$$SO_{3(g)} + H_2O \rightarrow H_2SO_{4(aq)} \rightarrow 2H^+ + SO_4^{2-} \quad (13)$$

$$2H_2SO_{3(aq)} + O_{2(g)} \rightarrow 2H_2SO_{4(aq)} \rightarrow 4H^+ + 2SO_4^{2-} \quad (14)$$

Also, chlorine present in the flue gas could react with water to form H_3O^+ and Cl^- (Eq. (15)):

$$HCl + H_2O \rightarrow H_3O^+ + Cl^- \quad (15)$$

Besides, part of Na^+ could react with SO_4^- and Cl^- according to Eqs. (16) and (17):

$$Na^+ + SO_4^- \rightarrow NaSO_4 \quad (16)$$

$$Na^+ + Cl^- \rightarrow NaCl \quad (17)$$

In order to model accurately the process, equilibrium reactions and salts formation were implemented in the computational model of our work. The salts formation reactions that can occur are (Eqs. (18)–(21)):

$$2Na^+ + CO_3^- + 10H_2O \rightarrow Na_2CO_3 \bullet 10H_2O \quad (18)$$

$$2Na^+ + CO_3^- + 7H_2O \rightarrow Na_2CO_3 \bullet 7H_2O \quad (19)$$

$$2Na^+ + CO_3^- + H_2O \rightarrow Na_2CO_3 \bullet H_2O \quad (20)$$

$$3Na^+ + CO_3^{--} + HCO_3^- + 2H_2O \rightarrow 2(Na_2CO_3 \bullet NaHCO_3 \bullet 2H_2O) \quad (21)$$

Thus, in addiction to sodium bicarbonate ($NaHCO_3$) other salts can be formed from the reactions involving CO_2, water and soda ash: sodium carbonate decahydrate ($Na_2CO_3.10H_2O$), sodium carbonate heptahydrate ($Na_2CO_3.8H_2O$), sodium carbonate monohydrate ($Na_2CO_3{\cdot}H_2O$), Wegscheider's salt ($Na_2CO_3{\cdot}3NaHCO_3$) and trona ($Na_2CO_3{\cdot}NaHCO_3{\cdot}2H_2O$) [91]. Fig. 4 shows the evolution of reaction equilibrium constants with temperature for the production of $NaHCO_3$ and other salts used in this work (adapted from [91]). The data was well fitted to the Eq. (22) [90]:

$$lnK_s = A + \frac{B}{T} + C\,ln(T) + DT \quad (22)$$

Best fitting parameters are shown in [90].

5. Case study: CFPP- dry-carbonate process (DCP) integration

5.1. Baseline CFPP

This section shows results from the simulation of the retrofitting of a 150 MW_e CFPP with a Dry Carbonate CO_2 capture system to assess the effects on the power plant and global system performance and to assess the feasibility of assisting sorbent regeneration by solar thermal energy.

Flue gas exiting the power plant is characterized by a dilute concentration of CO_2 and a large volumetric flow at ambient pressure. Thus, a typical 505 MW_e pulverized CFPP plant produces 28,300 m^3 of flue gas per minute with a CO_2 volume concentration between 10% and 15% [92]. In this work, a reference coal fired plant of 150 MW_e has been considered. The reference plant scheme is illustrated in Fig. 5 taking as a reference the integration model developed by Ortiz et al. [93]. The main data of the CFPP are given in Table 1.

Post-combustion flue gas characteristics are detailed in Table 2:

5.2. Dry carbonate process (DCP) integration

A schematic representation of the integrated process for CO_2 capture proposed in this work is shown in Fig. 6. Simulations were done using ASPEN PLUS™ environment [94]. Main units are indicated in the layout: for carbonation (CARB) and decarbonation (DECARB) of the sorbent, two separation units and heat exchangers for heat recovery and water

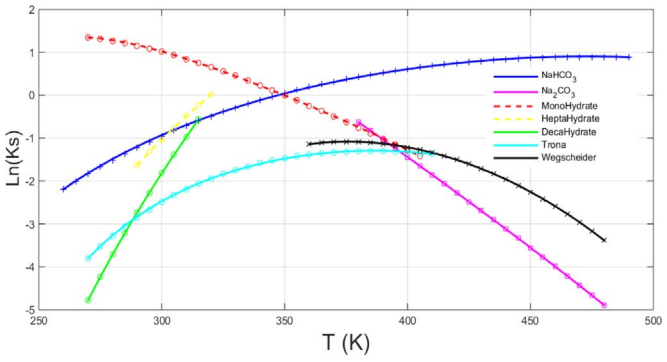

Fig. 4. Ln(Ks) values for reactions involved in $NaHCO_3$ production (derived from [90]).

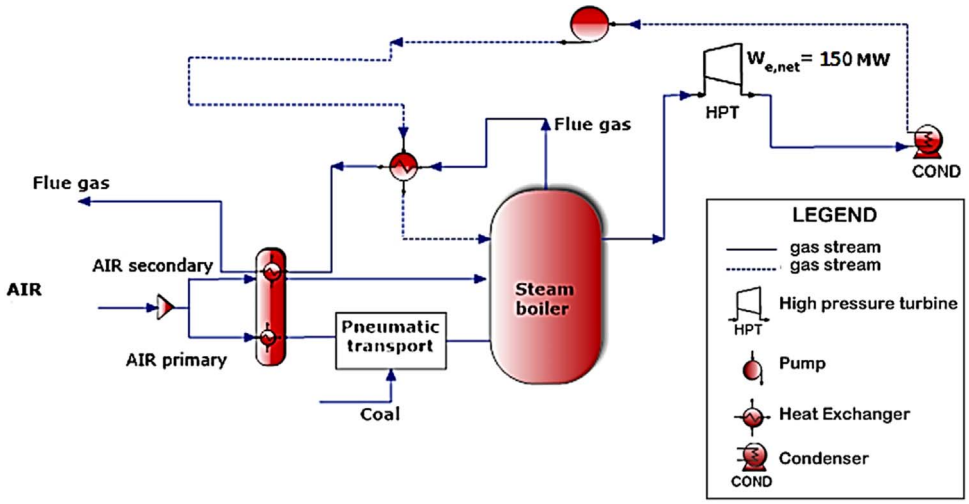

Fig. 5. Reference coal fired power plant scheme used in the present work.

Table 1
Reference data for a 150 MW_e coal fired plant (data scaled from [48]).

Item	Magnitude	Unit
Coal consumption	61	ton/h
Air intake	692	ton/h
Gross power introduced with fuel	447	MW_{th}
Net power supplied	397	MW_{th}
Net Power produced	150	MW_e
Net efficiency	33.5	%

Table 2
Flue gas flow for a 150 MW_e coal fired plant (data scaled from [48]).

Coal flue gas component	Mole flow (kmol/h)	Mass flow (tons/h)
N_2	17,154.21	529.71
CO_2	3085.62	135.96
H_2O	1471.86	29.4
O_2	781.8	27.57
CO	140.7	3.93
NO	135.36	4.47
SO_2	37.53	2.64

condensation at the end of the process are implemented. In the carbonator, inlet streams are water (WATHOT), sodium carbonate (NA_2CO_3) and cooled flue gas (FGPLAN4). The following assumptions have been considered in the simulation in ASPEN: i) ideal gas-solid separation, ii) auxiliaries are enough for heating and cooling necessities in the plant, iii) auxiliaries electric power consumption is not considered, iv) steady state operation is assumed, v) the regenerator reactor model is based on chemical and phase equilibrium through Gibbs' free energy minimization method, and iv) 90% isentropic efficiency is considered in the CO2 compressor

The carbonator works at 60 °C and absolute pressure 1.01 bar for CO_2 sorption. Under these conditions, formation of Weigscheider' salt is thermodynamically favored. The CO_2 input flow to the carbonator (FGPLANT) is 136 t/h (3080 kmol/h) while the CO_2 output flow (CARB-OUT) is 10.7 t/h CO_2. Efficiency of CO_2 capture in the carbonator is evaluated as:

$$\varepsilon_{ABS} = \frac{\dot{m}_{CO2,FGPLANT} - \dot{m}_{CO2,CARB-OUT}}{\dot{m}_{CO2,FGPLANT}} = 0,\ 92 \tag{23}$$

Here ε_{ABS} is the efficiency of absorption, while $m_{CO2,\ FGPLANT}$ and $m_{CO2,\ CARB.OUT}$ represent the CO_2 mass flows of flue gas exiting the CFPP and the carbonator, respectively.

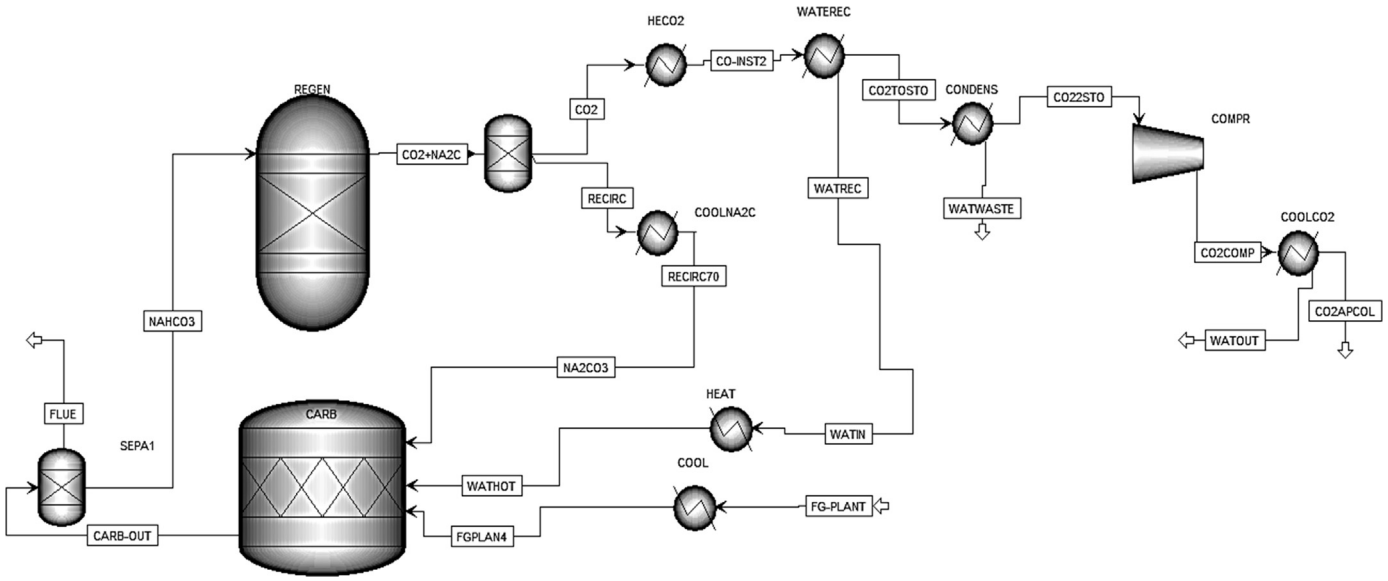

Fig. 6. Dry carbonate process layout.

Assuming a conservative value for Na_2CO_3 conversion (X = 0.75) in the carbonator ([74], see Fig. 3), the required mas flow of Na_2CO_3 is 430 t/h, which yields a mass ratio Na_2CO_3/CO_2 of 3.2 kg_{Na2CO3}/kg_{CO2}. In the best scenario (X = 1), this mass ratio would be 2.4 kg_{Na2CO3}/kg_{CO2}. Na_2CO_3 carbonation proceeds at an equimolar amount of CO_2 and H_2O, which yields a hot water requirement of at least 55.4 t/h. Within this amount, 27 t/h are taken directly from the residual steam in the post-combustion flue gas while the rest must be added from an external source. Table 3 shows the values of main operation parameters in the carbonator and calciner reactors.

Following the proposed layout (Fig. 6), the solids stream consists of $Na_2CO_3{\cdot}3NaHCO_3$ since $NaHCO_3$ and H_2O (NAHCO3C) is separated in the first separation unit from air and flue gas (FLUE) and is sent to the regenerator. Sorbent regeneration is carried out in this reactor, which releases a CO_2 concentrated stream. The amount of CO_2 released in the regenerator is 127 t/h at 140 °C with a 100% efficiency of CO_2 stripping from the sorbent.

From the energy balance in the regenerator, it may be calculated that a total 122.48 MW_{th} are required for maintaining the process. This heat can be obtained by burning additional coal or from another external source. In this work, the novel use of solar thermal power is proposed for that purpose. Pressurized hot water can be stored for a relatively long time at temperatures above 140 °C. Table 4 details the balances between the input and output flows in the calciner. It must be taken into account that part of the sorbent is lost during the overall process because of the irreversible reactions with SO_2 and HCl at the process conditions (Eqs. (5) and (6)). The loss of sorbent requires a make-up flow of 3 t/h of Na_2CO_3 in order to maintain the capture efficiency in the carbonator. After the regeneration stage, Na_2CO_3 is separated from the gas stream and it is recirculated into the carbonator at 80 °C.

From the calciner, a gas flow of 17.8 t/h (29% steam and 71% CO_2 by weight) is sent to a train of heat exchangers/coolers for heating and H_2O recovery. Finally, a flow of 12.7 t/h of pure CO_2 is compressed through three intercooled stages up to 70 bar, with a global power consumption of 1.5 MW_e, after which it is sent to storage. Considering the energy needed in the regenerator for sorbent regeneration, integration of the DCP yields a plant efficiency given by Eq. (24):

$$\eta_{plant} = \frac{\dot{W}_{CFPP} - \dot{W}_{cons,DC}}{\dot{Q}_{CFPP} + \dot{Q}_{DC}} \quad (24)$$

Here η_{plant} is the plant efficiency, W_{CFPP} and Q_{CFPP} are the net power production and the thermal power consumptions of the CFPP, while $W_{cons,\ DC}$ and Q_{DC} are the electric power consumption and the thermal power consumption in the DCP, respectively. By considering the work for CO_2 compression (W_{COMP}) and solids conveying (Wsolid), parasitic power consumption ($Wcons_{,DC}$) is given by Eq. (25):

$$\dot{W}_{cons,DC} = \dot{W}_{solid} + \dot{W}_{COMP} \quad (25)$$

Here a conservative value of W_{solid} = 5.5 kWh/ton can be used for estimating the solids conveying energy [95], which yields (Eq. (26)):

$$\dot{W}_{solid} = \dot{m}_{Na2CO3} \bullet 5,5 \frac{kwh}{ton} = 2.37 MWel \quad (26)$$

being Na_2CO_3 the sodium carbonate mass flow. A summary of the global plant data is given in Table 5.

By considering the extra-heat that must be supplied from coal to integrate the DCP, the global plant efficiency drops from 33.5% to 23.3%. The results obtained by imposing different carbonator and regenerator temperatures are shown in Fig. 7.

In the temperature range 50–70 °C for the carbonator, power consumption varies within the range 126.5–138.8 MW_{th}. As will be seen below, integration of solar thermal power to aid sorbent regeneration, as newly proposed in this work, could serve to mitigate significantly the efficiency penalty related to the carbon capture system.

5.3. Optimized plant configuration

The modified configuration proposed in this section is schematized in Fig. 8. A solid-solid heat exchanger (HEATEXCH) has been included between the two reactors with the aim of reducing the total amount of heat required in the regenerator. This heat exchanger allows for increased temperatures in the regenerator, which enhances the reaction rate with little additional expense of thermal power. The modified configuration also leads to a reduction of the power consumption for compression by introducing a multi-stage compression with inter-refrigeration included. A sensitivity analysis using this configuration has been also carried out to analyze the variation of power required for different carbonator/regenerator temperatures (Fig. 9).

In this case, the analysis shows (Fig. 9) that power consumption is in the range 111.9–116.4 MW_{th}. In this new configuration, it is possible to increase temperature in the regenerator with just a slight increase of power consumption and the advantage of enhancing reaction kinetics. Thus, heat recovery reduces the heat required for sorbent regeneration by about a 10%. The heat required using this new configuration (with working conditions in the regenerator set to 200 °C and 1.01 bar) is 114 MW_{th}.

The integration of solar thermal heat for aiding sorbent regeneration is a feasible option to achieve the required temperatures in the regenerator. This renewable heat source support would mitigate significantly the operational expenditure (OPEX) penalty associated to the carbon capture system integration.

In order to minimize the power consumption of CO_2 compression a multistage compression system is proposed. Configurations with two and three stages and different compression ratios were considered, Table 6. A three-stage compression with an inter-refrigeration stage at 20 °C reduces the compression power from 15 MW_e (baseline case) to 11.16 MW_e

Table 7 shows power consumption in the different parts of the system after introducing the proposed modifications:

With these modifications, the global efficiency of the plant (coal power plant + CCS) is increased by 0.9% (from 23.3% to 24.2%). In the above calculations, a constant value of sorbent conversion X = 0.75 was used. Table 8 shows the effect of sorbent conversion (X) on global efficiency. This parameter should be determined with further certainty from lab-scale thermogravimetric studies under realistic process conditions such as the solids residence time in the reactors in future works. Nevertheless, the efficiency variation is just around 1% in a wide range of sorbent conversions (between 0.4 and 0.95, Table 8).

To achieve a near to zero CO_2 emissions global system, renewable energy must be used for heating the regenerator, either solar or biomass when there is no availability of solar direct irradiation, which may be accomplished by storing heat. A number of storage materials for sensible storage systems are listed in Table 9. Solid storage and liquid storage media are presented for indirect storage of thermal energy, i.e. thermal energy from a heat transfer fluid (e.g. thermal oil, air) is transferred to a solid storage medium [96].

For this study, the storage volume needed for supplying the heat for regeneration during 12 h has been estimated. For example, a volume of 25 m × 25 m × 10 m is required for cast iron in order to cover a storage capacity of 12 h while if sand-rock mineral oil is used the required

Table 3
Carbonator and calciner working conditions.

	Carbonator	Calciner
Outlet temperature [°C]	60	140
Outlet pressure [bar]	1,01	1.01
Net heat duty [MW_{th}]	−101.240	122.480
Total feed stream CO2 flow [ton/h]	135.550	0
Total product stream CO2 flow [ton/h]	10.620	127.010
Net stream CO2 production [ton/h]	−124.930	127.010

Table 4
Calciner streams composition.

	CO_2+ NA	$NAHCO_3H$
Temperature (°C)	140	60
Pressure (bar)	1.01	1.01
Mass flow (ton/h)		
H_2O	50.28	1.44
CO_2	124	0
Na_2CO_3	323.25	442.7
$NaHCO_3$	0	11.39
Wegsheider's salt		44.39

Table 5
Power balance without heat recovery.

	Power production	Power consumption
CFFP	150 MW_e	447 MW_{th}
Decarbonator		122.5 MW_{th}
COMP		15 MW_e
Wsolid		2.37 MW_e
Net Power	132.53 MW_e	
Total heat requirement		569.5 MW_{th}

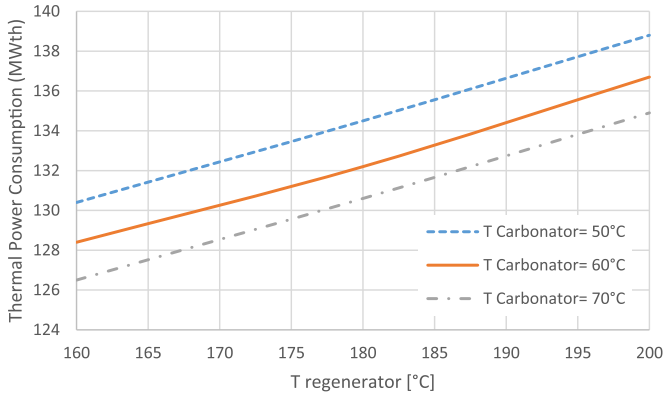

Fig. 7. Thermal power required for different carbonator and regenerator temperatures.

volume is 50 m × 50 m × 10 m (Table 9). Storage capacity has been estimated including a utilization coefficient $f_{utilization}$. This factor depends on the heat conductivity of the storage medium and the operational mode of the storage [97]:

$$Q_{storage} = f_{utilization} . m. c_p. \Delta T_{mix/max} \quad (27)$$

where m is the mass [kg], c_p is the mean heat capacity [J/(kg K)] and $\Delta T_{mix/max}$ is the temperature difference of the working fluid. Estimated associated costs of the solar system are included in the economic sensitivity analyses. These storage volume sizes constrain the applicability of the integrated CCS/solar solution as depending on space availability.

Another possibility for achieving the near to zero CO_2 emissions global system would be using biomass to meet power requirements for the regenerator. By considering an average heat capacity of biomass of 10.87 MJ/kg (Table 10), a biomass flow rate input of 44.5 t/h is necessary. If wood chips are used, the storage capacity for the biomass needed for one week of plant operation would be around 17,500 m^3.

Under the Carbon Emissions Reduction Target (CERT), a factor of 0.0249 kg_{CO2}/kWh is assumed for wood [99]. In the case study a factor of 0.03 ton_{CO2}/MWh is considered. Thus, an additional amount of 3.5 t/h (from 10.7 t/h to 14.2 t/h) must be taken into account in the analysis.

5.4. CFPP- dry-carbonate process integration: economic analysis

A detailed techno-economic analysis to assess the integration of medium temperature solar thermal technology to assist regeneration of the dry sorbent has been carried out. If heat for regenerator is obtained from solar thermal power the economic efficiency (defined in this case as the ratio between power production −136 MW_e- and fossil fuel consumption −447 MW_{th}- without considering solar thermal power) would be 30.5%. A number of assumptions according to different scenarios were made for the economic analysis. These different scenarios were defined in terms of:

- Electricity production, to take into account the penalty on electricity generation of the ancillary equipment consumption and parasitic loads (consumption in compressors, solids conveying and other ancillary equipment). All these factors have been considered by an electricity penalty of 10.1%.
- Variation of fuel costs, to include in the analyses the variability of fuel costs.
- Uncertainties in plant installation costs, to take into account uncertainty in the evolution of equipment costs. The maximum deviation has been taken as a ± 9% of the average installation price.
- DCP costs. As for any novel technology, there is uncertainty on the installation costs and its evolution. A range of ± 50% for CCS installation cost has been considered.
- Different fixed charge factors were in addition considered for the different scenarios.

Under these considerations, three scenarios were defined:

- Scenario **P** (Pessimistic Scenario). The pessimistic scenario implies a combination of the following factors: highest penalty in electricity generation (it has been taken as the maximum error in estimating parasitic electricity losses), highest costs and a fixed charge factor of 0.15.
- Scenario **BE** (Best Estimated Scenario). In this scenario, the values derived from the simulation above described were used to define the efficiency of the system. It considers a capital cost of 30 M€ [6] for the CCS technology and a fixed charge factor of 0.1.
- Scenario **O** (Optimistic Scenario). This optimistic scenario considers a range of minor fuel cost and minor costs of the CCS technology and plant installation. Furthermore, it considers the smallest change in electricity production and the smallest fixed charge factor of 0.075.

Table 11 summarizes the data used for calculating the costs according to the different scenarios for a total amount of 1089 kton/year avoided CO_2 emissions using the DCP.

Along with capital investment and operating and maintenance (O & M) cost, energy consumption is a main factor that determines the viability of a CO_2 capture technology. The specific energy consumption for CO_2 avoided (SPECCA) is usually employed to quantify the additional fuel consumption (in MJ) needed to avoid the emission of 1 kg of CO_2 into the atmosphere [42] (Eq. (28)):

$$SPECCA = 3600 \frac{\frac{1}{\eta_{CCS}} - \frac{1}{\eta_{ref}}}{E_{ref} - E_{CCS}} \left[\frac{MJ}{kg_{CO2}}\right] \quad (28)$$

where η_{ref} and η_{CCS} are the power plant efficiencies, and E_{ref} and E_{CCS} are the CO_2 emissions ratios (in kg_{CO2} /MWh_{el}) without and with the DCP integrated, respectively. Table 12 shows the results obtained from the SPECCA analysis for the different scenarios:

If the analysis is performed in terms of operational expenditures, and heat for regeneration of the sorbent is provided by solar (evaluated as a free energy intake from the point of view of OPEX), an operational efficiency ($\eta_{CCS,ECO}$) and a specific energy consumption for CO_2 avoided, considering only the fossil fuel ($SPECCA_{ECO}$) can be defined as:

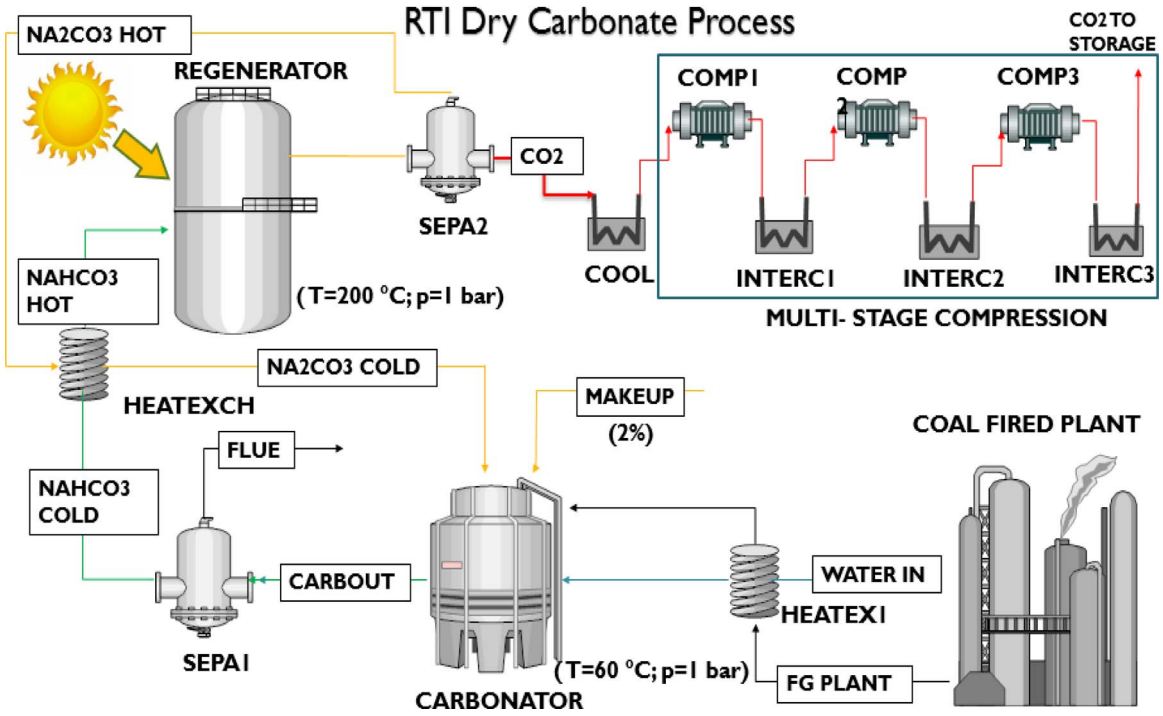

Acronyms (equipment and streams):

CARBONATOR: CO_2 capture reactor
CARBOUT: Final product from carbonator
CO_2: CO_2 recovered from the system
CO_2 TO STORAGE: CO_2 to the storage system (20 °C, 75 bar)
COAL FIRED PLANT: Coal fired plant for electricity production
COMP1: Compressor CO_2 (1-10 bar)
COMP2: Compressor CO_2 (10-25 bar)
COMP3: Compressor CO_2 (25-75 bar)
COOL: CO2 (20°C) intercooler
FGPLANT: Flue gas exits the coal fired plant
NA2CO3 COLD: Regenerated Na_2CO_3 (80°C)
NA2CO3 HOT: Regenerated Na_2CO_3 (200°C)
NAHCO3 COLD (fig.6): Solids exits the carbonator (60°C)
NAHCO3 HOT: Solids entering the regenerator (140°C)
HEATEX1 H_2O-flue gas heat exchanger
HEATEXCH: $NaHCO_3$-Na_2CO_3 heat exchanger
INTERC1: CO_2 (20°C) intercooler
INTERC2: CO_2 (20°C) intercooler
INTERC3: CO_2 (20°C) intercooler
MAKE UP: Sorbent Make up
REGENARATOR: Sorbent regenerator
SEPA1: Solid-gas separator
SEPA2: Solid-gas separator
WATER IN: Water to CO_2 capture reactor

Fig. 8. Optimized plant configuration proposed in this work.

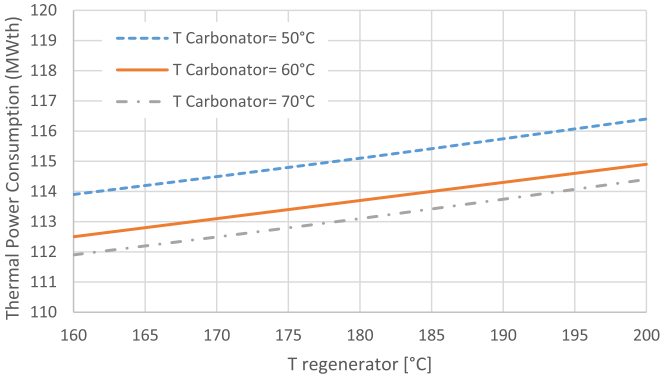

Fig. 9. Power consumption for different operating conditions (including heat recovery).

Table 6
CO_2 compression power.

Component	Two-stage compression		Three-stage compression	
	Exhaust pressure (bar)	Power (MW_e)	Exhaust pressure (bar)	Power (MW_e)
COMP1	9	6.29	4.2	3.78
COMP2	75	6.02	17.6	3.78
COMP3	–	–	75	3.6
Global W_{comp}		12.31		11.16

Table 7
Global plant energy balance.

	Power production	Power consumption
CFFP	150 MW_e	447 MW_{th}
Decarbonator		114.9 MW_{th}
COMP		11.16 MW_e
Wsolid		2.47 MW_e
Net Power	136.37 MW_e	
Total heat		561.9 MW_{th}

Table 8
Efficiency values for different sorbent conversion factors (X).

X	Na_2CO_3 flow (kmol/h)	Calciner (MW_{th})	Carbonator (MW_{th})	W_{solid} (MW_e)	Efficiency (%)
0.4	84.5	119.5	– 104	4.6	23.2
0.75	42.93	114.9	– 101	2.47	24.2
0.95	32.86	111	– 98	1.89	24.37

$$\eta_{CCS,ECO} = \frac{Net\ Power\ Production\,(MW_e)}{Fossil\ Fuel\ Consumption\,(MW_{th})} \tag{29}$$

$$SPECCA = 3600\frac{\frac{1}{\eta_{CCS,ECO}} - \frac{1}{\eta_{ref}}}{E_{ref} - E_{CCS}}\left[\frac{MJ}{kg_{CO2}}\right] \tag{30}$$

Table 9
Main properties of materials to store energy in the form of sensible heat [97,98].

	Temperature (°C) Cold	Hot	Average density (kg/m³)	Average heat conductivity (W/ (mK))	Average heat capacity (kJ/(kgK))	Thermal diffusivity (m^2/s)	Volume specific heat capacity (kWht/m^3)	Volume (m^3)
Solid storage media								
Sand-rock-mineral oil	200	300	1700	1.0	1.30	4.5 × 10–7	60	22,460.1
Reinforced concrete	200	400	2200	1.5	0.85	8.0 × 10–7	100	13,271.9
Cast iron	200	400	7200	37.0	0.56	9.2 × 10–6	160	6155.4
Liquid storage media								
Mineral oil	200	300	770	0.12	2.6	6.0 × 10–8	55	24,793.6
Synthetic oil	250	350	900	0.11	2.3	5.3 × 10–8	57	23,979.1
Silicone oil	300	400	900	0.10	2.1	5.3 × 10–8	52	Out of range
Nitrite salts	250	450	1825	0.57	1.5	2.1 × 10–7	152	Out of range

Table 10
Properties of different typologies of wood chips.

Wood chips	H_i[MJ/kg]	ρ[kg/m^3]	H_i[MJ/ m^3]
Chestnut	10.53	580	6106.24
Beech	13,45	750	10084.95
Spruce	7.90	450	3556.98
Larch	11.60	660	7654.88
Average	10.87	610	6630.29

The economic cost of CO_2 capture can be estimated in different ways, yet the most commonly used method contemplates incremental cost of electricity (€/kWh) and avoiding CO_2 cost (AC) expressed in terms of €/tonCO_2 avoided [100] (Eqs. (30) and (31)):

$$\Delta COE = COE_{CCS} - COE_{ref} \tag{31}$$

$$AC = \frac{\Delta COE}{\left(\frac{ton_{CO2}}{kWh}\right)_{CCS} - \left(\frac{ton_{CO2}}{kWh}\right)_{CCS}} \tag{32}$$

Here COE is the cost of electricity, the sub-index *CCS* represents the carbon capture and storage system and the sub-index *ref* refers to the reference plant (coal fired plant). For an accurate economic analysis, the lack of imposed taxes to CO_2 emissions has been taken into consideration. The costs of electricity in the three different scenarios for the reference plant are given by Eq. (33):

$$COE = Fixed\ Cost + Variable\ Cost + Fuel\ Cost = \frac{TCR \bullet FCF}{8760h} + VOM + \frac{FC}{\eta_{el}} \tag{33}$$

where η is the global plant efficiency (η = 0.335 for the reference plant).

Regarding the solar thermal power technology that would be used for producing the thermal power required for sorbent regeneration, a cost range between 1500 and 3500 €/kW [11] has been estimated for a parabolic trough plant with thermal energy storage [96]. This solar thermal technology can supply heat for regeneration of the dry sorbent at the required temperatures in the regenerator. Thus, to supply the heat required for the CCS system the expected cost has been calculated as (Eq. (34)):

$$E_{SOLAR}(M€) = c_{SOLAR}\left(\frac{M€}{MW}\right) \bullet \Phi_{REGENERATOR}(MW) \tag{34}$$

where c_{SOLAR} is the solar plant cost and $\Phi_{REGENERATOR}$ is the thermal power required by the regenerator.

The summarized COE costs for the three scenarios are shown in Table 13:

Table 14 shows the COE and investment costs for the three scenarios considered to facilitate the analysis on the effect of solar thermal power cost (in the range between 1500 €/kW_{th} and 3500 €/kWth). It includes the cost of the heat storage system. Regarding the cost of electricity with a CCS system, electric efficiency depends on power consumption for the different scenarios. Table 15 shows the variation of COE for different estimations of solar thermal power costs.

The costs of the other components and reactors are estimated in the range between 20 and 40 M€, estimated and extrapolated from the layouts presented in [6102]. Finally, maintenance and operation costs are assumed as 10% of the total investment cost. The total cost of the CCS system is given by Eq. (35):

$$E_{TOT} = E_{SOLAR} + E_{DRYCARBONATE} + E_{O\&M} \tag{35}$$

where E_{TOT} is the total investment cost, E_{SOLAR} is the solar plant installation cost, $E_{DRYCARBONATE}$ is the carbon capture system installation cost and $E_{O\&M}$ represents the cost due to operation and main-

Table 12
SPECCA analysis for different scenarios.

Item	Scen. P	Scen. BE	Scen. O
Net Power Production (MW_e)	125	136.37	137
CO_2 $_{CCS}$ (ton/h)	10.7	10.7	10.7
E_{CCS} (kg_{CO2}/kW h_{el})	85.60	78.46	78.10
η_{CCS}	0.232	0.242	0.244
SPECCA (MJ/kg_{CO2})	5.86	5.03	4.90
η_{CCS_ECO}	0.279	0.305	0.306
$SPECCA_{\_ECO}$(MJ/kg_{CO2})	2.65	1.29	1.24

Table 11
CO_2 emission data for different scenarios.

	Reference plant	Dry carbonate (P)	Dry carbonate (BE)	Dry carbonate (O)
Power (MW_e)	150	150	150	150
CCS Power consumption (MW_e)	–	25	13.63	13
Regenerator Heat requirement (MW_{th})	–	119	114.9	111
Net power (MW_e)	150	125	136.37	137
CO_2 Emissions (ton/h)	136	10.7	10.7	10.7
CO_2 Emissions (kmol/h)	3080	243.2	243.2	243.2
CO_2 Avoided Emissions (kton/year)		1089	1089	1089
CO_2 Emissions (tons/ MW h_e/h)	0.9	0.085	0.078	0.078

Table 13
COE for different scenarios.

Item	Item	Units	Scen. P	Scen. BE	Scen. O
Fuel cost [101]	FC	€/kW h	0.03	0.023	0.02
Capital cost	TCR	€/kWe	1200	1100	1000
Fixed charge factor [101]	FCF	$year^{-1}$	0.15	0.1	0.075
Variable cost	VOM	€/kWe	0.006	0.006	0.006
COE_{ref}		€/kW h	0.116	0.087	0.074

Table 14
COE for CCS system (as function of Solar Capital Costs).

Item	Item	Units	Scen. PE	Scen. BE	Scen. O
Net power production		MW_e	125	136.37	137
η_{el}			27.9	29.9	30.2
η_{system}		%	22.1	24.2	24.37
Dry Carb. Capital cost [6,102]	TCR	M€/ MW_e	0.32	0.223	0.148
Solar capital cost [103]	TCR	M€/MW_{th}	1.5		
COECCS		€/kW h	0.165	0.115	0.095
AC		€/ton_{CO2}	60.416	34.245	25.421
Solar capital cost [103]	TCR	M€/ MW_{th}	2		
COECCS		€/kW h	0.174	0.121	0.099
AC		€/ton_{CO2}	64.223	41.188	30.629
Solar capital cost [103]	TCR	M€/ MW_{th}	2.5		
COECCS		€/kWh	0.182	0.127	0.103
AC		€/ton_{CO2}	73.736	48.132	35.837
Solar capital cost [103]	TCR	M€/ MW_{th}	3		
COECCS		€/kW h	0.191	0.132	0.108
AC		€/ton_{CO2}	83.249	55.076	41.045
Solar capital cost [103]	TCR	M€/ MW_{th}	3.5		
COECCS		€/kW h	0.199	0.138	0.112
AC		€/ton_{CO2}	92.762	62.020	46.253

Table 15
ΔCOE (€/kWh_{el}) for different costs of solar thermal field.

Solar thermal cost (€/kW_{th})	Scen. P	Scen. BE	Scen. O
1500	0.0492	0.0281	0.0209
2000	0.0578	0.0339	0.0252
2500	0.0664	0.0396	0.0295
3000	0.0749	0.0453	0.0337
3500	0.0835	0.0510	0.0380

tenance including contingencies. Total CFPP retrofitting investment cost are shown in Table 16 as a function of investment costs for the three scenarios and solar field prices considered.

After the economic evaluation of electricity costs and avoided CO_2 emissions with the DCP assisted by medium temperature solar thermal power, net present value (NPV) and Simple Pay Back (SPB) are analyzed with the goal of assessing the effects of carbon taxes and installation funds for renewables technologies. To carry out these analyses, carbon taxes are assumed as fixed through the next years in the worst scenario (Scenario P) while they are assumed to increase in future years for the optimistic scenario (Scenario O). Additionally to these assumptions, for further viability analyses European or National funds could be considered because of the integration of solar thermal power to reduce CO_2 emissions. The net gain from avoided CO_2 emissions is given by Eq. (36):

$$E_{CO2,AVOIDED} = (ton_{CO2,ref} - ton_{CO2,CCS}) \bullet c_{CO2} \quad (36)$$

where $E_{CO2\ AVOIDED}$ is the avoided cost due to the avoided emission of CO_2, $ton_{CO2,\ ref}$ and $ton_{CO2,\ CCS}$ are the CO_2 emissions without and with the DCP integrated, respectively, while c_{CO2} is the carbon tax expressed in €/ton_{CO2}. The energy simple payback period, SPB, is the time to recover the initial investment in energy savings. SPB is calculated as the ratio of capital costs to the annual energy cost savings (Eq. (37)):

$$SPB = \frac{E_{TOT}}{E_{NET,GAIN,year}} \quad (37)$$

where E_{TOT} is the total investment of the plant while $E_{NET,\ GAIN,\ year}$ represents the annual economic gain due to the avoided emissions. Fig. 10 illustrates the SPB curves for the three scenarios as function of total CFPP retrofitting capital cost.

The net present value (NPV) is calculated as the discounted cash flow minus the capital cost (Eq. (38)):

$$NPV = \sum_{n=0}^{n} \frac{E_{NET,GAIN,year}}{(i+1)^n} - E_{TOT} \quad (38)$$

where n represents the year number and i is the discount rate. Fig. 11 illustrates the variation of NPV as a function of the carbon taxes value for fixed discount rate (i = 0.1) and different values of investment cost.

It shows the high dependence of NPV under different situations of carbon taxes. If the economic profit for the avoided CO_2 emissions is not enough to balance the additional investment cost an increase of electricity price ($\Delta PRICE_{EL}$) is required. The annual revenues due to this incremental cost is given by Eq. (39):

$$E_{INCR} = \Delta PRICE_{EL}\left(\frac{€}{kwh}\right) \bullet P_{NET,year}\left(\frac{MWh}{year}\right) \quad (39)$$

where E_{INCR}, expressed in M€/year, represents the revenues due to the incremented cost of selling electricity while $P_{NET,\ year}$ is the total electric energy per year produced by the plant. Thus, the total yearly revenue ($E_{TOT,\ REV}$) would be (Eq. (40)):

$$E_{TOT,REV} = E_{NET,GAIN,year} + E_{INCR} \quad (40)$$

The required rise of electricity price associated to each case is shown in Table 17:

Table 16
Total CFPP retrofitting cost calculated by considering several CSP plant prices.

Solar thermal cost 1.5 M€/ MW_{th}				
	Units	Scen. P	Scen. BE	Scen. O
ESOLAR	M€	179.25	172.35	166.5
EDRY	M€	40	30	20
EO & M	M€	21.92	20.23	18.65
ETOT	M€	241.17	222.58	205.15
Solar Thermal Cost 2 M€/ MW_{th}				
	Units	Scen. P	Scen. BE	Scen. O
ESOLAR	M€	239	229.8	222
EDRY	M€	40	30	20
EO & M	M€	27.9	25.98	24.2
ETOT	M€	306.9	285.78	266.2
Solar Thermal Cost 2.5 M€/ MW_{th}				
	Units	Scen. P	Scen. BE	Scen. O
ESOLAR	M€	298.75	287.25	277.5
EDRY	M€	40	30	20
EO & M	M€	33.87	31.725	29.75
ETOT	M€	372.62	348.975	327.25
Solar Thermal Cost 3 M€/ MW_{th}				
	Units	Scen. P	Scen. BE	Scen. O
ESOLAR	M€	358.5	344.7	333
EDRY	M€	40	30	20
EO & M	M€	39.85	37.47	35.3
ETOT	M€	438.35	412.17	388.3
Solar Thermal Cost 3.5 M€/ MW_{th}				
	Units	Scen. P	Scen. BE	Scen. O
ESOLAR	M€	418.25	402.15	388.5
EDRY	M€	40	30	20
EO & M	M€	45.82	43.21	40.85
ETOT	M€	504.07	475.36	449.35

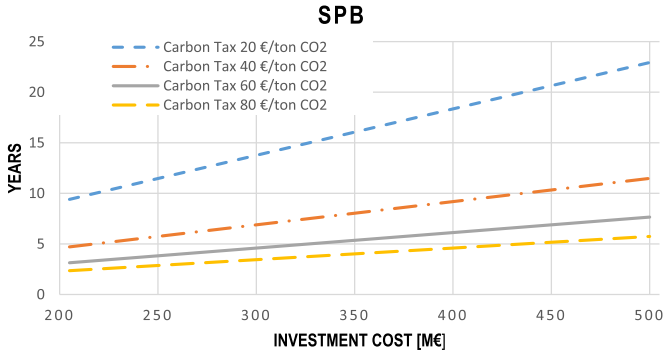

Fig. 10. SPB curves according to the three scenarios as function of CFPP retrofitting capital costs.

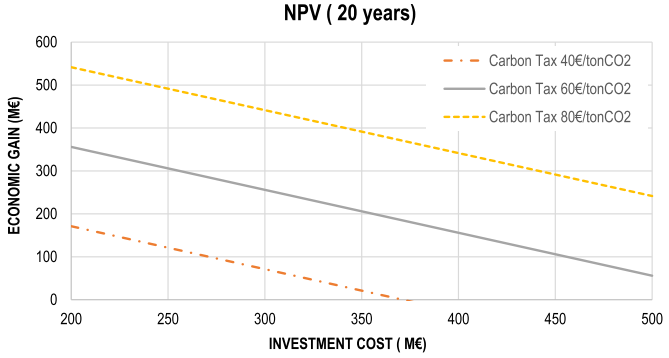

Fig. 11. NPV for different carbon tax values and different investment costs.

Table 17
Required increment of electricity sale price for maintaining a fixed value of IRR = 0.1.

	Total investment cost (M€)	E_{incr} (M €/year)	Δ Electricity price (c €/kW h)
Without carbon tax	200	23.5	1.967
	300	35.2	2.947
	400	47	3.934
	500	58.8	4.922
Carbon tax 20 €/tonCO2	200	0	0
	300	11.6	0.971
	400	23.4	1.959
	500	35.2	2.947
Carbon tax 40€/ tonCO2	200	0	0
	300	0	0
	400	0	0
	500	11.5	0.963

5.5. Heat storage for near zero CO_2 emissions

The use of heat storage for solar has been considered in the previous analyses by taking into account solar equipment costs. If biomass is alternatively employed, operating costs derive from the various stages of the supply chain (cutting, chipping, transportation). On average, a total cost of 50 €/ton [104] for M40 (M40 = 40% of humidity) wood chip can be estimated whereas the total cost would be 85 €/ton [105] for M20 wood chip. In the case study the LHV is near a M40 wood chip class. If a wood chip price of 60 €/ton is assumed, it would result a biomass annual cost of 31.18 M€. Under a scenario of 60 €/ton CO_2 for carbon taxes a yearly revenue of 32.31 M€ could be achieved. For these calculations, a total investment cost within the range of 80–110 €/kW [106] is considered for the biomass system, where O & M costs are estimated as a 40% of the capital costs.

5.6. Discussion

The above results suggest a potential interest of the DCP for CO_2 capture. The energy penalty that results from retrofitting a CFPP with this CCS technology (9%) is similar to that estimated for other technologies such as pre-combustion CO_2 capture (16%), amines scrubbing (8–12%), membranes (5–8.5%) and Calcium Looping (4–9%). However, because of the low temperature needed to regenerate the sorbent, a CO_2 neutral solar facility could be efficiently integrated to supply the heat required, which would reduce coal consumption and operation costs significantly. Solar energy integration would serve to decrease the energy penalty just to CO_2 compression and auxiliaries consumption, which leads to a near to zero CO_2 emissions power plant. The solar-CCS system penalty is estimated as just 3–4% points, with a SPECCA of only around 2 MJ/kg. Previous works based on thermodynamic analysis of the DCP report an energy consumption of about 3 MJ/kg [8]. For a 120 MWth CSP plant, as presented in this analysis, if parabolic through technology were considered the solar installation would require an area in the range of 60–70 ha [94]. Therefore applicability of the concept will be constrained by area availability in the surroundings of power plant for the development of solar field and energy storage integration.

The results obtained from the economic analysis strongly suggest the economic viability of using the DCP to retrofit a CFPP. Since the DCP is an emerging CCS technology, cost estimations are based on assumptions based on diverse scenarios. Thus, for a 150 MW_e CFPP, the most optimistic scenario leads the total investment cost of 205 M€ whereas for the pessimistic scenario the calculated investment is 449 M €. Thus, estimated costs are in the range between 25 and 46 €/ton_{CO2} (avoided CO_2) and from 0.095 to 0.112 € per kWh_e. Considering the results obtained for the Best Estimated Scenario case, the total investment cost of the proposed solar assisted DCP is estimated in the range of 1500–3200 $/$kW_e$ as function of solar facility cost. These values are higher than those estimated for other CO_2 capture technologies (the cost of a CFPP with a MEA system for post-combustion CO_2 capture would be about 700$/$kW_e$ [8]). According to Zhao et al. [8], the total capital cost of an Integrated Gasification Combined Cycle (IGCC) plant with a pre-combustion CO_2 capture system is about 1775–2567$/$kW_e$, the cost of a CFPP with a MEA system for post-combustion CO_2 capture would be about 1798$/$kW_e$, that of an oxy-combustion plant would be about 1810 $/$kW_e$ whereas that of a membrane/catalytic plant would be 2082 $/$kW_e$. However, OPEX will be notably reduced by replacing fuel by solar energy, with a SPECCA of 2 MJ/kgCO_2, meanwhile the SPECCA for MEA based systems is estimated in the double, around 4 MJ/kgCO_2 and similar values are obtained for other CCS technologies [42]. This very reduced value of SPECCA compensates the higher investment costs.

In this sense it is important to point out that the above analysis is based on different assumptions for a novel integration scheme and references to other applications. Solar field cost is estimated on the basis of solar power plants costs. For this CCS application, with a clearly lower temperature than in CSP parabolic trough power plants, and without an integrated power block, cheaper materials in the receiver and for heat transfer can be used. For instance, for the temperature range of CCS application, pressurized water perfectly could be used instead of the thermal oil system in CSP. Therefore, lower investment costs should be expected. In any case, the preliminary results obtained show an interesting potential to be further explored by a deeper analysis in future works. Future works should address in further depth a comparison between different CFPP-DCP-solar integration schemes to minimize energy penalty and investment costs. Since the carbonation reaction is exothermic, a proper use of the released energy is fundamental. Moreover, further work on the multi-cycle sorbent behavior at realistic process conditions is needed.

6. Conclusions

This paper is devoted in its first part to provide an overview of the currently most studied CO_2 capture systems. The performance of CCS technologies is assessed, highlighting advantages, drawbacks and challenges. In a second part a novel analysis is carried out for the integration of medium temperature solar thermal energy into the Dry Carbonate Process to assist sorbent regeneration. The Dry Carbonate Process to capture CO_2 is based on the use of a cheap, abundant and non-toxic material (Na_2CO_3) as dry sorbent at relatively low temperatures for both carbonation and sorbent regeneration. Our work shows that, when coupled with a medium temperature solar thermal power technology including thermal storage, the integration yields a nearly zero CO_2 emissions with a reduced global penalty in the power plant and avoiding also the generation of hazardous waste. The efficiency of the power plant coupled to the Dry Carbonate Process to capture CO_2 is decreased from 33.5% to 24.2% if fossil fuel is used to supply the heat for regeneration of the sorbent. This penalty is due to the amount of heat required for sorbent regeneration plus the power spent for CO_2 compression and solid conveying. If solar thermal power is used for sorbent regeneration, the penalty drops remarkably and the global efficiency, defined in terms of operational expenditures, is just decreased from 33.5% to 30%. Since additional fossil fuel would not be needed for sorbent regeneration most of this penalty is due to compression of the captured CO_2. A cost estimation of CO_2 capture by means of the Dry Carbonation Process coupled to solar thermal power (for the optimistic scenario) ranges from 25 to 46 €/ton_{CO2} (avoided CO_2) and from 0.095 to 0.112 € per kWh_e produced (compared to 0.087 €/kWh_e for the reference plant) as depending on the cost of the solar thermal technology. Thus, the highest costs are associated to the solar energy system. Although there is room for technology improvement and additional cost reductions could be expectedly achieved, especially in the solar field, the proposed integration based on solar thermal power and the Dry Carbonation Process can be considered as a promising technology as compared to other carbon capture technologies and renewable energy integrations recently proposed in the literature.

Acknowledgements

This work was supported by the Spanish Government Agency Ministerio de Economia y Competitividad and FEDER Funds (contracts CTQ2014-52763-C2-2-R and MAT2013-41233-R). The authors would like to thank the Spanish Ministry of Education, Culture and Sport for financial support via two pre-doctoral contracts: the FPU contract granted to Francisco Jesús Lizana Moral (FPU14/06583); and the FPI contract granted to Carlos Ortiz Dominguez (BES-2015–0703149).

References

[1] United Nations. Adoption of the Paris agreement; 2015.
[2] IRENA. REthinking Energy 2017: Accelerating the global energy transformation. IRENA; 2017.
[3] Arnette AN. Renewable energy and carbon capture and sequestration for a reduced carbon energy plan: an optimization model. Renew Sustain Energy Rev 2016;70:254–65. http://dx.doi.org/10.1016/j.rser.2016.11.218.
[4] Zhang X, Singh B, He X, Gundersen T, Deng L, Zhang S. Post-combustion carbon capture technologies: energetic analysis and life cycle assessment. Int J Greenh Gas Control 2014;27:289–98. http://dx.doi.org/10.1016/j.ijggc.2014.06.016.
[5] Annesini MC, Augelletti R, De Filippis P, Scarsella M, Verdone N. Sviluppo di un processo di separazione della CO_2 dal biogas mediante assorbimento con soluzioni amminiche in solvente organico (Report RdS/PAR2013/253); 2013.
[6] Nelson TO, Coleman LJI, Green DA, Gupta RP. The dry carbonate process: carbon dioxide recovery from power plant flue gas. Energy Procedia 2009;1:1305–11. http://dx.doi.org/10.1016/j.egypro.2009.01.171.
[7] Kondakindi RR, Aleksic S, Whittenberger W, Abraham MA. Na_2CO_3-based sorbents coated on metal foil: post testing analysis. Top Catal 2013;56:1944–51. http://dx.doi.org/10.1007/s11244-013-0131-1.
[8] Zhao C, Zhao C, Chen X, Anthony EJ, Jiang X, Duan L, et al. Capturing CO_2 in flue gas from fossil fuel-fired power plants using dry regenerable alkali metal-based sorbent. Prog Energy Combust Sci 2013;39:515–34. http://dx.doi.org/10.1016/j.pecs.2013.05.001.
[9] Bonaventura D, Chacartegui R, Valverde JM, Becerra JA, Verda V. Carbon capture and utilization for sodium bicarbonate production assisted by solar thermal power. Energy Convers Manag 2017. http://dx.doi.org/10.1016/j.enconman.2017.03.042.
[10] Change WGI of the IP on C. IPCC, 2005: Special report on carbon dioxide capture and storage; 2005.
[11] International Energy Agency. Technology roadmap solar thermal electricity; 2014:52. http://dx.doi.org/10.1007/SpringerReference_7300.
[12] Jansen D, Gazzani M, Manzolini G, Dijk E Van, Carbo M. Pre-combustion CO_2 capture. Int J Greenh Gas Control 2015;40:167–87. http://dx.doi.org/10.1016/j.ijggc.2015.05.028.
[13] Feron PHM, Hendriks CA. CO_2 Capture process principles and costs. Oil Gas Sci Technol – Rev IFP 2005;60:451–9. http://dx.doi.org/10.2516/ogst:2005027.
[14] Chacartegui R, Torres M, Sánchez D, Jiménez F, Muñoz a, Sánchez T. Analysis of main gaseous emissions of heavy duty gas turbines burning several syngas fuels. Fuel Process Technol 2011;92:213–20. http://dx.doi.org/10.1016/j.fuproc.2010.03.014.
[15] Chacartegui R, Sánchez D, de Escalona JMM, Monje B, Sánchez T. On the effects of running existing combined cycle power plants on syngas fuel. Fuel Process Technol 2012;103:97–109. http://dx.doi.org/10.1016/j.fuproc.2011.11.017.
[16] Sánchez D, Chacartegui R, Muñoz A, Sánchez T. Thermal and electrochemical model of internal reforming solid oxide fuel cells with tubular geometry. J Power Sources 2006;160:1074–87. http://dx.doi.org/10.1016/j.jpowsour.2006.02.098.
[17] IEAGHG. CO_2 Capture at gas fired power plant; 2012.
[18] Barelli L, Bidini G, Gallorini F, Servili S. Hydrogen production through sorption-enhanced steam methane reforming and membrane technology: a review. Energy 2008;33:554–70. http://dx.doi.org/10.1016/j.energy.2007.10.018.
[19] Perejon A, Romeo LM, Lara Y, Lisbona P, Valverde JM. The calcium-looping technology for CO_2 capture: on the important roles of energy integration and sorbent behavior. Appl Energy 2015;162:787–807. http://dx.doi.org/10.1016/j.apenergy.2015.10.121.
[20] Ochoa-Fernandez E, Haugen G, Zhao T, Ronning M, Aartun I, B?rresen B, et al. Process design simulation of H2 production by sorption enhanced steam methane reforming: evaluation of potential CO_2 acceptors. Green Chem 2007;9:654. http://dx.doi.org/10.1039/b614270b.
[21] Martínez I, Romano MC, Chiesa P, Grasa G, Murillo R. Hydrogen production through sorption enhanced steam reforming of natural gas: thermodynamic plant assessment. Int J Hydrog Energy 2013;38:15180–99. http://dx.doi.org/10.1016/j.ijhydene.2013.09.062.
[22] Ramkumar S, Fan LS. Calcium looping process (CLP) for enhanced noncatalytic hydrogen production with integrated carbon dioxide capture. Energy Fuels 2010;24:4408–18. http://dx.doi.org/10.1021/ef100346j.
[23] Wall T, Liu Y, Spero C, Elliott L, Khare S, Rathnam R, et al. An overview on oxyfuel coal combustion-State of the art research and technology development. Chem Eng Res Des 2009;87:1003–16. http://dx.doi.org/10.1016/j.cherd.2009.02.005.
[24] Pei X, He B, Yan L, Wang C, Song W, Song J. Process simulation of oxy-fuel combustion for a 300 MW pulverized coal-fired power plant using Aspen Plus. Energy Convers Manag 2013;76:581–7. http://dx.doi.org/10.1016/j.enconman.2013.08.007.
[25] Chen L, Yong SZ, Ghoniem AF. Oxy-fuel combustion of pulverized coal: characterization, fundamentals, stabilization and CFD modeling. Prog Energy Combust Sci 2012;38:156–214. http://dx.doi.org/10.1016/j.pecs.2011.09.003.
[26] Kather A, Scheffknecht G. The oxycoal process with cryogenic oxygen supply. Naturwissenschaften 2009;96:993–1010. http://dx.doi.org/10.1007/s00114-009-0557-2.
[27] Scheffknecht G, Al-Makhadmeh L, Schnell U, Maier J. Oxy-fuel coal combustion – a review of the current state-of-the-art. Int J Greenh Gas Control 2011;5:16–35. http://dx.doi.org/10.1016/j.ijggc.2011.05.020.
[28] Seepana S, Jayanti S. Steam-moderated oxy-fuel combustion. Energy Convers Manag 2010;51:1981–8. http://dx.doi.org/10.1016/j.enconman.2010.02.031.
[29] Romano M, Martínez I, Murillo R, Arstad B. Guidelines for modeling and simulation of Ca-looping processes; 2012.
[30] Martínez I, Murillo R, Grasa G, Abanades JC. Integration of a Ca-looping system for CO_2 capture in an existing power plant. Energy Procedia 2011;4:1699–706. http://dx.doi.org/10.1016/j.egypro.2011.02.043.
[31] Posch S, Haider M. Optimization of CO_2 compression and purification units (CO_2CPU) for CCS power plants. Fuel 2012;101:254–63. http://dx.doi.org/10.1016/j.fuel.2011.07.039.
[32] Romano MC. Ultra-high CO_2 capture efficiency in CFB oxyfuel power plants by calcium looping process for CO_2 recovery from purification units vent gas. Int J Greenh Gas Control 2013;18:57–67. http://dx.doi.org/10.1016/j.ijggc.2013.07.002.
[33] Escudero AI, Espatolero S, Romeo LM. Oxy-combustion power plant integration in an oil refinery to reduce CO_2 emissions. Int J Greenh Gas Control 2016;45:118–29. http://dx.doi.org/10.1016/j.ijggc.2015.12.018.
[34] Buhre BJP, Elliott LK, Sheng CD, Gupta RP, Wall TF. Oxy-fuel combustion technology for coal-fired power generation. Prog Energy Combust Sci 2005;31:283–307. http://dx.doi.org/10.1016/j.pecs.2005.07.001.
[35] Escudero AI, Espatolero S, Romeo LM, Lara Y, Paufique C, Lesort A-L, et al. Minimization of CO_2 capture energy penalty in second generation oxy-fuel power plants. Appl Therm Eng 2016;103:274–81. http://dx.doi.org/10.1016/j.applthermaleng.2016.04.116.
[36] Jin B, Zhao H, Zheng C. Thermoeconomic cost analysis of CO_2 compression and

purification unit in oxy-combustion power plants Bo. Energy 2015;83:416–30. http://dx.doi.org/10.1016/j.energy.2015.02.039.
[37] Mathekga HI, Oboirien BO, North BC. A review of oxy-fuel combustion in fluidized bed reactors; 2016. p. 878–902. http://dx.doi.org/10.1002/er.
[38] Lupion M, Alvarez I, Otero P, Kuivalainen R, Hotta A, Hack H. 30 MWth CIUDEN Oxy-CFB boiler – first experiences. Energy Procedia 2013;37:6179–88. http://dx.doi.org/10.1016/j.egypro.2013.06.547.
[39] De Diego LF, Obras-loscertales M De, Rufas A, Gayán P, Abad A, Adánez J. Pollutant emissions in a bubbling fluidized bed combustor working in oxy-fuel operating conditions: effect of flue gas recirculation. Appl Energy 2013;102:860–7. http://dx.doi.org/10.1016/j.apenergy.2012.08.053.
[40] El Hadri N, Quang DV, Goetheer ELV, Abu Zahra MRM. Aqueous amine solution characterization for post-combustion CO_2 capture process. Appl Energy 2015;185:1433–49. http://dx.doi.org/10.1016/j.apenergy.2016.03.043.
[41] Cohen SM, Webber ME, Rochelle GT. Utilizing solar thermal energy for post-combustion CO_2 capture. J Energy Power Eng 2011;3:195–208. http://dx.doi.org/10.1115/ES2010-90147.
[42] Politecnico di Milano – Alstom UK (CAESAR project). European best practice guidelines for assessment of CO_2 capture technologies; 2011.
[43] Aaron D, Tsouris C. Separation of CO_2 from flue gas: a review. Sep Sci Technol 2005;40:321–48. http://dx.doi.org/10.1081/SS-200042244.
[44] Luis P. Use of monoethanolamine (MEA) for CO_2 capture in a global scenario: consequences and alternatives. Desalination 2016;380:93–9. http://dx.doi.org/10.1016/j.desal.2015.08.004.
[45] Rey A, Gouedard C, Ledirac N, Cohen M, Dugay J, Vial J, et al. Amine degradation in CO_2 capture. 2. New degradation products of MEA. Pyrazine and alkylpyrazines: analysis, mechanism of formation and toxicity. Int J Greenh Gas Control 2013;19:576–83. http://dx.doi.org/10.1016/j.ijggc.2013.10.018.
[46] Fytianos G, Ucar S, Grimstvedt A, Hyldbakk A, Svendsen HF, Knuutila HK. Corrosion and degradation in MEA based post-combustion CO_2 capture. Int J Greenh Gas Control 2016;46:48–56. http://dx.doi.org/10.1016/j.ijggc.2015.12.028.
[47] Dean CC, Blamey J, Florin NH, Al-Jeboori MJ, Fennell PS. The calcium looping cycle for CO_2 capture from power generation, cement manufacture and hydrogen production. Chem Eng Res Des 2011;89:836–55. http://dx.doi.org/10.1016/j.cherd.2010.10.013.
[48] Wang W, Ramkumar S, Wong D, Fan LS. Simulations and process analysis of the carbonation-calcination reaction process with intermediate hydration. Fuel 2012;92:94–106. http://dx.doi.org/10.1016/j.fuel.2011.06.059.
[49] Manovic V, Anthony EJ. Competition of sulphation and carbonation reactions during looping cycles for CO_2 capture by cao-based sorbents. J Phys Chem A 2010;114:3997–4002. http://dx.doi.org/10.1021/jp910536w.
[50] Fennell PS, Davidson JF, Dennis JS, Hayhurst AN. Regeneration of sintered limestone sorbents for the sequestration of CO_2 from combustion and other systems. J Energy Inst 2007;80:116–9. http://dx.doi.org/10.1179/174602207X189175.
[51] Ylätalo J, Parkkinen J, Ritvanen J, Tynjälä T, Hyppänen T. Modeling of the oxy-combustion calciner in the post-combustion calcium looping process. Fuel 2013;113:770–9. http://dx.doi.org/10.1016/j.fuel.2012.11.041.
[52] Arias B, Diego ME, Abanades JC, Lorenzo M, Diaz L, Martínez D, et al. Demonstration of steady state CO_2 capture in a 1.7MWth calcium looping pilot. Int J Greenh Gas Control 2013;18:237–45. http://dx.doi.org/10.1016/j.ijggc.2013.07.014.
[53] Dieter H, Bidwe AR, Varela-duelli G, Charitos A, Hawthorne C. Development of the calcium looping CO_2 capture technology from lab to pilot scale at IFK, University of Stuttgart. Fuel 2014;127:23–37. http://dx.doi.org/10.1016/j.fuel.2014.01.063.
[54] Valverde JM. A model on the CaO multicyclic conversion in the Ca-looping process. Chem Eng J 2013;228:1195–206. http://dx.doi.org/10.1016/j.cej.2013.05.023.
[55] Valverde JM, Sanchez-Jimenez PE, Perez-Maqueda L. Calcium-looping for post-combustion CO_2 capture. On the adverse effect of sorbent regeneration under CO_2. Appl Energy 2014;126:161–71. http://dx.doi.org/10.1016/j.apenergy.2014.03.081.
[56] Shimizu T, Hirama T, Hosoda H, Kitano K, Inagaki M, Tejima K. A twin fluid-bed reactor for removal of CO_2 from combustion processes. Chem Eng Res Des 1999;77:62–8. http://dx.doi.org/10.1205/026387699525882.
[57] Abanades JC. The maximum capture efficiency of CO_2 using a carbonation/calcination cycle of CaO/$CaCO_3$. Chem Eng J 2002;90:303–6. http://dx.doi.org/10.1016/S1385-8947(02)00126-2.
[58] Borgwardt RH. Calcium oxide sintering in atmospheres containing water and carbon dioxide. Ind Eng Chem Res 1989;28:493–500. http://dx.doi.org/10.1021/ie00088a019.
[59] Ortiz C, Valverde JM, Chacartegui R, Benítez-Guerrero M, Perejón A, Romeo LM. The Oxy-CaL process: a novel CO_2 capture system by integrating partial oxy-combustion with the Calcium-Looping process. Appl Energy 2017;196:1–17. http://dx.doi.org/10.1016/j.apenergy.2017.03.120.
[60] Martínez Isabel, Grasa Gemma, Parkkinen Jarno, Tynjälä Tero, Hyppänen Timo, Murillo MCR Ramón. Review and research needs of Ca-Looping systems modelling for post-combustion CO_2 capture applications. Int J Greenh Gas Control 2016;50:1–101. http://dx.doi.org/10.1016/j.ijggc.2016.04.002.
[61] Ortiz C, Valverde JM, Chacartegui R. Energy consumption for CO_2 capture by means of the calcium looping process: a comparative analysis using limestone, dolomite, and steel slag. Energy Technol 2016:1–12. http://dx.doi.org/10.1002/ente.201600390.
[62] Ströhle J, Junk M, Kremer J, Galloy A, Epple B. Carbonate looping experiments in a 1 MWth pilot plant and model validation. Fuel 2014;127:13–22. http://dx.doi.org/10.1016/j.fuel.2013.12.043.
[63] Goto K, Yogo K, Higashii T. A review of efficiency penalty in a coal-fired power plant with post-combustion CO_2 capture. Appl Energy 2013;111:710–20. http://dx.doi.org/10.1016/j.apenergy.2013.05.020.
[64] Baker RW, Lokhandwala K. Natural gas processing with membranes: an overview; 2008. p. 2109–21.
[65] Merkel TC, Lin H, Wei X, Baker R. Power plant post-combustion carbon dioxide capture: an opportunity for membranes. J Memb Sci 2010;359:126–39. http://dx.doi.org/10.1016/j.memsci.2009.10.041.
[66] Favre E. Membrane processes and postcombustion carbon dioxide capture: challenges and prospects. Chem Eng J 2011;171:782–93. http://dx.doi.org/10.1016/j.cej.2011.01.010.
[67] Chacartegui R, Monje B, Sánchez D, Becerra J a, Campanari S. Molten carbonate fuel cell: towards negative emissions in wastewater treatment CHP plants. Int J Greenh Gas Control 2013;19:453–61. http://dx.doi.org/10.1016/j.ijggc.2013.10.007.
[68] Discepoli G, Milewski J, Desideri U. Off-design operation of coal power plant integrated with natural gas fueled molten carbonate fuel cell as CO_2 reducer. Int J Hydrog Energy 2016;41:4773–83. http://dx.doi.org/10.1016/j.ijhydene.2016.01.065.
[69] Milewski J, Bujalski W, Wołowicz M, Futyma K, Kucowski J, Bernat R. Experimental investigation of CO_2 separation from lignite flue gases by 100 cm2 single molten carbonate fuel cell. Int J Hydrog Energy 2014;39:1558–63. http://dx.doi.org/10.1016/j.ijhydene.2013.08.144.
[70] Barelli L, Bidini G, Campanari S, Discepoli G, Spinelli M. Performance assessment of natural gas and biogas fueled molten carbonate fuel cells in carbon capture configuration. J Power Sources 2016;320:332–42. http://dx.doi.org/10.1016/j.jpowsour.2016.04.071.
[71] Nataly Echevarria Huaman R, Xiu Jun T. Energy related CO_2 emissions and the progress on CCS projects: a review. Renew Sustain Energy Rev 2014;31:368–85. http://dx.doi.org/10.1016/j.rser.2013.12.002.
[72] Krieg JP, Winston AE. Dry carbonation process. United States Patent. US 06/487114 (US4459272 A); 1984.
[73] Falotico AJ. Dry carbonation of trona. PCT Application. PCT/US1992/006321 (WO1993/011070 A1); 1993.
[74] Nelson TO, Green DA, Box P, Gupta RP, Henningsen G, Turk BS. Carbon dioxide capture from flue gas using dry regenerable sorbents (Final Report). DOE cooperative agreement no. DE-FC26-00NT40923, RTI Project No. 0207887; 2009.
[75] Wang M, Lawal A, Stephenson P, Sidders J, Ramshaw C, Hill W, et al. Post-combustion CO_2 capture with chemical absorption: a state-of-the-art review. Chem Eng Res Des 2011;89:1609–24. http://dx.doi.org/10.1016/j.cherd.2010.11.005.
[76] Parvareh F, Sharma M, Qadir A, Milani D, Khalilpour R, Chiesa M, et al. Integration of solar energy in coal-fired power plants retrofitted with carbon capture: a review. Renew Sustain Energy Rev 2014;38:1029–44. http://dx.doi.org/10.1016/j.rser.2014.07.032.
[77] Qadir A, Mokhtar M, Khalilpour R, Milani D, Vassallo A, Chiesa M, et al. Potential for solar-assisted post-combustion carbon capture in Australia. Appl Energy 2013;111:175–85. http://dx.doi.org/10.1016/j.apenergy.2013.04.079.
[78] Liang Z, Fu K, Idem R, Tontiwachwuthikul P. Review on current advances, future challenges and consideration issues for post-combustion CO_2 capture using amine-based absorbents. Chin J Chem Eng 2016;24:278–88. http://dx.doi.org/10.1016/j.cjche.2015.06.013.
[79] Mokhtar M, Ali MT, Khalilpour R, Abbas A, Shah N, Hajaj A Al, et al. Solar-assisted post-combustion carbon capture feasibility study. Appl Energy 2012;92:668–76. http://dx.doi.org/10.1016/j.apenergy.2011.07.032.
[80] Li H, Yan J, Campana PE. Feasibility of integrating solar energy into a power plant with amine-based chemical absorption for CO_2 capture. Int J Greenh Gas Control 2012;9:272–80. http://dx.doi.org/10.1016/j.ijggc.2012.04.005.
[81] Wang F, Zhao J, Li H, Li H, Zhao L, Yan J. Experimental study of solar assisted post-combustion carbon capture. Energy Procedia 2015;75:2246–52. http://dx.doi.org/10.1016/j.egypro.2015.07.401.
[82] Wang F, Zhao J, Li H, Deng S, Yan J. Preliminary experimental study of post-combustion carbon capture integrated with solar thermal collectors. Appl Energy 2016:185. http://dx.doi.org/10.1016/j.apenergy.2016.02.040.
[83] Carapellucci R, Giordano L, Vaccarelli M. Analysis of CO_2 post-combustion capture in coal-fired power plants integrated with renewable energies. Energy Procedia 2015;82:350–7. http://dx.doi.org/10.1016/j.egypro.2015.11.801.
[84] Sharma M, Parvareh F, Abbas A. Highly integrated post-combustion carbon capture process in a coal-fired power plant with solar repowering. Int J Energy Res 2015;44. http://dx.doi.org/10.1002/er.3361.
[85] Zhang X, Liu Y. Performance assessment of CO_2 capture with calcination carbonation reaction process driven by coal and concentrated solar power. Appl Therm Eng 2014;70:13–24. http://dx.doi.org/10.1016/j.applthermaleng.2014.04.072.
[86] Zhai R, Li C, Qi J, Yang Y. Thermodynamic analysis of CO_2 capture by calcium looping process driven by coal and concentrated solar power. Energy Convers Manag 2016;117:251–63. http://dx.doi.org/10.1016/j.enconman.2016.03.022.
[87] Tregambi C, Montagnaro F, Salatino P, Solimene R. A model of integrated calcium looping for CO_2 capture and concentrated solar power. Sol Energy 2015;120:208–20. http://dx.doi.org/10.1016/j.solener.2015.07.017.
[88] Heda PK, Dollimore D, Alexander KS, Chen D, Law E, Bicknell P. A method of assessing solid state reactivity illustrated by thermal decomposition experiments on sodium bicarbonate. Thermochim Acta 1995;255:255–72. http://dx.doi.org/10.1016/0040-6031(94)02154-G.

[89] Otsubo Y, Yamaguchi K. Thermochemical properties and reaction processes of alkali carbonate-ferric oxide systems as investigated by means of differential thermal method. I-II. I. Li_2CO_3-Fe_2O_3 System. Chem Soc Jpn 1961;82:557–60. http://dx.doi.org/10.1246/nikkashi1948.82.5_557.
[90] Bonaventura D, Chacartegui R, Valverde JM, Becerra JA, Verda V. Carbon capture and utilization for sodium bicarbonate production assisted by solar thermal power. Energy Convers Manag 2017. http://dx.doi.org/10.1016/j.enconman.2017.03.042.
[91] Haynes HW. Thermodynamic solution model for trona brines. AIChE J 2003;49:1883–94. http://dx.doi.org/10.1002/aic.690490724.
[92] Ciferno JP, Fout TE, Jones AP, Murphy JT. Capturing carbon from existing coal-fired power plants. Chem Eng Prog 2009;105:33–41.
[93] Ortiz C, Chacartegui R, Valverde JM, Becerra JA. A new integration model of the calcium looping technology into coal fired power plants for CO_2 capture. Appl Energy 2016;169:408–20. http://dx.doi.org/10.1016/j.apenergy.2016.02.050.
[94] Chemical Process Optimization Software – Chemical process design | Aspen Plus n.d. ⟨http://www.aspentech.com/products/engineering/aspen-plus/⟩. [Accessed 11 June 2017].
[95] Mills D. Pneumatic conveying design guide; 2004. p. 80.
[96] Chacartegui R, Vigna L, Becerra JA, Verda V. Analysis of two heat storage integrations for an Organic Rankine Cycle Parabolic trough solar power plant. Energy Convers Manag 2016;125:353–67. http://dx.doi.org/10.1016/j.enconman.2016.03.067.
[97] Hoffschmidt PD-IB. Thermal heat storage systems; 2008.
[98] Winter Sizmann V-H. Solar power plants – fundamentals, technology, systems, economics. Springer-Verlag; 1991.
[99] Bates J, Henry S. Carbon factor for wood fuels for the supplier obligation. Final report (AEA/ED01858010/Issue 2); 2009.
[100] Carlos Abanades J, Grasa G, Alonso M, Rodriguez N, Anthony EJ, Romeo LM. Cost structure of a postcombustion CO2 capture system using CaO; 2007. http://dx.doi.org/10.1021/ES070099A.
[101] European coal prices slump to a record low - Bloomberg n.d.
[102] Green DA, Turk BS. Carbon dioxide capture from flue gas; 2005. doi:DOE Cooperative agreement no. DE-FC26-00NT40923.
[103] IRENA. Renewable energy technologies cost analysis series: concentrating solar power. vol. 1; 2012. http://dx.doi.org/10.1016/B978-0-08-087872-0.00319-X.
[104] Jacobson M. Project economics for wood energy. Common forms of biomass; 2011.
[105] Junginger M, Goh CS, Faaij A. International bioenergy trade: history, status & outlook on securing sustainable bioenergy supply, demand and markets. Dordrecht: Springer Science & Business Media; 2014. http://dx.doi.org/10.1007/978-94-007-6982-3, [Lecture No].
[106] Lizana J, Ortiz C, Soltero VM, Chacartegui R. District heating systems based on low-carbon. Energy Technol Mediterr Areas Energy 2016. http://dx.doi.org/10.1016/j.energy.2016.11.096.

ANNEX 9*: Ortiz C, Valverde JM, Chacartegui R, Perez-Maqueda LA. Carbonation of Limestone Derived CaO for Thermochemical Energy Storage: From Kinetics to Process Integration in Concentrating Solar Plants. ACS Sustain Chem Eng 2018;6:6404–17. doi:10.1021/acssuschemeng.8b00199.*

ACS Sustainable Chemistry & Engineering

Research Article

Cite This: ACS Sustainable Chem. Eng. 2018, 6, 6404−6417

pubs.acs.org/journal/ascecg

Carbonation of Limestone Derived CaO for Thermochemical Energy Storage: From Kinetics to Process Integration in Concentrating Solar Plants

C. Ortiz,*[,†] J. M. Valverde,[†] R. Chacartegui,[‡] and L. A. Perez-Maqueda[§]

[†]Facultad de Física, Universidad de Sevilla, Avenida Reina Mercedes s/n, 41012 Sevilla, Spain

[‡]Escuela Técnica Superior de Ingeniería, Universidad de Sevilla, Camino de los descubrimientos s/n, 41092 Sevilla, Spain

[§]Instituto de Ciencia de Materiales de Sevilla (C.S.I.C.-Univ. Sevilla), Américo Vespucio 49, 41092 Sevilla, Spain

ABSTRACT: Thermochemical energy storage (TCES) is considered as a promising technology to accomplish high energy storage efficiency in concentrating solar power (CSP) plants. Among the various possibilities, the calcium-looping (CaL) process, based on the reversible calcination−carbonation of $CaCO_3$ stands as a main candidate due to the high energy density achievable and the extremely low price, nontoxicity, and wide availability of natural CaO precursors such as limestone. The CaL process is already widely studied for CO_2 capture in fossil fuel power plants or to enhance H_2 production from methane reforming. Either one of these applications requires particular reaction conditions to which the sorbent performance (reaction kinetics and multicycle conversion) is extremely sensitive. Therefore, specific models based on the conditions of any particular application are needed. To get a grip on the optimum conditions for the carbonation of limestone derived CaO in the CaL-CSP integration, in the present work is pursued a multidisciplinary approach that combines theoretical modeling on reaction kinetics, lab-scale experimental tests at relevant CaL conditions for TCES, process modeling, and simulations. A new analytic equation to estimate the carbonation reaction rate as a function of CO_2 partial pressure and temperature is proposed and validated with experimental data. Using the kinetics analysis, a carbonator model is proposed to assess the average carbonation degree of the solids. After that, the carbonator model is incorporated into an overall process integration scheme to address the optimum operation conditions from thermodynamic and kinetics considerations. Results from process simulations show that the highest efficiencies for the CaL-CSP integration are achieved at carbonator absolute pressures of ∼3.5−4 bar, which leads to an overall plant efficiency (net electric power to net solar thermal power) around 41% when carbonation is carried out at 950 °C under pure CO_2.

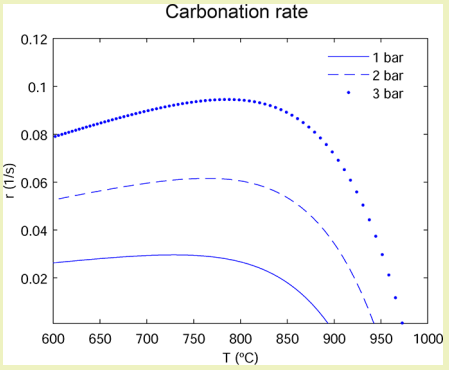

KEYWORDS: *Calcium looping, Carbonation kinetics, CSP, Energy storage, Limestone*

INTRODUCTION

The main challenge to increase the share of renewable energy in the global energy mix is dispatchability. Regarding this issue, concentrating solar power (CSP) shows several advantages over solar photovoltaic (PV) and wind due to the relatively low cost and feasible integration of thermal energy storage technologies in large-scale facilities compared to battery storage.[1−3] Thus, thermal energy storage (TES) in CSP plants has gained attention in the last years as demonstrated by the current data on commercial CSP facilities. A 42% of commercial CSP plants in operation incorporate TES systems while this percentage rises up to 83% for those planned and under development.[4]

Most commercial TES systems are based on sensible heat storage by means of molten salts, which allows plant operation for up to 15 h in the absence of direct solar irradiation. However, molten salt based systems have several drawbacks that penalize the performance of CSP plants. On one hand, the maximum working temperature is limited to ∼560 °C to avoid salt degradation, which reduces the power cycle efficiency.[5] On the other, there is a minimum working temperature of ∼200 °C to avoid salt solidification,[6] which demands a significant amount of energy to keep the molten salts from solidifying when the plant is out of operation. Thus, annual efficiencies for CSP plants with tower technology are currently found in the range 14−18%[7] with a power cycle efficiency usually lower than 38%.[4] Salt corrosiveness is also a serious issue that requires the use of expensive highly resistant materials for transport and storage.[8,9]

Thermochemical energy storage (TCES) is a promising alternative to TES to overcome these drawbacks in addition to providing other advantages such as the possibility to store energy in the long term and a relatively higher energy density.[10,11] Among the diverse TCES systems proposed, the $CaCO_3$/CaO

Received: January 14, 2018
Revised: March 1, 2018
Published: April 19, 2018

DOI: 10.1021/acssuschemeng.8b00199
ACS Sustainable Chem. Eng. 2018, 6, 6404−6417

system based on the cyclic calcination/carbonation of $CaCO_3$ (calcium-looping)

$$CaCO_{3(s)} \rightleftarrows CaO_{(s)} + CO_{2(g)} \quad \Delta H_r^0 = 178 \frac{kJ}{mol} \tag{1}$$

stands as a promising alternative for its high energy density and the extremely low price, nontoxicity, and wide availability of natural CaO precursors such as limestone or dolomite.[12] Thus, the calcium-looping (CaL) process shows a theoretical energy density around 3−4 GJ/m^3[13−16] depending on storage temperatures and pressure and the multicycle performance of the Ca-based materials employed. In the case of commercial CSP plants with tower technology based on a two tank molten salts system, the energy density is just around 0.4 GJ/m^3.[17]

The CaL process is initiated by $CaCO_3$ decomposition in the calciner to produce CaO and CO_2, which are stored separately. When energy is needed, CaO and CO_2 are brought together in a separate reactor to release the stored energy by means of the exothermic carbonation reaction. Before being considered as a potential TCES system in the late 1970s,[18−20] the use of CaO-based materials was already used for CO_2 capture to enhance H_2 production from methane reforming as early as 1933.[21] More recently, the CaL process has been widely studied for postcombustion CO_2 capture (PCC) in fossil power plants where it has been successfully demonstrated at the 1−2 MWth pilot scale.[22−26]

Importantly, the optimum conditions to carry out the CaL process depend on the particular application. They may vary notably from one case to another, which affects critically the CaO multicycle performance.[27] Thus, process conditions for postcombustion CO_2 capture involve decomposition of $CaCO_3$ at high temperature (around 950 °C) under high CO_2 partial pressure and carbonation at ∼650 °C under low CO_2 partial pressure (∼0.15 bar).[28−30] On the other hand, CaL conditions to achieve high overall efficiency for TCES and electricity generation in CSP plants are radically different.[31] In this application, carbonation would be carried out at high CO_2 partial pressure and high temperature (around or above 850 °C) whereas calcination could be performed at relatively low temperature (∼700 °C) using a gas easily separable from CO_2 under which the reaction kinetics is enhanced such as superheated steam or helium.[32−34] The diverse CaL conditions used for PCC and TCES lead also to different multicycle CaO performances[35,36] and reaction kinetics behavior.[33,37] In this regard, there are a wide number of carbonation kinetics studies focused on CO_2 capture conditions,[38−40] but those considering the specific conditions for TCES application are scarce.[41]

This manuscript presents a novel carbonation kinetics model focused on the conditions that lead to an efficient energy integration of CSP-CaL plants for TCES. A new analytic expression is proposed to estimate the carbonation reaction rate as a function of temperature and pressure. The new reaction kinetics expression shows a good agreement with experimental data and previous works.[41] Using the equation derived from this study together with thermogravimetric analysis results on the multicycle CaO conversion at relevant CaL conditions for TCES, a carbonator model is developed to analyze the carbonation behavior after a long number of cycles in the industrial process. Next, a CSP-CaL plant has been modeled to analyze the overall efficiency of the plant (defined as the ratio between net electric power production and net solar thermal power entering the calciner) and to envisage the conditions that maximize energy efficiency. Thus, our multidisciplinary approach combines reaction kinetics theory and lab-scale tests at relevant CaL conditions with process modeling and simulations in order to further explore the optimum process conditions for the integration of the CaL process into CSP plants.

The manuscript is structured as follows: A first section on carbonation kinetics describes in detail the kinetics model developed starting from the analysis of carbonation mechanism. Thermogravimetric analysis (TGA) experimental results on the carbonation kinetics are also presented and compared with theoretical predictions. The next section develops a carbonator model, which is built upon TGA and kinetics theory developed in previous sections. Later on, a section focused on the CSP-CaL integration describes a conceptual engineering process to incorporate TCES into CSP plants.

CARBONATION KINETICS

Let us consider an ideally flat surface of a CaO solid where carbonation proceeds in a gas environment at a given temperature and CO_2 partial pressure P. Arguably, the overall carbonation mechanism consists of two stages as usually observed in heterogeneous gas/solid reactions.[42] In the first stage, CO_2 molecules become physically adsorbed on the CaO surface after which a chemical reaction stage yields $CaCO_3$:

Stage I CO_2 adsorption

$$CaO + \underset{\theta}{L} + \underset{P}{CO_2} \overset{k_a}{\underset{k_d}{\rightleftarrows}} CaO + \underset{1-\theta}{L(CO_2)}$$

Stage II Chemical reaction

$$CaO + \underset{1-\theta}{L(CO_2)} \overset{k_2}{\underset{k_1}{\rightleftarrows}} CaCO_3 + \underset{\theta}{L}$$

Here L represents the active site wherein physical adsorption of a CO_2 molecule takes place before the chemical reaction occurs, k_i are the reaction rate constants, θ is the fraction of active empty sites, and $1 - \theta$ is the fraction of active sites filled with adsorbed CO_2 molecules.

According to the pseudosteady state hypothesis,[43] the rate of increase of the fraction of active sites filled with CO_2 by adsorption must balance the rate of decrease of filled active sites by chemical reaction in order not to have a net accumulation of reactive intermediates. Thus, the rates of adsorption r_a and chemical reaction r_2:

$$r_a = k_a\theta P - k_d(1 - \theta) \tag{2}$$

$$r_2 = k_2(1 - \theta) - k_1\theta \tag{3}$$

must balance out ($r_a = r_2$), which yields

$$\theta = \frac{k_2 + k_d}{k_a P + k_d + k_1 + k_2} \tag{4}$$

The microscopic reversibility principle determines that for the overall reaction to reach equilibrium ($\theta = \theta_{eq}$, $P = P_{eq}$), the rate of any process in each elementary step must be equal to the rate of its reverse process ($r_a = r_2 = 0$).[44] The microscopic reversibility principle has been successfully applied to the kinetics description of a number of reversible processes such as the dehydrogenation/hydrogenation of MgH_2.[45] This principle leads to

$$\left.\begin{aligned} k_a\theta_{eq}P_{eq} &= k_d(1 - \theta_{eq}) \\ k_2(1 - \theta_{eq}) &= k_1\theta_{eq} \end{aligned}\right\} \rightarrow P_{eq}(atm) = \frac{k_1}{k_2}\frac{k_d}{k_a} \tag{5}$$

DOI: 10.1021/acssuschemeng.8b00199
ACS Sustainable Chem. Eng. 2018, 6, 6404−6417

Assuming, as in most gas−solid heterogeneous reactions,[42] that the rate-limiting step is the chemical reaction stage (k_1, $k_2 \ll k_aP$, k_d) it is

$$\theta \approx \frac{k_d}{k_aP + k_d}$$

$$r \approx r_2 = k_2(1-\theta) - k_1\theta$$

Rearranging, we arrive at

$$r \approx a_2 e^{-E_2/RT}\left(\frac{P}{P_{eq}} - 1\right)\left(\frac{1}{\frac{P}{P_{eq}} + e^{\Delta S_2^0/R} e^{-\Delta H_2^0/RT}}\right) \quad (6)$$

where E_2 is the carbonation activation energy, a_2 is a pre-exponential factor, and R the gas constant ($k_2 = a_2\, e^{-E_2/RT}$). The Van't Hoff equation[42] has been used for the equilibrium constant $K_2 = k_2/k_1 = e^{-\Delta G_2^0/RT}$ being $\Delta G_2^0 = \Delta H_2^0 - T\Delta S_2^0$ the standard free energy change of carbonation.

By using eq 5, we obtain

$$P_{eq}(\text{atm}) = \frac{1}{K_2K_a} = e^{-(\Delta S_2^0 + \Delta S_a^0)/R} e^{(\Delta H_2^0 + \Delta H_a^0)/RT} \quad (7)$$

where the Van't Hoff equation has been used for the equilibrium constant $K_a = k_a/k_d = e^{-\Delta G_a^0/RT}$, with $\Delta G_a^0 = \Delta H_a^0 - T\Delta S_a^0$ the standard free energy change of adsorption. On the other hand, from thermochemical data,[46−48] the following is inferred:

$$P_{eq} = Ae^{-\alpha/T} \quad (8)$$

where $A = 4.083 \times 10^7$ atm, $\alpha = 20474$ K, which from eq 7 yields $\Delta S_2^0 + \Delta S_a^0 = -146$ J/mol·K and $\Delta H_2^0 + \Delta H_a^0 = -170$ kJ/mol. On the other hand, the sum of the standard enthalpy change of adsorption ΔH_a^0 and carbonation ΔH_2^0 is the standard enthalpy change of the overall reaction: $\Delta H_r^0 = \Delta H_a^0 + \Delta H_2^0 = -178$ kJ/mol as independently determined from the difference between the standard enthalpies of formation of the final product ($CaCO_3$(s)) and initial reactants (CO_2(g) and CaO(s)). Likewise, it is $\Delta S_r^0 = \Delta S_a^0 + \Delta S_2^0 = -160$ J/mol·K. As should be expected, these independently determined values are similar to those derived from comparison of eqs 7 and 8.

The standard entropy change of adsorption ΔS_a^0 may be obtained from the difference between the standard entropy of adsorbed CO_2 (S_{ad}^0) and the standard entropy of CO_2 in the gas phase ($S_{gas}^0 = 238$ J/mol·K for CO_2). According to Campbell and Sellers,[49] the standard entropy of adsorbed molecules on single crystal surfaces can be well fitted (up to $S_{gas}^0 \approx 60R$) to the universal law $S_{ad}^0 = 0.7S_{gas}^0 - 3.3R$. Thus, it is $\Delta S_a^0 = S_{ad}^0 - S_{CO2}^0 \cong -92$ J/mol·K. On the other hand, using $\Delta H_a^0 \cong -20$ kJ/mol as a typical value[50] in eq 7, it is

$$\frac{P}{P_{eq}} + e^{\Delta S_2^0/R} e^{-\Delta H_2^0/RT} = e^{\Delta S_2^0/R} e^{-\Delta H_2^0/RT}\left(1 + Pe^{\Delta S_a^0/R} e^{-\Delta H_a^0/RT}\right) \approx e^{\Delta S_2^0/R} e^{-\Delta H_2^0/RT} \quad (9)$$

for the typical range of carbonation temperatures and CO_2 partial pressures ($Pe^{\Delta S_a^0/R}\, e^{-\Delta H_a^0/RT} \ll 1$), which leads to (eq 6):

$$r \approx a_2 e^{-\Delta S_2^0/R} e^{-E_1/RT}\left(\frac{P}{P_{eq}} - 1\right) \quad (10)$$

where it has been used $\Delta H_2^0 = E_2 - E_1$, with E_1 the activation energy for chemical decomposition. Using, as estimated above, $\Delta S_a^0 = -92$ J/mol·K and $\Delta S_r^0 = \Delta S_a^0 + \Delta S_2^0 = -160$ J/mol·K, the standard entropy change of carbonation is $\Delta S_2^0 = -68$ J/mol·K whereas the activation energy for chemical decomposition is similar to the overall reaction enthalpy change as measured experimentally:[51] $E_1 \cong 180$ kJ/mol.

Note that for $\frac{P}{P_{eq}} \gg 1$ and using eq 7:

$$r \approx a_2 e^{\Delta S_a^0/R} e^{(-(E_2 - E_d)/RT)} P \quad (11)$$

where $\Delta H_a^0 = E_a - E_d$, being E_d the activation energy for desorption and the activation energy for adsorption E_a is assumed to be negligible.

EXPERIMENTAL RESULTS ON THE CARBONATION KINETICS

In this work, thermogravimetric analysis (TGA) tests have been carried out to analyze experimentally the carbonation reaction kinetics depending on the reaction temperatures under pure CO_2 and high temperature as relevant conditions in the CaL-CSP integration for TCES. Natural limestone of high purity (99.6 wt % $CaCO_3$) was used in the tests, which were carried out by employing two different thermogravimetric analyzers (TA Q600 and Setaram LABSYS evo). In all the tests, a small sample mass (10 mg) was employed to minimize mass/heat transfer undesired effects. The limestone samples were calcined at 750 °C under pure N_2 for 5 min after which the temperature was increased to the target carbonation temperature and pure CO_2 at atmospheric pressure was introduced for carbonation to proceed.

Results for the time evolution of CaO conversion during carbonation at different temperatures are shown in Figure 1. As can be seen, CaO conversion is hindered as the carbonation temperature approaches the equilibrium temperature ($T \sim 895$ °C under pure CO_2 at atmospheric pressure). As the reaction evolves, the carbonation rate is determined as a function of conversion degree X, and reaction temperature T and pressure P (eq 12). Note that the conversion degree X, which is usually employed to note the conversion of CaO during carbonation, is equivalent to the term α usually employed in kinetics studies.

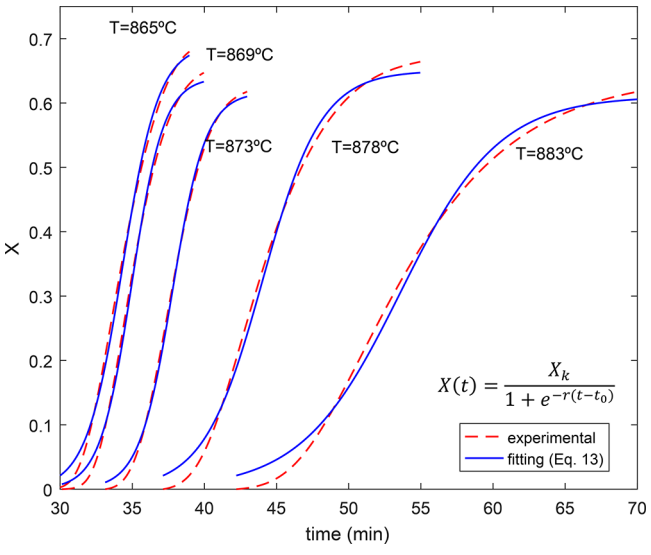

Figure 1. Time evolution of CaO conversion measured experimentally and best fit curves from eq 13. Values of the best fitting parameters (t_0, X_K, and r) are shown in Table 1. Best fitting parameters are plotted in Figure 2 (reaction rate r) and Figure 3 (conversion at the end of the reaction controlled stage X_K).

DOI: 10.1021/acssuschemeng.8b00199
ACS Sustainable Chem. Eng. 2018, 6, 6404−6417

Table 1. Best Fitting Parameters of Equation 13 to Experimental Data on CaO Conversion for Carbonation under CO_2 at Atmospheric Pressure and Several Carbonation Temperatures

	carbonation temperature				
$X(t) = \frac{X_k}{1+e^{-r(t-t_0)}}$	T = 865 °C	T = 869 °C	T = 873 °C	T = 878 °C	T = 883 °C
X_K	0.691	0.640	0.617	0.650	0.611
r (1/min)	0.798	0.9081	0.868	0.491	0.292
t_0 (min)	34.330	34.974	37.790	44.040	53.576

$$\frac{dX}{dt} = f(X)r(T, P) \tag{12}$$

where $f(X)$ is a mechanistic-rate function that takes into account solids' heterogeneities.[52] Our experimental results on the time evolution of conversion (Figure 1) show the typical sigmoidal shape of autocatalytic processes and are well fitted by a Prout−Tompkins model function $f(X) = X(1 - X)$[53] modified by introducing a conversion limit X_K, which is the CaO conversion at the end of the reaction controlled phase (after which carbonation becomes controlled by solid-state diffusion of CO_2 across de $CaCO_3$ layer built up on the CaO surface). Thus

$$\frac{dX}{dt} = X\left(1 - \frac{X}{X_k}\right)r(T, P) \leftrightarrow X(t) = \frac{X_k}{1 + e^{-r(t-t_0)}} \tag{13}$$

Equation 13 fits quite satisfactorily to our experimental data on CaO conversion (Figure 1), which allows us deriving experimental values for the reaction rate at different temperatures $r(T, P)$. Best fitting parameters are shown in Table 1. Reaction rates obtained in this way are compared to the theoretically predicted values (eq 6) in Figure 2. It should be noted that while the modified Prout−Tompkins model used here provides a good fitting to experimental data, it has been shown in the literature that the kinetics parameters, i.e. activation energy, obtained from the analysis of isothermal data, is independent of the assumed kinetic model, and in any case, it leads to the real value of the activation energy.[54]

As may be seen in Figure 2a, a rather good agreement can be found between experiments and theory (eq 6) by only adjusting the prefactor a_2 as a free parameter in the theoretical curve. Interestingly, data obtained using different commercial thermal analysis instruments with quite different experimental setups could be nicely fitted by eq 6. In view of these results, and even though technical limitations prevented us from carrying out carbonation experiments at pressures greater than atmospheric, we will use eq 6 and its approximate limit (eq 10) to estimate the reaction rate under CO_2 at pressurized conditions (predicted curves are shown in Figure 2b).

Table 2 summarizes the values used for the reaction enthalpies, entropies, and activation energies, as discussed in the previous section, that will be employed for the theoretical reaction rate in the modeling analysis ahead.

As seen in Figure 2b, there is a temperature at which the carbonation rate reaches a maximum and above which it rapidly decreases as the equilibrium temperature is approached. This same trend was already predicted by Kyaw et al.[41] The temperature at which the reaction rate is maximum is a relevant input for the CaL-CSP application. Plant efficiency will be higher the higher the carbonation temperature, but considering that temperatures nearby equilibrium affects negatively to kinetics. The plot in Figure 3 shows the equilibrium temperature and temperature at which the reaction rate is maximum for carbonation under pure CO_2 as a function of the absolute carbonator pressure calculated from the carbonation kinetics model developed above.

A further interesting parameter derived from the best fit of eq 13 to experimental data on conversion is X_K, namely the value of CaO conversion at the boundary between the fast reaction and solid-state diffusion stages. Values for the conversion at the end of the reaction-controlled stage X_K obtained in this way are shown in Figure 4.

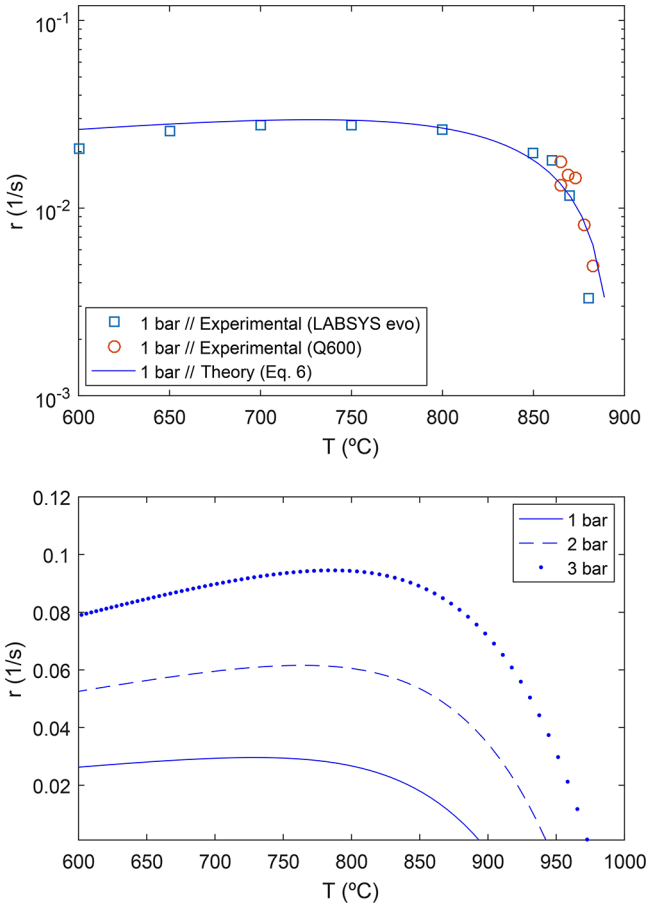

Figure 2. (top) Reaction rate obtained from experimental tests (using different TG analyzers as indicated) and theoretically predicted (eq. 6, with a_2 = 1160 1/s) for carbonation under pure CO_2 at atmospheric pressure as a function of the temperature. (bottom) Reaction rate as a function of temperature theoretically predicted by varying the carbonator absolute pressure (eq 6).

CARBONATOR MODEL

TGA Data Analysis. The behavior of CaO conversion X along multiple calcination/carbonation cycles is a critical input for the CaL cycle assessment. The CaL process applied to postcombustion CO_2 capture involves carbonation under low CO_2 partial pressure (around 0.15 bar for coal fired power plants) whereas calcination is carried out under high CO_2 concentration at temperatures around 950 °C. These harsh calcination conditions lead to a severe decay of CaO conversion in short residence times with the number of cycles due to progressive sintering of the regenerated CaO and the consequent drop of available surface area for carbonation in the fast reaction controlled stage.[55] Thus, conversion of limestone derived CaO in short residence times (of a few minutes) decays significantly after just a few cycles at CaL conditions for CO_2

DOI: 10.1021/acssuschemeng.8b00199
ACS Sustainable Chem. Eng. 2018, 6, 6404−6417

Table 2. CO_2 Values of Enthalpy−Entropy Changes in the Chemical Decomposition and Desorption Stages and Activation Energies

ΔH_r^0	180 kJ/mol
ΔH_1^0	160 kJ/mol
ΔH_d^0	20 kJ/mol
E_d	20 kJ/mol
E_1	180 kJ/mol
E_2	20 kJ/mol
ΔS_r^0	0.16 kJ/(mol·K)
ΔS_1^0	0.068 kJ/(mol·K)
ΔS_d^0	0.092 kJ/(mol·K)
a_2	1160 (1/s)

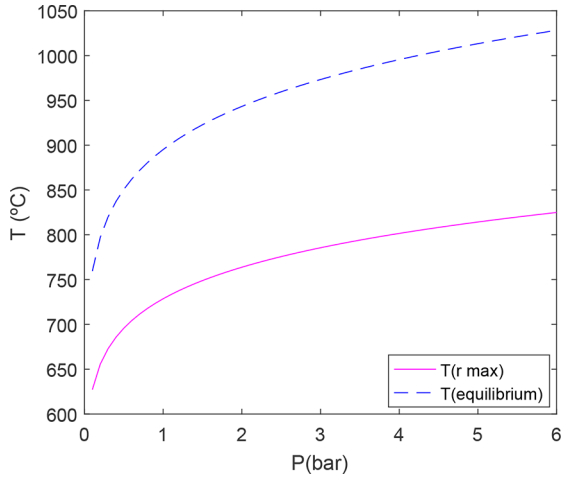

Figure 3. Values of temperature at which the carbonation reaction rate is maximum calculated from the kinetics model and at which the reaction is at equilibrium (carbonation under pure CO_2) as a function of the carbonator absolute pressure.

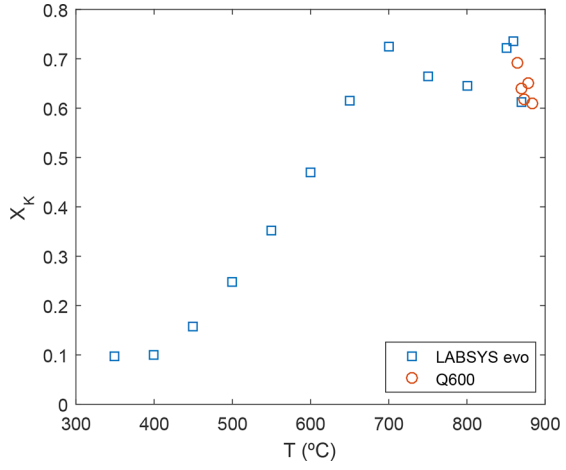

Figure 4. CaO conversion at the end of the reaction-controlled stage (X_K) for carbonation under pure CO_2 (at atmospheric pressure) as a function of temperature. Data are obtained from the best fits of eq 13 to experimental data on the time evolution of conversion.

capture and converges toward a residual value of just around 0.07−0.08.[26,55] Moreover, part of the CaO is irreversibly sulfated or deactivated by ashes. A number of methods to enhance the multicycle CaO conversion have been reported in the last years,[27] such as the formulation of synthetic sorbents,[56,57] thermal pretreatment,[58,59] mechanical pretreatment,[60] and using steam or helium in either the calcination or carbonation reactors.[32,61]

However, CaL conditions for TCES in CSP do not need to be identical to those employed for CO_2 capture. In previously proposed CaL-CSP integration schemes[12,31,62] carbonation is carried out under a pure CO_2 atmosphere whereas calcination can be carried out under low CO_2 partial pressure, which leads to a different multicycle behavior.[37] Moreover, SO_2 and ashes are not present in the reactors. Thus, the residual conversion of limestone derived CaO can be as large as 0.5 for carbonation under 100% CO_2 atmosphere and calcination at 725 °C in absence of CO_2 for residence times in both stages of 5 min and using limestone particles smaller than 45 μm.[35] Carbonation under these conditions is limited by pore plugging, which leads to a significant loss of activity for typical particle sizes to be employed in circulating fluidized beds (>100 μm).[37] Thus, pore plugging causes a drop of the residual conversion of limestone derived CaO to just about X = 0.2 for particles larger than about 45 μm. Nevertheless, it has been reported that pore plugging does not limit carbonation for large enough dolomite particles (>∼100 μm) reaching a residual effective conversion of about 0.4.[37]

Figure 5 shows thermogravimetric experimental data (see refs 35 and 37 for further details) on the multicycle conversion

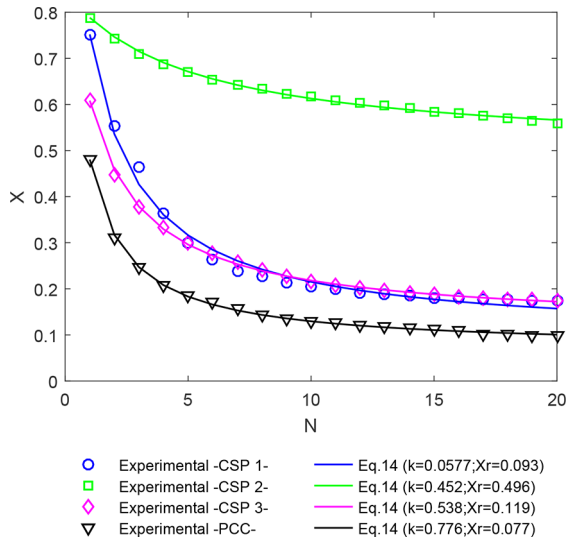

Figure 5. Thermogravimetric experimental data[35,37,65] on the multicycle conversion (X) of limestone derived CaO under typical calcination/carbonation conditions for postcombustion CO_2 capture (PCC) and thermochemical energy storage of CSP. Testing conditions are shown in Table 3. The lines are the best fit curves from eq 14 to data. Best fitting parameters are shown in the legend.

of limestone derived CaO for several carbonation/calcination conditions. Testing conditions (particle size range used, type of atmosphere, temperature, and residence time in both calcination and carbonation stages) are detailed in Table 3. As can be seen, the evolution of CaO conversion X with the number of cycles N is well-fitted by eq 14:[63]

$$\frac{X_N}{X_1} = \frac{X_r}{X_1} + \left(\frac{1}{\kappa(N-1) + \left(1 - \frac{X_r}{X_1}\right)^{-1}} \right) \quad (14)$$

where X_1 is CaO conversion in the first cycle, k is the deactivation rate constant, and X_r is the residual CaO conversion,

DOI: 10.1021/acssuschemeng.8b00199
ACS Sustainable Chem. Eng. 2018, 6, 6404−6417

Table 3. TGA Test Conditions Corresponding to Measured Multicycle CaO Conversion Data Plotted in Figure 5

reference	particle size	gas calciner−carbonator	temperature calciner−carbonator
CSP 1	>45 μm	He−CO_2	725−850 °C
CSP 2	<45 μm	He−CO_2	725−850 °C
CSP 3	>45 μm	CO_2−CO_2	950−850 °C
PCC	>45 μm	CO_2−N_2/CO_2 (15% v/v)	950−650 °C

which would be reached asymptotically after a very large number of cycles (as would occur in commercial CaL plants).

As shown in Figure 5, a higher CaO deactivation occurs for postcombustion CO_2 capture (PCC) conditions compared to CaL-CSP conditions. Thus, after 20 cycles, CaO conversion drops to 0.1 whereas under CaL-CSP3 conditions (calcination at 950 °C and carbonation at 850 °C, both under pure CO_2) conversion after 20 cycles remains at 0.18. A similar value of the residual conversion for CaO derived limestone is reported by Obermeier et al.,[64] who performed calcination at 800 °C in an air atmosphere and carbonation at 600 °C under a pure CO_2 atmosphere.

Carbonator Model. A carbonator model, previously employed to analyze the CaL process for CO_2 capture,[66] has been adapted in this work to study the CaL process for its integration in CSP plants. The model conforms to the flow diagram shown in Figure 6. The flow rate of CaO solids entering the carbonator (F_R) as well as the CaO present in the reactor bed (N_{Ca}) react with the pure CO_2 stream (flow rate F_{CO2}) to produce $CaCO_3$. As discussed above in the kinetics study, CaO conversion for a single particle in a certain residence time is dependent on carbonation temperature (Figure 1). Moreover, CaO conversion after several cycles decays close to a residual value, which is also dependent on process conditions. Thus, since carbonation is not completely achieved in short residence times, only a fraction of the total CaO flow rate (given by CaO conversion X) reacts to produce $CaCO_3$, the rest $(1 - X)$ remaining as unreacted CaO ($F_{CaO,unr}$). The model assumes a perfect mixing of solids in the reactor bed with a CO_2 stream passing in plug flow through it. At the carbonator exit, the CO_2 mass flow rate is decreased according to the CO_2 captured in the process (with an efficiency E_{CO2}).

By means of a mass balance, the maximum average conversion of the CaO particles in the carbonator can be expressed as

$$X_{max,ave} = \sum_{N=1}^{N=\infty} \phi_N X_N \tag{15}$$

Here X_N is the average CaO conversion at cycle N and ϕ_N is the fraction of solids that are cycled N times:[67]

$$\phi_N = \frac{F_0 F_R^{N-1}}{(F_0 + F_R)^N} \tag{16}$$

where F_0 is the flow rate of makeup fresh limestone introduced to the system in order to mitigate CaO deactivation. If this fresh material is not introduced into the system, the maximum conversion after many cycles would be just the residual CaO conversion ($X_{max,ave} \approx X_r$).

As is well-known from previous works,[38,67−69] carbonation takes place through two differentiated stages, a first fast stage in which the reaction occurs on the free surface of CaO particles (see reaction mechanism in the Carbonation Kinetics section) and a second stage, that takes place once a carbonate layer has been formed on the particles' surface, controlled by counter-current diffusion of CO_3^{2-} and O^{2-} across the $CaCO_3$ product layer and characterized by a much lower reaction rate. According to previous TGA studies, after calcination at 725 °C, most of the carbonation in short residence times on the regenerated CaO skeleton occurs in the fast stage due to the high CO_2 concentration and carbonation temperature, which promote the reaction kinetics.[37] Thus, carbonation in the diffusion-controlled phase is neglected in this model,[35] and therefore, $X_r = X_K$.

Accordingly, the present carbonator model assumes that carbonation occurs at a given rate until it reaches the maximum carbonation allowed in the fast carbonation stage, after which the particles remain inactive. Thus, only a fraction of particles, f_a, are active in the carbonator with the capacity to react in the fast reaction controlled stage:

$$f_a = (1 - e^{-t_K/\tau}) \tag{17}$$

where t_K is the fast carbonation stage time and τ is the average residence time of CaO solids in the carbonator:

$$\tau = \frac{N_{Ca}}{F_R} \tag{18}$$

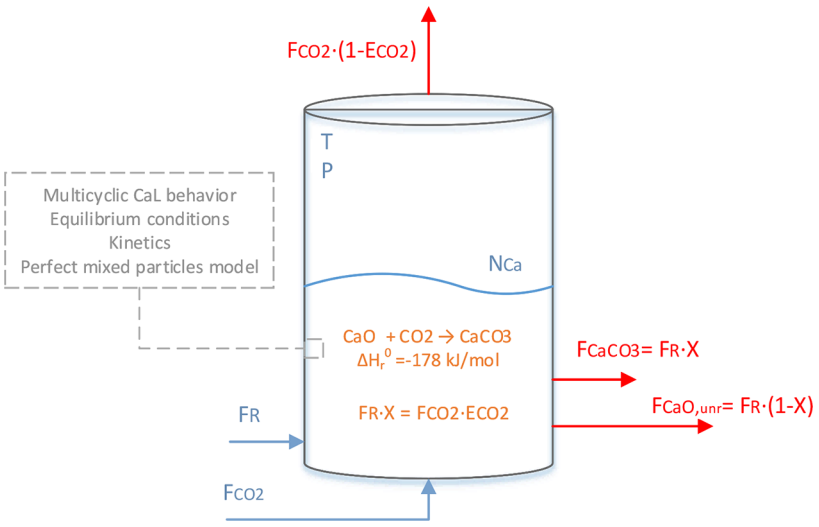

Figure 6. Carbonator model flow diagram.

DOI: 10.1021/acssuschemeng.8b00199
ACS Sustainable Chem. Eng. 2018, 6, 6404−6417

Considering a perfect mixing model, the average conversion of the particles leaving the carbonator (X) can be calculated using the followed equations:[66]

$$X = \frac{\int_0^{t_K} r_{ave} t \left(\frac{1}{\tau}\right) e^{-t/\tau}\, dt}{1 - e^{-t_K/\tau}} = X_{max,ave} \frac{f_a}{\ln\left(\frac{1}{1-f_a}\right)} \quad (19)$$

$$f_{carb} = \frac{X}{X_{max,ave}} \quad (20)$$

$$E_{CO2} = \frac{F_R}{F_{CO2}} X = \frac{N_{Ca} f_a r_{ave}}{F_{CO2}} \quad (21)$$

where f_{carb} is the average carbonation level in the carbonator and r_{ave} is the average reaction rate in the fast carbonation stage, which is calculated from the kinetics model theoretical prediction (eq 10).

The carbonator model allows us to carry out a sensitivity analysis to assess the effect of pressure, temperature and solids inventory in the carbonator on the average carbonation level (f_{carb}). Results are shown in Figure 7.

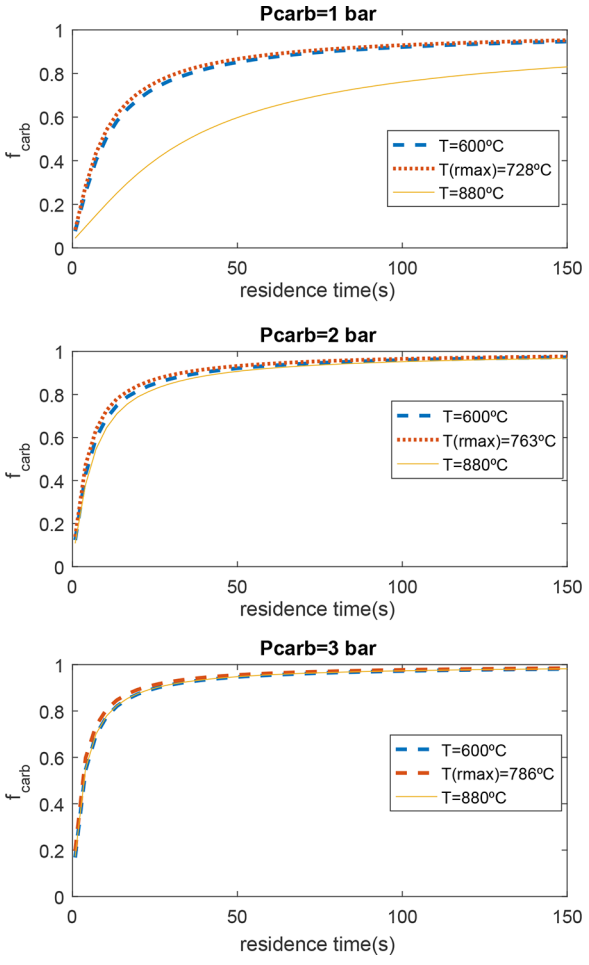

Figure 7. Carbonator model results. Average carbonation level (f_{carb}) for several carbonation conditions (P, T). T(rmax) is the temperature at which the reaction rate reaches a maximum (Figure 3).

As can be seen in Figure 7, the average carbonation level (f_{carb}) is enhanced by increasing the carbonator pressure due to faster reaction kinetics (Figure 2b). After a few of seconds in the carbonator, most of the CaO reaches the maximum conversion (according to eq 13) due to the very fast kinetics achieved in these CaL conditions. This is basically because of the high amount of CO_2 entering the carbonator (which exceeds the stoichiometric amount in order to use the effluent excess as heat carrier). According to the kinetics model, by increasing the carbonator temperature, the average carbonation level is slightly enhanced up to the temperature T(rmax)—Figure 3—is reached from which kinetics is penalized with the consequent curtailment of the average carbonation level. As shown in Figure 7, this effect is mitigated when the carbonator pressure is increased, which is beneficial in practice since working at higher carbonator temperatures will promote the power cycle efficiency. Next section analyses the CSP-CaL integration efficiency as a function of carbonator temperature and pressure in order to select the best conditions based on both experimental data and the theoretical reaction kinetics study.

CSP-CaL Plant. This section is devoted to a detailed analysis on the CSP-CaL integrated plant for TCES. As main novelties regarding previous works,[12,70] new CaL conditions, TGA experimental data and the carbonator model above-described will be introduced in the analysis. Calculations have been performed using the commercial software Aspen PlusTM.

The CSP-CaL plant (see Figure 8) works as follows: Direct solar irradiation is used to preheat the streams entering the calciner up to the reaction temperature to carry out the calcination reaction. Calcination occurs under helium atmosphere which allows reducing the calcination temperature to 725 °C[33] in short residence times to simulate conditions as tested in the Carbonation Kinetics section using limestone as a CaO precursor. Note that the proposed scheme (Figure 8) is a closed cycle in which any stream must be fed continuously to the plant. This is relevant for the recycling of helium in the system, which is a rare and expensive gas. Several solar calciner reactors have been already proposed in the literature.[71−74] By calcination under an He atmosphere, a reduction of the calcination temperature would lead to an increase in the solar receiver efficiency as a consequence of the lower radiative losses. Full calcination is assumed in our model.[64,75] After calcination, the CaO stream ($c1$ in Figure 8) is separated from the He-CO_2 stream ($g1$) by means of a cyclone. The He−CO_2 stream is passed through a separation system based on membranes. A detailed study on the membrane system is out of the scope of this work and an ideal separation is assumed. However, it may be noted that commercial H_2/CO_2 separation membranes are available, and since He molecule is similar to H_2, the He/CO_2 separation system could take advantage of H_2/CO_2 currently commercial technologies. The He stream ($g1$-2) is recirculated into the calciner while the pure CO_2 stream ($g1$-1) is passed through a heat recovery steam generator (HRSG) to use its high temperature as a previous step to be stored or used in the power cycle. Since heat input to the steam power cycle is moderate, a simple superheated steam cycle without reheat stages and moderate live steam conditions are assumed. Thus, the steam cycle is modeled by considering a condensing pressure of 0.075 bar, an evaporation pressure of 45 bar and a superheated steam temperature of 400 °C.

On the carbonator side of the plant, a CaO stream from the storage vessel (c_2) reacts with the CO_2 stream coming either from storage ($g7b$) or the calciner side ($g3$) according to the carbonation reaction at atmospheric pressure (carbonation at higher pressure will be also considered ahead). The CO_2 entering the carbonator ($g9$-2) exceeds the stoichiometric amount

DOI: 10.1021/acssuschemeng.8b00199
ACS Sustainable Chem. Eng. 2018, 6, 6404−6417

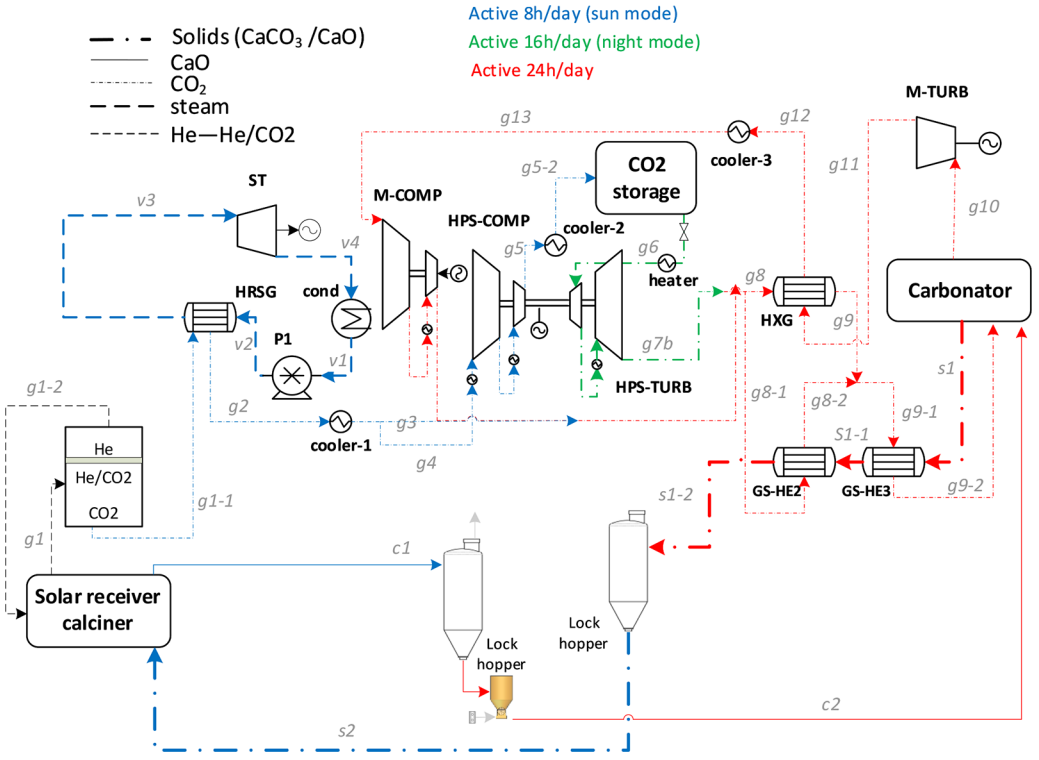

Figure 8. CSP-CaL plant scheme.

needed for carbonation. The CO_2 in excess that exits the carbonator acts as heat carrier to produce electrical power by means of a CO_2 closed Brayton cycle wherein a heat exchanger HXG is used as a recuperator.

Different operations in "sun" and "night" modes are simulated. A solar multiple (SM) equal to 3 is assumed for the system design and, for simplicity, the day is considered as composed by 8 sun h, which constantly provides 100 MWth to the calciner, and of 16 night h. Thus, in the "sun" operating mode, the CO_2 mass flow entering the carbonator side ($g3$ or $g7b$) is 1/3 the amount produced in the calciner ($g1$). Accordingly, the plant efficiency is determined as a weighted average of the performances in sun and night modes (eq 22). Although it is out of the scope of the present work, an additional analysis to consider real solar irradiance as well as off-design conditions would be required for further assessing equipment sizing and costs. Moreover, other plant operation modes could be considered as a function of solar irradiation, electricity prices, filling level of storage tanks, etc. On the other hand, a more detailed study on the different operation modes would be useful to estimate the penalty associated with daily start-up/shut-down of the plant. In this regard, lower start-up/shut-down penalties than in commercial CSP plants are expected since the system is designed to achieve a full working hours capacity. Note that efficiency in this model considers the heat input to the calciner and disregards the thermal efficiency of the solar receiver whose design and modeling is beyond the scope of this work. Concerning solids transport, a power consumption of 20 MJ/ton is assumed.[12] Thus, the global plant efficiency will be given by

$$\eta = \frac{\int_{24h} \dot{W}_{net}\, dt}{\int_{24h} \dot{Q}_{input}\, dt} = \frac{\dot{W}_{net,sun}\Delta t_{sun} + \dot{W}_{net,night}(24 - \Delta t_{sun})}{\dot{Q}_{input}\Delta t_{sun}} \quad (22)$$

where $\dot{W}_{net}$ is the net electrical power produced by the system and $\dot{Q}_{input}$ is the solar power input in the calciner. The electric power produced is computed for the sun mode ($\dot{W}_{net,sun}$) and the night mode ($\dot{W}_{net,night}$).

Several assumptions have been made to model the CSP-CaL plant, which are summarized in Table 4.

CSP-CaL Integration Model Results. The proposed CSP-CaL integration model has been simulated considering in the base case that the carbonator works at 850 °C/1 bar and with a solids inventory of 105 kmol, which allows to achieve a 95% of average carbonation level (f_{carb}) in the carbonator (Figure 7). An important benefit of working at atmospheric pressure in the carbonator is that high temperature lock hoppers for solids pressurization are not necessary. On the other hand, hermetic machines and heat exchangers must be employed. Tables 5 and 6 show the main streams and energy balance results.

The energy balance for the CSP-CaL integration shows an overall daily efficiency of 38% (Table 6). Since the main turbine (M-TURB) has been selected to work at constant power production, a higher net power output is achieved during the night mode compared to the sun mode. This is because the high-pressure CO_2 storage compressor (HPS-COMP) and auxiliaries' consumptions are not fully compensated by the steam turbine production in the sun mode. As shown in Table 6, main heat rejections to the ambient occur in the steam condenser (COND) and in the CO_2 cycle precooler (COOLER-3) while the main power consumption is caused by the CO_2 compressor in the carbonator side (M-COMP).

The CSP-CaL integration performance has been analyzed as a function of the pressure ratio (PR) defined as the ration of the carbonator pressure (1 bar) to the turbine outlet pressure. On one hand, by increasing the pressure ratio the power production in the CO_2 power cycle is enhanced, which increases the global cycle efficiency. On the other hand, by increasing PR, the temperature of the CO_2 exiting the turbine is lowered and a

DOI: 10.1021/acssuschemeng.8b00199
ACS Sustainable Chem. Eng. 2018, 6, 6404−6417

Table 4. Main Assumptions in the CSP-CaL Model

group/component	parameter		
turbomachinery	isentropic efficiency	mechanical-electric efficiencies	intercooling/ reheating stages and temperatures
main CO_2 turbine (M-TURB)	0.9	0.98	
main CO_2 compressor (M-COMP)	0.87	0.98	2/40 °C
high pressure storage turbine (HPS-TURB)	0.8	0.96	2 65 °C/100 °C
high pressure storage compressor (HPS-COMP)	0.8	0.96	5/40 °C
steam turbine (ST)	0.75	0.98	
component	parameter		
heat exchangers	minimum temperature difference	pressure drops	parasitic power consumption
coolers	15 °C	1%	0.8% of heat released[76]
HXG (both sides)	15 °C	5%	
HRSG (hot side)	15 °C	3%	
HRSG (cold side)	15 °C	11%	
solid−gas HX (both sides)	15 °C	3%	
component	parameter		
various	efficiency	heat input	heat losses
calciner	1	100 MWt	
carbonator			1% of heat transferred
storage vessels			0%

higher amount of energy is recovered in the recuperator (HXG), which translates into a higher amount of carbonation energy needed to bring the reactants to carbonation conditions. The effect of increasing the PR on the overall plant efficiency is illustrated in Figure 9.

As can be seen in Figure 9, a higher overall efficiency is calculated as the carbonation temperature is increased at a given value of PR. Thus, the benefits of increasing the carbonation temperature above $T_{carb} \sim 728$ °C (at which the reaction rate is maximum for atmospheric carbonation as shown in Figure 2b) compensates the penalty caused by the reduction of the reaction speed which yields a lower carbonation level and therefore a lower CaO conversion (X).

Table 6. Energy Balance for the CSP-CaL Integration (Figure 8)

parameter	sun mode	night mode
solar thermal power (MWth)	100	0
Heat Exchanger Thermal Power (MWth)		
HRSG	16.01	
COOLER-1	−0.37	
COND	−11.68	
HP-COMP (intercooler)	4.50	
COOLER-2	−4.01	
HEATER	2.07	
TURB1 (interheater)	-	0.97
COOLER-3	-	−5.63
HXG	88.81	88.81
GS-HE2	3.602	3.602
GS-HE3	4.782	4.782
Power Inlet (MWe)		
CO_2 storage turbine (HPS-TURB)		1.32
main CO_2 turbine (M-TURB)	25.35	25.35
steam turbine (ST)	4.27	
Power Outlet (MWe)		
steam cycle pump (P)	−0.03	
main CO_2 compressor (M-COMP)	−12.59	−12.50
CO_2 storage compressor (HPS-COMP)	−5.14	
auxiliaries heat calciner	−0.16	
auxiliaries heat carbonator	−0.11	−0.16
auxiliaries solids transport calciner	−0.87	
auxiliaries solids transport carbonator	−0.29	−0.29
Wnet		
$\dot{W}_{net,sun}$ (MWe)	**10.42**	
$\dot{W}_{net,night}$ (MWe)		**13.77**
overall plant efficiency (η)	**38%**	

The temperature limit imposed by the thermodynamic equilibrium (eq 8) for carbonation under pure CO_2 at atmospheric pressure is 895 °C (Figure 3). Thus, the carbonator pressure must be increased over atmospheric pressure to further increase the carbonator temperature above 895 °C. This would enhance the power plant efficiency (higher temperature at turbine inlet) as well as the carbonation kinetics (as shown in Figure 2a and Figure 7). The CSP-CaL integration (Figure 8) is also valid when the carbonator is operated under over atmospheric pressure. For that purpose, the only modification needed is that the

Table 5. Main Stream Data for the CSP-CaL Integration (Base Case)

ID	P (bar)	T (°C)	$\dot{m}$ (kg/s)	ID	P (bar)	T (°C)	$\dot{m}$ (kg/s)
s1	1.00	850	29.13	*g4*	1.14	44.43	14.69
s1-1	0.97	703.17	29.13	*g5*	75.75	123.63	14.69
s1-2	0.94	588.83	29.13	*g5-2*	75	25	14.69
s2	0.94	588.83	87.37	*g6*	74.25	130	7.34
c1	1.00	725	65.39	*g7b*	1.14	21.92	7.34
c2	1.00	725	21.79	*g8*	1.14	72.10	134.62
v1	0.074	40.13	5.27	*g8-1*	1.14	72.10	6.54
v2	45.00	40.53	5.27	*g8-2*	1.10	535.06	6.54
v3	40.00	400	5.27	*g9*	1.08	679.56	134.62
v4	0.075	40.31	5.27	*g9-1*	1.08	675.41	141.17
g1	1.00	725	440.58	*g9-2*	1.05	703.17	141.17
g1-1	1.00	725	22.03	*g10*	1.00	850	133.82
g1-2	1.00	725	418.55	*g11*	0.33	694.56	133.82
g2	0.97	58.99	22.03	*g12*	0.32	87.30	133.82
g3	1.14	44.43	7.34	*g13*	0.31	40	133.82

DOI: 10.1021/acssuschemeng.8b00199
ACS Sustainable Chem. Eng. 2018, 6, 6404−6417

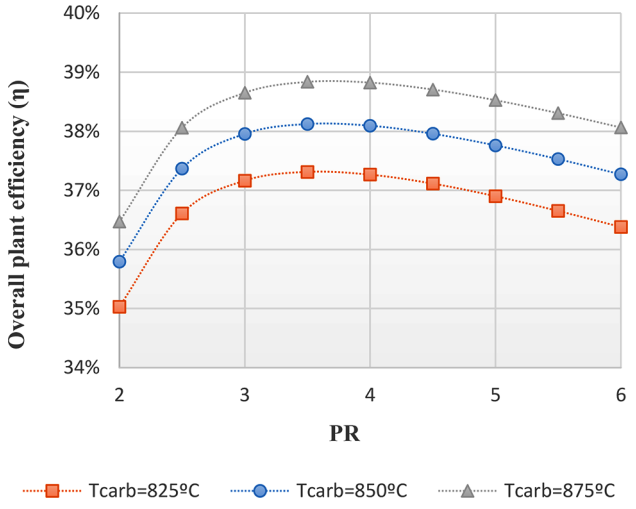

Figure 9. Overall plant efficiency as a function of pressure ratio (PR).

CO_2 stream coming from the calciner (*g*3 stream in Figure 8) in the day mode is passed through the main CO_2 compressor (M-COMP) up to reach the carbonator pressure (including the pressure drop) as a previous step to enter the recuperator (*HXG*). Note that the CO_2 exiting the main turbine (M-TURB) can be at atmospheric pressure working under pressurized carbonation conditions. Therefore, hermetic machines and heat exchangers would not be necessary. Figure 10 shows the overall

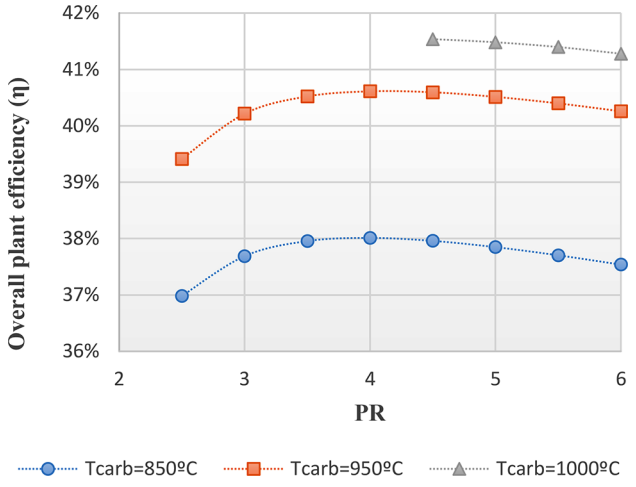

Figure 10. Overall plant efficiency as a function of the pressure ratio (PR) for carbonation at over atmospheric pressure (P_{carb}). The CO_2 exiting the turbine (M-TURB) is at atmospheric pressure, and therefore P_{carb} = PR.

CSP-CaL efficiency for the pressurized carbonator case. Except for the carbonator conditions (*P*, *T*), the rest of the parameters are the same as in the base case.

By comparing Figures 9 and 10 it is appreciated that the overall plant efficiency is significantly enhanced by increasing the carbonator temperature, which is facilitated when the carbonator works under pressurized conditions. In this way, overall plant efficiencies above 41% are achievable. Note that in the case of T_{carb} = 1000 °C the carbonator pressure must be higher than 4.21 bar due to thermodynamic equilibrium constraints.

Carbonator Presizing. At this point an important issue regarding the carbonator size must be addressed. The carbonator in the application of the CaL technology for post-combustion CO_2 capture (PCC) is characterized by a very large size (volume ~ 18 m^3/MWe; solids inventory ~ 1300 kg/MWe[77]), which significantly increases capital and operating costs (CAPEX and OPEX).[78,79] Previous works[80,81] have shown that the sizes of the carbonator and calciner play an important role on increasing the cost of the PCC technology. In contrast, the carbonator size in the application of the CaL technology for TCES in CSP would be remarkably reduced as evidenced by stream data (Table 5). Table 7 shows the carbonator reactor presizing for

Table 7. Carbonator Reactor Properties in the CSP-CaL Integration (Base Case)

parameter	base case (P_{carb} = 1 bar)	pressurized carbonation (P_{carb} = 3 bar)
power plant size (MW_{th})	100	100
Carbonator Operating Conditions		
P_{carb} (bar)	1	1
T_{carb} (°C)	850	950
$F_{R,crb}$ (kmol/h)	1399	1499
$F_{CO2crb,in}$ (kmol/h)	11547	10533
F_R/F_{CO2}	0.12	0.14
$\dot{V}_{CO2}$ (m^3/s)	248.5	85.44
W_s (kg)	8000	5000
Carbonator Preliminary Sizing		
reactor type	CFB	CFB
μ_0 (m/s)	4	4
particle size (μm)	100	100
A (m^2)	62.12	21.36
D (m)	8.89	5.21
W_s/A (kg/m^2)	128.78	234.08
H (m)	36.67	15.64

the case proposed in our study. Since gas and solids mass flow rates in the CSP-CaL case are relatively small, the cross-section surface area of the carbonator reactor (A ~ 21 m^2 for the pressurized carbonator case) is small as compared to the typical size of the carbonator in the PCC-CaL application (A ~ 175 m^2[77]) assuming the same superficial velocity for the fluidized bed to be operated in a circulation regime. Likewise, the carbonator height, which can be estimated from the ratio a H/D ~ 3[77] is much smaller in the CSP-CaL technology as compared to the PCC-CaL application.

The minimum amount of solids inventory needed can be estimated to achieve a 95% of average carbonation level in the carbonator while carbonation kinetics can be inferred from the Carbonation Kinetics section of this manuscript. As shown in Table 7, a solids inventory of ~128−234 kg/MWe is needed, which is significantly lower than in the case of the PCC-CaL application (~1300 kg/MWe). A direct consequence of a reduction in solids inventory in the carbonator, is a significant reduction of fan power consumption to ensure fluidization conditions. As would be expected, the base case requires a larger carbonator size as compared with the pressurized carbonator configuration. The atmospheric pressure carbonator in the base case involves a larger amount of CO_2 volume entering the reactor as well as a lower reaction rate, which would be enhanced with the carbonator pressure (Figure 2b).

CONCLUSIONS

This paper analyzes the carbonation of limestone derived CaO in the CaL process as for thermochemical energy storage in CSP plants. Since the carbonation behavior (kinetics and

DOI: 10.1021/acssuschemeng.8b00199
ACS Sustainable Chem. Eng. 2018, 6, 6404−6417

multicyclic CaO conversion) is highly dependent on the CaL conditions, which vary according to the type of application, a theoretical reaction kinetics study has been carried out to analyze the effect of the particular CaL carbonation conditions to be used in the CSP-CaL integration, which involve carbonation under high CO_2 partial pressure at high temperature. The reaction kinetics study is supported by TGA tests performed under these specific conditions. As a result, a new expression to estimate the carbonation conversion rate as a function of the carbonator pressure and temperature has been derived. A carbonator model based on the kinetics study is used to estimate the average carbonation level after a long number of cycles as would occur at industrial scale. Accordingly, the carbonation rate is enhanced with the carbonator temperature up to reach a maximum, from which a further increase of temperature is detrimental as the thermodynamic equilibrium temperature is approached. On the other hand, an increase in the carbonator pressure promotes significantly the conversion rate and therefore the average carbonation level in short residence times. Thus, an increase of the carbonator pressure yields an improved performance not only from a reaction kinetics perspective but also because a higher carbonator pressure allows for a higher carbonator temperature, which enhances the power cycle efficiency when stored energy is released. The CSP-CaL integration model explored in this work, which is based on power production by means of a closed CO_2 Brayton cycle, shows that the overall plant efficiency is significantly promoted as the carbonator temperature is increased. Thus, optimum carbonator pressures are in the range of ∼3.5−4 bar, which allow carbonator operation temperatures of 950 °C to yield global efficiencies of about 41%. As a final comment, it is remarkable that a fundamental understanding of physicochemical processes at the molecular level helped us tackle the industrial process with an extra degree of confidence.

AUTHOR INFORMATION

Corresponding Author

*Tel.: +34 655783930. E-mail address: cortiz7@us.es.

ORCID

C. Ortiz: 0000-0002-7795-676X

J. M. Valverde: 0000-0002-2345-8888

Notes

The authors declare no competing financial interest.

ACKNOWLEDGMENTS

This work has been supported by the Spanish Government Agency Ministerio de Economia y Competitividad (MINECO-FEDER funds), contracts CTQ2014-52763-C2, CTQ2017-83602-C2 (-1-R and -2-R). The research leading to these results has received funding from the European Union's Horizon 2020 research and innovation programme under grant agreement No 727348, project SOCRATCES. We acknowledge the characterization services of the Innovation, Technology and Research Center of the University of Seville (CITIUS) and of the Institute of Materials Science of Seville (ICMS).

NOTATION

A = carbonator cross-section, m^2
D = carbonator diameter, m
E_1 = activation energy for chemical decomposition, kJ/mol
f_a = fraction of CaO that reacts in the carbonator in the fast stage
f_{carb} = average carbonation level
F_i = molar flow rate of component i, kmol/s
F_{CaCO_3} = $CaCO_3$ molar flow rate
$F_{CaCO3,crb}$ = $CaCO_3$ molar flow rate (calciner side)
$F_{CaO,unr}$ = molar flow rate of unreacted CaO (calciner side)
$F_{CO_2,clc}$ = CO_2 molar flow rate at calciner outlet
$F_{CO_2,crb,in}$ = CO_2 molar flow rate at carbonator inlet
$F_{CO_2,crb,out}$ = CO_2 molar flow rate at carbonator outlet
F_O = mole flow rate of fresh makeup limestone, kmol/h
F_R = mole flow rate of CO_2 in flue gas entering the carbonator, kmol/h
$F_{R,crb}$ = recirculating molar flow rate (carbonator side)
$F_{R,clc}$ = recirculating molar flow rate (calciner side)
h_i = enthalpy, kJ/kmol
H = carbonator height, m
$\dot{m}$ = mass flow rate, kg/s
N = cycle number
N_{Ca} = mol of Ca in the carbonator, mol
P = pressure, bar
P_{carb} = absolute carbonator pressure, bar
P_{eq} = CO_2 partial pressure at equilibrium, bar
PR = pressure ratio
$\dot{Q}_{input}$ = solar power input
r = reaction rate, s^{-1}
r_{ave} = average reaction rate, s^{-1}
SM = solar multiple
t = time, s
T = temperature, °C
$T_{calciner}$ = calciner temperature, °C
T_{carb} = carbonator temperature, °C
T_{eq} = equilibrium temperature, °C
t_k = fast carbonation stage time, s
μ_0 = mean superficial velocity in the CFB riser, m/s
$\dot{V}_{CO2}$ = CO_2 volume flow rate, m^3/s
W_s = solid inventory in the carbonator per MW of a typical power plant, kg
$\dot{W}_{net}$ = average electrical power, MWe
$\dot{W}_{net,night}$ = net electrical power for the night mode, MWe
$\dot{W}_{net,sun}$ = net electrical power for the sun mode, MWe
$\dot{W}_{M\text{-}TURB}$ = power produced by the main CO_2 turbine, MWe
$\dot{W}_{M\text{-}COMP}$ = power consumed by the main CO_2 compressor, MWe
$\dot{W}_{HPS\text{-}TURB}$ = power produced by the high-pressure CO_2 turbine, MWe
$\dot{W}_{HPS\text{-}COMP}$ = power consumption of high pressure intercooled CO_2 compressor for the storage system, MWe
$\dot{W}_{ST}$ = power produced in the steam turbine cycle, MWe
$\dot{W}_P$ = power consumed in the steam turbine cycle, MWe
$\dot{W}_{PSOLCAL}$ = power consumptions for solids transport in the calciner side, MWe
$\dot{W}_{PSOLCAR}$ = power consumptions for solids transport in the carbonator side, MWe
$\dot{W}_{AUXPOWCA}$ = auxiliary power consumptions in the calciner side, MWe
$\dot{W}_{AUXPOWCR}$ = auxiliary power consumptions in the carbonator side, MWe
X = average CaO conversion
X_{ave} = average conversion of the sorbent
$X_{max,ave}$ = maximum average conversion of the sorbent
X_K = CaO conversion in the fast carbonation stage
X_N = CaO conversion at the N cycle
X_r = residual CaO conversion
ΔP = pressure drop at carbonator, bar

DOI: 10.1021/acssuschemeng.8b00199
ACS Sustainable Chem. Eng. 2018, 6, 6404−6417

ΔS_2^0 = carbonation entropy change, J/(mol·K)
Δt_{sun} = average daytime period, h
$\Delta H_r(T_{react})$ = reaction enthalpy at the reactor temperature, kJ/mol
ΔP = pressure drop at carbonator, bar
ΔS_2^0 = carbonation entropy change, J/(mol·K)
Δt_{sun} = average daytime period, h
$\Delta H_r(T_{react})$ = reaction enthalpy at the reactor temperature, kJ/mol
ΔH_r^0 = standard enthalpy of reaction, kJ/mol
η = overall net efficiency
κ = deactivation constant rate
τ = average residence time in the carbonator, s
ϕ_N = fraction of solids cycled N times

REFERENCES

(1) Gil, A.; Medrano, M.; Martorell, I.; Lázaro, A.; Dolado, P.; Zalba, B.; Cabeza, L. F. State of the Art on High Temperature Thermal Energy Storage for Power Generation. Part 1—Concepts, Materials and Modellization. *Renewable Sustainable Energy Rev.* **2010**, *14* (1), 31−55.
(2) Wagner, S. J.; Rubin, E. S. Economic Implications of Thermal Energy Storage for Concentrated Solar Thermal Power. *Renewable Energy* **2014**, *61*, 81−95.
(3) Denholm, P.; Wan, Y. Y. H.; Hummon, M.; Mehos, M. *An Analysis of Concentrating Solar Power with Thermal Energy Storage in a California 33% Renewable Scenario (Technical Report NREL/TP-6A20−58186)*; 2013.
(4) National Renewable energy laboratory (NREL). Concentrating Solar Power Projects https://www.nrel.gov/csp/solarpaces/ (accessed Apr 2, 2017).
(5) Kearney, D.; Kelly, B.; Herrmann, U.; Cable, R.; Pacheco, J.; Mahoney, R.; Price, H.; Blake, D.; Nava, P.; Potrovitza, N. Engineering Aspects of a Molten Salt Heat Transfer Fluid in a Trough Solar Field. *Energy* **2004**, *29* (5−6), 861−870.
(6) Vignarooban, K.; Xu, X.; Arvay, A.; Hsu, K.; Kannan, A. M. Heat Transfer Fluids for Concentrating Solar Power Systems − A Review. *Appl. Energy* **2015**, *146*, 383−396.
(7) Liu, M.; Steven Tay, N. H.; Bell, S.; Belusko, M.; Jacob, R.; Will, G.; Saman, W.; Bruno, F. Review on Concentrating Solar Power Plants and New Developments in High Temperature Thermal Energy Storage Technologies. *Renewable Sustainable Energy Rev.* **2016**, *53*, 1411−1432.
(8) Valverde, J. M.; Barea-López, M.; Perejón, A.; Sánchez-Jiménez, P. E.; Pérez-Maqueda, L. A. Effect of Thermal Pretreatment and Nanosilica Addition on Limestone Performance at Calcium-Looping Conditions for Thermochemical Energy Storage of Concentrated Solar Power. *Energy Fuels* **2017**, *31* (4), 4226−4236.
(9) Ho, C. K. A Review of High-Temperature Particle Receivers for Concentrating Solar Power. *Appl. Therm. Eng.* **2016**, *109*, 958−969.
(10) N'Tsoukpoe, K. E.; Liu, H.; Le Pierrès, N.; Luo, L. A Review on Long-Term Sorption Solar Energy Storage. *Renewable Sustainable Energy Rev.* **2009**, *13* (9), 2385−2396.
(11) Pardo, P.; Deydier, A.; Anxionnaz-Minvielle, Z.; Rougé, S.; Cabassud, M.; Cognet, P. A Review on High Temperature Thermochemical Heat Energy Storage. *Renewable Sustainable Energy Rev.* **2014**, *32*, 591−610.
(12) Chacartegui, R.; Alovisio, A.; Ortiz, C.; Valverde, J. M.; Verda, V.; Becerra, J. A. Thermochemical Energy Storage of Concentrated Solar Power by Integration of the Calcium Looping Process and a CO_2 Power Cycle. *Appl. Energy* **2016**, *173*, 589−605.
(13) Hanak, D. P.; Manovic, V.; Biliyok, C. Calcium Looping with Inherent Energy Storage for Decarbonisation of Coal-Fired Power Plant. *Energy Environ. Sci.* **2016**, *9*, 971−983.
(14) Abedin, A. H. A Critical Review of Thermochemical Energy Storage Systems. *Open Renewable Energy J.* **2011**, *4* (1), 42−46.
(15) Felderhoff, M.; Urbanczyk, R.; Peil, S. Thermochemical Heat Storage for High Temperature Applications − A Review. *Green* **2013**, *3* (2), 113−123.
(16) Kuravi, S.; Trahan, J.; Goswami, D. Y.; Rahman, M. M.; Stefanakos, E. K. Thermal Energy Storage Technologies and Systems for Concentrating Solar Power Plants. *Prog. Energy Combust. Sci.* **2013**, *39* (4), 285−319.
(17) Ortega-Fernández, I.; Calvet, N.; Gil, A.; Rodríguez-Aseguinolaza, J.; Faik, A.; D'Aguanno, B. Thermophysical Characterization of a by-Product from the Steel Industry to Be Used as a Sustainable and Low-Cost Thermal Energy Storage Material. *Energy* **2015**, *89*, 601−609.
(18) Barker, R. The Reactivity of Calcium Oxide towards Carbon Dioxide and Its Use for Energy Storage. *J. Appl. Chem. Biotechnol.* **1974**, *24* (4−5), 221−227.
(19) Flamant, G.; Hernandez, D.; Bonet, C.; Traverse, J.-P. Experimental Aspects of the Thermochemical Conversion of Solar Energy; Decarbonation of CaCO3. *Sol. Energy* **1980**, *24* (4), 385−395.
(20) Badie, J. M.; Bonet, C.; Faure, M.; Flamant, G.; Foro, R.; Hernandez, D. Decarbonation of Calcite and Phosphate Rock in Solar Chemical Reactors. *Chem. Eng. Sci.* **1980**, *35* (1−2), 413−420.
(21) Williams, R. Hydrogen Production. US 1938202 A, 1933.
(22) Shimizu, T.; Hirama, T.; Hosoda, H.; Kitano, K.; Inagaki, M.; Tejima, K. A Twin Fluid-Bed Reactor for Removal of CO_2 from Combustion Processes. *Chem. Eng. Res. Des.* **1999**, *77* (1), 62−68.
(23) Dean, C. C.; Blamey, J.; Florin, N. H.; Al-Jeboori, M. J.; Fennell, P. S. The Calcium Looping Cycle for CO_2 Capture from Power Generation, Cement Manufacture and Hydrogen Production. *Chem. Eng. Res. Des.* **2011**, *89* (6), 836−855.
(24) Charitos, a.; Hawthorne, C.; Bidwe, A. R.; Sivalingam, S.; Schuster, A.; Spliethoff, H.; Scheffknecht, G. Parametric Investigation of the Calcium Looping Process for CO_2 Capture in a 10kWth Dual Fluidized Bed. *Int. J. Greenhouse Gas Control* **2010**, *4* (5), 776−784.
(25) Arias, B.; Diego, M. E.; Abanades, J. C.; Lorenzo, M.; Diaz, L.; Martínez, D.; Alvarez, J.; Sánchez-Biezma, A. Demonstration of Steady State CO_2 Capture in a 1.7MWth Calcium Looping Pilot. *Int. J. Greenhouse Gas Control* **2013**, *18*, 237−245.
(26) Grasa, G. S.; Abanades, J. C. CO_2 Capture Capacity of CaO in Long Series of Carbonation/Calcination Cycles. *Ind. Eng. Chem. Res.* **2006**, *45* (26), 8846−8851.
(27) Perejón, A.; Romeo, L. M.; Lara, Y.; Lisbona, P.; Martínez, A.; Valverde, J. M. The Calcium-Looping Technology for CO_2 Capture: On the Important Roles of Energy Integration and Sorbent Behavior. *Appl. Energy* **2016**, *162*, 787−807.
(28) Sanchez-Jimenez, P. E.; Valverde, J. M.; Perez-Maqueda, L. A. Multicyclic Conversion of Limestone at Ca-Looping Conditions: The Role of Solid-Sate Diffusion Controlled Carbonation. *Fuel* **2014**, *127*, 131−140.
(29) Valverde, J. M.; Sanchez-Jimenez, P. E.; Perez-Maqueda, L. Calcium-Looping for Post-Combustion CO_2 Capture. On the Adverse Effect of Sorbent Regeneration under CO_2. *Appl. Energy* **2014**, *126*, 161−171.
(30) Hanak, D. P.; Anthony, E. J.; Manovic, V. A Review of Developments in Pilot-Plant Testing and Modelling of Calcium Looping Process for CO_2 Capture from Power Generation Systems. *Energy Environ. Sci.* **2015**, *8* (8), 2199−2249.
(31) Ortiz, C.; Chacartegui, R.; Valverde, J. M.; Alovisio, A.; Becerra, J. A. Power Cycles Integration in Concentrated Solar Power Plants with Energy Storage Based on Calcium Looping. *Energy Convers. Manage.* **2017**, *149*, 815−829.
(32) Berger, E. E. Effect of Steam on the Decomposition of Limestone. *Ind. Eng. Chem.* **1927**, *19* (5), 594−596.
(33) Valverde, J. M.; Medina, S. Reduction of Calcination Temperature in the Calcium Looping Process for CO_2 Capture by Using Helium: In Situ XRD Analysis. *ACS Sustainable Chem. Eng.* **2016**, *4* (12), 7090−7097.
(34) Valverde, J. M.; Medina, S. Limestone Calcination under Calcium-Looping Conditions for CO_2 Capture and Thermochemical

DOI: 10.1021/acssuschemeng.8b00199
ACS Sustainable Chem. Eng. 2018, 6, 6404−6417

Energy Storage in the Presence of H_2O: An in Situ XRD Analysis. *Phys. Chem. Chem. Phys.* **2017**, *19* (11), 7587−7596.
(35) Sarrion, B.; Valverde, J. M.; Perejon, A.; Perez-maqueda, L. A.; Sanchez-jimenez, P. E. On the Multicycle Activity of Natural Limestone/dolomite for Cheap, Efficient and Non-Toxic Thermochemical Energy Storage of Concentrated Solar Power. *Energy Technol.* **2016**, *4*, 1013.
(36) Benitez-Guerrero, M.; Valverde, J. M.; Sanchez-Jimenez, P. E.; Perejon, A.; Perez-Maqueda, L. A. Multicycle Activity of Natural $CaCO_3$ minerals for Thermochemical Energy Storage in Concentrated Solar Power Plants. *Sol. Energy* **2017**, *153*, 188−199.
(37) Benitez-Guerrero, M.; Sarrion, B.; Perejon, A.; Sanchez-Jimenez, P. E.; Perez-Maqueda, L. A.; Manuel Valverde, J. Large-Scale High-Temperature Solar Energy Storage Using Natural Minerals. *Sol. Energy Mater. Sol. Cells* **2017**, *168* (March), 14−21.
(38) Bhatia, S. K.; Perlmutter, D. D. Effect of the Product Layer on the Kinetics of the CO_2-Lime Reaction. *AIChE J.* **1983**, *29* (1), 79−86.
(39) Grasa, G.; Murillo, R.; Alonso, M.; Abanades, J. C. Application of the Random Pore Model to the Carbonation Cyclic Reaction. *AIChE J.* **2009**, *55* (5), 1246−1255.
(40) Gupta, H.; Fan, L.-S. Carbonation−Calcination Cycle Using High Reactivity Calcium Oxide for Carbon Dioxide Separation from Flue Gas. *Ind. Eng. Chem. Res.* **2002**, *41* (16), 4035−4042.
(41) Kyaw, K.; Kubota, M.; Watanabe, F.; Matsuda, H.; Hasatani, M. Study of Carbonation of CaO for High Temperature Thermal Energy Storage. *J. Chem. Eng. Jpn.* **1998**, *31* (2), 281−284.
(42) Moore, W. J. *Physical Chemistry*, 5th ed.; Prentice-Hall, 1999.
(43) Pijolat, M.; Soustelle, M. Experimental Tests to Validate the Rate-Limiting Step Assumption Used in the Kinetic Analysis of Solid-State Reactions. *Thermochim. Acta* **2008**, *478* (1−2), 34−40.
(44) Valverde, J. M.; Sanchez-Jimenez, P. E.; Perez-Maqueda, L. Limestone Calcination Nearby Equilibrium: Kinetics, CaO Crystal Structure, Sintering and Reactivity. *J. Phys. Chem. C* **2015**, *119* (4), 1623−1641.
(45) Perejón, A.; Sánchez-Jiménez, P. E.; Criado, J. M.; Pérez-Maqueda, L. A. Magnesium Hydride for Energy Storage Applications: The Kinetics of Dehydrogenation under Different Working Conditions. *J. Alloys Compd.* **2016**, *681*, 571−579.
(46) Barin, I. *Thermochemical Data of Pure Substances*; VCH: Weinheim, 1989.
(47) Stanmore, B. R.; Gilot, P. Review—calcination and Carbonation of Limestone during Thermal Cycling for CO_2 Sequestration. *Fuel Process. Technol.* **2005**, *86* (16), 1707−1743.
(48) García-Labiano, F.; Abad, A.; de Diego, L. F.; Gayán, P.; Adánez, J. Calcination of Calcium-Based Sorbents at Pressure in a Broad Range of CO_2 Concentrations. *Chem. Eng. Sci.* **2002**, *57* (13), 2381−2393.
(49) Campbell, C. T.; Sellers, J. R. V. The Entropies of Adsorbed Molecules. *J. Am. Chem. Soc.* **2012**, *134* (43), 18109−18115.
(50) Negi, A. S.; Anand, S. C. *A Textbook of Physical Chemistry*; Wiley Eastern, 1985.
(51) Criado, J.; González, M.; Málek, J.; Ortega, A. The Effect of the CO_2 Pressure on the Thermal Decomposition Kinetics of Calcium Carbonate. *Thermochim. Acta* **1995**, *254* (121), 121−127.
(52) Khawam, A.; Flanagan, D. R. Solid-State Kinetic Models: Basics and Mathematical Fundamentals. *J. Phys. Chem. B* **2006**, *110* (35), 17315−17328.
(53) Brown, M. E. The Prout-Tompkins Rate Equation in Solid-State Kinetics. *Thermochim. Acta* **1997**, *300* (1−2), 93−106.
(54) Sánchez-Jiménez, P. E.; Perejón, A.; Pérez-Maqueda, L. A.; Criado, J. M. New Insights on the Kinetic Analysis of Isothermal Data: The Independence of the Activation Energy from the Assumed Kinetic Model. *Energy Fuels* **2015**, *29* (1), 392−397.
(55) Valverde, J. M.; Sanchez-Jimenez, P. E.; Perez-Maqueda, L. Ca-Looping for Postcombustion CO_2 Capture: A Comparative Analysis on the Performances of Dolomite and Limestone. *Appl. Energy* **2015**, *138*, 202−215.
(56) Wang, K.; Hu, X.; Zhao, P.; Yin, Z. Natural Dolomite Modified with Carbon Coating for Cyclic High-Temperature CO_2 Capture. *Appl. Energy* **2016**, *165*, 14−21.
(57) Sun, R.; Li, Y.; Liu, H.; Wu, S.; Lu, C. CO_2 Capture Performance of Calcium-Based Sorbent Doped with Manganese Salts during Calcium Looping Cycle. *Appl. Energy* **2012**, *89* (1), 368−373.
(58) Manovic, V.; Anthony, E. J. Thermal Activation of CaO-Based Sorbent and Self-Reactivation during CO_2 Capture Looping Cycles. *Environ. Sci. Technol.* **2008**, *42* (11), 4170−4174.
(59) Valverde, J. M.; Sanchez-jimenez, P. E.; Perejon, A.; Perez-maqueda, L. A. Role of Looping-Calcination Conditions on Self-Reactivation of Thermally Pretreated CO_2 Sorbents Based on CaO. *Energy Fuels* **2013**, *27*, 3373−3384.
(60) Valverde, J. M. *Relevant Influence of Limestone Crystallinity on CO_2 Capture in The Ca-Looping Technology at Realistic Calcination Conditions*; 2014.
(61) Manovic, V.; Anthony, E. J. Carbonation of CaO-Based Sorbents Enhanced by Steam Addition. *Ind. Eng. Chem. Res.* **2010**, *49* (19), 9105−9110.
(62) Alovisio, A.; Chacartegui, R.; Ortiz, C.; Valverde, J. M.; Verda, V. Optimizing the CSP-Calcium Looping Integration for Thermochemical Energy Storage. *Energy Convers. Manage.* **2017**, *136*, 85−98.
(63) Valverde, J. M. A Model on the CaO Multicyclic Conversion in the Ca-Looping Process. *Chem. Eng. J.* **2013**, *228*, 1195−1206.
(64) Obermeier, J.; Sakellariou, K. G.; Tsongidis, N. I.; Baciu, D.; Charalambopoulou, G.; Steriotis, T.; Müller, K.; Karagiannakis, G.; Konstandopoulos, A. G.; Stubos, A.; et al. Material Development and Assessment of an Energy Storage Concept Based on the CaO-Looping Process. *Sol. Energy* **2017**, *150*, 298−309.
(65) Valverde, J. M.; Sanchez-Jimenez, P. E.; Perez-Maqueda, L. Role of Precalcination and Regeneration Conditions on Postcombustion CO_2 Capture in the Ca-Looping Technology. *Appl. Energy* **2014**, *136*, 347−356.
(66) Alonso, M.; Rodríguez, N.; Grasa, G.; Abanades, J. C. Modelling of a Fluidized Bed Carbonator Reactor to Capture CO_2 from a Combustion Flue Gas. *Chem. Eng. Sci.* **2009**, *64* (5), 883−891.
(67) Abanades, J. C. The Maximum Capture Efficiency of CO_2 Using a Carbonation/calcination Cycle of CaO/CaCO3. *Chem. Eng. J.* **2002**, *90* (3), 303−306.
(68) Arias, B.; Abanades, J. C.; Grasa, G. S. An Analysis of the Effect of Carbonation Conditions on CaO Deactivation Curves. *Chem. Eng. J.* **2011**, *167* (1), 255−261.
(69) Mess, D.; Sarofim, A. F.; Longwell, J. P. Product Layer Diffusion during the Reaction of Calcium Oxide with Carbon Dioxide. *Energy Fuels* **1999**, *13* (5), 999−1005.
(70) Edwards, S. E. B.; Materić, V. Calcium Looping in Solar Power Generation Plants. *Sol. Energy* **2012**, *86* (9), 2494−2503.
(71) Fidaros, D. K.; Baxevanou, C. a.; Vlachos, N. S. A Parametric Study of a Solar Calcinator Using Computational Fluid Dynamics. *Energy Convers. Manage.* **2007**, *48* (11), 2784−2791.
(72) Meier, A.; Bonaldi, E.; Cella, G. M.; Lipinski, W.; Wuillemin, D. Solar Chemical Reactor Technology for Industrial Production of Lime. *Sol. Energy* **2006**, *80* (10), 1355−1362.
(73) Reich, L. Towards Solar Thermochemical Carbon Dioxide Capture via Calcium Oxide Looping: A Review. *Aerosol Air Qual. Res.* **2014**, *14* (2), 500−514.
(74) Koepf, E.; Alxneit, I.; Wieckert, C.; Meier, A. A Review of High Temperature Solar Driven Reactor Technology: 25years of Experience in Research and Development at the Paul Scherrer Institute. *Appl. Energy* **2017**, *188*, 620−651.
(75) Meier, A.; Gremaud, N.; Steinfeld, A. Economic Evaluation of the Industrial Solar Production of Lime. *Energy Convers. Manage.* **2005**, *46* (6), 905−926.
(76) Kvamsdal, H. M.; Romano, M. C.; van der Ham, L.; Bonalumi, D.; van Os, P.; Goetheer, E. Energetic Evaluation of a Power Plant Integrated with a Piperazine-Based CO_2 Capture Process. *Int. J. Greenhouse Gas Control* **2014**, *28*, 343−355.
(77) Romano, M. C. Modeling the Carbonator of a Ca-Looping Process for CO_2 Capture from Power Plant Flue Gas. *Chem. Eng. Sci.* **2012**, *69* (1), 257−269.
(78) MacKenzie, A.; Granatstein, D. L.; Anthony, E. J.; Abanades, J. C. Economics of CO_2 Capture Using the Calcium Cycle with a

DOI: 10.1021/acssuschemeng.8b00199
ACS Sustainable Chem. Eng. 2018, 6, 6404−6417

Pressurized Fluidized Bed Combustor. *Energy Fuels* **2007**, *21* (2), 920−926.
(79) Abanades, J. C.; Grasa, G.; Alonso, M.; Rodriguez, N.; Anthony, E. J.; Romeo, L. M. Cost Structure of a Postcombustion CO_2 Capture System Using CaO. *Environ. Sci. Technol.* **2007**, *41* (15), 5523−5527.
(80) Romano, M. C.; Spinelli, M.; Campanari, S.; Consonni, S.; Cinti, G.; Marchi, M.; Borgarello, E. The Calcium Looping Process for Low CO_2 Emission Cement and Power. *Energy Procedia* **2013**, *37*, 7091−7099.
(81) Cormos, C.-C. Economic Evaluations of Coal-Based Combustion and Gasification Power Plants with Post-Combustion CO_2 Capture Using Calcium Looping Cycle. *Energy* **2014**, *78*, 665−673.

DOI: 10.1021/acssuschemeng.8b00199
ACS Sustainable Chem. Eng. 2018, 6, 6404−6417

***ANNEX 10**: Ortiz C, Romano MC, Valverde JM, Binotti M, Chacartegui R. Process integration of Calcium-Looping thermochemical energy storage system in concentrating solar power plants. Energy 2018;155:535–51. doi:10.1016/j.energy.2018.04.180.*

Energy 155 (2018) 535–551

Contents lists available at ScienceDirect

Energy

journal homepage: www.elsevier.com/locate/energy

Process integration of Calcium-Looping thermochemical energy storage system in concentrating solar power plants

C. Ortiz [a, *], M.C. Romano [b], J.M. Valverde [a], M. Binotti [b], R. Chacartegui [c]

[a] Facultad de Física, Universidad de Sevilla, Avenida Reina Mercedes s/n, 41012, Sevilla, Spain
[b] Politecnico di Milano - Dipartimento di Energia, Via Lambruschini 4, 20156, Milano, Italy
[c] Escuela Técnica Superior de Ingeniería, Universidad de Sevilla, Camino de los Descubrimientos s/n, 41092, Sevilla, Spain

ARTICLE INFO

Article history:
Received 23 October 2017
Received in revised form
8 April 2018
Accepted 28 April 2018
Available online 30 April 2018

Keywords:
Calcium looping
CO_2 cycle
CSP
Energy storage

ABSTRACT

The Calcium-Looping process is a promising thermochemical energy storage method based on the multicycle calcination-carbonation of $CaCO_3$-CaO to be used in concentrated solar power plants. When solar energy is available, the $CaCO_3$ solids are calcined at high temperature to produce CaO and CO_2, which are stored for subsequent utilization. When power is needed, these reaction by-products are fed into a carbonator reactor where energy is released from the exothermic carbonation reaction. In comparison with currently commercial energy storage systems, such as solar salts, the Calcium-Looping process presents several benefits such as the feasibility to work at significantly higher power cycle temperatures, a higher energy storage density and the possibility to store energy in the medium-long term. The present manuscript analyzes a number of novel Calcium-Looping configurations for energy storage combined with CO_2 cycles in a solar tower plant. The high overall efficiencies achieved (32–44%, defined as the ratio of net electric power production to net solar thermal power entering the calciner) indicate a potential interest for the integration of the Calcium-Looping process in Concentrating Solar Power Plants, although major technological challenges related to the design of the solar receiver and of the high temperature solids handling devices remain to be faced.

1. Introduction

Dispatchability is a main challenge for the commercial deployment of intrinsically variable major renewable energies such as wind and solar. Thus, efficient, cheap and non-toxic thermal energy storage (TES) is a key issue for Concentrating Solar Power (CSP) plants to provide a significant share of electricity generation. Currently, over 40% of commercial CSP plants around the world incorporate TES systems typically based on a two-tank TES system to use the sensible heat stored in molten salts, which allows CSP plants to operate up to 15 h in the absence of solar radiation [1].

In the last years, research on Thermochemical Energy Storage (TCES) systems as an alternative to molten salts has gained a considerable momentum [2]. TCES applied to CSP uses the heat available in the solar receiver to drive an endothermic reaction. When energy is needed, the by-products of the reaction are brought together at the necessary conditions for the reverse exothermic reaction to occur, which releases the previously stored chemical energy for power production. Main advantages of TCES over TES and PCMs are the possibility of storing energy in the long term [3] and the high energy density potentially achievable [4]. Many TCES systems are being analyzed as candidates for energy storage in CSP plants [5], among which we find systems based on hydroxides (e.g. $Ca(OH)_2$ [6]), metal redox (e.g. Co_3O_4 [7]), carbonates (e.g. $CaCO_3$ [8], $SrCO_3$ [9,10]), hydrides (e.g. MgH_2 [11]), ammonia [12], sulfur [13] or organic compounds (e.g. CH_4 [14]). A proper selection of the TCES system is crucial. In order to compare the different TCES systems, a general criterion was proposed by Wentworth and Chen [15].

Among the diverse thermochemical systems for energy storage, the cyclic calcination-carbonation of $CaCO_3$-CaO (Eq. (1)) stands as a promising method for CSP applications [16–20].

$$CaCO_{3(s)} \rightleftarrows CaO_{(s)} + CO_{2(g)} \quad \Delta H_r^0 = 178\ kJ/mol \tag{1}$$

The Calcium-Looping (CaL) process shows a number of important benefits for TCES in CSP such as: i) high turning temperature, which allows using high efficiency power cycles [21] thus

* Corresponding author.
E-mail address: cortiz7@us.es (C. Ortiz).

https://doi.org/10.1016/j.energy.2018.04.180
0360-5442/

overcoming the limitations imposed by the degradation of molten salts at temperatures near ~600 °C, ii) high energy density [19], iii) the use of a well-known process and already mature technology originally developed for the cement and lime industry [22–24], iv) the low price, wide availability and non toxicity of natural limestone (near 100% $CaCO_3$) that may be employed as CaO precursor [25–27].

The CSP-CaL integrated process starts with the decomposition of $CaCO_3$ in a solar calcination reactor (calciner) where heat is supplied by concentrated solar radiation. In this regard, the CaL process is especially suited for CSP plants with tower technology where the attainable temperatures fit in the necessary range to achieve fast $CaCO_3$ decomposition (above 700 °C depending on the CO_2 partial pressure in the calciner environment [28]). The calcination by-products (CaO and CO_2) are sent to storage vessels and, when needed, circulated into a carbonator reactor wherein energy is recovered from the exothermic carbonation reaction.

The CSP-CaL integration, although already proposed as a concept in the late 1970s [29], has not been analyzed in detail until quite recently. Several solar calcination reactors have been proposed and tested [30–33]. Moreover, a number of studies have been reported regarding Ca-based materials behavior for TCES [20,34,35]. Edwards et al. [36] developed a CSP-CaL integration scheme in which the carbonator heat is transferred to a CO_2/air stream used as working fluid in a Joule-Brayton open cycle. Chacartegui et al. [8] have more recently proposed a higher efficiency (up to 45%) CSP-CaL scheme optimized by a pinch analysis [37] wherein the TCES system is coupled to a closed CO_2 power cycle [21]. Another possibility would be integrating a supercritical CO_2 cycle (s-CO_2) [38–40] in an indirect way, as was analyzed in a previous work [21]. Previous schemes [38,41] take advantage of the energy storage capacity of CaL process within a post-combustion CO_2 system. Other works [42,43] have presented diverse schemes in which CSP is used to aid calcination when the CaL process is employed for CO_2 capture in a coal fired power plant.

The present manuscript goes beyond previous analyses on the CSP-CaL integration by investigating the performance of new process schemes. Regarding to previous works, the novel schemes analyzed in the present work consider high temperature solids storage, which simplifies the heat integration process while maintaining a high-energy storage potential. In this regard, a new expression to estimate the energy density of a thermochemical system based on gas-solid reactions is proposed, which considers not just the reaction enthalpy but also the size of the vessels needed for solids storage and material properties such as the bulk porosity of the granular solids. A simpler heat integration allows to use novel integration schemes with a design similar to state-of-the-art equipment. Starting from a simplified base case each modified layout seeks to increase the overall plant efficiency at the expense of introducing an additional degree of complexity and therefore a higher investment cost.

The manuscript is structured as follows: first a CSP-CaL plant is generally described. Main concepts, possibilities and limitations of the cycle, as well as the assumptions made along the analisys are addressed. In section 3, four novel CSP-CaL integration schemes are analyzed from mass and energy balances. Afterwards, a sensitivity analisys is carried out in order to assess the impact of the different assumptions on cycle efficiency. Results show that overall plant efficiencies, defined as the ratio of net electrical production to net thermal input entering the calciner (and therefore without considering solar receiver efficiency) vary in a wide range of 32–44% depending on the system complexity and cycle parameters.

2. CSP-CaL plant

2.1. Overall description

Fig. 1 shows a flow diagram of the CSP-CaL integrated system. The process starts in the calciner, where solar energy is used to carry out the calcination reaction that releases gaseous CO_2 and solid CaO as products. In the present work it is assumed that calcination can be fully achieved in the calciner [17,22]. According to chemical equilibrium [28], a temperature around 900 °C is sufficiently high to drive calcination at atmospheric pressure in short residence times. Such temperature can be attained, for example, in a solar particle receiver [44,45]. Several solar calciner reactors have been already proposed in literature [30–32,46] and experimentally tested up to 50 kW scale [47].

CaO generated in the solar calciner is stored in a CaO storage vessel, while hot CO_2 is cooled down in a heat exchanger network consisting in a heat recovery steam generator for a bottoming steam cycle and in possible solids preheater. Cooled CO_2 is stored in a pressurized CO_2 vessel or used as working fluid in the power cycle.

On the carbonator side, preheated CO_2 reacts with CaO by exothermic carbonation, which produces $CaCO_3$. The CO_2 mass flow rate entering in the carbonator ($F_{CO2,crb,in}$) is well above the stoichiometric need and the excess CO_2 ($F_{CO2,crb,out}$) is used as fluid carrier to evacuate the heat released by carbonation. Hot CO_2 effluent from the carbonator is expanded in the main CO_2 turbine (M-TURB) driving the CO_2 compressors and producing electric power. Expanded CO_2 stream is cooled in a heat exchanger network, which consists of a CO_2 cycle regenerator and may include solids preheaters. The cooled CO_2 is mixed with the cooled CO_2 generated in the calciner or from the CO_2 storage vessel and then compressed up to the carbonator pressure.

One of the main drawbacks of the CaL process is the progressive loss of activity toward carbonation in short residence times of the regenerated CaO as the number of cycles increases depending on the carbonation/calcination conditions employed [48]. Thus, only a fraction *X* of the total flow of CaO entering the carbonator ($F_{R,crb,in}$) reacts to produce $CaCO_3$ ($F_{CaCO3,crb}$), while *1-X* remains as unreacted CaO ($F_{CaO,unr}$). The average CaO conversion X is thus a critical material property for the simulations. CaO conversion is highly dependent on the carbonation-calcination conditions as well as on the CaO precursor [49]. The CaL process applied to post-combustion CO_2 capture, which most of the CaL research focused on, involves carbonation under low CO_2 partial pressure whereas calcination is carried out under high CO_2 concentration at temperatures around 950 °C. These conditions lead to a severe drop of the CaO conversion with the number of cycles, reaching a residual value of just around $X = 0.07–0.08$ [50]. However, CaL conditions for TCES in CSP are not the same as those employed for CO_2 capture. In the proposed CaL-CSP integration scheme (Fig. 1) both carbonation and calcination are carried out under a pure CO_2 atmosphere. According to previous works, CaO residual conversion is about $X = 0.2$ for carbonation under 100%CO_2 atmosphere and calcination at 725 °C (under low CO_2 partial pressure) for $CaCO_3$ particles larger than 45 μm [18]. A similar value of the residual conversion for CaO derived limestone is reported by Obermeier et al. [17], who performed calcination at 800 °C in air atmosphere and carbonation at 600 °C under pure CO_2 atmosphere. In the present work, a baseline value of $X = 0.15$ is assumed for the process simulations at stationary conditions, which means that about 85% by weight of the CaO entering into the carbonator exits it as unreacted CaO. Nevertheless, a sensitivity analysis on the average conversion will be performed in Section 4 to assess the dependency of the plant performance on the CaO conversion.

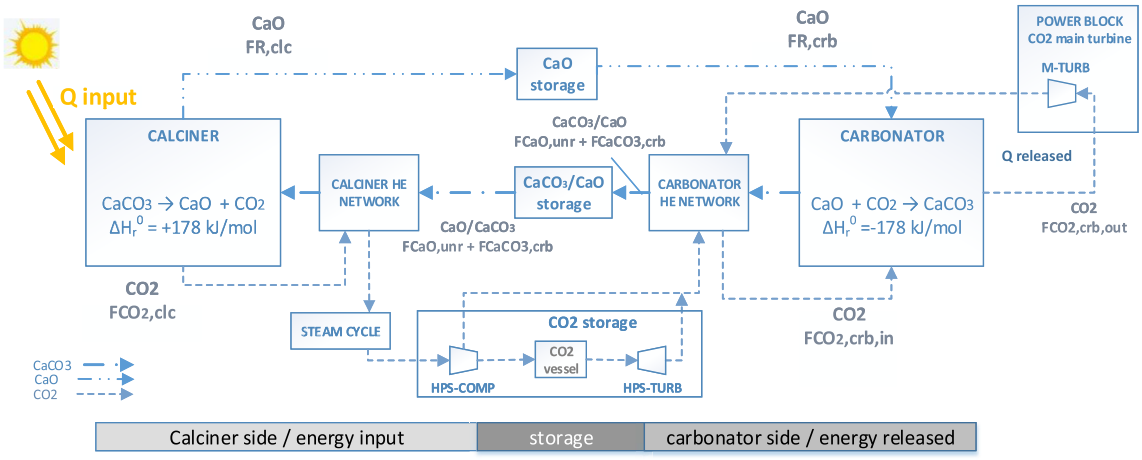

Fig. 1. CSP-CaL conceptual scheme.

Energy density values found in the literature for the CaL system vary widely. Some authors [4,38,51–53] report values around of 3–4 GJ/m^3 from the reaction enthalpy while other works [38,54,55] give values in the range of 0.9–2 GJ/m^3 by considering gas and solids vessels and/or that carbonation is not complete. Rhodes et al. [10] use an expression to calculate the energy density in each cycle as a function of the mass change observed in thermogravimetric experiments. However, it is interesting for practical purposes to address the size of the vessels needed for solids storage (i.e. taking into account the particles porosity and the packing density of solids), which is more closely connected with the capital costs of the energy storage system. To this end we propose Eq. (2), which can be applied to gas-solid TCES systems with the structure $AB_{(s)} \rightleftarrows A_{(s)} + B_{(g)}$ (for the CaL case: $AB = CaCO_3$; A = CaO; B=CO_2):

$$E_{den}\left[\frac{GJ}{m^3}\right] = \frac{X\cdot\left(\Delta H_R + \int_{T_{B,\ vessel}}^{T_{reactor}} c_{p,\ B}\,dT + \int_{T_{AB,\ vessel}}^{T_{A,\ vessel}} c_{p,AB}dT\right) + (1-X)\cdot\int_{T_{AB,\ vessel}}^{T_{A,\ vessel}} c_{p,A}dT}{\left(\frac{v_{AB}}{(1-\varepsilon_{AB})} + \frac{v_A}{(1-\varepsilon_A)}\right)\frac{1}{\varnothing} + X\cdot v_B} \tag{2}$$

where ΔH_R is the reaction enthalpy (GJ/kmol), $c_{p,\ i}$ is the specific heat of the component i (MJ/kmol·K), $T_{reactor}$ is the decomposition reaction temperature (K),$T_{i,\ vessel}$ is the storage temperature for of the component i (K), v_i is the specific volume (m^3/kmol) of the component i at storage conditions, ε_i is the internal porosity of the component i and $\varnothing$ is the particle packing density, whose value is set to 0.6 as a typical value for the random loose packing fraction of irregularly shaped particles under gravity [56]. For the CaL specific case, it is assumed that particle size does not change by reversible reaction (which would affect mainly to its internal porosity) and therefore $v_{AB} = v_A$.

The CO_2 tank volume is a critical factor depending on the gas temperature and pressure. In the CSP-CaL integration scheme proposed elsewhere [8] CO_2 is stored at high pressure (75 bar) and atmospheric temperature (25 °C) to guarantee supercritical conditions and therefore minimize vessel size. The solids vessels capacity is highly influenced by the CaO conversion, since a high CaO reactivity reduces storage volume needs. Thus, the volumetric energy density of the entire CaL system is mainly dependent on the CO_2 storage conditions (pressure and temperature) and CaO conversion as shown in Fig. 2.

As shown in Fig. 2, considering supercritical conditions for CO_2 storage, the energy density of the entire system varies in a range of ~ 0.39–0.9 GJ/m^3 depending on CaO conversion. Fig. 2 also shows the energy storage density of a molten salt system by considering a two-tank configuration [57] and typical values of the temperature change (DT) in CSP plants [1]. As can be seen, the energy storage density of the entire CaL system is comparable to the molten salt technology for CaO conversions of 0.15, whereas it can be well above that of the molten salts system for higher CaO conversion.

2.2. Model assumptions

The main assumptions made to model the CSP-CaL plant are summarized in Table 1. All gas-gas heat exchangers are characterized by a minimum temperature difference (ΔT_{min}) of 15 °C, whereas gas-solids heat exchangers are assumed to achieve the same outlet temperature in both streams, assuming fluidized bed or entrained flow gas solid contactors. Auxiliaries power consumption in the carbonator and calciner sides are calculated as 0.8% of the heat rejected in coolers [58]. Solids transport is carried out by means of pneumatic conveying, which is an already mature technology to transport high temperature granular solids [59]. For Ca based particles and a typical transport length of 200 m, the estimated energy consumption is 20 MJ/ton [8]. Thermal loss in the storage system is highly dependent on the type of insulation employed. Thus, a thermal uncertainty parameter (including receiver and storage efficiencies) will be considered in the calculation of the solar to electric power efficiency.

In regard to the turbomachinery efficiencies, different values

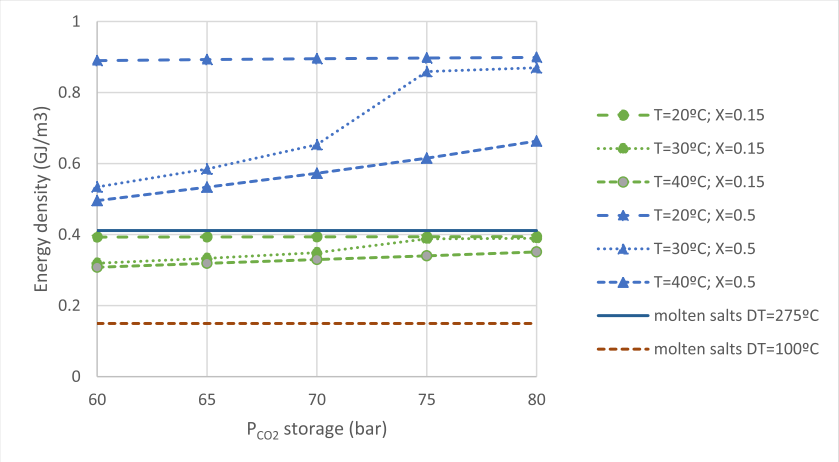

Fig. 2. Overall CaL energy storage density as a function of CO_2 storage conditions (pressure and temperature) and CaO conversion X. Solids storage temperature is assumed at 600 °C.

Table 1
Main assumptions in the CSP-CaL model.

Group	Parameter	Component	Value
Turbomachinery	Isentropic efficiency	Main CO_2 turbine (M-TURB)	0.9
		Main CO_2 compressor (M-COMP)	0.87
		High pressure storage turbine (HPS-TURB)	0.8
		High pressure storage compressor (HPS-COMP)	0.8
	Mechanical-electric efficiencies	Main CO_2 turbine (M-TURB)	0.98
		Main CO_2 compressor (M-COMP)	0.98
		CO_2 turbine (HPS-TURB)	0.96
		High pressure storage compressor (HPS-COMP)	0.96
	number of intercooling/reheating stages	High pressure storage compressor (HPS-COMP)	5
		Main CO_2 compressor (M-COMP)	0
		CO_2 turbine (HPS-TURB)	2
	Intercooling/reheating temperature	High pressure storage compressor (HPS-COMP)	40 °C
		High pressure storage turbine (HPS-TURB)	65 °C/100 °C
Heat exchangers	minimum temperature difference	gas-gas HX	15 °C
		CO_2-cooler	15 °C
	Pressure drops	coolers	1%
		HXG (both sides)	5%
		HRSG (hot side)	3%
		HRSG (cold side)	11%
		solid-gas HX (both sides)	3%
Reactors	Efficiency	Calciner	1
	Heat input	Calciner	100 MW
	Heat losses	Carbonator	1% of heat transferred
Storage vessels	Temperature losses	All	0 °C
	CO_2 storage conditions	CO_2 vessel	75 bar
			25 °C
Steam cycle	isentropic efficiency	Steam turbine (ST)	0.75
	Mechanical-electric efficiencies	Steam turbine (ST)	0.98
	condensing pressure	COND	0.075 bar
	evaporation pressure	HRSG	45 bar
	Super-heated steam temperature	HRSG	400 °C
Heat rejection	Auxiliaries electric power consumption	All coolers	0.8% of heat released

have been considered as a function of turbomachinery size and type (Table 1). Thus, higher isentropic and mechanical efficiencies are assumed for turbomachines with larger volume flow rate (M-TURB and M-COMP). The moderate heat input does not justify the adoption of complex configurations with high steam parameters for the heat recovery steam cycle. Thus, a simple superheated steam cycle with no reheat and moderate pressure and temperatures has been assumed.

Different operations in "sun" and "night" modes are simulated in this work. As previously stated, a Solar Multiple (SM) equal to 3 is assumed for the system design and for simplicity the day is considered composed by 8 h of sun, constantly providing 100 MWth to the calciner, and of 16 h of night. In the "sun" operating mode the CO_2 mass flow entering the carbonator side ($F_{CO2,crb,in}$) is thus 1/3 the amount produced in the calciner ($F_{CO2,clc}$) whereas the remaining 2/3 are sent to a CO_2 storage vessel that is discharged during the "night" mode operations (2/3 of the day). In this simplified approach, the plant efficiency is therefore determined as a weighted average of the performances in "sun" mode and "night" mode (Eq. (3)). A more detailed hour-by-hour calculation with real solar radiation data and off-design plant analysis should be pursued for a rigorous yearly analysis.

$$\eta = \frac{\int_{24h} \dot{W}_{net}\, dt}{\int_{24h} \dot{Q}_{input}\, dt} = \frac{\dot{W}_{net,sun}\Delta t_{sun} + \dot{W}_{net,night}\,(24 - \Delta t_{sun})}{\dot{Q}_{input}\,\Delta t_{sun}} \quad (3)$$

In Eq. (4), $\dot{W}_{net}$ is the net electrical power produced by the system and $\dot{Q}_{input}$ is the solar power input in the calciner (100 MW for Δt_{sun} of 8 h). The electric power produced is computed for the "*sun mode*" ($\dot{W}_{net,sun}$) and the "*night mode*"($\dot{W}_{net,night}$), (Eqs. (4) and (5)):

$$\dot{W}_{net,sun} = \dot{W}_{M-TURB} + \dot{W}_{ST} - \dot{W}_{P} - \dot{W}_{M-COMP} - \dot{W}_{HPS-COMP} - \dot{W}_{PSOLCAL} - \dot{W}_{PSOLCAR} - \dot{W}_{AUXPOWCA} - \dot{W}_{AUXPOWCR} \quad (4)$$

$$\dot{W}_{net,night} = \dot{W}_{M-TURB} + \dot{W}_{HPS-TURB} - \dot{W}_{M-COMP} - \dot{W}_{PSOLCAR} - \dot{W}_{AUXPOWCR} \quad (5)$$

where $\dot{W}_{M-TURB}$ is the power produced by the main CO_2 turbine; $\dot{W}_{ST}$ and $\dot{W}_{P}$ are the power produced and consumed by the steam turbine and the pump of the steam cycle, respectively; $\dot{W}_{M-COMP}$ is the power consumed by the main CO_2 compressor; $\dot{W}_{HPS-COMP}$ is the power consumption by the high pressure intercooled CO_2 compressor for the storage system; $\dot{W}_{PSOLCAL}$ and $\dot{W}_{PSOLCAR}$ are the power consumptions due to solids transport in the calciner and carbonator sides, respectively; $\dot{W}_{AUXPOWCA}$ and $\dot{W}_{AUXPOWCR}$ are the auxiliary power consumptions in the calciner and carbonator sides, respectively; $\dot{W}_{HPS-TURB}$ is the power produced by the high pressure CO_2 turbine for expanding CO_2 from the storage to the carbonator pressure.

It is important to note that efficiency in our work strictly refers to the heat input to the calciner and therefore it does not take into account the thermal efficiency of the solar receiver, whose design and modelling is beyond the scope of this work.

3. CSP-CaL schemes

In order to analyze the most beneficial configuration as a tradeoff between efficiency and complexity 4 layouts have been analyzed. Case 1 is the base case, gas-solid heat exchangers are introduced in Case 2, an intercooled compression is added to Case 3 and, in Case 4, an ambient pressure carbonator is also employed. Calculations have been performed using the commercial software Aspen Plus™.

3.1. Base case

The proposed configuration for the base case is shown in Fig. 3. In the "sun" operation mode, solar energy is used in the calciner to bring the $CaCO_3$-rich solids stream up to reaction temperature (900 °C) for the calcination reaction to be achieved. The CO_2 produced in the calcination (*g1* in Fig. 3) is sent to a heat recovery steam generator (HRSG) in order to use its sensible heat for power production by means of a simple superheated steam Rankine cycle. The cooled CO_2 stream (*g3*) is then compressed up to 3 bar in the main CO_2 compressor (M-COMP) and is split in two streams. A fraction of the CO_2 (1/3 of total) is sent directly to the carbonator (*g7a*), whereas the rest (*g4*) is further compressed up to 75 bar (HPS-COMP) and stored (CO_2 storage) for its use during the "night" operation mode. The CaO produced in the calciner (*c1*) is directly stored in the high temperature CaO storage vessel. Solids are stored at ambient pressure and therefore lock hoppers are needed for decoupling the pressure of the atmospheric solar receiver and of the storage vessel from the pressurized carbonator.

On the carbonator side, electric power is produced by means of a CO_2 closed Brayton cycle wherein a heat exchanger *HXG* is used as recuperator. For this base case, CO_2 is expanded from carbonator pressure to atmospheric pressure in the turbine with a pressure ratio of 3 ($PR = P_{carbonator}/P_{out,\ MTURB}$). The CO_2 mass flow rate entering the carbonator (*g9*) is well above the stoichiometric need for CaO carbonation and is controlled to achieve the target turbine inlet temperature. Thus, the CO_2 flow rate that does not react (*g10*) takes the heat released by the carbonation reaction. Carbonation has been modelled in the base case by considering a residual value of CaO conversion X = 0.15. Then, with the aim of analyzing the effect of CaO conversion on the plant performance a sensitivity analysis has been carried out. After the recuperator, the CO_2 stream is cooled by heat rejection to ambient and then compressed again in the low-pressure compressor (M-COMP) to close the Brayton power cycle.

As can be seen in Fig. 3, only gas-gas heat exchangers (HRSG, HXG) and coolers are considered in this base case, which simplifies the plant as compared to previously proposed CSP-CaL integrations [8], which made use of counter-flow gas-solid and solid-solid heat exchangers. This new configuration is therefore advantageous from the point of view of plant engineering, construction and operation. Main stream data for the base case is given in Appendix.

The energy balance resulting from the simulation of the base case is summarized in Table 2. This configuration shows an overall plant efficiency of 32.1%. As a consequence of the design criteria to keep a constant power production by the main turbine (M-TURB), a higher net power output is obtained in the "night mode" compared to the "sun mode". This is because the power consumed by the high-pressure CO_2 storage compressor (HPS-COMP) and by the auxiliaries for solids transport is not fully compensated by the power generated by the steam turbine. On the other hand, part of the CO_2 compression power is recovered in the "night mode" by the high-pressure CO_2 storage turbine (HPS-TURB). As a result, net power output in the "night mode" operation is 44% higher than in "sun mode" operation.

The third column in Table 2 (*"sun mode w/o storage"*) shows the energy balance of the plant when operated without storage. This case can be representative of i) the same plant designed with SM = 3 when operating with a solar radiation absorbed by the calciner equal to 1/3 of the design heat input or of ii) a plant designed with the same gross turbine power (M-TURB), SM = 1 and no TES. In this case, heat input to the calciner is 1/3 of the design power and the flow rate of CO_2 produced in the calciner matches the flow rate sent to the CO_2 cycle to compensate the CO_2 captured in the carbonator. In this operating mode, the power related to the turbomachines linked to the storage system (HPS-COMP and HPS-TURB) is zero. The overall plant efficiency obtained for this case is 33.9%. Thus, the efficiency penalty associated to the storage system sized with a solar multiple of 3 is 1.8% points.

As shown in Table 2, main heat rejections to ambient occur in the CO_2 cycle precooler (COOLER-3 in Fig. 3) and in the steam condenser (COND). In the case of COOLER-3, the CO_2 stream exiting the recuperator HXG (g12) is cooled from 154 °C down to 40 °C and part of this heat is used to heat up the CO_2 coming from the storage (HEATER). A non-negligible thermal power is also rejected to ambient by the high-pressure CO_2 cooler (COOLER-2), which is used to cool the compressed CO_2 (g5 stream) from the HP compressor (HPS-COMP) to a storage temperature of 25 °C and by the HPS-COMP intercoolers.

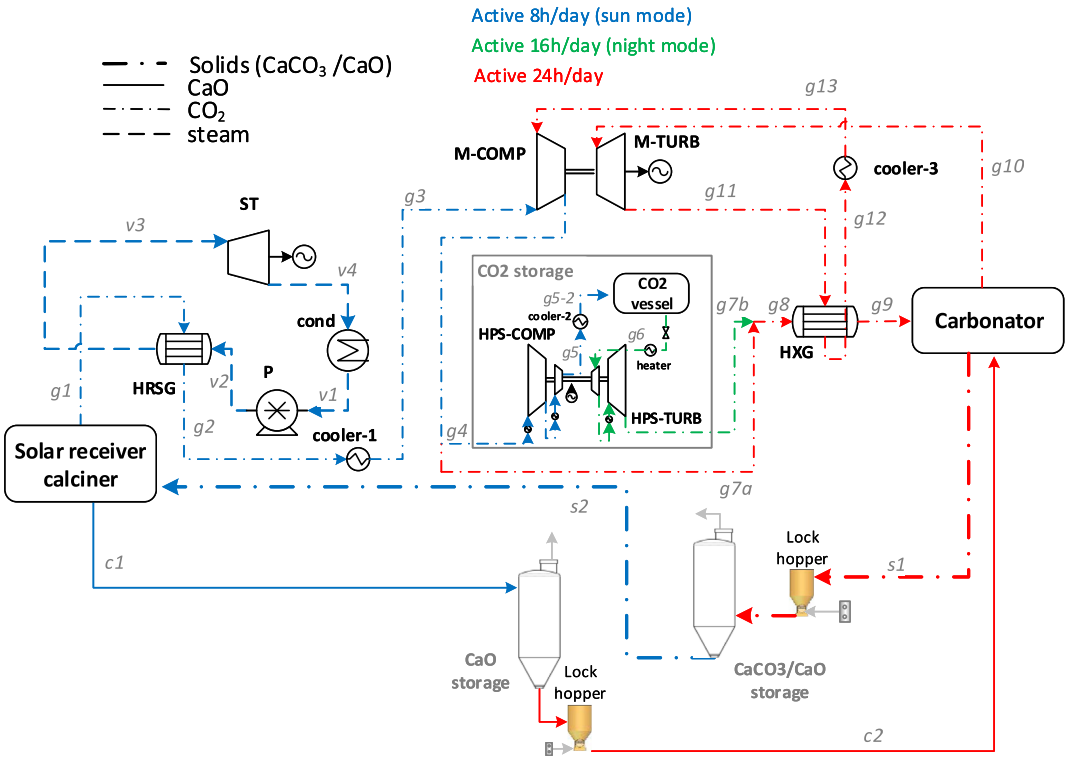

Fig. 3. Proposed configuration in this work for the CSP-CaL base case.

Table 2
Energy balance resulting from the simulations of the base case.

	Parameter	Base case (Fig. 3)		
		"sun mode"	"night mode"	"sun mode w/o storage"
	Solar thermal power to the calciner (MW_{th})	100	0	33.33
Heat exchangers Thermal Power(MWth)	HRSG	21.73	–	7.24
	COOLER-1	0.24	–	0.08
	COND	15.85	–	5.28
	HP-COMP (intercooler)	4.66	–	–
	COOLER-2	4.15	–	–
	HEATER	–	2.14	–
	TURB1 (interheater)	–	0.77	–
	COOLER-3	13.24	13.24	13.24
	HXG	75.91	75.91	75.91
Power production (MWe)	CO_2 storage turbine (HPS-TURB)	–	1.05	–
	Main CO_2 turbine (M-TURB)	23.92	23.92	23.92
	Steam Turbine (ST)	5.80	–	1.93
Power consumptions(MWe)	Steam cycle pump (P)	−0.04	–	−0.01
	Main CO_2 compressor (M-COMP)	−12.94	−12.22	−12.94
	CO_2 storage compressor (HPS-COMP)	−5.33	–	–
	Auxiliaries for heat rejection (calciner side)	−0.20	–	−0.04
	Auxiliaries for heat rejection (carbonator side)	−0.11	−0.11	−0.11
	Auxiliaries for solids transport calciner	−2.17	–	−0.72
	Auxiliaries for solids transport carbonator	−0.72	−0.72	−0.72
Net power (MWe)	$\dot{W}_{net,sun}$	**8.27**	**-**	**11.31**
	$\dot{W}_{net,night}$	**-**	**11.93**	**0**
Overall plant efficiency	η	**0.321**		**0.339**

3.2. Case 2: addition of solid-gas heat exchangers

Compared to the base case, case 2 (Fig. 4) incorporates the use of solid-gas heat exchangers on both calciner and carbonator sides. In this way, it is possible to make a more profitable use of the high temperature heat stored in the streams exiting the reactors, which leads to an improved thermal integration. Solids heating could be performed in a suspension preheater where gas and solids are sequentially contacted in risers and separated by cyclones, as usually performed in raw meal preheaters of cement plants [60]. All solid-gas heat exchangers have been modelled by assuming a co-flow arrangement and a same exit temperature of the gas and solids streams (as shown in Fig. 5).

GS-HE1 is used to exchange heat between the CO_2 stream exiting the calciner at 900 °C and the solids stream entering it, which must be brought to the calcination temperature, while heat

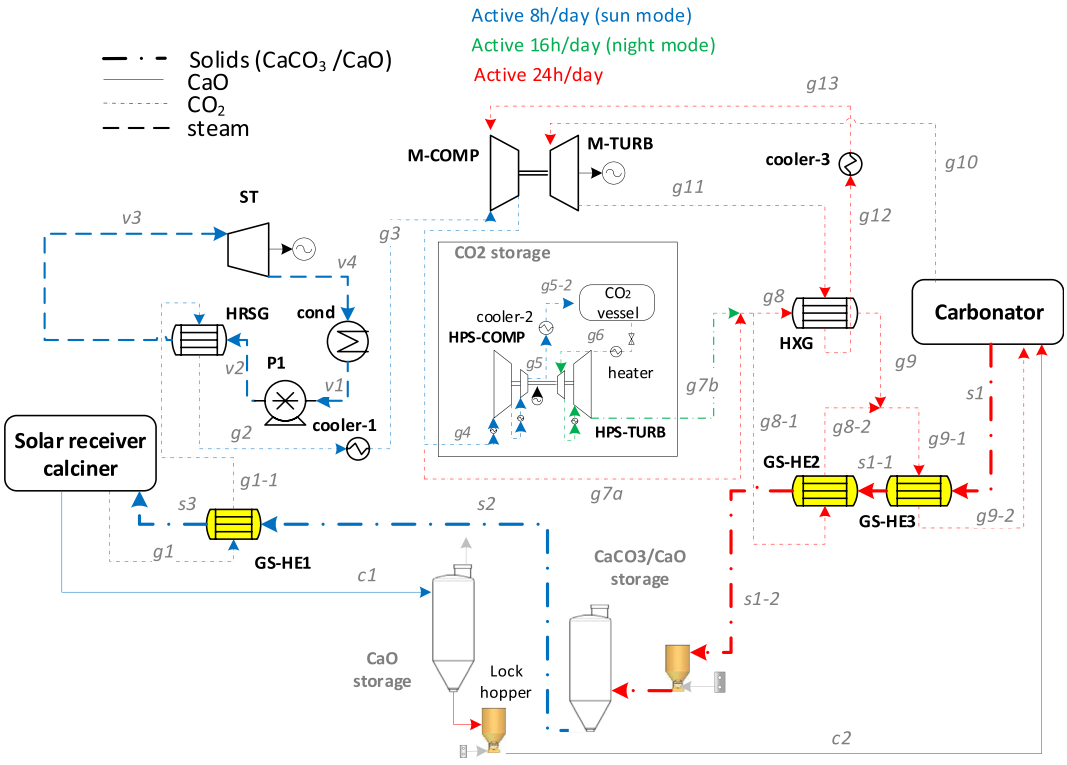

Fig. 4. CSP-CaL modified integration scheme (case 2).

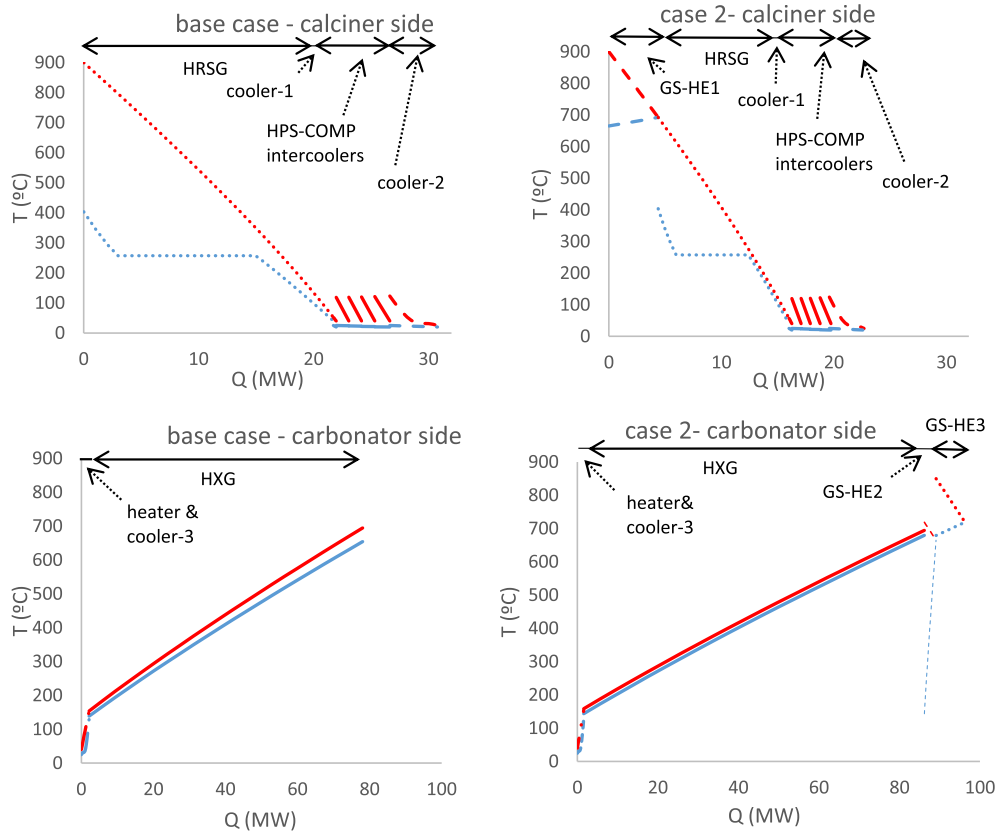

Fig. 5. TQ diagrams for calciner/carbonator sides in both the base case and case 2 configurations.

Table 3
Energy balance for the cases 2,3 and 4.

Parameter		Case 2			Case 3			Case 4		
		Including: solids heat exchangers			Including: solids heat exchangers Intercooled compression			Including: solids heat exchangers Intercooled compression P=Patm carbonation		
		"sun mode"	"night mode"	"sun mode w/o storage"	"sun mode"	"night mode"	"sun mode w/o storage"	"sun mode"	"night mode"	"sun mode w/o storage"
Solar thermal power (MW_{th})		100	0	33.33	100	0	33.33	100	0	33.33
Heat exchangers thermal Power (MWth)	HRSG	11.63	–	3.88	11.37	–	3.80	11.51	–	3.84
	GS-HE1	4.39	–	1.46	4.45	–	1.48	4.42	–	1.47
	COOLER-1	0.25	–	0.08	0.32	–	0.11	0.28	–	0.09
	COND	8.49	–	2.830	8.23	–	2.78	8.40	–	2.80
	HP-COMP (intercooler)	3.47	–	–	3.45	–	–	3.46	–	–
	COOLER-2	3.08	–	–	3.06	–	–	3.07	–	–
	HEATER	–	1.58	–	–	1.57	–	–	1.58	–
	TURB1 (interheater)	–	0.57	–	–	0.56	–	–	0.74	–
	COOLER-3	15.54	15.54	15.54	6.02	6.02	6.02	6.04	6.04	6.04
	HXG	84.60	84.60	84.60	93.27	93.27	93.27	93.68	93.68	93.68
	GS-HE2	2.91	2.91	2.91	3.17	3.17	3.17	3.04	3.04	3.04
	GS-HE3	7.19	7.19	7.19	7.15	7.15	7.15	7.17	7.17	7.17
Power inlet (MWe)	CO_2 storage turbine (HPS-TURB)	–	0.77	–	–	0.76	–	–	1.01	–
	Main CO_2 turbine (M-TURB)	26.87	26.87	26.87	26.64	26.64	26.64	26.77	26.77	26.77
	Steam Turbine (ST)	3.10	–	1.03	3.03	–	1.01	3.07	–	1.02
Power outlet (MWe)	Steam cycle pump (P)	−0.02	–	−0.01	−0.02	–	−0.01	−0.02	–	−0.01
	Main CO_2 compressor (M-COMP)	−14.67	−14.11	−14.67	−13.26	−12.75	−13.26	−13.28	−13.20	−13.28
	CO_2 storage compressor (HPS-COMP)	−3.98	–	0.00	−3.95	–	0.00	−3.96	–	0.00
	Auxiliaries heat calciner	−0.12	–	−0.02	−0.12	–	−0.02	−0.12	–	−0.02
	Auxiliaries heat carbonator	−0.12	−0.12	−0.12	−0.12	−0.12	−0.12	−0.12	−0.12	−0.12
	Auxiliaries solids transport calciner	−1.60	–	−0.53	−1.59	–	−0.53	−1.60	–	−0.53
	Auxiliaries solids transport carbonator	−0.53	−0.53	−0.53	−0.53	−0.53	−0.53	−0.53	−0.53	−0.53
Wnet	$\dot{W}_{net,sun}$	**8.94**	–	**12.01**	**10.09**	–	**13.18**	**10.21**	–	**13.30**
	$\dot{W}_{net,night}$	–	**12.88**	–	–	**14.01**	–	–	**13.92**	**-**
Overall plant efficiency	η		**0.347**	**0.360**		**0.381**	**0.395**		**0.381**	**0.399**

exchangers GS-HE2 and GS-HE3 are used to preheat the CO_2 stream entering the carbonator. As a consequence, solids are stored in the vessels at lower temperature and lock hoppers also operate at lower temperatures. Streams properties is reported in Appendix while the energy balance for this case is shown in Table 3.

Because of the preheating of the gas in GS-HE2 and GS-HE3, this enter the carbonator at higher temperature compared to the base case (719 °C instead 654 °C) and a higher CO_2 flow rate can pass across this reactor to carry the heat released by the carbonation reaction. As a result, the power produced by the main CO_2 turbine increases by a 12%. Fig. 5 shows the temperature-heat (TQ) diagrams for both the base case and case 2.

As shown in Fig. 5, a better heat integration is achieved in the calciner side for the case 2. An enhanced utilization of high-temperature stream temperature is achieved, with the consequent reduction in exergy loses. The lower storage temperature in the $CaCO_3$/CaO storage vessel also causes a reduction of the solids temperature at the inlet of the calciner (stream s3). Therefore, in the "sun mode", a higher portion of the heat provided to the calciner is taken as sensible heat of the solids stream and less power is available for the calcination reaction, which lowers the production of CaO and CO_2. The reduced flow rate of CO_2 combined with the lower temperature at the HRSG inlet (stream g1-1) after the solids preheater GS-HE1 causes a reduction of the steam generated and of the steam turbine power (−47% compared to the base case). The reduction of the solids flow rate and of the CO_2 flow rate generated in the calciner also lead to a reduction of consumption of the HP CO_2 storage compressor and the auxiliaries for calciner solids transport (−26%).

Regarding the energy balance, an overall plant efficiency of 34.7% has been obtained, i.e. 2.6% points higher than the base case efficiency. The calculated net efficiency without energy storage also increases to 36.0%. Due to the reduced consumption for CO_2 storage compression, the differences between these two calculated efficiencies and between the net power produced in "sun" and "night" modes are also reduced.

3.3. Case 3: introduction of solid-gas heat exchangers and intercooled compression

Compared with case 2, case 3 contemplates the use of an intercooled main CO_2 compressor, which allows reducing the consumption for CO_2 compression and achieving a higher cycle efficiency thanks to the presence of the regenerator. The low-pressure intercooled compressor is used to compress around 140 kg/s of CO_2 from atmospheric pressure to the carbonator pressure. In this case, two intercoolers are assumed with an intercooled temperature of 40 °C, leading to compressor outlet temperatures of 73 °C from each stage. This leads to a reduction of the CO_2 stream temperature at compressor outlet (*g8*) compared to case 2 (73 °C instead 143 °C), which allows for a higher heat exchange in HXG and therefore a reduced need for cooling in cooler-3. Results for this configuration can be seen in Table 3. By using a 2 intercooled-stages main compressor (M-comp), electric

consumption is reduced by 6.8% and 8.8% in the "sun" and "night" modes, respectively, which implies an overall plant efficiency increase of 3.4%.

3.4. Case 4: carbonator at ambient pressure

Case 4 allows operating the carbonator at ambient pressure. As a benefit, high temperature lock hoppers for solids pressurization would not be necessary. On the other hand, hermetic machines and heat exchangers to avoid air in-leakages as well as larger turbomachines (to handle the higher volume flow rate), larger carbonator and larger heat exchangers (to compensate the decrease of heat transfer coefficient with gas density) must be employed. Moreover, it is expected to achieve a lower reaction rate in the carbonator, which is favored by high CO_2 pressure [61].

Fig. 6 shows the case 4 scheme. M-comp compresses the CO_2 stream coming from the carbonator (*g13*) up to atmospheric pressure (plus about 0.1 bar to overcome pressure drops). Unlike in previous layouts in which *g3* and *g13* compressions were made completely in the M-compressor, in case 4 the CO_2 coming from the calciner (*g3*) is simply blown by a fan and is directly sent to the carbonator side, without passing through the M-comp.

As shown in Table 3, there are no big differences in terms of efficiency between cases 3 and 4. Therefore, the most advantageous configuration between pressurized and atmospheric pressure carbonator must be chosen based on techno-economic considerations depending on the technical challenge and cost of a high temperature lock hopper system or the sealed components for a specific facility. The techno-economic analysis is being carried out by considering a quasi-stationary simulation to better assess the equipment sizes and costs and will be reported in a future publication. Note that all configurations have been modelled with $PR = 3$.

A higher temperature is achieved at the carbonator inlet in all cases where solid-gas heat exchangers are integrated (as shown in Appendix), which leads to a higher temperature of heat introduced in the thermodynamic cycle and therefore to a higher cycle efficiency. As a consequence, a larger mass flow rate of CO_2 can be heated up to 850 °C for power production. Thus, 133.5 kg/s of CO_2 enter in the main turbine for the base case whereas in case 4 this value is increased up to 151 kg/s.

Compared to the base case (where the global efficiency is 32.1%), the overall plant efficiency increases for all the modified configurations. As mentioned in the base case, also in these schemes an efficiency increase is achieved when no storage and SM = 1 are considered as the high-pressure compressor is not used. Thus, it is important to point out that the base operation mode selected for the simulations ("*sun mode*", SM = 3) represents the worst scenario since throughout the day the solar power hitting the solar receiver will vary and therefore most of the time less than 100 MW_{th} will be produced in the solar field. In practical operation conditions, the net global efficiency achieved in each case will be comprised between the weighed efficiency (1/3–2/3) and the efficiency in "*sun mode w/o storage*" depending on the characteristics of solar radiation for the selected site and on the solar field off-design performance.

4. Sensitivity analysis and discussion

This section is devoted to compare the performance of the four configurations proposed for different gas cycle pressure ratio and

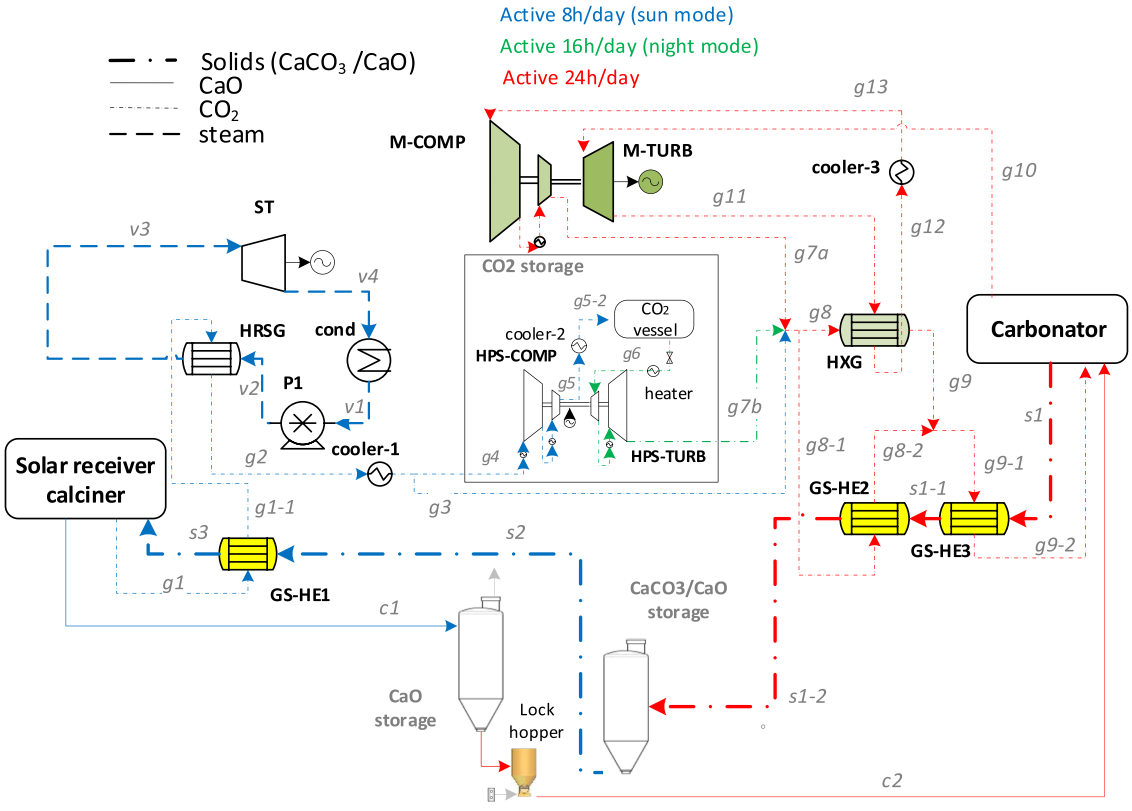

Fig. 6. CSP-CaL modified integration scheme (case 4).

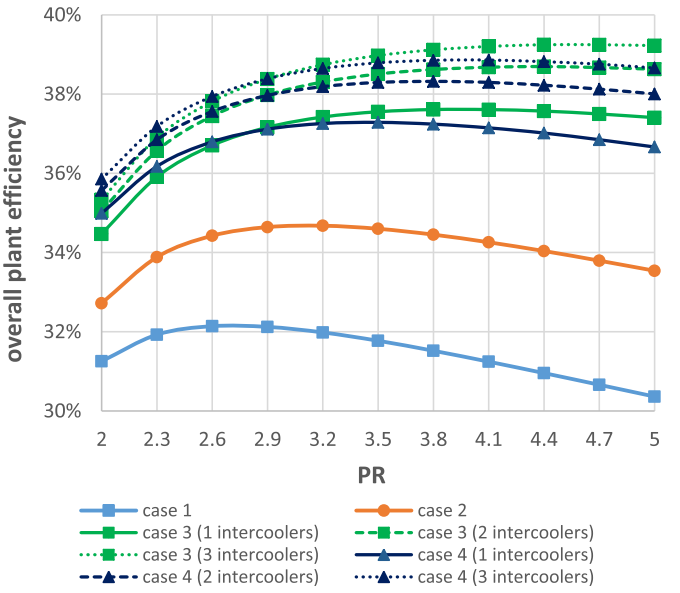

Fig. 7. Sensitivity analysis on pressure ratio (PR).

number of main compressor intercoolers from the overall efficiency perspective. Moreover, to further explore the CSP-CaL integration, a sensitivity analysis has been carried out on case 3 about the effect of the turbine inlet temperature, CaO conversion, steam cycle conditions, turbomachinery efficiency, minimum ΔT in the main CO_2 heat exchanger, and CaO-CO_2 storage conditions.

4.1. Effect of pressure ratio

In this section, all previous schemes are compared to analyze the most advantageous configuration. To this end, the pressure ratio (*PR*), defined as the ratio of the carbonator pressure to the turbine outlet pressure, has been chosen as dependent variable. Note that in the previous section all configurations are analyzed at $PR = 3$.

Fig. 7 shows the resulting overall plant efficiency as a function of the pressure ratio for the different cases and assuming a different number of intercooling stages in the main CO_2 compressor (for cases 3 and 4 only). As can be seen, cases 3 and 4 clearly show a higher efficiency than cases 1 and 2, particularly for higher pressure ratios. This illustrates the benefits of using the multi-stage inter-cooled compression combined with the gas cycle regenerator HXG.

The simplest configuration (base case) reaches the maximum efficiency with PR of about 2.8, whereas in case 2 (where gas-solids heat exchangers are considered) efficiency is enhanced to near 35% at PR = 3.2. Gas-solids preheating allows increasing the temperature of solids stream entering the carbonator and a higher CO_2 flow rate can be expanded in the main turbine (M-TURB). Thanks to the inter-cooled compression, the overall efficiency is further increased in case 3, reaching a value near 40% at PR between 4 and 5. Compared to previously reported CSP-CaL schemes [8,21], this relatively high efficiency is achieved in case 3 with a configuration of lower technical complexity and based on equipment already used in the cement industry, which would imply also a lower system cost.

4.2. Effect of turbine inlet temperature (TIT), CaO average conversion (X) and pressure ratio

As it was shown in Fig. 7, there is a carbonator pressure for which the integration efficiency reaches a maximum, which justifies the relevance of an analysis on the pressure and temperature conditions in the carbonator to determine the optimal CaL-power cycle integration.

Since the carbonator is directly connected to the turbine inlet, increasing the carbonator temperature leads to a higher power cycle efficiency. However, the maximum temperature in the carbonator is limited by the thermodynamic equilibrium of the calcination-carbonation reaction (Eq. (1)). According to thermochemical data, the equilibrium temperature T_{eq} is related to the CO_2 partial pressure in the carbonator environment P by means of Eq. (6) [28]:

$$T_{eq} = -\frac{20474}{\ln\left(\frac{P}{4.137 \cdot 10^7}\right)} \tag{6}$$

where P is measured in bar and T_{eq} in K. Thus, for a given value of P there is a maximum carbonator temperature ($T_{max}=T_{eq}$) above which the CO_2 partial pressure is not sufficiently high for the reaction to be shifted toward carbonation (Fig. 8). Since in all considered cases carbonation is carried out under a pure CO_2 atmosphere, CO_2 partial pressure coincides with the carbonator absolute pressure.

In order to get a grip on the role of turbine inlet temperature and pressure ratio, case 3 was simulated by considering the cycle without storage, thus all the CO_2 and CaO exiting the calciner side is sent to power production (SM = 1). The analysis also contemplates several values of the average CaO conversion (X). This analysis is important because of the high uncertainty on the CO_2 carrying capacity of CaO under the carbonation and calcination conditions assumed in this work. Moreover, as discussed in section 2, CaO conversion is highly dependent on the carbonator-calciner conditions as well as on the CaO precursor.

Table 4 shows the energy balance obtained by varying the carbonator temperature (and therefore the TIT) and the CaO average conversion. Note that for a better understanding, these balances are referred to the conditions without storage and therefore consumption of CO_2 storage compressor and power generated by the CO_2 storage turbine are zero.

As expected, an increase in either CaO conversion or TIT leads to a higher overall plant efficiency. If TIT is raised from 850 °C to 950 °C the overall efficiency is enhanced by about 1.2% and 2.7% points for X = 0.1 and X = 0.4, respectively. As shown in Table 4,

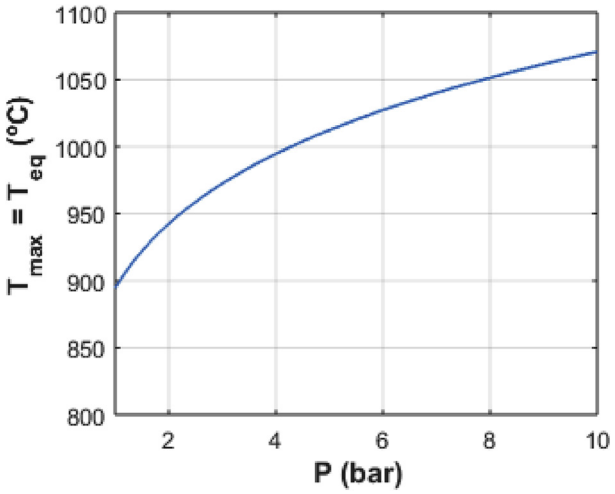

Fig. 8. Maximum carbonator temperature as a function of CO_2 partial pressure in the carbonator atmosphere according to thermodynamic equilibrium (Eq. (6)).

Table 4
Energy balance for the case 3 as a function of TIT and X (SM = 1, PR = 3.5).

	Parameter	X = 0.1		X = 0.4	
		TIT = 850 °C	TIT = 950 °C	TIT = 850 °C	TIT = 950 °C
	Solar thermal power (MW_{th})	33.33	33.33	33.33	33.33
Heat exchangers (MWth)	HRSG	3.368	4.796	4.138	4.859
	GS-HE1	1.279	0.868	2.072	1.693
	COOLER-1	−0.097	−0.111	−0.128	−0.137
	COND	−2.457	−3.499	−3.019	−3.545
	COOLER-3	−5.943	−5.157	−5.719	−5.104
	HXG	80.923	83.050	78.760	82.764
	GS-HE2	2.891	4.299	3.261	4.077
	GS-HE3	9.108	10.804	4.975	5.601
Power inlet (MWe)	Main CO_2 turbine (M-TURB)	27.226	26.044	26.479	25.943
	Steam Turbine (ST)	0.899	1.280	1.105	1.297
Power outlet (MWe)	Steam cycle pump (P)	−0.006	−0.009	−0.008	−0.009
	Main CO_2 compressor (M-COMP)	−13.523	−12.030	−13.335	−12.083
	Auxiliaries heat calciner	−0.020	−0.029	−0.025	−0.029
	Auxiliaries heat carbonator	−0.120	−0.105	−0.117	−0.105
	Auxiliaries solids transport calciner	−0.677	−0.824	−0.275	−0.291
	Auxiliaries solids transport carbonator	−0.677	−0.824	−0.275	−0.291
Carbonator heat (MWth)	carbonation heat	19.253	23.442	25.717	27.137
	reactants preheating (sensible heat)	2.217	−4.698	−0.320	−2.573
	losses	−0.194	−0.234	−0.252	−0.274
	carbonator heat to power cycle	21.276	18.510	25.145	24.290
Power output CO_2 cycle (MWe)		13.704	14.014	13.144	13.860
Power output steam cycle (MWe)		0.893	1.271	1.097	1.288
Overall plant efficiency (η)		**0.393**	**0.405**	**0.406**	**0.433**

Table 5
Trends in selected streams by varying X and TIT.

X	TIT = 850 °C				TIT = 950 °C			
	g10 (kg/s)	g1 (kg/s)	s2 (T°C)	s3 (T°C)	g10 (kg/s)	g1 (kg/s)	s2 (T°C)	s3 (T°C)
0.1	127.43	4.93	673.17	692.25	111.75	6.00	769.82	780.31
0.15	126.18	5.49	647.71	676.88	111.73	6.28	736.96	755.71
0.2	125.39	5.86	627.67	666.43	111.59	6.48	712.35	738.90
0.25	124.87	6.11	611.42	659.11	111.51	6.64	692.97	726.95
0.3	124.48	6.31	597.72	653.70	111.42	6.76	676.86	717.88
0.35	124.19	6.46	586.25	649.83	111.37	6.86	663.22	710.84
0.4	123.95	6.58	576.19	646.81	111.32	6.94	651.52	705.28

power consumptions due to solids conveying are the same in the calciner and carbonator sides since storage is not considered in this analysis.

As can be seen, the steam cycle production is enhanced with the carbonator temperature. As the carbonator temperature is raised, the temperature of the solids entering the calciner (s2) increases as well, reducing the sensible heat required to heat them up to 900 °C or, equivalently, increasing the $CaCO_3$ flow rate to achieve full calcination. Thus, a higher amount of CO_2 can be produced in the calciner (see *g1* stream in Table 5). Furthermore, the net power produced by the CO_2 closed cycle is also enhanced with the carbonator temperature. An increase in CaO conversion enhances the steam cycle production albeit it does not lead to a higher net power output in the CO_2 closed cycle. This is mainly due to the reduction of CO_2 temperature at the carbonator inlet (Table 5) because of the lower solids to gas ratio in the CO_2 preheaters, which leads to a lower temperature of heat introduction into the gas cycle and therefore to a decrease of the cycle efficiency. A reduction of the CO_2 temperature at the carbonator inlet causes that a higher amount of carbonation heat is used to bring the reactants to the carbonation temperature and therefore, a lower amount of CO_2 can be recirculated (*g10)*. Table 4 shows the carbonator heat used to preheat the reactants to the carbonator temperature. By considering TIT = 850 °C and X = 0.1, a high amount of solids (compared with the X = 0.4 case) is circulated from the calciner (at 900 °C) to the carbonator, whose temperature is reduced. Therefore, this solids stream carries additional heat from the calciner to be used in the power cycle (as can be seen by the positive sign of the reactants pre-heating thermal power in Table 4).

Fig. 9 shows the global CSP-CaL efficiency as a function of X and TIT.

The different trends followed by the overall efficiency with X in the cases of TIT = 850 °C and 950 °C may be explained by an analysis of the CaO temperature entering the carbonator from the calciner at 900 °C. In the case of TIT = 950 °C, a part of the energy released in the carbonator must be used to bring the solids up to the carbonator temperature, being this effect more important when X is reduced (see reactants preheating power in Table 4). In the case of TIT = 850 °C, it is not necessary to heat up the solids since these come from the calciner at higher temperature, and therefore the loss of efficiency by reducing the CaO conversion is mitigated. Fig. 9 shows also efficiency results obtained by including or not auxiliaries' consumption. In regard to increasing the CaO conversion, the energy consumption linked to solids conveying is decreased, which

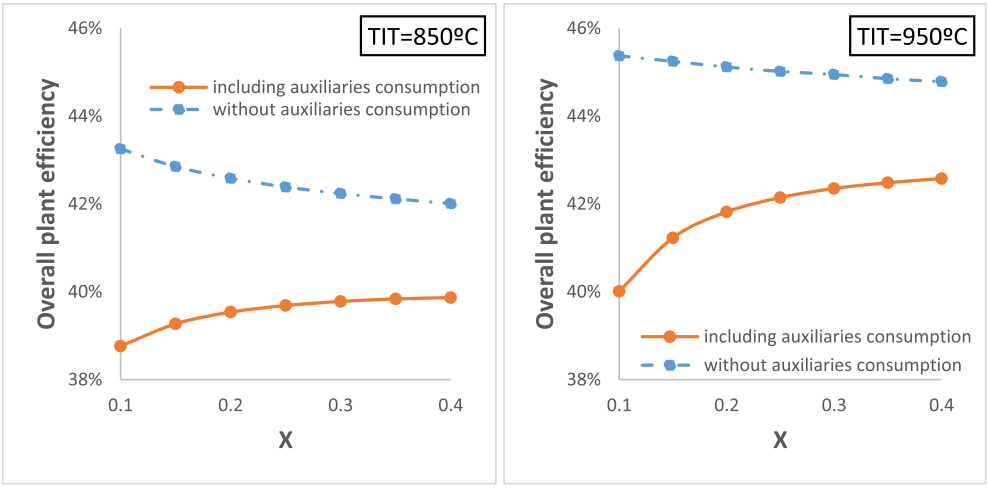

Fig. 9. Overall plant efficiency as a function of X for two different TIT (no storage is considered: SM = 1).

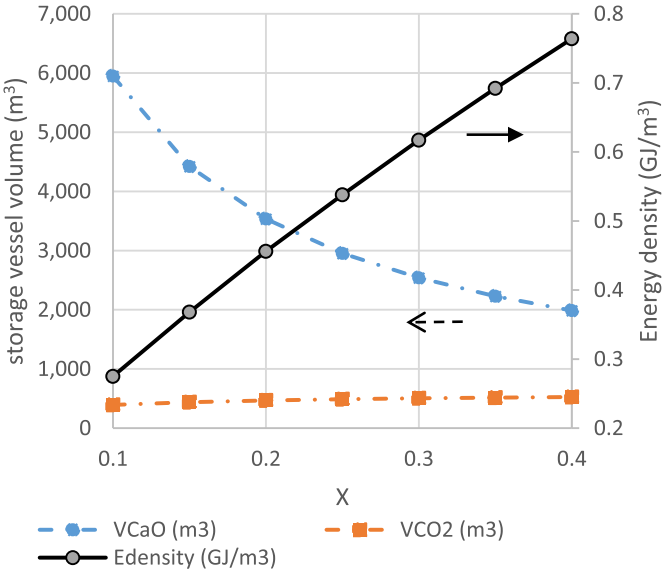

Fig. 10. Storage vessels and energy density as a function of CaO conversion. CO_2 is stored at 25 °C; 75 bar.

serves to enhance the overall net efficiency. These trends are also appreciated when overall average daily performance is considered.

As showed in section 2, the energy density of the storage system is highly influenced by the CaO conversion, as shown in Fig. 10. CO_2 vessel volume is not affected by X, but is only dependent on pressure and temperature conditions. Note that the energy density is calculated by using Equation (2), and therefore considers not only the CaCO3 as solid material, but also the CO_2 and CaO vessels, the bulk porosity and packing density of the granular solids. Thus, energy density of the storage system infrastructure varies between 0.27 and 0.77 GJ/m^3.

In Table 6 three more cases, in which temperature and pressure in the carbonator are varied taking into account thermodynamic equilibrium restrictions (Fig. 8), are analyzed.

As can be seen in Table 6, an increase of the carbonator temperature (and therefore of TIT) from 950 °C up to 1050 °C serves to enhance the overall plant efficiency by 0.8% points due to the increase of net power output in both the CO_2 and steam power cycles. As expected, an increase of the carbonator pressure (keeping fixed temperature) does not improve the cycle efficiency (as seen in Fig. 7 for other conditions). According to these results, the increase of the carbonator temperature improves the overall efficiency, albeit it would also add a higher degree of complexity for the turbine and the solid filtration system. On the other hand, varying the PR from 3 to 9 has an important effect on the heat exchanged in HXG (Table 6). This effect is caused by the reduction of the CO_2 temperature at the carbonator inlet, which decreases from 820 °C (at PR = 3) to 749 °C (at PR = 9) as a consequence of the isentropic CO_2 expansion process. A higher CO_2 temperature inlet allows a higher CO_2 mass flow rate to enter the power cycle since less carbonator heat is used to preheat the reactants to the carbonator temperature. Thus, the CO_2 mass flow rate decreases from 395 kg/s (at PR = 3) to 231.3 kg/s (at PR = 9).

As a summary, case 3 simulation results indicate that increasing the temperature in the carbonator, and therefore the TIT, systematically leads to a higher overall plant efficiency. However, the maximum temperature in the carbonator is limited by the thermodynamic reaction equilibrium, which depends on the carbonator pressure. The process efficiency is also enhanced as the PR is increased up to a certain value of around 3–3.5 from which a further increase of the PR does not improve efficiency. Moreover, increasing the CaO conversion enhances the overall efficiency (reaching values about 43% at X = 0.4) mainly because of the significant reduction of auxiliaries power consumption for solids transport.

4.3. Effect of steam cycle conditions, auxiliaries consumption and turbomachinery-heat exchangers efficiencies

Following with the sensitivity analysis, this section assesses how the overall efficiency is affected by important parameters whose values were fixed in previous calculations (Table 1). Reference case conditions as well as the range of variation of these parameters are shown in Table 7. The values of those parameters not specified in Table 7 are left unchanged. Results of the sensitivity analysis on overall CSP-CaL efficiency are shown in Fig. 11.

Compared to CSP-CaL schemes reported in previous papers [8,21,37] a main novelty of the present work is the introduction of a steam power cycle to take advantage of the high temperature CO_2

Table 6
Energy balance for case 3 as a function of TIT and PR (without energy storage).

	Parameter	X = 0.15		
		$T_{carb} = 950\,^{\circ}C$ $P_{carb} = 3$ bar	$T_{carb} = 950\,^{\circ}C$ $P_{carb} = 9$ bar	$T_{carb} = 1050\,^{\circ}C$ $P_{carb} = 9$ bar
	Solar thermal power (MW_{th})	33.33	33.33	33.33
Heat exchangers (MWth)	HRSG	4.951	4.032	5.482
	GS-HE1	1.082	1.401	0.885
	COOLER-1	−0.128	−0.110	−0.128
	COND	−3.613	−2.941	−3.999
	COOLER-3	−5.283	−4.914	−4.232
	HXG	96.221	40.601	41.844
	GS-HE2	4.388	3.794	5.241
	GS-HE3	8.329	11.420	12.917
Power inlet (MWe)	Main CO_2 turbine (M-TURB)	25.702	27.245	25.974
	Steam Turbine (ST)	1.322	1.076	1.463
Power outlet (MWel)	Steam cycle pump (P)	−0.009	−0.008	−0.010
	Main CO_2 compressor (M-COMP)	−11.860	−13.503	−12.167
	Auxiliaries heat calciner	−0.030	−0.024	−0.033
	Auxiliaries heat carbonator	−0.105	−0.112	−0.100
	Auxiliaries solids transport calciner	−0.607	−0.546	−0.640
	Auxiliaries solids transport carbonator	−0.607	−0.546	−0.640
Carbonator heat (MWth)	carbonation heat	25.010	22.496	26.361
	reactants preheating (sensible heat)	−3.714	−3.893	−10.062
	losses	−0.250	−0.226	−0.258
	carbonator heat to power cycle	21.046	18.376	16.041
Power output CO_2 cycle (MWe)		13.842	13.741	13.807
Power output steam cycle (MWe)		1.313	1.069	1.453
Overall plant efficiency (η)		**0.414**	**0.407**	**0.415**

Table 7
Parameters variation throughout the sensitivity analysis on the overall CSP-CaL efficiency.

Selected scheme		case 3 (section 3.3)				
Main fixed parameters		TIT		950 °C		
		PR		3.5		
		X		0.15		
		SM		3		
Sensitivity analysis		Parameter	Ref. value	Variation		ID-Fig. 11
				lower limit	upper limit	
	Rankine cycle	live steam	400 °C;40 bar	360 °C; 40 bar	540 °C; 40 bar	**Rankine 1**
				360 °C;100 bar	540 °C; 100 bar	**Rankine 2**
	Turbomachinery isentropic efficiency	M-TURB	0.9	−5%	+5%	**Isentropic 1**
		HPS-TURB	0.8	−5%	+5%	**Isentropic 2**
		M-COMP	0.87	−5%	+5%	**Isentropic 3**
		HPS-COMP	0.8	−5%	+5%	**Isentropic 4**
	Turbomachinery mechanical efficiency	M-TURB	0.98	−2%	+2%	**Mechanical 1**
		HPS-TURB	0.96	−2%	+2%	**Mechanical 2**
		M-COMP	0.98	−2%	+2%	**Mechanical 3**
		HPS-COMP	0.96	−2%	+2%	**Mechanical 4**
	Turbomachinery intercooled stages	HPS-COMP	5	3	7	**HP-ic-stage**
		M-COMP	2	0	4	**LP-ic-stage**
	Heat exchangers minimum DT	HXG (regenerator)	15 °C	10 °C	20 °C	**HXG**
	Cooling temperature	Intercoolers	40 °C	30 °C	50 °C	**T-cooling**
		Cooler-2				
		Cooler-3				
	Heat exchangers pressure drops	Coolers	1%	−10%	+10%	**P-drops**
		HXG	5%			
		solid-gas HX	3%			
	Auxiliaries	Heat rejection	0.8% of heat released	0.4%	1.2%	**Heat-rejec**
		Solids conveying consumption	10 MJ/ton	5 MJ/ton	15 MJ/ton	**Solids**

stream exiting the calciner for power production. For this purpose, a simple Rankine cycle with moderate live steam conditions (400 °C/40 bar) has been considered from the small power output of this cycle (around 3 MW_e at plant design point). Considering these conditions, the net electric efficiency remains at 26.5% whereas for 540 °C/100 bar live steam conditions the efficiency increases by 5% points. By computing the overall efficiency after this live steam conditions change, the new efficiency value is 0.6%

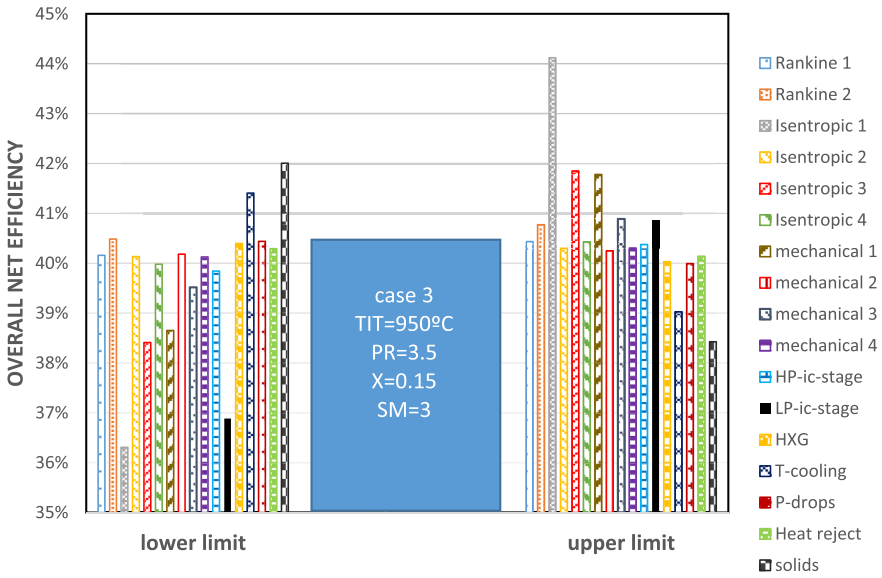

Fig. 11. Sensitivity analysis on overall CSP-CaL efficiency results (see ID definition in Table 7). For an easier understanding, bars are presented in the same order than legend and a colour code is used. The reader is referred to the web version of this article. (For interpretation of the references to colour in this figure legend, the reader is referred to the Web version of this article.)

higher than for the reference case.

As shown in Fig. 11, the most critical parameters on the overall efficiency are those related to turbomachinery efficiency. Thus, increasing by 5% the reference isentropic efficiency value for the main CO_2 compressor (M-COMP) the overall efficiency rises up to 44%. Regarding the number of intercooled stages, variations in low-pressure compressor have a stronger effect on the overall efficiency compared to the high-pressure compressor since the penalty over the cycle caused by the former is higher. Fig. 11 shows also that variations in energy consumption linked to solids transport plays a significant role in the plant efficiency, as was also seen in Fig. 9. Regarding heat exchangers, a reduction by 5 °C of the minimum temperature difference in the regenerator (HXG) leads to an enhancement of efficiency by 1%.

5. Conclusions

The present work is focused on an energy integration analysis of a CSP-CaL plant. Four novel integration schemes have been developed by progressively increasing the level of complexity. Plant operation considering solar multiples (SM) of 3 (design-point for a constant power production throughout the day) and SM = 1 (avoiding the energy storage equipment consumptions since lower solar radiation is assumed) were tested. As no high-pressure compressor is needed in the second case, the overall efficiency is increased by 1.8% points and therefore showing the penalty associated to the proposed high-pressure CO_2 storage system.

The base case presents an overall efficiency of 32.1%. By adding gas-solid heat exchangers on both the calciner and carbonator sides (case 2) the overall plant efficiency reaches a 34.7%. Furthermore, if a 2-intercooled stage compression is used in the low-pressure compressor (which is the equipment with greater energy consumption in the plant) efficiency is enhanced up to 38.1%. Cases 3 and 4 present similar efficiencies. The optimum configuration for a specific plant will depend on techno-economic considerations. Results from a sensitivity analysis on the pressure ratio (PR) in the Brayton cycle shows that the highest efficiency is achieved for PR around 3–4.5 in all cases.

A sensitivity analysis on the effect of CaO conversion and carbonator pressure/temperature shows that increasing the TIT under the limits posed by thermodynamic equilibrium enhances the overall plant efficiency. The overall efficiency is also enhanced as CaO conversion is increased (reaching values about 43% at X = 0.4), mainly because of the significant reduction of auxiliaries power consumption. A new expression for the energy density is proposed in this paper, which takes into account the size of the infrastructure (including all vessels and the packing density of solids). For the proposed cases, the energy storage density, mainly dependent on CO_2 pressure, CO_2 temperature and CaO conversion, varies between 0.2 and 0.9 GJ/m^3.

Our study gives support to the potential benefits of using the Calcium-Looping process for thermochemical energy storage in CSP plants. Major technological challenges are yet to be faced for the plant assessed in this work, especially related to the design of the solar receiver/calciner and to the high temperature solids pressurization and depressurization system. In future works, a design study of the solar receiver, hour-by-hour simulations of the plant considering variable heat input in the solar calciner and techno-economic analysis need to be undertaken to further assess the feasibility and competiveness of the CSP– CaL integration.

Acknowledgments

This work has been supported by the Spanish Government Agency Ministerio de Economia y Competitividad (MINECO-FEDER funds), contracts CTQ2014-52763-C2-2-R, CTQ2017-83602-C2-2-R and FPI contract granted to Carlos Ortiz Dominguez (BES-2015-0703149) within the project: Hybrid thermochemical storage of concentrated solar power (CTQ2014-52763-C2-2-R).

Appendix

Table 8 shows the main stream data for all simulated cases.

Table 8
Main stream data for the CSP-CaL integration

ID	Base case			Case 2			Case 3			Case 4		
	P (bar)	T (°C)	$\dot{m}$ (kg/s)	P (bar)	T (°C)	$\dot{m}$ (kg/s)	P (bar)	T (°C)	$\dot{m}$ (kg/s)	P (bar)	T (°C)	$\dot{m}$ (kg/s)
s1	1.10	850	72.19	1.20	850	53.47	1.20	850	53.06	1.00	850	53.27
s1-1	–	–	–	1.17	718.92	53.47	1.17	718.81	53.06	0.97	718.90	53.27
s1-2	–	–	–	1.14	665.03	53.47	1.14	659.62	53.06	0.94	662.40	53.27
s2	1.10	850	216.56	1.14	665.03	160.40	1.14	659.62	159.17	0.94	662.40	159.80
s3	–	–	–	1.11	692.17	160.40	1.11	687.39	159.17	0.91	689.84	159.80
c1	1.00	900	193.75	1.00	900	143.51	1.00	900	142.41	1.00	900	142.97
c2	1.00	900	64.58	1.00	900	47.84	1.00	900	47.47	1.00	900	47.66
v1	0.074	40.13	7.14	0.074	40.13	3.82	0.074	40.32	3.74	0.074	40.32	3.78
v2	45	40.53	7.14	45.00	40.53	3.82	45.00	40.72	3.74	45.00	40.72	3.78
v3	40	400	7.14	40.00	400	3.82	40.00	400	3.74	40.00	400	3.78
v4	0.075	40.32	7.14	0.075	40.32	3.82	0.075	40.32	3.74	0.075	40.32	3.78
g1	1.00	900	22.81	1.00	900	16.89	1.00	900	16.76	1.00	900	16.83
g1-1	–	–	–	0.97	692.17	16.89	0.97	687.39	16.76	0.97	689.84	16.83
g2	0.97	52.03	22.81	0.94	56.92	16.89	0.94	62.03	16.76	0.94	58.95	16.83
g3	0.96	40	22.81	0.93	40	16.89	0.93	40	16.76	0.93	40	16.83
g4	3.21	142.69	15.21	3.31	148.29	11.26	3.31	74.36	11.18	1.14	40	11.22
g5	75.75	123.66	15.21	75.75	124.27	11.26	75.75	124.27	11.18	75.75	124.27	11.22
g6	74.25	130	7.60	75.00	130	5.64	75.00	130	5.59	75.00	130	5.61
g7a	3.21	142.69	126.25	3.31	148.29	141.8	3.31	74.36	140.58	1.14	45.28	141.30
g7b	3.21	38.57	7.60	3.31	39.08	5.64	3.31	39.08	5.59	1.14	21.92	5.61
g8	3.21	138.83	133.72	3.31	143.44	142.38	3.31	72.78	141.19	1.14	72.81	142.14
g8-1	–	–	–	3.31	143.44	5.05	3.31	72.78	4.98	1.14	72.81	4.77
g8-2	–	–	–	3.21	665.03	5.05	3.21	659.52	4.98	1.10	662.39	4.77
g9	3.05	654.1	133.72	3.14	679.55	142.38	3.14	679.54	141.19	1.08	679.56	142.14
g9-1	–	–	–	3.14	679.05	147.43	3.14	678.87	146.17	1.08	679.00	146.91
g9-2	–	–	–	3.05	718.93	147.43	3.05	718.81	146.17	1.05	718.94	146.91
g10	3.00	850	126.25	3.00	850	141.8	3.00	850	140.58	1.00	850	141.30
g11	1.00	694.53	126.25	1.00	694.54	141.8	1.00	694.54	140.58	0.33	694.56	141.30
g12	0.95	153.83	126.25	0.95	158.65	141.8	0.95	87.98	140.58	0.32	88.01	141.30
g13	0.94	40	126.25	0.94	40	141.8	0.94	40	140.58	0.31	40	141.30

Notation

A	carbonator cross-section, m^2	$T_{i,\ vessel}$	storage temperature for of the i-component, °C
$c_{p,i}$	specific heat, kJ/(kmol·K)	TIT	turbine temperature inlet, °C
E_{den}	energy density, GJ/m^3	v_i	specific volume for the i-component, m3/kmol
ε_i	porosity of the i-component	V_i	storage vessel volume for the i-component, m^3
F_i	molar flow rate of component i, kmol/s	$\dot{V}_{CO2}$	CO_2 volume flow rate, m^3/s
F_{CaCO_3}	$CaCO_3$ molar flow rate	$\dot{W}_{net}$	average electrical power, MWe
$F_{CaCO3,crb}$	$CaCO_3$ molar flow rate (calciner side)	$\dot{W}_{net,night}$	net electrical power for the night mode, MWe
$F_{CaO,unr}$	molar flow rate of unreacted CaO (calciner side)	$\dot{W}_{net,sun}$	net electrical power for the sun mode, MWe
$F_{CO_2,clc}$	CO_2 molar flow rate at calciner outlet	$\dot{W}_{M-TURB}$	power produced by the main CO_2 turbine, MWe
$F_{CO_2,crb,in}$	CO_2 molar flow rate at carbonator inlet	$\dot{W}_{M-COMP}$	power consumed by the main CO_2 compressor, MWe
$F_{CO_2,crb,\ out}$	CO_2 molar flow rate at carbonator outlet	$\dot{W}_{HPS-TURB}$	power produced by the high-pressure CO_2 turbine, MWe
$F_{R,crb}$	recirculating molar flow rate (carbonator side)	$\dot{W}_{HPS-COMP}$	power consumption of high pressure intercooled CO_2 compressor for the storage system, MWe
$F_{R,clc}$	recirculating molar flow rate (calciner side)	$\dot{W}_{ST}$	power produced in the steam turbine cycle, MWe
h_i	Enthalpy, kJ/kmol	$\dot{W}_P$	power consumed in the steam turbine cycle, MWe
$\dot{m}$	mass flow rate, kg/s	$\dot{W}_{PSOLCAL}$	Power consumptions for solids transport in the calciner side, MWe
N	cycle number	$\dot{W}_{PSOLCAR}$	Power consumptions for solids transport in the carbonator side, MWe
P	pressure, bar	$\dot{W}_{AUXPOWCA}$	auxiliary power consumptions in the calciner side, MWe
P_{carb}	absolute carbonator pressure, bar	$\dot{W}_{AUXPOWCR}$	auxiliary power consumptions in the carbonator side, MWe
P_{eq}	CO_2 partial pressure at equilibrium, bar	X	average CaO conversion
PR	pressure ratio	X_r	residual CaO conversion
$\dot{Q}_{input}$	solar power input	ΔP	pressure drop at carbonator, bar
SM	solar multiple	Δt_{sun}	average daytime period (h)
T	temperature, °C	$\Delta H_R(T_{react})$	reaction enthalpy at the reactor temperature, kJ/mol
$T_{calciner}$	calciner temperature, °C	ΔH_R^0	standard enthalpy of reaction, kJ/mol
T_{carb}	carbonator temperature, °C	η	global net efficiency
T_{eq}	equilibrium temperature, °C	ϕ	packing density

References

[1] National Renewable energy laboratory (NREL). Concentrating solar power projects n.d. https://www.nrel.gov/csp/solarpaces/. [Accessed 2 April 2017].

[2] Li TX, Wu S, Yan T, Xu JX, Wang RZ. A novel solid–gas thermochemical multilevel sorption thermal battery for cascaded solar thermal energy storage. Appl Energy 2016;161:1–10. https://doi.org/10.1016/j.apenergy.2015.09.084.

[3] N'Tsoukpoe KE, Liu H, Le Pierrès N, Luo L. A review on long-term sorption solar energy storage. Renew Sustain Energy Rev 2009;13:2385–96. https://doi.org/10.1016/j.rser.2009.05.008.

[4] Kuravi S, Trahan J, Goswami DY, Rahman MM, Stefanakos EK. Thermal energy storage technologies and systems for concentrating solar power plants. Prog Energy Combust Sci 2013;39:285–319. https://doi.org/10.1016/j.pecs.2013.02.001.

[5] Pardo P, Deydier A, Anxionnaz-Minvielle Z, Rougé S, Cabassud M, Cognet P. A review on high temperature thermochemical heat energy storage. Renew Sustain Energy Rev 2014;32:591–610. https://doi.org/10.1016/j.rser.2013.12.014.

[6] Schmidt M, Linder M. Power generation based on the Ca(OH)2/CaO thermochemical storage system – experimental investigation of discharge operation modes in lab scale and corresponding conceptual process design. Appl Energy 2017;203:594–607. https://doi.org/10.1016/j.apenergy.2017.06.063.

[7] Singh A, Tescari S, Lantin G, Agrafiotis C, Roeb M, Sattler C. Solar thermochemical heat storage via the Co 3 O 4/CoO looping cycle: storage reactor modelling and experimental validation. Sol Energy 2017;144:453–65. https://doi.org/10.1016/j.solener.2017.01.052.

[8] Chacartegui R, Alovisio A, Ortiz C, Valverde JM, Verda V, Becerra JA. Thermochemical energy storage of concentrated solar power by integration of the calcium looping process and a CO2 power cycle. Appl Energy 2016;173:589–605. https://doi.org/10.1016/j.apenergy.2016.04.053.

[9] Bagherisereshki E, Tran J, Lei F, AuYeung N. Investigation into SrO/SrCO 3 for high temperature thermochemical energy storage. Sol Energy 2018;160:85–93. https://doi.org/10.1016/j.solener.2017.11.073.

[10] Rhodes NR, Barde A, Randhir K, Li L, Hahn DW, Mei R, et al. Solar thermochemical energy storage through carbonation cycles of SrCO3/SrO supported on SrZrO3. ChemSusChem 2015. https://doi.org/10.1002/cssc.201501023. n/a-n/a.

[11] Qu X, Li Y, Li P, Wan Q, Zhai F. The development of metal hydrides using as concentrating solar thermal storage materials. Front Mater Sci 2015;9:317–31. https://doi.org/10.1007/s11706-015-0311-y.

[12] Chen C, Aryafar H, Lovegrove KM, Lavine AS. Modeling of ammonia synthesis to produce supercritical steam for solar thermochemical energy storage. Sol Energy 2017;155:363–71. https://doi.org/10.1016/j.solener.2017.06.049.

[13] Sattler C, Roeb M, Agrafiotis C, Thomey D. Solar hydrogen production via sulphur based thermochemical water-splitting. Sol Energy 2017;156:30–47. https://doi.org/10.1016/j.solener.2017.05.060.

[14] Edwards JH, Do KT, Maitra AM, Schuck S, Fok W, Stein W. The use if solar-based CO2/CH4 reforming for reducing greenhouse gas emissions ruding the generation of electricity and process heat. Energy Convers Manag 1996;37(6–8):1339–44.

[15] Wentworth WE, Chen E. Simple thermal decomposition reactions for storage of solar thermal energy. Sol Energy 1976;18:205–14. https://doi.org/10.1016/0038-092X(76)90019-0.

[16] Barker R. The reactivity of calcium oxide towards carbon dioxide and its use for energy storage. J Appl Chem Biotechnol 2007;24:221–7. https://doi.org/10.1002/jctb.2720240405.

[17] Obermeier J, Sakellariou KG, Tsongidis NI, Baciu D, Charalambopoulou G, Steriotis T, et al. Material development and assessment of an energy storage concept based on the CaO-looping process. Sol Energy 2017;150:298–309. https://doi.org/10.1016/j.solener.2017.04.058.

[18] Benitez-Guerrero M, Sarrion B, Perejon A, Sanchez-Jimenez PE, Perez-Maqueda LA, Manuel Valverde J. Large-scale high-temperature solar energy storage using natural minerals. Sol Energy Mater Sol Cells 2017;168:14–21. https://doi.org/10.1016/j.solmat.2017.04.013.

[19] Kyaw K, Matsuda H, Hasatani M. Applicability of carbonation/decarbonation reactions to high-temperature thermal energy storage and temperature upgrading. J Chem Eng Jpn 1996;29:119–25. https://doi.org/10.1252/jcej.29.119.

[20] Sakellariou KG, Karagiannakis G, Criado YA, Konstandopoulos AG. Calcium oxide based materials for thermochemical heat storage in concentrated solar power plants. Sol Energy 2015;122:215–30. https://doi.org/10.1016/j.solener.2015.08.011.

[21] Ortiz C, Chacartegui R, Valverde JM, Alovisio A, Becerra JA. Power cycles integration in concentrated solar power plants with energy storage based on calcium looping. Energy Convers Manag 2017;149:815–29. https://doi.org/10.1016/j.enconman.2017.03.029.

[22] Meier A, Gremaud N, Steinfeld A. Economic evaluation of the industrial solar production of lime. Energy Convers Manag 2005;46:905–26. https://doi.org/10.1016/j.enconman.2004.06.005.

[23] Atsonios K, Grammelis P, Antiohos SK, Nikolopoulos N, Kakaras E. Integration of calcium looping technology in existing cement plant for CO2 capture: process modeling and technical considerations. Fuel 2015;153:210–23. https://doi.org/10.1016/j.fuel.2015.02.084.

[24] Dean CC, Blamey J, Florin NH, Al-Jeboori MJ, Fennell PS. The calcium looping cycle for CO2 capture from power generation, cement manufacture and hydrogen production. Chem Eng Res Des 2011;89:836–55. https://doi.org/10.1016/j.cherd.2010.10.013.

[25] Romeo LM, Lara Y, Lisbona P, Martínez A. Economical assessment of competitive enhanced limestones for CO2 capture cycles in power plants. Fuel Process Technol 2009;90:803–11. https://doi.org/10.1016/j.fuproc.2009.03.014.

[26] Martínez A, Lara Y, Lisbona P, Romeo LM. Energy penalty reduction in the calcium looping cycle. Int J Greenh Gas Control 2012;7:74–81. https://doi.org/10.1016/j.ijggc.2011.12.005.

[27] Cormos C-C. Economic evaluations of coal-based combustion and gasification power plants with post-combustion CO 2 capture using calcium looping cycle. Energy 2014;78:665–73. https://doi.org/10.1016/j.energy.2014.10.054.

[28] Barin I. Thermochemical data of pure substances. Weinheim: VCH; 1989. p. 1989.

[29] Flamant G, Hernandez D, Bonet C, Traverse J-P. Experimental aspects of the thermochemical conversion of solar energy; Decarbonation of CaCO3. Sol Energy 1980;24:385–95. https://doi.org/10.1016/0038-092X(80)90301-1.

[30] Fidaros DK. Baxevanou C a., Vlachos NS. A parametric study of a solar calcinator using computational fluid dynamics. Energy Convers Manag 2007;48:2784–91. https://doi.org/10.1016/j.enconman.2007.07.025.

[31] Meier A, Bonaldi E, Cella GM, Lipinski W, Wuillemin D. Solar chemical reactor technology for industrial production of lime. Sol Energy 2006;80:1355–62. https://doi.org/10.1016/j.solener.2005.05.017.

[32] Reich L. Towards solar thermochemical carbon dioxide capture via calcium oxide looping: a review. Aerosol Air Qual Res 2014;14:500–14. https://doi.org/10.4209/aaqr.2013.05.0169.

[33] Abanades S, André L. Design and demonstration of a high temperature solar-heated rotary tube reactor for continuous particles calcination. Appl Energy 2018;212:1310–20. https://doi.org/10.1016/j.apenergy.2018.01.019.

[34] Valverde JM, Barea-López M, Perejón A, Sánchez-Jiménez PE, Pérez-Maqueda LA. Effect of thermal pretreatment and nanosilica addition on limestone performance at calcium-looping conditions for thermochemical energy storage of concentrated solar power. Energy Fuels 2017;31:4226–36. https://doi.org/10.1021/acs.energyfuels.6b03364.

[35] Benitez-Guerrero M, Valverde JM, Perejon A, Sanchez-Jimenez PE, Perez-Maqueda LA. Low-cost Ca-based composites synthesized by biotemplate method for thermochemical energy storage of concentrated solar power. Appl Energy 2018;210:108–16. https://doi.org/10.1016/j.apenergy.2017.10.109.

[36] Edwards SEB, Materić V. Calcium looping in solar power generation plants. Sol Energy 2012;86:2494–503. https://doi.org/10.1016/j.solener.2012.05.019.

[37] Alovisio A, Chacartegui R, Ortiz C, Valverde JM, Verda V. Optimizing the CSP-calcium looping integration for thermochemical energy storage. Energy Convers Manag 2017;136:85–98. https://doi.org/10.1016/j.enconman.2016.12.093.

[38] Hanak DP, Manovic V. Calcium looping with inherent energy storage for decarbonisation of coal-fired power plant. Energy Environ Sci 2016;9:971–83. https://doi.org/10.1016/j.energy.2016.02.079.

[39] Le Moullec Y. Conceptual study of a high efficiency coal-fired power plant with CO2capture using a supercritical CO2Brayton cycle. Energy 2013;49:32–46. https://doi.org/10.1016/j.energy.2012.10.022.

[40] Binotti M, Astolfi M, Campanari S, Manzolini G, Silva P. Preliminary assessment of sCO2cycles for power generation in CSP solar tower plants. Appl Energy 2017;204:1007–17. https://doi.org/10.1016/j.apenergy.2017.05.121.

[41] Criado YA, Arias B, Abanades JC. Calcium looping CO2 capture system for back-up power plants. Energy Environ Sci 2017;10:1994–2004. https://doi.org/10.1039/C7EE01505D.

[42] Tregambi C, Montagnaro F, Salatino P, Solimene R. A model of integrated calcium looping for CO2 capture and concentrated solar power. Sol Energy 2015;120:208–20. https://doi.org/10.1016/j.solener.2015.07.017.

[43] Zhai R, Li C, Qi J, Yang Y. Thermodynamic analysis of CO2 capture by calcium looping process driven by coal and concentrated solar power. Energy Convers Manag 2016;117:251–63. https://doi.org/10.1016/j.enconman.2016.03.022.

[44] Hoffschmidt B. Receivers for solar tower systems. 2014.

[45] Ho CK. A review of high-temperature particle receivers for concentrating solar power. Appl Therm Eng 2016;109:958–69. https://doi.org/10.1016/j.applthermaleng.2016.04.103.

[46] Koepf E, Alxneit I, Wieckert C, Meier A. A review of high temperature solar driven reactor technology: 25years of experience in research and development at the Paul Scherrer Institute. Appl Energy 2017;188:620–51. https://doi.org/10.1016/j.apenergy.2016.11.088.

[47] SOLPART project. Temperature solar-heated reactors for industrial production of reactive particulates n.d. http://www.solpart-project.eu/(accessed June 1, 2017).

[48] Perejón A, Romeo LM, Lara Y, Lisbona P, Martínez A, Valverde JM. The Calcium-Looping technology for CO 2 capture: on the important roles of energy integration and sorbent behavior. Appl Energy 2016;162:787–807. https://doi.org/10.1016/j.apenergy.2015.10.121.

[49] Valverde JM, Sanchez-Jimenez PE, Perez-Maqueda L. Role of precalcination and regeneration conditions on postcombustion CO 2 capture in the Ca-looping technology. Appl Energy 2014;136:347–56. https://doi.org/10.1016/j.apenergy.2014.09.052.

[50] Valverde JM, Sanchez-Jimenez PE, Perez-Maqueda L. Ca-looping for post-combustion CO2 capture: a comparative analysis on the performances of dolomite and limestone. Appl Energy 2015;138:202–15. https://doi.org/

10.1016/j.apenergy.2014.10.087.
[51] Gil A, Medrano M, Martorell I, Lázaro A, Dolado P, Zalba B, et al. State of the art on high temperature thermal energy storage for power generation. Part 1—concepts, materials and modellization. Renew Sustain Energy Rev 2010;14:31–55. https://doi.org/10.1016/j.rser.2009.07.035.
[52] Abedin AH. A critical review of thermochemical energy storage systems. Open Renew Energy J 2011;4:42–6. https://doi.org/10.2174/1876387101004010042.
[53] Felderhoff M, Urbanczyk R, Peil S. Thermochemical heat storage for high temperature applications – a review. Green 2013;3:113–23. https://doi.org/10.1515/green-2013-0011.
[54] Guy E. Solar heat storage using chemical reactions. J Solid State Chem 1977;22:51–61.
[55] Prieto C, Cooper P, Fernandez AI, Cabeza LF. Review of technology: thermochemical energy storage for concentrated solar power plants. Renew Sustain Energy Rev 2016;60:909–29. https://doi.org/10.1017/CBO9781107415324.004.
[56] Valverde JM, Castellanos A. Random loose packing of cohesive granular materials. Europhys Lett 2007;75:985–91. https://doi.org/10.1209/epl/i2006-10208-4.
[57] Ortega-Fernández I, Calvet N, Gil A, Rodríguez-Aseguinolaza J, Faik A, D'Aguanno B. Thermophysical characterization of a by-product from the steel industry to be used as a sustainable and low-cost thermal energy storage material. Energy 2015;89:601–9. https://doi.org/10.1016/j.energy.2015.05.153.
[58] Kvamsdal HM, Romano MC, van der Ham L, Bonalumi D, van Os P, Goetheer E. Energetic evaluation of a power plant integrated with a piperazine-based CO 2 capture process. Int J Greenh Gas Control 2014;28:343–55. https://doi.org/10.1016/j.ijggc.2014.07.004.
[59] Mills D. Pneumatic conveying design guide. 2004. p. 80.
[60] Schorcht F, Kourti I, Scalet BM, Roudier S, Sancho LD. Best available techniques (BAT). Reference document for the production of cement. Lime and Magnesium Oxide 2015. https://doi.org/10.2788/12850.
[61] Kyaw K, Kubota M, Watanabe F, Matsuda H, Hasatani M. Study of carbonation of CaO for high temperature thermal energy storage. J Chem Eng Jpn 1998;31:281–4. https://doi.org/10.1252/jcej.31.281.